MACROMOLECULAR STRUCTURE UNDERLYING RECOGNITION IN INNATE IMMUNITY

EDITED BY: Uttara SenGupta, Uday Kishore and Maha Ahmed Al-Mozaini
PUBLISHED IN: Frontiers in Immunology

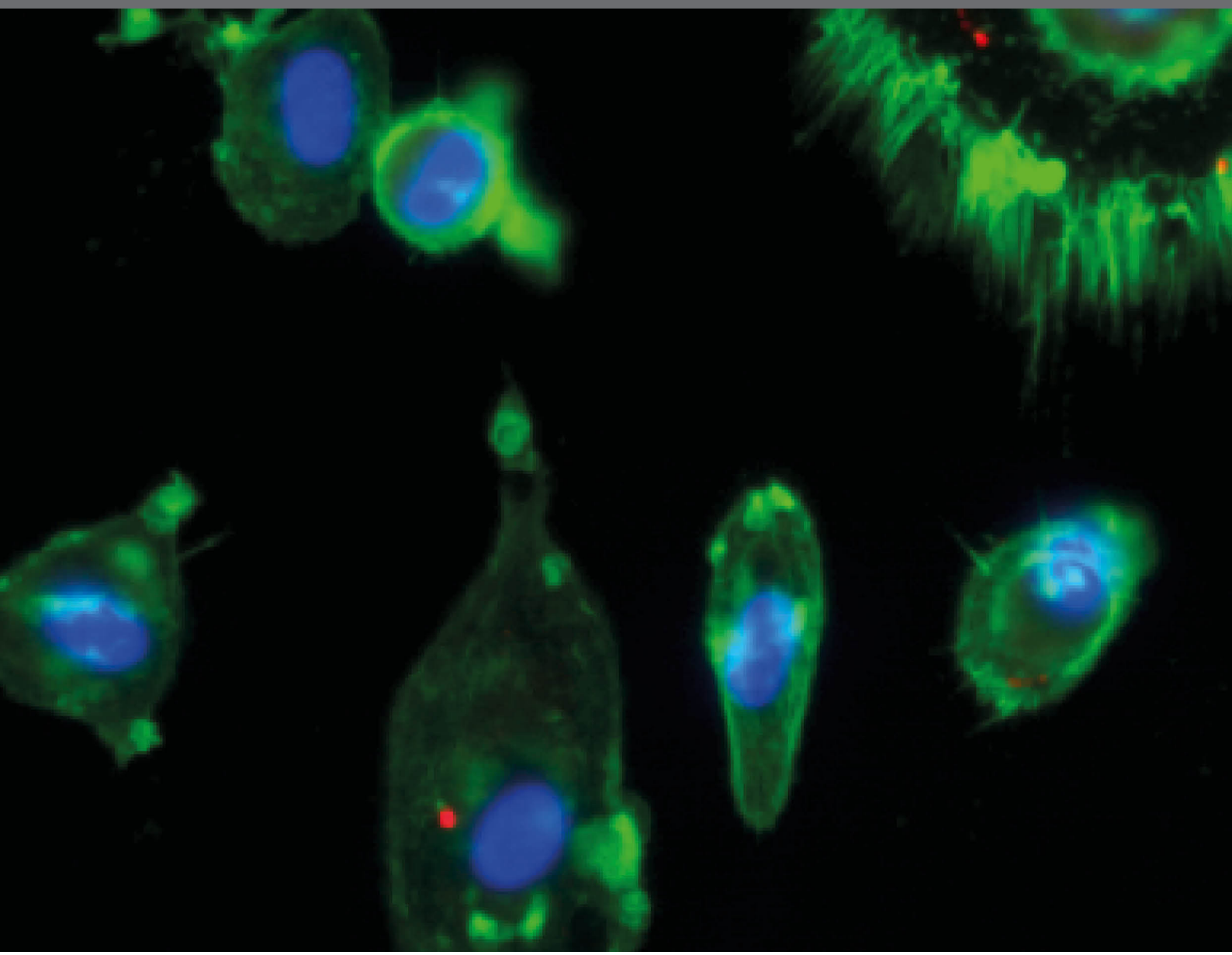

frontiers Research Topics

frontiers

ISSN 1664-8714
ISBN 978-2-88945-527-0
DOI 10.3389/978-2-88945-527-0

About Frontiers

Frontiers is more than just an open-access publisher of scholarly articles: it is a pioneering approach to the world of academia, radically improving the way scholarly research is managed. The grand vision of Frontiers is a world where all people have an equal opportunity to seek, share and generate knowledge. Frontiers provides immediate and permanent online open access to all its publications, but this alone is not enough to realize our grand goals.

Frontiers Journal Series

The Frontiers Journal Series is a multi-tier and interdisciplinary set of open-access, online journals, promising a paradigm shift from the current review, selection and dissemination processes in academic publishing. All Frontiers journals are driven by researchers for researchers; therefore, they constitute a service to the scholarly community. At the same time, the Frontiers Journal Series operates on a revolutionary invention, the tiered publishing system, initially addressing specific communities of scholars, and gradually climbing up to broader public understanding, thus serving the interests of the lay society, too.

Dedication to quality

Each Frontiers article is a landmark of the highest quality, thanks to genuinely collaborative interactions between authors and review editors, who include some of the world's best academicians. Research must be certified by peers before entering a stream of knowledge that may eventually reach the public - and shape society; therefore, Frontiers only applies the most rigorous and unbiased reviews.
Frontiers revolutionizes research publishing by freely delivering the most outstanding research, evaluated with no bias from both the academic and social point of view. By applying the most advanced information technologies, Frontiers is catapulting scholarly publishing into a new generation.

What are Frontiers Research Topics?

Frontiers Research Topics are very popular trademarks of the Frontiers Journals Series: they are collections of at least ten articles, all centered on a particular subject. With their unique mix of varied contributions from Original Research to Review Articles, Frontiers Research Topics unify the most influential researchers, the latest key findings and historical advances in a hot research area! Find out more on how to host your own Frontiers Research Topic or contribute to one as an author by contacting the Frontiers Editorial Office: researchtopics@frontiersin.org

MACROMOLECULAR STRUCTURE UNDERLYING RECOGNITION IN INNATE IMMUNITY

Topic Editors:
Uttara SenGupta, Northwick Park Institute for Medical Research, United Kingdom
Uday Kishore, Brunel University, United Kingdom
Maha Ahmed Al-Mozaini, King Faisal Specialist Hospital & Research Centre, Saudi Arabia

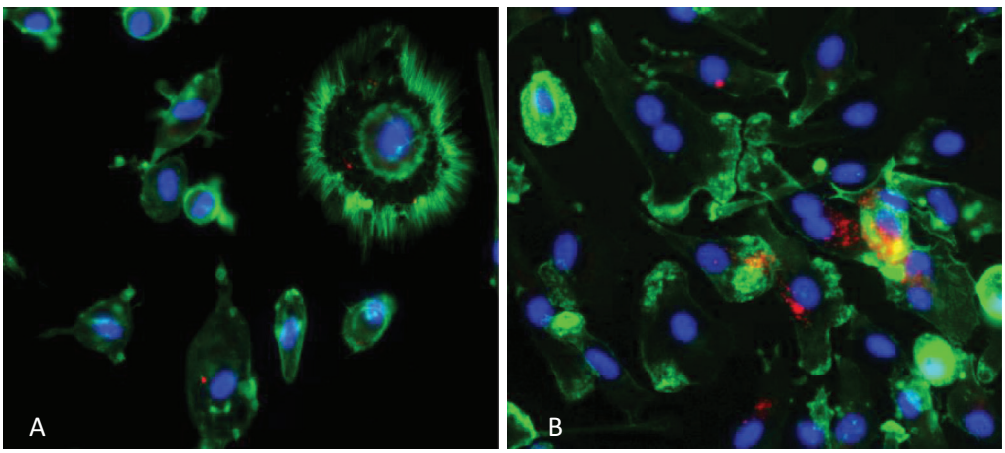

Human peripheral monocytes (green: plasma membrane; blue: nucleus) incubated with biotin-labelled carbon nanotubes (A: no complement B: complement deposited).
Image: Gudrun Stenbeck and Uday Kishore.

Citation: SenGupta, U., Kishore, U., Al-Mozaini, M. A., eds. (2018). Macromolecular Structure Underlying Recognition in Innate Immunity. Lausanne: Frontiers Media. doi: 10.3389/978-2-88945-527-0

Table of Contents

frontiers in Immunology

EDITORIAL
published: 15 May 2018
doi: 10.3389/fimmu.2018.00980

Editorial: Macromolecular Structure Underlying Recognition in Innate Immunity

*Uday Kishore**

Biosciences, College of Health and Life Sciences, Brunel University London, Uxbridge, United Kingdom

Keywords: pattern recognition, innate immunity, host–pathogen interactions, protein–protein interaction, HIV-1, malaria, zebrafish model system

Editorial on the Research Topic

Macromolecular Structure Underlying Recognition in Innate Immunity

Our innate immune system has evolved to distinguish between self, non-self, altered self, and intrinsic as well as extrinsic danger signals. Recognition is mediated *via* interactions between pattern recognition receptor molecules (PPRs) and their ligands, which include hydrophobic and electrostatic interactions between amino acid residues on the PPRs and uncharged or charged groups on amino acid residues, sugar rings, or DNA/RNA molecules. These PRRs can be phagocytic, sensors, and humoral. Recognition in innate immunity can involve interaction between many ligands with one receptor molecule, and the density and the number of glycans, charge patterns or epitopes dictate a strong and specific recognition, distinct from weak non-specific binding (1). In the case of toll-like receptors (TLRs) and nucleotide-binding oligomerization domain-like receptors (NLRs), the ligand recognition is followed by oligomerization of the receptor molecules. This special topic issue has made an effort to somewhat highlight the complexity of such biological interactions and their, sometimes unexpected, consequences.

Bessa Pereira et al. have taken up the case of a scavenger receptor, SSc5D, which belongs to the scavenger receptor cysteine-rich (SRCR) family, and have made an effort to localize domains involved in pathogen-associated molecular patterns (PAMPs) recognition. SRCR proteins can be membrane-bound or secreted that contain type I macrophage scavenger receptor domain/s. SSc5D is a soluble SRCR composed of an N-terminal, five SRCR domains (N-SSc5D) and a C-terminal mucin-like domain. Based on surface plasmon resonance-measurements of interaction kinetics, N-SSc5D was found to have a better ability to bind *Escherichia coli* strains RS218 and IHE3034, and *Listeria monocytogenes*. This paper speculates on the importance of differential SRCR binding on the strain specificity. An associated commentary on this paper by Lozano and Martínez-Florensa, however, sounds a cautionary note on the interpretation of the data, especially with respect to CD6 that does not seem to be functional in the studies by Bessa Pereira et al. The scientific exchange between the two research groups (Lozano and Martínez-Florensa; Oliveira and Carmo) raises an important issue that a number of variations reported in the literature could owe to the design of the constructs and choice of domains used.

The study and critique on SRCR (Bessa Pereira et al.; Lozano and Martínez-Florensa; Oliveira and Carmo) are followed by some excellent, though diverse, papers that highlight the importance of understanding protein–ligand and protein–protein interactions in innate and adaptive immunity. Two papers (Hellmuth et al.; Wan et al.) dwell upon the modalities of modulating intracellular PRRs (sensors) and their immunological consequences. Hellmuth et al. have made a synthetic bid to impede TLR7 activation by conjugating single-stranded RNA (ssRNA for TLR7 stimulation), small molecules TLR7 agonists (smTLRa for immune potentiation of candidate vaccines), and an interference RNA (siRNA). Contrary to an expected synergistic effect, the authors reported a reduced TLR7 activation and encouraged the notion of shielding effect of the conjugates on TLR7 stimulation

OPEN ACCESS

Edited and Reviewed by:
Thomas A. Kufer, University of Hohenheim, Germany

***Correspondence:**
Uday Kishore
ukishore@hotmail.com, uday.kishore@brunel.ac.uk

Specialty section:
This article was submitted to Molecular Innate Immunity, a section of the journal Frontiers in Immunology

Received: *17 March 2018*
Accepted: *20 April 2018*
Published: *15 May 2018*

Citation:
Kishore U (2018) Editorial: Macromolecular Structure Underlying Recognition in Innate Immunity. Front. Immunol. 9:980. doi: 10.3389/fimmu.2018.00980

(Hellmuth et al.). Wan et al. have examined, using a grass carp model, downstream signaling and interferon (IFN) response involving two intracellular sensors: retinoic acid-inducible gene I (RIG-I) and melanoma differentiation-associated gene 5 (MDA5). Following grass carp reovirus infection, MDA5 induced an elaborate type I IFN response; both MDA5 and RIG-I facilitated the total phosphorylation levels of IFN regulatory factor (IRF) 3 and 7 (IRF7). Whereas MDA5 enhanced the heterodimerization of IRF3 and IRF7 and homodimerization of IRF7, RIG-I facilitated the heterodimerization and attenuated IRF7 homodimerization. The consequence of this differential multimerization renders MDA5 a more effective modulator of IFN response compared to RIG-1 (Wan et al.). In an exciting paper on zebrafish innate immunity, García-Valtanen et al. have investigated, *via* transcriptomics and immunohistochemistry, the immune responses of *Rag1* gene knock-out ($^{-/-}$) phenotype (zebrafish deficient in its adaptive immune wing) to Spring Viremia Carp Virus (SVCV) infection. Remarkably, *Rag1*$^{-/-}$ zebrafish showed resistance to SVCV in an age-dependent manner, compared to their *Rag1*$^{+/+}$ counterparts. The analysis of the microarray data revealed that genes related to apoptotic functions, immune-related multigene families, and IFN-related components were constitutively upregulated in adult *Rag1*$^{-/-}$ zebrafish, thus preparing the host for the impending pathogen insult. In addition, in the absence of T and B cell functions, the *Rag1*$^{-/-}$ mice relied heavily on the infiltration of macrophages and natural killer cells, and IFNs for achieving a sustainable anti-viral state (García-Valtanen et al.; García-Valtanen et al.). Next, Kajla et al. report that heme peroxidase HPX15, which is found in the midgut of mosquito *Anopheles stephensi*, encourages development of *Plasmodium* parasite by suppressing local immune mechanisms. The orthologs of HPX15 are absent in non-*Anopheles* mosquitoes, insects, or human. Silencing of this gene *via* iRNA reduced the midgut parasite load in the mosquito, suggesting that interference with HPX15 gene can be exploited to contain the *Plasmodium* within the vector and minimize its dissemination.

There are five papers that take up a range of issues related to two key complement proteins, C1q and properdin. C1q is the first subcomponent of the complement classical pathway that binds to IgG or IgM containing immune complexes and a number of self and non-self target ligands *via* its globular (gC1q) domain. The gC1q domain is located C-terminal to a triple-helical collagen-like domain, which offers sites for interaction with C1r and C1s subcomponents, in addition to binding to its putative receptors, including calreticulin-CD91 complex (2). C1q is a versatile soluble charge pattern recognition molecule of the innate immunity. The gC1q domain is a heterotrimeric structure, which is composed of C-terminal ends of the three chains of C1q (A, B, and C chains). Individually expressed globular head (gh) modules of the three chains (ghA, ghB, and ghC) have been functionally characterized previously (3), which established the concept of structural and functional modularity within the heterotrimeric structure of the gC1q domain. However, in this volume, generation of a recombinant form of heterotrimeric gC1q domain is being reported by Gaboriaud et al. using a mammalian expression system (Moreau et al.), which is functionally active and its crystal structure mirrors that of the native gC1q domain generated *via* collagenase digestion of an intact human C1q molecule. Thus, this recombinant gC1q domain can be of great help in basic and clinical research on human C1q, in addition to being an excellent reagent/tool for the complement research community. On the continuing theme of gC1q domain, Pednekar et al. have examined the nature of interaction of the recombinant ghA, ghB, and ghC modules as well their substitution mutants with a gC1q putative receptor molecule, gC1qR. Another paper examines interaction between dendritic cell-specific intercellular adhesion molecule-3-grabbing non-integrin (DC-SIGN; CD209), C1q and gC1qR, and its implication on HIV-1 infection (Pednekar et al.). It sheds an interesting light on host–pathogen interaction involving three immune molecules and one pathogen component. C1q, by virtue of its ability to bind DC-SIGN, appears to suppress DC-SIGN mediated transfer of HIV-1 to $CD4^+$ T cells while gC1qR appears to enhance trans-infection, raising the possibility that HIV-1 may recruit/exploit gC1qR in order to negate the protective effect of C1q (Pednekar et al.).

The final two papers in this issue report pattern recognition properties of human properdin, an upregulator of the complement alternative pathway. Properdin stabilizes C3bBb convertase in the alternative pathway, and its functions have largely been considered to be reliant on C3b deposition on the complement-activating surfaces (4). However, there are recent evidences to suggest that local production of properdin by immune cells including dendritic cells, neutrophils, and T cells may be geared at complement-independent functions of properdin. Kouser et al. report that human properdin can opsonize nanoparticles using its thrombospondin repeats 4 and 5 (TSR4 + 5) and mount a robust pro-inflammatory immune response *via* recruitment of NF-κB. One of the major findings reported in this paper is that a recombinant form of TSR4 + 5, expressed in tandem and coated on the nanoparticles, can act as an inhibitor of the alternative pathway, thus paving a way forward for *in vivo* preclinical trials of such nanoparticles for dampening exaggerated complement activation in a range of disease models (5; Kouser et al.). Al-Mozaini et al. have examined complement-independent interaction between human properdin and *Mycobacterium bovis* BCG. Contrary to their behavior when coated on nanoparticles, properdin, and recombinant TSR4 + 5 appear to exert an anti-opsonic effect on *M. bovis* BCG, thus, reducing micro-organism uptake by phagocytic cells (Al-Mozaini et al.). These two papers (Kouser et al.; Al-Mozaini et al.) appear to highlight that properdin can act as a soluble PRR, it does not always require the availability of C3b bound to target ligands, and that properdin on its own can modulate local inflammatory response. However, in the case of nanoparticles, properdin seems to enhance phagocytosis; whereas in the case of *M. bovis* BCG, it appears to reduce uptake: a contrasting and intriguing set of observations. Clearly, specific ligands need to be identified on *Mycobacterium* whose masking by properdin may interfere with surface receptors on macrophages that are used by this pathogen to enter its intracellular habitat.

AUTHOR CONTRIBUTIONS

UK reflected on the papers published within the volume and wrote the manuscript.

REFERENCES

1. Dam TK, Brewer CF. Lectins as pattern recognition molecules: the effects of epitope density in innate immunity. *Glycobiology* (2010) 20(3):270–9. doi:10.1093/glycob/cwp186
2. Kishore U, Gaboriaud C, Waters P, Shrive AK, Greenhough TJ, Reid KB, et al. C1q and tumor necrosis factor superfamily: modularity and versatility. *Trends Immunol* (2004) 25(10):551–61. doi:10.1016/j.it.2004.08.006
3. Kishore U, Gupta SK, Perdikoulis MV, Kojouharova MS, Urban BC, Reid KB. Modular organization of the carboxyl-terminal, globular head region of human C1q A, B, and C chains. *J Immunol* (2003) 171(2):812–20. doi:10.4049/jimmunol.171.2.812
4. Kouser L, Abdul-Aziz M, Nayak A, Stover CM, Sim RB, Kishore U. Properdin and factor H: opposing players on the alternative complement pathway "see-saw". *Front. Immunol* (2013) 4:93. doi:10.3389/fimmu.2013.00093
5. Kouser L, Abdul-Aziz M, Tsolaki AG, Singhal D, Schwaeble WJ, Urban BC, et al. A recombinant two-module form of human properdin is an inhibitor of the complement alternative pathway. *Mol Immunol* (2016) 73:76–87. doi:10.1016/j.molimm.2016.03.005

Conflict of Interest Statement: The author declares that the research was conducted in the absence of any commercial or financial relationships that could be construed as a potential conflict of interest.

frontiers in Immunology

ORIGINAL RESEARCH
published: 13 October 2016
doi: 10.3389/fimmu.2016.00416

The Scavenger Receptor SSc5D Physically Interacts with Bacteria through the SRCR-Containing N-Terminal Domain

Catarina Bessa Pereira[1,2,3†], Markéta Bocková[4†], Rita F. Santos[1,2], Ana Mafalda Santos[5], Mafalda Martins de Araújo[1,2], Liliana Oliveira[1,2], Jiří Homola[4‡] and Alexandre M. Carmo[1,2,3‡]*

[1] *i3S-Instituto de Investigação e Inovação em Saúde, Universidade do Porto, Porto, Portugal,* [2] *IBMC – Instituto de Biologia Molecular e Celular, Porto, Portugal,* [3] *ICBAS – Instituto de Ciências Biomédicas Abel Salazar, Universidade do Porto, Porto, Portugal,* [4] *Institute of Photonics and Electronics of the Czech Academy of Sciences, Prague, Czech Republic,* [5] *MRC Human Immunology Unit, Nuffield Department of Clinical Medicine, Weatherall Institute of Molecular Medicine, University of Oxford, Oxford, UK*

OPEN ACCESS

Edited by:
Uday Kishore,
Brunel University London, UK

Reviewed by:
Simon John Clark,
University of Manchester, UK
Bernardo Louis Trigatti,
McMaster University, Canada

****Correspondence:***
Alexandre M. Carmo
acarmo@ibmc.up.pt

†Catarina Bessa Pereira and Markéta Bocková are co-first authors.

‡Jiří Homola and Alexandre M. Carmo are co-senior authors.

Specialty section:
This article was submitted to Molecular Innate Immunity, a section of the journal Frontiers in Immunology

Received: *08 July 2016*
Accepted: *26 September 2016*
Published: *13 October 2016*

Citation:
Bessa Pereira C, Bocková M, Santos RF, Santos AM, Martins de Araújo M, Oliveira L, Homola J and Carmo AM (2016) The Scavenger Receptor SSc5D Physically Interacts with Bacteria through the SRCR-Containing N-Terminal Domain. Front. Immunol. 7:416. doi: 10.3389/fimmu.2016.00416

The scavenger receptor cysteine-rich (SRCR) family comprises a group of membrane-attached or secreted proteins that contain one or more modules/domains structurally similar to the membrane distal domain of type I macrophage scavenger receptor. Although no all-inclusive biological function has been ascribed to the SRCR family, some of these receptors have been shown to recognize pathogen-associated molecular patterns (PAMP) of bacteria, fungi, or other microbes. SSc5D is a recently described soluble SRCR receptor produced by monocytes/macrophages and T lymphocytes, consisting of an N-terminal portion, which contains five SRCR modules, and a large C-terminal mucin-like domain. Toward establishing a global common role for SRCR domains, we interrogated whether the set of five SRCR domains of SSc5D displayed pattern recognition receptor (PRR) properties. For that purpose, we have expressed in a mammalian expression system the N-terminal SRCR-containing moiety of SSc5D (N-SSc5D), thus excluding the mucin-like domain likely by nature to bind microorganisms, and tested the capacity of the SRCR functional groups to physically interact with bacteria. Using conventional protein–bacteria binding assays, we showed that N-SSc5D had a superior capacity to bind to *Escherichia coli* strains RS218 and IHE3034 compared with that of the extracellular domains of the SRCR proteins CD5 and CD6 (sCD5 and sCD6, respectively), and similar *E. coli*-binding properties as Spα, a proven PRR of the SRCR family. We have further designed a more sensitive, real-time, and label-free surface plasmon resonance (SPR)-based assay and examined the capacity of N-SSc5D, Spα, sCD5, and sCD6 to bind to different bacteria. We demonstrated that N-SSc5D compares with Spα in the capacity to bind to *E. coli* and *Listeria monocytogenes*, and further that it can distinguish between pathogenic *E. coli* RS218 and IHE3034 strains and the non-pathogenic laboratory *E. coli* strain BL21(DE3). Our work thus advocates the utility of SPR-based assays as sensitive tools for the rapid screening of interactions between immune-related receptors and PAMP-bearing microbes. The analysis of our results suggests that SRCR domains of different members of the family have a differential capacity to interact with bacteria, and further that the same receptor can discriminate between different bacteria strains and species.

Keywords: surface plasmon resonance, scavenger receptor cysteine-rich, pattern recognition receptors, bacteria

INTRODUCTION

Pattern recognition receptors (PRR) are membrane-bound or cytosolic receptors of plants and animals that are capable of interacting with pathogen-associated molecular patterns (PAMP), including lipopolysaccharide (LPS) of Gram-negative bacteria, the Gram-positive bacteria lipotheicoic acid (LTA) and peptydoglycan (PGN), as well as the fungi polysaccharides Zymosan or β-glucan, thus providing a first line of immune defense against microbes or their secreted toxins. Several families of PRR have been reported to be specific for pathogens or virulence factors, and they include Toll-like receptors, nucleotide-binding oligomerization domain (NOD)-like receptors, retinoic acid-inducible gene I (RIG-I)-like receptors, and C-type lectin receptors, among others (1). In contrast, receptors belonging to yet another group, the scavenger receptor cysteine-rich superfamily (SRCR-SF), are seldom referred to as pathogen-recognition molecules, despite the fact that several SRCR receptors have been shown to bind to and clear bacteria, fungi, or viruses from infected hosts (2).

Scavenger receptor cysteine-rich members are present in all animal phyla and although individual proteins may have various roles in, for example, cell differentiation, iron metabolism, homeostasis, or apoptosis, most SRCR proteins are thought to serve immune-related functions (3). A subfamily (group B) of the SRCR-SF consists of members present only in vertebrates (4), and four of the nine receptors described in humans have been shown to bind to bacteria or bacterial components. CD6 and CD163 are membrane-bound receptors of T cells and macrophages, respectively; DMBT1, which has a broad expression profile, and Spα, a soluble glycoprotein expressed by macrophages in the lymphoid tissues and highly present in the serum [detection levels of microgram per milliliter (5)], are molecular sensors of Gram-positive and Gram-negative bacteria (6–9). Although shown not to bind to either Gram-positive or -negative bacteria, the T cell surface SRCR protein CD5 is reported to interact with conserved fungal components and to aggregate fungal cells (10).

After bacterial challenges, the soluble SRCR protein Spα is immediately released from human macrophages to control bacteria spreading and inflammatory cytokine secretion by PRR-expressing innate cells (9). *In vivo* studies of PAMP-induced septic shock have shown that the levels of the Spα mouse homolog (mAIM/Api6/Cd5L) increase rapidly upon injection of LPS or Zymosan, further suggesting that this SRCR protein can act as a circulating PRR (11). SSc5D is a recently described soluble SRCR protein that shares many features with Spα. SSc5D is expressed in macrophages, T cells, and several epithelial cells, especially from placenta, spleen, and colon (12). It is also highly abundant in the serum and shows increased levels in inflammatory conditions (13). The mouse homolog of SSc5D [S5D-SRCRB (14)] is also upregulated upon infection and seems capable to bind bacteria (15), although this has not been reported for the human counterpart. A major difference between SSc5D and Spα relates not only to the number of SRCR domains (5 and 3, respectively) but also to the existence of a large mucin-like sequence located at the C-terminus of SSc5D. In the human molecule, this domain represents about 40% of the amino acid content of the whole protein, and it is expected that, similar to other *O*-glycosylated mucin-like proteins, it may bind and modulate pathogen behavior.

Label-free biosensors have revolutionized the qualitative and quantitative analysis of biomolecular interactions (e.g., protein–protein or protein–nucleic acids interactions) and are also broadly used in medical diagnostics, environmental monitoring, or food safety and security (16). Highly sensitive detection technology, such as surface plasmon resonance (SPR) that allows real-time studies of molecular binding processes, has been recently applied to the detection of bacteria and other microbial pathogens (17–19). These early studies have relied on the use of high-affinity antibodies recognizing particular components of bacterial surfaces. Despite the considerably weaker binding affinities for common receptor–ligand pairs when compared with antibody–antigen interactions, we hypothesized that an analogous strategy could be set up to scrutinize the interaction of secreted SRCR proteins with whole cell bacteria if these interactions were strong enough, reflecting a potential PRR nature of SRCR proteins.

In this work, we demonstrate the ability of SPR biosensor technology to monitor the interaction of secreted SRCR proteins with whole cell bacteria of different types. We have assessed the bacteria-binding capacity of the N-terminal moiety of SSc5D (excluding the mucin-like sequence likely to bind bacteria *per se*) and compared with the equivalent domains of other SRCR-family proteins, soluble Spα, and the extracellular domains of CD5 and CD6. The SPR experiments demonstrate the differential bacteria-binding capacity of N-SSc5D compared with the other SRCR proteins, and that globally these receptors can qualitatively distinguish between different types of bacteria.

MATERIALS AND METHODS

Recombinant Protein Production and Purification

The soluble extracellular domain of CD6 (sCD6) was produced as previously described (20), and the remaining recombinant proteins (N-SSc5D, Spα, and sCD5) were expressed and purified as follows. A cDNA corresponding to the N-terminal half of SSc5D (exons 1–12), which includes the five SRCR domains (N-SSc5D) (12), was amplified by PCR from human placenta cDNA using forward 5′-TATAATGGATCCGAGCGCCTGCG CCTGGCCGAT and reverse 5′-AATAGGATCCCTCTTGTGTC CGGCAGGCGCCTTATTGCTGG primers (*Bam*HI restriction sites are underlined). The Spα cDNA was amplified by PCR from human spleen cDNA using forward 5′-TTAGGATCCTCTCC ATCTGGTGTGCGGCTG and reverse 5′-CAAGGATCCACC TGAGCAGATGACAGCCAC primers. A cDNA fragment encoding the extracellular domain of human CD5 (residues Arg^{25}-Ser^{348}; sCD5) was amplified by PCR from a template CD5-pGFP-N1 kindly provided by G. Bismuth (Institut Cochin, Paris) using forward 5′-TAGGGATCCCGGCTCAGCTGGTATGAC and reverse 5′-CTAGGATCCCGGGGTTTGGATCTTGGCAT primers. Each cDNA was inserted into the *Bam*HI sites of the lab-modified version of pEE14 in order to obtain chimeric cDNAs encoding, in the following order, signal peptide, HA-tag,

the specific protein sequence (Spα, N-SSc5D, or sCD5), a BirA recognition sequence, and 6·His tag sequences.

The sCD5, N-SSc5D, and Spα vectors were transfected into CHO-K1 cells using Lipofectamine (Invitrogen). Clones resistant to 30-μM methionine sulfoximine (MSX) were selected (21) and screened for soluble CD5 (HA-sCD5-BirA-His), N-SSc5D (HA-N-SSc5D-BirA-His), and Spα (HA-Spα-BirA-His) expression using dot blots and western blots. The best clones expressing HA-sCD5-BirA-His, HA-N-SSc5D-BirA-His, and HA-Spα-BirA-His were selected for large-scale production of protein and grown in cell factories (Nunc). Proteins secreted into tissue culture supernatants were harvested after approximately 4 weeks and purified by metal-chelate chromatography using Ni Sepharose High Performance (HisTrap HP, GE Life Sciences). HA-sCD5-BirA-His was eluted from the Ni column with 250 mM imidazole in PBS, while HA-N-SSc5D-BirA-His and HA-Spα-BirA-His were eluted with 40 mM imidazole in PBS. Fractions containing the HA-N-SSc5D-BirA-His and HA-Spα-BirA-His were further purified by anionic chromatography (UNO Q column BioRad) with 1 M NaCl. The previously produced recombinant protein sCD6 also conformed to a similar structure as the newly produced proteins, having a HA-sCD6-BirA-His sequence.

Protein purity was analyzed by SDS-PAGE (Figure S1 in Supplementary Material). Samples of the fractions obtained by chromatography were run for 1 h at 150 V, and the gels were stained with Bio-Safe Coomassie Premixed Staining Solution (Bio-Rad Laboratories) for visualization of the protein products.

For N-SSc5D immunoblotting, samples were run in SDS-PAGE for 1 h at 150 V with Tris/glycine/SDS running buffer (Bio-Rad Laboratories). Samples were transferred to the nitrocellulose membrane using the iBlot™ Gel Transfer Device (Invitrogen) following the manufacturer's instructions. Then, the membrane was blocked with TBS, 0.1% Tween 20 (TBS-T), containing 5% non-fat dried milk, for 1 h with shaking. N-SSc5D was subsequently detected with rabbit anti-SSc5D (Abgent, 1:5,000) primary antibody in TBS-T with 3% non-fat dried milk, for 1 h at RT, followed by peroxidase-conjugated goat anti-rabbit IgG antibody (Sigma, 1:30,000) for 1 h at RT. The immunoblot was developed using ECL detection reagent (GE Healthcare Life Sciences), and the image was acquired in a ChemiDoc XRS+ system (Bio-Rad Laboratories).

Bacteria Strains

Listeria monocytogenes EGD-e was grown in brain heart infusion (BHI) medium (BD-Difco) at 37°C to an optical density of 0.6 at 600 nm (OD_{600}; exponential phase), and *Escherichia coli* strains [BL21(DE3), IHE3034, RS218] were grown in LB medium at 37°C to an OD_{600} of 0.45.

Conventional Bacteria–Protein Binding Assays

Recombinant proteins Spα, N-SSc5D, sCD6, and sCD5 (5 μg per assay) were incubated for 1 h at 4°C with the indicated cell suspensions of live bacteria (1×10^8 cells) in binding buffer (TBS, 1% BSA, 5 mM $CaCl_2$). Suspensions were centrifuged at 4,000 × *g* for 5 min at 4°C. Cell pellets were washed thoroughly, then resuspended in 40-μl Laemmli's sample buffer, and denatured by heating at 95°C for 10 min. Next, 20 μl of this lysate and pure recombinant proteins (25 or 100 ng) were separated in 6% SDS-PAGE. The gel was run for 1 h at 150 V with Tris/glycine/SDS running buffer (Bio-Rad Laboratories). After the SDS-PAGE, proteins were transferred to the nitrocellulose membrane using the iBlot™ Gel Transfer Device (Invitrogen) following the manufacturer's instructions. Then, the membrane was blocked with TBS-T containing 5% non-fat dried milk, for 1 h. Cell-bound protein was subsequently detected using mouse IgG1 anti-HA (clone 16B12) from Covance (0.1 μg/ml) in TBS-T with 3% non-fat dried milk, for 1 h at RT, followed by goat anti-mouse HRP-conjugated (Santa Cruz Biotechnology) (0.02 μg/ml) in the same conditions. The immunoblot was developed using ECL detection reagent (GE Healthcare Life Sciences), and the image was acquired in a ChemiDoc XRS+ system (Bio-Rad Laboratories).

SPR-Based Detection of Whole Bacterial Cell Interaction with SRCR Proteins

We used a laboratory four-channel SPR platform based on the wavelength spectroscopy of surface plasmons (Plasmon IV) (22) developed at the Institute of Photonics and Electronics, Czech Republic. In this SPR biosensor, the sensor response is expressed as a shift in the wavelength of SPR resonance and is directly proportional to the mass of biomolecules attached to the surface of the sensor. Using the calibration procedure described in Ref. (23), the surface density of both the immobilized receptors and the subsequently attached molecules can be determined. For an SPR resonance of around 750 nm, the shift of 1 nm in the SPR wavelength represents a change in the protein surface coverage of 17 ng/cm^2 (23). All the experiments were performed at 25°C. Buffers used were SA_{10} (10 mM sodium acetate, pH 4.0/5.0), PBS (10 mM phosphate, 2.9 mM KCl, 137 mM NaCl, pH 7.4), PBNa (10 mM phosphate, 2.9 mM KCl, 750 mM NaCl, pH 7.4), and Tris (10 mM Tris-HCl, pH 7.4).

Functionalization of the Sensor Chip

The sensor chip was functionalized with a mixed self-assembled monolayer (SAM) by incubating the cleaned gold chip in degassed absolute ethanol with a mixture (7:3) of $HSC_{11}(EG)_4OH$ and $HSC_{11}(EG)_6OCH_2COOH$ alkanethiols at a final concentration of 200 μM. The $HSC_{11}(EG)_6OCH_2COOH$ alkanethiols terminated with a carboxylic head group were used to anchor a receptor by amino coupling, while $HSC_{11}(EG)_4OH$ alkanethiols terminated with hydroxylic group were used to form a stable non-fouling background. For that purpose, the sensor chip was immersed in a mixed thiol solution at a temperature of 40°C for 10 min and then stored overnight in the dark at RT. After the formation of the mixed SAM, the chip was removed from the solution, rinsed with absolute ethanol and deionized water, and dried with nitrogen. The chip was then immediately mounted to the prism on the SPR sensor. The activation of carboxylic terminal groups was performed *in situ* by injecting deionized water followed by a 1:1 mixture of NHS and EDC for 5 min and deionized water again.

Conditions for immobilization have been optimized in terms of running buffer composition and pH, as well as sufficient surface coverage. Immobilization of proteins *via* covalent attachment to

COOH/OH SAM was performed at a flow rate of 30 µl/min and a temperature of 25°C. To immobilize the receptors, sodium acetate (SA_{10}) pH 4.0 (Spα, N-SSc5D, and sCD6) or 5.0 (sCD5) was flowed trough the activated surface until a baseline was achieved. Then, the SA_{10} solutions containing the receptors (2–5 µg/ml) were flowed across the activated surface until a desired surface coverage was achieved. To remove the non-covalently bound receptors, the high ionic strength PBNa buffer was flowed along the sensor surface. Finally, the sensor surface was treated with 1 M EA to deactivate residual carboxylic groups.

Detection of the Interaction of SRCRs with Bacteria

Bacteria cells were pelleted by centrifugation (4,000 × *g*, 5 min) and resuspended in PBS. Then, to preserve bacterial cell morphology and to increase the sensitivity of the detection, cell aliquots were exposed to isopropanol (final concentration, 70% v/v) for 20 min at RT. The pellets of isopropanol-fixed cells were obtained by centrifugation at 7,000 × *g* for 5 min and washed twice with PBS. Next, running buffer was flowed along the sensor surface until the baseline was achieved. Bacteria were resuspended in the running buffer at a concentration of 1×10^7 CFU/ml (or as indicated in the text) and delivered at a flow rate of 50 µl/min to the sensor surfaces with the immobilized proteins. Then, the running buffer was introduced again. The binding of bacteria to the sensor surface was detected as the difference in the sensor response between the equilibrium level after washing the bound surface with the running buffer and the baseline level obtained before the injection of the bacteria solution.

In this work, we used reference-compensated measurements and tested several different surfaces to be used as a reference surface. These included a surface without receptors, surfaces covered with blocking molecules such as BSA, casein, or NeutrAvidin, and a surface with immobilized reference protein (sCD5). The study revealed that there was considerable adsorption of bacteria to a bare alkylthiolate SAM (used as a functional layer) without any receptors/molecules immobilized and that the binding of bacteria to the surface coated with blocking molecules was significantly higher than that observed in case of surface coated with a reference protein. Therefore, this approach was selected as the best option.

RESULTS

Detection of N-SSc5D Binding to Bacteria in Conventional Bacteria–Protein Binding Assays

We first assessed the binding of the SRCR-containing extracellular domains of Spα, SSc5D, CD6, and CD5 (respectively, Spα, N-SSc5D, sCD6, and sCD5) to *E. coli* strains BL21(DE3), IHE3034, and RS218, and to *L. monocytogenes* strain EGD-e, using conventional bacteria-protein binding assays. Although Spα, sCD5, and sCD6 had previously been tested for bacteria binding (6, 9, 10), no experiments had been performed for SSc5D. We incubated 5 µg of each recombinant SRCR protein with bacterial suspensions of 1×10^8 live cells (colony-forming units, CFU) at 4°C, followed by centrifugation and immunoblotting of the pelleted bacteria.

We confirmed the interaction of recombinant Spα with all bacterial samples tested, having an enhanced capacity to bind *E. coli* RS218 comparing with the other bacteria strains (**Figure 1**). However, and in contrast with previous studies, no detectable sCD6 was recovered in association with the bacterial pellets, using our experimental setup. There was also no bacteria-bound sCD5 detected, but this was expected, given that CD5 was reported not to bind to bacteria (10). As observed from the experiments, N-SSc5D distinctly detected *E. coli* RS218 and IHE3034, although there was no conclusive evidence at this stage that it could bind to *E. coli* BL21(DE3) or to *L. monocytogenes*.

N-SSc5D and Spα Binding to Bacteria Is Measurable by SPR

The results from the previous experiment suggested that different SRCR proteins had distinct binding properties to different bacterial strains, which might not have been highlighted in previous publications, each addressing a different SRCR protein at a time. Aware that western blot detection might not be the most sensitive method to emphasize these differences, we designed a new SPR-based assay to enhance the sensitivity of detection of extracellular proteins binding to bacteria. In this assay, the proteins are directly attached to the sensor chip by amine coupling. Suspensions of isopropanol-fixed bacteria, resuspended at a concentration of 1×10^7 CFU/ml or lower, are then delivered to the sensor surface containing the immobilized proteins. The output of the SPR sensor (expressed in nanometer of resonant wavelength) is directly proportional to the amount of biomolecules attached to the active surface of the sensor. The difference in the sensor output before

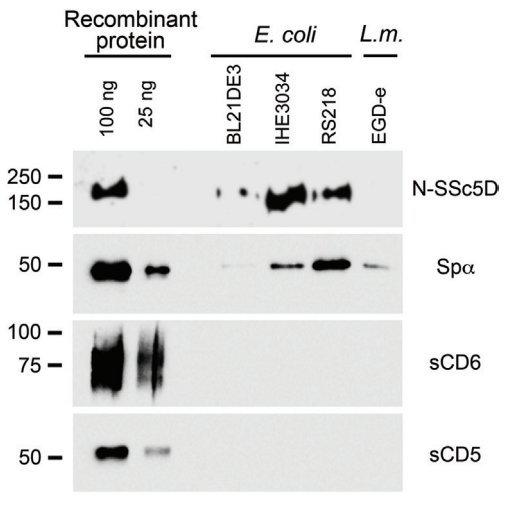

FIGURE 1 | Spα and N-SSc5D bind bacteria. Recombinant Spα, N-SSc5D, sCD6, and sCD5 were incubated (5 µg each sample) with suspensions of 1×10^8 CFU of live *E. coli*, strains BL21(DE3), IHE3034, or RS218, or with *L. monocytogenes*, strain EGD-e. Cell-bound proteins were detected by immunoblotting using anti-HA mAb. Pure recombinant proteins were also run (100 and 25 ng, left lanes) to determine the sensitivity of the assay.

injection of bacteria (baseline level) and after washing the surface with captured bacteria in buffer is therefore proportional to the amount of bacteria captured (irreversibly bound) by the proteins immobilized on the sensor surface. This quantity was used to characterize the ability of the respective immobilized proteins to bind bacteria.

We considered the following as references for the binding spectra: (a) the positive interaction of Spα with neuropathogenic *E. coli* K1 RS218 and with *L. monocytogenes* EGD-e and (b) the null interaction of sCD5 with both bacteria species (**Figure 2A**). Spα and sCD5 were immobilized in alternate flow chambers, bacteria were injected at 1×10^7 CFU/ml, and SPR plots registered.

Next, we tested whether the interactions of N-SSc5D with *E. coli* RS218 and *L. monocytogenes* EGD-e were measurable by SPR. As illustrated in **Figure 2B**, the interaction levels of N-SSc5D with bacteria were lower than those of Spα in both cases (between 15 and 40% across several experiments), but quite distinct from the profiles obtained for sCD5. These results confirmed the WB detection of the N-SSc5D-*E. coli* RS218 interactions seen in **Figure 1**, but further advanced in the detection of a subtle interaction between N-SSc5D with *L. monocytogenes*.

The results were reliable and qualitatively consistent among experiments, with only small variations in the absolute values of the responses. The chip-to-chip reproducibility of the interaction was >82% and >95% for N-SSc5D and sCD5 binding, respectively. The reproducibility values were determined from three independent experiments for each protein.

N-SSc5D Can Distinguish between Bacterial Strains

To test whether N-SSc5D could have a different capacity to bind different *E. coli* strains, we immobilized N-SSc5D and simultaneously injected, in separate flow channels, the non-pathogenic laboratory BL21(DE3) strain, and the meningitis-causing RS218 and IHE3034 *E. coli* strains. As another control of null-binding, we used in the fourth flow channel, heat-killed IHE3034. In parallel, we performed the same experiment with immobilized Spα. As seen in **Figure 3**, *E. coli* RS218 gave the best binding curve to N-SSc5D, followed by IHE3034, and finally BL21(DE3). Heat-killed IHE3034 only marginally bound to N-SSc5D, suggesting that the bacterial determinants recognized by N-SSc5D are destroyed by heat. The binding profile of Spα to the different *E. coli* strains was not too different, binding marginally better to RS218 and BL21(DE3) than N-SSc5D, and less to IHE3034 than N-SSc5D, indicating that these proteins have slightly distinct

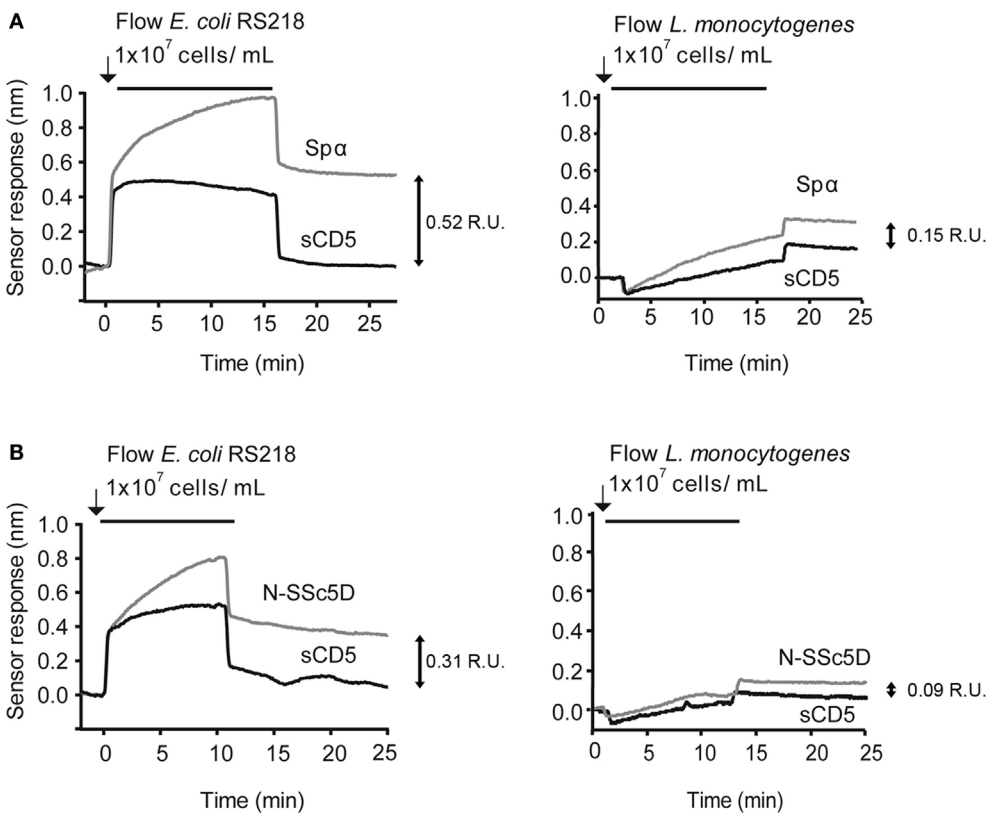

FIGURE 2 | SPR detection of N-SSc5D binding to *E. coli* RS218 and *L. monocytogenes* EGD-e. Recombinant Spα **(A)** or N-SSc5D **(B)**, as well as the control sCD5 were immobilized in sensorchips and flowed with *E. coli* RS218 (left) or *L. monocytogenes* EGD-e (right) suspensions of 1×10^7 CFU/ml. After injection stopped, bacteria were retained in the different surfaces containing the SRCR proteins according to the strength of binding. Data are representative of multiple experiments with similar results. R.U., response units.

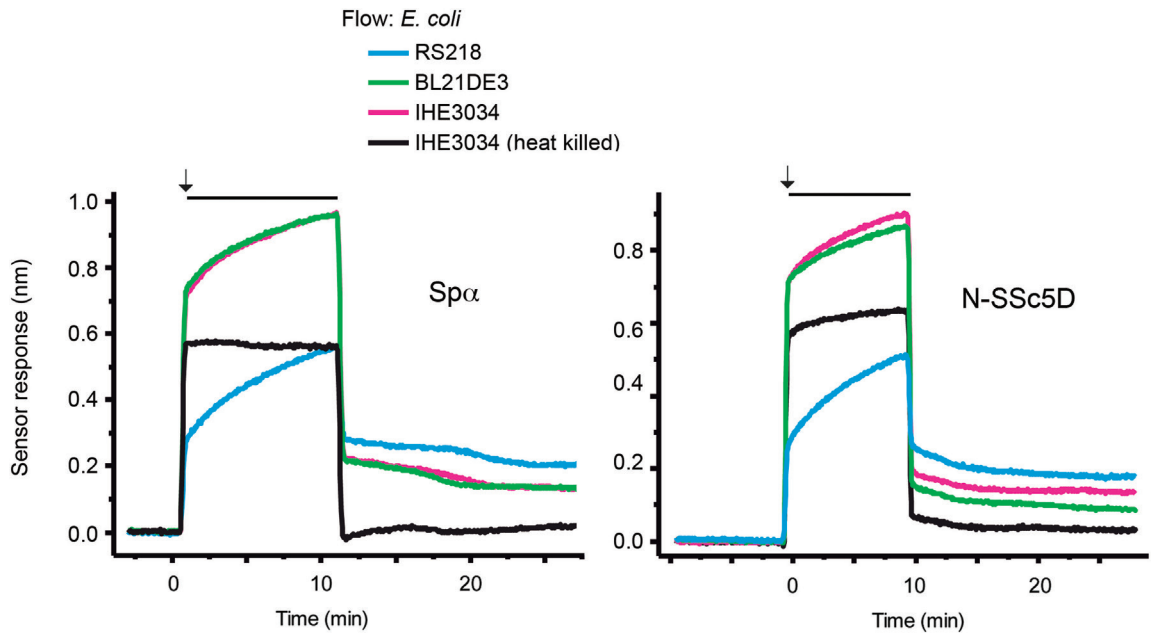

FIGURE 3 | Temporal sensor response to the differential binding of N-SSc5D and Spα to different *E. coli* strains. Recombinant N-SSc5D (and Spα in parallel experiments) was immobilized in the four sensing channels and simultaneously injected suspensions of 1×10^7 CFU/ml of *E. coli* RS218, IHE3034, or *E. coli* BL21(DE3). The fourth flow channel was used to flow heat-killed IHE3034. After 10 min of injection, bacteria were differently retained in the four different sensor chambers. Data are representative of multiple experiments with similar results.

recognition profiles but can nevertheless distinguish between different bacterial strains.

Differential Binding of SRCR Proteins to a Same Bacterial Strain

To directly assess the differential binding capacity of the different SRCR receptors to a same bacterial preparation, we immobilized Spα, N-SSc5D, sCD6, and sCD5 in the four sensing channels and simultaneously injected *E. coli* RS218 at 1×10^7 CFU/ml to all channels. As depicted in **Figure 4A**, RS218 bound with the highest level to Spα, followed by N-SSc5D. As expected, sCD5 displayed the lowest level of RS218 binding; however, binding of the bacteria to immobilized sCD6 was, although relatively low, noticeably higher than that binding to sCD5. This indicates that despite the apparent negative result of **Figure 1**, there is some above-background level of binding of sCD6 to *E. coli* RS218 measurable by this SPR-based method.

Finally, we evaluated the sensitivity of the method by analyzing the interaction of *E. coli* RS218 with N-SSc5D using suspensions with decreasing bacteria concentration. **Figure 4B** represents again the profiles of binding of *E. coli* RS218 at 1×10^7 CFU/ml to immobilized N-SSc5D and sCD5. Then, the specific binding was obtained by subtracting the signals arising from the measuring channels with immobilized N-SSc5D from those measured in the sCD5-immobilized reference channels. Three different concentrations of bacteria were used, 3, 5, and 10×10^6 CFU/ml, and for each concentration, the subtractive plots are represented in **Figure 4C**, indicating that the method clearly detects specific binding of *E. coli* RS218 to N-SSc5D even when using bacteria concentrations as low as 3×10^6 CFU/ml.

DISCUSSION

The SRCR-B family comprises a group of proteins that have a very high level of genetic conservation and remarkable structural similarity of the SRCR domains. However, each member has been described with very exclusive functions, as diverse as roles in signal transduction, regulation of inflammation, cell survival and apoptosis, differentiation, detoxification in iron metabolism, to name just a few, to such an extent that the structural properties of the SRCR modules may be so far the only proven unifying feature of the family. This diversity in functions can be in part explained from the fact that each protein has unique features (different number of SRCR domains), is expressed in different contexts and architectures (membrane bound in different cell types, carrying cytoplasmic domains of variable lengths and compositions, or is secreted), may have additional domains of other types, and can display different degrees of posttranslational modifications, such as *O*- and/or *N*-glycosylation.

Recently, the description of a physical interaction between Spα, which is a small soluble protein almost exclusively composed of the three SRCR domains, and several strains of bacteria (9) projected an explicit PRR function for such type of domain. Similar microbe-binding properties of other SRCR proteins have indeed been assigned to their own SRCR domains (6–8). To further explore this possible unifying role for SRCR domains, we thus

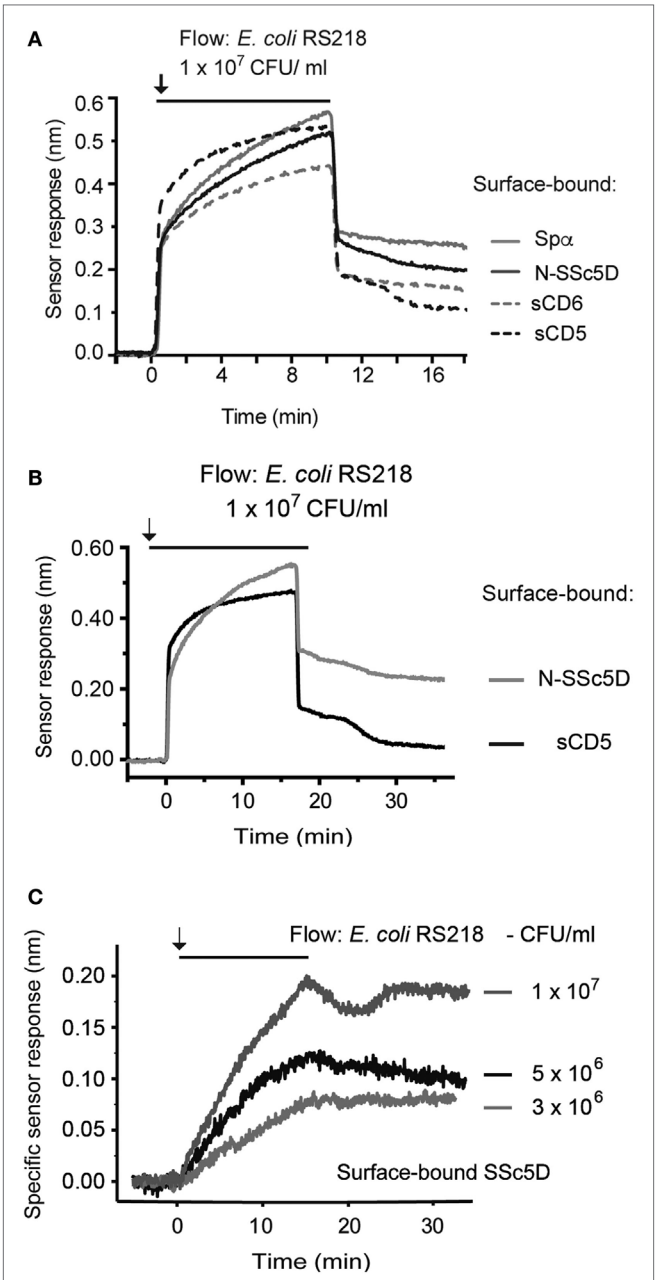

FIGURE 4 | Temporal sensor response to the binding of SRCR proteins to *E. coli* RS218. **(A)** Recombinant Spα, N-SSc5D, sCD6, and sCD5 were immobilized in the four sensing channels and simultaneously injected with an *E. coli* RS218 suspension of 1×10^7 CFU/ml. **(B)** Recombinant N-SSc5D and sCD5 were immobilized on alternate chambers, and *E. coli* RS218 was flowed at 1×10^7 CFU/ml. **(C)** The specific binding of *E. coli* RS218 to N-SSc5D was obtained by the subtraction of the non-specific response registered for sCD5 from the measured signals of *E. coli* RS218 binding to N-SSc5D, for bacterial concentrations of 3, 5, and 10×10^6 CFU/ml.

investigated the PRR-type properties of the recently described protein SSc5D, and more specifically of its SRCR-containing moiety. For this purpose, we designed an SPR-based assay for rapid and direct detection of immune receptor–bacteria interactions.

Conventional methods used previously to assay the interaction of bacteria with secreted recombinant SRCR (or other) proteins, such as flow cytometry or immunoblotting, rely on the labeling of proteins with a fluorescent dye, such as FITC (24), or with biotin targeting the sulfhydryl groups of cysteine residues (6, 9, 10). Among the many practical advantages of the SPR method compared with conventional ones, there is no requirement for receptor labeling, and only minute amounts of protein are needed to generate distinct or differential signals. In our conventional assays shown in **Figure 1**, we used 5 μg of recombinant protein and 1×10^8 CFU per individual receptor–bacteria assay, and some of these interactions were on the borderline of western blot sensitivity. By comparison, 2 μg of recombinant protein could be used in a single SPR assay testing the interaction with up to four bacteria types, these also used at smaller amounts (typically at 1×10^7 CFU/ml, but feasibly down to 3×10^6 CFU/ml), which represent an improvement of the detection of protein–bacteria interactions. Moreover, the versatility of our setup allows having up to four different immobilized proteins and simultaneously comparing the binding of each protein to the same bacterial suspension as analyte, or conversely, comparing directly in the same assay suspensions of four different bacteria binding to the same immobilized protein.

Surface plasmon resonance biosensor technology-based affinity and kinetic measurements are typically performed with analytes that are monovalent (25). Although through complex analyses it is possible to obtain such parameters in the case of multivalent (bacterial) contacts (26), we have utilized SPR to detect interaction *per se* and to make synchronized measurements, obtaining direct comparable data for sets of four different receptors, or four different bacteria samples. Detection of binding of bacteria to macromolecules, including lipids and carbohydrates, has been accomplished before (26, 27), but to the best of our knowledge, this is the first SPR study addressing the interaction between a host PRR and bacteria. It should be noted that we chose to consider the amount of captured (irreversibly bound) bacteria to characterize the ability of the respective proteins to bind selected bacteria, as the reported experiments with bacteria are complex, and the binding curves in response to bacteria are not determined only by kinetic parameters of the interactions; they are also affected by other factors, such as background refractive index changes (due to differences in the composition of samples containing bacteria and running buffer), the non-specific adsorption of bacteria, or other non-target molecules onto the sensing surface and mass transport (due to rather slow diffusion of bacteria to the sensing surface).

From the experiments described in the present work, we show for the first time that, like some other human SRCR proteins, SSc5D, through its set of SRCR domains, has the capacity to bind bacteria and, from the direct comparisons established using the multichannel SPR apparatus, that N-SSc5D and Spα can distinguish between different types of bacteria on one hand and different strains of one type of bacteria on the other. Binding of N-SSc5D and Spα to *E. coli* RS218 gave higher sensor responses than binding to BL21(DE3). While BL21(DE3) is a well-characterized non-pathogenic research model commonly used in academic laboratories and in the biotech industry, RS218 is a pathogenic

strain belonging to the serotype O18ac:H7:K1 and displaying virulence factors that contribute to the onset of meningitis. The IHE3034 strain also belongs to the same serotype and although N-SSc5D binds better to IHE3034 than to BL21(DE3), the same behavior is not observed for Spα, suggesting that SRCR proteins may have very defined discriminatory properties on different, still undefined, extracellular components of bacteria. Likewise, the response signals for N-SSc5D and Spα binding to *L. monocytogenes* were significantly lower than to *E. coli*, possibly reflecting a differential sensing of Gram-positive vs. Gram-negative bacteria, but at this stage and with very few bacteria types tested, it is premature to establish any categorization.

The interactions of N-SSc5D and Spα with *E. coli* RS281 were relatively strong and specific and, as shown for N-SSc5D, the sensor responses increased proportionally to the concentration of the bacterial suspensions used. Comparing with the conventional assays, binding to *E. coli* IHE3034, also a meningitis-causing pathogen, did not give the same precise results, as N-SSc5D bound less and Spα bound better in the SPR experiments than in the bacteria-binding assays. SPR offers substantial benefits when compared with these methods, because it allows real-time detection of bacteria and, moreover, since bacteria are delivered under conditions of continuous hydrodynamic flow, the SPR technique is expected to better mimic the protein–bacteria interaction under physiological conditions where shear forces promoted by the body fluids are likely present (28, 29). As measurements are obtained simultaneously for the different proteins/bacteria within the same experiment, we can be confident that they truly reflect quantitative differences in binding of SRCR proteins to bacteria.

An important aspect in the design of the assay is the choice of a reference, which allows for the compensation of the binding of non-target molecules to the sensing surface. In the context of our study, sCD5 was defined as such based on the literature and on the result obtained with our conventional assay. Additionally, we chose to use sCD5 in experiments, as this protein is genetically and structurally related with the query molecules N-SSc5D and Spα, and thus it would account for intrinsic unspecific binding features that can be particular to the SRCR family of molecules.

CD6, on the other hand, was reported to bind to Gram-positive and Gram-negative bacterial strains (6). CD6 is a receptor of T lymphocytes that has characterized roles in the regulation of T cell signaling and in inflammatory responses (20, 30), so its role as a pathogen sensor was unexpected. From the results of our conventional assay shown in **Figure 1**, we would have concluded that either sCD6 does not bind to the tested bacteria or that it binds with such low affinity that the interaction does not survive the pelleting and washing of the bacteria. The lack of binding could not be attributed to any functional defect of our produced sCD6 protein, as this was shown to clearly bind its natural ligand CD166 by flow cytometry (Figure S2 in Supplementary Material). However, our improved SPR assays may highlight a slightly different conclusion: although the level of binding of sCD6 to *E. coli* RS218 (**Figure 4**) or to *L. monocytogenes* (data not shown) was significantly lower than that of either N-SSc5D or Spα, it stayed clearly above the level of the sCD5 negative profile. Apart from the higher sensitivity over the previous methods, SPR is run at the more adequate temperature of 25°C, whereas conventional protein–bacteria binding assays are customarily performed at 4°C. Notwithstanding the fact that the bacteria-binding capacities of sCD6 are reduced comparing with N-SSc5D or Spα, it is nonetheless very plausible that sCD6 may have true microbe-sensing properties, which are highlighted by its capacity to protect animals from LPS-induced septic shock (6).

In conclusion, we have demonstrated through the use of a dynamic, antibody-free, SPR-based assay that N-SSc5D, like Spα, is capable to physically interact with whole bacteria cells. This new approach can be adapted to screen for interactions with a wide range of bacteria and once the best bacterial targets of N-SSc5D are identified, this will hopefully allow to better characterize and more deeply explore the role of this SRCR protein in pathogen sensing and in driving immune responses. The results obtained in this study using the SRCR-containing moiety of SSc5D will undoubtedly further our understanding of the specific function of SRCR domains as the functional parts of a family of mammalian proteins that have enhanced capabilities to recognize and eventually fight bacterial pathogens.

AUTHOR CONTRIBUTIONS

CP designed and produced recombinant proteins, executed SPR experiments, and wrote the paper; MB designed and executed SPR experiments and wrote the paper; RS produced recombinant proteins and bacteria strains; AS and MA designed and produced recombinant proteins; LO performed experiments with bacteria strains; JH designed the SPR experiments and wrote the paper; AC planned and designed the study and wrote the paper.

ACKNOWLEDGMENTS

We thank Frederico Silva for technical assistance in protein purification, Pedro Madureira for providing the *E. coli* strains, and Filipe Carvalho for providing the *L. monocytogenes* strain. This work is funded by National Funds through FCT – Fundação para a Ciência e a Tecnologia under the project SRecognite Infect-ERA/0003/2015, by the project Norte-01-0145-FEDER-000012 – structured program on bioengineered therapies for infectious diseases and tissue regeneration, supported by Norte Portugal Regional Operational Programme (NORTE 2020), under the PORTUGAL 2020 Partnership Agreement, through the European Regional Development Fund, by Praemium Academiae of the Academy of Sciences of the Czech Republic and the Czech Science Foundation (contract # P205/12/G118). CP was the recipient of a studentship from FCT (SFRH/BD/47107/2008). AS is funded by the Wellcome Trust. RS was the recipient of a fellowship from the American Portuguese Biomedical Research Fund (APBRF) and is funded by an FCT studentship (SFRH/BD/110691/2015). LO is funded by FCT-PTDC.

SUPPLEMENTARY MATERIAL

The Supplementary Material for this article can be found online at http://journal.frontiersin.org/article/10.3389/fimmu.2016.00416

FIGURE S1 | **Proteins purified and used in SPR assays**. **(A)** Coomassie-staining of sCD5, sCD6, and Spα proteins purified from TCS with Ni-NTA resin and imidazole elution. Gels of sCD6 and sCD5 (12%) and Spα (10%) were run under reducing conditions. Identity of the proteins was confirmed by immunoblotting (not shown). **(B)** Anionic chromatography of N-SSc5D recovered from TCS samples and further purification. **(C)** N-SSc5D fractions 43–46 were collected and run on 7.5% SDS-PAGE and stained with Coomassie. N-SSc5D expression was confirmed by immunoblotting (bottom).

FIGURE S2 | **sCD6 binds to cells expressing its ligand, CD166**. Panel of cells screened using recombinant sCD6 tetramers for binding to CD166. Cells were incubated with streptavidin-PE as an isotype control (red), sCD6 tetramers (blue), and sCD58 tetramers (green). **(A)** Jurkat and K562 cells do not express CD166, and therefore sCD6 tetramers showed no binding. sCD58 tetramers bind to CD2, which is highly expressed at the surface of the Jurkat T cell line. **(B)** The THP-1 (monocytic) and Raji (B cell) lines express CD166 at their surface (but not CD2) and therefore displayed binding of the sCD6 tetramers.

REFERENCES

1. Blander JM, Sander LE. Beyond pattern recognition: five immune checkpoints for scaling the microbial threat. *Nat Rev Immunol* (2012) 12:215–25. doi:10.1038/nri3167
2. Martínez VG, Moestrup SK, Holmskov U, Mollenhauer J, Lozano F. The conserved scavenger receptor cysteine-rich superfamily in therapy and diagnosis. *Pharmacol Rev* (2011) 63:967–1000. doi:10.1124/pr.111.004523
3. Sarrias MR, Grønlund J, Padilla O, Madsen J, Holmskov U, Lozano F. The scavenger receptor cysteine-rich (SRCR) domain: an ancient and highly conserved protein module of the innate immune system. *Crit Rev Immunol* (2004) 24:1–37. doi:10.1615/CritRevImmunol.v24.i1.10
4. Carmo AM, Sreenu VB. A systematic and thorough search for domains of the scavenger receptor cysteine-rich group B family in the human genome. In: Mahdavi MA, editor. *Bioinformatics – Trends and Methodologies*. Rijeka, Croatia: InTech (2011). p. 195–210.
5. Sarrias MR, Padilla O, Monreal Y, Carrascal M, Abian J, Vives J, et al. Biochemical characterization of recombinant and circulating human Spalpha. *Tissue Antigens* (2004) 63:335–44. doi:10.1111/j.0001-2815.2004.00193.x
6. Sarrias MR, Farnós M, Mota R, Sánchez-Barbero F, Ibáñez A, Gimferrer I, et al. CD6 binds to pathogen-associated molecular patterns and protects from LPS-induced septic shock. *Proc Natl Acad Sci U S A* (2007) 104:11724–9. doi:10.1073/pnas.0702815104
7. Fabriek BO, van Bruggen R, Deng DM, Ligtenberg AJ, Nazmi K, Schornagel K, et al. The macrophage scavenger receptor CD163 functions as an innate immune sensor for bacteria. *Blood* (2009) 113:887–92. doi:10.1182/blood-2008-07-167064
8. Prakobphol A, Xu F, Hoang VM, Larsson T, Bergstrom J, Johansson I, et al. Salivary agglutinin, which binds *Streptococcus mutans* and *Helicobacter pylori*, is the lung scavenger receptor cysteine-rich protein gp-340. *J Biol Chem* (2000) 275:39860–6. doi:10.1074/jbc.M006928200
9. Sarrias MR, Roselló S, Sánchez-Barbero F, Sierra JM, Vila J, Yélamos J, et al. A role for human Sp alpha as a pattern recognition receptor. *J Biol Chem* (2005) 280:35391–8. doi:10.1074/jbc.M505042200
10. Vera J, Fenutría R, Cañadas O, Figueras M, Mota R, Sarrias MR, et al. The CD5 ectodomain interacts with conserved fungal cell wall components and protects from zymosan-induced septic shock-like syndrome. *Proc Natl Acad Sci U S A* (2009) 106:1506–11. doi:10.1073/pnas.0805846106
11. Martínez VG, Escoda-Ferran C, Tadeu Simões I, Arai S, Orta Mascaró M, Carreras E, et al. The macrophage soluble receptor AIM/Api6/CD5L displays a broad pathogen recognition spectrum and is involved in early response to microbial aggression. *Cell Mol Immunol* (2014) 11:343–54. doi:10.1038/cmi.2014.12
12. Gonçalves CM, Castro MA, Henriques T, Oliveira MI, Pinheiro HC, Oliveira C, et al. Molecular cloning and analysis of SSc5D, a new member of the scavenger receptor cysteine-rich superfamily. *Mol Immunol* (2009) 46:2585–96. doi:10.1016/j.molimm.2009.05.006
13. Balakrishnan L, Bhattacharjee M, Ahmad S, Nirujogi RS, Renuse S, Subbannayya Y, et al. Differential proteomic analysis of synovial fluid from rheumatoid arthritis and osteoarthritis patients. *Clin Proteomics* (2014) 11:1. doi:10.1186/1559-0275-11-6
14. Miró-Julià C, Roselló S, Martínez VG, Fink DR, Escoda-Ferran C, Padilla O, et al. Molecular and functional characterization of mouse S5D-SRCRB: a new group B member of the scavenger receptor cysteine-rich superfamily. *J Immunol* (2011) 186:2344–54. doi:10.4049/jimmunol.1000840
15. Miró-Julià C, Escoda-Ferran C, Carrasco E, Moeller JB, Vadekaer DF, Gao X, et al. Expression of the innate defense receptor S5D-SRCRB in the urogenital tract. *Tissue Antigens* (2014) 83:273–85. doi:10.1111/tan.12330
16. Homola J. Surface plasmon resonance sensors for detection of chemical and biological species. *Chem Rev* (2008) 108:462–93. doi:10.1021/cr068107d
17. Bergwerff AA, van Knapen F. Surface plasmon resonance biosensors for detection of pathogenic microorganisms: strategies to secure food and environmental safety. *J AOAC Int* (2006) 89:826–31.
18. Homola J, Dostálek J, Chen S, Rasooly A, Jiang S, Yee SS. Spectral surface plasmon resonance biosensor for detection of staphylococcal enterotoxin B in milk. *Int J Food Microbiol* (2002) 75:61–9. doi:10.1016/S0168-1605(02)00010-7
19. Taylor AD, Ladd J, Yu Q, Chen S, Homola J, Jiang S. Quantitative and simultaneous detection of four foodborne bacterial pathogens with a multi-channel SPR sensor. *Biosens Bioelectron* (2006) 22:752–8. doi:10.1016/j.bios.2006.03.012
20. Oliveira MI, Gonçalves CM, Pinto M, Fabre S, Santos AM, Lee SF, et al. CD6 attenuates early and late signaling events, setting thresholds for T-cell activation. *Eur J Immunol* (2012) 42:195–205. doi:10.1002/eji.201040528
21. Davis SJ, Ward HA, Puklavec MJ, Willis AC, Williams AF, Barclay AN. High level expression in Chinese hamster ovary cells of soluble forms of CD4 T lymphocyte glycoprotein including glycosylation variants. *J Biol Chem* (1990) 265:10410–8.
22. Pimková K, Bocková M, Hegnerová K, Suttnar J, Cermák J, Homola J, et al. Surface plasmon resonance biosensor for the detection of VEGFR-1 – a protein marker of myelodysplastic syndromes. *Anal Bioanal Chem* (2012) 402:381–7. doi:10.1007/s00216-011-5395-3
23. Homola J. *Surface Plasmon Resonance Based Sensors*. Berlin: Springer-Verlag (2006).
24. Kneidl J, Löffler B, Erat MC, Kalinka J, Peters G, Roth J, et al. Soluble CD163 promotes recognition, phagocytosis and killing of *Staphylococcus aureus* via binding of specific fibronectin peptides. *Cell Microbiol* (2012) 14:914–36. doi:10.1111/j.1462-5822.2012.01766.x
25. van der Merwe PA. Surface plasmon resonance. In: Harding S, Chowdry B, editors. *Protein-Ligand Interactions: Hydrodynamics and Calorimetry*. Oxford, UK: Oxford Univ Press (2001). p. 137–70.
26. Chung KH, Park JS, Hwang HS, Kim JC, Lee KY. Detection and kinetics of mucosal pathogenic bacteria binding with polysaccharides. *J Microbiol Biotechnol* (2007) 17:1191–7.
27. Bérubé LR, Schur MK, Latta RK, Hirama T, McKenzie CR, Jarrell HC. Phosphatidyl choline-mediated inhibition of *Streptococcus pneumoniae* adherence to type II pneumocytes in vitro. *Microb Pathog* (1999) 26:65–75. doi:10.1006/mpat.1998.0254
28. Salminen A, Loimaranta V, Joosten JA, Khan AS, Hacker J, Pieters RJ, et al. Inhibition of P-fimbriated *Escherichia coli* adhesion by multivalent galabiose derivatives studied by a live-bacteria application of surface plasmon resonance. *J Antimicrob Chemother* (2007) 60:495–501. doi:10.1093/jac/dkm251
29. Bustanji Y, Arciola CR, Conti M, Mandello E, Montanaro L, Samorí B. Dynamics of the interaction between a fibronectin molecule and a living bacterium under mechanical force. *Proc Natl Acad Sci U S A* (2003) 100:13292–7. doi:10.1073/pnas.1735343100
30. Pinto M, Carmo AM. CD6 as a therapeutic target in autoimmune diseases: successes and challenges. *BioDrugs* (2013) 27:191–202. doi:10.1007/s40259-013-0027-4

Conflict of Interest Statement: The authors declare that the research was conducted in the absence of any commercial or financial relationships that could be construed as a potential conflict of interest.

frontiers in Immunology

GENERAL COMMENTARY
published: 28 March 2017
doi: 10.3389/fimmu.2017.00366

Commentary: The Scavenger Receptor SSc5D Physically Interacts with Bacteria through the SRCR-Containing N-Terminal Domain

Francisco Lozano[1,2,3] and Mario Martínez-Florensa[1]*

[1] Grup d'Immunoreceptors del Sistema Innat i Adaptatiu, Institut d'Investigacions Biomèdiques August Pi i Sunyer (IDIBAPS), Barcelona, Spain, [2] Servei d'Immunologia, Hospital Clínic de Barcelona, Barcelona, Spain, [3] Facultat de Medicina, Departament de Biomedicina, Universitat de Barcelona, Barcelona, Spain

Keywords: SSc5D, S5D-SRCRB, scavenger receptor cysteine-rich, bacterial binding, CD6

A commentary on

The scavenger receptor SSc5D physically interacts with bacteria through the SRCR-containing N-terminal domain
by Bessa Pereira C, Bocková M, Santos RF, Santos AM, Martins de Araújo M, Oliveira L, et al. Front Immunol (2016) 7:416. doi: 10.3389/fimmu.2016.00416

OPEN ACCESS

Edited by:
Uday Kishore,
Brunel University London, UK

Reviewed by:
Taruna Madan,
National Institute for Research in Reproductive Health, India
Simon John Clark,
University of Manchester, UK

****Correspondence:***
Francisco Lozano
flozano@clinic.ub.es

Specialty section:
This article was submitted to Molecular Innate Immunity, a section of the journal Frontiers in Immunology

Received: *19 January 2017*
Accepted: *14 March 2017*
Published: *28 March 2017*

Citation:
Lozano F and Martínez-Florensa M (2017) Commentary: The Scavenger Receptor SSc5D Physically Interacts with Bacteria through the SRCR-Containing N-Terminal Domain. Front. Immunol. 8:366. doi: 10.3389/fimmu.2017.00366

The recently published article by Bessa Pereira et al. reports that the human SSc5D receptor physically interacts with some bacterial species (1), thus basically confirming previous available information on its mouse homolog (S5D-SRCRB) (2). The interspecies conservation of such a basic innate immune function (bacterial binding) has been noticed for other members of the scavenger receptor cysteine-rich superfamily (SRCR-SF) (e.g., human Spα and its mouse homolog AIM/Api6/CD5L) (3, 4). This advocates for its functional physiological relevance in innate defense of body surfaces as it has been proposed for the urogenital tract (5).

A substantive part of the work by Bessa Pereira et al. is also devoted to explore putative qualitative and/or quantitative differences on the bacterial-binding properties of SSc5D with other human SRCR-SF proteins, namely, CD5, Spα, and CD6 by using conventional protein–bacteria binding assays and surface plasmon resonance-based assays. They were chosen based on previously reported information showing that Spα (4) and CD6 (6–8) but not CD5 (9) exhibit broad bacterial-binding properties. While the authors confirmed the work on Spα and CD5, they were unable to replicate that on CD6. Exclusively based on a single experimental evidence, the authors cast doubt on the well-documented bacterial-binding properties of CD6 (6–8). These properties were unveiled by using a recombinant soluble form of human CD6 (rshCD6) encompassing from D^{25} to M^{400} and, indistinctly, produced in different mammalian cell expression systems (NSO, HEK293-EBNA, and CHO cells). Further confirmation was obtained by demonstrating similar properties displayed by a natural soluble CD6 form isolated from human serum, as well as by Jurkat cell transfectants expressing a membrane-bound full-length form of CD6 (6). Accordingly, it was later reported that rshCD6 infusion significantly reduces mouse mortality following septic shock induced by intraperitoneal monobacterial infection of Gram-positive (*S. aureus*) or Gram-negative (*A. baumannii*) origin (7). More recently, new evidence shows that not only rshCD6 but also adenovirally expressed mouse sCD6 have protective survival effects on polymicrobial septic shock induced by cecal ligation and puncture (8), the gold standard model for experimental sepsis.

The only shCD6 protein assayed by Bessa Pereira et al. was the chimerical HA–sCD6–BirA–His, which differed from rshCD6 in several aspects: (1) the CD6 component from HA–sCD6–BirA–His

was slightly shorter than that of rshCD6 (D25 to E398 vs D25 to M400, respectively), (2) in contrast to rshCD6, the chimerical HA–sCD6–BirA–His protein included N- and/or C-terminal protein tags (e.g., HA, BirA, or His tail), and (3) the chimerical HA–sCD6–BirA–His protein was tetrameric whereas rshCD6 was monomeric under native conditions (our unpublished observations). While differences in shCD6 sequence length can be considered functionally meaningless in our opinion, the introduction of protein tags and/or the formation of tetramerical structures could impose important steric limitations preventing shCD6 interaction with bacterial surfaces. Indeed, the spatial organization of the three consecutive SRCR domains in the CD6 receptor is non-linear (horseshoe-like shaped) (10), and such a topology would explain how monoclonal antibodies against the CD6 domain 1 might impede access of CD166/ALCAM—the CD6 ligand—to its binding site at the membrane-proximal domain (D3) of CD6 (10). The reason by which similar chimerical versions of the other receptors in study (Spα and SSc5D) do still bind to bacteria and do not undergo putative steric hindrance issues is uncertain. However, the presence sialylated *O*-linked glycans interspacing their SRCR domains of Spα and SSc5D (but not CD6) could impose them to adopt a rigid rod-like shaped conformation similar to that previously reported for CD5 (11). This would minimize steric problems when tetramerized.

The higher avidity of chimerical protein tetramers compared to untagged monomeric proteins could certainly make them advantageous for unraveling low-affinity receptor–ligand interactions. However, the physiological meaning of data generated with them should always be taken cautiously, especially when the original receptor is monomeric and does not contain any similar protein tag, as it the case of both the membrane-bound and the soluble-circulating CD6 forms. Reasonably, Bessa Pereira et al. validated the functionality of the chimerical HA–sCD6–BirA–His protein by means of flow cytometry analyses showing its specific binding to CD166/ALCAM-expressing human cell lines, a property also shared by the rshCD6 protein used in our studies (6). In our opinion, this minimal *sine qua non-condition* should not be taken as an absolute criterion of full shCD6 functionality, particularly when the bacterial-binding site/s has/ve not yet been identified and there is no evidence for its mapping or close relationship with the CD166/ALCAM-binding site.

AUTHOR CONTRIBUTIONS

FL and MM-F discussed and wrote the commentary.

FUNDING

The work by FL and MM-F is supported by grants from the Spanish Ministerio de Economía y Competitividad (Plan Nacional de I+D+i, SAF2013-46151-R), Instituto de Salud Carlos III (ISCIII)—co-financed by European Development Regional Fund "A way to achieve Europe" ERDF (Spanish Network for Research in Infectious Diseases, REIPI, RD12/0015/0018).

REFERENCES

1. Bessa Pereira C, Bocková M, Santos RF, Santos AM, Martins de Araújo M, Oliveira L, et al. The scavenger receptor SSc5D physically interacts with bacteria through the SRCR-containing N-terminal domain. *Front Immunol* (2016) 7:416. doi:10.3389/fimmu.2016.00416
2. Miró-Julià C, Roselló S, Padilla O, Fink DR, Escoda C, Vázquez-Echeverría C, et al. Molecular and functional characterization of mouse S5D-SRCRB, a new member of the group B scavenger receptor cysteine-rich superfamily. *J Immunol* (2011) 186:2344–54. doi:10.4049/jimmunol.1000840
3. Sarrias MR, Roselló S, Sánchez-Barbero F, Sierra JM, Vila J, Yélamos J, et al. A role for Sp alpha as a pattern-recognition receptor. *J Biol Chem* (2005) 280:35391–8. doi:10.1074/jbc.M505042200
4. Martínez VG, Escoda-Ferran C, Simoes IT, Arai S, Orta M, Carreras E, et al. The macrophage soluble receptor AIM/Api6/CD5L displays a broad pathogen recognition spectrum and is involved in early response to microbial aggression. *Cell Mol Immunol* (2014) 11:343–54. doi:10.1038/cmi.2014.12
5. Miró-Julià C, Escoda-Ferran C, Carrasco E, Bonet J, Fink D, Gao X, et al. Expression of the innate defense receptor S5D-SRCRB in the urogenital tract. *Tissue Antigens* (2014) 83:273–85. doi:10.1111/tan.12330
6. Sarrias MR, Farnós M, Mota R, Sánchez-Barbero F, Ibañez A, Gimferrer I, et al. CD6 binds to pathogen-associated molecular patterns and protects from lipopolysaccharide-induced septic shock. *Proc Natl Acad Sci U S A* (2007) 104:11724–9. doi:10.1073/pnas.0702815104
7. Martínez-Florensa M, Consuegra-Fernández M, Martínez VG, Cañadas O, Armiger-Borràs N, Bonet-Roselló L, et al. Targeting of key pathogenic factors from Gram-positive bacteria by the soluble ectodomain of the scavenger-like lymphocyte receptor CD6. *J Infect Dis* (2014) 209:1077–86. doi:10.1093/infdis/jit624
8. Martínez-Florensa M, Consuegra-Fernández M, Aranda F, Armiger N, Muñoz L, Di Scala M, et al. Beneficial effects of a soluble CD6 form in experimental polymicrobial sepsis. *Antimicrob Agents Chemother* (2017) 61:e1391–416. doi:10.1128/AAC.01391-16
9. Vera J, Fenutría R, Cañada O, Figueras MT, Mota RA, Sarrias MR, et al. The ectodomain of CD5 interacts with conserved fungal structures and protects from zymosan-induced septic-like shock. *Proc Natl Acad Sci U S A* (2009) 106:1506–11. doi:10.1073/pnas.0805846106
10. Chappell PE, Garner LI, Yan J, Metcalfe C, Hatherley D, Johnson S, et al. Structures of CD6 and its ligand CD166 give insight into their interaction. *Structure* (2015) 23:1426–36. doi:10.1016/j.str.2015.05.019
11. McAlister MS, Brown MH, Willis AC, Rudd PM, Harvey DJ, Aplin R, et al. Structural analysis of the CD5 antigen-expression, disulphide bond analysis and physical characterisation of CD5 scavenger receptor superfamily domain 1. *Eur J Biochem* (1998) 257(1):131–41. doi:10.1046/j.1432-1327.1998.2570131.x

Conflict of Interest Statement: FL is founder and ad honorem scientific advisor of ImmunNovative Developments. The remaining authors declare that the research was conducted in the absence of any commercial or financial relationships that could be construed as a potential conflict of interest.

frontiers in Immunology

GENERAL COMMENTARY
published: 23 August 2017
doi: 10.3389/fimmu.2017.01004

Response: Commentary: The Scavenger Receptor SSc5D Physically Interacts with Bacteria through the SRCR-Containing N-Terminal Domain

Liliana Oliveira[1,2] *and Alexandre M. Carmo*[1,2]*

[1] *i3S – Instituto de Investigação e Inovação em Saúde, Universidade do Porto, Porto, Portugal,* [2] *IBMC – Instituto de Biologia Molecular e Celular, Porto, Portugal*

Keywords: scavenger receptor cisteine-rich, CD6, bacteria, pattern recognition receptors, surface plasmon resonance

A commentary on

Commentary: the Scavenger Receptor SSc5D Physically Interacts with Bacteria through the SRCR-Containing N-Terminal Domain
by Lozano F and Martínez-Florensa M, Front. Immunol. (2017) 8:366. doi:10.3389/fimmu.2017.00366

OPEN ACCESS

Edited by:
Uday Kishore,
Brunel University London,
United Kingdom

Reviewed by:
Uttara SenGupta,
Northwick Park Institute for Medical Research,
United Kingdom
Miki Nakao,
Kyushu University, Japan

***Correspondence:**
Alexandre M. Carmo
acarmo@ibmc.up.pt

Specialty section:
This article was submitted to Molecular Innate Immunity, a section of the journal Frontiers in Immunology

Received: *24 April 2017*
Accepted: *04 August 2017*
Published: *23 August 2017*

Citation:
Oliveira L and Carmo AM (2017) Response: Commentary: The Scavenger Receptor SSc5D Physically Interacts with Bacteria through the SRCR-Containing N-Terminal Domain. Front. Immunol. 8:1004. doi: 10.3389/fimmu.2017.01004

While until recently there were no known common functional features shared between different scavenger receptor cysteine-rich (SRCR) group B glycoproteins, between 2000 and 2009 the receptors DMBT1, Spα, CD6, and CD163 were reported to bind bacteria, thus suggesting a potential broad role of SRCR proteins as pattern recognition receptors (PRRs) (1–4). The reports came from three different teams, each using different approaches and in the context of their specific research.

Having cloned the five-SRCR domain-containing soluble protein SSc5D (5), we addressed in the paper by Bessa Pereira et al. (6) a possible PRR function for SSc5D, but introduced additionally a question not commonly asked: do all SRCR proteins bind equally to the same bacteria strains or species? The very fact that the different authors published their reports logically means that their studied receptors did bind bacteria; but how each receptor fared comparing with the others in the bacteria-binding properties was not fully weighed.

To perform an unbiased analysis of binding to bacteria of the SRCR domain-containing parts of CD5, CD6, Spα, and SSc5D, we produced all receptors using the same vectors introducing the same tags and used the same mammalian expression and protein purification systems. The analysis was performed using two methods, in the first incubating proteins with bacteria, followed by lysis and protein detection using immunoblotting, and in the second using the more sensitive technique surface plasmon resonance (SPR).

Given the impartial and balanced nature of our study, we were surprised to understand that Lozano and Martínez-Florensa consider in their commentary that we "cast doubt on the well-documented bacterial-binding properties of CD6." This statement is simply not accurate, because analyzing the spirit of our paper and reinforced in its conclusions, we never challenged Lozano's previous findings. On the contrary, we have always assumed as definitive that CD6 can recognize and bind to bacteria in several of our publications, including a recent editorial (7).

The fact that in one of the methods we used, the traditional protein–bacteria binding assays, we did not detect interactions between recombinant CD6 with the *E. coli* and *L. monocytogenes* strains tested does not change our perception of the bacteria-binding potential of CD6. Relevantly, this observation was produced at the very same stage in the paper where we were also not able to detect interactions of our own query receptor SSc5D with *Listeria* and one of the *E. coli* strains. A main aim

of the study was precisely to develop a more sensitive and reliable novel method to tackle a difficult and controversial problem. The conclusions of the SPR analysis and thus of our paper are categorical in that the binding of CD6 to the tested *E. coli* RS218 and *L. monocytogenes* EGD-e strains is "clearly above the level of the sCD5 negative profile."

Lozano and Martínez-Florensa's commentary contains other factual inaccuracies. We find bizarre the argument that our alleged doubts are "Exclusively based on a single experimental evidence" when in fact our study involved two types of experiments. Also, the suggestion that we used tetrameric instead of unconjugated CD6 for bacteria-binding assays is incorrect: all recombinant SRCR receptors, including CD6, were used as monomeric proteins in the receptor–bacteria binding assays and nothing in the text from start to finish could suggest otherwise or mislead the reader. Tetrameric CD6 was assembled as a cytometry useful reagent in supplementary data for the sole purpose of confirming that recombinant CD6 retained its natural ability to bind the membrane-expressed ligand CD166, as we had previously demonstrated (8).

Why, then, are our and Lozano's results not concordant in one type of experiment? There are countless possible reasons given that the experimental models differ in a number of aspects, such as that we detected the bacteria-bound proteins using anti-HA primary antibodies followed by secondary HRP-conjugated goat anti-mouse antibodies, whereas they biotinylated their proteins and detected them using HRP-conjugated streptavidin. However, this does not explain why by comparison we could easily detect Spα and SSc5D, but not CD6, binding to bacteria. Although unlikely, it is also possible as they suggest that the introduction of tags could impede any CD6 binding to bacteria; but the exact same modifications were introduced in Spα and SSc5D as well. A simpler straightforward possibility to explain the different patterns of binding is that the bacteria strains used are not the same.

As it is shown in our paper and also illustrated in previous studies, the binding profiles of a given receptor to different strains of a same bacterial species can vary dramatically (1, 6). Therefore and objectively, using receptors produced by the same way and incubated with the same bacteria in identical conditions, we can state that in our system Spα and N-SSc5D attach better to the bacterial strains used than does sCD6. This is consistent with the notion that different SRCR may have dissimilar pathogen recognition spectra, or that some are more specialized in bacteria recognition than others. None of this excludes that CD6 interacts with bacteria.

However, it should be noted that for CD6 to have a biological protective function, there needs to be no proportional correlation of the binding strength to pathogens namely when the model addressing the protective effect of CD6 is sepsis. As Lozano and colleagues convincingly described, CD6 protects mice from LPS-induced septic shock and from polymicrobial sepsis (3, 9). While this effect can be mediated by direct binding of sCD6 to LPS and/or bacteria, which by aggregation could facilitate clearance and consequently lead to lower inflammatory cytokine release, a strong anti-inflammatory role of CD6 *per se* ought not to be excluded. By competing with T cell-surface CD6 binding to antigen-presenting cell (APC)-expressed CD166, sCD6 may hamper or weaken T–APC interactions, thus diminishing inflammatory responses and having an impact on the outcome of the septic process.

Notwithstanding the widely demonstrated pathogen-sensing properties of CD6, or likewise of Spα or SSc5D, to reduce their prophylactic or curative function to the microbe-binding properties is, in our opinion, an oversimplification. The biological functions of soluble circulating SRCR proteins will undoubtedly be further clarified in the near future.

AUTHOR CONTRIBUTIONS

LO and AC wrote the response to the commentary.

FUNDING

This work is funded by National Funds through FCT—Fundação para a Ciência e a Tecnologia under the project SRecognite Infect-ERA/0003/2015, by the project Norte-01-0145-FEDER-000012—structured program on bioengineered therapies for infectious diseases and tissue regeneration, supported by Norte Portugal Regional Operational Programme (NORTE 2020), under the PORTUGAL 2020 Partnership Agreement, through the European Regional Development Fund.

REFERENCES

1. Prakobphol A, Xu F, Hoang VM, Larsson T, Bergstrom J, Johansson I, et al. Salivary agglutinin, which binds *Streptococcus mutans* and *Helicobacter pylori*, is the lung scavenger receptor cysteine-rich protein gp-340. *J Biol Chem* (2000) 275(51):39860–6. doi:10.1074/jbc.M006928200
2. Sarrias MR, Roselló S, Sánchez-Barbero F, Sierra JM, Vila J, Yélamos J, et al. A role for human Sp alpha as a pattern recognition receptor. *J Biol Chem* (2005) 280(42):35391–8. doi:10.1074/jbc.M505042200
3. Sarrias MR, Farnós M, Mota R, Sánchez-Barbero F, Ibáñez A, Gimferrer I, et al. CD6 binds to pathogen-associated molecular patterns and protects from LPS-induced septic shock. *Proc Natl Acad Sci U S A* (2007) 104(28):11724–9. doi:10.1073/pnas.0702815104
4. Fabriek BO, van Bruggen R, Deng DM, Ligtenberg AJ, Nazmi K, Schornagel K, et al. The macrophage scavenger receptor CD163 functions as an innate immune sensor for bacteria. *Blood* (2009) 113(4):887–92. doi:10.1182/blood-2008-07-167064
5. Gonçalves CM, Castro MA, Henriques T, Oliveira MI, Pinheiro HC, Oliveira C, et al. Molecular cloning and analysis of SSc5D, a new member of the scavenger receptor cysteine-rich superfamily. *Mol Immunol* (2009) 46(13):2585–96. doi:10.1016/j.molimm.2009.05.006
6. Bessa Pereira C, Bockova M, Santos RF, Santos AM, de Araujo MM, Oliveira L, et al. The scavenger receptor SSc5D physically interacts with bacteria through the SRCR-containing N-terminal domain. *Front Immunol* (2016) 7:9. doi:10.3389/fimmu.2016.00416
7. Carmo AM. Heads or tails: betting on CD6 as a resurged target for autoimmune diseases and sepsis. *Curr Drug Targets* (2016) 17(6):618. doi:10.2174/1389450117706160324153314
8. Oliveira MI, Gonçalves CM, Pinto M, Fabre S, Santos AM, Lee SF, et al. CD6 attenuates early and late signaling events, setting thresholds for T-cell activation. *Eur J Immunol* (2012) 42(1):195–205. doi:10.1002/eji.201040528
9. Martínez-Florensa M, Consuegra-Fernández M, Aranda F, Armiger-Borràs N, Di Scala M, Carrasco E, et al. Protective effects of human and mouse soluble scavenger-like CD6 lymphocyte receptor in a lethal model of polymicrobial

sepsis. *Antimicrob Agents Chemother* (2017) 61(1):e01391–16. doi:10.1128/AAC.01391-16

Conflict of Interest Statement: The authors declare that the research was conducted in the absence of any commercial or financial relationships that could be construed as a potential conflict of interest.

frontiers in Immunology

ORIGINAL RESEARCH
published: 24 March 2017
doi: 10.3389/fimmu.2017.00312

Bioconjugation of Small Molecules to RNA Impedes Its Recognition by Toll-Like Receptor 7

*Isabell Hellmuth[1], Isabel Freund[2], Janine Schlöder[3], Salifu Seidu-Larry[1], Kathrin Thüring[1], Kaouthar Slama[1], Jens Langhanki[4], Stefka Kaloyanova[5], Tatjana Eigenbrod[2], Matthias Krumb[4], Sandra Röhm[5], Kalina Peneva[5], Till Opatz[4], Helmut Jonuleit[3], Alexander H. Dalpke[2] and Mark Helm[1]**

[1] Institute of Pharmacy and Biochemistry, Johannes Gutenberg-University Mainz, Mainz, Germany, [2] Department of Infectious Diseases, Medical Microbiology and Hygiene, University of Heidelberg, Heidelberg, Germany, [3] Department of Dermatology, University Medical Center of the Johannes Gutenberg-University Mainz, Mainz, Germany, [4] Institute of Organic Chemistry, Johannes Gutenberg-University Mainz, Mainz, Germany, [5] Max Planck Institute for Polymer Research (MPG), Mainz, Germany

A fundamental mechanism of the innate immune system is the recognition, *via* extra- and intracellular pattern-recognition receptors, of pathogen-associated molecular patterns. A prominent example is represented by foreign nucleic acids, triggering the activation of several signaling pathways. Among these, the endosomal toll-like receptor 7 (TLR7) is known to be activated by single-stranded RNA (ssRNA), which can be specifically influenced through elements of sequence structure and posttranscriptional modifications. Furthermore, small molecules TLR7 agonists (smTLRa) are applied as boosting adjuvants in vaccination processes. In this context, covalent conjugations between adjuvant and vaccines have been reported to exhibit synergistic effects. Here, we describe a concept to chemically combine three therapeutic functions in one RNA bioconjugate. This consists in the simultaneous TLR7 stimulation by ssRNA and smTLRa as well as the therapeutic function of the RNA itself, e.g., as a vaccinating or knockdown agent. We have hence synthesized bioconjugates of mRNA and siRNA containing covalently attached smTLRa and tested their function in TLR7 stimulation. Strikingly, the bioconjugates displayed decreased rather than synergistically increased stimulation. The decrease was distinct from the antagonistic action of an siRNA bearing a Gm motive, as observed by direct comparison of the effects in the presence of otherwise stimulatory RNA. In summary, these investigations showed that TRL7 activation can be impeded by bioconjugation of small molecules to RNA.

Keywords: bioconjugate, click chemistry, immunostimulation, mRNA, siRNA, small molecules, toll-like receptor

OPEN ACCESS

Edited by:
Uday Kishore,
Brunel University London, UK

Reviewed by:
Tom Peter Monie,
University of Cambridge, UK
Lubna Kouser,
Imperial College London, UK

****Correspondence:***
Mark Helm
mhelm@uni-mainz.de

Specialty section:
This article was submitted to Molecular Innate Immunity, a section of the journal Frontiers in Immunology

Received: *07 December 2016*
Accepted: *06 March 2017*
Published: *24 March 2017*

Citation:
Hellmuth I, Freund I, Schlöder J, Seidu-Larry S, Thüring K, Slama K, Langhanki J, Kaloyanova S, Eigenbrod T, Krumb M, Röhm S, Peneva K, Opatz T, Jonuleit H, Dalpke AH and Helm M (2017) Bioconjugation of Small Molecules to RNA Impedes Its Recognition by Toll-Like Receptor 7. Front. Immunol. 8:312. doi: 10.3389/fimmu.2017.00312

INTRODUCTION

Recognition of nucleic acids by the innate immune system results in the activation of signaling cascades that drive animal immune responses. Pattern-recognition receptors (PRRs) are tasked to discriminate between non-infectious self and potentially infectious non-self nucleic acids. This may be achieved by differences in structure, localization, and modification (1, 2). Recognition of non-self nucleic acids typically leads to an immune response that ultimately also shapes adaptive

immunity. Precise definition of the structural details in nucleic acids that correspond to pathogen-associated molecular patterns (PAMPs) has important impact on our understanding of immune responses in bacterial and viral infections, autoimmune diseases, and cancer biology (2). Immediate impact of new insights will also affect the field of therapeutic nucleic acids (3, 4). Understanding the molecular details of innate nucleic acid recognition has made significant progress in the last couple of years with respect to cytosolic factors like retinoic acid inducible gene I (5–7), melanoma differentiation-associated protein 5 (8), absent in melanoma 2 (9–12), and more recently, cGAS (13, 14). Another class of membrane associated PRRs are toll-like receptors (TLRs), among which a subset is located to endosomes. These are thought to inspect exogenous material during the process of uptake and endocytosis. While TLR9 recognizes DNA; TLR3, TLR7/8, and murine TLR13 recognize microbial RNA. TLR3 recognizes double-stranded RNA above a minimal helix length of ~40 nucleotides (15), yet short siRNA might also induce activation in a different binding manner (16). TLR13 is activated by a 13-base sequence from bacterial 23S rRNA, and activation is sensitive to *N6*-methylation of a specific adenosine (17–20). PAMP recognition by the TLR7/8 system is particular in that RNA as well as a series of small molecules with structural elements from purine nucleobases are both recognized (21–26), albeit apparently associated to slightly different signaling modes (27, 28). Indeed, TLR7 and TLR8 were reported to bind degradation products of RNA at two different sites. A crystal structure of toll-like receptor 7 (TLR7) showed a presumed RNA degradation product, namely, guanosine (G), bound to a region that overlaps with a small molecules TLR7 agonists (smTLRa) binding site. Similarly, uridine was found in a TLR8 structure. Furthermore, a single-stranded RNA (ssRNA) was found binding to a distinct second binding site (28, 29). From these structures came the inspiration for a bioconjugate molecule offering ligands that might bind in both of the above binding sites. Whereas both TLR7 and TLR8 recognize RNA, their expression patterns in leukocytes differ (30). TLR7 is highly expressed in plasmacytoid dendritic cells (pDCs), which secrete type I IFN. Of note, pDCs are very nearly the exclusive contributors to IFN secretion from PBMCs, which is why PBMC preparations are popular in measurements of TLR7 stimulation *via* ELISA-based quantification of IFN in the supernatant after exposure of PBMCs to stimulating agents. In contrast, TLR8 is found in monocytes where stimulation induces TNF (31). While RNA recognition of this system has long been described as specific for ssRNA (2), recent results suggest that this simplified review is in need for some refinement. The recognition of mRNA (32) may still be attributed to its single-stranded regions, but tRNA contains very few truly single-stranded regions. Recognition of tRNA was evidenced in three domains of its structure, only one of which is truly single stranded (33, 34). These studies have also unraveled a particular mode of action of posttranscriptional modifications in the discrimination of self and non-self RNA. Ribose methylations in a specific sequence context (35) where shown to act as TLR7 antagonists (36), which do not only prevent the modified RNA from being sensed by TLR7 but also dampen response to additional unmodified, otherwise stimulatory RNA. Such modulation of TLR7 activation is of high interest in the design and development of therapeutic RNA, e.g., siRNA for diverse RNAi approaches (37, 38) or mRNA for tumor vaccine (39). In some approaches, an inhibition of TLR7 response is desirable, e.g., limiting immunostimulatory side effects by siRNA (40–42). In contrast, nucleic acid-derived adjuvants are frequently used to deliberately induce a boost of innate immune response, which, in turn, is known to increase the efficiency of certain vaccines (4, 43, 44). Ideally, it would be possible to fine-tune stimulatory properties *via* the nature and density of synthetic modifications on a therapeutic RNA. As a step in this direction, we decided to test, if the aforementioned TLR7 stimulation by mRNA and smTLRa could be further modulated by covalent conjugation to form a bidentate ligand reaching both binding sites of the receptor. Successful stimulation of innate immunity has been reported for covalent conjugates of various TLR ligands. In particular, ligands for TLR4, TLR7, and TLR9 have been combined by covalent conjugation in a single molecular entity and used to stimulate secretion of NFκB, IL-12, and other cytokines from bone-marrow derived DCs (45). Small molecule TLR7/8 agonists have been conjugated to various polymeric carriers thereby retaining their stimulatory properties. For example, the adenine derivative 1V270 was conjugated to a phospholipid *via* its *N*9 on the purine ring (46). *Via* the same site, another adenine derivative 1V209 was attached to polysaccharides (47). The same nitrogen, numbered *N*1 in tricyclic derivatives of the -quimod series (numbered I or 1 in Figure S1 in Supplementary Material), was used for conjugation of an imiquimod derivative to nanogels (48). In a similar concept, *N*1-derivatives of resiquimod (R848) to alkane and PEG chains leading to self-assembly of the compounds in to nanosized particles (49). Further, derivatives of the same compound class explored the *C*8 position (VIII in Figure S1 in Supplementary Material), the *C*2 position (II in Figure S1 in Supplementary Material), and exocyclic *N*4 (IV in Figure S1 in Supplementary Material), finding derivatization at these sites compatible with TLR7 stimulation (50, 51).

Based on the above findings, our concept, as depicted in **Figure 1**, aimed at the synthesis of a trifunctional mRNA, comprising two types of TLR agonists and the vaccine contained in the mRNA sequence itself. We chose the exocyclic *N*4 of resiquimod and the secondary amine in the *C*2-side chain of gardiquimod as attachment points for a bioconjugation approach that made use of click chemistry of the Cu(I)-catalyzed azide-alkyne 1,3-dipolar cycloaddition (CuAAC) type. Derivatization of this site, according to the recently published structure of TLR7 (28), is expected to disrupt only a single of the hydrogen bonds involved in the recognition of resiquimod, suggesting minimal interference with activity. The same structure suggested that a PEG chain might bridge the two identified binding sites in this receptor, one for resiquimod, and the other for RNA, potentially causing a cooperative effect from a bidentate ligand made of RNA and a small molecule derivative of resiquimod. Since RNAs bearing terminal alkyne groups are readily accessible, we synthesized azide derivatives with 1*H*-imidazo-[4,5-*c*]-purine structure (52–54), i.e., derivatives of imidazoquinolines of the quimod

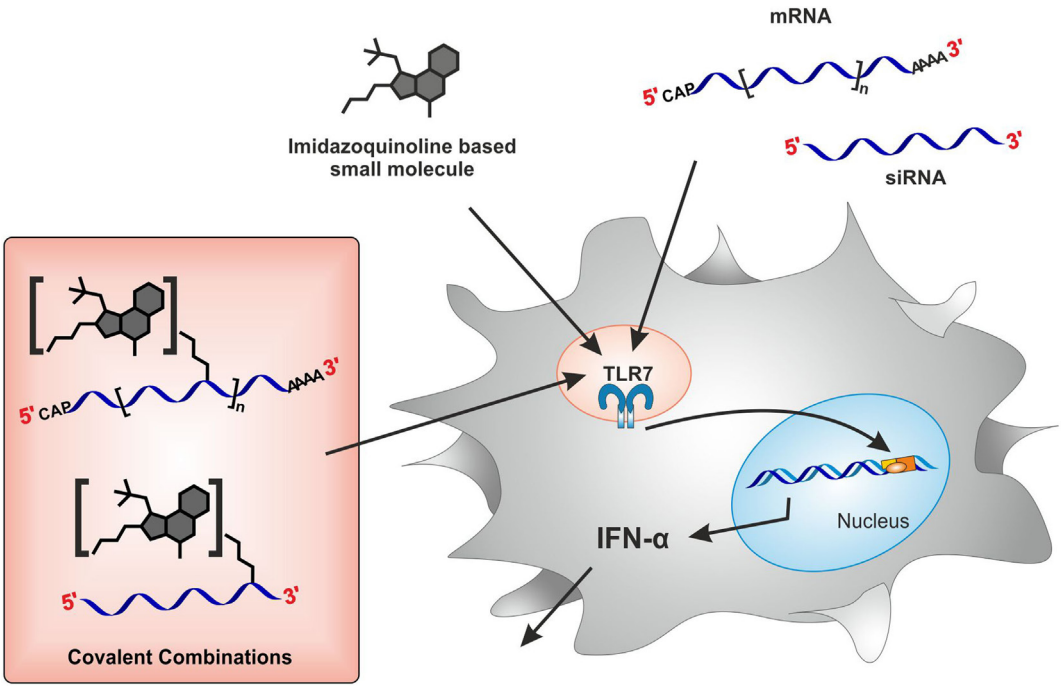

FIGURE 1 | Study conceptualization. Stimulation of toll-like receptor 7 (TLR7) with either imidazoquinoline-based small molecules or RNA species such as mRNA and siRNA results in cytokine (IFNα) secretion from plasmacytoid DCs within PBMCs. How is TLR7 activity modulated upon covalent conjugation of both TLR7 ligands?

series and produced the respective bioconjugates for testing. While the anticipated cooperativity could not be evidenced, we observed that covalent modifications of RNA effectively decrease TLR7-mediated signaling.

MATERIALS AND METHODS

Details to the synthesis procedures of azide-modified TLR ligands, mannose- and dye-derivatives can be found in the supplementary section.

Working with DNA and RNA

All DNA and RNA samples were handled in DNase/RNase- and endotoxin-free water (Zymo Research). Concentrations of DNA and RNA samples were determined using a NanoDrop™ spectrophotometer (Thermo Scientific). Additional confirmation of RNA concentration was carried out with a Qubit™ fluorometer (Thermo Scientific), excluding false positive results.

pDNA Amplification and Preparation

For plasmid DNA, we used the transcription vector pGEM4Z64A-eGFP (55), which was transformed into competent DH5α *Escherichia coli* strain (Invitrogen) according to the manufacturer's instructions and selected *via* an ampicillin resistance gene. pDNA was isolated from *E. coli* overnight culture following the Spin Format Protocol Modification of a GenElute™ high performance endotoxin-free plasmid maxiprep kit (Sigma-Aldrich). Plasmid linearization was carried out with the restriction enzyme *Bcu*I (Thermo Scientific) as described by the manufacturer, purified *via* phenol/chloroform extraction and followed by ethanol precipitation.

mRNA Synthesis

mRNAs were transcribed *in vitro* from 5.0 µg linearized pDNA template using in house expressed and purified T7 RNA polymerase at 37°C for 4 h in a total volume of 100 µL Tris–HCl (40 mM, pH 8.1). Nucleoside triphosphates were applied in a 5 mM final concentration, whereas alkyne-modified 5-ethynyluridine-5′-triphosphate (EUTP) (Jena Bioscience, Germany) was used in indicated percentages of 5 mM and UTP in the remaining amount. Additionally, the reaction contained $MgCl_2$ (30 mM), dithiothreitol (DTT 5 mM), spermidine (1 mM), and 0.01% Triton X-100. *In vitro* transcriptions (IVTs) were stopped by DNaseI treatment as described by the manufacturer (Thermo Scientific). Subsequent capping reactions were carried out using the combination of *Vaccinia* Capping System and mRNA Cap 2′-*O*-methyltransferase (NEB) following the one-step capping and 2′-*O*-methylation protocol (NEB) prolonged to 2 h. All *in vitro* transcripts and capped mRNA-constructs were purified using the MEGAclear™ Kit (Ambion™).

Click Functionalization

All copper-catalyzed click reactions were performed in aqueous solutions containing up to 5% (v/v) dimethyl sulfoxide. The solutions were buffered to pH 8 with NaH_2PO_4 (100 mM) and contained 50 µg (5 µM) mRNA or 1 nmol sense siRNA (MH662;

sequence see Supplementary Material, p. 26; IBA, Goettingen/Germany), respectively, 120–200 µM azido-functionalized ligand [synthesis and characterization for azide-compounds gardiquimod-diethylene-glycol-azide (GDA), resiquimod-polyethylene-glycol-azide (RPA), MMA, TMA, and PDI are given in the supplement]; SCy5-azide (Jena Bioscience, Germany), 250 µM $CuSO_4 \cdot 5H_2O$, 1.25 mM *tris*-[4-(3-hydroxypropyl)-(1,2,3) triazolyl-1-methyl]amine, and 2.5 mM sodium ascorbate. The reaction mixtures were agitated under light protection at 25°C for 2 h. Reactions were stopped through addition of equivalent volumes of a 1 mM EDTA solution and purified through ethanol precipitation.

Polyacrylamide Gel Electrophoresis (PAGE)

mRNA samples (1 µg) were dissolved in gel loading buffer [containing 20% glycerol in 1× TBE (Carl Roth®)] and loaded onto a 6% polyacrylamide gel. Electrophoresis was carried out in 1× TBE (Rotiphorese®, Carl Roth®) buffer at 12 W for 4 h. Gels were post-stained for 20 min with Stains-all (Sigma-Aldrich) and destained overnight in 75% isopropanol. Nucleic acid bands were visualized on a Typhoon 9400 (GE Healthcare) using 633 nm. Emission signals were recorded at 670 nm.

Single-stranded siRNA samples were analyzed by denaturing PAGE. Twenty-five picomoles of oligonucleotides were loaded onto a 20% denaturing polyacrylamide gel containing 1× TBE (compounds for denaturing PAGE from Carl Roth®). PAGE was performed in 1× TBE buffer (12 W/4 h), gels were then post-stained for 20 min with Stains-all (Sigma-Aldrich) and destained overnight in 75% isopropanol. Detection was carried out on a Typhoon 9400 (GE Healthcare), before and after staining, using 532 and 633 nm for excitation. Emission signals were recorded at settings 610BP30 nm and 670 nm.

HPLC Analysis of EU-Containing mRNA

Sample Preparation

Prior to HPLC analysis, 20 pmol of each mRNA sample were digested to the nucleosides level according to the following protocol (56): samples were incubated in presence of 1/10 volume of 10× nuclease P1 buffer (0.2 M NH_4OAc pH 5.0, $ZnCl_2$ 0.2 mM), 0.3 U nuclease P1 (Sigma-Aldrich, Munich, Germany), and 0.1 U snake venom phosphodiesterase (Worthington, Lakewood, CO, USA) at 37°C for 2 h. Next, 1/10 volume of 10× fast alkaline phosphatase buffer (Fermentas, St. Leon-Roth, Germany) and 1 U fast alkaline phosphatase (Fermentas, St. Leon-Roth, Germany) were added, and samples were incubated for additional 60 min at 37°C. For the calibration series of EU, commercially available EU triphosphate was digested analogously.

HPLC Method

The digested mRNA samples were analyzed on an Agilent 1260 HPLC series equipped with a diode array detector (DAD). A Synergi Fusion-RP column (4 µm particle size, 80 Å pore size, 250 mm length, and 2 mm inner diameter) from Phenomenex (Aschaffenburg, Germany) was used at 35°C column temperature for the chromatographic separation of the nucleosides. The solvents applied were a 5 mM ammonium acetate buffer adjusted to pH 5.3 using acetic acid (solvent A) and pure acetonitrile (solvent B). The elution was performed at a flow rate of 0.35 mL/min using a linear gradient from 0 to 8% solvent B at 10 min, 40% solvent B at 20 min, and 0% solvent B at 23 min. For additional 7 min, the column was rinsed with 100% solvent A to restore the initial conditions. The detection of EU and the four canonical nucleosides was performed by measuring the column effluent photometrically at 254 nm using the DAD. For analysis of the recorded UV chromatograms and extracting the respective peak areas of EU and G, the Agilent MassHunter Qualitative Analysis software was used. The exact retention times of EU and the main nucleosides were determined using commercially available standard substances.

Quantification of EU in mRNA by HPLC Analysis

For quantification of EU in the mRNA samples, external calibration series were run for both EU (calibration range 2–120 pmol) and the G (calibration range 50–3,500 pmol) using commercially available reference substances. The detected peak areas for each calibration solution were plotted against the injected amount of EU or the G, and the slope of the linear fit of the resulting curves was used for calculation of the EU and G amounts in each sample. The amount of G was divided by the number of its sites per mRNA molecule, yielding the injected amount of mRNA molecules. The result was then used to calculate the amount of EU residues per mRNA (mol EU per mol mRNA).

Stimulation of PBMCs

Human PBMCs were isolated from blood from voluntary healthy donors: informed consent was signed by each donor, and blood drawing was approved by the Ethic Committee of the Medical Faculty of the University Heidelberg (Permit S-157/2006). Heparinized blood was submitted to standard Ficoll-Hypaque density gradient centrifugation (Ficoll 1.078 g/mL) (42). PBMCs were resuspended in complete medium prepared of RPMI 1640 (Biochrom, Berlin, Germany) supplemented with 10% heat inactivated (1 h, 56°C) FCS (Gibco/Thermo Fisher Scientific, Schwerte, Germany). For stimulation, mRNA was encapsulated with DOTAP (*N*-[1-(2, 3-dioleoyloxy)propyl]-*N*,*N*,*N*-trimethylammonium-205 methylsulfate) (Carl Roth, GmbH Karlsruhe, Germany) at a ratio of 3 µL DOTAP per 1 µg of RNA in Opti-MEM Reduced Serummedium (Life Technologies) and incubation for 10 min at room temperature. As a control, cells were incubated with the individual clickable small molecule-, dye-, and mannose-derivatives only at indicated concentrations. Additionally, cells were co-stimulated with unmodified mRNA in the presence or absence of small molecules and their respective clickable derivatives. All stimulations were performed in duplicates per individual donor at a density of 4×10^5 cells/well PBMCs in a 96-well flat bottom plate. Cells were incubated in a humidified 5% CO_2 atmosphere at 37°C for 16–20 h. Cell-free supernatants were analyzed by sandwich ELISA for secretion of IFN-α (Affymetrix eBioscience, Frankfurt, Germany) according to the manufacturer's protocol. Cytokines were detected by measuring the absorbance at 490 nm with a 650 nm reference in a photometer (Sunrise reader, Tecan, Salzburg, Austria).

Cytokine concentration was calculated according to a standard dilution of recombinant cytokine using Magellan V 5.0 software (Tecan, Salzburg, Austria). Each experiment was repeated minimum three times. Cytokine secretion of individual donors was normalized to a stimulation with 1 µg/mL eGFP-mRNA or R848, respectively, which served as internal calibrator. Cell viability of stimulated PBMCs was assessed by MTS assay using CellTiter 96 Aqueous One solution proliferation kit (Promega, Madison, WI, USA) according to the manufacturer's instructions. Cells were incubated for 3 h at 37°C in a humidified, 5% CO_2 atmosphere. Viable cells were detected by measuring the absorbance at 492 nm in a photometer (Sunrise reader, Tecan, Salzburg, Austria).

Generation and Transfection of Human Dendritic Cells

Myeloid DCs were generated from buffy coats of healthy volunteers as described previously (57, 58). In brief, PBMCs were isolated by Ficoll density gradient centrifugation, and monocytes were isolated by plastic adherence and cultured in X-VIVO-15 (Lonza) supplemented with 1% heat-inactivated autologous plasma, 800 IU/mL GM-CSF (Leukine, Berlex), and 100 IU/mL IL-4 (CellGenix). Fresh media with GM-CSF (1,600 U/mL) and IL-4 (100 IU/mL) were given at day 2 and day 4. Immature DCs were harvested at day 6 and subsequently used for further electroporation experiments. All electroporation experiments with human DCs were performed with Neon Transfection System (Thermo Fisher Scientific). According to the manufacturer's instruction, 0.5–1 × 10^6 DCs were electroporated with various amounts of mRNA in a total volume of 100 µL of electroporation buffer. To achieve high transfection efficiencies, the following program was used: pulse voltage: 1,500 V; pulse width: 30 ms; pulse number: 1. Afterward, DCs were cultured in pre-warmed X-VIVO-15 supplemented with 1% heat-inactivated autologous plasma, 800 IU/mL GM-CSF and 100 IU/mL IL-4 for 24 h at 37°C, 5% CO_2. RNA translation was analyzed by flow cytometry (BD Accuri™ C6 Cytometer).

Knockdown in HeLa MAZ

Cells

HeLa MAZ cells (59) contain the episomal vector pMARS-mODC-AZ, which encodes for a destabilized eGFP. Cells were a kind gift from Dr. Andriy Khobta from the group of Prof. B. Epe (Institute of Pharmacy and Biochemistry, Mainz).

Hybridization

siRNA single strands (antisense MH533 and sense MH662; sequences see Supplementary Material) were obtained from IBA (Göttingen, Germany). The hybridization experiments were carried out in 1× phosphate-buffered saline (pH 7.4), with the two complementary strands in a 1:1 ratio, to result in a final duplex concentration of 5 µM. The strands were first incubated at 70°C for 3 min, and duplex formation was allowed at 37°C over 1 h. The prepared duplex siRNA was stored at −20°C.

Knockdown Experiments

Prior to transfection, 5 × 10^4 HeLa MAZ cells were seeded in 24-well plate in 1 mL DMEM (Thermo Fisher) with 10% fetal bovine serum (Sigma-Aldrich). After 1 day, medium was replaced by 500 µL of 10% FCS DMEM, and cells were transfected with siRNA. Briefly, to prepare siRNA/lipid transfection mixture, 40 pmol from a starting 5 µM siRNA duplex was diluted in Opti-MEM® (Thermo Fisher) in twofold dilution series and mixed with transfection agent Lipofectamine™ (Thermo Fisher) according to the manufacturer's instruction. In the transfection time, 100 µL of siRNA was added in dropwise to the wells. Transfection experiment was realized in duplicate, and each experiment was repeated three times. Cells were incubated 24 h, after which the medium was replaced by 185 µL of 10% FCS medium and 65 µL of 2 M MG115 (proteasome inhibitor, Sigma-Aldrich). This was followed by another 6 h incubation. For FACS analysis, cells were washed with 500 µL DPBS, trypsinized with 200 µL trypsin/EDTA, resuspended in 400 µL DPBS, and the eGFP signal measured by flow cytometry instrument (LSR-FortessaSORP, BD Biosciences) with excitation at 488 nm and a 530BP30 nm emission filter. Data were used for IC_{50} curves. The calculated eGFP signal corresponds to the product of the percentage of eGFP positive cells and their median fluorescence intensity, normalized to the value of positive controls (untreated with siRNA duplex). For acquisition and analysis, the FACSDiva Software (BD Biosciences) was used.

Statistical Analysis

Data were analyzed using GraphPad Prism 7.0 (GraphPad Software Inc.). Significant differences were assessed by two-way ANOVA followed by multiple comparisons tests. In all figures, the P values are indicated by ns (not significant; $P > 0.05$), $^*P \leq 0.05$, $^{**}P \leq 0.01$, $^{***}P \leq 0.001$, $^{****}P \leq 0.0001$.

RESULTS

The original question we sought to address, derived from the recent report of two distinct signaling pathways originating from TLR7 stimulation, one triggered by small molecules of the imiquimod series, and the other triggered by RNA (27, 28). We wondered, if it was possible to simultaneously stimulate both pathways by chemically combining both sorts of PAMPs in the same molecule. Hence, we designed small molecule derivatives of the -quimod series with two alternative sites for immobilization on RNA molecules by CuAAC-click chemistry. RNA molecules could then be viewed as scaffolds to present both types of TLR7-activating molecular patterns. To this end, we used alkyne-modified siRNA as well as alkyne-modified mRNA, thus a small and a large RNA, both considered for therapeutic purposes (4, 39, 60) and both reported to be TLR7 ligands (61, 62).

Azide-Functionalized Small Molecule TLR Agonists: TLR7 Activity Depends on Conjugation Site

The synthesis route to azide-bearing small molecule TLR ligands is depicted in **Figure 2** below. In order to equip gardiquimod **1** (GQI) with an azido-ethylene glycol linker at its aliphatic amine, the hydroxyl group of the latter was converted into a good leaving group, a methane sulfonyl moiety. This linker was attached to the small molecule *via* substitution at the exocyclic secondary amine

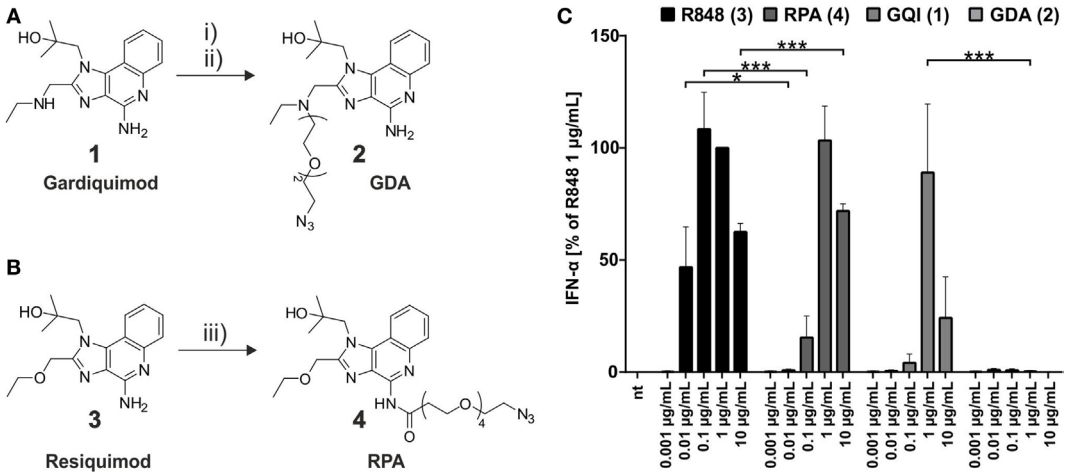

FIGURE 2 | Synthesis of azide-functionalized small molecule toll-like receptor agonists. **(A)** gardiquimod-diethylene-glycol-azide (GDA) (2) from gardiquimod (1): (i) mesylation of HO-TEG-N_3, 80%; (ii) SO_2MeO-TEG-N_3, acetonitrile, RT, 50%. **(B)** Resiquimod-polyethylene-glycol-azide (RPA) (resiquimod-PEG_4-N_3) (4) from resiquimod (R848) (3): (iii) NHS-PEG_4-N_3, DCM, RT, 25%. **(C)** Titration of PBMCs with the commercial small molecules and their respective azide derivatives (nt, non-treated). IFN-α production was measured by ELISA as technical duplicate of biological triplicates (three donors). Due to donor variation in the absolute amount of IFN-α secreted, data from each individual were normalized to 1.0 µg/mL R848 (=100%) of the respective (n = 3; mean + SD). [Asterisks above bars indicate the respective P values evaluated by ANOVA and Sidak's multiple comparisons test; no declaration = not significant (ns).]

to give the desired product GDA **2**. Resiquimod **3** (R848) was equipped with an azido-polyethylene-glycol linker by applying standard NHS-ester chemistry (63) between its primary amine and the reactive *N*-hydroxysuccinimide-group of the linker to yield the product RPA **4**. The purity of both products was confirmed by ^1H-NMR, full range and high resolution MS (Figures S2–9 in Supplementary Material), which was a prerequisite for subsequent experiments, to exclude residual starting material of the smTLRa.

The impact on immunostimulatory activity arising from the conjugates in contrast to the original agonists was evaluated by an ELISA-based measurement of IFN-α secretion from incubated PBMCs, which reflects activation of pDCs through TLR7 (33, 64). As the highly significant comparison in **Figure 2C** (all results of significance evaluation given in Table S1 in Supplementary Material) shows attachment of an azide-conjugated PEG-linker at the *C*-2-ethyl-amino-methyl-group of the 1*H*-imidazo-[4,5-*c*]-quinolin scaffold (see also Figure S1 in Supplementary Material) ablated TLR7 stimulation of the gardiquimod derivative 2. This finding was in keeping with a previous study reporting diminished IFN secretion upon variation at the *C*-2 site (51), although others reported the *N*-9-position as a "tolerant" linker site upon structure–activity relationship measurements (52–54). In contrast, attachment of the PEG-linker to the *C*-4-NH_2-group of 3, which resulted in the resiquimod derivative 4, led to less stimulation than 3 at a concentration of 0.1 µg/mL, but to an equal outcome at a concentration of 1 µg/mL and even higher at 10 µg/mL (see also Table S1 in Supplementary Material). Thus, the conjugation to a PEG chain, while it indeed did diminish the activity of 4, still allowed to retain activity that showed no difference up to a significant enhancement to unconjugated gardiquimod (Table S1 in Supplementary Material), which itself is a potent agent originally developed as a potential successor of imiquimod. The activity of 4 is in keeping with the conjugation chemistry interfering with receptor binding only at a single hydrogen bond (28). The linker-equipped resiquimod 4 is therefore a valid smTLRa for later comparison with its mRNA-conjugate. Of note, an MTS-based cell viability assay (Figure S15 in Supplementary Material) showed decreased metabolic activity after exposure to 10 µg/mL resiquimod, which likely explains the reduced IFN secretion under these conditions. However, cells showed normal viability under all other conditions.

Synthesis of Alkyne-Modified mRNA and Posttranscriptional Functionalization

Using eGFP encoding mRNA as a model that allowed reporting its functionality in protein biosynthesis, we synthesized alkyne-modified mRNA by IVT with T7 RNA polymerase from a linearized plasmid-DNA template comprising a poly-dT sequence of 64 dTs for the *in situ* synthesis of a 3′-poly-A-tail. For alkyne-modified mRNAs, 1 or 10% of the standard UTP reaction concentration were substituted with EUTP (65, 66), with no discernible impact on the IVT yield. The 5′-end of the purified IVT-construct was subsequently equipped with a 7-methylguanosine-ppp-Gm cap structure (Cap1) (Figure S16A in Supplementary Material). This was effected by means of combined enzymatic reactions of the *vaccinia* capping enzyme and 2′-*O*-methyltransferase (67, 68) after optimization employing a tritium incorporation assay with ^{3}H-*S*-adenosyl-methionine (Figure S16B in Supplementary Material).

With an mRNA equipped with terminal alkyne moieties and azide-functionalized small molecule derivatives (**Figure 3A**) in hand, CuAAC-click reactions were conducted according to Hong et al. (69). Integrity of the mRNA after click reaction was verified by PAGE (Figure S17 in Supplementary Material).

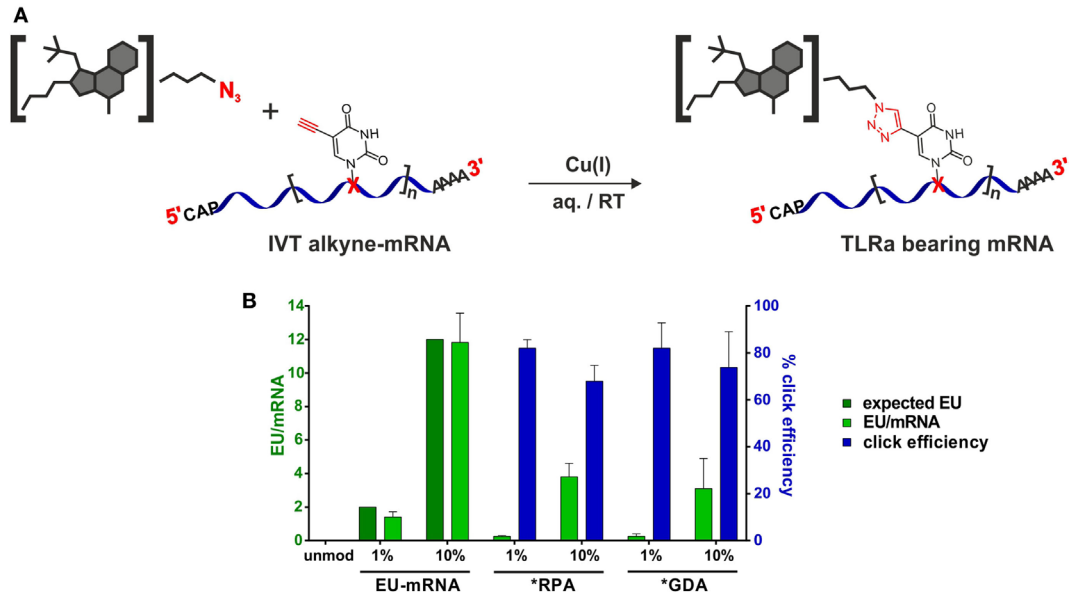

FIGURE 3 | Synthesis of small molecule-TLRa bearing eGFP-mRNA. **(A)** Symbolic synthesis scheme of Cu(I)-catalyzed azide-alkyne-cycloaddition between azide-functionalized toll-like receptor (TLR) agonists and *in vitro* transcribed (n)alkyne-modified eGFP-mRNA. **(B)** HPLC-quantification of EU content (light green) in *in vitro* transcription (IVT)- and TLRa-eGFP-mRNA including click efficiency (blue) ($n = 5$; mean + SD).

To assess incorporation of clickable nucleoside and click efficiency, both, alkyne-containing *in vitro* transcripts and products from click reactions, were analyzed on the nucleoside level with respect to their existing/remaining EU content. Therefore, the RNA oligonucleotides were digested to nucleosides by stepwise incubation with nuclease P1, snake venom phosphodiesterase, and alkaline phosphatase and subjected to quantitative HPLC analysis. With the sequence of the unmodified mRNA containing 119 uridines (Supplementary Material, p. 26), it was expected to find 1–2 and 12, respectively, of them replaced by 5-ethynyluridine in IVT syntheses when employing 1 and 10% EU, respectively. **Figure 3B** shows quantification results (light-green bars for EU-mRNA) confirming this assumption.

The yield of the implemented click reactions was determined from residual EU (light green and blue bars in **Figure 3B**). For both ligands, click modification of 1% EU-mRNA proceeded to 82% completion, corresponding to 1–2 conjugated small molecules per molecule mRNA, and to 70% of the 10% EU-mRNA, equaling 8–9 conjugated small molecules per molecule mRNA.

To gauge the dynamic range of a potential cooperative stimulation by both types of TLR7 agonists, they were tested together. Therefore, unmodified mRNA concentration was varied at a constant concentration (0.1 µg/µL) of the smTLRa. **Figure 4** shows that smTLRa based IFN-α secretion can be increased by addition of mRNA (dark blue bars). In particular, the maximum effect of resiquimod, determined to be at 0.1 µg/mL in **Figure 2C**, was increased as a function of the concentration of additional mRNA (**Figure 4**; Figure S18 in Supplementary Material). Similarly, IFN-α secretion based on RPA, gardiquimod, or GDA alone, was increased upon addition of mRNA.

According to the working hypothesis, a relative increase upon stimulation with the covalent conjugates was expected. As shown in **Figure 4**, the impact on covalent attachment of the TLRa derivatives to mRNA in terms of TLR7 stimulation contradicted this original hypothesis. Rather than showing an amplification or synergistic effect, the TLRa moieties clicked onto the mRNA (yellow and orange bars) dampen the emission of IFN-α in comparison to free mRNA (gray bars) or the combined mRNA and smTLRa (dark blue bars). The effect is mild at 1–2 TLRa moieties per molecule mRNA but clearly more pronounced at a higher degree of modification, i.e., 8–9 moieties per mRNA.

Non-TLR-Binding Moieties also Shield RNA-Conjugate Molecules from Stimulating TLR7

Since the mRNA bioconjugates tested so far all contained substructures known to interact with TLR7, we decided to expand the scope of these investigations to include structures that are *bona fide* non-PAMPs. **Figure 5A** shows four azides employed in this perspective, which did indeed not cause any IFN-α secretion in stimulation tests (not shown). Two are highly hydrophilic sugar moieties of divergent size, and two are fluorescent dyes of planar structure, whose lipophilicity is partially mitigated by sulfonyl groups. Synthesis of mRNA conjugates was performed as above. Click yields ranged from 50 to 60%, corresponding to 1 or 6 clicked moieties per mRNA molecule, for 1 and 10% EU content, respectively (**Figure 5B**). As detailed in **Figure 5C**, the corresponding mRNA conjugates showed a dampened immune response, although to varying degrees. As before, any observable effects increase with the number of attached moieties. The most

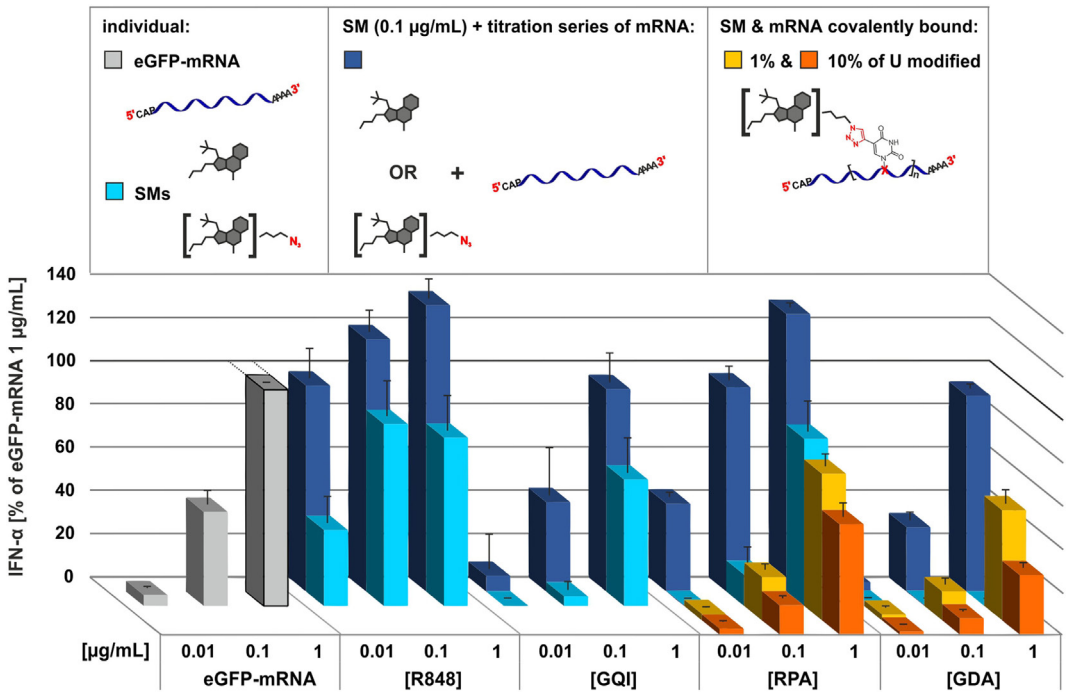

FIGURE 4 | Comparison of the effect of small molecules TLR7 agonists, RNA, and covalent conjugates of both in immunostimulation. Titration of PBMCs with eGFP-mRNA (gray), commercial small molecules and their respective azide derivatives (light blue), 0.1 µg/mL of SMs titrated individually with eGFP-mRNA (dark blue), 1% (yellow) and 10% (orange) alkyne-eGFP-mRNA clicked with resiquimod-polyethylene-glycol-azide (RPA) and gardiquimod-diethylene-glycol-azide (GDA), respectively. IFN-α production was measured by ELISA as technical duplicate of biological triplicates (three donors). Due to donor variation in the absolute amount of IFN-α secreted, data from each individual were normalized to 1.0 µg/mL eGFP-mRNA (=100%) of the respective (n = 3; mean + SD). Numeric P values are given in Figure S18 in Supplementary Material.

pronounced effect was seen for the PDI dye, which also has the largest molecular weight. This conjugate is also the only one with a clear effect at 1% EU.

Transfer to siRNA

The above findings suggest that conjugation of small molecules to mRNA reduces the potency of RNA to trigger TLR7-mediated IFN-α secretion and that the degree of reduction depends on the size and the number of small molecules attached to the RNA. This implies a certain dependence on the modification density, i.e., the number of conjugation sites per length unit of the RNA. Consequently, the effect would be expected to be more pronounced even for single attachment sites on smaller RNAs such as siRNAs. We therefore synthesized siRNA conjugates by CuAAC using the same azides as before (**Figures 2** and **5**). We used an siRNA sequence that previously had been shown to stimulate TLR7 (42). In contrast to mRNA, siRNA conjugates had the additional advantage that they could be separated from unreacted material, hence the immunostimulation data can be attributed to molecules carrying exactly one conjugation site per 22 nucleotides ssRNA, illustrated in **Figure 6A**. The purified sense strands (**Figure 6B**) were tested for IFN-α secretion as described before. As shown in **Figure 6C**, the alkyne-bearing control sense strand (MH662) gives the most prominent amplitude in IFN-α secretion at a concentration of 1 µg/mL. In contrast, all siRNA conjugates show at least a decrease to 55% in TLR7 activation, with the strongest outcome being a sixfold reduction to 20% for the TMA conjugate.

Influence of RNA Modification on Biologic Activity

The biological activities of both types of RNA after CuAAC conjugation were investigated bearing in mind that both are being actively investigated as therapeutic agents. Translation efficacies of click-conjugated mRNA derivatives were compared to their untreated controls by measuring the fluorescence of the encoded reporter protein eGFP. Therefore, immature DCs were electroporated with differentially treated mRNA samples. Fluorescence intensity was measured 24 h later by flow cytometry. The introduction of an alkyne moiety *via* IVT did not have any negative impact on protein expression at neither 1% (Figure S19 in Supplementary Material) nor 10 EU% (not shown). However, CuAAC-mediated conjugation of any azide compound featured in **Figures 2** and **5** ablated translational activity completely. Testing of material from mock reactions, i.e., click reactions without azide compound, confirmed that this effect is due to the conjugation and not a consequence of the reaction conditions of the CuAAC (Figure S19 in Supplementary Material). We conclude

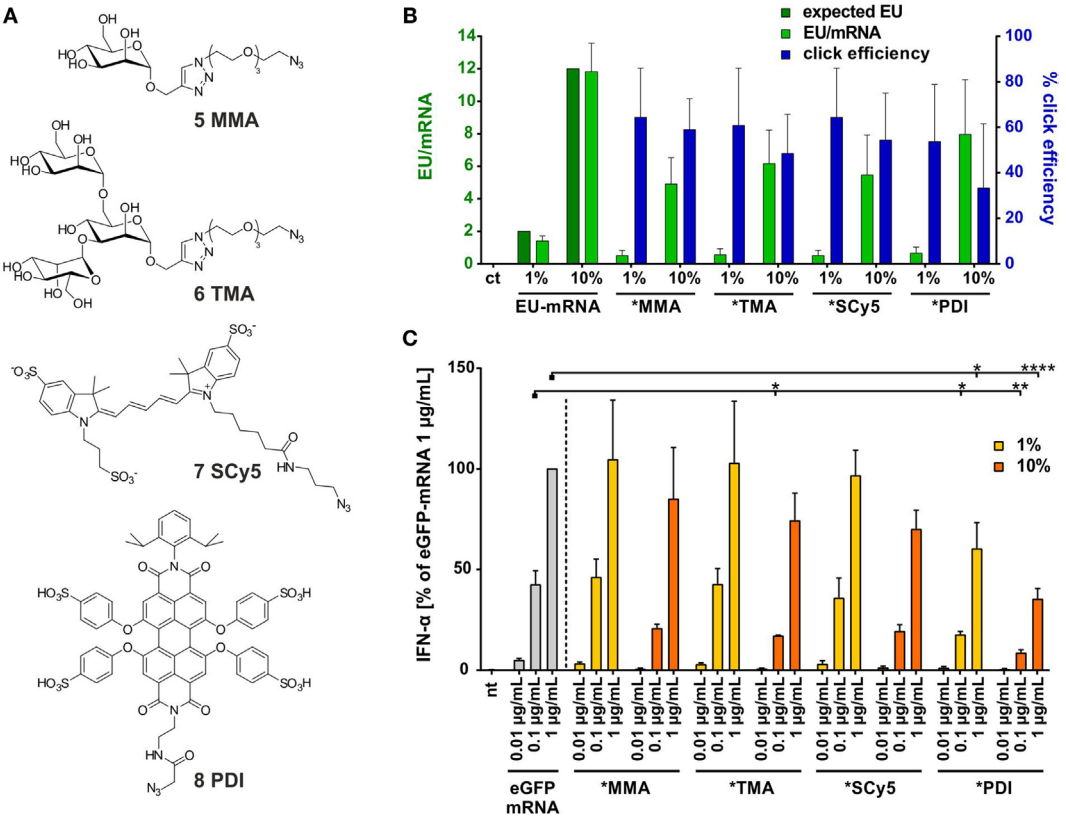

FIGURE 5 | **(A)** Selected azide-bearing molecules of different molecular weight: sugar moieties mono- and trimannose (5, 6), fluorescent dyes Sulfo-Cy5 (7), and perylene-derivative PDI (8). **(B)** HPLC quantification of EU content (light green) in *in vitro* transcription- and clicked-eGFP-mRNA including click efficiency (blue) (n = 2–5; mean + SD) (ct = unmodified control eGFP-mRNA). **(C)** Titration of PBMCs with eGFP-mRNA, 1 and 10% alkyne-eGFP-mRNA clicked with molecules 5–8 (nt, non-treated). IFN-α production was measured by ELISA as technical duplicate of biological triplicates (three donors). Due to donor variation in the absolute amount of IFN-α secreted, data from each individual were normalized to 1.0 µg/mL eGFP-mRNA (=100%) of the respective donor (n = 3; mean + SD). [Asterisks above bars indicate the respective P values evaluated by ANOVA and Sidak's multiple comparisons test; no declaration = not significant (ns).].

that even a single lateral conjugation anywhere onto an mRNA is incompatible with the translation apparatus.

In order to assess how the respective bioconjugations would influence the RNAi efficiency of an siRNA, IC_{50} values were determined in HeLa MAZ cells (59) *via* the knockdown of a destabilized eGFP with selected constructs (**Figure 6D**). After hybridization of clicked sense-strand derivatives to the appropriate antisense strand, cells were incubated with a concentration series of siRNA double strands and eGFP fluorescence emission measured by FACS 24 h later. In keeping with our previously reported identification of a permissive attachment site on the 3′-end of the sense strand (70), conjugation of various azides did not significantly increase the IC_{50} values (**Figure 6D**). Indeed, the *PDI derivative (pink in **Figure 6**) showed an IC_{50} value improved by ~3-fold.

The Effect of Bioconjugates on TLR7-Mediated Immunostimulation Is Distinct from Inhibition by Ribose Methylation

Given that the bioconjugates of smTLRa ligands, as well as all other conjugates showed a decreased stimulation of TLR7, the question arose, if this decrease was comparable to that known from RNA carrying a Gm residue. This residue, a G nucleotide with a 2′-*O*-methylation, when placed in the right sequence context, was previously shown to act as a TLR7 antagonist when applied together with otherwise stimulatory RNA (33, 35). A corresponding assay was carried out with four of the above siRNA conjugates, namely, of RPA, GDA, TMA, and PDI. A constant concentration of stimulatory siRNA was co-incubated with increasing amounts of the conjugates, and for comparison an siRNA carrying a Gm modification was investigated under the same conditions. **Figure 7** shows a striking and clear inhibition of the Gm-RNA in comparison to the stimulatory RNA alone. In contrast, all mixtures of stimulatory RNA and conjugates showed a moderate and concentration dependent increase of IFN-α emission relative to the standard, presumably as a result of an overall increased amount of applied RNA. Hence, the effect of bioconjugation on stimulation of TLR7 is neither inhibitory, nor as pronounced as that of Gm.

DISCUSSION

The work described here was based on the working hypothesis that TLR7 activation might be synergistically increased by the combination of two known but distinct TLRa, namely, ssRNA

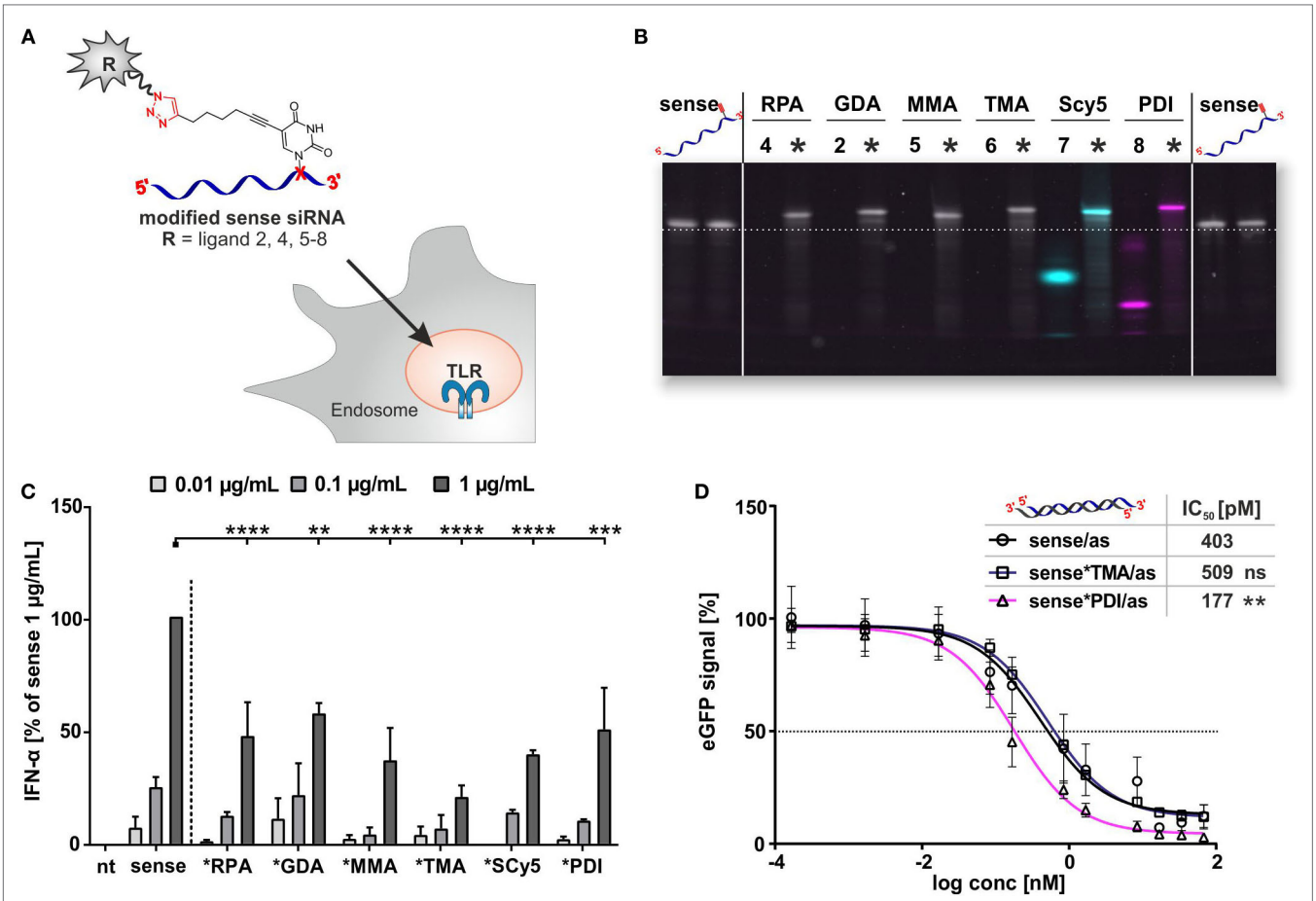

FIGURE 6 | Application on commercial mono-alkyne-functionalized sense eGFP-siRNA. **(A)** Sense siRNA constructs for PBMC stimulation. **(B)** Denaturing polyacrylamide gel electrophoresis for comparison of the click efficiency of the single-stranded, alkyne-modified oligonucleotide MH662 (sense), free azides (**4, 2, 5–8**), and purified clicked (*) oligonucleotides, showing band shift after click reaction and additional fluorescent signals for SCy5 (blue) and PDI (purple). Before staining, excitation for dye-carrying constructs was done at 532 nm (PDI) and 633 nm (SCy5). Stains-all (gray/633 nm) was used as loading control to visualize non-fluorescent bands. Emission signals were recorded at 610BP30 nm and 670 nm (superimposition shown). **(C)** Titration of PBMCs with sense siRNA, clicked with molecules 2, 4, and 5–8 (nt, non-treated). IFN-α production was measured by ELISA as technical duplicate of biological triplicates (three donors). To account for donor variation in the absolute amount of IFN-α secreted, data from each individual were normalized to 1.0 µg/mL unmodified siRNA MH662 (=100%) of the respective donor ($n = 3$; mean + SD). (Asterisks above bars indicate P values evaluated by ANOVA and Sidak's multiple comparisons test; no declaration = ns.) **(D)** eGFP-knockdown experiments with unlabeled control- (sense), TMA (6)- and PDI (8)-siRNA double strands [with antisense-strand MH533 (as)] in HeLa MAZ (stably expressing eGFP). IC_{50} ($n = 3$; mean + SD). (Respective P values for IC_{50} were evaluated by ANOVA and Dunnett's multiple comparisons test.)

and small molecules of the -quimod series. Previous work by the Weber group provided experimental evidence that these two classes of TLRa engage TLR7 in different recognition modes, since they lead to different signaling cascades (27), which could be confirmed by resent investigations on TLR7-crystal structures by Zhang et al. (28). Our attempts to unite both patterns in a single bidentate molecular entity clearly failed, since the covalent conjugates of resiquimod to RNA decreased the TLR7-mediated interferon response, rather than increasing it. One interesting result is contained within the control reactions performed in this context, though: combined administration of mRNA and (unconjugated) resiquimod can still increase the interferon response that was already saturated with respect to resiquimod—compare light blue and dark blue bars in the R848 panel in **Figure 4**. This indicates additional capacity for activation not accessible by R848 alone. Synergistic but also anti-synergistic effects of stimulation by nucleic acid in combination with imidazoquinolines have been described for DNA in the context of human and murine TLR7/8 systems (71–73). For example, poly(T) ODNs inhibited TLR7 activation but enhanced TLR8 signaling by imidazoquinoline derivatives optimized to trigger either TLR7 or TLR8. Those effects seemed to be independent from DNA receptor TLR9. Here, experiments with GDA, a non-stimulatory derivate, show that the opposite also occurs: coupling GDA to mRNA (**Figure 4**) inhibited activation by otherwise stimulatory RNA nucleic acid.

This modification scheme by CuAAC chemistry on mRNA was explored, to our best knowledge, for the first time concerning immunostimulation and protein expression. The complete ablation of mRNA translation on the 5-position of uridines, even by a single modification, is somewhat surprising. It suggests that, besides the coding region, the entire length of the RNA (with the possible exception of the poly-A tail) is subject to some kind of

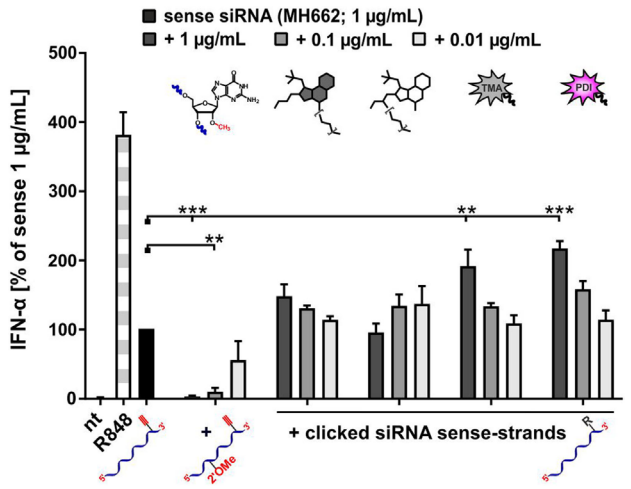

FIGURE 7 | A new distinct type of prevention of toll-like receptor 7-mediated immunostimulation: steric shielding acts different from ribose methylation. PBMCs were incubated with 1.0 µg/mL sense siRNA (MH662) and simultaneously with a titration series of MH662 bearing either a Gm motive (2′-OMe) at position 8, or MH662 clicked to azides of resiquimod-polyethylene-glycol-azide (4), gardiquimod-diethylene-glycol-azide (2), TMA (6), or PDI (8) (nt, non-treated). IFN-α production was measured by ELISA as technical duplicate of biological triplicates (three donors). To account for donor variation in the absolute amount of IFN-α secreted, data from each individual were normalized to 1.0 µg/mL unmodified siRNA MH662 (=100%) of the respective donor (n = 3; mean + SD). (Asterisks above bars indicate the respective P values evaluated by ANOVA and Dunnett's multiple comparisons test; no declaration = ns.)

steric surveillance, which is unlikely to be effected by ribosomes alone, since the 3′-UTR is also concerned. More promising is the continued function of siRNA conjugates, whose potentially undesired immunostimulation can be partially shielded by bulky conjugates. A serendipitous discovery is the actual improvement of RNAi efficiency upon addition of the large perylene dye. While one might speculate this to be related to issues of membrane penetration from the endosomal compartment into the cytosol, detailed follow-up studies are required to determine the extent of this effect.

The recurrent observation of a moderately decreased response to conjugates containing small molecules attached to the RNA chain laterally (mRNA) or terminally (siRNA) are in contrast to our previous observations of a truly active antagonist mode displayed by naturally occurring ribose methylations in defined nucleotide contexts, which, despite being much smaller, block activation even in the presence of otherwise potently stimulatory RNA (33, 35). Because we have ruled out a similar effect for the RNA bioconjugates synthesized here (see comparative data in **Figure 7**), we conclude that it is likely that the bioconjugated small molecule residues provide some amount of steric shielding to the RNA, reducing TLR activation simply by blocking access to recognition notices in the RNA proper. In contrast, the antagonistic action of ribose-methylated RNAs is more in keeping with a mechanism in which the methylated RNA is bound by TRL7 but inhibits a conformational rearrangement conductive to signaling. Given that our work failed to identify a new structural principle for the activation of TLR7, we feel that it would mean over-interpretation to excessively discuss solely negative data in the context of the published X-ray structures of TLR/and TLR8 (28, 29).

In summary, in failing to show cooperative TLR7 stimulation by R848-RNA conjugates, we have described a general steric shielding effect to reduce TLR7 stimulation by RNA. Our concluding experiment (**Figure 7**) has shown that the steric shielding effect discovered here is of fundamentally different nature than the inhibition known from ribose methylation (33, 35). Although, the latter is already an elegant method to prevent RNA molecules from immunostimulation, our findings are by no means negligible in RNA-bioconjugate chemistry as any label may potentially influence TLR7 stimulation. Of note, siRNA conjugates to trimeric sugar moieties similar to the trimannose conjugate (*TMA in **Figures 5** and **6**) are in preclinical trials (74), and their immunogenic potential is likely to be affected in a similar way.

AUTHOR CONTRIBUTIONS

IH—contributions to design of the work, performed research, acquisition and analysis of data, illustration, initial drafting of the manuscript, critical revision, and final approval; IF—performed research, acquisition and analysis of data, critical revision, and final approval; JS, SS-L, KT, KS, JL, SK, MK, and SR—performed research and final approval; TE—contributions to critical discussion and analysis of data and final approval; KP—contributions to design of the work, supervision, and final approval; TO and HJ—contributions to design of the work, critical revision, supervision, and final approval; AD—contributions to design of the work, illustration, critical revision, supervision, and final approval; MH—design of the work, illustration, writing of the manuscript, critical revision, supervision, and final approval.

ACKNOWLEDGMENTS

The authors would like to thank the Cytometry Core Facility of the Institute of Molecular Biology gGmbH (IMB, Mainz), Yolanda Kleiner B.Sc., and Jasmin Hertler B.Sc.

FUNDING

The authors acknowledge funding by the German Research Foundation (DFG) to MH, HJ, and TO (SFB1066, Projects B7 and A2), MH (He3397/9-1), and AD (Da592/5-1).

SUPPLEMENTARY MATERIAL

The Supplementary Material for this article can be found online at http://journal.frontiersin.org/article/10.3389/fimmu.2017.00312/full#supplementary-material.

REFERENCES

1. Brencicova E, Diebold SS. Nucleic acids and endosomal pattern recognition: how to tell friend from foe? *Front Cell Infect Microbiol* (2013) 3:37. doi:10.3389/fcimb.2013.00037
2. Dalpke A, Helm M. RNA mediated toll-like receptor stimulation in health and disease. *RNA Biol* (2012) 9:828–42. doi:10.4161/rna.20206
3. Barchet W, Wimmenauer V, Schlee M, Hartmann G. Accessing the therapeutic potential of immunostimulatory nucleic acids. *Curr Opin Immunol* (2008) 20:389–95. doi:10.1016/j.coi.2008.07.007
4. Junt T, Barchet W. Translating nucleic acid-sensing pathways into therapies. *Nat Rev Immunol* (2015) 15:529–44. doi:10.1038/nri3875
5. Hornung V, Ellegast J, Kim S, Brzozka K, Jung A, Kato H, et al. 5'-Triphosphate RNA is the ligand for RIG-I. *Science* (2006) 314:994–7. doi:10.1126/science.1132505
6. Schuberth-Wagner C, Ludwig J, Bruder AK, Herzner AM, Zillinger T, Goldeck M, et al. A conserved histidine in the RNA sensor RIG-I controls immune tolerance to N1-2'O-methylated self RNA. *Immunity* (2015) 43:41–52. doi:10.1016/j.immuni.2015.06.015
7. Yoneyama M, Kikuchi M, Natsukawa T, Shinobu N, Imaizumi T, Miyagishi M, et al. The RNA helicase RIG-I has an essential function in double-stranded RNA-induced innate antiviral responses. *Nat Immunol* (2004) 5:730–7. doi:10.1038/ni1087
8. Kato H, Takeuchi O, Sato S, Yoneyama M, Yamamoto M, Matsui K, et al. Differential roles of MDA5 and RIG-I helicases in the recognition of RNA viruses. *Nature* (2006) 441:101–5. doi:10.1038/nature04734
9. Fernandes-Alnemri T, Yu J-W, Datta P, Wu J, Alnemri ES. AIM2 activates the inflammasome and cell death in response to cytoplasmic DNA. *Nature* (2009) 458:509–13. doi:10.1038/nature07710
10. Hornung V, Ablasser A, Charrel-Dennis M, Bauernfeind F, Horvath G, Caffrey DR, et al. AIM2 recognizes cytosolic dsDNA and forms a caspase-1-activating inflammasome with ASC. *Nature* (2009) 458:514–8. doi:10.1038/nature07725
11. Roberts TL, Idris A, Dunn JA, Kelly GM, Burnton CM, Hodgson S, et al. HIN-200 proteins regulate caspase activation in response to foreign cytoplasmic DNA. *Science* (2009) 323:1057–60. doi:10.1126/science.1169841
12. Burckstummer T, Baumann C, Bluml S, Dixit E, Durnberger G, Jahn H, et al. An orthogonal proteomic-genomic screen identifies AIM2 as a cytoplasmic DNA sensor for the inflammasome. *Nat Immunol* (2009) 10:266–72. doi:10.1038/ni.1702
13. Sun L, Wu J, Du F, Chen X, Chen ZJ. Cyclic GMP-AMP synthase is a cytosolic DNA sensor that activates the type I interferon pathway. *Science* (2013) 339:786–91. doi:10.1126/science.1232458
14. Ablasser A, Goldeck M, Cavlar T, Deimling T, Witte G, Rohl I, et al. cGAS produces a 2'-5'-linked cyclic dinucleotide second messenger that activates STING. *Nature* (2013) 498:380–4. doi:10.1038/nature12306
15. Liu L, Botos I, Wang Y, Leonard JN, Shiloach J, Segal DM, et al. Structural basis of toll-like receptor 3 signaling with double-stranded RNA. *Science* (2008) 320:379–82. doi:10.1126/science.1155406
16. Pirher N, Ivicak K, Pohar J, Bencina M, Jerala R. A second binding site for double-stranded RNA in TLR3 and consequences for interferon activation. *Nat Struct Mol Biol* (2008) 15:761–3. doi:10.1038/nsmb.1453
17. Li XD, Chen ZJ. Sequence specific detection of bacterial 23S ribosomal RNA by TLR13. *Elife* (2012) 1:456. doi:10.7554/eLife.00102
18. Oldenburg M, Krüger A, Ferstl R, Kaufmann A, Nees G, Koedel U, et al. TLR13 recognizes bacterial 23S rRNA devoid of erythromycin resistance-forming modification. *Science* (2012) 337:1111–5. doi:10.1126/science.1220363
19. Hidmark A, von Saint Paul A, Dalpke AH. Cutting edge: TLR13 is a receptor for bacterial RNA. *J Immunol* (2012) 189:2717–21. doi:10.4049/jimmunol.1200898
20. Song W, Wang J, Han Z, Zhang Y, Zhang H, Wang W, et al. Structural basis for specific recognition of single-stranded RNA by toll-like receptor 13. *Nat Struct Mol Biol* (2015) 22:782–7. doi:10.1038/nsmb.3080
21. Hemmi H, Kaisho T, Takeuchi O, Sato S, Sanjo H, Hoshino K, et al. Small anti-viral compounds activate immune cells via the TLR7 MyD88-dependent signaling pathway. *Nat Immunol* (2002) 3:196–200. doi:10.1038/ni758
22. Jurk M, Heil F, Vollmer J, Schetter C, Krieg AM, Wagner H, et al. Human TLR7 or TLR8 independently confer responsiveness to the antiviral compound R-848. *Nat Immunol* (2002) 3:499. doi:10.1038/ni0602-499
23. Heil F, Hemmi H, Hochrein H, Ampenberger F, Kirschning C, Akira S, et al. Species-specific recognition of single-stranded RNA via toll-like receptor 7 and 8. *Science* (2004) 303:1526–9. doi:10.1126/science.1093620
24. Diebold SS, Kaisho T, Hemmi H, Akira S, Reis e Sousa C. Innate antiviral responses by means of TLR7-mediated recognition of single-stranded RNA TL-303. *Science* (2004) 303:1529–31. doi:10.1126/science.1093616
25. Lund JM, Alexopoulou L, Sato A, Karow M, Adams NC, Gale NW, et al. Recognition of single-stranded RNA viruses by toll-like receptor 7. *Proc Natl Acad Sci U S A* (2004) 101:5598–603. doi:10.1073/pnas.0400937101
26. Gorden KB, Gorski KS, Gibson SJ, Kedl RM, Kieper WC, Qiu X, et al. Synthetic TLR agonists reveal functional differences between human TLR7 and TLR8. *J Immunol* (2005) 174:1259–68. doi:10.4049/jimmunol.174.3.1259
27. Colak E, Leslie A, Zausmer K, Khatamzas E, Kubarenko AV, Pichulik T, et al. RNA and imidazoquinolines are sensed by distinct TLR7/8 ectodomain sites resulting in functionally disparate signaling events. *J Immunol* (2014) 192:5963–73. doi:10.4049/jimmunol.1303058
28. Zhang Z, Ohto U, Shibata T, Krayukhina E, Taoka M, Yamauchi Y, et al. Structural analysis reveals that toll-like receptor 7 is a dual receptor for guanosine and single-structural analysis reveals that toll-like receptor 7 is a dual receptor for guanosine and single-stranded RNA. *Immunity* (2016) 45:737–48. doi:10.1016/j.immuni.2016.09.011
29. Tanji H, Ohto U, Shibata T, Taoka M, Yamauchi Y, Isobe T, et al. Toll-like receptor 8 senses degradation products of single-stranded RNA. *Nat Struct Mol Biol* (2015) 22:109–15. doi:10.1038/nsmb.2943
30. Hornung V, Rothenfusser S, Britsch S, Krug A, Jahrsdörfer B, Giese T, et al. Quantitative expression of toll-like receptor 1-10 mRNA in cellular subsets of human peripheral blood mononuclear cells and sensitivity to CpG oligodeoxynucleotides. *J Immunol* (2002) 168:4531–7. doi:10.4049/jimmunol.168.9.4531
31. Eigenbrod T, Dalpke AH. Bacterial RNA: an underestimated stimulus for innate immune responses. *J Immunol* (2015) 195:411–8. doi:10.4049/jimmunol.1500530
32. Karikó K, Ni H, Capodici J, Lamphier M, Weissman D. mRNA is an endogenous ligand for toll-like receptor 3. *J Biol Chem* (2004) 279:12542–50. doi:10.1074/jbc.M310175200
33. Gehrig S, Eberle M-E, Botschen F, Rimbach K, Eberle F, Eigenbrod T, et al. Identification of modifications in microbial, native tRNA that suppress immunostimulatory activity. *J Exp Med* (2012) 209:225–33. doi:10.1084/jem.20111044
34. Jöckel S, Nees G, Sommer R, Zhao Y, Cherkasov D, Hori H, et al. The 2'-O-methylation status of a single guanosine controls transfer RNA-mediated toll-like receptor 7 activation or inhibition. *J Exp Med* (2012) 209:235–41. doi:10.1084/jem.20111075
35. Kaiser S, Rimbach K, Eigenbrod T, Dalpke AH, Helm M. A modified dinucleotide motif specifies tRNA recognition by TLR7. *RNA* (2014) 20:1351–5. doi:10.1261/rna.044024.113
36. Rimbach K, Kaiser S, Helm M, Dalpke AH, Eigenbrod T. 2'-O-methylation within bacterial RNA acts as suppressor of TLR7/TLR8 activation in human innate immune cells. *J Innate Immun* (2015) 7:482–93. doi:10.1159/000375460
37. Sridharan K, Gogtay NJ. Therapeutic nucleic acids: current clinical status. *Br J Clin Pharmacol* (2016) 82:1–14. doi:10.1111/bcp.12987
38. Manoharan M, Akinc A, Pandey RK, Qin J, Hadwiger P, John M, et al. Unique gene-silencing and structural properties of 2′-fluoro-modified siRNAs. *Angew Chem Int Ed Engl* (2011) 50:2284–8. doi:10.1002/anie.201006519
39. Sahin U, Kariko K, Tureci O. mRNA-based therapeutics – developing a new class of drugs. *Nat Rev Drug Discov* (2014) 13:759–80. doi:10.1038/Nrd4278
40. Judge AD, Sood V, Shaw JR, Fang D, McClintock K, MacLachlan I. Sequence-dependent stimulation of the mammalian innate immune response by synthetic siRNA. *Nat Biotechnol* (2005) 23:457–62. doi:10.1038/nbt1081
41. Judge AD, Bola G, Lee ACH, MacLachlan I. Design of noninflammatory synthetic siRNA mediating potent gene silencing in vivo. *Mol Ther* (2006) 13:494–505. doi:10.1016/j.ymthe.2005.11.002
42. Eberle F, Giessler K, Deck C, Heeg K, Peter M, Richert C, et al. Modifications in small interfering RNA that separate immunostimulation from RNA interference. *J Immunol* (2008) 180:3229–37. doi:10.4049/jimmunol.180.5.3229
43. Desmet CJ, Ishii KJ. Nucleic acid sensing at the interface between innate and adaptive immunity in vaccination. *Nat Rev Immunol* (2012) 12:479–91. doi:10.1038/nri3247

44. Bagnoli F, Fontana MR, Soldaini E, Mishra RPN, Fiaschi L, Cartocci E, et al. Vaccine composition formulated with a novel TLR7-dependent adjuvant induces high and broad protection against *Staphylococcus aureus*. *Proc Natl Acad Sci U S A* (2015) 112:3680–5. doi:10.1073/pnas.1424924112
45. Tom JK, Dotsey EY, Wong HY, Stutts L, Moore T, Davies DH, et al. Modulation of innate immune responses via covalently linked TLR agonists. *ACS Cent Sci* (2015) 1:439–48. doi:10.1021/acscentsci.5b00274
46. Goff PH, Hayashi T, Martínez-Gil L, Corr M, Crain B, Yao S, et al. Synthetic toll-like receptor 4 (TLR4) and TLR7 ligands as influenza virus vaccine adjuvants induce rapid, sustained, and broadly protective responses. *J Virol* (2015) 89:3221–35. doi:10.1128/JVI.03337-14
47. Shinchi H, Crain B, Yao S, Chan M, Zhang SS, Ahmadiiveli A, et al. Enhancement of the immunostimulatory activity of a TLR7 ligand by conjugation to polysaccharides. *Bioconjug Chem* (2015) 26:1713–23. doi:10.1021/acs.bioconjchem.5b00285
48. Nuhn L, Vanparijs N, De Beuckelaer A, Lybaert L, Verstraete G, Deswarte K, et al. pH-degradable imidazoquinoline-ligated nanogels for lymph node-focused immune activation. *Proc Natl Acad Sci U S A* (2016) 113:8098–103. doi:10.1073/pnas.1600816113
49. Lynn GM, Laga R, Darrah PA, Ishizuka AS, Balaci AJ, Dulcey AE, et al. In vivo characterization of the physicochemical properties of polymer-linked TLR agonists that enhance vaccine immunogenicity. *Nat Biotechnol* (2015) 33:1201–10. doi:10.1038/nbt.3371
50. Shukla NM, Mutz CA, Malladi SS, Warshakoon HJ, Balakrishna R, David SA. Toll-like receptor (TLR)-7 and -8 modulatory activities of dimeric imidazoquinolines. *J Med Chem* (2012) 55:1106–16. doi:10.1021/jm2010207
51. Shukla NM, Malladi SS, Mutz CA, Balakrishna R, David SA. Structure-activity relationships in human toll-like receptor 7-active imidazoquinoline analogues. *J Med Chem* (2010) 53:4450–65. doi:10.1021/jm100358c
52. Russo C, Cornella-Taracido I, Galli-Stampino L, Jain R, Harrington E, Isome Y, et al. Small molecule toll-like receptor 7 agonists localize to the MHC class II loading compartment of human plasmacytoid dendritic cells. *Blood* (2011) 117:5683–91. doi:10.1182/blood-2010-12-328138
53. Jones P, Pryde DC, Tran TD, Adam FM, Bish G, Calo F, et al. Discovery of a highly potent series of TLR7 agonists. *Bioorg Med Chem Lett* (2011) 21:5939–43. doi:10.1016/j.bmcl.2011.07.076
54. Nakamura T, Wada H, Kurebayashi H, McInally T, Bonnert R, Isobe Y. Synthesis and evaluation of 8-oxoadenine derivatives as potent toll-like receptor 7 agonists with high water solubility. *Bioorg Med Chem Lett* (2013) 23:669–72. doi:10.1016/j.bmcl.2012.11.114
55. Schaft N, Dörrie J, Thumann P, Beck VE, Müller I, Schultz ES, et al. Generation of an optimized polyvalent monocyte-derived dendritic cell vaccine by transfecting defined RNAs after rather than before maturation. *J Immunol* (2005) 174:3087–97. doi:10.4049/jimmunol.174.5.3087
56. Thüring K, Schmid K, Keller P, Helm M. Analysis of RNA modifications by liquid chromatography-tandem mass spectrometry. *Methods* (2016) 107:1–9. doi:10.1016/j.ymeth.2016.03.019
57. Jonuleit H, Kühn U, Müller G, Steinbrink K, Paragnik L, Schmitt E, et al. Pro-inflammatory cytokines and prostaglandins induce maturation of potent immunostimulatory dendritic cells under fetal calf serum-free conditions. *Eur J Immunol* (1997) 27:3135–42. doi:10.1002/eji.1830271209
58. Hubo M, Trinschek B, Kryczanowsky F, Tuettenberg A, Steinbrink K, Jonuleit H. Costimulatory molecules on immunogenic versus tolerogenic human dendritic cells. *Front Immunol* (2013) 4:82. doi:10.3389/fimmu.2013.00082
59. Kitsera N, Khobta A, Epe B. Destabilized green fluorescent protein detects rapid removal of transcription blocks after genotoxic exposure. *Biotechniques* (2007) 43:222–7. doi:10.2144/000112479
60. Sullenger BA, Nair S. From the RNA world to the clinic. *Science* (2016) 352:1417–20. doi:10.1126/science.aad8709
61. Hornung V, Guenthner-Biller M, Bourquin C, Ablasser A, Schlee M, Uematsu S, et al. Sequence-specific potent induction of IFN-alpha by short interfering RNA in plasmacytoid dendritic cells through TLR7. *Nat Med* (2005) 11:263–70. doi:10.1038/nm1191
62. Fotin-Mleczek M, Duchardt KM, Lorenz C, Pfeiffer R, Ojkić-Zrna S, Probst J, et al. Messenger RNA-based vaccines with dual activity induce balanced TLR-7 dependent adaptive immune responses and provide antitumor activity. *J Immunother* (2011) 34:1–15. doi:10.1097/CJI.0b013e3181f7dbe8
63. Mattson G, Conklin E, Desai S, Nielander G, Savage MD, Morgensen S. A practical approach to crosslinking. *Mol Biol Rep* (1993) 17:167–83. doi:10.1007/BF00986726
64. Eberle F, Sirin M, Binder M, Dalpke AH. Bacterial RNA is recognized by different sets of immunoreceptors. *Eur J Immunol* (2009) 39:2537–47. doi:10.1002/eji.200838978
65. Jao CY, Salic A. Exploring RNA transcription and turnover in vivo by using click chemistry. *Proc Natl Acad Sci U S A* (2008) 105:15779–84. doi:10.1073/pnas.0808480105
66. Karikó K, Buckstein M, Ni H, Weissman D. Suppression of RNA recognition by toll-like receptors: the impact of nucleoside modification and the evolutionary origin of RNA. *Immunity* (2005) 23:165–75. doi:10.1016/j.immuni.2005.06.008
67. Shuman S. Catalytic activity of vaccinia mRNA capping enzyme subunits coexpressed in *Escherichia coli*. *J Biol Chem* (1990) 265:11960–6.
68. Langberg SR, Moss B. Post-transcriptional modifications of mRNA. *J Biol Chem* (1981) 256:10054–60.
69. Hong V, Presolski SI, Ma C, Finn MG. Analysis and optimization of copper-catalyzed azide-alkyne cycloaddition for bioconjugation. *Angew Chem Int Ed Engl* (2009) 48:9879–83. doi:10.1002/anie.200905087
70. Seidu-Larry S, Krieg B, Hirsch M, Helm M, Domingo O. A modified guanosine phosphoramidite for click functionalization of RNA on the sugar edge. *Chem Commun* (2012) 48:11014–6. doi:10.1039/c2cc34015a
71. Jurk M, Kritzler A, Schulte B, Tluk S, Schetter C, Krieg AM, et al. Modulating responsiveness of human TLR7 and 8 to small molecule ligands with T-rich phosphorothiate oligodeoxynucleotides. *Eur J Immunol* (2006) 36:1815–26. doi:10.1002/eji.200535806
72. Gorden KK, Qiu X, Battiste JJ, Wightman PP, Vasilakos JP, Alkan SS. Oligodeoxynucleotides differentially modulate activation of TLR7 and TLR8 by imidazoquinolines. *J Immunol* (2006) 177:8164–70. doi:10.4049/jimmunol.177.11.8164
73. Kuznik A, Bencina M, Svajger U, Jeras M, Rozman B, Jerala R. Mechanism of endosomal TLR inhibition by antimalarial drugs and imidazoquinolines. *J Immunol* (2011) 186:4794–804. doi:10.4049/jimmunol.1000702
74. Nair JK, Willoughby JLS, Chan A, Charisse K, Alam MR, Wang Q, et al. Multivalent N-acetylgalactosamine-conjugated siRNA localizes in hepatocytes and elicits robust RNAi-mediated gene silencing. *J Am Chem Soc* (2014) 136:16958–61. doi:10.1021/ja505986a

Conflict of Interest Statement: The authors declare that the research was conducted in the absence of any commercial or financial relationships that could be construed as a potential conflict of interest.

frontiers in Immunology

ORIGINAL RESEARCH
published: 24 February 2017
doi: 10.3389/fimmu.2017.00189

MDA5 Induces a Stronger Interferon Response than RIG-I to GCRV Infection through a Mechanism Involving the Phosphorylation and Dimerization of IRF3 and IRF7 in CIK Cells

*Quanyuan Wan[1], Chunrong Yang[2], Youliang Rao[1], Zhiwei Liao[1] and Jianguo Su[1]**

[1] College of Fisheries, Huazhong Agricultural University, Wuhan, China, [2] College of Veterinary Medicine, Huazhong Agricultural University, Wuhan, China

OPEN ACCESS

Edited by:
Uday Kishore,
Brunel University London, UK

Reviewed by:
Yunhao Tan,
Harvard Medical School, USA
Nicola Tamassia,
University of Verona, Italy

***Correspondence:**
Jianguo Su
sujianguo@mail.hzau.edu.cn

Specialty section:
This article was submitted to Molecular Innate Immunity, a section of the journal Frontiers in Immunology

Received: *03 November 2016*
Accepted: *09 February 2017*
Published: *24 February 2017*

Citation:
Wan Q, Yang C, Rao Y, Liao Z and Su J (2017) MDA5 Induces a Stronger Interferon Response than RIG-I to GCRV Infection through a Mechanism Involving the Phosphorylation and Dimerization of IRF3 and IRF7 in CIK Cells. Front. Immunol. 8:189. doi: 10.3389/fimmu.2017.00189

Retinoic acid-inducible gene I (RIG-I) and melanoma differentiation-associated gene 5 (MDA5) are critical cytosolic sensors that trigger the production of interferons (IFNs). Though their recognition functions are well identified, their unique roles in the downstream signal transduction remain to be elucidated. Herein, we report the differential effect between grass carp (*Ctenopharyngodon idella*) MDA5 (CiMDA5) and CiRIG-I on the production of various IFNs upon grass carp reovirus (GCRV) infection in *C. idella* kidney (CIK) cell line. In CIK cells, grass carp IFN1 (CiIFN1) and CiIFN3 are relatively highly expressed while CiIFN2 and CiIFN4 are relatively slightly expressed. Following GCRV infection, CiMDA5 induces a more extensive type I IFN response than CiRIG-I. Further investigation reveals that both CiMDA5 and CiRIG-I facilitate the expression and total phosphorylation levels of grass carp IFN regulatory factor (IRF) 3 (CiIRF3) and CiIRF7 upon GCRV infection or poly(I:C) stimulation. However, the difference is that CiRIG-I decreases the threonine phosphorylation level of CiIRF7. As a consequence, CiMDA5 enhances the heterodimerization of CiIRF3 and CiIRF7 and homodimerization of CiIRF7, whereas CiRIG-I facilitates the heterodimerization but attenuates homodimerization of CiIRF7. Moreover, the present study suggests that CiIRF3 and CiIRF7 heterodimers and CiIRF7 homodimers are able to induce more extensive IFN-I responses than CiIRF3 homodimers under GCRV infection. Additionally, CiMDA5 induces a stronger type II IFN (IFN-II) response against GCRV infection than CiRIG-I. Collectively, these results demonstrate that CiMDA5 plays a more potent role than CiRIG-I in IFN response to GCRV infection through differentially regulating the phosphorylation and dimerization of CiIRF3 and CiIRF7.

Keywords: grass carp (*Ctenopharyngodon idella*), grass carp reovirus, RIG-I, MDA5, IRF3, IRF7, IFN

HIGHLIGHTS

1. CiMDA5 and CiRIG-I increase the phosphorylation levels rather than the mRNA and protein expressions of CiIRF3 and CiIRF7.
2. CiMDA5 enhances the heterodimerization of CiIRF3 and CiIRF7 and homodimerization of CiIRF7, whereas CiRIG-I facilitates the heterodimerization but attenuates the homodimerization of CiIRF7.
3. CiMDA5 induces a stronger IFN response against GCRV infection than CiRIG-I.

INTRODUCTION

Vertebrates are armed with innate and adaptive immune systems to withstand invasive viruses and other microbes. The interferon (IFN)-mediated innate immune response is the first line of defense against various pathogens (1). In which, pattern recognition receptors that detect the conserved patterns or structures, including bacterial cytoderm components, non-self nucleic acids, and certain highly conserved proteins, play a vital role in initiating IFN signaling pathways. The retinoic acid-inducible gene I (RIG-I)-like receptors (RLRs), including RIG-I, melanoma differentiation-associated protein 5 (MDA5), and laboratory of genetics and physiology 2 (LGP2), are crucial PRRs in the recognition of viral RNA in the cytosol (2). They share a DExD/H-box RNA helicase domain that hydrolyzes ATP to unwind RNA and a C-terminal autoregulatory domain (CTD or RD) that is responsible for initial RNA binding (3). Another pivotal domain, i.e., tandem N-terminal caspase recruitment domains (CARDs) that exist in MDA5 and RIG-I but not in LGP2 are the essential components in the signal transduction. Upon binding with ligands, MDA5 and RIG-I undergo reconfiguration to release the RD-repressed CARDs, which then recruit and interact with the CARD in mitochondrion-adherent adaptor named as mitochondrial antiviral signaling protein (MAVS, also known as IPS-1, VISA, and Cardif) (4). Once the CARD–CARD interaction shapes, MAVS forms functional prion-like aggregates and recruits several tumor receptor-associated factors (TRAFs) to activate IκB kinases (IKKs) and TRAF-associated NF-κB activator-binding kinase (TBK) 1 (5, 6), and thereby recruits IFN regulatory factor (IRF) 3 for its phosphorylation activation and the subsequent nucleus translocation (7). In this regard, another major transcription factor IRF7, a typical IFN-stimulated gene (ISG), is implicated in RLR signaling pathway as well (8, 9). Similar to IRF3, phosphorylation-activated IRF7 undergoes nucleus translocation and then cooperates with activated IRF3 to bind the promoter regions of IFN genes for the expression initiation following viral infection (10).

As key cytokines in the innate immune response, IFNs exhibit various biological functions, including antiviral activity, antitumor activity and immunomodulatory effects (11). In mammals, most of the IFN family members are well characterized and classified into three types, namely type I (IFN-I), II (IFN-II), and III (IFN-III), according to their structures and receptor complexes (1, 11). Since IFNs are vital and complicated players in antiviral immunity, much attention has been paid on their evolution characterization, which gives rise to broad identification studies on fish IFNs (12–14). As the two excellent review literature studies summarized, teleost fishes possess IFN-I and IFN-II, and IFN-I is further classified into group I and II according to the number of cysteines they contained (15, 16). In zebrafish (*Danio rerio*), group I IFN-I includes IFN1 and IFN4, while group II IFN-I includes IFN2 and IFN3, and IFN-II contains two members: IFNγ1 and IFNγ2 (16). Each kind of IFN performs its own functions: group I IFN-I is responsible for inducting most of the ISGs, while group II IFN-I as rapid and transient agonist antiviral genes serves as a complement of group I IFN-I (17), and IFN-II contributes to the phagocytic and nitric oxide responses of phagocytes and the regulation of some cytokines and chemokines (16).

Another member of RLRs, LGP2 does not possess a CARD, which leads to an incessant controversy about its functions in antiviral immunity (18–20). Although the function of LGP2 and the shared functions of MDA5 and RIG-I are subjects of great interest to immunologist, the different roles of MDA5 and RIG-I should be paid more attention as well, which may contribute to better understanding of the fine regulation of RLRs. At present, overwhelming reports have focused on the similar and different roles of MDA5 and RIG-I in the recognition of pathogens (21–23), which state that MDA5 and RIG-I play a complementary and non-redundant role in the pattern recognition. However, it is interesting that RIG-I cannot be identified in some fishes, such as Japanese pufferfish (*Takifugu rubripes*), medaka (*Oryzias latipes*), stickleback (*Gasterosteus aculeatus*), and large yellow croaker (*Pseudosciaena crocea*) (24–26), which arouses an interest in the investigation on the shared and unique roles of fish MDA5 and RIG-I in the downstream signal transduction. In addition, considering the complexity of fish IFNs in antiviral immunity, it is of great interest to investigate the different IFNs induced by fish MDA5 and RIG-I.

Previously, we attested the critical roles of full-length MDA5 and RIG-I and their domains in antiviral immunity in grass carp (*Ctenopharyngodon idella*) (27–30), but the differential roles of MDA5 and RIG-I were not well characterized. And recently, the IFN system in grass carp was clarified, which suggests that there are six grass carp IFNs (CiIFNs): CiIFN1 and CiIFN4 belong to group I IFN-I; CiIFN2 and CiIFN3 belong to group II IFN-I; while CiIFNγ1 and CiIFNγ2 belong to IFN-II (31). Based on these available data, the present study reveals that *C. idella* MDA5 (CiMDA5) and CiRIG-I differentially induce the production of IFNs. Further investigations show that CiMDA5 and CiRIG-I facilitate the protein phosphorylation rather than mRNA and protein expression levels of *C. idella* IRF3 (CiIRF3) and CiIRF7 and give rise to different dimerization forms of CiIRF3 and CiIRF7 under immunostimulation. Our findings demonstrate that CiMDA5 plays a more potent role in the pathway of IFN induction than CiRIG-I in *C. idella* kidney (CIK) cells.

MATERIALS AND METHODS

Cell Culture, Virus, and Reagents

C. idella kidney cells were provided by China Center for Type Culture Collection. Fathead minnow cell line (FHM) was a kind

gift from Dr. Junfa Yuan, Huazhong Agricultural University, Wuhan, China. Previous established overexpression cells, i.e., stably transfected MDA5 (MDA5+), RIG-I (RIG-I+), and enhanced GFP (EGFP+) cells, were renewedly cultured (27, 30). Cells were grown in DMEM (Gibco) supplemented with 10% FBS (Gibco), 100 U/ml penicillin, and 100 U/ml streptomycin and maintained at 28°C in a humidified atmosphere of 5% CO_2 incubator (Thermo Scientific). Geneticin (G418) (200 μg/ml) (Sigma-Aldrich) was added to maintain MDA5+, RIG-I+, and EGFP+ cells. Grass carp reovirus (GCRV) was propagated in CIK cells and stored at −80°C.

Polyinosinic:polycytidylic acid [poly(I:C)], isopropyl-D-1-thiogalactopyranoside (IPTG), serine/threonine phosphatase inhibitor, tyrosine phosphatase inhibitor, and protease inhibitor cocktails were purchased from Sigma-Aldrich. Hoechst 33342 was from AAT Bioquest. FuGENE® 6 transfection reagent was purchased from Promega. Calf intestinal alkaline phosphatase (CIP) was purchased from NEB. All the restriction enzymes were purchased from Thermo Scientific. Lysis buffer [20 mM Tris (pH 7.5), 150 mM NaCl, 1% Triton X-100, and a handful of compounds containing sodium pyrophosphate, β-glycerophosphate, sodium orthovanadate, sodium fluoride, EDTA, and leupeptin] was purchased from Beyotime, Shanghai, China. Nuclear and cytoplasmic protein extraction kit was purchased from Beyotime. All the primer synthesis and DNA sequencing were carried out in AuGCT biotechnology Co., Ltd., Wuhan, China.

Expression Vectors/Recombinant Plasmids

The whole open reading frames of CiIRF3 gene (GenBank accession no. KC898261) and CiIRF7 gene (GenBank accession no. GQ141741) were amplified from cDNA derived from head kidney tissue of grass carp. Then the CiIRF3 or CiIRF7 overexpression vectors (pIRF3 or pIRF7) and tag-labeled vectors (pIRF3-Flag, pIRF3-*myc*, pIRF7-Flag, and pIRF7-*myc*) were singly constructed by insertion of the corresponding PCR amplicons into the *Eco*RI/*Kpn*I sites of pdCMV vector (Figure S1A in Supplementary Material) as described in our previous report (27). For subcellular localization experiment, EGFP-fused vectors of CiIRF3 (or CiIRF7), i.e., pIRF3-EGFP and pIRF7-EGFP were constructed by insertion of the PCR amplicons into *Kpn*I/*Bam*HI and *Kpn*I/*Apa*I sites of psCMV (Figure S1B in Supplementary Material). The 5′-flanking sequences of CiIRF3, CiIRF7, CiIFN3, and CiIFN4 genes were obtained from the genome data of grass carp (32) and confirmed using Sanger sequencing (ABI 3730 DNA Analyzer). The promoter regions of them were predicted using PROSCAN program (version 1.7) (33). For promoter identification, pIRF3pro-EGFP, pIRF7pro-EGFP, pIFN3pro-EGFP, and pIFN4pro-EGFP plasmids were singly constructed by substituting the CMV promoter with either the 516 bp fragment of CiIRF3, 901 bp fragment of CiIRF7, 1,023 bp fragment of CiIFN3, or 1,610 bp fragment of CiIFN4, which contained the corresponding predicted promoter region in the *Xho*I/*Hin*dIII sites of psCMV. Subsequently, the validated 5′-flanking sequences were singly inserted into the *Xho*I/*Hin*dIII sites of pGL3-basic luciferase reporter vector (Promega), and the constructed plasmids were named as pIRF3pro-Luc, pIRF7pro-Luc, pIFN3pro-Luc, and pIFN4pro-Luc, respectively. The primers used for constructs are listed in Table S1 in Supplementary Material, and all the PCR amplicons were validated by Sanger sequencing. Additionally, pMDA5-HA, pRIG-I-HA, pIFN1pro-Luc, pIFN2pro-Luc, pIFNγ1pro-Luc, and pIFNγ2pro-Luc plasmids were constructed before in our laboratory.

Transfection, Infection, Confocal Fluorescence Microscopy, and Luciferase Activity Assay

To establish stably overexpressed and EGFP fusion-expressed cells, 0.8 μg of either pIRF3, pIRF7, pIRF3-EGFP, or pIRF7-EGFP vector was transfected into CIK cells, respectively, as previous description in detail (34). Meanwhile, pIRF3pro-EGFP and pIRF4pro-EGFP were transfected into CIK cells as well, and the expression of EGFP was assessed by imaging with a fluorescence microscope (Leica). For GCRV infection or poly(I:C) stimulation, cells were equally aliquoted into 12-well or 6-well plates in advance. After washing the monolayer cells thrice with fresh serum-free DMEM, serum-free DMEM with GCRV [multiplicity of infection (MOI) = 1] or poly(I:C) (final concentration is 5 μg/ml) was added into the wells of experiment group, while serum-free DMEM with commensurate phosphate-buffered saline (PBS) was added into the wells of control group. For confocal fluorescence microscopy, pIRF3-EGFP and pIRF7-EGFP stably transfected cells were equably seeded on microscope coverslips (Fisher Scientific) in 12-well plates for 24 h, then washed with fresh DMEM for either GCRV infection, poly(I:C) stimulation or PBS treatment (control). Twenty-four hours later, those cells were washed thrice with PBS and fixed with 4% (v/v) paraformaldehyde for 15 min at room temperature. For nuclear staining, cells were incubated in 0.1 mg/ml Hoechst 33342 for 10 min in a darkroom. The observation of subcellular location was performed using an UltraVIEW VoX 3D Live Cell Imaging System (PerkinElmer).

For luciferase reporter assays, either CIK or FHM cells were seeded in 24-well plates overnight, followed by being co-transfected with the overexpressed plasmid, target promoter-luciferase plasmid, and pRL-TK (internal control reporter vector) at a ratio of 10:10:1 using FuGENE® 6 transfection reagents (Promega). Simultaneously, pdCMV, objective promoter-luciferase plasmid, and pRL-TK vectors were co-transfected as vehicle control. Luciferase activities were measured using the Dual-Luciferase Reporter Assay System (Promega) and a VICTOR™ X Series Multilabel Plate Reader (PerkinElmer). Data were normalized to the amounts of Renilla luciferase activities according to the protocol.

Preparations of Polyclonal Antisera and Commercial Antibodies

For the acquisition of anti-IRF7 polyclonal antiserum, the full-length coding sequence of CiIRF7 gene was cloned into *Eco*RI/*Xho*I sites of pET-32a(+) vector (Novagen) for prokaryotic expression. The plasmid pET-32a(+)-IRF7 was transformed into the *Escherichia coli* BL21(DE3) pLysS cells (Novagen). A single isolated colony of transformant was inoculated in 5 ml

of LB medium containing 100 μg/ml ampicillin and incubated for 12 h. The overnight culture was diluted 1:100 in 400 ml of LB medium containing same antibiotics. The culture was grown to an A600 of 0.6 and induced by addition of 1 mM IPTG. The bacteria were harvested after 5 h induction. The recombinant protein was extracted according to the classical protocol (35) and purified using Ni-IDA-Sefinose™ Resin Kit (Sangon Biotech, Shanghai, China). The purified protein was confirmed by Western blotting with Anti-His tag mouse monoclonal primary antibody (1:2000) (Abbkine), and then applied to immunize New Zealand white rabbits to acquire the polyclonal anti-IRF7 antiserum according to the protocols mentioned in previous reports (36). As a kind gift, anti-IRF3 rabbit polyclonal antiserum was previously prepared by Professor Yibing Zhang, Institute of Hydrobiology, Chinese Academy of Sciences, Wuhan, China (37). Phosphoserine, phosphothreonine, and phosphotyrosine antibodies were purchased from ImmuneChem. Anti-Flag tag (ab45766), anti-HA tag (ab18181), anti-*myc* tag (ab32) mouse monoclonal antibodies, and anti-β-tubulin primary rabbit polyclonal antibody (ab6046) were purchased from Abcam. Anti-H3 primary rabbit polyclonal antibody was purchased from Beyotime. IRDye® 800CW Donkey anti-rabbit-IgG and anti-mouse-IgG (H+L) secondary antibodies were purchased from LI-COR.

Western Blotting and Immunoprecipitation (IP)

For Western blotting analysis, cells were plated in 6-well plates, incubated overnight, and subsequently treated with PBS, GCRV, or poly(I:C). At 24 h posttreatment, cells were washed with PBS and lysed in lysis buffer supplemented with 1 mM phenylmethylsulfonyl fluoride, serine/threonine phosphatase inhibitor, tyrosine phosphatase inhibitor, and protease inhibitor cocktails. After clarification by centrifugation at 12,000 rpm for 15 min, 30 μg of supernatant proteins was separated by 8–12% SDS-PAGE. The separated polypeptides were electroblotted onto nitrocellulose (NC) filter membranes (Millipore) using a trans-blot SD semidry electrophoretic transfer cell (Jim-X, Dalian, China), and then the blotted membranes were incubated with blocking TBST buffer (0.5 M Tris-Cl, 150 mM NaCl, 0.5% Tween 20, and 1% bovine serum albumin) at room temperature for 2 h or 4°C overnight. Subsequently, the membranes were incubated with appropriate primary antibodies for 2 h at room temperature or overnight at 4°C in blocking TBST buffer, washed thrice with TBST buffer, and then incubated with secondary antibody for 1 h at room temperature. After again washing thrice with TBST buffer, the NC membranes were scanned and imaged by an Odyssey® CLx Imaging System (LI-COR). For hybridization, the anti-IRF3 and anti-IRF7 antisera were diluted 1:1,000, commercial primary antibodies 1:5,000, and secondary antibodies 1:10,000.

To determine the phosphorylation and dimerization status of CiIRF3 and CiIRF7, IP and Co-IP were performed. Whole-cell lysates were prepared in the presence of abovementioned lysis buffer, and the cellular debris was removed by centrifugation at 12,000 rpm for 30 min at 4°C. The supernatant was transferred to a fresh tube and incubated with 1 μg antibodies overnight at 4°C, followed by incubation with 30 μl protein A+G sepharose beads (Beyotime) for 2 h at 4°C. Then the beads were washed with lysis buffer four times and eluted with 20 μl 2 × SDS loading buffer by boiling for 10 min. The precipitates were detected by immunoblotting with the corresponding antibodies.

Viability Tests of CiIRF3 and CiIRF7 Overexpressed Cells upon GCRV Infection

C. idella kidney cells that overexpressed either CiIRF3, CiIRF7, or EGFP were severally seeded in 96-well plates (1×10^4 cells/well). After being incubated overnight, the cells were infected with GCRV. At the scheduled time, 20 μl of 3-(4,5-dimethylthiazol-2-yl)-2,5-dimethyltetrazolium bromide (5 mg/ml in PBS) was added to each well. After 4 h of incubation at 28°C, DMSO (100 μl/well) was added at 28°C for 10 min. The OD was measured by a microplate reader (Infinite F200, Tecan) at 490 nm. Data were expressed as viability index, which is the ratio of the mean OD value of quartic wells measured at corresponding time point to the mean value of quartic wells measured at 0 h postinfection (p.i.).

Semi-Quantitative and Real-time Quantitative RT-PCR (RT-qPCR)

Total cellular RNA isolation and cDNA synthesis were performed according to the protocol described in the previous reports (38). For semiquantitative RT-PCR, 200 ng of cDNA for each target gene amplification was used according to the following procedure: 5 min predenaturation at 94°C, amplification and extension for 35 cycles (20 cycles for internal control) at 94°C for 30 s, 60°C for 30 s, and 72°C for 20 s. The amplicons were analyzed by agarose electrophoresis and imaged using Gel Doc XR system (Bio-Rad). For RT-qPCR, the mRNAs of target genes were quantified using SYBR Premix Ex Taq II reagent (Takara) and a LightCycler 480 II Real-time PCR system (Roche). The PCR reactions were cycled during the real-time detection. Primers are listed in **Table 1.** The mRNA expression levels were normalized to the expression level of EF1α, and the data were analyzed using the $2^{-\Delta\Delta Ct}$ method as described previously (39).

Data Analysis

Statistical analysis and presentation graphics were carried out using Graphpad Prism 6.0 software. Unpaired Student's *t*-test was used in the data analysis, and the *P* value <0.05 was considered as a statistically significant difference ($^*P < 0.05$, $^{**}P < 0.01$, $^{***}P < 0.001$).

RESULTS

CiMDA5 and CiRIG-I Differentially Induce the Production of CiIFNs

To explore the differential role of CiMDA5 and CiRIG-I, MDA5+ and RIG-I+ cells were cultured, and the mRNA expression levels of CiMDA5 and CiRIG-I were detected. The result showed that CiMDA5 and CiRIG-I were overexpressed in MDA5+ and RIG-I+

TABLE 1 | Primers for real-time quantitative RT-PCR analysis.

Gene	Primer name	Forward primer (5′–3′)	Primer name	Reverse primer (5′–3′)
EF1α	EF125	CGCCAGTGTTGCCTTCGT	ER126	CGCTCAATCTTCCATCCCTT
Retinoic acid-inducible gene I	RF230	ACTACACTGAACACCTGCGGAA	RR231	GCATCTTTAGTGCGGGCG
Melanoma differentiation-associated gene	MF150	CAGGAGCGACTCTTGGACTATG	MR151	AAAGACGGTTTATTTGAATGGAAG
IFN regulatory factor 3 (IRF3)	IF960	ACTTCAGCAGTTTAGCATTCCC	IR961	GCAGCATCGTTCTTGTTGTCA
IRF7	IF767a	CGCCTGTGTTCGTCACTCGT	IR768a	GGTGGTTGGAAAGCGTATTGG
Interferon 1 (IFN1)	IF590	AAGCAACGAGTCTTTGAGCCT	IR591a	GCGTCCTGGAAATGACACCT
IFN2	IF439	TCTTTTTCCTCGTGAATGCTTG	IR433	TCACAACGATGTTCTGACTGGA
IFN3	IF435	TACATTTATAGAGACTGCGGGTGG	IR357	TGGAGTGTCTGGTAAACAGCCTT
IFN4	IF354	GTTCGTCATTCAGGCTCTGGTAG	IR436	TCCCTCCATCCTCCTTGTTCA
IFNγ1	IgF339	CGAGATGACCCATTTGGAGAC	IR390	CTTTGAAACCCATTCTGTGCC
IFNγ2	WF79	CAGCGAACACCTGAAACTAACA	WR80	CCATCCCAAAGTCATCAAACAT
IL-4	ILF559	GCACTGACATTTGTAGCCGTTA	ILR560	ATGGTTATGTAGGGTCTGGTTCA
IL-10	ILF561	TTGCCATTGTGACATTTTCCAG	ILR562	ATGATGACGTGAGTCGAGTTTGA
IL-12	ILF1702b	CTTTGTCGGGGTCCTAATTATGT	ILR1552	GTGCTTTTGCTTTGATGATGGA
GCRV-induced gene 1	GigF598	CTGCCCCTGCTGAAATGCT	GigR599	AGCCAAAGTTTCCATTCTGAGG
IFI56	IFIF596	TCTGGAGGGACTGAAGATTGGT	IFIR597	TGCGTTCGTTTCGTTCTTGTAG
ISG15	ISGF604	CCCCTTTCCAAGTGTTCGTC	ISGR605	ATGGTGCTTCCAGATGTGATGT
Mx2	MF428	ACATTGACATCGCCACCACT	MR429	TTCTGACCACCGTCTCCTCC

cells, respectively (**Figure 1A**). Interestingly, it was unexpected that stable overexpressed CiRIG-I decreases the mRNA expression of endogenic CiMDA5, while CiMDA5 stable overexpression has no obvious effect on that of endogenic CiRIG-I. Next, we investigated the mRNA expression patterns of IFNs in CIK, MDA5+, and RIG-I+ cells. The result showed that CiIFN1 and CiIFN3 were the most abundant IFNs, followed by CiIFNγ1 and CiIFNγ2, while CiIFN2 and CiIFN4 were slightly expressed in CIK cells without immunostimulation (**Figure 1B**). Additionally, CiMDA5 and CiRIG-I were not able to affect the expression of CiIFNs without any immunostimulation. Subsequently, we asked whether CiMDA5 and CiRIG-I played an identical role in the induction of CiIFNs after immunostimulation. For sampling, a preexperiment was implemented, which indicated that 0.5 h, 6 h, 12 h, and 24 h were suitable for the detection of mRNA expression profiles of CiIFN1, CiIFN4, CiIFNγ1, and CiIFNγ2 and that 0.5 h, 6 h, and 12 h were suitable for that of CiIFN2 and CiIFN3. The following results showed that CiIFN1, CiIFN2 and CiIFN4 and CiIFNγ2 were slightly induced, while CiIFN3 was inhibited in GCRV-infected CIK cells at the early stage (0.5 h and 6 h p.i.) (**Figures 1C–H**, upper panels). Particularly, CiIFNγ1 could be detected just at 24 h p.i. or poststimulation, indicating that CiIFNγ1 is relatively insensitive to GCRV infection and poly(I:C) stimulation. These data suggest that the seldom expressed CiIFN2 and CiIFN4 play a positive role in GCRV infection or poly(I:C) stimulation in CIK cells.

To clarify the different roles of CiMDA5 and CiRIG-I in the induction of IFNs production, we tested the expression patterns of various IFNs in MDA5+, RIG-I+ and CIK cells by RT-qPCR. Relative to the expression levels in CIK cells, CiMDA5 overexpression strongly induced the expression of CiIFN1 at 6 h p.i., CiIFN2 at 6 h p.i. and 12 h p.i.; CiIFN3 and CiIFN4 at 0.5 h p.i.; CiIFNγ2 at 0.5 h p.i. and 6 h p.i., while inhibited CiIFNγ1 at 24 h p.i. under GCRV infection or poly(I:C) stimulation (**Figures 1C–H**, middle panels). Likewise, in CiRIG-I overexpressed cells infected with GCRV or stimulated with poly(I:C), the expression trend of each CiIFN could be described as that: CiIFN1 was not obviously affected; CiIFN2, CiIFN3, CiIFN4, and CiIFNγ2 was moderately induced at 6 h p.i., 0.5 h p.i., 12 h p.i., and 6 h p.i., respectively, while CiIFNγ1 was inhibited at 24 h p.i. (**Figures 1C–H**, lower panels). Subsequently, luciferase reporter assays were conducted to examine the effects of CiMDA5 and CiRIG-I on the promoter activities of CiIFNs. As shown in **Figure 2**, transient overexpressed CiMDA5-HA and CiRIG-I-HA did not affect the promoter activities of CiIFN-I at steady state, while enhanced the promoter activities of CiIFN-I under GCRV infection. Importantly, CiMDA5 induced a higher promoter activities than CiRIG-I. However, transient overexpressed CiMDA5-HA and CiRIG-I-HA decreased the promoter activities of CiIFN-II at steady state, while had no effects on them under GCRV infection. Furthermore, the expression levels of ISG, including GCRV-induced gene 1 (Gig1), IFN-induced gene 56 (IFI56), ISG15, and Mx2, were examined. As expected, CiMDA5 overexpression induced higher expression levels of CiGig1, CiIFI56, and CiMx2 than CiRIG-I overexpression under GCRV infection or poly(I:C) stimulation (Figure S2 in Supplementary Material). However, CiRIG-I and CiMDA5 overexpression did not have a significant induction effect on CiISG15 under immunostimulations. Collectively, these data illustrate that CiMDA5 induced a stronger IFN response than CiRIG-I in CIK cells under GCRV infection or poly(I:C) stimulation.

CiMDA5 and CiRIG-I Have No Significant Effect on the Expression Levels of CiIRF3 and CiIRF7

Next, we examined whether the dissimilar effect between CiMDA5 and CiRIG-I on IFN inducing was attributed to CiIRF3 and CiIRF7. To this end, we investigated the influence of CiMDA5 and CiRIG-I on CiIRF3 and CiIRF7 by luciferase activity assay, semiquantitative RT-PCR, and Western blotting. Before

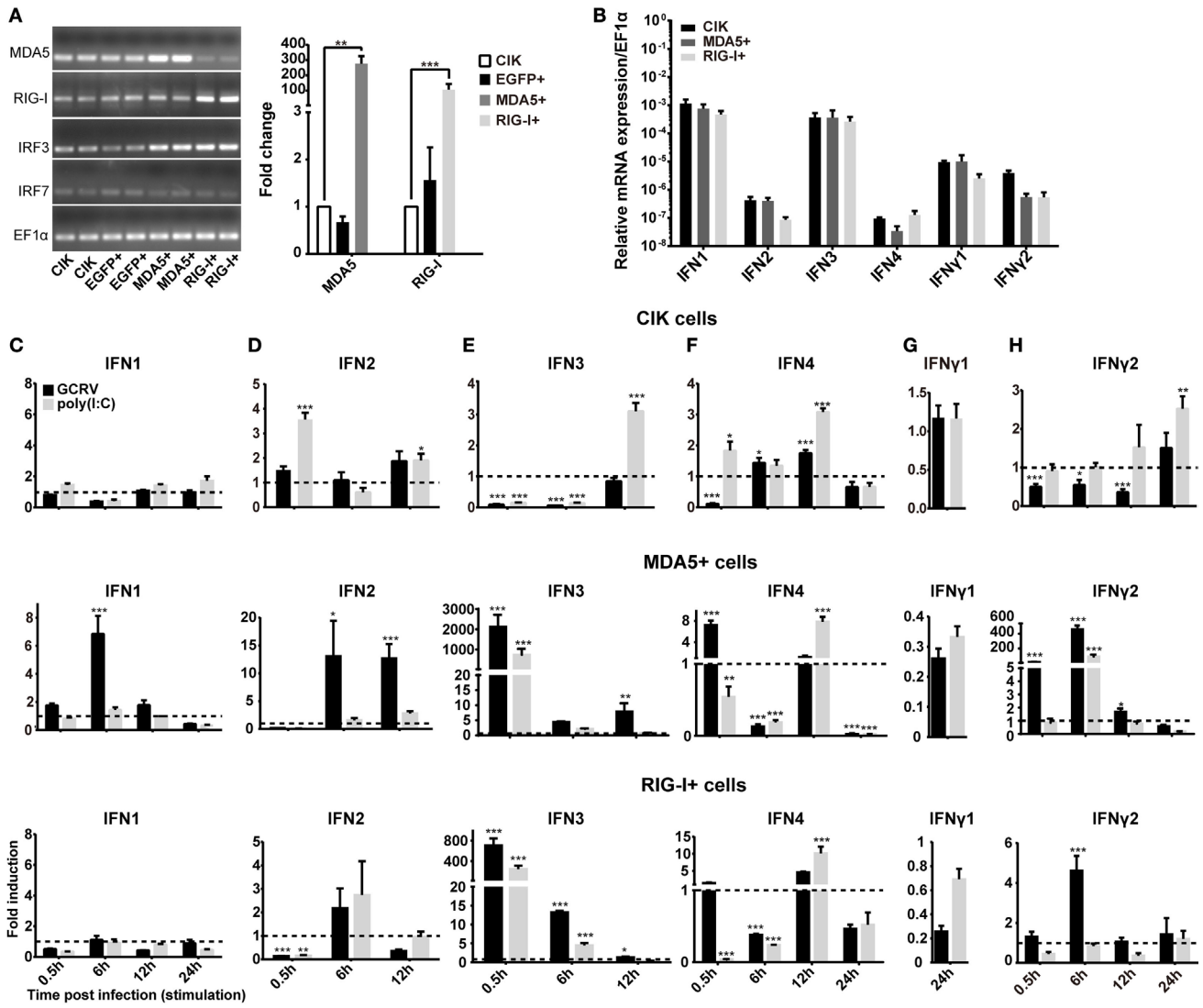

FIGURE 1 | ***Ctenopharyngodon idella*** **melanoma differentiation-associated gene 5 (CiMDA5) and** ***C. idella*** **retinoic acid-inducible gene I (CiRIG-I) differentially induce the production of interferons (IFNs)**. **(A)** EGFP+, MDA5+, and retinoic acid-inducible gene I (RIG-I)+ cells were seeded in 12-well plates for 24 h cultivation, and then total RNA samples were isolated from these cells for semiquantitative RT-PCR or RT-qPCR. **(B)** Total RNA samples isolated from *C. idella* kidney (CIK), MDA5+, and RIG-I+ cells were used to measure the relative expression levels of IFNs. Relative mRNA expression levels were normalized to *EF1*α in CIK cells. **(C–H)** CIK, MDA5+, and RIG-I+ cells were seeded in 12-well plates, and then were either phosphate-buffered saline (PBS) treated, grass carp reovirus (GCRV) infected, or polyinosinic:polycytidylic acid [poly(I:C)] stimulated. Total RNA samples were isolated at the scheduled time postchallenge. The relative expression levels of these genes were normalized by *EF1*α. Fold induction of gene expression level in CIK cells was obtained by comparing the normalized gene expression level in GCRV- or poly(I:C)-treated cells with that in PBS-treated cells (defined as 1) at the same time point, while those in MDA5+ and RIG-I+ cells were determined relative to corresponding treated CIK cells at the same time point. Data represent mean ± SEM of four independent wells of cells. $^{*}P < 0.05$; $^{**}P < 0.01$; $^{***}P < 0.001$.

luciferase activity assay, the 5′-flanking sequences of CiIRF3 gene and CiIRF7 gene were proved to promote the expression of EGFP (Figure S3 in Supplementary Material). Following luciferase activity assay performed in FHM cells, we demonstrated that CiMDA5 inhibited the promoter activity of CiIRF3, but had no effect on that of CiIRF7 and that CiRIG-I enhanced the promoter activity of CiIRF3, but inhibited that of CiIRF7 (**Figures 3A,B**). Next, we investigated whether CiMDA5 and CiRIG-I affected the mRNA and protein expression levels of CiIRF3 and CiIRF7. Thus, total RNA samples from MDA5+ cells, RIG-I+ cells, and EGFP+ cells were isolated for the subsequent semiquantitative RT-PCR analysis. The result revealed that both CiMDA5 and CiRIG-I were able to positively regulate the mRNA expression of CiIRF3, but had no obvious effect on that of CiIRF7 (**Figure 1A**).

On the other hand, CiIRF7-His fusion protein was well expressed and purified, and then the purified protein was successfully identified by Western blotting (Figure S4A in Supplementary Material). With approximately one and half

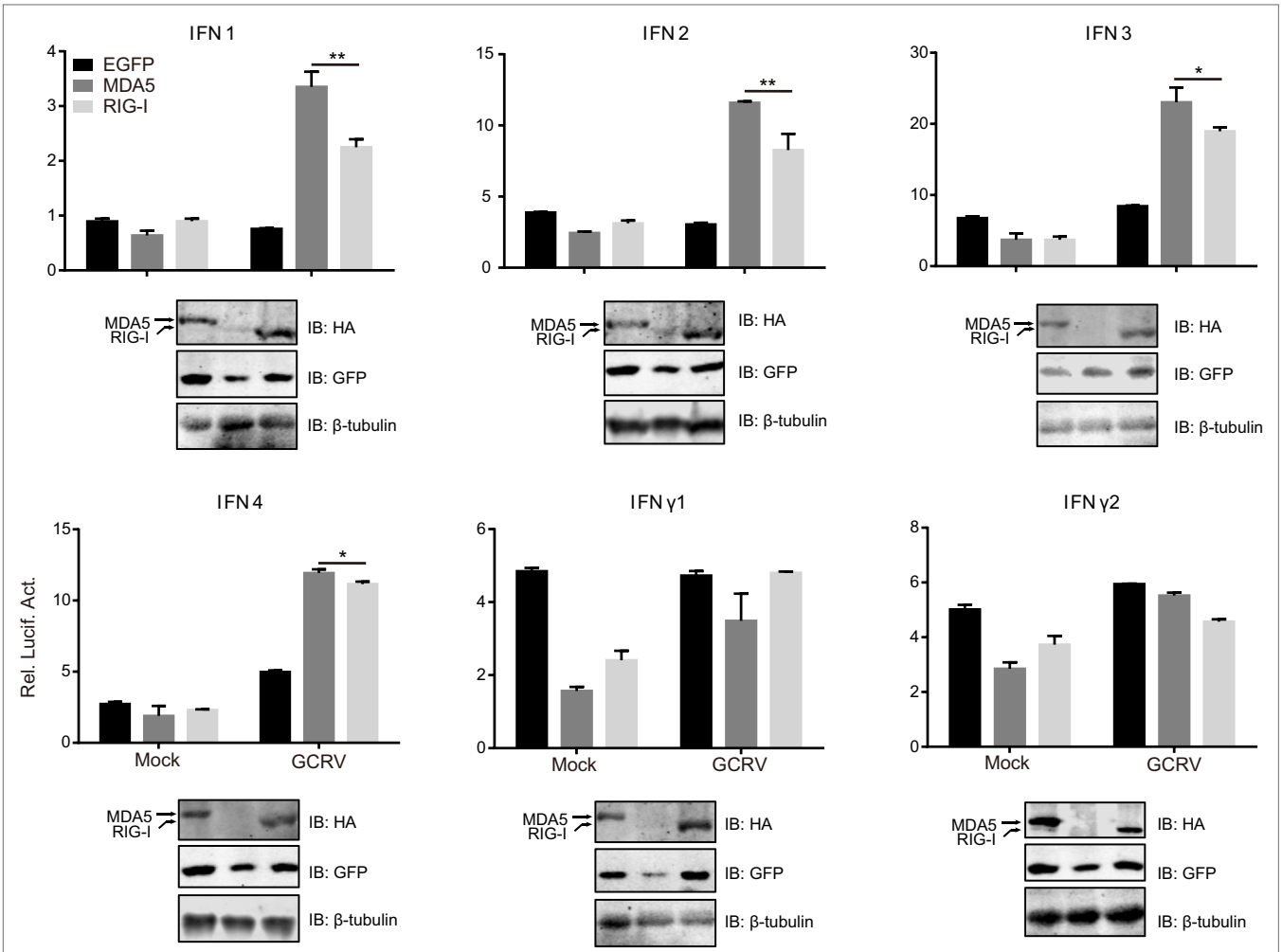

FIGURE 2 | Melanoma differentiation-associated gene 5 (MDA5) and retinoic acid-inducible gene I (RIG-I) differentially induce the promoter activities of various IFNs. *Ctenopharyngodon idella* kidney cells seeded in 24-well plates were co-transfected with 380 ng pMDA5-HA or pRIG-I-HA, 380 ng pIFNpro-Luc (either pIFN1pro-Luc, pIFN2pro-Luc, pIFN3pro-Luc, pIFN4pro-Luc, pIFNγ1pro-Luc, or pIFNγ2pro-Luc), and 38 ng pRL-TK. Twenty-four hours later, one half of the cells were infected with grass carp reovirus, and the other half of the cells were treated with phosphate-buffered saline. Luciferase activities were detected at 6 h p.i. The remaining cell lysates were used for subsequent Western blotting tests to detect the overexpression of *C. idella* RIG-I-HA or CiMDA5-HA. Error bars represent ±SEMs obtained by testing each sample in quadruplicate. *$P < 0.05$; **$P < 0.01$.

months of immunoreaction, the rabbit antiserum was collected. Before the subsequent Western blotting analysis, the rabbit anti-CiIRF7 antiserum was detected for its specificity according to the methods mentioned in the previous report (37), which showed that the anti-CiIRF7 antiserum rather than negative serum from the preimmunized rabbit was able to recognize a cellular protein with a molecular mass of ~49 kDa. When we preabsorbed anti-IRF7 antiserum with fusion protein IRF7-His as primary antibodies, the target protein band disappeared (Figure S4B in Supplementary Material). These data proved that the anti-CiIRF7 antiserum could be employed for further investigation. The following Western blotting analysis manifested that CiMDA5 and CiRIG-I affected the protein expression of neither CiIRF3 nor CiIRF7 (**Figures 3C,D**). Taken together, these data indicate that CiMDA5 and CiRIG-I influence CiIRF3 and CiIRF7 at the promoter activities and mRNA expression levels but not at protein expression levels.

CiIRF3 and CiIRF7 Undergo Phosphorylation to Protect CIK Cells against GCRV Infection

In consideration of the void effect of CiMDA5 and CiRIG-I on the protein expressions of CiIRF3 and CiIRF7, we wondered that whether CiIRF3 or CiIRF7 played a role in GCRV infection. Thus, either pIRF3 or pIRF7 was stably transfected into CIK cells (**Figure 4A**), and the viability of the stably transfected CiIRF3 (IRF3+) and CiIRF7 (IRF7+) cells upon GCRV infection was determined using an *ex vivo* cell viability assay. Cell proliferation in IRF3+ and IRF7+ cells, but cell death in EGFP+ cells were observed (**Figure 4B**), which attested the positive roles of CiIRF3

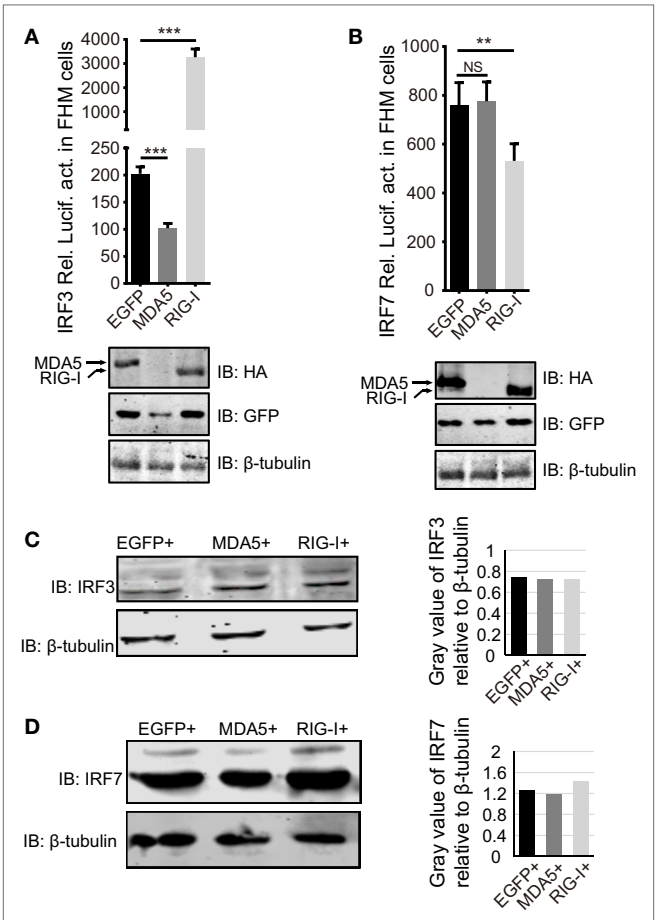

FIGURE 3 | Effect of *Ctenopharyngodon idella* retinoic acid-inducible gene I (CiRIG-I) and *C. idella* melanoma differentiation-associated gene 5 (CiMDA5) on the expression levels of *C. idella* IFN regulatory factor 3 (CiIRF3) and CiIRF7. **(A,B)** Fathead minnow cells seeded in 24-well plates were co-transfected with 380 ng pRIG-I-HA (or pMDA5-HA or pCMV), 380 ng pIRF3pro-Luc (or pIRF7pro-Luc), and 38 ng pRL-TK. Twenty-four hours later, cells were harvested for detection of luciferase activity, and the remaining cell lysates were used for subsequent Western blotting tests to detect the overexpression of CiRIG-I-HA or CiMDA5-HA. **(C,D)** EGFP+, MDA5+, and RIG-I+ cells were seeded in 6-well plates for 24 h cultivation, and then the cell lysate was used for Western blotting analysis. The histograms beside the Western blotting results exhibit the relative expression levels, which were quantified using ImageJ software. Data represent mean ± SEM of four experiments. $^{**}P < 0.01$; $^{***}P < 0.001$.

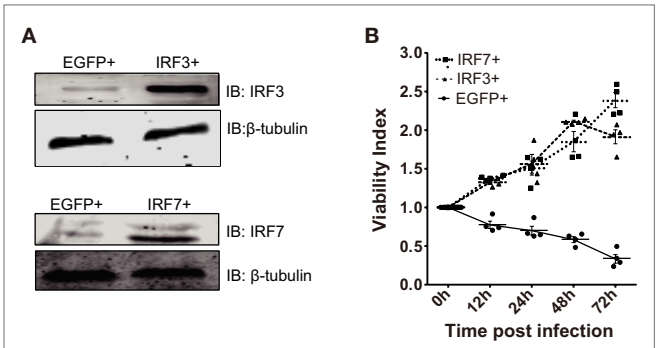

FIGURE 4 | *Ctenopharyngodon idella* IFN regulatory factor 3 (CiIRF3) and CiIRF7 play positive roles in *C. idella* kidney cells under grass carp reovirus (GCRV) infection. **(A)** IRF3+, IRF7+, and EGFP+ cells were seeded in 6-well plates for 24 h cultivation, and then the cell lysate was used for Western blotting analysis. **(B)** 3-(4,5-Dimethylthiazol-2-yl)-2,5-dimethyltetrazolium bromide (MTT) cell viability assay for GCRV-resistant testing in IRF3+, IRF7+, and EGFP+ cells. IRF3+, IRF7+, and EGFP+ cells were seeded in 96-well plates and then infected with GCRV. At each scheduled time, cell viability was analyzed by the MTT colorimetric method and expressed as viability index. Data represent mean ± SEM of four experiments.

and CiIRF7 in CIK cells against GCRV infection. Next, we sought to investigate whether the expression levels and subcellular localization of CiIRF3 and CiIRF7 were affected by GCRV infection or poly(I:C) stimulation. At first, mRNA expression levels of CiIRF3 and CiIRF7 were detected by RT-qPCR. The mRNA level of CiIRF3 was provisionally inhibited at 12 h and then induced post-GCRV infection, while it was induced post-poly(I:C) stimulation in a time-dependent manner (**Figure 5A**). In contrast, the mRNA level of CiIRF7 was depressed under GCRV infection or poly(I:C) stimulation (**Figure 5C**). Second, in accordance with the mRNA expression patterns of CiIRF3 and CiIRF7, we performed the Western blotting at 24 h poststimulation. The results revealed that CiIRF3 and CiIRF7 were not visibly affected by GCRV infection or poly(I:C) stimulation, though the data analyzed by ImageJ software showed that CiIRF3 was inhibited and CiIRF7 was slightly increased (**Figures 5B,D**). Third, confocal fluorescence microscopy analysis was employed to investigate the subcellular localization of CiIRF3 and CiIRF7, which showed that CiIRF3 translocated from cytoplasm into nucleus (**Figure 5E**), while CiIRF7 persistently existed in the whole cell (**Figure 5F**). To verify the result of confocal fluorescence microscopy, we investigated the levels of CiIRF3 and CiIRF7 in the nucleus. The result showed that little CiIRF3 and much more CiIRF7 existed in the nucleus without immunostimulations, but they were aggregated into the nucleus under GCRV infection or poly(I:C) stimulation (**Figure 5G**). These results suggested that CiIRF3 and CiIRF7 were implicated into the immune response provoked by GCRV or poly(I:C) in CIK cells.

Accidently, we noticed that there were blurry blotting bands above the corresponding objective bands of CiIRF3 and CiIRF7, which might be the phosphorylation forms of CiIRF3 or CiIRF7. Therefore, a verification test was carried out. Briefly, the whole-cell lysis was incubated with or without 10 U of CIP before incubating with phosphoserine antibody, and the precipitates were detected by Western blotting. As anticipated, bands in the untreated group were abundant, while there was no band in the CIP treated group (Figure S4C in Supplementary Material). Subsequently, when we treated the whole-cell lysis with CIP, the larger bands above CiIRF7 disappeared (Figure S4D in Supplementary Material). Based on these confirmations, the Western blotting analysis revealed that the phosphorylated CiIRF3 and CiIRF7 were induced by GCRV infection or poly(I:C) stimulation. Taken together, these data show that CiIRF3 and CiIRF7 play positive roles through the phosphorylation and subsequent nuclear translocation (CiIRF3) in CIK cells infected with GCRV or stimulated with poly(I:C).

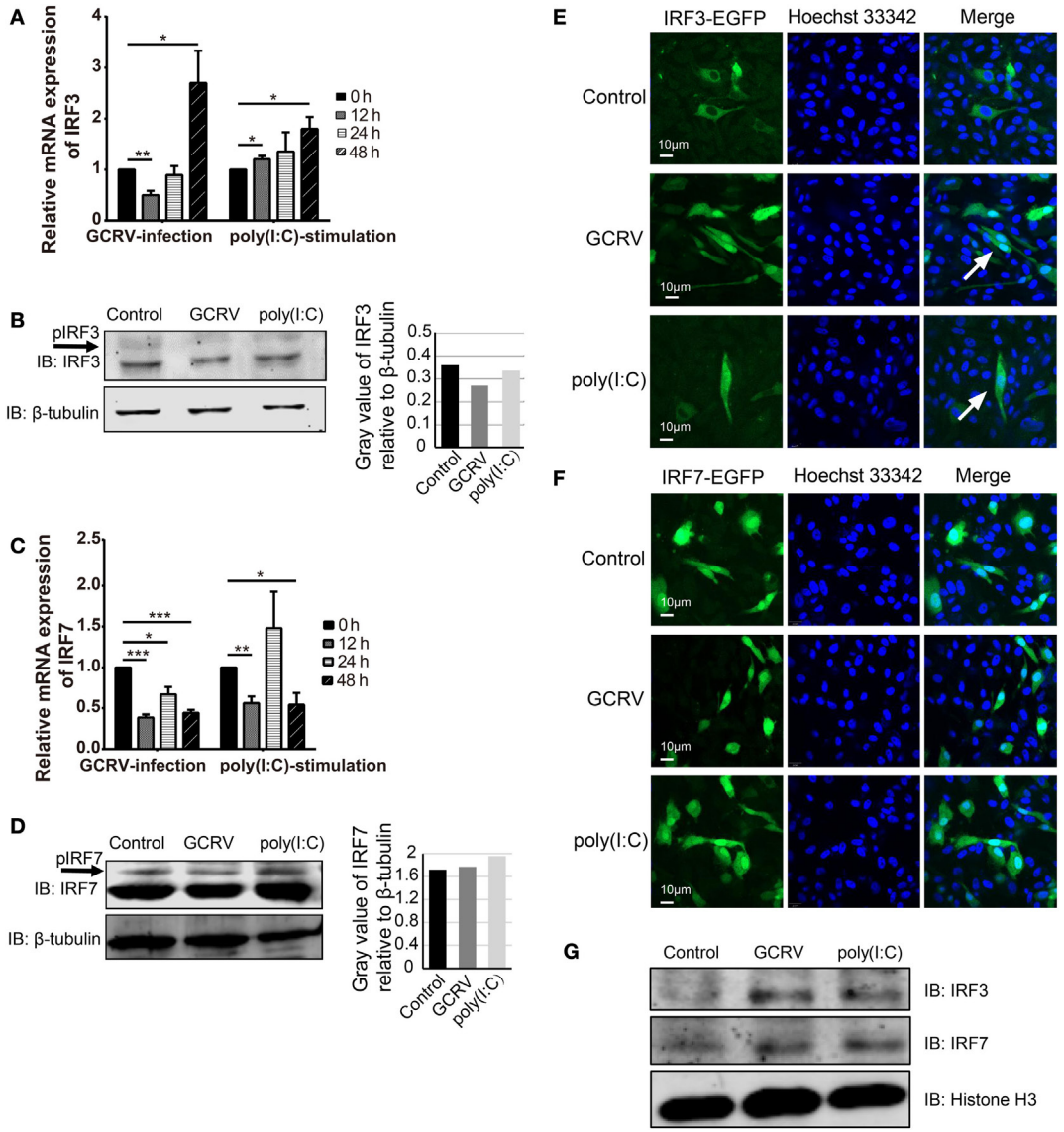

FIGURE 5 | **Expression and subcellular localizations of grass crap IFN regulatory factor 3 (CiIRF3) and CiIRF7 are affected by grass carp reovirus (GCRV) infection or polyinosinic:polycytidylic acid [poly(I:C)] stimulation**. For mRNA expression, *Ctenopharyngodon idella* kidney (CIK) cells were seeded in 12-well plates and then infected with GCRV or stimulated with poly(I:C). At the scheduled time, total RNAs were isolated, and RT-qPCR assay for CiIRF3 **(A)** and CiIRF7 **(C)** was performed. The data are presented in relative expression units where *EF1*α was used to normalize all samples, and fold change was determined relative to cells before infection (0 h). Data represent mean ± SEM of four independent wells of cells. **P* < 0.05; ***P* < 0.01; ****P* < 0.001. For protein expression, CIK cells seeded in 6-well plates were lysed at 24 h post-GCRV infection or poly(I:C) stimulation, and then Western blotting analysis for CiIRF3 **(B)** and CiIRF7 **(D)** was carried out. The histograms exhibit the relative protein expression levels, which are quantified using ImageJ software. "p" in the front of IFN regulatory factor 3/7 indicates the phosphorylation. **(E,F)** Subcellular localization of CiIRF3 and CiIRF7. CIK cells that stably transfected with pIRF3-EGFP **(E)** or pIRF7-EGFP **(F)** were seeded on microscope coverslips in 12-well plates, followed by either phosphate-buffered saline (PBS), GCRV, or poly(I:C) treatment for 24 h. Then those cells were observed using a confocal fluorescence microscope (PerkinElmer). Arrows indicate nucleus translocation of CiIRF3. **(G)** CIK cells seeded in 6-well plates were either treated with PBS, GCRV, or poly(I:C). Twenty-four hours later, cells were harvested, and the nucleoprotein was prepared for the subsequent Western blotting analysis.

CiMDA5 and CiRIG-I Differentially Regulate the Phosphorylation Status of CiIRF3 and CiIRF7 Post-GCRV Infection

To further explore whether CiMDA5 and CiRIG-I are correlative with CiIRF3 and CiIRF7 and the mechanism by which CiMDA5 and CiRIG-I influence CiIRF3 and CiIRF7, MDA5+, RIG-I+, and EGFP+ cells were either infected with GCRV or stimulated with poly(I:C). Twenty-four hours later, we found that the phosphorylation and protein expression levels of CiIRF3 and CiIRF7 were higher in MDA5+ and RIG-I+ cells than those in EGFP+ cells (**Figures 6A,C**). Subsequent IP assay showed that the serine,

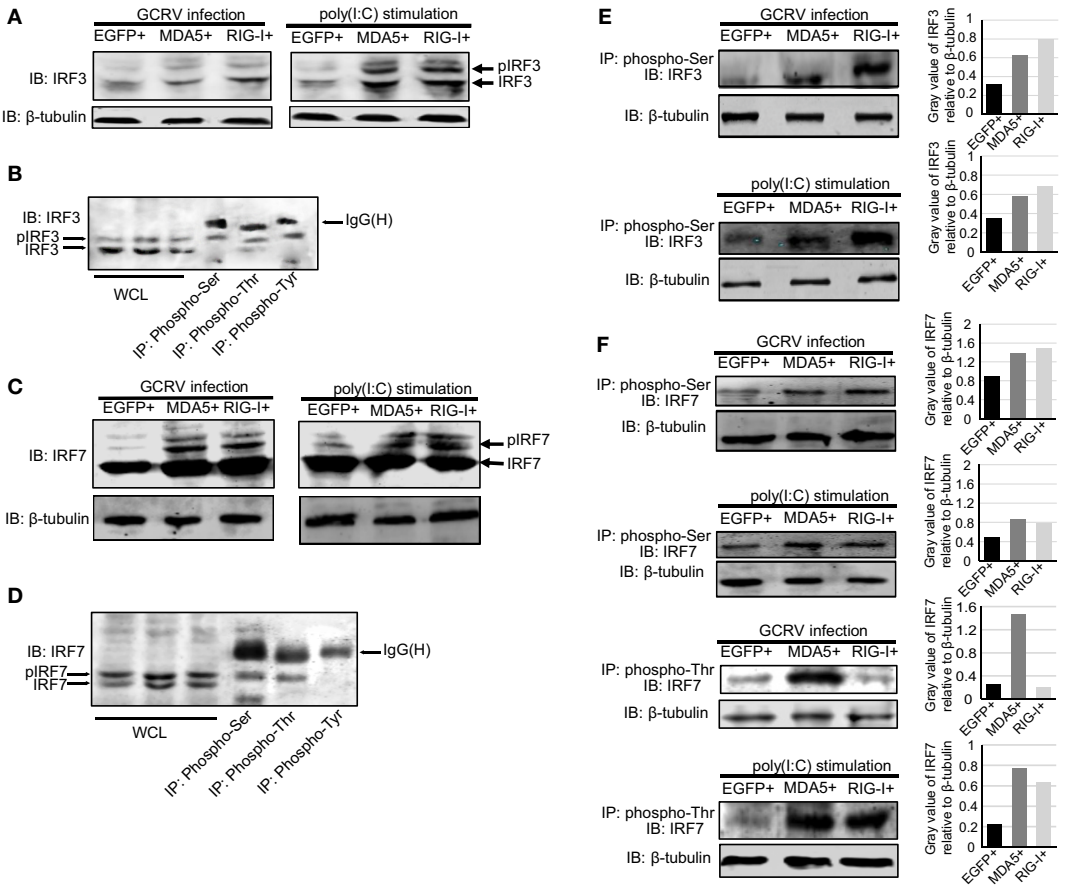

FIGURE 6 | *Ctenopharyngodon idella* melanoma differentiation-associated gene 5 (CiMDA5) and *C. idella* retinoic acid-inducible gene I (CiRIG-I) affect the phosphorylation levels of grass carp IFN regulatory factor 3 (CiIRF3) and CiIRF7 under grass carp reovirus (GCRV) infection or polyinosinic:polycytidylic acid [poly(I:C)] stimulation. **(A,C)** MDA5+, retinoic acid-inducible gene I (RIG-I)+, and EGFP+ cells were seeded into 6-well plates, and then either treated with phosphate-buffered saline, infected with GCRV, or stimulated with poly(I:C) for 24 h. Whole-cell lysates (WCL) were prepared for Western blot analysis. "p" in the front of IRF3\7 indicates the phosphorylation. **(B,D)** *C. idella* kidney cells were seeded in 10-cm plates, and then infected with GCRV for 24 h. WCL were subjected to immunoprecipitation (IP) with 1 μg of corresponding antiphosphorylation antibodies, followed by Western blotting analysis. **(E,F)** MDA5+, RIG-I+, and EGFP+ cells were seeded into 10-cm plates, and then either infected with GCRV or stimulated with poly(I:C). Twenty-four hours later, IP assays were performed with antiphosphoserine antibody or antiphosphothreonine antibody. The histograms exhibit the relative expression levels, which are quantified using ImageJ software. All the immunoblots were performed using anti-IRF3 or anti-IRF7 anti-rabbit polyclonal antibody.

threonine, and tyrosine phosphorylation events occurred on CiIRF3, while serine and threonine phosphorylation events happened on CiIRF7 (**Figures 6B,D**). To verify the auxo-action of CiMDA5 and CiRIG-I on the phosphorylated activation of CiIRF3 and CiIRF7, we performed IP assay using phosphoserine and phosphothreonine antibodies. As expected, under GCRV infection or poly(I:C) stimulation, the phosphorylation levels of CiIRF3 and CiIRF7 in MDA5+ and RIG-I+ cells were higher than those in EGFP+ cells (**Figures 6E,F**). Moreover, CiRIG-I was able to facilitate a stronger phosphorylation of CiIRF3 than CiMDA5, while on the contrary, CiMDA5 facilitated a stronger phosphorylation of CiIRF7 than CiRIG-I. Taken together, these data strongly suggest that CiMDA5 and CiRIG-I facilitate not only the protein expressions but also the phosphorylated levels of CiIRF3 and CiIRF7 under GCRV infection or poly(I:C) stimulation.

CiMDA5 and CiRIG-I Distinguishingly Modulate the Dimerization of CiIRF3 and CiIRF7, Leading to the Differential Production of IFNs

As described above, CiMDA5 and CiRIG-I facilitated the phosphorylation levels of CiIRF3 and CiIRF7 at different degrees. Notably, we noticed that CiMDA5 increased but CiRIG-I reduced the threonine phosphorylation level of CiIRF7 upon GCRV infection, and CiMDA5 more potently enhanced it under poly(I:C) stimulation. Given that phosphorylation is a crucial step for the dimerization of IRF3 or IRF7 (10), CiMDA5 and CiRIG-I may differentially affect the dimerization of CiIRF3 and CiIRF7. To address this, we investigated the dimerization of CiIRF3 and CiIRF7 in either CiMDA5 or CiRIG-I overexpressed cells by Co-IP using tag antibodies whose applicability in CIK

cells was verified. As shown in **Figure 7A**, in the respective target regions, proteins from CIK and EGFP+ cells could not be recognized by either anti-HA, anti-Flag, or anti-*myc* antibody, indicating these tag antibodies can be employed for subsequent experiments. Two sets of IRF3/7 constructs carrying the Flag or *myc* tag were co-transfected into CIK cells. In CiIRF3-Flag and CiIRF3-*myc*, CiIRF3-Flag and CiIRF7-*myc*, CiIRF7-Flag and CiIRF7-*myc* overexpressing cells, anti-*myc* antibody immunoprecipitated protein complex was immunoblotted by anti-Flag Ab. The anti-*myc* antibody immunoprecipitated protein complex

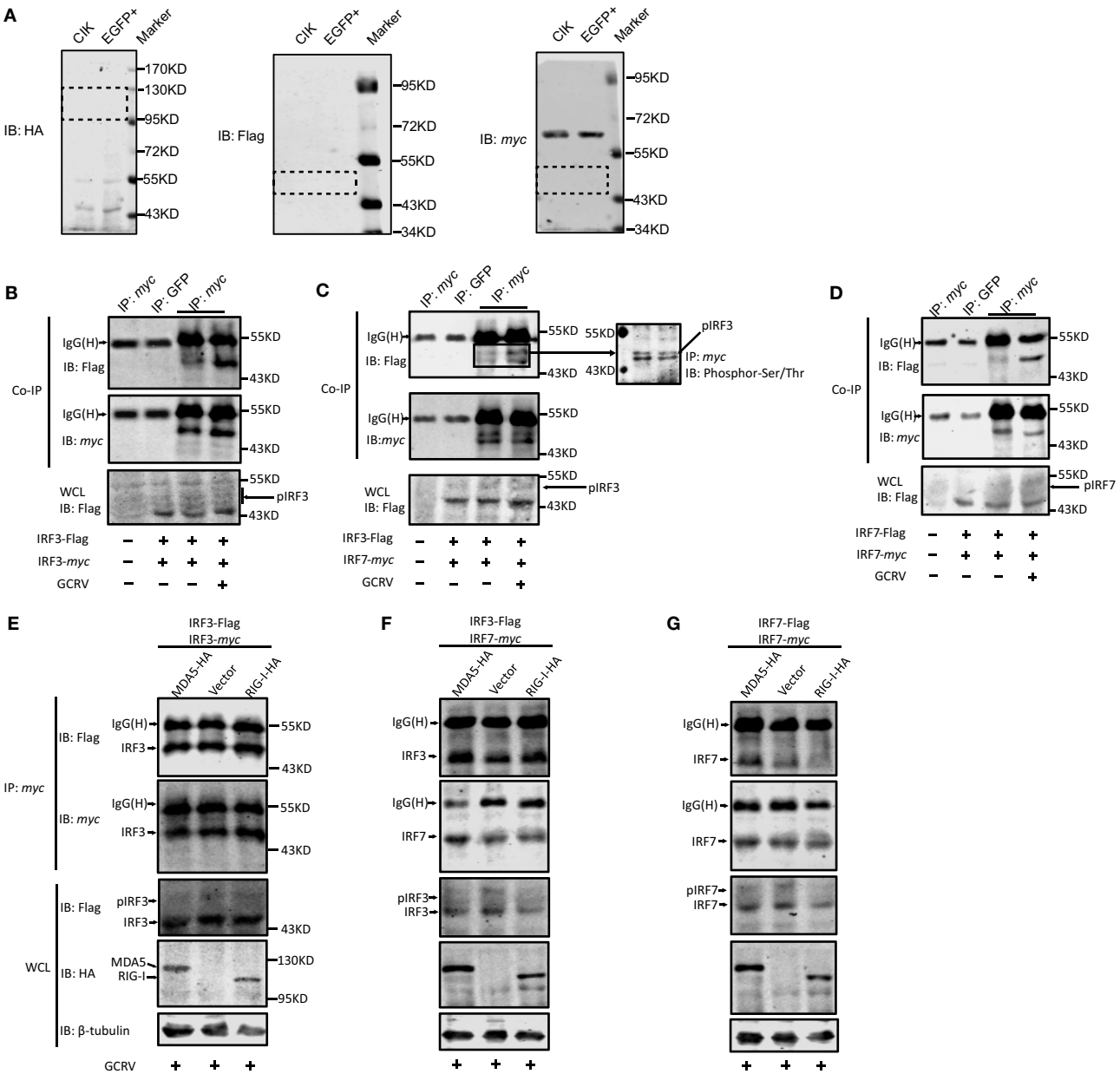

FIGURE 7 | **The same and differential effects of *Ctenopharyngodon idella* melanoma differentiation-associated gene 5 (CiMDA5) and *C. idella* retinoic acid-inducible gene I (CiRIG-I) on the dimerization of grass carp IFN regulatory factor 3 (CiIRF3) and CiIRF7**. **(A)** Applicability test for anti-HA, -Flag, *-myc* antibodies. *C. idella* kidney (CIK) and EGFP+ cells seeded in 6-well plates were harvested for Western blot assay. Anti-HA, -Flag, *-myc* antibodies were used. Dotted boxes show the areas of corresponding target protein bands. **(B–D)** Grass carp reovirus (GCRV) infection facilitates the homo- and heterodimerization of IRF3 and IRF7. CIK cells seeded in 10-cm dishes were co-transfected with 4 μg pIRF3-Flag and 4μg pIRF3-*myc* **(B)**, pIRF3-Flag and pIRF7-*myc* **(C)**, and pIRF7-Flag and pIRF7-*myc* **(D)**. Twenty-four hours later, the transfected cells were infected with GCRV. At 24 h postinfection, cells were harvested for Co-IP assay with anti-*myc* antibody and subsequently immunoblotted with the indicated antibodies. **(E–G)** Effect of CiMDA5 and CiRIG-I on the dimerization of CiIRF3 and CiIRF7. CIK cells seeded in 10-cm dishes were co-transfected with 2.6 μg of pMDA5-HA (or pRIG-I-HA, or pdCMV), 2.6 μg of pIRF3-Flag and 2.6 μg of pIRF3-*myc* **(E)**, pIRF3-Flag and pIRF7-*myc* **(F)**, pIRF7-Flag and pIRF7-*myc* **(G)**. The subsequent experiments were carried out as described above.

from non-transfected cells and anti-GFP antibody immunoprecipitated protein complex from transfected cells were not able to be recognized by anti-Flag antibody (**Figures 7B–D**). The results indicated that CiIRF3 and CiIRF7 were able to shape homodimers and heterodimers. Notably, in anti-*myc* antibody immunoprecipitated protein complex from CiIRF3-Flag and CiIRF7-*myc* overexpressing cells, two protein bands were immunoblotted by anti-*myc* and anti-Flag antibodies. As shown in **Figure 7C**, the anti-*myc* antibody immunoprecipitated protein complex was recognized by serine- and threonine phosphorylation antibodies, indicating that both bands were phosphorylated proteins. Furthermore, it was observed that CiIRF3-Flag was weakly combined with CiIRF3-*myc* in the steady state, whereas they strongly combined under GCRV infection in CIK cells (**Figure 7B**). The same was true for the combinations between CiIRF3-Flag and CiIRF7-*myc* and between CiIRF7-Flag and CiIRF7-*myc* (**Figures 7C,D**), thus demonstrating that GCRV infection strengthened both homo- and heterodimerization of CiIRF3 and CiIRF7.

Considering that dimerization of CiIRF3 and CiIRF7 was strengthened by GCRV infection, the dimerization in grass carp plays a critical role in IFN induction, same as that in mammalian. Hereupon, we wondered whether CiMDA5 and CiRIG-I differentially affected the dimerization of CiIRF3 and CiIRF7. Therefore, constructs were transiently co-transfected into CIK cells, IP of *myc*-tagged protein was performed, followed by immunoblotting analysis of the immunoprecipitate with anti-Flag antibody and anti-*myc* antibody, respectively. As shown in **Figure 7E**, the amount of Flag-tagged CiIRF3 in anti-*myc* antibody immunoprecipitate from CiMDA5- or CiRIG-I overexpressed cells was equal to that from empty vector transfected cells, revealing that CiMDA5 and CiRIG-I were not able to affect the homodimerization of CiIRF3. Similar experiments illuminated that CiMDA5 and CiRIG-I facilitated the heterodimerization of CiIRF3 and CiIRF7 (**Figure 7F**). Dissimilarly, CiMDA5 facilitated but CiRIG-I impeded the homodimerization of CiIRF7 (**Figure 7G**).

Based on the abovementioned data, we ought to verify the assumption that the homodimer and heterodimer of CiIRF3 and CiIRF7 differentially induce CiIFNs production. As a consequent, luciferase assays were employed to test the expression regulation of CiIFNs by CiIRF3 and CiIRF7. To examine the synergistic effect between CiIRF3 and CiIRF7, pIRF3 and pIRF7 were co-transfected into CIK cells at a ratio of1:4, which had been proved to be the perfect ratio in zebrafish (40). As shown in **Figure 8**, single CiIRF3 overexpression significantly activated the promoter of CiIFN1, but suppressed the promoter of CiIFN3, and failed to activate the promoters of CiIFN2 and CiIFN4. Single CiIRF7 overexpression or both CiIRF3 and CiIRF7 overexpression widely activated the promoters of IFN-I, and the synergy between CiIRF3 and CiIRF7 was embodied in the activation of CiIFN1 promoter. Consistent with previous theory that IRF3 and IRF7 induced the production of IFN-I but not IFN-II, overexpressed CiIRF3/7 alone or collectively were not able to activate the promoters of

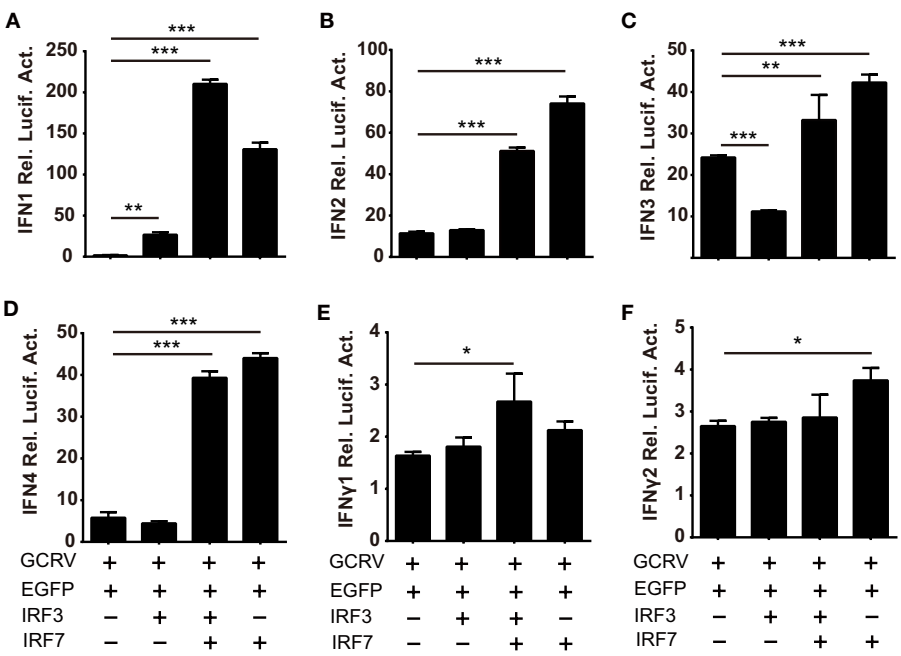

FIGURE 8 | Differential responses of IFN promoters to *Ctenopharyngodon idella* IFN regulatory factor 3/7 (CiIRF3/7) individually and collectively. *C. idella* kidney cells seeded in 24-well plates were co-transfected with 380 ng pIFNpro-Luc [either pIFN1pro-Luc **(A)**, pIFN2pro-Luc **(B)**, pIFN3pro-Luc **(C)**, pIFN4pro-Luc **(D)**, pIFNγ1pro-Luc **(E)**, or pIFNγ2pro-Luc **(F)**], and 380 ng indicated plasmids [pIRF3 the second bar of each figure, pIRF3:pIRF7 = 1:4 the third bar of each figure, pIRF7 the fourth bar of each figure] and 38 ng pRL-TK. Twenty-four hours later, the cells were infected with GCRV. The luciferase activities were detected at 6 h p.i. Error bars represent SEMs obtained by testing each sample in quadruplicate. *$P < 0.05$; **$P < 0.01$; ***$P < 0.001$.

IFNγ1 and IFNγ2 (**Figures 8E,F**). These data demonstrate that the different effect between CiMDA5 and CiRIG-I on IFN-I inducing is involved in the phosphorylation and dimerization of CiIRF3 and CiIRF7.

CiMDA5 and CiRIG-I Differentially Affect the mRNA Expressions of CiIL-4 and CiIL-12p40

We further attempted to inquire the possible mechanism by which CiMDA5 and CiRIG-I differentially induced the expression of CiIFN-II. Given that certain cytokines such as IL-4, IL-10, IL-12, and IL-18 can regulate IFN-II production (41), we wondered whether CiMDA5 and CiRIG-I differentially affected the expression of such cytokines. Hence, we obtained the sequences of CiIL-4 gene (GenBank accession no. KP896505) and CiIL-10 gene (GenBank accession no. HQ388294), but did not find the sequence of CiIL-18 gene in GenBank or the genomic database of grass carp (32). Subsequently, we designed primers of CiIL-4 and CiIL-10 and used available primers of CiIL-12p40 (38) for the following RT-qPCR assay (**Table 1**). As shown in **Figure 9**, compared to the expression levels in CIK cells, CiIL-4 and CiIL-12p40 were significantly highly expressed in MDA5+ cells at 12 h post-GCRV infection or poly(I:C) stimulation. However, the expression of CiIL-4 was repressed in RIG-I+ cells, the expression of CiIL-12p40 in RIG-I+ cells was same as that in CIK cells. Unexpectedly, CiIL-10 was not detected in all samples, suggesting that CiIL-10 was hardly expressed in CIK cells. These data reveal that CiMDA5 increases the expression of CiIL-4 and CiIL-12p40, while CiRIG-I represses that of CiIL-4, which may provide clues for the further studies on the correlation between RLRs and IFN-II.

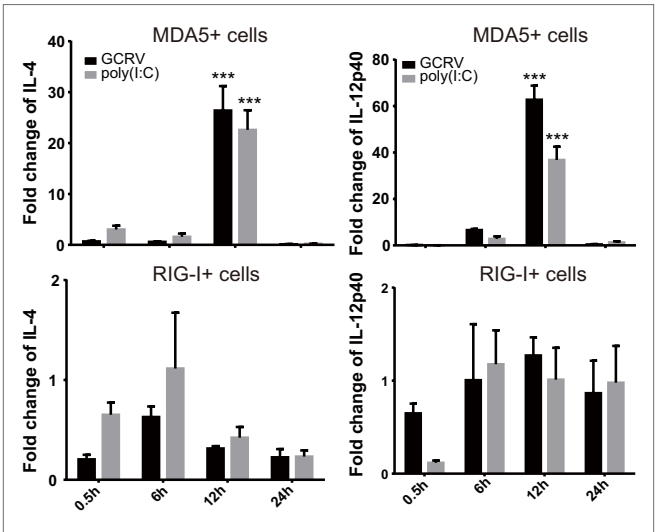

FIGURE 9 | *Ctenopharyngodon idella* melanoma differentiation-associated gene 5 (CiMDA5) and *C. idella* retinoic acid-inducible gene I (CiRIG-I) differentially affect the mRNA expression levels of CiIL-4 and CiIL-12p40 genes. *C. idella* kidney (CIK), MDA5+, and RIG-I+ cells were seeded in 12-well plates, and then infected with GCRV or stimulated with polyinosinic:polycytidylic acid. At the scheduled time, total RNA samples were isolated for RT-qPCR analysis. The relative expression levels of these genes were normalized by *EF1α*. Fold change of gene expression level was determined relative to corresponding treated CIK cells at the same time point. Data represent mean ± SEM of four independent wells of cells. ***$P < 0.001$.

DISCUSSION

As critical intracellular sensors, the recognition mechanisms of MDA5 and RIG-I were broadly investigated in the past few years. To date, a widespread theory considers that MDA5 and RIG-I play non-redundant roles in pathogen recognition: MDA5 recognizes positive single strand RNA (ssRNA) or long double strand RNA (dsRNA) virus, while RIG-I recognizes negative ssRNA or short dsRNA virus (2). This conclusion signifies that MDA5 and RIG-I jointly recognize those viruses whose genome is composed of different-sized segmented dsRNA, such as reovirus. In this case, MDA5 and RIG-I are seemingly redundant sensors in antiviral immunity upon such virus invasion, and thus their shared and/or unique functions in the downstream signal pathway should be elucidated. Moreover, previous studies had stated or identified that distinct pathogens or virus MOI affected IFN-I subtype induction (42, 43), but the mechanisms are unclear. Based on the abovementioned observations, it is presumed that MDA5 and RIG-I induce differential IFN subtypes in antiviral immunity. Fish can be served as an appropriate research object because RIG-I homologs are absent in some fish genomes. To this end, a dsRNA reovirus named GCRV, which was previously proved to induce the expression of CiMDA5 and CiRIG-I *in vivo* and *in vitro,* served as stimulus of CIK cells in the present study (28, 29), aiming at revealing the similar and different roles between CiMDA5 and CiRIG-I in the induction of IFN system.

Though our previous studies reported that either CiMDA5 or CiRIG-I overexpression plays a positive role in antiviral response in CIK cells (27, 30), the distinction in IFN induction between them has yet to be clarified. CiIFN genes are recently sorted out by bioinformatics analysis (31), the expression patterns of CiIFNs were first investigated in the present study. The expression pattern of IFN-I in CIK cells is different from that in salmon cells, in which group I IFN-I (IFN-a, IFN-d, and IFN-e) but not group II IFN-I (IFN-b, IFN-c, and IFN-f) are ubiquitously produced and are inducible (IFN-a, IFN-d, IFN-e, and IFN-f) in response to viral infection (12). CiIFN3 is downregulated until 12 h p.i., indicating that CiIFN3 is inhibited at the early stage of GCRV infection. Besides, CiIFN4 is different from IFN-d (CiIFN4 homolog) in Atlantic salmon, which was identified to have no response to poly(I:C) (44). Likewise, IFN4 in rhabdoviruses infected zebrafish expressed lowly and shows low biological activity (45). Though the specific biological activity of CiIFN4 has yet to be investigated, its expression pattern implies that CiIFN4 plays a positive role in antiviral immunity. These data reveal that IFN1 and IFN3 are the major functional IFN-I, and the four IFN-I subtypes may play mutual synergistic and supplementary roles in CIK cells as previously reviewed (16). With regard to IFN-II, the moderate expression patterns may indicate their indispensable roles. Under immunostimulation, CiIFNγ1 could not be detected

until 24 h p.i., and CiIFNγ2 is inhibited until 24 h p.i., implying that CiIFNγ1 and CiIFNγ2 play critical roles in antiviral immunity and are restrained at early stage in CIK cells. On the other hand, either CiMDA5 or CiRIG-I overexpression does not lead to the upregulation of IFNs at steady state in CIK cells, but significantly induces the expression of IFN-I upon GCRV or poly(I:C) stimulation, which may be attributed to the autoinhibition and phosphorylation of CiMDA5 and CiRIG-I at the steady state (46). Previous study on IFN-I in Atlantic salmon showed that IFN-a (CiIFN1 homolog) is the main IFN subtype induced by the RIG-I/MDA5 pathway (44). However, we found that CiIFN3 is dramatically induced by overexpressed CiMDA5 and CiRIG-I, indicating that RIG-I and MDA5 mainly induce the expression of IFN3 in grass carp. Comparing the expression patterns of various IFNs in MDA5+ cells with those in RIG-I+ cells, we found that the relative expression levels of IFNs in MDA5+ cells are higher than those in RIG-I+ cells. More obviously, CiMDA5 but not CiRIG-I overexpression upregulated the expression of CiIFN1, implying that the downstream signal pathway of MDA5 is not identical with that of RIG-I in grass carp. Subsequently, these consequences are validated by a luciferase reporter assay. CiMDA5 and CiRIG-I overexpressions are not able to activate the promoters of CiIFN-I at the steady state, but they activate the promoters under GCRV infection and, more importantly, CiMDA5 is more potent to activate CiIFN-I promoters than CiRIG-I. Furthermore, the expression patterns of ISG also underscored this conclusion. CiMDA5 overexpression induced higher expression levels of CiGig1, CiIFI56, and CiMx2 than CiRIG-I overexpression under immunostimulations. Of note is that, CiMDA5 and CiRIG-I overexpression cannot upregulate the expression of CiISG15. Previous study identified that ISG15 was able to conjugate with RIG-I to negatively regulate RIG-I-mediated antiviral signaling (47). Thus, we deduce that ISG15 is mainly induced by other signaling pathways to regulate the RLR pathway in grass carp. Additionally, we also noticed that CiMDA5 and CiRIG-I induce the mRNA expression of IFNγ2. Considering that IL-4 and IL-10 negatively regulate while IL-12 and IL-18 positively regulate the production of IFNγ, we attempted to detect the expression of these ILs. Since IL-18 is not retrieved in grass carp genome and the expression of CiIL-10 is not detected, we showed the expression profiles of CiIL-4 and CiIL-12p40. Considering NF-κB which initiates the transcriptions of various cytokines including some ILs and is a critical downstream transcription factor for MAVS (48, 49), CiMDA5 and CiRIG-I may affect the expressions of these ILs to regulate the production of IFN-II through the NF-κB pathway.

One probable mechanism for the differential effects between CiMDA5 and CiRIG-I is that CiRIG-I inhibits the expression of CiMDA5 (**Figure 1A**). The inhibition mechanism can be speculated from the distinct structures between MDA5 and RIG-I. As is well known that RIG-I but not MDA5 in a strictly autoinhibited conformation in the ligand-free state, the superabundant MDA5 in cytosol can lead to overactive immune response or apoptosis to threaten the cell survival (50, 51). Therefore, to maintain the intracellular balance, MDA5 was downregulated by a present unknown mechanism when RIG-I overexpressed. However, the autoinhibited RIG-I posed no threat to the cell survival, thus it is needless to regulate the expression of RIG-I when MDA5 overexpressed. This observation may result from a host adaption mechanism defined as "PRR reprogramming" (52). This finding indicates that the expression levels of MDA5 and RIG-I were in dynamic equilibrium in cytosol, and sometimes they play reciprocal inhibited roles. On the other hand, as key transcription factors of IFN-I in the RLR signaling pathway, IRF3 and IRF7 may be responsible for the functional differentiation between CiMDA5 and CiRIG-I. In zebrafish, IRF3 overexpression effectively activates IFN1, while IRF7 overexpression activates IFN3 (9), which implies that fish IRF3 and IRF7 play distinct roles in IFN signaling. Thus, it is doubtful whether CiMDA5 and CiRIG-I differently affect the expression of CiIRF3 and CiIRF7. Though the promoter activity and mRNA level of CiIRF3 and the promoter activity of CiIRF7 were affected by CiRIG-I and/or CiMDA5, the protein levels of CiIRF3 and CiIRF7 were not affected. Two research findings can be employed to understand the discordance among the promoter activity, mRNA and protein levels. First, transiently transfection can result in temporal changes in the expression of many transcripts (53). CiMDA5 and CiRIG-I were transiently overexpressed in the luciferase activity assay, while they were stably overexpressed in the RT-qPCR and Western blotting tests. Thus, we deduce that this discordance is caused by the overexpressed modes of CiMDA5 and CiRIG-I. Second, the discordance between protein and mRNA expression is prevalent in human, especially for genes of regulation in terms of biological process, which refers to many posttranscriptional mechanisms (54, 55). Overall, we found that CiRIG-I and CiMDA5 overexpression were able to affect the expression of CiIRF3 and CiIRF7 in CIK cells without immunostimulations. It is well known that immune system should stay in homeostasis without xenogeneic invasion. To avoid provoking the IFN response in the steady state, excrescent IRF3 and IRF7 should be degraded by certain mechanisms such as RNA degradation and protein ubiquitylation (56–58). On the other hand, considering IRF7 is majorly induced by IFN-I (59), the non-effect of CiMDA5 and CiRIG-I on CiIRF7 might be caused by the non-effect of CiMDA5 and CiRIG-I on IFN-I without immunostimulation. Based on such findings, we wondered whether CiIRF3 and CiIRF7 play roles in antiviral response in CIK cells. The subsequent investigation demonstrates that CiIRF3 and CiIRF7 indeed play protective roles in GCRV infection and that the expression levels of CiIRF3 and CiIRF7, as well as the subcellular location of CiIRF3, were affected by GCRV infection or poly(I:C) stimulation.

Since CiIRF3 and CiIRF7 participated in the antiviral response, it was still a puzzle that how CiMDA5 and CiRIG-I differently affected the downstream signals. Excitedly, we noticed that there are some faint slow-migrating bands above the target bands. Considering that IRF3 and IRF7 may be activated by phosphorylation, those larger bands might be the phosphorylation forms of CiIRF3 or CiIRF7. Subsequently, this hypothesis is verified by the IP and Western blotting assays. Therefore,

we demonstrated that GCRV infection or poly(I:C) stimulation facilitates the phosphorylation levels of CiIRF3 and CiIRF7, which leads to CiIRF3 and CiIRF7 translocation from cytoplasm to the nucleus. More importantly, the expression and phosphorylation levels of CiIRF3 and CiIRF7 are higher in MDA5+ and RIG-I+ cells than those in EGFP+ cells under GCRV infection or poly(I:C) stimulation (**Figure 6**), indicating that the immunostimulation but not the expression of immune-related genes is the key to initiate immune responses. Subsequently, the effects of CiMDA5 and CiRIG-I on the phosphorylation levels of CiIRF3 and CiIRF7 are explored. The result shows that CiMDA5 and CiRIG-I significantly facilitate the serine phosphorylation levels of CiIRF3 and CiIRF7 under GCRV infection or poly(I:C) stimulation. Differently, since RIG-I is able to interact with STING to specify IRF3 phosphorylation (60, 61), CiRIG-I induces a higher phosphorylation level of CiIRF3 than CiMDA5. Interestingly, the threonine phosphorylation of CiIRF7 was facilitated by CiMDA5 but inhibited by CiRIG-I under GCRV infection, and the threonine phosphorylation level of CiIRF7 in CiRIG-I overexpressed cells was slightly lower than that in CiMDA5 overexpressed cells under poly(I:C) stimulation.

As it is well-known that phosphorylated IRF3 and IRF7 translocate into the nucleus and then form dimers to bind various IFN promoters, Teleost IRF3 prefers to bind the promoter and induce the production of IFN1, while IRF7 has a preference to induce IFN3 (9, 40). Therefore, the different dimerization forms of IRF3 and IRF7 induce different IFNs. However, which factor determines the dimerization form namely homo- or heterodimer

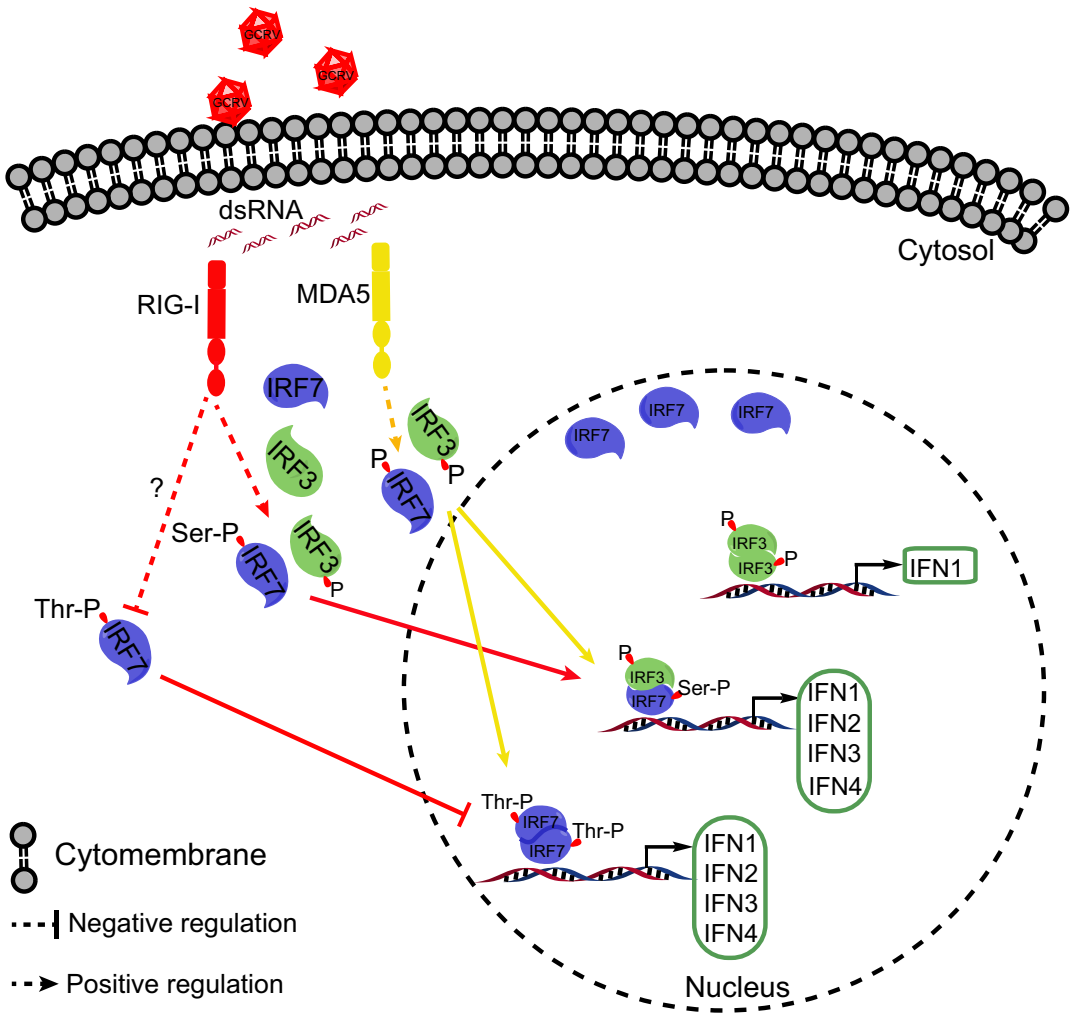

FIGURE 10 | Schematic representation of the difference between *Ctenopharyngodon idella* melanoma differentiation-associated gene 5 (CiMDA5) and *C. idella* retinoic acid-inducible gene I (CiRIG-I) in inducing grass carp IFNs (CiIFN) genes. The red arrows indicate the RIG-I pathway, while yellow arrows indicate the MDA5 pathway. Under grass carp reovirus (GCRV) infection, CiMDA5 and CiRIG-I facilitate the holistic phosphorylation levels of grass carp IFN regulatory factor 3 (CiIRF3) and CiIRF7. Both CiMDA5 and CiRIG-I enhance heterodimerization of CiIRF3 and CiIRF7. Differently, CiMDA5 facilitates but CiRIG-I weakens the threonine phosphorylation level of CiIRF7, which results in the status that CiMDA5 facilitates but CiRIG-I weakens the homodimerization of CiIRF7. This mechanism explains that CiMDA5 induces a stronger CiIFN-I response than CiRIG-I under GCRV infection in *Ctenopharyngodon idella* kidney cells.

is unknown. We posit that this factor is phosphorylation form. In light of the different effects between CiMDA5 and CiRIG-I on the production of CiIFNs and the phosphorylation of CiIRF3 and CiIRF7, we deduced that CiMDA5 and CiRIG-I differentially affect the dimerization of CiIRF3 and CiIRF7. Subsequent Co-IP assays verify this assumption. CiMDA5 and CiRIG-I facilitate the phosphorylation of CiIRF3 but have no obvious effect on the homodimerization of CiIRF3, while enhance the heterodimerization of CiIRF3 and CiIRF7, indicating that most CiIRF3 is employed to shape heterodimers with CiIRF7. More importantly, CiRIG-I increases the serine phosphorylation but decreases the threonine phosphorylation levels of CiIRF7, leading to the upregulation of the heterodimerization level of CiIRF3 and CiIRF7 but the downregulation of the homodimerization level of CiIRF7 under GCRV infection. It was previously stated that RIG-I but not MDA5 is autoinhibited, which gives MDA5 a greater propensity to form filaments along dsRNA (62). This difference may result in the more potent role of MDA5 than that of RIG-I in the immune response. Herein, the present results show the differential effect between CiMDA5 and CiRIG-I on the regulation of phosphorylation and dimerization of CiIRF3 and CiIRF7, revealing that CiMDA5 is more potent to modulate IFN-I production than CiRIG-I and, to a certain extent, CiMDA5 and CiRIG-I play redundant and complementary roles in the immune response against the invasion of some viruses which can be recognized by MDA5 and RIG-I. On the other hand, these results suggest that threonine phosphorylation of CiIRF7 is required to shape CiIRF7 homodimers, while serine phosphorylation of CiIRF7 is required to shape CiIRF7 heterodimers with CiIRF3. According to this inference, CiIRF7 may dominate the heterodimerization between CiIRF3 and CiIRF7. Notably, subsequent dual luciferase reporter assay reveals that the heterodimer of CiIRF3 and CiIRF7 strongly activate the promoters of IFN-I genes, emphasizing the critical role of the heterodimerization in IFN-I induction. In the process of heterodimerization, another unknown protein modification is required. The direct evidence for this statement is that there are two different sizes of phosphorylated CiIRF3-Flag and phosphorylated CiIRF7-*myc* in the immunoprecipitate from CiIRF3-Flag and CiIRF7-*myc* overexpressed cells (**Figure 7C**). Coincidentally, similar result is found in zebrafish (40). Given that most phosphorylation residues of human and mouse IRF3/7 are not conservative in CiIRF3/7 (Figure S5 in Supplementary Material), to clarify the phosphorylation residues of CiIRF3/7 may be of great interest in the future, which may contribute to understanding the fine regulatory mechanisms of the dimerization. Similar to previous reports in zebrafish (9, 40), IRF3 prefers to activate IFN1, while IRF7 widely activates IFN-I genes in grass carp. Previously, Honda and Taniguchi deduced that the homodimer of IRF7 or the heterodimer of IRF7 and IRF3, rather than the homodimer of IRF3, might be more important for the cytosolic pathway of IFN-I gene induction by viruses (10). Consistently, we found that IRF7 is more efficient in IFN-I promoter activation than IRF3 in grass carp. In light of the abovementioned results, we approved the viewpoint that IRF7 plays a more important role in the pathway of production of IFN-I than IRF3 under virus infection (10, 63). Thus, the IFN-I response to GCRV infection in CIK cells can be conceived as that: IRF3 is activated for the shaping of homodimer to induce IFN1 production, and then IFN1 induces the expression and activation of IRF7 which then forms homodimers and heterodimers with IRF3 to induce stronger expression of IFN1, IFN2, IFN3, and IFN4.

Collectively, the present study revealed that CiMDA5 induces a more extensive IFN response than CiRIG-I under GCRV infection. As shown in **Figure 10**, the differential effect is ascribed to the following mechanisms. CiMDA5 facilitates the total phosphorylation levels of CiIRF3 and CiIRF7, while CiRIG-I facilitates the total phosphorylation level of CiIRF3 and serine phosphorylation level of CiIRF7 but decreases the threonine phosphorylation level of CiIRF7. This difference gives rise to the observation that CiMDA5 enhances the heterodimerization of CiIRF3 and CiIRF7, and the homodimerization of CiIRF7; while CiRIG-I strengthens the heterodimerization of CiIRF3 and CiIRF7, but impairs the homodimerization of CiIRF7. Since CiIRF7 homodimer broadly induces the production of IFN-I, CiRIG-I induces a weaker IFN-I response than CiMDA5 upon GCRV infection. These findings imply that CiMDA5 is crucial for the cytosolic pathway in induction of IFN genes by GCRV, and that the contribution of CiRIG-I is minor. This may be another evidence to explain why MDA5 is able to completely substitute RIG-I in Chinese tree shrew (64). Under this situation, the matter that RIG-I cannot be identified in certain fishes can be well explained.

AUTHOR CONTRIBUTIONS

JS and QW conceived and designed the experiments. QW, CY, and YR performed the experiments and analyzed the data. ZL contributed to the bioinformatics analysis of correlative gene sequences. QW and JS wrote the manuscript. All authors reviewed the manuscript.

ACKNOWLEDGMENTS

The authors highly appreciate Professor Yibing Zhang (Institute of Hydrobiology, Chinese Academy of Sciences, Wuhan, China) for kindly providing rabbit anti-IRF3 antiserum, Dr. Junfa Yuan (Huazhong Agricultural University, Wuhan, China) for kindly providing FHM cells. Our thanks equally go to Mr. Tianle Gu, Miss Xueying Shang, Miss Juanjuan Su, Mr. Xun Xiao, and Mr. Jianfei Ji for helpful technical assistance.

FUNDING

This work was supported by Huazhong Agricultural University Scientific & Technological Self-innovation Foundation (Program No. 2014RC019) and National Natural Science Foundation of China (31572648).

SUPPLEMENTARY MATERIAL

The Supplementary Material for this article can be found online at http://journal.frontiersin.org/article/10.3389/fimmu.2017.00189/full#supplementary-material.

REFERENCES

1. Sadler AJ, Williams BR. Interferon-inducible antiviral effectors. *Nat Rev Immunol* (2008) 8(7):559–68. doi:10.1038/nri2314
2. Kato H, Takahasi K, Fujita T. RIG-I-like receptors: cytoplasmic sensors for non-self RNA. *Immunol Rev* (2011) 243:91–8. doi:10.1111/j.1600-065X.2011.01052.x
3. Cui S, Eisenacher K, Kirchhofer A, Brzozka K, Lammens A, Lammens K, et al. The C-terminal regulatory domain is the RNA 5'-triphosphate sensor of RIG-I. *Mol Cell* (2008) 29(2):169–79. doi:10.1016/j.molcel.2007.10.032
4. West AP, Shadel GS, Ghosh S. Mitochondria in innate immune responses. *Nat Rev Immunol* (2011) 11(6):389–402. doi:10.1038/nri2975
5. Liu S, Chen J, Cai X, Wu J, Chen X, Wu YT, et al. MAVS recruits multiple ubiquitin E3 ligases to activate antiviral signaling cascades. *Elife* (2013) 2:e00785. doi:10.7554/eLife.00785.001
6. Hou F, Sun L, Zheng H, Skaug B, Jiang QX, Chen ZJ. MAVS forms functional prion-like aggregates to activate and propagate antiviral innate immune response. *Cell* (2011) 146(3):448–61. doi:10.1016/j.cell.2011.06.041
7. Liu S, Cai X, Wu J, Cong Q, Chen X, Li T, et al. Phosphorylation of innate immune adaptor proteins MAVS, STING, and TRIF induces IRF3 activation. *Science* (2015) 347(6227):aaa2630. doi:10.1126/science.aaa2630
8. Paz S, Sun Q, Nakhaei P, Romieu-Mourez R, Goubau D, Julkunen I, et al. Induction of IRF-3 and IRF-7 phosphorylation following activation of the RIG-I pathway. *Cell Mol Biol* (2006) 52(1):17–28. doi:10.1170/t694
9. Sun F, Zhang YB, Liu TK, Shi J, Wang B, Gui JF. Fish MITA serves as a mediator for distinct fish IFN gene activation dependent on IRF3 or IRF7. *J Immunol* (2011) 187(5):2531–9. doi:10.4049/jimmunol.1100642
10. Honda K, Taniguchi T. IRFs: master regulators of signalling by Toll-like receptors and cytosolic pattern-recognition receptors. *Nat Rev Immunol* (2006) 6(9):644–58. doi:10.1038/nri1900
11. Takaoka A, Yanai H. Interferon signalling network in innate defence. *Cell Microbiol* (2006) 8(6):907–22. doi:10.1111/j.1462-5822.2006.00716.x
12. Zou J, Gorgoglione B, Taylor NG, Summathed T, Lee PT, Panigrahi A, et al. Salmonids have an extraordinary complex type I IFN system: characterization of the IFN locus in rainbow trout *Oncorhynchus mykiss* reveals two novel IFN subgroups. *J Immunol* (2014) 193(5):2273–86. doi:10.4049/jimmunol.1301796
13. Langevin C, Aleksejeva E, Passoni G, Palha N, Levraud JP, Boudinot P. The antiviral innate immune response in fish: evolution and conservation of the IFN system. *J Mol Biol* (2013) 425(24):4904–20. doi:10.1016/j.jmb.2013.09.033
14. Zou J, Tafalla C, Truckle J, Secombes CJ. Identification of a second group of type I IFNs in fish sheds light on IFN evolution in vertebrates. *J Immunol* (2007) 179(6):3859–71. doi:10.4049/jimmunol.179.6.3859
15. Zhang YB, Gui JF. Molecular regulation of interferon antiviral response in fish. *Dev Comp Immunol* (2012) 38(2):193–202. doi:10.1016/j.dci.2012.06.003
16. Zou J, Secombes CJ. Teleost fish interferons and their role in immunity. *Dev Comp Immunol* (2011) 35(12):1376–87. doi:10.1016/j.dci.2011.07.001
17. Lopez-Munoz A, Roca FJ, Meseguer J, Mulero V. New insights into the evolution of IFNs: zebrafish group II IFNs induce a rapid and transient expression of IFN-dependent genes and display powerful antiviral activities. *J Immunol* (2009) 182(6):3440–9. doi:10.4049/jimmunol.0802528
18. Moresco EM, Beutler B. LGP2: positive about viral sensing. *Proc Natl Acad Sci U S A* (2010) 107(4):1261–2. doi:10.1073/pnas.0914011107
19. Chen X, Yang C, Su J, Rao Y, Gu T. LGP2 plays extensive roles in modulating innate immune responses in *Ctenopharyngodon idella* kidney (CIK) cells. *Dev Comp Immunol* (2015) 49(1):138–48. doi:10.1016/j.dci.2014.10.012
20. Childs K, Randall R, Goodbourn S. Paramyxovirus V proteins interact with the RNA Helicase LGP2 to inhibit RIG-I-dependent interferon induction. *J Virol* (2012) 86(7):3411–21. doi:10.1128/JVI.06405-11
21. Kato H, Takeuchi O, Sato S, Yoneyama M, Yamamoto M, Matsui K, et al. Differential roles of MDA5 and RIG-I helicases in the recognition of RNA viruses. *Nature* (2006) 441(7089):101–5. doi:10.1038/nature04734
22. Loo YM, Fornek J, Crochet N, Bajwa G, Perwitasari O, Martinez-Sobrido L, et al. Distinct RIG-I and MDA5 signaling by RNA viruses in innate immunity. *J Virol* (2008) 82(1):335–45. doi:10.1128/JVI.01080-07
23. David RYS, Combredet C, Sismeiro O, Dillies MA, Jagla B, Coppee JY, et al. Comparative analysis of viral RNA signatures on different RIG-I-like receptors. *Elife* (2016) 5:e11275. doi:10.7554/eLife.11275.001
24. Zou J, Chang M, Nie P, Secombes CJ. Origin and evolution of the RIG-I like RNA helicase gene family. *BMC Evol Biol* (2009) 9:85. doi:10.1186/1471-2148-9-85
25. Mu Y, Li M, Ding F, Ding Y, Ao J, Hu S, et al. *De novo* characterization of the spleen transcriptome of the large yellow croaker (*Pseudosciaena crocea*) and analysis of the immune relevant genes and pathways involved in the antiviral response. *PLoS One* (2014) 9(5):e97471. doi:10.1371/journal.pone.0097471
26. Ao J, Mu Y, Xiang LX, Fan D, Feng M, et al. Genome sequencing of the perciform fish *Larimichthys crocea* provides insights into molecular and genetic mechanisms of stress adaptation. *PLoS Genet* (2015) 11(4):e1005118. doi:10.1371/journal.pgen.1005118
27. Chen L, Su J, Yang C, Peng L, Wan Q, Wang L. Functional characterizations of RIG-I to GCRV and viral/bacterial PAMPs in grass carp *Ctenopharyngodon idella*. *PLoS One* (2012) 7(7):e42182. doi:10.1371/journal.pone.0042182
28. Yang C, Su J, Huang T, Zhang R, Peng L. Identification of a *retinoic acid-inducible gene I* from grass carp (*Ctenopharyngodon idella*) and expression analysis *in vivo* and *in vitro*. *Fish Shellfish Immunol* (2011) 30(3):936–43. doi:10.1016/j.fsi.2011.01.020
29. Su J, Huang T, Dong J, Heng J, Zhang R, Peng L. Molecular cloning and immune responsive expression of *MDA5* gene, a pivotal member of the RLR gene family from grass carp *Ctenopharyngodon idella*. *Fish Shellfish Immunol* (2010) 28(4):712–8. doi:10.1016/j.fsi.2010.01.009
30. Gu T, Rao Y, Su J, Yang C, Chen X, Chen L, et al. Functions of MDA5 and its domains in response to GCRV or bacterial PAMPs. *Fish Shellfish Immunol* (2015) 46(2):693–702. doi:10.1016/j.fsi.2015.08.005
31. Liao Z, Wan Q, Su J. Bioinformatics analysis of organizational and expressional characterizations of the IFNs, IRFs and CRFBs in grass carp *Ctenopharyngodon idella*. *Dev Comp Immunol* (2016) 61:97–106. doi:10.1016/j.dci.2016.03.020
32. Wang Y, Lu Y, Zhang Y, Ning Z, Li Y, Zhao Q, et al. The draft genome of the grass carp (*Ctenopharyngodon idellus*) provides insights into its evolution and vegetarian adaptation. *Nat Genet* (2015) 47(6):625–31. doi:10.1038/ng.3280
33. Prestridge DS. Predicting Pol II promoter sequences using transcription factor binding sites. *J Mol Biol* (1995) 249(5):923–32. doi:10.1006/jmbi.1995.0349
34. Rao Y, Su J, Yang C, Yan N, Chen X, Feng X. Dynamic localization and the associated translocation mechanism of HMGBs in response to GCRV challenge in CIK cells. *Cell Mol Immunol* (2015) 12(3):342–53. doi:10.1038/cmi.2014.55
35. Palmer I, Wingfield PT. Preparation and extraction of insoluble (inclusion-body) proteins from *Escherichia coli*. In: Coligan JE, Dunn BM, Speicher DW, Wingfield PT, editors. *Current Protocols in Protein Science*. United States: Wiley Interscience (1995). p. 6.3.1–6.3.15.
36. Hu YX, Guo JY, Shen L, Chen Y, Zhang ZC, Zhang YL. Get effective polyclonal antisera in one month. *Cell Res* (2002) 12(2):157–60. doi:10.1038/sj.cr.7290122
37. Sun F, Zhang YB, Liu TK, Gan L, Yu FF, Liu Y, et al. Characterization of fish IRF3 as an IFN-inducible protein reveals evolving regulation of IFN response in vertebrates. *J Immunol* (2010) 185(12):7573–82. doi:10.4049/jimmunol.1002401
38. Wan Q, Su J. Transcriptome analysis provides insights into the regulatory function of alternative splicing in antiviral immunity in grass carp (*Ctenopharyngodon idella*). *Sci Rep* (2015) 5:12946. doi:10.1038/srep12946
39. Su J, Zhang R, Dong J, Yang C. Evaluation of internal control genes for qRT-PCR normalization in tissues and cell culture for antiviral studies of grass carp (*Ctenopharyngodon idella*). *Fish Shellfish Immunol* (2011) 30(3):830–5. doi:10.1016/j.fsi.2011.01.006
40. Feng H, Zhang QM, Zhang YB, Li Z, Zhang J, Xiong YW, et al. Zebrafish IRF1, IRF3, and IRF7 differentially regulate IFNφ1 and IFNφ3 expression through assembly of homo- or heteroprotein complexes. *J Immunol* (2016) 197(5):1893–904. doi:10.4049/jimmunol.1600159
41. Schroder K, Hertzog PJ, Ravasi T, Hume DA. Interferon-gamma: an overview of signals, mechanisms and functions. *J Leukoc Biol* (2004) 75(2):163–89. doi:10.1189/jlb.0603252

42. Zaritsky LA, Bedsaul JR, Zoon KC. Virus multiplicity of infection affects type I interferon subtype induction profiles and interferon-stimulated genes. *J Virol* (2015) 89(22):11534–48. doi:10.1128/JVI.01727-15
43. Baig E, Fish EN. Distinct signature type I interferon responses are determined by the infecting virus and the target cell. *Antivir Ther* (2008) 13(3): 409–22.
44. Svingerud T, Solstad T, Sun B, Nyrud ML, Kileng O, Greiner-Tollersrud L, et al. Atlantic salmon type I IFN subtypes show differences in antiviral activity and cell-dependent expression: evidence for high IFNb/IFNc-producing cells in fish lymphoid tissues. *J Immunol* (2012) 189(12):5912–23. doi:10.4049/jimmunol.1201188
45. Aggad D, Mazel M, Boudinot P, Mogensen KE, Hamming OJ, Hartmann R, et al. The two groups of zebrafish virus-induced interferons signal via distinct receptors with specific and shared chains. *J Immunol* (2009) 183(6):3924–31. doi:10.4049/jimmunol.0901495
46. Wies E, Wang MK, Maharaj NP, Chen K, Zhou S, Finberg RW, et al. Dephosphorylation of the RNA sensors RIG-I and MDA5 by the phosphatase PP1 is essential for innate immune signaling. *Immunity* (2013) 38(3):437–49. doi:10.1016/j.immuni.2012.11.018
47. Kim MJ, Hwang SY, Imaizumi T, Yoo JY. Negative feedback regulation of RIG-I-mediated antiviral signaling by interferon-induced ISG15 conjugation. *J Virol* (2008) 82(3):1474–83. doi:10.1128/JVI.01650-07
48. Seth RB, Sun L, Ea CK, Chen ZJ. Identification and characterization of MAVS, a mitochondrial antiviral signaling protein that activates NF-κB and IRF3. *Cell* (2005) 122(5):669–82. doi:10.1016/j.cell.2005.08.012
49. Lauksund S, Svingerud T, Bergan V, Robertsen B. Atlantic salmon IPS-1 mediates induction of IFNa1 and activation of NF-kappaB and localizes to mitochondria. *Dev Comp Immunol* (2009) 33(11):1196–204. doi:10.1016/j.dci.2009.06.012
50. Besch R, Poeck H, Hohenauer T, Senft D, Hacker G, Berking C, et al. Proapoptotic signaling induced by RIG-I and MDA-5 results in type I interferon-independent apoptosis in human melanoma cells. *J Clin Invest* (2009) 119(8):2399–411. doi:10.1172/JCI37155
51. Yu X, Wang H, Li X, Guo C, Yuan F, Fisher PB, et al. Activation of the MDA-5–IPS-1 viral sensing pathway induces cancer cell death and type I interferon-dependent antitumor immunity. *Cancer Res* (2016) 76(8):2166–76. doi:10.1158/0008-5472.can-15-2142
52. Hotz C, Roetzer LC, Huber T, Sailer A, Oberson A, Treinies M, et al. TLR and RLR signaling are reprogrammed in opposite directions after detection of viral infection. *J Immunol* (2015) 195(9):4387–95. doi:10.4049/jimmunol.1500079
53. Jacobsen L, Calvin S, Lobenhofer E. Transcriptional effects of transfection: the potential for misinterpretation of gene expression data generated from transiently transfected cells. *Biotechniques* (2009) 47(1):617–24. doi:10.2144/000113132
54. Guo Y, Xiao P, Lei S, Deng F, Xiao GG, Liu Y, et al. How is mRNA expression predictive for protein expression? A correlation study on human circulating monocytes. *Acta Biochim Biophys Sin (Shanghai)* (2008) 40(5):426–36. doi:10.1111/j.1745-7270.2008.00418.x
55. Chen G, Gharib TG, Huang CC, Taylor JM, Misek DE, Kardia SL, et al. Discordant protein and mRNA expression in lung adenocarcinomas. *Mol Cell Proteomics* (2002) 1(4):304–13. doi:10.1074/mcp.M200008-MCP200
56. Yu Y, Hayward GS. The ubiquitin E3 ligase RAUL negatively regulates type i interferon through ubiquitination of the transcription factors IRF7 and IRF3. *Immunity* (2010) 33(6):863–77. doi:10.1016/j.immuni.2010.11.027
57. Higgs R, Gabhann JN, Larbi NB, Breen EP, Fitzgerald KA, Jefferies CA. The E3 ubiquitin ligase Ro52 negatively regulates IFN-β production post-pathogen recognition by polyubiquitin-mediated degradation of IRF3. *J Immunol* (2008) 181(3):1780–6. doi:10.4049/jimmunol.181.3.1780
58. Rigby RE, Rehwinkel J. RNA degradation in antiviral immunity and autoimmunity. *Trends Immunol* (2015) 36(3):179–88. doi:10.1016/j.it.2015.02.001
59. Ning S, Pagano JS, Barber GN. IRF7: activation, regulation, modification and function. *Genes Immun* (2011) 12(6):399–414. doi:10.1038/gene.2011.21
60. Ishikawa H, Barber GN. STING is an endoplasmic reticulum adaptor that facilitates innate immune signalling. *Nature* (2008) 455(7213):674–8. doi:10.1038/nature07317
61. Tanaka Y, Chen ZJ. STING specifies IRF3 phosphorylation by TBK1 in the cytosolic DNA signaling pathway. *Sci Signal* (2012) 5(214):ra20. doi:10.1126/scisignal.2002521
62. Reikine S, Nguyen JB, Modis Y. Pattern recognition and signaling mechanisms of RIG-I and MDA5. *Front Immunol* (2014) 5:342. doi:10.3389/fimmu.2014.00342
63. Feng X, Zhang Y, Yang C, Liao L, Wang Y, Su J. Functional characterizations of IPS-1 in CIK cells: potential roles in regulating IFN-I response dependent on IRF7 but not IRF3. *Dev Comp Immunol* (2015) 53(1):23–32. doi:10.1016/j.dci.2015.06.005
64. Xu L, Yu D, Fan Y, Peng L, Wu Y, Yao YG. Loss of RIG-I leads to a functional replacement with MDA5 in the Chinese tree shrew. *Proc Natl Acad Sci U S A* (2016) 113(39):10950–5. doi:10.1073/pnas.1604939113

Conflict of Interest Statement: The authors declare that the research was conducted in the absence of any commercial or financial relationships that could be construed as a potential conflict of interest.

frontiers in Immunology

ORIGINAL RESEARCH
published: 13 February 2017
doi: 10.3389/fimmu.2017.00121

Zebra Fish Lacking Adaptive Immunity Acquire an Antiviral Alert State Characterized by Upregulated Gene Expression of Apoptosis, Multigene Families, and Interferon-Related Genes

*Pablo García-Valtanen[1†], Alicia Martínez-López[1†], Azucena López-Muñoz[2], Melissa Bello-Perez[1], Regla M. Medina-Gali[1], María del Mar Ortega-Villaizán[1], Monica Varela[3], Antonio Figueras[3], Víctoriano Mulero[2], Beatriz Novoa[3], Amparo Estepa[1] and Julio Coll[4]**

[1] Departamento de Bioquímica, Universidad Miguel Hernández de Elche (UMH), Alicante, Spain, [2] Facultad de Biología, Departamento de Biología Celular e Histología, Universidad de Murcia, IMIB-Arrixaca, Murcia, Spain, [3] Instituto de Investigaciones Marinas (IIM), Consejo Superior de Investigaciones Científicas (CSIC), Vigo, Spain, [4] Departamento de Biotecnología, Instituto Nacional Investigación y Tecnología Agraria y Alimentaria (INIA), Madrid, Spain

OPEN ACCESS

Edited by:
Francesca Granucci,
University of Milano-Bicocca, Italy

Reviewed by:
Michaela Semeraro,
Institut Necker Enfants Malades, France
Silke Paust,
Baylor College of Medicine, USA

***Correspondence:**
Julio Coll
juliocoll@inia.es

†These authors have contributed equally to this work.

Specialty section:
This article was submitted to Molecular Innate Immunity, a section of the journal Frontiers in Immunology

Received: 14 October 2016
Accepted: 25 January 2017
Published: 13 February 2017

Citation:
García-Valtanen P, Martínez-López A, López-Muñoz A, Bello-Perez M, Medina-Gali RM, Ortega-Villaizán M, Varela M, Figueras A, Mulero V, Novoa B, Estepa A and Coll J (2017) Zebra Fish Lacking Adaptive Immunity Acquire an Antiviral Alert State Characterized by Upregulated Gene Expression of Apoptosis, Multigene Families, and Interferon-Related Genes. Front. Immunol. 8:121. doi: 10.3389/fimmu.2017.00121

To investigate fish innate immunity, we have conducted organ and cell immune-related transcriptomic as well as immunohistologic analysis in mutant zebra fish (*Danio rerio*) lacking adaptive immunity (*rag1*$^{-/-}$) at different developmental stages (egg, larvae, and adult), before and after infection with spring viremia carp virus (SVCV). The results revealed that, compared to immunocompetent zebra fish (*rag1*$^{+/+}$), *rag1*$^{-/-}$ acquired increased resistance to SVCV with age, correlating with elevated transcript levels of immune genes in skin/fins and lymphoid organs (head kidney and spleen). Gene sets corresponding to apoptotic functions, immune-related multigene families, and interferon-related genes were constitutively upregulated in uninfected adult *rag1*$^{-/-}$ zebra fish. Overexpression of activated CASPASE-3 in different tissues before and after infection with SVCV further confirmed increased apoptotic function in *rag1*$^{-/-}$ zebra fish. Concurrently, staining of different tissue samples with a pan-leukocyte antibody marker showed abundant leukocyte infiltrations in SVCV-infected *rag1*$^{-/-}$ fish, coinciding with increased transcript expression of genes related to NK-cells and macrophages, suggesting that these genes played a key role in the enhanced immune response of *rag1*$^{-/-}$ zebra fish to SVCV lethal infection. Overall, we present evidence that indicates that *rag1*$^{-/-}$ zebra fish acquire an antiviral alert state while they reach adulthood in the absence of adaptive immunity. This antiviral state was characterized by (i) a more rapid response to viral infection, which resulted in increased survival, (ii) the involvement of NK-cell- and macrophage-mediated transcript responses rather than B- and/or T-cell dependent cells, and (iii) enhanced apoptosis, described here for the first time, as well as the similar modulation of multigene family/interferon-related genes previously associated to fish that survived lethal viral infections. From this and other studies, it might be concluded that some of the characteristics of mammalian trained immunity are present in lower vertebrates.

Keywords: zebra fish *rag1*$^{-/-}$ adaptive deficient mutants, spring viremia carp viral infections, multigene families and apoptosis in resistance to viral infections, trained immunity NK/macrophages in fish, antiviral alert state

INTRODUCTION

Immunity against infections in vertebrate species includes both innate (early and unspecific) and adaptive (late and specific) responses. However, how these responses interact to exert coordinated immune responses during infection remains poorly understood, especially in primitive vertebrates such as fish. In contrast to the mammalian immune system, fish have only tetrameric IgM in their sera, which does not undergo IgM affinity maturation or isotype switch, elicit rapid but less-efficient adaptive secondary responses (1), and possess mucosal IgT and unique phagocytic B-cells (2). On the other hand, protection against fish pathogens seems to rely more heavily on innate rather than adaptive responses (2–4). Thus, fish species are suitable models to study the specific role of innate immunity during infections.

Recent research conducted in mammal species has revealed that cells of the innate immune system can be primed so that upon a secondary immune challenge they are capable of eliciting more efficient immune responses, a characteristic previously attributed only to the adaptive arm of the immune system. These types of innate responses have been termed trained immunity (5–10). Mammalian trained immunity has the following properties: (a) it enhances the speed and magnitude of the responses to second pathogen encounter similar to adaptive immunity, (b) it is acquired after exposure to a pathogen, not inherited, (c) it protects against unrelated pathogens, (d) it is mediated by macrophages (11, 12) and/or natural killer (NK)-cells (13–16) rather than by lymphocytes (17–19), and (e) it is generated by epigenetic reprogramming (alternative splicing, DNA/histone modifications, miRNA, etc.) rather than by genetic recombination (12, 20). Trained immunity phenomena are largely unexplored in fish species despite the fact that these primitive vertebrates offer suitable models to study the innate immune system. Nevertheless, some examples of innate immune responses presenting characteristics similar to those of mammalian trained immunity have been reported. For instance, salmonid vaccines against novirhabdoviruses also protect against unrelated nodaviruses (21) or spring viremia carp virus (SVCV) (22). Likewise, β-glucans, widely present in the cell wall of bacteria and fungi, have long-term effects on fish innate immune responses (23). Additionally, mutant zebra fish lacking adaptive immune responses maintain protective immune memory against secondary bacterial infections (24, 25), and the modulation of several innate immune multigene families was implicated in the rapid memory responses to rhabdoviral infection in fish that had previously survived infection with the same virus (26, 27). Further characterization of trained immunity or its equivalent innate immune response in fish species has the potential to drive research to develop new vaccine concepts. Thus, traditionally, successful vaccines candidates for vertebrate species are selected on the basis that they both contain the pathogen antigen(s) that elicit strong pathogen-specific T and B cell-mediated responses and confer protection. With increasing evidence that innate, unspecific protective responses are also elicited by some vaccines (28, 29), the possibility to develop vaccines against wider pathogen spectra (non-specific or heterologous vaccines) is actively being explored (30–32). For instance, non-specific vaccines could be obtained by (i) triggering still unknown multiple receptors to improve the simultaneous recognition of different pathogens (32) and/or generate immune synergies (33, 34), (ii) activating long-term specific NK cells to increase IFNγ and Th1 responses (13–15, 35), and/or (iii) designing novel molecular adjuvants. Innate trained immunity is likely to mediate some of vaccine unspecific, protective effects associated to epigenetic changes (19, 29, 36). Such non-specific vaccine strategies will be most practical for farmed fish vaccination because with short lifespans, heterologous vaccines would represent a more cost-effective alternative than traditional vaccines.

Mutant *rag1*$^{-/-}$ zebra fish (37) offer a new opportunity to explore innate responses to pathogens in the absence of adaptive immunity (24) and therefore explore trained immunity and new vaccination strategies. These mutants were generated by introducing a premature stop codon at *rag1t26683*, which resulted in the expression of a truncated, inactivated form of RAG1 (38, 39). Zebra fish *rag1*$^{-/-}$ mutants fail to undergo germ line V(D)J recombination in both immunoglobulin (*ig*) and T-cell receptor (*tcr*) gene variable segments (40–42). In turn, this leads to the absence of mature *igs/tcr* transcripts and reduced B- and T-cell numbers in lymphoid organs (head kidney and spleen), rendering *rag1*$^{-/-}$ zebra fish deficient in adaptive immunity (43–45). Despite this and the problems associated with breeding these fish compared with similar mutants in mice (46), *rag1*$^{-/-}$ zebra fish are capable of surviving in non-sterile aquarium facilities (47). In addition to this, *rag1*$^{-/-}$ zebra fish exhibit relatively enhanced immune responses to bacterial infections (25, 48, 49). However, whether the overall immune phenotype resulting from the *rag1*$^{-/-}$ genotype is acquired or inherited and whether similar phenotypes are also acquired after fish viral infections remains unclear. To investigate this, we have used *rag1*$^{-/-}$ zebra fish to correlate resistance to viral infection with innate gene expression levels (transcriptomic and cellular responses) in eggs, larvae, and adult *rag1*$^{-/-}$ zebra fish. Probably, due to the difficulties encountered when breeding *rag1*$^{-/-}$ zebra fish, their gene expression profiles, including changes in their transcriptome in response to viral infection, has yet to be compared to *rag1*$^{+/+}$ (49). Here, we have successfully raised enough numbers of *rag1*$^{-/-}$ zebra fish and compared their gene expression profiles in response to SVCV with those of *rag1*$^{+/+}$.

For this work, SVCV was chosen for the infection model because zebra fish are susceptible to this pathogen (50, 51), and the transcriptomic responses of zebra fish to SVCV infection by bath immersion have been investigated (52). SVCV is a rhabdovirus, recently classified within the *Sprivivirus* genus (53) that naturally infects cyprinid species, mainly carp species such as *Cyprinus carpio* (54, 55). The progress of the SVCV infection is externally associated with exophthalmia, abdominal distension, and petechial hemorrhages of the skin and gills. Moreover, most important fish lymphoid organs such as head kidney, spleen, and liver are also affected (55, 56). As with other rhabdoviruses, SVCV enters the fish *via* the base of the fins and skin (57). These tissues are of special importance in the initial response to infection of

rag1$^{-/-}$ by mycobacterial (47) or SVCV (17, 51). High zebra fish mortalities occur 5–10 days after SVCV water-born infection at 10–17°C, but at 26°C infected fish generate neutralizing antibodies increasing survival to the disease (52). At later stages of infection, SVCV virions are shed mostly with the feces and urine and may infect other fish (55, 56). *In vitro* replication of SVCV takes place in the cytoplasm of cells from different origins, including mammalian cells, but to obtain replication in these cells, temperatures must be maintained within 10–30°C with optimal virus growth at 20°C (56).

Our results suggest that while aging, and particularly during the period of time when *rag1*$^{-/-}$ zebra fish reach adulthood, the innate immune system gradually shifts from one that is underdeveloped and incapable of eliciting protective responses against SVCV infection (in the egg and larval stages) to one that exerts enhanced, antiviral protective responses, compared to adult age-matched *rag1*$^{+/+}$ zebra fish. This acquired antiviral alert state was characterized by constitutively upregulated transcripts (i.e., *fas, fasl, hsp90, casp7*, and *hspb*) and protein (activated CASPASE-3) levels of apoptosis effector molecules, which is described here for the first time. Additionally, *rag1*$^{-/-}$ zebra fish presented abundant infiltration of leukocytes in different non-lymphoid organs, and this coincided with elevated transcript expression of NK-cell, macrophage, apoptosis-, immune-related multigene families, and interferon-related genes. Partial resistance to SVCV challenge observed in naïve adult *rag1*$^{-/-}$ zebra fish suggests that in these fish innate immunity was enhanced and was able to mount efficient responses shortly after exposure to SVCV by bath immersion, contrary to their immunocompetent counterparts. Acquired, non-specific, enhanced innate immune responses in *rag1*$^{-/-}$ zebra fish resemble trained immunity responses in other vertebrate species. While the mechanisms of trained immunity or its equivalent in fish species have not been described yet, our work shows that the occurrence of similar immune phenomena is facilitated in *rag1*$^{-/-}$ zebra fish, indicating that this model could be particularly well suited for further studies of these immunological responses.

MATERIALS AND METHODS

Zebra Fish (*Danio rerio*)

Wild-type AB family founder zebra fish (*D. rerio*) were originally obtained from David Raible's fish facility at the University of Washington (USA). Mutant adult zebra fish recombinant activation gene (*rag1*$^{-/-}$) and wild type (*rag1*$^{+/+}$) were reproduced and characterized at the University of Murcia (Dr. Víctoriano Mulero). Adult zebra fish *rag1*$^{-/-}$ and *rag1*$^{+/+}$ were raised and genotyped when they reached 0.5–1 g (~6 months of age). Figure S1 in Supplementary Material shows the smaller size and apparent accelerated aging in *rag1*$^{-/-}$ fish, compared to *rag1*$^{+/+}$ fish. As we have experienced in three different laboratories (CSIC, UM, and UMH), *rag1*$^{-/-}$ zebra fish mutants are difficult to raise and even more to reproduce compared to similar mutants in mice (46). These difficulties may explain why few people could make experiments with them and why only heterozygous *rag1*$^{\pm}$ rather than homozygous *rag1*$^{-/-}$ have been used for microarray analysis (49). Zebra fish were maintained at 28°C in 30 l aquaria with tap-dechlorinated carbon-filtered water with 1 g of $CaCl_2$, 1 g of $NaHCO_3$, and 0.5 g of Instant Ocean sea salts added to water resulting in a conductivity of 200–300 μS and pH of 7.8–8.2. The aquaria were provided with biological filters and fish fed daily with a commercial feed diet. Previously to the infection experiments, all fish were acclimatized to 22°C for 2 weeks.

ZF4 Cell Culture and SVCV

The zebra fish embryonic fibroblast (ZF4) cell line (58) was purchased from the American Type Culture Collection (number CRL-2050). ZF4 cells were maintained at 28°C in a 5% CO_2 atmosphere in RPMI 1640-Dutch modified culture medium (Gibco, Invitrogen Co., UK) supplemented with 20 mM HEPES, 10% fetal calf serum (Sigma, St. Louis, MO, USA), 1 mM piruvate, 2 mM glutamine, 50 μg/ml of gentamicin, and 2.5 μg/ml of fungizone.

The SVCV isolate 56/70 (59, 60) was grown in ZF4 cells at 22°C in the presence of 2% fetal calf serum. Supernatants from ZF4 cell monolayers infected with SVCV were clarified by centrifugation at 4,000 × *g* for 30 min and kept in aliquots at −70°C until used as described before (22, 61, 62). Viral titers of SVCV were determined by methylcellulose plaque assays (56). Briefly, ZF4 cell monolayers were infected with different dilutions of SVCV in 24-well plates for 90 min. Then, the cell culture media were removed, wells covered with 2% methyl cellulose (Sigma, St. Louis, USA) in cell culture media and plates incubated at 22°C. After 5 days, the media were removed and cell monolayers stained with 1% crystal violet-formalin to count plaque forming units (pfu). Please note that SVCV was recently renamed *Carp Sprivivirus* (53). However, to avoid confusion we have kept the traditional name for this publication.

In Vivo Infection (Challenge) of Zebra Fish with SVCV

Spring viremia carp virus infections were conducted as in previous studies (22, 61, 62). Briefly, zebra fish were exposed to SVCV (10^3, 10^4, or 10^5 pfu/ ml) by bath immersion for 90 min at 22°C (optimal temperature for SVCV replication). Mock-infected zebra fish were incubated with cell culture medium in parallel experiments. After SVCV infection, zebra fish were transferred to tanks with clean water and kept at 22°C to allow the progress of SVCV infection to until tissues were harvested or challenges ended.

Transcript expression folds were evaluated at 2 days after infection. At this time point, higher percentages of genes are differentially transcribed in virally infected fish (63–71), no new viruses are yet released into the water and external SVCV infection symptoms start to appear (52).

To evaluate mortalities, SVCV infections were allowed to proceed during 33 days. From days 2 to 33, infected and non-infected zebra fish were monitored daily to remove those fish that presented external hemorrhages.

Ethic Statement of Zebra Fish Handling

During SVCV-induced mortalities, zebra fish were monitored 2–4 times per day and those with external hemorrhages killed by

an overdose of anesthetics (methanesulfonate 3-aminobenzoic acid ethyl ester, MS-222) (Sigma-Aldrich) to minimize their suffering (72). Zebra fish were killed by an overdose of MS-222 to extract their tissues. To date, there is no evidence that short exposure to MS-222 has measurable effects on gene expression (since maximum changes are found >2 days of infection) and the use of differential expression fold calculations should eliminate any small differences; however, this cannot be completely rule out since it may affect different genes differentially. Fish were handled in accordance with the National and European guidelines and regulations on laboratory animal care. All the experiments were performed using protocols approved by the European Union Council Guidelines (86/609/EU). Animal work was approved by the UMH, CSIC, UMU, or INIA corresponding Ethic Committees.

Determination of SVCV Titers in Zebra Fish Organs after Infection with SVCV

Viral titers in zebra fish were determined as described previously (61). Briefly, pooled internal organs, skin, and fins from four fish culled by exposure to MS-222 (see above) were disrupted and homogenized using a pestle, homogenized using a sterile nylon cell strainer (BD Falcon, MA, USA), resuspended in 3 ml of cell culture medium and passed through 0.2 μm sterile filters to remove bacterial contamination. Virus containing suspensions were assessed using the same methylcellulose method as above.

RNA Isolation from Different Zebra Fish Tissues

To evaluated transcript expression in zebra fish organs by reverse transcriptase and quantitative polymerase chain reaction (RTqPCR), caudal and pectoral fins and adjacent skin were excised from four to six adult zebra fish per group before and after SVCV infection. Additionally, whole larvae and embryo eggs were pooled ($n = 10$–20 fish) in each group. RNA was extracted using the E.Z.N.A HP Tissue RNA kit (Omega Bio-tek, Norcross, GA, USA) following manufacturer's instructions. Isolated RNAs were stored at −80°C until used.

For microarray analysis of *rag*$^{-/-}$ and *rag*$^{+/+}$ zebra fish 2 (SVCV infection) or 4 [poly(I:C) injection] experiments were carried out. In each group, head kidney and spleen from individual zebra fish were pooled to obtain enough RNA for hybridization. Pooled head kidneys and spleens ($n = 3$ fish) were immediately immersed in RNAlater (Ambion, Austin, TX, USA) at 4°C overnight before being frozen at −70°C until processed. RNA was extracted from sonicated (1 min × 3 times at 40 W in ice) organs using a commercial RNA isolation kit (RNeasy kit, Qiagen, Hilden, Germany). RNA concentrations were estimated with Nanodrop and the presence of 18 and 28 S bands confirmed by denatured RNA agar electrophoresis (Sigma, Che. Co, MS, USA).

Differential Expression of Selected Gene Set (sGS) by RTqPCR

To study innate/adaptive immune responses by RTqPCR in embryo eggs, larvae, and adult zebra fish in *rag1*$^{-/-}$ versus *rag1*$^{+/+}$ groups, a selected gene set (sGS) was chosen as representative genes of innate and adaptive responses based in our own and also other studies. The sGS contained the following groups of immune-related genes: (i) pro-inflammatory cytokines interleukin-1β (*il1b*) and tumor necrosis α (*tnfa*), (ii) innate immunity-related genes such as the virus-induced transcription factor interferon regulatory factor-3 (*irf3*), tank-binding kinase-1 (*tbk1*), which induces IRF3 in mammalian models, tripartite-motif-21 (*trim21*), which directs virions to the proteasome for proteolysis, interferon PHI3 (*ifnphi3*) implicated in antiviral alert innate/adaptive responses in zebra fish, and interferon-induced myxovirus resistance isoforms A–B (*mxab*) and C (*mxc*) important in the zebra fish response to rhabdoviral infections (26), (iii) effector proteins such as the antimicrobial peptide defensin 2-like (*defbl2*), which exhibits antiviral properties against SVCV (73), and the antibacterial protein released from NK-cells NK-LYSIN (*nklysin*) and, (iv) adaptive immunity-related genes such as the markers of helper and cytotoxic T lymphocytes cluster of differentiation 4 and 8 (*cd4* and *cd8a*, respectively), NK cell- and T cell-generated interferon gamma (*ifng*) produced after viral infections and finally immunoglobulin M (*igm*) a marker of mature B-cells. Their corresponding primers are listed in Table S1 in Supplementary Material.

To perform RTqPCR assays 1 μg of RNA was used to obtain cDNA using reverse transcriptase (Moloney murine leukemia virus, Invitrogen) as previously described (73). Quantitative PCR was performed using ABI PRISM 7300 (Applied Biosystems, NJ, USA) and SYBR Green PCR master mix (Life Technologies, UK). Reactions were prepared in 20 μl volume with 2 μl of cDNA, 900 nM of each primer (Table S1 in Supplementary Material) and 10 μl of SYBR Green PCR master mix. Non-template controls were included for each gene analysis. The cycling conditions were 95°C for 10 min, followed by 40 cycles at 65°C 1 min, 95°C for 1 min, and extension of 10 min. The results were analyzed using the $2^{-\delta\delta Ct}$ method (74). Each gene expression value was normalized by the formula, expression of each gene/expression of *ef1a*. Similar results were obtained using the sum of all gene expression values for normalization (not shown). Differential folds were then calculated by the formula, normalized expression of each *rag1*$^{-/-}$ gene/normalized expression of each *rag1*$^{+/+}$ gene.

Microarray Hybridization, GSEA, and mMPG Analysis

To target a larger amount of immune-related genes even those which are found in the lowest concentrations, we employed two formats of zebra fish 60-mer oligo microarrays: (i) immune-targeted in-house-designed microarray, Agilent's ID47562 in a 8 × 15 K format-containing 14,541 fully annotated sequences, previously described, validated (26, 52), and deposited in Gene Expression Omnibus GEO's GPL17670 (SVCV-infected zebra fish) and (ii) genome-wide commercial microarray Agilent's ID019161 in a 4 × 44 K format vs2-containing 43,803 partially annotated sequences.

To account for the biological effects arising from small changes in several related genes, we used our previously designed 104 gene

set (GS) collection (26). The GS collection was designed from immune-related sequences obtained from key-word searches at the GeneBank, KEGG, and WIKI human/zebra fish pathways (as accessed in 2012) plus new fish GS resulting from leading edge gene analysis (LEGA) of previously studied microarray results in VHSV (a rhabdovirus related to SVCV) survivors (26). Our GS collection was used here for analysis of *rag1*$^{-/-}$ and *rag1*$^{+/+}$ by gene set enrichment analysis (GSEA) (http://www.broad.mit.edu/GSEA) (75–77). GSEA assigns a normalized enrichment score (NES) to each GS calculating its corresponding false discovery rates (FDR) for significance evaluation of differential expression folds. The most stringent cut-off value of <0.05 (**) or <0.25 FDR (*) were used in this work for NES to determine statistical significance.

Samples labeled from 2 µg of high quality RNA (50 µg/ml) were hybridized to the microarrays by Nimgenetics (Cantoblanco, Madrid, Spain). Raw and normalized data were deposited in the GEO bank at http://www.ncbi.nlm.nih.gov/geo/query/acc.cgi?acc, at GSE54096 (SVCV-infected zebra fish) for the experiments performed at the INIA laboratory and at GSE91397 [poly(I:C)-injected zebra fish] for the experiments performed at the CSIC laboratory. Biological replicates were obtained from head kidney/spleens from 3 pooled zebra fish per replica. Normalized data from two (SVCV-infection) or four [poly(I:C) injection] biological replicas were downsized to about 2,000 unique annotated genes after removing repeated and non-annotated genes and/or genes having outlier fold values. The resulting gene lists were compared and ranked by the *t*-test statistic metric to calculate GSEA NES. The different genotype or phenotypes comparisons were labeled as A, *rag1*$^{-/-}$ versus *rag1*$^{+/+}$ genotypes; B, SVCV-infected or poly(I:C) injected *rag1*$^{-/-}$ phenotypes versus *rag1*$^{-/-}$ genotypes; or C, SVCV-infected or poly(I:C)-injected *rag1*$^{+/+}$ phenotypes versus *rag1*$^{+/+}$ genotype.

To search for modulated MultiPath Genes (mMPG), those genes present in >6 pathways were extracted as described before using the software Origin pro vs8.6 (Northampton, MA, USA) (52). After normalization, fluorescence outliers defined as values outside the means ± SDs, were first masked from mean calculations ($n = 2$). Folds were then calculated by applying the formula, normalized gene fluorescence value for each biological replica/non-infected mean. Fold outliers were then eliminated and their mean and SDs recalculated. Those MPG with folds >1.5 or <0.66, significant at the $p > 0.05$ level ($n = 2$ or 4) using the two-tail independent *t*-test, were considered modulated (mMPG).

Cellular Gene Sets Defining Specific Immune-Related Cells

We used the cellular gene sets (cGS) described before (26), for Th1, T helper 1 cells; Th2, T helper 2 cells; Th17, T helper 17 cells; Treg, T regulatory cells; BZ cells, mucosal IgZ producing cells; B-cells, IgM-producing cells; Dendritic, dendritic cells; CTL, antigen-specific cytotoxic cells; NK-cells, NK cells; macrophages, monocyte and macrophages; and Neutrophil, neutrophil and granulocyte cells. To define the cGS, activating, membrane, and secreted genes were searched for each cellular type from different sources. The resulting cGS were used as inputs for GSEA.

Histology and Immunohistochemistry

Zebra fish were euthanized with MS-222 (as described above) and a small incision made on the ventral body from the anus to the anterior part of the body cavity. They were then fixed in 10% buffered formalin, embedded in paraffin and cut in sections of 3 µm. Sections were stained with anti-human/mouse active CASPASE-3 antibody (R&D Systems, MN, USA), which recognizes a fully conserved epitope of zebra fish CASPASE-3 (78) or anti-human L-plastin antibody (Gene Tex, CA, USA). All sections were slightly counterstained with hematoxylin.

RESULTS

Embryos and Larvae *rag1*$^{-/-}$ Zebra Fish Do Not Possess Enhanced Innate Immunity

In non-sterile aquaria both *rag1*$^{-/-}$ and *rag1*$^{+/+}$ zebra fish survive early stages of development (egg/larvae) and reach adulthood. However, adult fish in each group present differences in their physical appearance. Commonly, *rag1*$^{-/-}$ are smaller and present features that are indicative of accelerated physical deterioration or aging (Figure S1 in Supplementary Material), in contrast to mice *rag1*$^{-/-}$ mutants. The contrast between the cleanliness of mouse rooms and that of fish tanks may explain such difficulties. Based on the above mentioned observations, we asked the question, is the innate immune function at early stages of development different in *rag1*$^{-/-}$ zebra fish?

To answer this question, we selected some immune genes that, based on our own and other publications, are regulated when zebra fish are exposed to pathogens. Our resulting selected gene set (sGS) included the genes of inflammatory cytokines (*il1b, tnfa*), innate immune transcription factors and effector molecules (*irf3, tbk1, trim21, ifnphi3, mxab, mxc*), antimicrobial peptides (*defbl2*, *nklysin*), and molecules involved in adaptive immune responses (*cd4, cd8, ifng, igm*).

Except for *ifnphi3*, and *mxab*, the all of the genes were downregulated (folds < 1) in *rag1*$^{-/-}$ egg embryos at 24 h post-fertilization (hpf), compared to *rag1*$^{+/+}$ eggs (**Figure 1A**). This indicated that immune factors directly inherited from the mother were less efficiently passed or absent in *rag1*$^{-/-}$ egg embryos, compared to embryos in the *rag1*$^{+/+}$group. Similarly, we evaluated the transcript expression folds (*rag1*$^{-/-}$ versus *rag1*$^{+/+}$) in hatched larvae at 72 hpf. The differential expression in *rag1*$^{-/-}$ larvae had increased relative to egg embryos, reaching levels similar to those of *rag1*$^{+/+}$ larvae (compare results from **Figure 1A** to those of **Figure 1B**). Next, we tested the resistance of zebra fish larvae to SVCV infection. In the conditions used for infection (10^4 pfu of SVCV per ml, 22°C), both *rag1*$^{-/-}$ and *rag1*$^{+/+}$ larvae were susceptible. However, survival rates were modest, 4.4% in *rag1*$^{-/-}$ and 16.6% in *rag1*$^{+/+}$ (**Figure 1C**), similar to those previously reported for *rag1*$^{+/+}$ larvae (51).

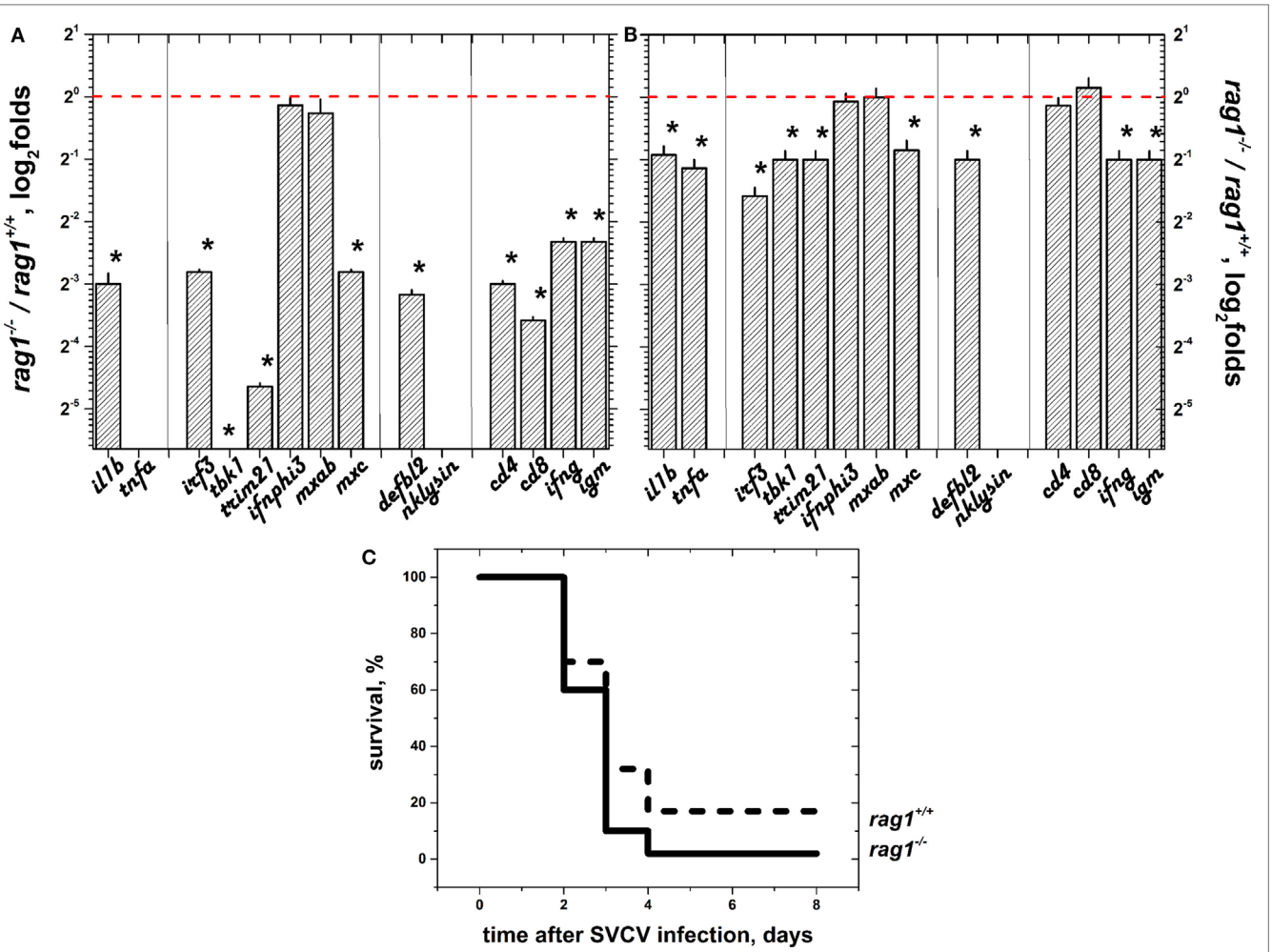

FIGURE 1 | Selected gene sets (sGS) were downregulated in *rag1*$^{-/-}$ egg embryos but were similar in early hatched larvae and both showed high mortalities when infected by spring viremia carp virus (SVCV). **(A)** Expression folds in embryo eggs 1 day after fertilization ($n = 60$). Reverse transcriptase and quantitative polymerase chain reaction data were first normalized by the formula, expression of each gene/expression of *ef1a*. Differential folds were then calculated by the formula, normalized expression of each *rag1*$^{-/-}$ gene/normalized expression of each *rag1*$^{+/+}$ gene. *Tbk1* fold was lower than 2^{-6} (not shown). *Tnfa* and *nklysin* were not done. Red dashed line, onefold boundary. *Statistically different from onefold with $p < 0.05$ by the *t*-test. **(B)** Expression folds in hatched larvae 3 days after fertilization ($n = 45$) calculated as in **(A)**. **(C)** Kaplan–Meier survival curves of naïve *rag1*$^{-/-}$ ($n = 90$) and *rag*$^{+/+}$ ($n = 90$) recently hatched larvae after bath infection in 10^4 pfu of SVCV per ml ($n = 2$) at 22°C (optimal replication for SVCV). Differences between *rag1*$^{-/-}$ and *rag*$^{+/+}$ survival curves of SVCV-infected larvae as determined by the Gehan–Breslow–Wilcoxon test were significant with $p < 0.05$ (*). Solid lines, *rag1*$^{-/-}$ larvae. Dashed lines, *rag*$^{+/+}$ larvae.

The fact that neither egg embryos nor larvae in the *rag1*$^{-/-}$ group showed upregulation in the expression of immune-related genes prior to SVCV infection or increased survival after SVCV infection, supports the idea that zebra fish need more time to develop an innate immune system to survive prolonged exposure to microorganisms in the water. To test this hypothesis, we then studied the innate immune response to SVCV infection in adult zebra fish.

SVCV Infection of Adult Zebra Fish Shows That Naïve *rag1*$^{-/-}$ Fish Are More Resistant Than Their *rag1*$^{+/+}$ Counterparts

When naïve *rag1*$^{-/-}$ or *rag1*$^{+/+}$ zebra fish of 6 months of age were infected by bath immersion with 10^4 pfu/ml of SVCV, there were neither infection symptoms nor deaths for the first 2 days after infection. At 3 days post-infection, zebra fish began to show external hemorrhagic symptoms in mouth, gills, lateral skin, and/or fin bases. Later on, 40–45% of adult *rag1*$^{-/-}$ zebra fish survived infection, while 100% of *rag1*$^{+/+}$ died in the first 12 days after infection (**Figure 2A**). Lower viral titers (~100-fold lower) observed in *rag1*$^{-/-}$ fish organs correlated with their delayed and lower mortality, compared to *rag1*$^{+/+}$ zebra fish (**Figure 2B**). Together, the mortality rates and viral loads observed in the viral challenge experiments suggest that *rag1*$^{-/-}$ individuals were capable of mounting an enhanced innate immune response in the absence of adaptive immunity, compared to fully immunocompetent *rag1*$^{+/+}$ zebra fish. Alternatively, the absence of antibody responses in *rag1*$^{-/-}$ could have caused less non-specific inflammation

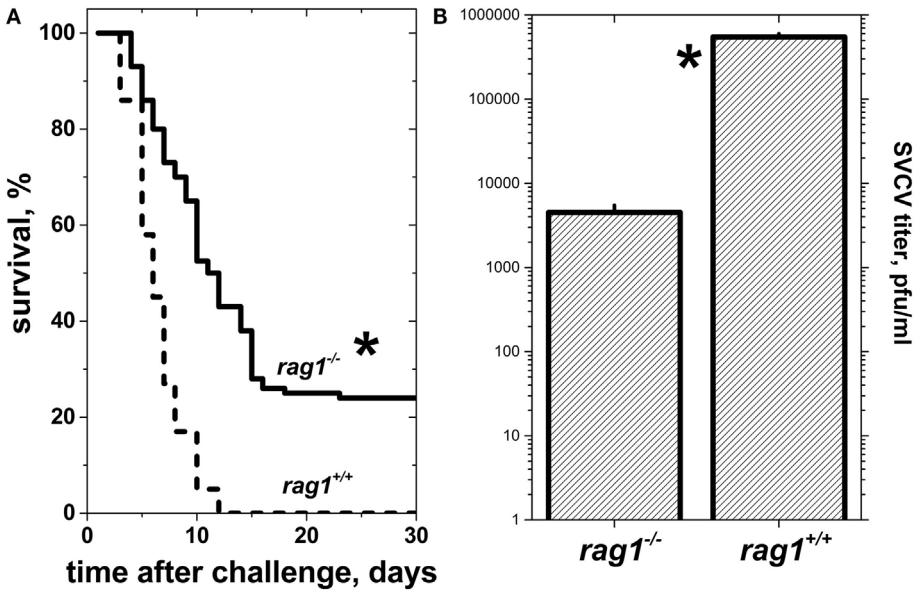

FIGURE 2 | **Naïve adult *rag1*$^{-/-}$ zebra fish are more resistant to lethal spring viremia carp virus (SVCV) infection than *rag1*$^{+/+}$ zebra fish**. **(A)** Kaplan–Meier survival curves of naïve *rag1*$^{-/-}$ ($n = 84$) and *rag*$^{+/+}$ ($n = 100$) adult zebra fish after exposure to a lethal dose of 10^4 pfu/ml of SVCV under the same challenge conditions as in panel **(A)**. *Statistically significant differences between survival curves between *rag1*$^{-/-}$ and *rag*$^{+/+}$ as determined by the Gehan–Breslow–Wilcoxon test with $p < 0.05$ ($n = 2$). Solid lines, *rag1*$^{-/-}$ zebra fish larvae. Dashed lines, *rag*$^{+/+}$ zebra fish larvae. **(B)** SVCV titers from pooled whole zebra fish ($n = 4$ zebra fish per genotype) 3 days after SVCV infection as determined by plaque forming unit (pfu) assays.

and less organ damage resulting in lower the mortality in this group. On the other hand, it is also possible that limitations of the antiviral innate response imposed by the adaptive immune system (i.e., antibodies) could explain higher mortalities in the *rag1*$^{+/+}$.

Increased Resistance to SVCV Infection in *rag1*$^{-/-}$ Adult Zebra Fish Is Accompanied by Increased Transcript Expression of Innate Immune-Related Genes in Skin and Fins

Because previous reports suggested the importance of the skin barrier in protecting zebra fish against viral infection and skin and fins are principal entry sites for SVCV (17, 47, 51), we studied the selected transcript differential expression in these organs. Before infection, all of the genes in the sGS except *irf3* were upregulated in skin/fins of adult *rag1*$^{-/-}$ (**Figure 3A**) with *nklysin* and *cd8* being the most upregulated. After SVCV infection, however, most of the individual gene differential expressions were reduced except for *irf3* and *nklysin* (**Figure 3B**). To note that *cd8* and *nklysin*, a marker for T cytotoxic cells and a gene highly expressed in both cytotoxic and NK-cells, respectively (79), were both upregulated before and after SVCV infection in *rag1*$^{-/-}$ zebra fish, suggesting that the participation of these cellular types are important in the antiviral response in these fish. These results indicate that transcription of the sGS genes is more active in naïve *rag1*$^{-/-}$ skin/fins fish than in *rag1*$^{+/+}$, an advantage for resisting SVCV infection. It is also worth noting that transcript expression folds for the genes upregulated in adult *rag1*$^{-/-}$ skin/fins correlated with folds of *rag1*$^{-/-}$ larvae with a Pearson's coefficient of 0.63 (using a polynomial fit) but not with those from embryo eggs (data not shown). Presently, whether the mechanisms that lead to the acquired overexpression of these genes in *rag1*$^{-/-}$ larvae involve epigenetic changes or other mechanisms is being evaluated but, for now, this is beyond the scope of this study.

Apoptosis-, Multigene Family, and Interferon-Related Genes Are Upregulated in Uninfected *rag1*$^{-/-}$ Adult Zebra Fish Lymphoid Organs

To further investigate the transcriptomic profile behind the enhanced survival of naïve adult *rag1*$^{-/-}$ after SVCV infection, transcript expression was estimated using both immune-targeted, in-house-designed, and commercially available genome wide microarrays. Analysis was performed in transcripts from pooled head kidneys (the analog of mammalian bone marrow) and spleens before and after SVCV infection or after poly(I:C) injection (to mimic viral replication intermediates). A total of 104 immune-related GSs and/or pathways obtained from keyword searches, KEGG, WIKI, and LEGA (see methods) were used to perform GS enrichment analysis (GSEA) and modulated multi-pathway gene (mMPG) analysis.

Table 1 shows that 25 out of the 104 GS were significantly modulated in at least one of the genotype/SVCV-infected phenotypes analyzed by GSEA using data obtained from the immune-targeted, in-house-designed microarrays. Of those 25 modulated GS, 18 (72%) were upregulated in uninfected *rag1*$^{-/-}$ fish, including 3 GS containing genes related to apoptosis.

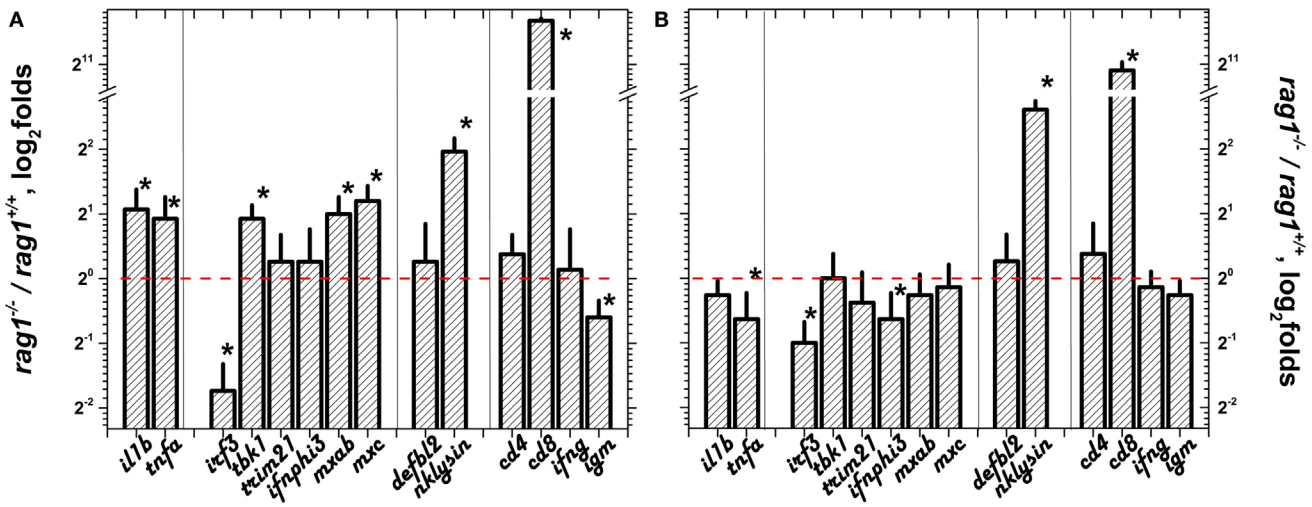

FIGURE 3 | Differential expression in skin/fins of adult zebra fish before and after spring viremia carp virus (SVCV) infection. The transcript differential expression folds of *rag1*$^{-/-}$/*rag1*$^{+/+}$ adult zebra fish in skin/fins were calculated as in **Figure 1**: **(A)** before infection and **(B)** 3 days after SVCV infection. Means and SDs were represented (n = 4–6 zebra fish). Red dashed line, onefold boundary. *Statistically different from onefold with $p < 0.05$ by the t-test.

TABLE 1 | Comparison of significant normalized enrichment scores (NESs) of gene sets (GSs) for *rag1*$^{-/-}$ genotype/spring viremia carp virus (SVCV)-infected phenotypes of adult zebra fish by gene set enrichment analysis (GSEA).

GS	GSor	A	B	C	1	2	3	4
5IFN + 4MX	L	2.31**	−1.53*	1.63*	X			X
7IFN + 5MX5 + 8TLR	L	2.25**	−1.50*	1.22	X			X
2348TLR + 12IFN	L	2.20**	−1.83**	0.77	X			
9CXCS (chemokines)	L	2.13**	−1.42	0.96				
MX (myxovirus-induced proteins)	KW	2.13**	−1.56	0.95	X			X
IFN (interferon)	KW	1.93**	−1.25	1.50	X			
278CASP (caspases)	L	1.88**	−1.86**	−0.97		X		
NITR (novel immune-type receptors)	KW	1.88**	−1.88**	1.04				X
Type II interferon signaling (ifng)	W	1.84**	−1.43	−0.76	X			
MHC (major histocompatibility complex)	KW	1.83**	−0.88	−0.99				
7ONCOS (oncogenes)	L	1.76**	−2.01**	0.85				
7TLR7CASP (toll-like recpt + caspases)	L	1.74**	−1.28	2.20**		X		
Cytosolic DNA-sensing pathway	K	1.69**	−1.42	0.84				
Intestinal immune network IgA	K	1.62**	−1.40	1.34				
AMP (antimicrobial peptides)	KW	1.61**	1.18	1.74**				
Apoptosis modulation by hsp70	W	1.59**	−1.16	0.79		X		
CHK (chemokines)	KW	1.57**	−0.72	1.37				
1CREB (transcription factors)	L	1.46*	−1.93**	−1.43				
Proteasome degradation	W	1.19	1.98**	1.16				X
COM (complement)	KW	0.82	1.37**	1.23			X	
Complement and coagulation cascades	K	−1.03	1.94**	1.79**			X	
1NFKB2NFKBIAB (NF-kB related)	L	−1.60*	−1.06	−3.07**				
CRP (c-reactive proteins)	KW	−2.20**	1.60**	−0.68				X
7MAPKS (MAP kinases)	L	−2.30**	2.33**	−1.10				
1IG3MAPK (MAP kinases)	L	−2.40**	2.01**	−2.05**				

*The immune-targeted in-house-designed microarray, Agilent's ID47562 in a 8 × 15 K format deposited in GEO's GPL17670 was used. Raw and normalized data were deposited in the GEO's GSE54096. GSor, GS origin. K, GS retrieved from human orthologous KEGG pathways. W, GS retrieved from human orthologous WIKI pathways. KW, GS retrieved from the GenBank data by searching zebra fish (Danio rerio) mRNA with key-words, briefly described within parenthesis. L, novel GS proposed by leading edge gene analysis (LEGA) of the differential transcription profiles from different zebra fish genotypes/phenotypes, including those previously described (26). The numbers before the LEGA gene names indicate the number of those genes in each GS. The significantly modulated GS were ordered by their NES values in (A). **False discovery rate (FDR) q value < 0.05. *FDR q value < 0.25. (A) rag1*$^{-/-}$ *versus rag1*$^{+/+}$ *genotypes. (B) SVCV-infected rag1*$^{-/-}$ *phenotype versus rag1*$^{-/-}$ *genotype. (C) SVCV-infected rag1*$^{+/+}$ *phenotype versus rag1*$^{+/+}$ *genotype. 1, GS of interferon-related TLR + IFN + MX genes. 2, GS related to apoptosis/caspases (gray rows). 3, GS related to complement. 4, GS related to multigene families modulated in VHSV survivors. 5, GS related to multigene families modulated in VHSV survivors.*

Upregulation of apoptosis-related genes in adult *rag1*$^{-/-}$ zebra fish is described here for the first time (**Table 1**, gray rows, columns A and 2). In addition to apoptosis, the multigene families "NITR" and "MX" (upregulated) or "CRP" and protein degradation *psm* genes (downregulated), which were previously associated to transcriptional changes in VHSV-survivor zebra fish phenotypes before and after reinfection (26), were also modulated in *rag1*$^{-/-}$ fish (**Table 1**, columns A and 4). Additionally, six upregulated GS contained well known interferon-related genes such as Toll-like receptors (*tlr*), interferons (*ifn*), and myxovirus-induced (*mx*) (**Table 1**, columns A and 1) or complement-related genes (**Table 1**, columns A and 3). Upregulation of interferon-related genes confirmed some of the data obtained in skin/fins in uninfected *rag1*$^{-/-}$ fish (**Figure 3A**), strongly suggesting that a systemic upregulation of many genes traditionally implicated in the response to viral infection occurred in the absence of virus. Other GS described here for the first time in relation to uninfected *rag1*$^{-/-}$ innate immunity were two GS related to chemokines ("CXCS" and "CHK") (**Table 1**, column A).

We then compared the modulated GS after SVCV infection in both genotypes (*rag1*$^{-/-}$ and *rag1*$^{+/+}$) using genotype-matched uninfected zebra fish to calculate differential expression folds. In *rag1*$^{-/-}$ fish, all of the GS that were upregulated in naïve fish were downregulated after SVCV infection (compare the 18 GS with upregulated NES in **Table 1**, column A with those in **Table 1**, column B). One possible explanation for such infection-induced downregulation could be that cell migration from internal lymphoid organs to peripheral tissues (i.e., viral entry tissues), reduces immune gene transcript levels in internal organs. On the contrary, GS that were downregulated in uninfected *rag1*$^{-/-}$ became upregulated after SVCV infection. For example, "Proteosome degradation" and "CRP" (**Table 1**, columns B and 4), complement (**Table 1**, columns B and 3), and others (**Table 1**, columns B) indicating an infection-induced response. On the other hand, SVCV infection of *rag1*$^{+/+}$ upregulated complement (**Table 1**, columns C and 4), 7TLR7CASP and AMP antimicrobial peptides (**Table 1**, columns C) GS.

Because some SVCV proteins have immunosuppressive effects (52, 80), we decided to study the differential expression fold profiles before and after injection of poly(I:C), a model for viral double-stranded RNA short-lived replication intermediates, in the absence of viral protein and their associated immunosuppressive effects. Thirty GS were modulated in at least one of the genotype/phenotypes when tested by GSEA using genome-wide microarrays (**Table 2**). In *rag1*$^{-/-}$ fish, 10 GS were upregulated, 4 of them containing genes related to apoptosis, coinciding with some of the results obtained in the same fish infected with SVCV (**Table 1** gray rows, columns A and 2). In addition, 3 GS contained interferon-related genes such as *tlr, ifn*, and/or *mx* genes (**Table 2**, columns A and 1). Poly (I:C) exclusively upregulated the GS "EGFR1 signaling pathway", "P13K-AKT signaling pathway" and "TGFB signaling wikipathway" (**Table 2**, columns A). It is worth noting that after being injected with poly(I:C), *rag1*$^{-/-}$ fish maintained similarly modulated GS than naïve fish (**Table 2**, columns B, 1, and 3), as opposed to what occurred in the same fish when infected with SVCV (**Table 1**, columns B). Interestingly, after injection with Poly (I:C), *rag1*$^{-/-}$ fish upregulated 5 GS participating in protein degradation pathways including, "Heat shock proteins," "Ubiquitin mediated proteolysis," "Protein processing in endoplasmic reticulum,", "Proteosome degradation," and "Protein export" (**Table 2**, columns B and 3). This suggests that there is a relationship between viral RNA intermediates and protein degradation pathways. In sharper contrast with SVCV infection, poly(I:C) injection of *rag1*$^{+/+}$ zebra fish, downregulated GS related to complement (**Table 2**, columns C and 4), suggesting opposite effects of SVCV and poly(I:C) regarding this pathway.

Gene set enrichment analysis of the data obtained in the SVCV infection and poly(I:C) injection experiments revealed important contributions of immune-related multigene families to the rapid defense mechanisms observed in *rag1*$^{-/-}$ fish. To some extent these results are in agreement with those from a previous study carried out with zebra fish which survived lethal VHSV infections. When reinfected, VHSV-survivor zebra fish responded more rapidly to infection due to a preceding modulation of specific innate multigene families, rather than to gene regulation in response to the virus (26). These multigene families containing 7–15 different genes each, included c-reactive proteins (*crp*), myxovirus-induced proteins (*mx*), novel immunoglobulin-type receptors (*nitr*), and proteasome subunit macropain proteins (*psm*). The regulation of these innate multigene families was indicative of responses similar to fish adaptive secondary responses, characterized by shorter lag times (1), rather than by both increased speed and magnitude of the response, as it ensues in mammal species. Because these multigene families present these similarities with adaptive memory responses and abundant gene polymorphisms (which allow for a higher variability), they are candidates for mediators of trained immunity or its equivalent in fish. Based on all the above commented results, it could be argued that in the absence of adaptive immunity, the continuous exposure to microorganisms present in the water activates compensatory innate immune mechanisms that lead to an antiviral alert state characterized by the modulation of apoptosis, multigene family and interferon-related transcripts that facilitate a more rapid and fish "adaptive"/memory-like response to pathogens, in this case a rhabdovirus.

Identification of Modulated Genes Common to Multiple Pathways (mMPG)

To identify modulated genes with high impact on network regulation in *rag1*$^{-/-}$ fish before and after viral infection, we performed a modulated MultiPath Gene (mMPG) analysis. In order to do this, fold data were extracted for genes that (i) were common to > 6 pathways, (ii) had a fold >1.5 or <0.66, and (iii) were significantly different ($p < 0.05$) from one of the 1.5/0.66-fold thresholds. The results showed that in uninfected *rag1*$^{-/-}$ fish several apoptosis-related mMPG were regulated, being *fas, faslg, hsp90, casp7*, and *hspb* the most upregulated (**Table 3** gray rows, column A, genes labeled with +), which confirms the importance of apoptosis for the survival of this genotype. Other important genes upregulated in the same fish included pro-inflammatory cytokine *il1b*, and the highly pleiotropic transcription factors *stat1a* and *stat3*. After infection with SVCV most of these mMPG were downregulated in *rag1*$^{-/-}$ fish (**Table 1**, column B), while

TABLE 2 | Comparison of significant normalized enrichment scores (NESs) of gene sets (GSs) for genotype/poly(I:C)-injected phenotypes of adult zebra fish by gene set enrichment analysis (GSEA).

GS	GSor	A	B	C	1	2	3	4	5
EGFR1 signaling pathway	W	1.92**	−0.68	0.62					
7IFN + 5MX5 + 8TLR	L	1.88**	2.17**	0.97	X				X
APO (Apoptosis)	KW	1.82*	1.82**	0.7		X			
Type II interferon signaling (IFNG)	W	1.77*	1.00	−1.03	X				
5IFN + 4MX	L	1.70*	2.17**	0.82	X				X
Apoptosis	K	1.69*	−0.42	0.65		X			
ApoptosisW	W	1.67*	0.78	0.67		X			
Apoptosis modulation by HSP70	W	1.65*	1.34	−0.89		X			
PI3K-AKT signaling pathway	K	1.64*	−0.63	0.55					
TGFB signaling wikipathway	W	1.64*	−1.25	−0.65					
7ONCOS (oncogenes)	L	1.59	−1.03	−0.76					
MAPK cascade	W	1.57	−0.72	0.77					
Interleukin5	W	1.56	−0.42	1.3					
BAC.MAPK + PIK	L	1.54	−1.40	−0.47					
23789CASPS	L	1.53	−0.80	0.81		X			
Alha6-beta4 integrin signaling	W	1.50	−1.62	−0.83					
278CASP	L	1.47	0.98	−1.16		X			
ONG (oncogenes)	KW	1.46	−1.02	−1.13					
FGF signaling pathway	W	1.45	−0.51	1.71					
P38 MAPK signaling pathway	W	1.44	0.74	−0.82					
MX (Myxovirus-induced proteins)	KW	1.39	1.66*	0.91	X				X
IFN (interferon)	KW	1.36	1.77*	−0.67	X				
COM (complement)	KW	1.13	−1.81*	−1.89*				X	
Complement and coagulation cascades	K	0.84	−1.15	−1.95*				X	
TLR (Toll-like receptors)	KW	0.17	1.54*	−1.18	X				
HSP (heat shock proteins)	KW	−0.76	1.55*	0.98			X		
Ubiquitin-mediated proteolysis	K	−1.12	1.66*	1.67			X		
Protein processing in endoplasmic reticulum	K	−1.14	1.56*	0.84			X		
Proteosome degradation	W	−1.43	2.55**	0.88			X		X
Protein export	K	−1.91**	2.14**	1.27			X		

The genome-wide microarray Agilent's ID019161 in a 4 × 44 K format vs2 was used. Raw and normalized data were deposited in the GEO's GSE91397. GSEA was performed as described in the legend of **Table 1**. ***False discovery rate (FDR) q value < 0.05. *FDR q value < 0.25. (A) rag1*$^{-/-}$ *versus rag1*$^{+/+}$ *genotypes. (B) Poly(I:C)-injected rag1*$^{-/-}$ *phenotype versus rag1*$^{-/-}$ *genotype. (C) Poly(I:C)-injected rag1*$^{+/+}$ *phenotype versus rag1*$^{+/+}$ *genotype. 1, GS of interferon-related TLR + IFN + MX genes. 2, GS related to apoptosis/caspases (gray rows). 3, GS related to proteolysis. 4, GS related to complement. 5, GS related to multigene families modulated in VHSV survivors.*

only *il1b*, *irf6*, and *hspb* were upregulated in SVCV-infected *rag1*$^{+/+}$ fish (**Table 3**, column C).

As expected, the level of immunoglobulin *igm* (probes designed against its heavy chain constant domain) was downregulated in uninfected *rag1*$^{-/-}$, compared to *rag1*$^{+/+}$ fish. However, the most intriguing data was the upregulation of *igm* in *rag1*$^{-/-}$ fish after infection with SVCV. This might reflect a host desperate attempt to activate *igm* constant domains in the presence of a pathogen, despite the absence of recombination of the variable domains. Thus, it is also possible that although there is no V(D)J recombination in *rag1*$^{-/-}$ mutants, some *igm* sterile transcription occurs, as previously suggested by others (81).

Active CASPASE-3 Contributes to the Antiviral Alert State before and after SVCV Infection in Adult rag1$^{-/-}$ Zebra Fish

Because apoptosis was likely to be important for the survival of *rag1*$^{-/-}$ fish based on the transcript upregulations of apoptosis-related GS (**Tables 1** and **2**) and mMPG (**Table 3**), we tested whether apoptosis was activated also at the protein level. To that end, we stained zebra fish head kidney, gut, skin, and liver with an anti-apoptosis protein antibody. For those experiments, we chose active CASPASE-3 because of its amplifying role in CASPASE-8-mediated mammalian/fish apoptosis (82, 83). Staining of uninfected histological sections revealed augmented positive staining in *rag1*$^{-/-}$ tissues compared to *rag1*$^{+/+}$ (**Figure 4A**). When tissues from SVCV-infected zebra fish were stained, active CASPASE-3 positive staining increased in both *rag1*$^{-/-}$ and *rag1*$^{+/+}$ fish (**Figure 4B**). Therefore, it could be argued that as part of the *rag1*$^{-/-}$ antiviral alert state both transcripts and proteins facilitate the rapid induction of apoptosis, which would help to eliminate virus-infected cells and increase survival.

Both the Level of Immune Cell-Specific Transcripts and Leukocyte Infiltration Are Increased in Uninfected *rag1*$^{-/-}$ Fish Tissues

Because of the lack of molecular markers for zebra fish immune cells, cGS including immune cell type-representative genes were designed as alternative markers in a previous study. The same

TABLE 3 | Modulated MultiPath Genes (mMPG) in genotype/spring viremia carp virus (SVCV)-infected phenotypes of adult zebra fish.

Gene		A		B		C		Gene description	Accession numbers
Symbols	#	Mean	SD	Mean	SD	Mean	SD		
hsp90+	8	5.03*	0.79	0.20*	0.16	0.79	0.15	Heat shock protein 90. beta	NM_198210
fas+	9	4.09*	0.27	0.61*	0.09	1.27	0.16	Fas (TNF receptor superfamily, member 6)	XM_685355
il1b	14	3.71*	0.47	0.42*	0.05	2.05*	0.34	Interleukin 1, beta	NM_212844
hspb+	7	3.51*	0.33	0.52*	0.04	2.27*	0.32	Heat shock protein. alpha-crystalline-related	NM 001008615
Ifih	7	2.78*	0.47	0.48*	0.02	0.78	0.04	Novel protein similar to vertebrate interferon	XM_689032
irf7	8	2.65*	0.17	0.80	0.05	1.29	0.16	Interferon regulatory factor 7	NM_200677
faslg+	11	2.38*	0.28	0.84	0.05	0.91	0.26	Fas ligand (TNF superfamily, member 6)	NM_001042701
casp7+	7	2.23*	0.07	0.55*	0.04	1.36	0.11	Caspase 7, apoptosis cysteine peptidase	NM_001020607
jak1	17	2.21*	0.14	0.76	0.07	1.25	0.12	Janus kinase 1	NM_131073
stat3	13	2.17*	0.24	0.80	0.10	1.18	0.07	Signal transduction/activation transcription 3	XM_002661113
stat1a	23	1.93*	0.15	1.00	0.18	1.21	0.17	Signal transduction/activation transcription 1a	NM_131480
Ikbke	9	1.90*	0.12	0.69	0.03	1.65	0.19	Inhibitor of kappa light polypeptide gene	NM_001002751
Tnfsf	8	1.82*	0.54	0.73	0.21	1.16	0.39	Tumor necrosis factor (ligand) superfamily	NM_001002593
inpp5d	7	1.75*	0.11	0.79	0.01	1.09	0.08	Inositol polyphosphate-5-phosphatase	XM_001922972
irf6	8	0.73	0.12	0.90	0.29	2.15*	0.56	Interferon regulatory factor 6	NM_200598
Igm	7	0.03*	0.01	0.73	0.04	0.51*	0.02	Ig heavy chain constant region home design	AY643753

*Modulated (differential expression folds > 1.5 or < 0.66) genes present in > 6 KEGG pathways (mMPG) were filtered/extracted from the microarray data. The mMPG were tabulated together with their corresponding mean folds (n = 2) and SDs, ordered by fold values in A. #, number of pathways per mMPG. The rest of the 154 MPG in the microarray were not modulated. *Significatively <0.66 or >1.5-fold at the p < 0.05 level by the t-test. (A) rag1*$^{-/-}$ *versus rag1*$^{+/+}$ *genotypes. (B) SVCV-infected rag1*$^{-/-}$ *phenotype versus rag1*$^{-/-}$ *genotype. (C) SVCV-infected rag1*$^{+/+}$ *phenotype versus rag1*$^{+/+}$*genotype. + and gray rows, apoptosis-related mMPG.*

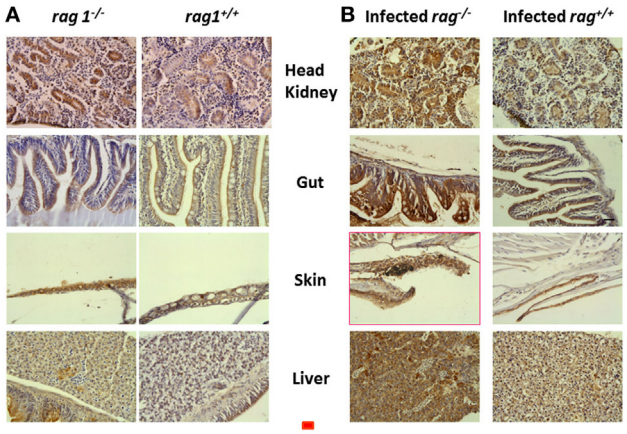

FIGURE 4 | Active CASPASE-3 staining in different tissues from uninfected and spring viremia carp virus (SVCV)-infected *rag1*$^{-/-}$ and *rag1*$^{+/+}$ adult zebra fish. Tissue sections from **(A)** uninfected and **(B)** SVCV-infected *rag1*$^{-/-}$ and *rag1*$^{+/+}$ adult zebra fish were stained by anti-human active CASPASE-3 antibody. Dark-stained areas in all *rag1*$^{-/-}$ tissues indicate the presence of active CASPASE-3. Images are representative of at least two independent experiments. Horizontal red line, 30 μm.

TABLE 4 | Comparison of normalized enrichment scores (NESs) obtained by using gene set enrichment analysis (GSEA) of cellular gene sets (cGS).

cGS	No. of genes per cGS	A	B	C
NK-cells	35	1.83**	−1.61**	−1.03
Macrophages	31	1.60*	−1.48*	0.96
TH17	37	1.51*	−1.58**	1.19
TH2	31	1.47*	−1.51*	1.11
Dendritic	10	1.29	−1.28*	1.05
BZ-cells	23	1.25	−1.08	1.51
B-cells	23	1.18	−1.03	1.47*
TH1	30	1.17	−1.64*	−0.93
Neutrophil	16	1.11	−0.86	1.44*
Treg	25	0.96	−1.44*	−1.12
CTL	12	−0.84	−1.04	−1.40

*The table shows the NES of each cGS on the different zebra fish genotype/spring viremia carp virus (SVCV)-infected phenotypes ordered by those of A. NK-cells, natural killer cells; macrophages, monocyte/macrophages; Th17, T-helper 17 cells; Th2, T-helper 2 cells; dendritic, dendritic cells; BZ cells, mucosal IgZ producing cells; B cells, serum IgM producing cells; Th1, T-helper 1 cells; Neutrophil, neutrophil and granulocyte cells; Treg, T regulatory cells; CTL, antigen-specific cytotoxic cells. **False discovery rate (FDR) q value < 0.05. *FDR q value < 0.25. (A) rag1*$^{-/-}$ *versus rag1*$^{+/+}$ *genotypes. (B) SVCV-infected rag1*$^{-/-}$ *phenotype versus rag1*$^{-/-}$ *genotype. (C) SVCV-infected rag1*$^{+/+}$ *phenotype versus rag1*$^{+/+}$ *genotype. Note that B-cells were upregulated only in SVCV-infected rag1*$^{+/+}$.

analysis was applied here to evaluate the relative importance of each particular cell type in the *rag1*$^{-/-}$ genotype before and after SVCV infection.

Transcripts from NK-cells and macrophages were the most upregulated cGS in uninfected *rag1*$^{-/-}$ fish (**Table 4**). Both NK-cells and macrophages have been identified in higher vertebrate models, as mediators of trained immunity (9, 11, 16, 18). In partial agreement with our results, *rag1*$^{-/-}$ zebra fish developed immune memory when immunized to *Edwardsiella ictaluri* (a pathogenic bacterium) through the participation of NK-cells (25). NK-cells are traditionally defined as cells of the innate immune system because they lack RAG recombinase-dependent antigen receptors. The comparison of candidate mechanisms for mediating mammalian antigen-specific NK cell memory with other examples of RAG-independent pathways that generate antigen receptor diversity in non-mammalian species such as

zebra fish, suggests that specific subsets of NK cells can develop long-lived and specific memory to a variety of antigens independent of B cells and T cells (13, 84). Most recently, antigen-specific NK cell responses to influenza and HIV viruses were induced in primates after infection and/or vaccination, an important opening for human vaccine improvement (13–15). T helper cell 17 (TH17) and TH2 were also upregulated in uninfected *rag1*$^{-/-}$ fish, contrary to other cellular types such as B-cells and neutrophils. Interestingly, all head kidney/spleen cellular types studied were downregulated in *rag1*$^{-/-}$ fish after SVCV infection, suggesting again that cellular migration to peripheral tissues ensues after infection. In contrast, in *rag1*$^{+/+}$ fish, B-cells and neutrophils were upregulated (**Table 4**).

Since the transcript data suggested that NK-cells and/or macrophages might infiltrate *rag1*$^{-/-}$ tissues, we stained the corresponding zebra fish tissue sections with an anti-L-plastin polyclonal antibody, a pan-leukocyte marker (85, 86), to explore for the presence of leukocytes in peripheral tissues. Leukocytes were abundant in significant amounts in zebra fish muscle and skin from uninfected *rag1*$^{-/-}$ fish (**Figure 5**). In contrast, equivalent tissue sections from *rag1*$^{+/+}$ fish showed limited leukocyte presence (**Figure 5**), confirming previous reports (45).

After recognizing different pathogen-associated molecular patterns, mammalian NK-cells and macrophages undergo epigenetic changes to become effector cells for trained immunity (9, 18). Our results showed that cell-specific gene expression and immunohistology data from *rag1*$^{-/-}$ zebra fish confirmed the increased function and/or activation of NK-cells/macrophages and leukocytes, respectively. Therefore, it could be argued that in *rag1*$^{-/-}$ zebra fish these cellular types mediate a shorter lag time responses that resemble adaptive responses in fish, consistent with trained immunity responses mediated by similar cells in other vertebrate models.

DISCUSSION

In this work, we show that the *rag1*$^{-/-}$ genotype that results in deficient adaptive immunity in zebra fish, favored the development of an acquired antiviral alert state that correlated with increased resistance to lethal infection with SVCV. A plausible explanation for the pre-existing antiviral alert state observed in uninfected *rag1*$^{-/-}$ fish could be that the continuous exposure to aquatic microbiota (present in the aquaria) induces increased and perhaps species-specific variation in transcriptional levels. Similarly, a continuous exposure to the remaining, latent virus could be the cause for the maintenance of similar antiviral states in immunocompetent zebra fish that survived VHSV infection (a related fish rhabdovirus infection) (26). Alternatively, the lower viral loads in *rag1*$^{-/-}$ fish could be reflecting that in the absence of adaptive immunity and antibodies, the innate immune response develops unchecked. On the contrary, in immunocompetent *rag1*$^{+/+}$ zebra fish, adaptive mechanisms (e.g., antibodies) would limit the innate antiviral response. In this hypothesis, the *rag1*$^{+/+}$ downregulation of innate genes may occur as a feed-back mechanism to prevent the host cell damage otherwise induced by uncontrolled upregulation of the innate response. If such feedback mechanisms are mediated by IgM antibodies, they would involve immunoglobulin receptors, hypothesis which could be tested by injecting zebra fish IgM into *rag1*$^{-/-}$ fish. In this context, it is known that in mammalians secreted IgG levels sensed by B-cell receptors (FcγRIIB) regulate IgM plasma levels (87). Since in zebra fish (88) or in any other fish (89, 90), only polymeric Ig receptors (PIGR/*pigr*) have been identified, any IgM feedback fish mechanism to control innate response levels through antibodies would, in principle require PIGR receptors. Therefore, anti-PIGR antibodies could also be used to block an hypothetical IgM feedback. Future experimentation addressing this and/or other hypothesis will help clarify the mechanism for maintaining the acquired adult *rag1*$^{-/-}$ fish antiviral alert state.

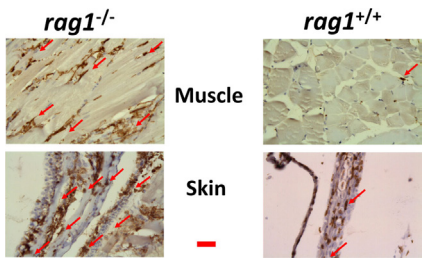

FIGURE 5 | Leukocyte infiltration in muscle and skin tissues in *rag1*$^{-/-}$ and *rag1*$^{+/+}$ adult zebra fish. Histological sections from muscle and skin tissues of *rag1*$^{-/-}$ and *rag1*$^{+/+}$ were stained with an antibody anti-L-plastin, a pan-leukocyte marker (dark-stained areas). Red arrows, examples of L-plastin stained cells. Images are representative of at least two independent experiments. Horizontal red line, 30 μm.

This acquired *rag1*$^{-/-}$ antiviral alert state included modulation of previously described immune multigene families and interferon-related genes in VHSV-survivor zebra fish, but the participation of apoptosis and putative NK-cells/macrophages (some of the characteristics of mammalian trained immunity) is described here for the first time. Nevertheless, although we introduced an original way to detect putative NK cells by using their transcript expression profiles (26), at present we cannot validate those results, since there are no zebra fish specific reagents available. On the other hand, resemblance in the modulation of multigene families (*mx*, *crp*, *nitr*, *psm*) between *rag1*$^{-/-}$ fish and VHSV-survivor *rag1*$^{+/+}$ zebra fish, suggests that those genes are important contributors to similar acquired antiviral alert states in both cases (genotypic and phenotypic, respectively). Because, some of the multigene families modulated in *rag1*$^{-/-}$ and survivor rag1$^{+/+}$ zebra fish (i.e., *nitr*) have orthologs linked to NK-cell memory in mammalian trained immunity (35), they might also be candidates for mediators of trained immunity or its equivalent in fish species.

As mentioned above, we have described apoptosis in *rag1*$^{-/-}$ fish as a factor that may contribute to the maintenance of their acquired antiviral alert state. The inhibition of early immune response of fish hosts by species-specific non-virion novirhabdoviral proteins (80, 91) or by other viral proteins in fish herpes virus CyHV-3 and/or SVCV (92), underline the importance that apoptosis or other alternative immune pathways may have as rapid mechanisms of defense against viruses in fish. The

presence of high levels of apoptosis-related transcripts and activated CASP-3 protein strongly suggests that apoptosis is associated with enhanced viral protection of *rag1*$^{-/-}$ zebra fish, possibly by eliminating viral-infected cells at an early stage of infection. In this regard, recent system biology approaches have confirmed that similar early pathogen/zebra fish crosstalks may explain the final outcome of many infections (93). In contrast, late apoptosis-dependent lysis of host cells favors viral spread, as described for several fish rhabdoviruses, including SVCV (92, 94–96), which indicates that a prompt activation is crucial for apoptosis to exert its antiviral role during rhabdoviral infections.

In this work, we have gathered immunohistochemical evidence that demonstrates that *rag1*$^{-/-}$ zebra fish maintain elevated numbers of leukocytes in peripheral tissues, compared to *rag1*$^{+/+}$ zebra fish. The differences are maintained before and after SVCV infection correlating with the increased resistance of *rag1*$^{-/-}$ fish to infection and the transcriptional downregulation of some immune genes in internal, lymphoid organs. All these results could be indicative of zebra fish cell migration (from lymphoid organs) as one of the mechanisms for eliciting rapid responses to viral infection. Thus, similar leukocyte cell migration has been previously shown to be altered in zebra fish during disease (97) and B-cell migration explained the high levels of plasma neutralizing antibodies in VHSV-survivor zebra fish coinciding with B-cell (IgM + cells by flow cytometry) depletion in lymphoid organs (26).

A growing number of studies in mammalian models have identified vaccine non-specific side effects, which may be explained by trained immunity. Non-specific effects of viral (e.g., measles or oral polio) and bacterial (BCG vaccine against tuberculosis or the diphtheria-tetanus-pertussis) vaccines have been shown to affect the survival of children with different outcomes (i.e., increased or decreased mortality) depending on the vaccine (98). Most recently, human studies showed that BCG immunization primes the immune system of adult individuals so that the subsequent BCG-unrelated immune responses to an influenza vaccine are enhanced, a phenomenon attributed to trained immunity (99). These studies and others suggest that non-specific vaccination effects could be harnessed to improve overall health. Our work shows how adult, adaptive immunity-deficient zebra fish exhibit increased resistance to a lethal viral infection with SVCV, contrary to larvae and most importantly adult, immunocompetent zebra fish. However, regardless of what event(s) or cue(s) trigger the development of enhanced immunity to SVCV in *rag1*$^{-/-}$ zebra fish, this model, integrating *rag1*$^{-/-}$ zebra fish and subsequent infections reproduces, at least to some extent, the development of non-specific, protective immunity *in vivo*. However, challenges with heterologous pathogens should be performed in the future to obtain evidence for such protectio against non-specific pathogens.

On the other hand, trained immunity in mammalians is associated to epigenetic reprogramming (e.g., cytosine methylations, histone acetylation/hypermethylation, or miRNA) (10, 12, 100) rather than genetic recombination of adaptive immune receptors (20). Here, we described permanent changes in the expression of immune genes in *rag1*$^{-/-}$ zebra fish, which resemble gene expression profile changes in zebra fish that survive lethal viral infections. Epigenetic changes in the vicinity of the promoters of these genes could explain, at least partially, how the baseline transcript expression is changed permanently in response to environmental stimuli (e.g., virus infection or microorganisms present in the water), as these genomic regions would be more or less accessible to transcription factors resulting in up or downregulation of specific genes. However, our knowledge of fish trained immunity (or its equivalent) and the availability of reagents and methods to investigate epigenetics in fish models remain scarce. For instance, in mammals, both the adaptive and trained immunity secondary responses (memory) are characterized by increased speed and magnitude, compared to primary responses (10, 12, 100). In contrast, fish adaptive secondary responses have been defined as more rapid but not bigger in magnitude than primary responses (1). Therefore, it would not be surprising that the observed increased survival of uninfected *rag1*$^{-/-}$ zebra fish, which clearly exhibit an antiviral alert state, was a product of the promptness and not magnitude of the response to SVCV. Overall, our results strongly indicate that maintaining elevated levels of innate immune transcripts/proteins, including apoptosis effector molecules, may be an efficient mechanism to provide rapid protection against lethal virus infections in the aquatic environment, at least in the absence of adaptive immunity (this work) and in fish, which have survived virus infections (26). The possible epigenetics that may be implicated remains to be investigated. The results of the studies reported here, in turn, raise unexpected questions, such as, is there a common on/off epigenetic switch triggering a unique antiviral alert state in both uninfected *rag1*$^{-/-}$ and viral survivor fish? Or, is the premature physical deterioration/aging observed in adult *rag1*$^{-/-}$ fish (Figure S1 in Supplementary Material) a physiological cost for maintaining a permanent antiviral alert state? In the future, studies such as this and similar future experimental setups using *rag1*$^{-/-}$ zebra fish should help answer these questions and other in relation to innate immunity in fish species.

AUTHOR CONTRIBUTIONS

PG-V performed infection experiments, RTqPCR at Elche and help in writing the MS. AM-L performed infection experiments and RTqPCR at Elche and wrote the first drafts. AL-M performed larval infection and immunohistochemical experiments at Murcia. MB-P performed infection experiments and care of rag mutants at Elche. RM-G performed infection experiments and care of rag mutants at Elche. MO-V controlled infection experimental set up at Elche. MV performed injection experiments and care of rag mutants at Vigo. AF analyzed the microarray data at Vigo. VM coordinated the larval infection and immunohistochemical experiments at Murcia and contributed to the writing of the MS. BN coordinated rag production at Vigo and contributed to the writing of the ms. AE coordinated the whole work at Elche and contributed to the writing of the MS. JC performed and analyzed microarray data at Madrid and coordinated and wrote the final MS.

ACKNOWLEDGMENTS

Thanks are especially due to co-author Dr. Amparo Estepa, who recently passed away. Dr. Amparo Estepa was a key contributor to the conception, direction, writing, and financing of this work for years. We thank the editor and two anonymous reviewers for their constructive commentaries which greatly contributed to improving the initially submitted manuscript. This work was supported by INIA project RTA2013-00008-00-00, CICYT project AGL2014-51773-C3, AGL2014-53190 REDC, BIO2011-23400, and BIO2014-52655-R of the Ministerio de Economía y Competitividad of Spain.

SUPPLEMENTARY MATERIAL

The Supplementary Material for this article can be found online at http://journal.frontiersin.org/article/10.3389/fimmu.2017.00121/full#supplementary-material.

REFERENCES

1. Bengten E, Wilson M. Antibody repertoires in fish. *Results Probl Cell Differ* (2015) 57:193–234. doi:10.1007/978-3-319-20819-0_9
2. Sunyer JO. Fishing for mammalian paradigms in the teleost immune system. *Nat Immunol* (2013) 14:320–6. doi:10.1038/ni.2549
3. Magnadottir B. Innate immunity of fish (overview). *Fish Shellfish Immunol* (2006) 20:137–51. doi:10.1016/j.fsi.2004.09.006
4. Ye J, Kaattari IM, Ma C, Kaattari S. The teleost humoral immune response. *Fish Shellfish Immunol* (2013) 35:1719–28. doi:10.1016/j.fsi.2013.10.015
5. Sun JC, Beilke JN, Lanier LL. Adaptive immune features of natural killer cells. *Nature* (2009) 457:557–61. doi:10.1038/nature07665
6. Sun Z, Cheng Z, Taylor CA, Mcconkey BJ, Thompson JE. Apoptosis induction by eIF5A1 involves activation of the intrinsic mitochondrial pathway. *J Cell Physiol* (2010) 223:798–809. doi:10.1002/jcp.22100
7. Netea MG, Quintin J, Van Der Meer JW. Trained immunity: a memory for innate host defense. *Cell Host Microbe* (2011) 9:355–61. doi:10.1016/j.chom.2011.04.006
8. Benn CS, Netea MG, Selin LK, Aaby P. A small jab – a big effect: nonspecific immunomodulation by vaccines. *Trends Immunol* (2013) 34:431–9. doi:10.1016/j.it.2013.04.004
9. Netea MG. Immunological memory in innate immunity. *J Innate Immun* (2014) 6:117–8. doi:10.1159/000357283
10. Netea MG, Joosten LA, Van Der Meer JW. Adaptation and memory in innate immunity. *Semin Immunol* (2016) 28:317–8. doi:10.1016/j.smim.2016.07.002
11. Holmes TD, Bryceson YT. Natural killer cell memory in context. *Semin Immunol* (2016) 28:368–76. doi:10.1016/j.smim.2016.05.008
12. Netea MG, Joosten LA. Master and commander: epigenetic regulation of macrophages. *Cell Res* (2016) 26:145–6. doi:10.1038/cr.2016.5
13. O'Leary JG, Goodarzi M, Drayton DL, Von Andrian UH. T cell- and B cell-independent adaptive immunity mediated by natural killer cells. *Nat Immunol* (2006) 7:507–16. doi:10.1038/ni1332
14. Paust S, Gill HS, Wang BZ, Flynn MP, Moseman EA, Senman B, et al. Critical role for the chemokine receptor CXCR6 in NK cell-mediated antigen-specific memory of haptens and viruses. *Nat Immunol* (2010) 11:1127–35. doi:10.1038/ni.1953
15. Reeves RK, Li H, Jost S, Blass E, Li H, Schafer JL, et al. Antigen-specific NK cell memory in rhesus macaques. *Nat Immunol* (2015) 16:927–32. doi:10.1038/ni.3227
16. Logie C, Stunnenberg HG. Epigenetic memory: a macrophage perspective. *Semin Immunol* (2016) 28:359–67. doi:10.1016/j.smim.2016.06.003
17. Vivier E, Raulet DH, Moretta A, Caligiuri MA, Zitvogel L, Lanier LL, et al. Innate or adaptive immunity? The example of natural killer cells. *Science* (2011) 331:44–9. doi:10.1126/science.1198687
18. Quintin J, Cheng SC, Van Der Meer JW, Netea MG. Innate immune memory: towards a better understanding of host defense mechanisms. *Curr Opin Immunol* (2014) 29:1–7. doi:10.1016/j.coi.2014.02.006
19. Sun JC, Ugolini S, Vivier E. Immunological memory within the innate immune system. *EMBO J* (2014) 33:1295–303. doi:10.1002/embj.201387651
20. Quintin J, Saeed S, Martens JH, Giamarellos-Bourboulis EJ, Ifrim DC, Logie C, et al. Candida albicans infection affords protection against reinfection via functional reprogramming of monocytes. *Cell Host Microbe* (2012) 12:223–32. doi:10.1016/j.chom.2012.06.006
21. Sommerset I, Lorenzen E, Lorenzen N, Bleie H, Nerland AH. A DNA vaccine directed against a rainbow trout rhabdovirus induces early protection against a nodavirus challenge in turbot. *Vaccine* (2003) 21:4661–7. doi:10.1016/S0264-410X(03)00526-7
22. Martinez-Lopez A, Garcia-Valtanen P, Ortega-Villaizan M, Chico V, Gomez-Casado E, Coll JM, et al. VHSV G glycoprotein major determinants implicated in triggering the host type I IFN antiviral response as DNA vaccine molecular adjuvants. *Vaccine* (2014) 32:6012–9. doi:10.1016/j.vaccine.2014.07.111
23. Petit J, Wiegertjes GF. Long-lived effects of administering beta-glucans: indications for trained immunity in fish. *Dev Comp Immunol* (2016) 64:93–102. doi:10.1016/j.dci.2016.03.003
24. Meijer AH, Spaink HP. Host-pathogen interactions made transparent with the zebrafish model. *Curr Drug Targets* (2011) 12:1000–17. doi:10.2174/138945011795677809
25. Hohn C, Petrie-Hanson L. Rag1$^{-/-}$ mutant zebrafish demonstrate specific protection following bacterial re-exposure. *PLoS One* (2012) 7:e44451. doi:10.1371/journal.pone.0044451
26. Estepa A, Coll J. Innate multigene family memories are implicated in the viral-survivor zebrafish phenotype. *PLoS One* (2015) 10:e0135483. doi:10.1371/journal.pone.0135483
27. Bello M, Falco A, Medina R, Encinar JA, Novoa B, Perez L, et al. Structure and functionalities of the human C-reactive protein compared to the zebrafish multigene family of c-reactive-like proteins. *Dev Comp Immunol* (2017) 69:33–40. doi:10.1016/j.dci.2016.12.001
28. Jensen KJ, Benn CS, Van Crevel R. Unravelling the nature of non-specific effects of vaccines-A challenge for innate immunologists. *Semin Immunol* (2016) 28:377–83. doi:10.1016/j.smim.2016.05.005
29. Netea MG, Joosten LA, Latz E, Mills KH, Natoli G, Stunnenberg HG, et al. Trained immunity: a program of innate immune memory in health and disease. *Science* (2016) 352:aaf1098. doi:10.1126/science.aaf1098
30. Lerm M, Netea MG. Trained immunity: a new avenue for tuberculosis vaccine development. *J Intern Med* (2016) 279:337–46. doi:10.1111/joim.12449
31. Saadatian-Elahi M, Aaby P, Shann F, Netea MG, Levy O, Louis J, et al. Heterologous vaccine effects. *Vaccine* (2016) 34:3923–30. doi:10.1016/j.vaccine.2016.06.020
32. Bowdish DM, Loffredo MS, Mukhopadhyay S, Mantovani A, Gordon S. Macrophage receptors implicated in the "adaptive" form of innate immunity. *Microbes Infect* (2007) 9:1680–7. doi:10.1016/j.micinf.2007.09.002
33. Napolitani G, Rinaldi A, Bertoni F, Sallusto F, Lanzavecchia A. Selected Toll-like receptor agonist combinations synergistically trigger a T helper type 1-polarizing program in dendritic cells. *Nat Immunol* (2005) 6:769–76. doi:10.1038/ni1223
34. Querec T, Bennouna S, Alkan S, Laouar Y, Gorden K, Flavell R, et al. Yellow fever vaccine YF-17D activates multiple dendritic cell subsets via TLR2, 7, 8, and 9 to stimulate polyvalent immunity. *J Exp Med* (2006) 203:413–24. doi:10.1084/jem.20051720
35. Martin-Fontecha A, Thomsen LL, Brett S, Gerard C, Lipp M, Lanzavecchia A, et al. Induced recruitment of NK cells to lymph nodes provides IFN-gamma for T(H)1 priming. *Nat Immunol* (2004) 5:1260–5. doi:10.1038/ni1138
36. Locati M, Mantovani A, Sica A. Macrophage activation and polarization as an adaptive component of innate immunity. *Adv Immunol* (2013) 120:163–84. doi:10.1016/B978-0-12-417028-5.00006-5
37. Wienholds E, Schulte-Merker S, Walderich B, Plasterk RH. Target-selected inactivation of the zebrafish rag1 gene. *Science* (2002) 297:99–102. doi:10.1126/science.1071762

38. Greenhalgh P, Steiner LA. Recombination activating gene 1 (Rag1) in zebrafish and shark. *Immunogenetics* (1995) 41:54–5. doi:10.1007/BF00188438
39. Willett CE, Cherry JJ, Steiner LA. Characterization and expression of the recombination activating genes (rag1 and rag2) of zebrafish. *Immunogenetics* (1997) 45:394–404. doi:10.1007/s002510050221
40. Willett CE, Zapata AG, Hopkins N, Steiner LA. Expression of zebrafish rag genes during early development identifies the thymus. *Dev Biol* (1997) 182:331–41. doi:10.1006/dbio.1996.8446
41. Li Z, Chang Y. V(D)J recombination in zebrafish: normal joining products with accumulation of unresolved coding ends and deleted signal ends. *Mol Immunol* (2007) 44:1793–802. doi:10.1016/j.molimm.2006.07.295
42. Zhong H, Li Z, Lin S, Chang Y. Initiation of V(D)J recombination in zebrafish (*Danio rerio*) ovaries. *Mol Immunol* (2007) 44:1784–92. doi:10.1016/j.molimm.2006.08.012
43. Steiner LA, Willett CE, Cherry JJ, Zapata A, Hopkins N. Expression of the rag genes of zebrafish identifies the thymus. *J Allergy ClinImmunol* (1997) 99:797–797.
44. Huttenhuis HB, Huising MO, Van Der Meulen T, Van Oosterhoud CN, Sanchez NA, Taverne-Thiele AJ, et al. Rag expression identifies B and T cell lymphopoietic tissues during the development of common carp (*Cyprinus carpio*). *Dev Comp Immunol* (2005) 29:1033–47. doi:10.1016/j.dci.2005.03.005
45. Petrie-Hanson L, Hohn C, Hanson L. Characterization of rag1 mutant zebrafish leukocytes. *BMC Immunol* (2009) 10:8. doi:10.1186/1471-2172-10-8
46. Mombaerts P, Iacomini J, Johnson RS, Herrup K, Tonegawa S, Papaioannou VE. RAG-1-deficient mice have no mature B and T lymphocytes. *Cell* (1992) 68:869–77. doi:10.1016/0092-8674(92)90030-G
47. Swaim LE, Connolly LE, Volkman HE, Humbert O, Born DE, Ramakrishnan L. *Mycobacterium marinum* infection of adult zebrafish causes caseating granulomatous tuberculosis and is moderated by adaptive immunity. *Infect Immun* (2006) 74:6108–17. doi:10.1128/IAI.00887-06
48. Trede NS, Langenau DM, Traver D, Look AT, Zon LI. The use of zebrafish to understand immunity. *Immunity* (2004) 20:367–79. doi:10.1016/S1074-7613(04)00084-6
49. Jima DD, Shah RN, Orcutt TM, Joshi D, Law JM, Litman GW, et al. Enhanced transcription of complement and coagulation genes in the absence of adaptive immunity. *Mol Immunol* (2009) 46:1505–16. doi:10.1016/j.molimm.2008.12.021
50. Sanders GE, Batts WN, Winton JR. Susceptibility of zebrafish (*Danio rerio*) to a model pathogen, spring viremia of carp virus. *Comp Med* (2003) 53:514–21.
51. Lopez-Munoz A, Roca FJ, Sepulcre MP, Meseguer J, Mulero V. Zebrafish larvae are unable to mount a protective antiviral response against waterborne infection by spring viremia of carp virus. *Dev Comp Immunol* (2010) 34:546–52. doi:10.1016/j.dci.2009.12.015
52. Encinas P, Garcia-Valtanen P, Chinchilla B, Gomez-Casado E, Estepa A, Coll J. Identification of multipath genes differentially expressed in pathway-targeted microarrays in zebrafish infected and surviving spring viremia carp virus (SVCV) suggest preventive drug candidates. *PLoS One* (2013) 8:e73553. doi:10.1371/journal.pone.0073553
53. ICTV Rhabdoviridae Study Group. *Implementation of Taxon-Wide Non-Latinized Binomial Species Names in the Family Rhabdoviridae*. Technical Report. Report number: ICTV [International Committee for Taxonomy of Viruses] Proposal (Taxoprop) No. 2015.006aM (2015). 9 p. Available from: https://talk.ictvonline.org/
54. Goodwin AE. Spring viremia of carp virus (SVCV): global status of outbreaks, diagnosis, surveillance, and research. *Isr J Aquac Bamidgeh* (2009) 61:180–7.
55. Ashraf U, Lu Y, Lin L, Yuan J, Wang M, Liu X. Spring viremia of carp virus: recent advances. *J Gen Virol* (2016) 97:1037–51. doi:10.1099/jgv.0.000436
56. Ahne W, Bjorklund HV, Essbauer S, Fijan N, Kurath G, Winton JR. Spring viremia of carp (SVC). *Dis Aquat Organ* (2002) 52:261–72. doi:10.3354/dao052261
57. Harmache A, Leberre M, Droineau S, Giovannini M, Bremont M. Bioluminescence imaging of live infected salmonids reveals that the fin bases are the major portal of entry for novirhabdovirus. *J Virol* (2006) 103:3655–9. doi:10.1128/JVI.80.7.3655-3659.2006
58. Driever W, Rangini Z. Characterization of a cell line derived from zebrafish (*Brachydanio rerio*) embryos. *In vitro Cell Dev Biol Anim* (1993) 294:749–54. doi:10.1007/BF02631432
59. Fijan N, Petrinec Z, Sulimanovic D, Zwillenberg LO. Isolation of the viral causative agent from the acute form of infectious dropsy of carp. *Vet Arch* (1971) 41:125–38.
60. Stone DM, Ahne W, Denham KL, Dixon PF, Liu CT, Sheppard AM, et al. Nucleotide sequence analysis of the glycoprotein gene of putative spring viraemia of carp virus and pike fry rhabdovirus isolates reveals four genogroups. *Dis Aquat Organ* (2003) 53:203–10.
61. Garcia-Valtanen P, Ortega-Villaizan Mdel M, Martinez-Lopez A, Medina-Gali R, Perez L, Mackenzie S, et al. Autophagy-inducing peptides from mammalian VSV and fish VHSV rhabdoviral G glycoproteins (G) as models for the development of new therapeutic molecules. *Autophagy* (2014) 10:1666–80. doi:10.4161/auto.29557
62. Ruyra A, Cano-Sarabia M, Garcia-Valtanen P, Yero D, Gibert I, Mackenzie SA, et al. Targeting and stimulation of the zebrafish (*Danio rerio*) innate immune system with LPS/dsRNA-loaded nanoliposomes. *Vaccine* (2014) 32:3955–62. doi:10.1016/j.vaccine.2014.05.010
63. Aoki T, Nam BH, Hirono II, Yamamoto E. Sequences of 596 cDNA clones (565,977 bp) of Japanese flounder (*Paralichthys olivaceus*) leukocytes infected with hirame rhabdovirus. *Mar Biotechnol (NY)* (1999) 1:477–88. doi:10.1007/PL00011804
64. Nam BH, Yamamoto E, Hirono I, Aoki T. A survey of expressed genes in the leukocytes of Japanese flounder, *Paralichthys olivaceus*, infected with hirame rhabdovirus. *Dev Comp Immunol* (2000) 24:13–24. doi:10.1016/S0145-305X(99)00058-0
65. Byon JY, Ohira T, Hirono I, Aoki T. Use of a cDNA microarray to study immunity against viral hemorrhagic septicemia (VHS) in Japanese flounder (*Paralichthys olivaceus*) following DNA vaccination. *Fish Shellfish Immunol* (2005) 18:135–47. doi:10.1016/j.fsi.2004.06.008
66. Kurobe T, Yasuike M, Kimura T, Hirono I, Aoki T. Expression profiling of immune-related genes from Japanese flounder *Paralichthys olivaceus* kidney cells using cDNA microarrays. *Dev Comp Immunol* (2005) 29:515–23. doi:10.1016/j.dci.2004.10.005
67. von Schalburg KR, Rise ML, Cooper GA, Brown GD, Gibbs AR, Nelson CC, et al. Fish and chips: various methodologies demonstrate utility of a 16,006-gene salmonid microarray. *BMC Genomics* (2005) 6:126. doi:10.1186/1471-2164-6-126
68. Byon JY, Ohira T, Hirono I, Aoki T. Comparative immune responses in Japanese flounder, *Paralichthys olivaceus* after vaccination with viral hemorrhagic septicemia virus (VHSV) recombinant glycoprotein and DNA vaccine using a microarray analysis. *Vaccine* (2006) 24:921–30. doi:10.1016/j.vaccine.2005.08.087
69. Purcell MK, Nichols KM, Winton JR, Kurath G, Thorgaard GH, Wheeler P, et al. Comprehensive gene expression profiling following DNA vaccination of rainbow trout against infectious hematopoietic necrosis virus. *Mol Immunol* (2006) 43:2089–106. doi:10.1016/j.molimm.2005.12.005
70. Yasuike M, Kondo H, Hirono I, Aoki T. Difference in Japanese flounder, *Paralichthys olivaceus* gene expression profile following hirame rhabdovirus (HIRRV) G and N protein DNA vaccination. *Fish Shellfish Immunol* (2007) 23:531–41. doi:10.1016/j.fsi.2006.12.006
71. MacKenzie S, Balasch JC, Novoa B, Ribas L, Roher N, Krasnov A, et al. Comparative analysis of the acute response of the trout, *O. mykiss*, head kidney to in vivo challenge with virulent and attenuated infectious hematopoietic necrosis virus and LPS-induced inflammation. *BMC Genomics* (2008) 9:141. doi:10.1186/1471-2164-9-141
72. Huang WC, Hsieh YS, Chen IH, Wang CH, Chang HW, Yang CC, et al. Combined use of MS-222 (tricaine) and isoflurane extends anesthesia time and minimizes cardiac rhythm side effects in adult zebrafish. *Zebrafish* (2010) 7:297–304. doi:10.1089/zeb.2010.0653
73. Garcia-Valtanen P, Martinez-Lopez A, Ortega-Villaizan M, Perez L, Coll JM, Estepa A. In addition to its antiviral and immunomodulatory properties, the zebrafish beta-defensin 2 (zfBD2) is a potent viral DNA vaccine molecular adjuvant. *Antiviral Res* (2014) 101:136–47. doi:10.1016/j.antiviral.2013.11.009
74. Livak KL, Schmittgen TD. Analysis of relative gene expression data using real-time quantitative PCR and the 2-DDCT method. *Methods* (2001) 25:402–8. doi:10.1006/meth.2001.1262
75. Subramanian A, Tamayo P, Mootha VK, Mukherjee S, Ebert BL, Gillette MA, et al. Gene set enrichment analysis: a knowledge-based approach for

interpreting genome-wide expression profiles. *Proc Natl Acad Sci U S A* (2005) 102:15545–50. doi:10.1073/pnas.0506580102
76. Subramanian A, Kuehn H, Gould J, Tamayo P, Mesirov JP. GSEA-P: a desktop application for Gene Set Enrichment Analysis. *Bioinformatics* (2007) 23:3251–3. doi:10.1093/bioinformatics/btm369
77. Tamayo P, Steinhardt G, Liberzon A, Mesirov JP. The limitations of simple gene set enrichment analysis assuming gene independence. *Stat Methods Med Res* (2012) 25:472–87. doi:10.1177/0962280212460441
78. Roca FJ, Mulero I, Lopez-Munoz A, Sepulcre MP, Renshaw SA, Meseguer J, et al. Evolution of the inflammatory response in vertebrates: fish TNF-alpha is a powerful activator of endothelial cells but hardly activates phagocytes. *J Immunol* (2008) 181:5071–81. doi:10.4049/jimmunol.181.7.5071
79. Andersson M, Gunne H, Agerberth B, Boman A, Bergman T, Sillard R, et al. NK-lysin, a novel effector peptide of cytotoxic T and NK cells. Structure and cDNA cloning of the porcine form, induction by interleukin 2, antibacterial and antitumour activity. *EMBO J* (1995) 14:1615–25.
80. Chinchilla B, Encinas P, Estepa A, Coll JM, Gomez-Casado E. Transcriptome analysis of rainbow trout in response to non-virion (NV) protein of viral haemorrhagic septicaemia virus (VHSV). *Appl Microbiol Biotechnol* (2015) 99:1827–43. doi:10.1007/s00253-014-6366-3
81. Calame KL. Mechanisms that regulate immunoglobulin gene expression. *Annu Rev Immunol* (1985) 3:159–95. doi:10.1146/annurev.iy.03.040185.001111
82. Hong JR, Huang LJ, Wu JL. Aquatic birnavirus induces apoptosis through activated caspase-8 and -3 in a zebrafish cell line. *J Fish Dis* (2005) 28:133–40. doi:10.1111/j.1365-2761.2004.00604.x
83. Rojas V, Guzmán F, Valenzuela C, Marshall SG, Mercado L. Development of a caspase-3 antibody as a tool for detecting apoptosis in cells from rainbow trout (*Oncorhynchus mykiss*). *Electron J Biotechnol* (2012) 15:12. doi:10.2225/vol15-issue5-fulltext-16
84. Paust S, von Andrian UH. Natural killer cell memory. *Nat Immunol* (2011) 12:500–8. doi:10.1038/ni.2032
85. Crowhurst MO, Layton JE, Lieschke GJ. Developmental biology of zebrafish myeloid cells. *Int J Dev Biol* (2002) 46:483–92.
86. Berman JN, Kanki JP, Look AT. Zebrafish as a model for myelopoiesis during embryogenesis. *Exp Hematol* (2005) 33:997–1006. doi:10.1016/j.exphem.2005.06.010
87. Montaudouin C, Anson M, Hao Y, Duncker SV, Fernandez T, Gaudin E, et al. Quorum sensing contributes to activated IgM-secreting B cell homeostasis. *J Immunol* (2013) 190:106–14. doi:10.4049/jimmunol.1200907
88. Akula S, Mohammadamin S, Hellman L. Fc receptors for immunoglobulins and their appearance during vertebrate evolution. *PLoS One* (2014) 9:e96903. doi:10.1371/journal.pone.0096903
89. Hamuro K, Suetake H, Saha NR, Kikuchi K, Suzuki Y. A teleost polymeric Ig receptor exhibiting two Ig-like domains transports tetrameric IgM into the skin. *J Immunol* (2007) 178:5682–9. doi:10.4049/jimmunol.178.9.5682
90. Zhang YA, Salinas I, Li J, Parra D, Bjork S, Xu Z, et al. IgT, a primitive immunoglobulin class specialized in mucosal immunity. *Nat Immunol* (2010) 11:827–35. doi:10.1038/ni.1913
91. Ammayappan A, Vakharia VN. Nonvirion protein of novirhabdovirus suppresses apoptosis at the early stage of virus infection. *J Virol* (2011) 85:8393–402. doi:10.1128/JVI.00597-11
92. Miest JJ, Adamek M, Pionnier N, Harris S, Matras M, Rakus KL, et al. Differential effects of alloherpesvirus CyHV-3 and rhabdovirus SVCV on apoptosis in fish cells. *Vet Microbiol* (2015) 176:19–31. doi:10.1016/j.vetmic.2014.12.012
93. Wu CC, Chen BS. A systems biology approach to the coordination of defensive and offensive molecular mechanisms in the innate and adaptive host-pathogen interaction networks. *PLoS One* (2016) 11:e0149303. doi:10.1371/journal.pone.0149303
94. Imajoh M, Hirayama T, Oshima S. Frequent occurrence of apoptosis is not associated with pathogenic infectious pancreatic necrosis virus (IPNV) during persistent infection. *Fish Shellfish Immunol* (2005) 18:163–77. doi:10.1016/j.fsi.2004.07.002
95. Chiu CL, Wu JL, Her GM, Chou YL, Hong JR. Aquatic birnavirus capsid protein, VP3, induces apoptosis via the Bad-mediated mitochondria pathway in fish and mouse cells. *Apoptosis* (2010) 15:653-68. doi:10.1007/s10495-010-0468-x
96. Kim MS, Lee JA, Kim KH. Effects of a broad-spectrum caspase inhibitor, Z-VAD(OMe)-FMK, on viral hemorrhagic septicemia virus (VHSV) infection-mediated apoptosis and viral replication. *Fish Shellfish Immunol* (2016) 51:41–5. doi:10.1016/j.fsi.2016.02.021
97. Deng Q, Huttenlocher A. Leukocyte migration from a fish eye's view. *J Cell Sci* (2012) 125:3949–56. doi:10.1242/jcs.093633
98. Sankoh O, Welaga P, Debpuur C, Zandoh C, Gyaase S, Poma MA, et al. The non-specific effects of vaccines and other childhood interventions: the contribution of INDEPTH health and demographic surveillance systems. *Int J Epidemiol* (2014) 43:645–53. doi:10.1093/ije/dyu101
99. Leentjens J, Kox M, Stokman R, Gerretsen J, Diavatopoulos DA, Van Crevel R, et al. BCG vaccination enhances the immunogenicity of subsequent influenza vaccination in healthy volunteers: a randomized, placebo-controlled pilot study. *J Infect Dis* (2015) 212:1930–8. doi:10.1093/infdis/jiv332
100. Topfer E, Boraschi D, Italiani P. Innate immune memory: the latest frontier of adjuvanticity. *J Immunol Res* (2015) 2015:478408. doi:10.1155/2015/478408

Conflict of Interest Statement: The authors declare that the research was conducted in the absence of any commercial or financial relationships that could be construed as a potential conflict of interest.

frontiers in Immunology

CORRECTION
published: 13 June 2017
doi: 10.3389/fimmu.2017.00668

Corrigendum: Zebra Fish Lacking Adaptive Immunity Acquire an Antiviral Alert State Characterized by Upregulated Gene Expression of Apoptosis, Multigene Families, and Interferon-Related Genes

*Pablo García-Valtanen[1†], Alicia Martínez-López[1†], Azucena López-Muñoz[2], Melissa Bello-Perez[1], Regla M. Medina-Gali[1], María del Mar Ortega-Villaizán[1], Monica Varela[3], Antonio Figueras[3], Víctoriano Mulero[2], Beatriz Novoa[3], Amparo Estepa[1] and Julio Coll[4]**

[1] Departamento de Bioquímica, Universidad Miguel Hernández de Elche (UMH), Alicante, Spain, [2] Facultad de Biología, Departamento de Biología Celular e Histología, Universidad de Murcia, IMIB-Arrixaca, Murcia, Spain, [3] Instituto delnvestigaciones Marinas (IIM), Consejo Superior de Investigaciones Científicas (CSIC), Vigo, Spain, [4] Departamento de Biotecnología, Instituto Nacional Investigación y Tecnología Agraria y Alimentaria (INIA), Madrid, Spain

Keywords: zebra fish rag1$^{-/-}$ adaptive deficient mutants, spring viremia carp viral infections, multigene families and apoptosis in resistance to viral infections, trained immunity NK/macrophages in fish, antiviral alert state

OPEN ACCESS

Edited and Reviewed by:
Francesca Granucci, University of Milano-Bicocca, Italy

****Correspondence:***
Julio Coll
juliocoll@inia.es

[†]These authors have contributed equally to this work.

Specialty section:
This article was submitted to Molecular Innate Immunity, a section of the journal Frontiers in Immunology

Received: *29 April 2017*
Accepted: *23 May 2017*
Published: *13 June 2017*

Citation:
García-Valtanen P, Martínez-López A, López-Muñoz A, Bello-Perez M, Medina-Gali RM, del Mar Ortega-Villaizán M, Varela M, Figueras A, Mulero V, Novoa B, Estepa A and Coll J (2017) Corrigendum: Zebra Fish Lacking Adaptive Immunity Acquire an Antiviral Alert State Characterized by Upregulated Gene Expression of Apoptosis, Multigene Families, and Interferon-Related Genes. Front. Immunol. 8:668. doi: 10.3389/fimmu.2017.00668

A corrigendum on

Zebra Fish Lacking Adaptive Immunity Acquire an Antiviral Alert State Characterized by Upregulated Gene Expression of Apoptosis, Multigene Families, and Interferon-Related Genes
by García-Valtanen P, Martínez-López A, López-Muñoz A, Bello-Perez M, Medina-Gali RM, Ortega-Villaizán M, et al. Front Immunol (2017) 8:121. doi: 10.3389/fimmu.2017.00121

In the original article there were two inaccurate statements, in the introduction and method sections, which may lead to misunderstanding the way previous microarray profiles of uninfected rag1$^{-/-}$ zebrafish were studied by Jima et al. 2009 (ref 49 in the paper). The meaning should be clear that in previous work, rag1$^{-/-}$ zebrafish were compared to heterozygous rag$^{+/-}$ while in the present work they were compared to homozygous rag1$^{+/+}$. The authors sincerely apologize for those inaccurate statements. These errors did not change the scientific conclusions of the article in any way.

The correct version of the introduction 3rd paragraph, statement on line 25 should more accurately read:

Probably, due to the difficulties encountered when breeding rag1$^{-/-}$ zebra fish, their gene expression profiles in response to viral infection, has yet to be compared to rag1$^{+/+}$.

The correct version of the materials and methods, zebra fish (*Danio rerio*) section, statement on line 13 should now be more accurate as:

These difficulties may explain why few people could make experiments with them and why only comparisons of rag1$^{-/-}$ to heterozygous rag1$^{+/-}$ have been used for microarray analysis (49).

Conflict of Interest Statement: The authors declare that the research was conducted in the absence of any commercial or financial relationships that could be construed as a potential conflict of interest.

frontiers in Immunology

ORIGINAL RESEARCH
published: 14 March 2017
doi: 10.3389/fimmu.2017.00249

Anopheles stephensi Heme Peroxidase HPX15 Suppresses Midgut Immunity to Support *Plasmodium* Development

*Mithilesh Kajla[1], Parik Kakani[1], Tania Pal Choudhury[1], Vikas Kumar[1], Kuldeep Gupta[1], Rini Dhawan[1], Lalita Gupta[1,2] and Sanjeev Kumar[1,3]**

[1] Molecular Parasitology and Vector Biology Laboratory, Department of Biological Sciences, Birla Institute of Technology and Science (BITS), Pilani, India, [2] Department of Zoology, Ch. Bansi Lal University, Bhiwani, India, [3] Department of Biotechnology, Ch. Bansi Lal University, Bhiwani, India

The heme peroxidase HPX15 is an evolutionary conserved anopheline lineage-specific gene. Previously, we found that this gene is present in the genome of 19 worldwide distributed different species of *Anopheles* mosquito and its orthologs are absent in other mosquitoes, insects, or human. In addition, 65–99% amino acid identity among these 19 orthologs permitted us to hypothesize that the functional aspects of this gene might be also conserved in different anophelines. In this study, we found that *Anopheles stephensi* AsHPX15 gene is mainly expressed in the midgut and highly induced after uninfected or *Plasmodium berghei*-infected blood feeding. RNA interference-mediated silencing of midgut AsHPX15 gene drastically reduced the number of developing *P. berghei* oocysts. An antiplasmodial gene nitric oxide synthase was induced 13-fold in silenced midguts when compared to the unsilenced controls. Interestingly, the induction of antiplasmodial immunity in AsHPX15-silenced midguts is in absolute agreement with *Anopheles gambiae*. In *A. gambiae*, AgHPX15 catalyzes the formation of a dityrosine network at luminal side of the midgut that suppresses the activation of mosquito immunity against the bolus bacteria. Thus, a low-immunity zone created by this mechanism indirectly supports *Plasmodium* development inside the midgut lumen. These indistinguishable functional behaviors and conserved homology indicates that HPX15 might be a potent target to manipulate the antiplasmodial immunity of the anopheline midgut, and it will open new frontiers in the field of malaria control.

Keywords: *Anopheles stephensi*, heme peroxidase, HPX15, mucin barrier, midgut, *Plasmodium*, innate immunity, vectorial capacity

OPEN ACCESS

Edited by:
Uday Kishore,
Brunel University London, UK

Reviewed by:
Kenneth Reid,
University of Oxford, UK
Anthony George Tsolaki,
Brunel University London, UK

****Correspondence:***
Sanjeev Kumar
sanjeevnih@gmail.com

Specialty section:
This article was submitted to Molecular Innate Immunity, a section of the journal Frontiers in Immunology

Received: *18 November 2016*
Accepted: *20 February 2017*
Published: *14 March 2017*

Citation:
Kajla M, Kakani P, Choudhury TP, Kumar V, Gupta K, Dhawan R, Gupta L and Kumar S (2017) Anopheles stephensi Heme Peroxidase HPX15 Suppresses Midgut Immunity to Support Plasmodium Development. Front. Immunol. 8:249. doi: 10.3389/fimmu.2017.00249

INTRODUCTION

Plasmodium completes its sexual life cycle inside the mosquito where various stages of parasite develop in different body compartments of the insect host. *Plasmodium* gametocytes start the insect cycle in mosquito midgut and produce male and female gametes. Subsequently, the fertilization leads to the formation of zygote that after 16–20 h of ingestion is transformed into the motile ookinete (1). Approximately after 24 h of ingestion, the ookinetes traverse the midgut epithelium and are then

transformed into the oocysts. Furthermore, in the next 10 days, several rounds of mitosis produce thousands of sporozoites. Mature sporozoites are released into the mosquito hemocoel and reach the salivary glands. Inoculation of these sporozoites into a vertebrate host continues the asexual cycle of *Plasmodium* development.

The success of *Plasmodium* sexual cycle depends on its interactions with the host immunity and internal environment. Thus, to develop transmission blocking strategies, the molecular understanding of these interactions is greatly demanded. So far, a large number of mosquito immune molecules have been identified that regulate mouse malaria parasite *Plasmodium berghei* development; however, they are ineffective against human malaria parasite *Plasmodium falciparum* (2–4). Thus, the discovery of those mosquito molecules, which can regulate the development of human malaria, requires sincere efforts. Recent studies identified that, in African mosquito *Anopheles gambiae*, the heme peroxidases play an important role in the regulation of *Plasmodium* development. One of the *A. gambiae* heme peroxidase, AgHPX2, along with AgNOX5 (NADPH Oxidase 5) catalyzes the nitration of epithelial cells that reduces the development of *P. berghei* ookinetes (5). In addition, another *A. gambiae* heme peroxidase AgHPX15 cross-links the mucins barrier on the luminal side of the midgut epithelium and that, in turn, blocks the recognition of *Plasmodium* by the mosquito innate immunity (6, 7). This mechanism, in fact, is an innate process that protects naturally acquired midgut microbes against the mosquito immunity and *Plasmodium* takes an advantage of this event (6–8). Silencing of AgHPX15 gene suppressed *P. berghei* as well as *P. falciparum* oocysts development due to the reduced integrity of the mucin barrier and activation of antiplasmodial midgut immunity (6).

Our previous studies identified AgHPX15 ortholog in major Indian malaria vector *Anopheles stephensi*, and we termed it as AsHPX15 (9, 10). In addition, putative orthologs of AsHPX15 gene were also found in the genome of 17 other anophelines with no orthology in other insects, mosquitoes (*Aedes* and *Culex*), or human. These findings revealed that HPX15 is an anopheline lineage-specific unique gene. Interestingly, these 19 HPX15 orthologs are also highly conserved and reveal 65–99% amino acid identity among them (10, 11). Based on these facts, we hypothesized that HPX15 might be functionally conserved in anophelines and can be considered as a general target to block the insect cycle of *Plasmodium* development. However, this hypothesis demands further investigations to establish the aforesaid regulatory role of HPX15 gene, in terms of *Plasmodium* development, in other anophelines. Thus, in the present study, we used the gene-silencing approach to determine the antiplasmodial role of AsHPX15 gene in the Indian malaria vector *A. stephensi*.

MATERIALS AND METHODS

Rearing of Mosquitoes

Mosquito colony was maintained in insectory at 28°C, 80% relative humidity, and 12 h light–dark cycle as described before (12). Larvae were fed on a 1:1 mixture of dog food (PetLover's crunch milk biscuit, India) and fish food (Gold Tokyo, India) as before (11, 12). Adult mosquitoes were fed on 10% sugar solution *ad libitum*. For colony propagation, 3–4 days old, starved females were fed on anesthetized mice. The eggs laid by these blood-fed (BF) females were collected in moist condition, and the hatched larvae were floated in water to continue the cycle.

Malaria Parasite *P. berghei* Maintenance

The transgenic *P. berghei* ANKA strain that expresses GFP (PbGFP) in all developmental stages (13) was a gift from Dr. Agam Prasad Singh, National Institute of Immunology, New Delhi, India. The *Plasmodium* strain was maintained in Swiss albino mice following the standard protocols as before (6, 14, 15). The parasitemia of the infected mice was determined from Giemsa-stained blood smears as mentioned before (14, 15). For blood stage passages, 100–150 µl of blood from an infected mouse (containing ~10–15% parasitemia) was injected intraperitoneal into the healthy mice. Parasitemia and potential infectivity of the *Plasmodium* to the mosquitoes was determined by exflagellation assays as before (16). In brief, 2 µl blood from the tail of the infected mouse was mixed with 20 µl of exflagellation buffer that was prepared by mixing equal parts of solution A (10mM Tris-Cl, 150mM NaCl, and 10mM glucose, pH 8) and heat-inactivated fetal bovine serum. In all the experiments, mice containing ~5–7% parasitemia and 2–3 exflagellations per field under 40× objective were used to infect the mosquitoes.

P. berghei Infection in Mosquito

The 4- to 5-day-old and overnight-starved 200 female mosquitoes were allowed to feed on an anesthetized Swiss albino mouse infected with the GFP expressing *P. berghei*. The mosquitoes fed on an uninfected mouse served as control. The unfed mosquitoes were removed and only fully engorged females were maintained at 21°C and 80% humidity, the permissive conditions for *P. berghei* development as discussed before (6, 11, 15, 17). Midguts samples were collected from 20 mosquitoes at different time points (3, 6, 12, 18, and 24 h) as mentioned below.

dsRNA Synthesis

A 218-bp fragment of the lacZ gene was amplified using the following primers (5′ to 3′) Fw-GAGTCAGTGAGCGAGGAAGC and Rev-TATCCGCTCACAATTCCACA and cloned into the pCRII-TOPO vector as before (18). In parallel, a 428-bp cDNA fragment of AsHPX15 gene that reported in our previous publication (10) was also cloned in the same vector. These recombinant plasmids were used individually as a template for *in vitro* transcription. The recombinant plasmid already had a T7 promoter site at M13F primer end, thus, a T7 promoter site was added to the other end of the fragment through amplifying M13R primer. The sequences (5′-3′) for these primers are following: M13F-GTAAAACGACGGCCAGT and T7-M13R-CTCGAGTAATACGACTCACTATAGGGCAGGAAACAGC TATGAC. PCR amplification using M13F and M13R primers was started with 94°C for 5 min followed by 40 cycles at 94°C for 30 s, 55°C for 30 s, 72°C for 30 s, and final extension was carried at 72°C for 10 min. Amplicons were purified with the QIA quick PCR purification kit (Qiagen, Valencia, CA, USA). PCR-purified amplicons tailed with T7 promoter sequences were used to synthesize dsRNAs with the MEGAscript kit

(Cat No. AM1626, Ambion, Austin, TX, USA) following the manufacturer's instructions. dsRNA was further purified using a Microcon YM-100 filter (Millipore) and finally concentrated to 3 µg/µl in DNase and RNase free water.

The Effect of dsRNA-Mediated HPX15 Gene Silencing on *Plasmodium* Development

The 1- to 2-day-old female mosquitoes were injected with 69 nl of 3 µg/µl dsAsHPX15 RNA (finally 207 ng/mosquito). Control mosquitoes were injected with dsLacZ RNA in the same manner. The gene silencing efficiency of the method was analyzed in sugar fed (SF), blood fed (BF), and *P. berghei*-infected midguts through qPCR against the respective controls. In these samples, on an average, we could achieve 98% silencing. To evaluate the effect of gene silencing on *Plasmodium* development, 4 days post dsRNA injected females were fed on transgenic GFP-*P. berghei*-infected mice, and the number of oocysts per midgut was determined after 7 days post infection. Furthermore, the midguts were dissected in Ashburner's PBS (3mM sodium chloride, 7mM disodium hydrogen phosphate, and 3mM sodium dihydrogen phosphate, pH 7.2), fixed for 15 min with 4% paraformaldehyde, washed thrice in PBS, and mounted on glass slides in Vectashield mounting medium. The numbers of green fluorescent oocysts were counted in each midgut under a fluorescent microscope (Olympus).

Sample Collection

Midguts from 20 uninfected or *P. berghei*-infected blood fed mosquitoes were dissected at different time points (3, 6, 12, 18, and 24 h) after the blood feeding. The dissected midguts or carcasses (rest of the body except midgut) were kept in RNAlater solution (Qiagen) and stored at −80°C. The midguts from randomly collected 20 SF mosquitoes were also dissected in similar way.

RNA Isolation, cDNA Synthesis, and qPCR

Total RNA from the midgut samples was isolated using RNeasy Mini Kit (Qiagen Cat no. 74104) following manufacturer's instructions. First-strand cDNA was synthesized from total RNA using QuantiTect Reverse Transcription kit (Qiagen Cat no. 205311). Expression profile of different genes was carried through semi-quantitative real-time PCR using SYBR Green supermix in a CFX Connect™ real-time PCR detection system (Bio-Rad) where ribosomal protein subunit S7 mRNA was used as internal loading control for normalization as described before (11, 19). The PCR primer pairs used for different genes are mentioned in **Table 1**. The PCR started with an initial denaturation at 95°C for 3 min and followed by 35 additional cycles at 94°C for 10 s, 57°C for 30 s, and 72°C for 50 s. Fluorescence for the PCR products was read at 72°C after each cycle. A final extension at 72°C for 10 min was completed before deriving a melting curve. Each experiment was performed in three independent biological replicates. Relative mRNA levels were calculated using $^{\Delta\Delta}C_t$ method by dividing the technical replicates in the control or test groups by the mean of the control group. This adjusted the control groups to a value of 1.0 as discussed before (6, 20–22).

Statistical Analysis of the Data

Statistical analysis was performed using GraphPad Prism 3.0 software (25). All these data were expressed as mean ± SD. Differences between test samples and their respective controls were evaluated by unpaired Student's *t*-test and considered to be significant if the *p*-Value was less than 0.05. Each experiment was performed at least thrice to validate the findings.

RESULTS

Tissue-Specific Expression Analysis of AsHPX15 Gene

To understand the organ-specific expression of AsHPX15 gene, we compared its relative mRNA levels in different body compartments. For that, we collected 24 h post uninfected or *P. berghei*-infected BF midguts and carcasses separately from 20 mosquitoes and analyzed the mRNA levels of AsHPX15 gene. We selected the 24 h post fed samples because it corresponds to the time when ookinetes invade the midgut epithelium (1, 6). Results shown in **Figure 1** revealed that in SF midguts the basal levels of AsHPX15 mRNA were ~40-fold higher than carcasses. Furthermore, its expression in 24 h BF midguts was induced ~17-folds against SF midguts (**Figure 1**). However, the expression of AsHPX15 gene was downregulated approximately twofold in *P. berghei*-infected midguts when compared to the uninfected BF controls ($p = 0.008$, **Figure 1**). Interestingly, the relative mRNA levels of AsHPX15 gene were indifferent in the carcass of SF or

TABLE 1 | List of primers used for real-time PCR.

S. no.	Primer sets	Primer sequence (5′–3′)	PCR product (bp) from cDNA template	Purpose	Reference
1	AsHPX15 Fw2 AsHPX15 Rev2	GAGAAGCTTCGCACGAGATTA GAATGTCGATTGCTTTCAGGTC	329	Real-time PCR	Kajla et al. (10)
2	Suppressor of cytokine signaling (SOCS) Fw SOCS Rev	CGTCGTACGTCGTATTGCTC CGGAAGTACAATCGGTCGTT	456	Real-time PCR	Dhawan et al. (15)
3	Nitric oxide synthase (NOS) Fw NOS Rev	ACATCAAGACGGAAATGGTTG ACAGACGTAGATGTGGGCCTT	250	Real-time PCR	Luckhart et al. (23)
4	Thioester-containing protein 1 (TEP1) Fw TEP1 Rev	GCTATCAAAATCAGATGCGCTATC ATCACAACCGCATGCTTCA	325	Real-time PCR	Present study
5	S7 Fw S7 Rev	GGTGTTCGGTTCCAAGGTGA GGTGGTCTGCTGGTTCTTATCC	487	PCR internal loading controls	Vijay et al. (24)

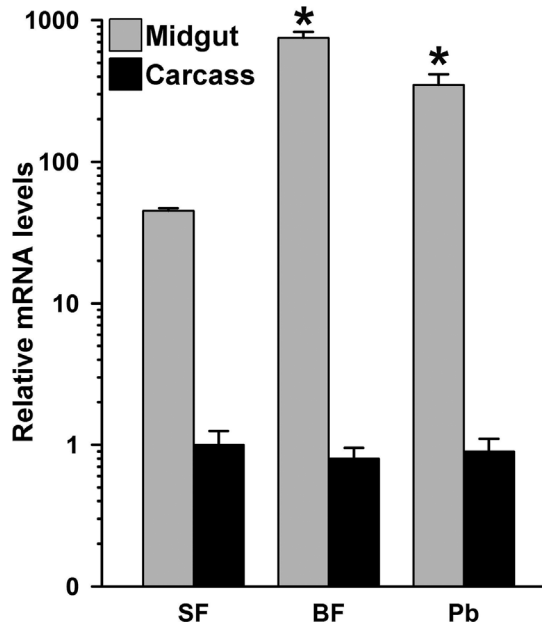

FIGURE 1 | Mosquito body compartment-specific expression of AsHPX15 gene. Relative mRNA levels of AsHPX15 gene were analyzed in midgut and carcass of sugar fed, 24 h post normal blood fed (BF) or *Plasmodium berghei*-infected BF females. The data are presented in $\log_{10}$ scale, and significant differences in the relative mRNA levels of AsHPX15 gene are indicated by an asterisk.

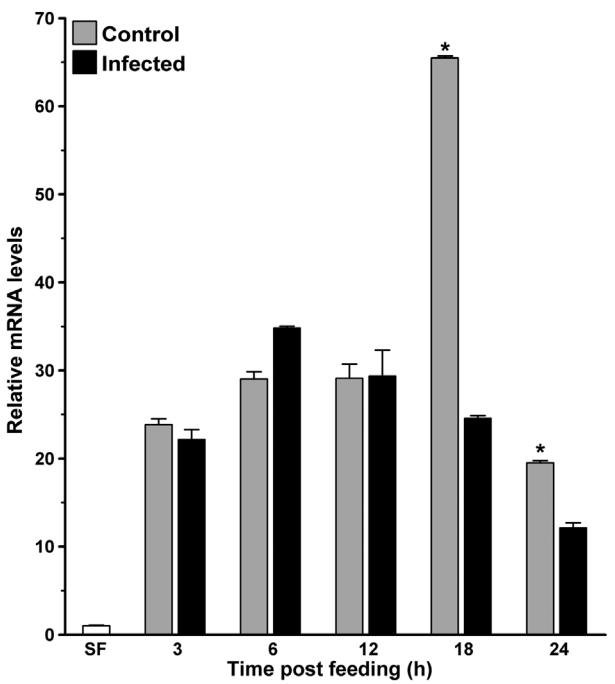

FIGURE 2 | Kinetics of AsHPX15 expression in mosquito midguts. Relative mRNA expression levels of AsHPX15 were analyzed at different time points after normal (Control) or *P. berghei*-infected blood feeding in *Anopheles stephensi* midguts. Relative fold inductions of the gene were calculated against sugar fed midguts. Significant differences between controls and infected midguts are indicated by an asterisk.

uninfected BF mosquitoes and also remained unaffected after *Plasmodium* infection (**Figure 1**). From these results, we concluded that AsHPX15 is a blood induced midgut-specific gene and suppressed during the *Plasmodium* ookinete invasion of the midgut epithelium. These findings are in agreement with the previous reports where *A. gambiae* AgHPX15 gene, an ortholog of AsHPX15, is induced in BF midguts and negatively regulated after malaria parasite infection (6, 26).

In parallel, we also analyzed the kinetics of AsHPX15 expression in *P. berghei*-infected midguts to understand its regulation during various stages of malaria parasite development. For that, the control or *P. berghei*-infected BF midguts were collected at different time points (3, 6, 12, 18, and 24 h) after the feeding and expression levels of AsHPX15 gene were analyzed through qPCR. Results presented in **Figure 2** revealed that the relative mRNA levels of AsHPX15 gene were similar in control and infected midguts for first 12 h ($p = 0.328$, $p = 0.091$, and $p = 0.945$ at 3, 6, and 12 h post blood feeding, respectively). However, there was a significant reduction of AsHPX15 mRNA levels in *P. berghei*-infected midguts at 18 h ($p < 0.0001$) and 24 h ($p = 0.0054$) post feeding when compared to the BF controls (**Figure 2**). These results indicated that the expression of AsHPX15 gene remains unaffected during the initial hours (up to 12 h) in infected midguts when the pre-ookinete stages of *Plasmodium* development predominate in the blood bolus (1). However, at later time points, the expression of this gene is suppressed when the mature ookinetes start invading the midgut epithelium (**Figure 2**).

AsHPX15 Silencing Has a Negative Effect on *Plasmodium* Development

Our previous findings revealed that *A. gambiae* heme peroxidase AgHPX15 catalyzes the cross-linking of a mucin layer at the luminal side of the midgut epithelium (6). This cross-linked mucin barrier does not allow the bolus antigens, especially, the naturally acquired microbes, to interact with the immune reactive midgut epithelium that subsequently suppresses the activation of innate immunity in this body compartment (6, 7). Thus, we hypothesized that the reduction of AsHPX15 mRNA levels through gene-silencing approaches might accelerate the recognition and killing of *Plasmodium* by the mosquito innate immunity. To test these assumptions, we injected a group of mosquitoes with dsLacZ (controls) or dsAsHPX15 (silenced) RNA and, after 5 days, these mosquitoes were fed on *P. berghei*-infected mice. After 24 h post infected blood feeding, our analysis revealed 98% reduction of AsHPX15 mRNA levels in silenced midguts when compared to the sham-treated controls (**Figure 3A**).

Subsequently, we counted the number of developing oocysts in the above-mentioned control and silenced midguts after 7 days post blood feeding. Results presented in **Figure 3B** revealed that the variable number of oocysts were observed in controls (oocysts range 0–1,800) and silenced (oocysts range 0–600) midguts. However, the median value for the oocysts numbers in controls and AsHPX15 silenced midguts was 329 and 89, respectively. This

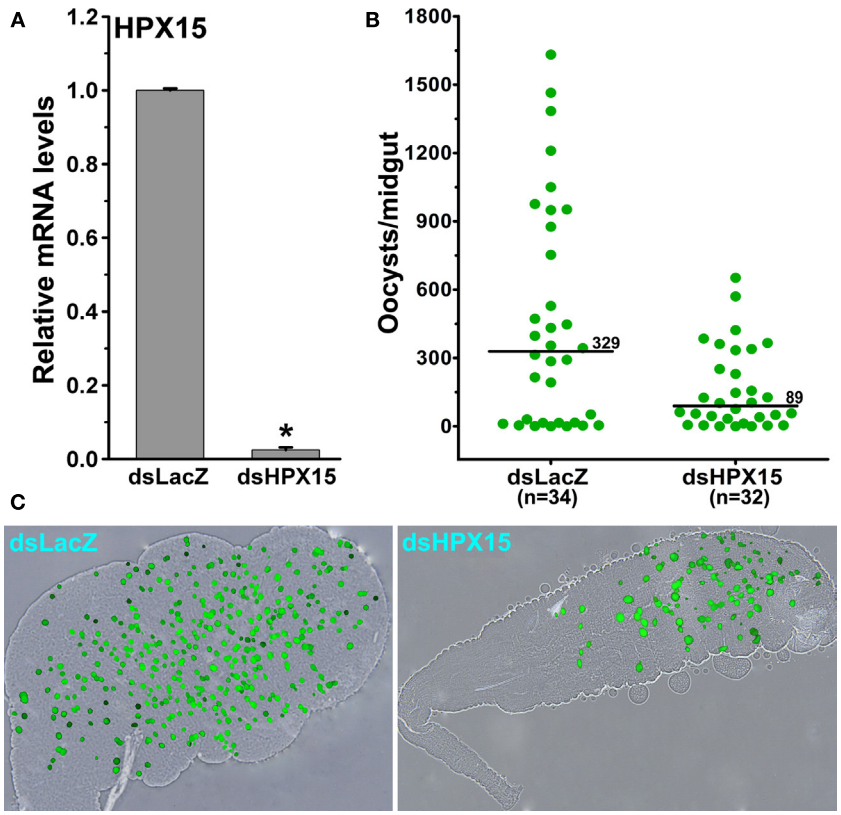

FIGURE 3 | **Effect of AsHPX15 silencing on *Plasmodium berghei* development in *Anopheles stephensi*. (A)** Relative abundance of AsHPX15 mRNA in control (dsLacZ) and silenced (dsAsHPX15) midguts that were collected 24 h post *P. berghei* infection. **(B)** Effect of AsHPX15 silencing on the number of live oocysts (green dots) in 7 days post infected blood fed midguts. Dots represent the number of parasites present in individual midguts, and the median number of oocysts is indicated by the horizontal line. Distributions are compared using the Kolmogorov–Smirnov test ($p = 0.027$); n = number of mosquitoes. **(C)** Representative *A. stephensi* midgut showing *P. berghei* oocysts in dsLacZ or dsHPX15-injected mosquitoes.

indicated that the numbers of developing oocysts were reduced significantly in the silenced midguts against controls (**Figure 3B**, $p = 0.027$). Based on these data, we concluded that AsHPX15 is a natural agonist that positively regulates *Plasmodium* development inside the mosquito midgut. These findings are in agreement with the previous reports where silencing of the AgHPX15 gene in *A. gambiae* also reduced *Plasmodium* survival (6).

AsHPX15-Silenced Midguts Induced Antiplasmodial Immunity

The development of *Plasmodium* was suppressed in AsHPX15-silenced midguts (**Figure 3**). We assumed that the induction of an antiplasmodial immunity in the silenced midgut might be responsible for the negative regulation of *Plasmodium* development. This may be simply due to the reduced or defective cross-linking of AsHPX15-mediated mucin barrier that, in turn, allowed the interaction and recognition of parasites by the immune reactive midgut epithelium. These assumptions were confirmed through expression analysis of various known antiplasmodial genes (6, 27) in the silenced and *P. berghei*-infected BF midguts that are mentioned in **Figure 3A**. Our analyses revealed that the relative mRNA levels of thioester-containing protein 1 (TEP1), an antiplasmodial immune gene (27), were similar in controls and dsHPX15-injected (silenced) mosquito midguts (**Figure 4**, $p = 0.106$). In addition, the relative levels of TEP1 mRNA were also indifferent between uninfected or *P. berghei*-infected BF midguts (**Figure 5**, $p = 0.091$).

Furthermore, the comparative analysis of another antiplasmodial immune gene nitric oxide synthase (NOS) in above samples revealed that this gene was induced ~13-folds in the silenced midguts against the controls (**Figure 4**, $p = 0.005$). These findings suggested that the induced NOS is most probably playing an antiplasmodial role in HPX15 silenced midguts as reported before (6, 28, 29). NOS catalyzed the formation of nitric oxide, a highly diffusable and reactive immune molecule that modifies and inactivates the biological marcomolecules (23). In mosquitoes, the induction of NOS gene is regulated by the Janus kinase/signal transducers and activators of transcription (JAK/STAT) pathway. Previous studies revealed that the suppressor of cytokinin signaling (SOCS) is also induced in parallel to the NOS and regulates the over activation of JAK/STAT pathway (6, 15, 28, 29). Thus, we also analyzed the induction of SOCS gene in the above-mentioned AsHPX15 silenced midguts to understand the activation of NOS through JAK/STAT pathway. Results presented in **Figure 4** revealed that the SOCS gene was induced approximately twofold in the silenced midguts against controls ($p = 0.001$). Thus, the induction of NOS, an effector gene, and SOCS, a suppressor gene, indicated that the activation

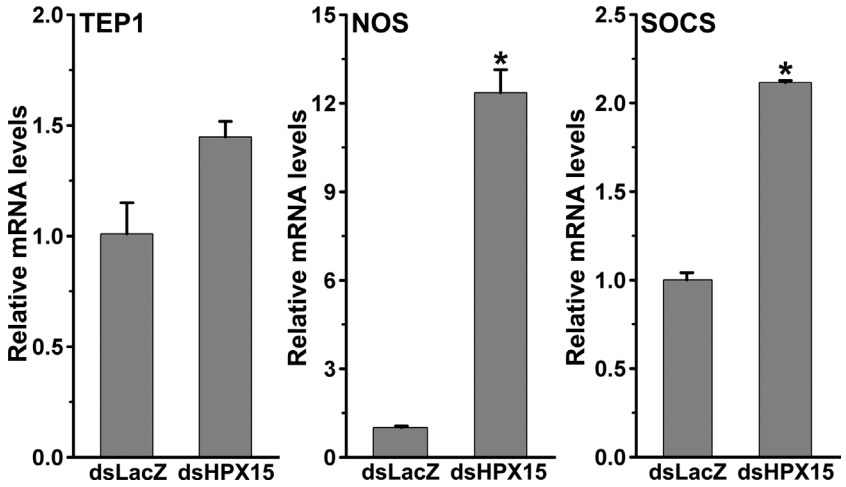

FIGURE 4 | Expression of immune genes in *Plasmodium berghei*-infected AsHPX15-silenced *Anopheles stephensi* midguts. Relative mRNA levels of various immune genes such as, thioester-containing protein 1, nitric oxide synthase, and suppressor of cytokine signaling in 24 h post *P. berghei* infected blood fed *A. stephensi* mosquito midguts that were injected with dsLacZ or dsAsHPX15. Significant differences in mRNA levels between dsLacZ and dsAsHPX15 are indicated by asterisk.

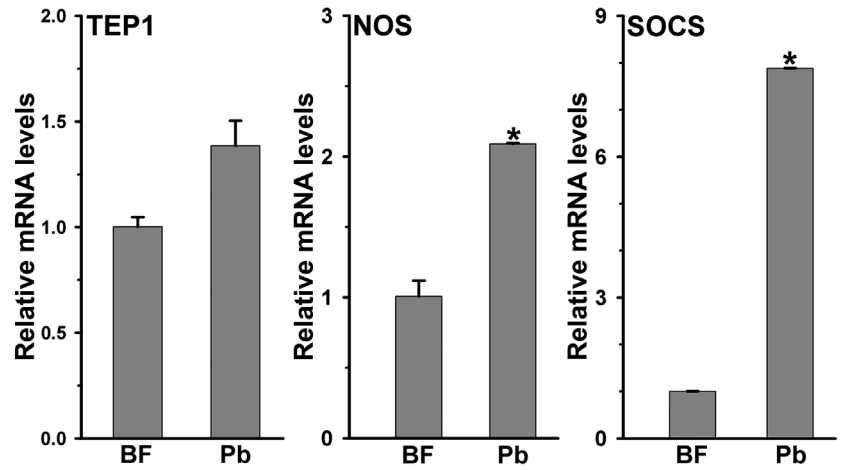

FIGURE 5 | Expression of immune genes in *Plasmodium berghei*-infected *Anopheles stephensi* midguts. Relative mRNA expression levels of various immune genes such as, thioester-containing protein 1 (TEP1), nitric oxide synthase (NOS), and suppressor of cytokine signaling (SOCS) in 24 h post normal blood fed and *P. berghei*-infected midguts. Significant differences are indicated by asterisk.

of JAK/STAT pathway might regulate antiplasmodial immunity in AsHPX15 silenced midguts. In addition, both NOS and SOCS genes were also induced twofold and eightfold, respectively in *Plasmodium*-infected unsilenced midguts when compared to the BF controls (**Figure 5**, $p = 0.011$ for NOS and $p < 0.0001$ for SOCS). These results collectively indicated that, in general, the JAK/STAT pathway is induced in *Plasmodium*-infected midguts (**Figure 5**). However, an additional induction of the same pathway in HPX15-silenced midguts seems to be the major regulator of *Plasmodium* development (**Figure 4**).

In conclusion, the absence of HPX15-catalyzed mucin barrier in infected midgut provides a better opportunity for the innate immune system to recognize the malaria parasite that, in turn, activates JAK/STAT pathway to regulate *Plasmodium* development negatively.

DISCUSSION

Mosquito midgut is the organ for digestion and also plays an important role in immunity. The midgut is housed by a large variety of microbes as well as it is the first organ that encounters blood-borne pathogens. The mutualistic association between the midgut and naturally acquired microbes is important for digestion and nutrition (6, 7, 30). Endogenous microbes proliferate in the lumen of BF midgut. Therefore, this organ is equipped with the mechanism(s) that maintain(s) a remarkable balance between

microbial homeostasis and immunity against the bolus antigens. One of the mechanisms that balances these events has been discussed in the African malaria vector *A. gambiae* (6, 7). In this mosquito, a tyrosine cross-linked mucins barrier is formed on the luminal surface of the BF midgut that blocks the recognition of bolus antigens or microbial elicitors by the immune reactive epithelial cells. Importantly, the cross-linking of mucins barrier is catalyzed by a heme peroxidase AgHPX15, which is also a blood feeding-induced midgut-specific gene [Ref. (6, 7); also **Figure 1** of this study].

Gene silencing studies carried in *A. gambiae* revealed that midgut bacteria as well as *Plasmodium* is recognized and killed by the midgut immunity in AgHPX15-silenced midguts. This effect was due to the reduced cross-linking of the mucin barrier, recognition of lumen bacteria and *Plasmodium* by the immune reactive midgut epithelium, and induction of antigen-specific innate immunity. It is of note that the suppressive effects of AgHPX15 silencing were identical against *P. falciparum* (human malaria) and *P. berghei* (murine malaria) (6).

Recent studies from our laboratory identified AgHPX15 ortholog in the Indian malaria vector *A. stephensi* and named it as AsHPX15 (10, 11). Interestingly, AsHPX15 and AgHPX15 are true orthologs and exhibit identical characteristics in several ways. For example, both orthologs are (a) midgut-specific and induced after blood feeding, (b) unique anopheline lineage-specific genes and do not have their orthologs in arthropods, including other mosquitoes, and human, (c) highly conserved and their putative ortholgs are present in the genome of 17 other worldwide distributed anophelines and share 65–99% amino acids identity, and (d) having same putative transcription factors binding sites in their regulatory region (10, 11). We assumed that due to the shared common features, *A. stephensi* AsHPX15 and *A. gambiae* AgHPX15 should be functionally identical in terms of modulating midgut immunity against bolus antigens. If it is true, then HPX15 can be considered as a common target to manipulate the midgut antiplasmodial immunity of anopheline mosquitoes (10, 11).

Thus, in the present study, we explored the role of *A. stephensi* AsHPX15 gene in regulation of *Plasmodium* development and replicating the findings reported earlier in case of AgHPX15 (6). We found that AsHPX15 gene is exclusively expressed in *A. stephensi* midgut, induced as early as 3 h post blood feeding and its mRNA levels remain elevated for first 12 h post blood feeding. Interestingly, the expression of AsHPX15 is significantly reduced during ookinete invasion of the midgut epithelium (24 h post infected blood feeding) (**Figures 1** and **2**). These findings are in agreement with the previous reports where AgHPX15 gene followed similar expression profile in BF midguts (6).

Furthermore, our analysis of AsHPX15 role in regulation of *Plasmodium* development revealed that parasite number was drastically reduced in silenced midguts (**Figure 3**). We believed that the absence of HPX15 protein would have resulted in the formation of a defective mucin barrier and that, in turn, induced antiplasmodial immunity in silenced midguts. Interestingly, we found that NOS, a downstream effector gene of JAK/STAT pathway, is highly induced in these samples (**Figure 4**) and might be one of the important negative regulators of *Plasmodium* development in the similar way as reported in *A. gambiae* (6). These results collectively indicated that the silencing of HPX15 gene has negative effects on *Plasmodium* development at least in two anophelines, *A. stephensi* and *A. gambiae*.

As we discussed earlier, the formation of HPX15-mediated mucin barrier is important for suppressing the midgut immunity against bolus antigens. It is believed that this mechanism is necessary to augment the process of digestion without activating immunity against food particles. Thus, the low-immunity zone created in this body compartment is also exploited by the pathogens to support their own development. Our study demonstrated that the HPX15 gene is conserved in anopheline mosquitoes in terms of its functional properties to modulate antiplasmodial immunity of the midgut. Therefore, it upholds a promising future to block mosquito cycle of *Plasmodium* development.

CONCLUSION

HPX15 is a unique, highly conserved protein among 19 anophelines. Its functional properties in terms of regulating the malaria parasite development are identical in two anophelines, *A. stephensi* and *A. gambiae*. Thus, we propose that anopheline HPX15 might serve as a "potent candidate" that can be targeted to manipulate mosquito vectorial capacity and blocking the transmission of malaria infection.

ETHICS STATEMENT

The protocol for using mice in this study was approved by Institutional Animal Ethics Committee (protocol number: IAEC/RES/13/01/REV/15/1) under the guidelines of Committee for the Purpose of Control and Supervision of Experiments on Animals, Minisrty of Environment, Forests and Climate Change, Government of India.

AUTHOR CONTRIBUTIONS

MK, LG, and SK designed experiments for this work. MK, TC, PK, KG, and RD collected samples to perform experiments. MK, TC, PK, KG, RD, LG, and SK performed expression kinetics of different immune genes. MK, TC, PK, LG, and SK performed HPX15-silencing experiments. MK, LG, VK, and SK analyzed these data and wrote the manuscript with input from all authors. All the authors read and approved the manuscript.

ACKNOWLEDGMENTS

The authors wish to thank the laboratory staff for maintaining the insectory and institute administration for providing all other facilities to accomplish the research and central animal facilities for providing mice during the study.

FUNDING

This work was supported by the research grants from the Department of Science and Technology (DST), Government

of India (grant number SR/SO/HS-0131/2010). University Grants Commission (UGC), India, provided Basic Science Research (BSR) fellowship to MK and KG. PK, RD, and TC would like to acknowledge the Department of Science and Technology (DST), Government of India, for providing the fellowship. VK acknowledges the Department of Biotechnology (DBT) for providing the research fellowship (grant number BT/PR8758/AGR/36/744/2013).

REFERENCES

1. Smith RC, Rodríguez JV, Jacobs-Lorena M. The *Plasmodium* bottleneck: malaria parasite losses in the mosquito vector. *Mem Inst Oswaldo Cruz* (2014) 109:644–61. doi:10.1590/0074-0276130597
2. Dimopoulos G, Seeley D, Wolf A, Kafatos FC. Malaria infection of the mosquito *Anopheles gambiae* activates immune-responsive genes during critical transition stages of the parasite life cycle. *EMBO J* (1998) 17:6115–23. doi:10.1093/emboj/17.21.6115
3. Povelones M, Waterhouse RM, Kafatos FC, Christophides GK. Leucine-rich repeat protein complex activates mosquito complement in defense against *Plasmodium* parasites. *Science* (2009) 324:258–61. doi:10.1126/science.1171400
4. Fraiture M, Baxter RH, Steinert S, Chelliah Y, Frolet C, Quispe-Tintaya W, et al. Two mosquito LRR proteins function as complement control factors in the TEP1-mediated killing of *Plasmodium*. *Cell Host Microbe* (2009) 5:273–84. doi:10.1016/j.chom.2009.01.005
5. Oliveira GA, Lieberman J, Barillas-Mury C. Epithelial nitration by a peroxidase/NOX5 system mediates mosquito antiplasmodial immunity. *Science* (2012) 335:856–9. doi:10.1126/science.1209678
6. Kumar S, Molina-Cruz A, Gupta L, Rodrigues J, Barillas-Mury C. A peroxidase/dual oxidase system modulates midgut epithelial immunity in *Anopheles gambiae*. *Science* (2010) 327:1644–8. doi:10.1126/science.1184008
7. Kajla M, Gupta K, Gupta L, Kumar S. A fine-tuned management between physiology and immunity maintains the gut microbiota in insects. *Biochem Physiol* (2015) 4:182. doi:10.4172/2168-9652.1000182
8. Kakani P, Suman S, Gupta L, Kumar S. Ambivalent outcomes of cell apoptosis: a barrier or blessing in malaria progression. *Front Microbiol* (2016) 7:302. doi:10.3389/fmicb.2016.00302
9. Kajla M, Kakani P, Choudhury TP, Gupta K, Dhawan R, Gakhar SK, et al. Characterization of anopheline unique peroxidase and its role in the regulation of *Plasmodium* development. *Malar J* (2014) 13:49. doi:10.1186/1475-2875-13-S1-P49
10. Kajla M, Gupta K, Kakani P, Dhawan R, Choudhury TP, Gupta L, et al. Identification of an *Anopheles* lineage-specific unique heme peroxidase HPX15: a plausible candidate for arresting malaria parasite development. *J Phylogenetics Evol Biol* (2015) 3:160. doi:10.4172/2329-9002.1000160
11. Kajla M, Kakani P, Gupta K, Choudhury TP, Gupta L, Kumar S. Characterization and expression analysis of gene encoding heme peroxidase HPX15 in major Indian malaria vector *Anopheles stephensi* (Diptera: Culicidae). *Acta Trop* (2016) 158:107–16. doi:10.1016/j.actatropica.2016.02.028
12. Kajla M, Bhattacharya K, Gupta K, Banerjee U, Kakani P, Gupta L, et al. Identification of temperature induced larvicidal efficacy of *Agave angustifolia* against *Aedes*, *Culex* and *Anopheles* larvae. *Front Public Health* (2016) 3:286. doi:10.3389/fpubh.2015.00286
13. Franke-Fayard B, Trueman H, Ramesar J, Mendoza J, van der Keur M, van der Linden R, et al. A *Plasmodium berghei* reference line that constitutively expresses GFP at a high level throughout the complete life cycle. *Mol Biochem Parasitol* (2004) 137:23–33. doi:10.1016/j.molbiopara.2004.04.007
14. Dong Y, Aguilar R, Xi Z, Warr E, Mongin E, Dimopoulos G. *Anopheles gambiae* immune responses to human and rodent *Plasmodium* parasite species. *PLoS Pathog* (2006) 2:e52. doi:10.1371/journal.ppat.0020052
15. Dhawan R, Gupta K, Kajla M, Kumar S, Gakhar SK, Kakani P, et al. Molecular characterization of SOCS gene and its expression analysis on *Plasmodium berghei* infection in *Anopheles culicifacies*. *Acta Trop* (2015) 152:170–5. doi:10.1371/journal.pntd.0001317
16. Billker O, Shaw MK, Margos G, Sinden RE. The roles of temperature, pH and mosquito factors as triggers of male and female gametogenesis of *Plasmodium berghei* in vitro. *Parasitology* (1997) 115:1–7. doi:10.1017/S0031182097008895
17. Dixit R, Sharma A, Mourya DT, Kamaraju R, Patole MS, Shouche YS. Salivary gland transcriptome analysis during *Plasmodium* infection in malaria vector *Anopheles stephensi*. *Int J Infect Dis* (2009) 13:636–46. doi:10.1016/j.ijid.2008.07.027
18. Gupta L, Noh JY, Jo YH, Oh SH, Kumar S, Noh MY, et al. Apolipophorin-III mediates antiplasmodial epithelial responses in *Anopheles gambiae* (G3) mosquitoes. *PLoS One* (2010) 5:e15410. doi:10.1371/journal.pone.0015410
19. Salazar CE, Mills-Hamm D, Kumar V, Collins FH. Sequence of a cDNA from the mosquito *Anopheles gambiae* encoding a homologue of human ribosomal protein S7. *Nucleic Acids Res* (1993) 21:4147. doi:10.1093/nar/21.17.4147
20. Livak KJ, Schmittgen TD. Analysis of relative gene expression data using real-time quantitative PCR and the 2(-Delta Delta C (T)) method. *Methods* (2001) 25:402–8. doi:10.1006/meth.2001.1262
21. Kajla M, Choudhury TP, Kakani P, Gupta K, Dhawan R, Gupta L, et al. Silencing of *Anopheles stephensi* heme peroxidase HPX15 activates diverse immune pathways to regulate the growth of midgut bacteria. *Front Microbiol* (2016) 7:1351. doi:10.3389/fmicb.2016.01351
22. Garver LS, de Almeida OG, Barillas-Mury C. The JNK pathway is a key mediator of *Anopheles gambiae* antiplasmodial immunity. *PLoS Pathog* (2013) 9:e1003622. doi:10.1371/journal.ppat.1003622
23. Luckhart S, Vodovotz Y, Cui L, Rosenberg R. The mosquito *Anopheles stephensi* limits malaria parasite development with inducible synthesis of nitric oxide. *Proc Natl Acad Sci U S A* (1998) 12:5700–5. doi:10.1073/pnas.95.10.5700
24. Vijay S, Rawat M, Adak T, Dixit R, Nanda N, Srivastava H, et al. Parasite killing in malaria non-vector mosquito *Anopheles culicifacies* species B: implication of nitric oxide synthase upregulation. *PLoS One* (2011) 6:e18400. doi:10.1371/journal.pone.0018400
25. Motulsky HJ. *Analyzing Data with GraphPad Prism*. San Diego, CA: GraphPad Software Inc. (1999). Available from: http://www.graphpad.com
26. Kumar S, Gupta L, Han YS, Barillas-Mury C. Inducible peroxidases mediate nitration of *Anopheles* midgut cells undergoing apoptosis in response to *Plasmodium* invasion. *J Biol Chem* (2004) 279:53475–82. doi:10.1074/jbc.M409905200
27. Blandin S, Shiao SH, Moita LF, Janse CJ, Waters AP, Kafatos FC, et al. Complement-like protein TEP1 is a determinant of vectorial capacity in the malaria vector *Anopheles gambiae*. *Cell* (2004) 116:661–70. doi:10.1016/S0092-8674(04)00173-4
28. Bahia AC, Kubota MS, Tempone AJ, Araujo HR, Guedes BA, Orfano AS, et al. The JAK-STAT pathway controls *Plasmodium vivax* load in early stages of *Anopheles aquasalis* infection. *PLoS Negl Trop Dis* (2011) 5:e1317. doi:10.1371/journal.pntd.0001317
29. Gupta L, Molina-Cruz A, Kumar S, Rodrigues J, Dixit R, Zamora RE, et al. The STAT pathway mediates late-phase immunity against *Plasmodium* in the mosquito *Anopheles gambiae*. *Cell Host Microbe* (2009) 5:498–507. doi:10.1016/j.chom.2009.04.003
30. Minard G, Mavingui P, Moro CV. Diversity and function of bacterial microbiota in the mosquito holobiont. *Parasit Vectors* (2013) 6:146. doi:10.1186/1756-3305-6-146

Conflict of Interest Statement: The authors declare that the research was conducted in the absence of any commercial or financial relationships that could be construed as a potential conflict of interest.

The reviewer AT and handling editor declared their shared affiliation, and the handling editor states that the process nevertheless met the standards of a fair and objective review.

frontiers in Immunology

ORIGINAL RESEARCH
published: 02 March 2016
doi: 10.3389/fimmu.2016.00079

Structural and Functional Characterization of a Single-Chain Form of the Recognition Domain of Complement Protein C1q

Christophe Moreau[1,2,3†], Isabelle Bally[1,2,3†], Anne Chouquet[1,2,3], Barbara Bottazzi[4], Berhane Ghebrehiwet[5], Christine Gaboriaud[1,2,3] and Nicole Thielens[1,2,3*]*

[1] IBS, University of Grenoble Alpes, Grenoble, France, [2] CNRS, IBS, Grenoble, France, [3] IBS, CEA, Grenoble, France, [4] Immunopharmacology Laboratory, Humanitas Research Hospital, Rozzano, Italy, [5] Department of Medicine, Stony Brook University, Stony Brook, NY, USA

OPEN ACCESS

Edited by:
Uday Kishore,
Brunel University London, UK

Reviewed by:
Kenneth Reid,
University of Oxford, UK
Lubka T. Roumenina,
INSERM UMRS 1138, France

***Correspondence:**
Christine Gaboriaud
christine.gaboriaud@ibs.fr;
Nicole Thielens
nicole.thielens@ibs.fr

†Christophe Moreau and Isabelle Bally contributed equally to this work.

Specialty section:
This article was submitted to Molecular Innate Immunity, a section of the journal Frontiers in Immunology

Received: *15 January 2016*
Accepted: *18 February 2016*
Published: *02 March 2016*

Citation:
Moreau C, Bally I, Chouquet A, Bottazzi B, Ghebrehiwet B, Gaboriaud C and Thielens N (2016) Structural and Functional Characterization of a Single-Chain Form of the Recognition Domain of Complement Protein C1q. Front. Immunol. 7:79. doi: 10.3389/fimmu.2016.00079

Complement C1q is a soluble pattern recognition molecule comprising six heterotrimeric subunits assembled from three polypeptide chains (A–C). Each heterotrimer forms a collagen-like stem prolonged by a globular recognition domain. These recognition domains sense a wide variety of ligands, including pathogens and altered-self components. Ligand recognition is either direct or mediated by immunoglobulins or pentraxins. Multivalent binding of C1q to its targets triggers immune effector mechanisms mediated *via* its collagen-like stems. The induced immune response includes activation of the classical complement pathway and enhancement of the phagocytosis of the recognized target. We report here, the first production of a single-chain recombinant form of human C1q globular region (C1q-scGR). The three monomers have been linked in tandem to generate a single continuous polypeptide, based on a strategy previously used for adiponectin, a protein structurally related to C1q. The resulting C1q-scGR protein was produced at high yield in stably transfected 293-F mammalian cells. Recombinant C1q-scGR was correctly folded, as demonstrated by its X-ray crystal structure solved at a resolution of 1.35 Å. Its interaction properties were assessed by surface plasmon resonance analysis using the following physiological C1q ligands: the receptor for C1q globular heads, the long pentraxin PTX3, calreticulin, and heparin. The 3D structure and the binding properties of C1q-scGR were similar to those of the three-chain fragment generated by collagenase digestion of serum-derived C1q. Comparison of the interaction properties of the fragments with those of native C1q provided insights into the avidity component associated with the hexameric assembly of C1q. The interest of this functional recombinant form of the recognition domains of C1q in basic research and its potential biomedical applications are discussed.

Keywords: innate immune recognition, complement, C1q, protein engineering, X-ray crystallography, surface plasmon resonance

Abbreviations: C1q-GR, globular region of C1q; C1q-scGR, single-chain globular region of C1q; CRT, calreticulin; gC1qR, receptor for the globular head of C1q; SPR, surface plasmon resonance.

INTRODUCTION

The soluble defense collagens are oligomeric innate immune pattern recognition receptors (PRRs), which are composed of N-terminal collagen-like stems prolonged by C-terminal globular trimeric pattern recognition domains [reviewed in Ref. (1)]. According to the nature of their recognition domain, these PRRs can be divided into three families in human, namely, proteins with gC1q domains (C1q and adiponectin), C-type lectin carbohydrate recognition domains (lung surfactant proteins A and D, mannan-binding lectin (MBL), collectins kidney 1 and liver 1), and fibrinogen-like domains (ficolins). Following target recognition, C1q and collectins (except surfactant proteins) or ficolins have the capacity to trigger activation of the classical and lectin pathways of complement for microbial killing and phagocytosis, through proteases associated with their collagen stems.

The C1q molecule is a complex defense collagen, being assembled from six heterotrimeric subunits, each consisting of three homologous, yet distinct polypeptide chains (A–C) encoded by the *C1QA*, *C1QB*, and *C1QC* genes oriented in the A–C–B order on human chromosome 1p (2). C1q also features the most versatile recognition properties, being able to identify not only bacterial and viral pathogens, either directly or through other immune proteins such as antibodies and pentraxins, but also many altered self elements, including β-amyloid fibrils (3), the pathological form of the prion protein (4, 5), modified low-density lipoproteins (6), and apoptotic cells (7–9).

Production of the C1q globular region (C1q-GR) by limited proteolysis of the serum-derived protein with collagenase allowed resolution of its X-ray crystal structure. The resulting compact heterotrimeric structure revealed differences in the surface charges of the subunits, a key factor for the versatility of C1q binding properties (10, 11). A further step toward understanding C1q binding properties was accomplished with the production of recombinant forms of the individual gC1q domains fused to maltose-binding protein, which revealed that these domains are functionally autonomous modules with differential ligand-binding properties (12). Site-directed mutagenesis studies provided information about the residues involved in the interaction of C1q with some of its ligands (13–16). However, elucidation of the C1q recognition properties in the more physiological context of the heterotrimeric globular regions still awaits the availability of the corresponding recombinant fragment.

We report here, the production of a single-chain recombinant form of human C1q globular region (C1q-scGR). The three monomers have been linked in tandem to generate a single continuous polypeptide, based on a strategy previously used to generate a single-chain form of the homotrimeric globular domain of adiponectin, a protein structurally related to C1q (17). The C1q-scGR recombinant protein was produced at high yield in stably transfected mammalian cells. Its physicochemical, structural, and functional analysis shows that it is correctly folded and retains the ability to associate with physiological C1q ligands, including the long pentraxin PTX3, the receptor for the globular heads of C1q (gC1qR), calreticulin (CRT), and heparin. The interest of this fragment in basic research and its potential biomedical applications will be discussed.

MATERIALS AND METHODS

Proteins and Reagents

C1q was purified from human serum and quantified, as described previously (18). The globular regions of C1q were prepared by collagenase digestion of C1q, as described previously (3), and their molar concentration estimated using a Mw value of 48,000 and an absorption coefficient (A1%, 1 cm) at 280 nm of 0.93. Recombinant human PTX3, gC1qR, and CRT were produced, as described previously (19–21). Streptavidin and heparin-biotin sodium salt (Mw 15 kDa) were procured from Sigma-Aldrich. Oligonucleotides were purchased from Eurogentec. Restriction and modification enzymes were from New England Biolabs.

Cloning of the Single-Chain Globular Domain of Human C1q

For recombinant protein expression in the baculovirus/insect cells system, a synthetic cDNA encoding residues 85–223 of mature C1qA, a Gly–Ser–Gly linker, residues 87–217 of mature C1qC (gC1qC), a Gly–Ser–Ala linker, and residues 90–226 of mature C1qB (gC1qB), cloned in frame with the melittin signal peptide of the pNT-Bac vector (22) (pNT-Bac–C1q-scGR), was purchased from GeneCust.

For expression in mammalian 293-F cells, an intermediate construct was generated from the pcDNA3.1–C1qA vector (23) by removing residues 1–87 of mature C1qA by site-directed mutagenesis, allowing in frame cloning of residues 88–223 of C1qA with the native signal peptide of C1qA (pcDNA3.1–gC1qA). A DNA fragment encoding the Gly–Ser–Gly linker, gC1qC, the Gly–Ser–Ala linker, and gC1qB was amplified using VentR polymerase and pNT-Bac–C1q-scGR as a template and inserted into pcDNA3.1–gC1qA by site-directed mutagenesis. The resulting construct (called pcDNA3.1–C1q-scGR) was characterized by restriction mapping and checked by double-stranded DNA sequencing (GATC Biotech).

Production of C1q-scGR in Eukaryotic Cells and Protein Purification

Generation of a recombinant baculovirus from the pNT-Bac–C1q-scGR plasmid using the Bac-to-Bac system (Invitrogen) and infection of *Trichoplusia ni* (High Five) insect cells was performed, as described previously (24). Stably transfected cells producing C1q-scGR were obtained by transfection of FreeStyle 293-F cells with the pcDNA3.1–C1q-scGR plasmid using 293-fectin and subsequent selection with 400 μg/ml G418 as recommended by the manufacturer (Invitrogen). The cells were expanded in the Freestyle expression medium (Invitrogen) and the culture supernatant harvested and replaced every 72 h up to three times.

The insect and mammalian cell culture supernatants containing C1q-scGR (500 ml) were dialyzed against 50 mM MES, 25 mM NaCl, pH 6.4, and loaded at 1.5 ml/min onto a SP Sepharose Fast Flow column (GE Healthcare) (50 ml) equilibrated in the same buffer. Elution was carried out by applying a 1-l linear gradient from 25 to 500 mM NaCl in the same buffer. The fractions containing the recombinant protein were identified by SDS-PAGE analysis, pooled, dialyzed against 50 mM Tris–HCl, 150 mM

NaCl, pH 7.4, and concentrated to 1–5 mg/ml by ultrafiltration on a PM-10 membrane (Amicon). The molar concentration of C1q-scGR was estimated using an absorption coefficient (A1%, 1 cm) at 280 nm of 0.93 and a Mr value of 47,534, as determined by mass spectrometry.

SDS-PAGE, N-Terminal Sequence, and Liquid Chromatography–Electrospray Ionization–Time-of-Flight Mass Spectrometry Analyses

Recombinant C1q-scGR was analyzed by SDS-PAGE under non-reducing or reducing conditions using Tris–HCl gels containing 10% polyacrylamide. N-terminal sequence determination was performed using an Applied Biosystems gas-phase sequencer model 492 coupled online with an Applied Biosystems Model 140C HPLC system. Liquid chromatography–electrospray ionization–time-of-flight (LC–ESI–TOF) mass spectrometry analyses of purified C1q-scGR, before and after treatment with *Clostridium perfringens* type X neuraminidase (Sigma) (0.3 U/mg) for 5 h at 25°C, were performed using a 6210 LC–TOF mass spectrometer interfaced with LC pump system (Agilent Technologies). Samples were desalted on-line on a protein trap (Zorbax 300SB-C8, 5 µm, 5 mm × 0.3 mm, Agilent Technologies) before analysis.

Analytical Ultracentrifugation

Sedimentation velocity analysis was performed using a Beckman XL-I analytical ultracentrifuge and an AN-50 TI rotor (Beckman Coulter, Palo Alto, CA, USA). Three C1q-scGR samples at 0.9, 2.5, and 5 mg/ml were loaded into 12, 3, and 1.5 mm pathlength double-sector cells and centrifuged at 42,000 rpm at 6°C in 50 mM Tris–HCl, 150 mM NaCl, and pH 7.4. Data acquisition was done in absorbance (at 280 nm) and interference modes. The sedimentation coefficients were obtained by fitting the sedimentation velocity profiles to the non-interacting species model using the SEDFIT program,[1] and the continuous distribution of sedimentation coefficients was obtained considering globular proteins. Solvent density was calculated at 1.00739 g/ml, and the partial specific volume was estimated at 0.724 ml/g, using the SEDNTERP program.[2]

Crystallization, Data Collection, and Structure Determination

Single-chain recombinant form of human C1q globular region was concentrated to 5 mg/ml, and standard crystallization kits were screened through the EMBL HTX Lab platform at 20°C. Several initial hits were reproduced manually, using the hanging drop method by mixing equal volumes (2 µl) of the protein and reservoir solutions and adding calcium in some reservoir solutions. The crystallization conditions used and the resulting crystal morphology were very similar to those obtained previously for plasma-derived C1q-GR (10). To obtain the crystal structures presented here, the following reservoir solutions were used: (1) 30% PEG 8000, 0.1M Hepes, pH 7.5; (2) 23% PEG 3350, 0.1M Tris, 0.2M NaCl, 50 mM $CaCl_2$, pH 8.5. Diffraction data were recorded up to 1.35 or 1.55 Å resolution at the European Synchrotron Radiation facility (ESRF) beamline ID23-eh1 and auto-processed in the C2 space group (25). The data collection statistics are provided in **Table 1**.

The position and orientation of the C1q-scGR trimeric globular domain in the asymmetric unit were determined with the molecular replacement software Phaser (26). Alternative cycles of refinement and graphics edition were performed using Refmac5 (27) and Coot (28), respectively. The final refinement cycles were performed using Phenix (29). Refinement statistics are provided in **Table 1**. Illustrations were prepared using Pymol (30).

Surface Plasmon Resonance Studies

Analyses were performed at 25°C using a Biacore 3000 instrument (GE Healthcare).

SPR Analyses on Immobilized C1q Protein Ligands

Calreticulin, gC1qR, and PTX3 were diluted to 20, 68, and 100 µg/ml in 10 mM sodium acetate pH 4.0, 4.0, and 3.5, respectively, and immobilized on a CM5 sensor chip (GE Healthcare) using the amine coupling chemistry in 10 mM Hepes, 150 mM NaCl, 3 mM EDTA, 0.005% surfactant P20, pH 7.4. The reference surface was submitted to the coupling steps without immobilized protein. Binding of C1q-scGR, C1q-GR, and C1q to immobilized CRT (3000–4700 RU), gC1qR (500–3400 RU), and PTX3 (5300–6200 RU) was measured at a flow rate of 20 µl/min in 50 mM Tris–HCl, 150 mM NaCl, 2 mM $CaCl_2$, 0.005% surfactant P20, pH 7.4. The specific binding signal was obtained by subtracting the background signal over the reference surface. Regeneration of the surfaces was achieved by 10 µl injections of 10–20 mM NaOH.

TABLE 1 | Data collection and refinement statistics for C1q-scGR.

Reservoir solution PDB ID	Without calcium 5HZF	With calcium 5HKJ
Data collection statistics		
Unit cell lengths (Å)	81.0, 52.9, 89.9	81.1, 52.7, 89.9
Unit cell angles (°)	90, 115.2, 90	90, 115.2, 90
Resolution (Å)[a]	100.0–1.55 (1.61–1.55)	100.0–1.35 (1.4–1.35)
Rsym[a]	5.6 (75.3)	7.0 (67.1)
% completeness[a]	98.4 (96.7)	98.7 (94.7)
I/sigma (I) average[a]	14.8 (1.9)	11.3 (1.8)
No. of observed reflections[a]	243,827 (25,061)	363,221 (31,079)
No. of unique reflections[a]	49,348 (5211)	74,618 (7346)
CC ½[a]	99.9 (56)	99.8 (68.2)
Mean Wilson B	27	21
Model refinement statistics		
R_{work}	0.169	0.175
R_{free}	0.185	0.2021
Root mean square deviation bonds (Å)	0.011	0.016
Root mean square deviation angles (°)	1.19	1.64

[a]*Statistics for the high-resolution bin are in parentheses.*

[1]https://sedfitsedphat.nibib.nih.gov/software

[2]www.bbri.org/RASMB/rasmb.html

SPR Analyses on Immobilized Heparin

Streptavidin (approximately 4000 RU) was immobilized on two flow cells of a CM5 sensor chip, as described previously (31). Biotinylated heparin was captured on the streptavidin surface in 10 mM Hepes, 150 mM NaCl, 0.005% surfactant P20, pH 7.4 (HBS-P) until a coupling level of 250–300 RU was obtained. Serum C1q-GR and recombinant C1q-scGR were injected over the heparin-bound surface at 20 µl/min in HBS-P. Surfaces were regenerated with 10 µl of 1M NaCl. The streptavidin surface without bound heparin was used as a reference.

SPR Data Evaluation

Data were analyzed by global fitting either to a 1:1 Langmuir binding model or to a two-state reaction binding model of both the association and dissociation phases for at least five concentrations simultaneously, using the BIAevaluation 3.2 software (GE Healthcare). Buffer blanks were subtracted from the data sets used for kinetic analysis (double referencing). Chi² values were below 3.5 in all cases. For the two-state reaction (conformational change) model, the apparent dissociation constants were calculated from the rate constants: $K_D = 1/[(k_{a1}/k_{d1})\ (1 + k_{a2}/k_{d2})]$. For the Langmuir binding model, the apparent equilibrium dissociation constants (K_D) were calculated from the ratio of the dissociation and association rate constants (k_d/k_a).

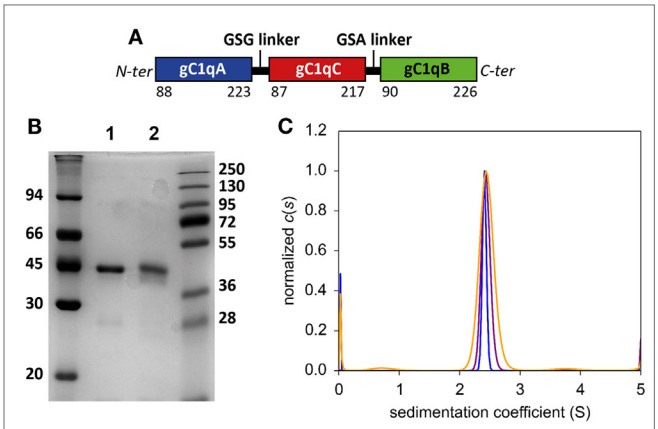

FIGURE 1 | Biochemical characterization of purified C1q-scGR. (A) Schematic representation of mature recombinant C1q-scGR protein. **(B)** SDS-PAGE analysis of C1q-scGR, unreduced (lane 1) and reduced (lane 2). The molecular masses of unreduced and reduced markers (expressed in kilodaltons) are shown on the left and right sides of the gel, respectively. **(C)** Sedimentation velocity analysis of C1q-scGR. Analysis was performed as described in Section "Materials and Methods" and the continuous distribution of sedimentation coefficients is shown. Orange, purple and blue traces correspond to C1q-scGR samples at 0.9, 2.5, and 5 mg/ml, respectively (data acquisition in absorbance mode).

RESULTS AND DISCUSSION

Generation of a Single-Chain Recombinant Form of gC1q

A strategy derived from that used for expression of a single polypeptide protein containing three consecutive copies of the globular domain of adiponectin was chosen to produce C1q-scGR (17). As revealed by the X-ray crystal structures of the globular domains of adiponectin (32) and of C1q (10), the N- and C-termini of the three gC1q modules emerge at the base of the trimer. Short 3-amino acid linkers can thus connect the adjacent monomers A–C and C–B. The 5′-3′ A–C–B order chosen to generate C1q-scGR also corresponds to that of the three C1q genes on chromosome 1p (33) (**Figure 1A**).

A first attempt to produce recombinant C1q-scGR was performed using a baculovirus/insect cells expression system, but the production yield was rather low since only 1 mg purified protein was recovered per liter of cell culture supernatant. In addition, the recombinant material was heterogeneous, consisting of a mixture of glycosylated and unglycosylated species (data not shown). Recombinant C1q-scGR was next produced in stably transfected 293-F mammalian cells and purified by cation-exchange chromatography. Up to 50 mg C1q-scGR could be purified from one liter of 293-F cells supernatant, which represents a 50-times higher yield compared to the baculovirus-infected insect cells. SDS-PAGE analysis showed a single band with an apparent mass of approximately 45 kDa under reducing and non-reducing conditions (**Figure 1B**).

N-terminal sequence analysis yielded the single sequence Lys–Asp–Gln–Pro–Arg, starting as expected at residue Lys 88 of C1qA chain. Mass spectrometry analysis yielded three peaks with masses of 47,749.84, 47,897.45, and 48,043.18 Da, accounting for a polypeptide chain with a predicted mass of 45,691.89 Da, and additional masses of 2059, 2205, and 2350 Da, corresponding to the three types of biantennary *N*-glycans (monosialylated, monosialylated fucosylated, and bisialylated) identified previously in serum-derived C1q (34, 35). The single N-glysosylation site at Asn 124 of C1qA is thus glycosylated in recombinant C1q-scGR. Sialidase treatment resulted in the appearance of two peaks with masses of 47,615.55 and 47,453.09 Da, compatible with asialylated biantennary *N*-glycans, fucosylated, or not (expected masses 1914 and 1768 Da).

Analysis of C1q-scGR by sedimentation velocity at three protein concentrations (0.9, 2.5, and 5 mg/ml) yielded a major peak accounting for 95 ± 3% of the signal with a sedimentation coefficient of 2.14 ± 0.4 S. Analysis in non-interacting species yielded a molecular mass of 41.4 ± 2 kDa, which is close to the mass measured by mass spectrometry, indicating that C1q-scGR is a monomer (**Figure 1C**).

X-ray Crystal Structure of C1q-scGR

Although sialidase treatment of serum-derived C1q-GR had been required to obtain crystals of this protein suitable for structure determination (10), the presence of sialic acids in C1q-scGR was not an obstacle to the determination of its crystal structure. Its X-ray structure, refined at 1.35 Å resolution (**Table 1**), allowed us to check that the linkers did not introduce any distortion. The recombinant and serum-derived C1q globular domains are indeed almost identical, as shown by their very small 0.1 Å RMS deviation on the 331 Cα common positions (**Figure 2A**). The main-chain trace of the segment encompassing the C–B linker and the first two residues of gC1qB (GSAKA) were modeled into the electron density (**Figure 2B**). This more rigid C–B linker only slightly alters the main-chain position of the two preceding and

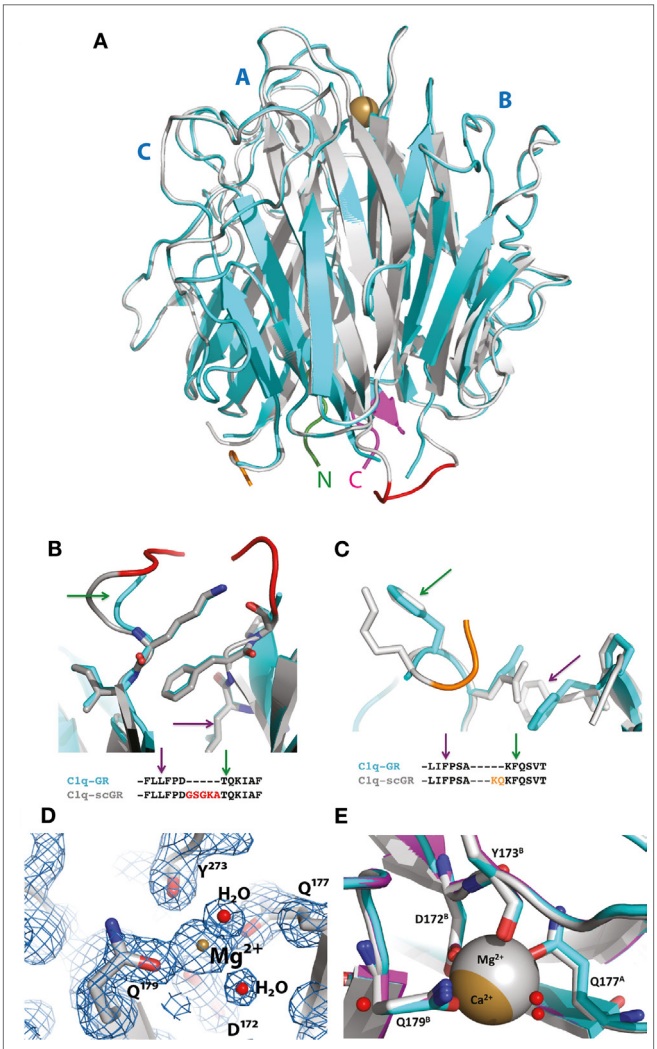

FIGURE 2 | Crystal structure of C1q-scGR and its comparison with C1q-GR. **(A)** The global superposition of C1q-scGR (gray) and C1q-GR (cyan) structures illustrates their similarity, with only 0.1 Å RMS deviation on 331 common Cα positions. The A–C labels corresponding to the three C1q-GR subunits are shown in blue. The calcium ion is shown as a golden sphere. The N-terminal and C-terminal ends are shown in green and magenta, respectively. More details of the C–B (red) and A–C (orange) linkers are provided in **(B)** and **(C)**, respectively. The green and magenta arrows link the details in these zooming sections with the positions in the sequences shown below. **(D)** In the absence of calcium in the crystallization reservoir, the calcium-binding site is occupied by a magnesium ion, as illustrated here in the 2mFo–DFc map contoured at 2 σ level. Introducing a calcium ion in the model at this position deteriorates the R_{free} factor by 2% and introduces a negative peak at this position in the Fo–Fc electron density map (not shown). **(E)** The ion substitution does not alter the structure of the calcium-binding site environment, as illustrated by the superposition of the structures of C1q-GR (cyan), C1q-scGR with calcium (magenta), and C1q-scGR with magnesium (gray).

following residues, but the positions of their side-chains are conserved (**Figure 2B**). The A–C linker is more flexible, and only the first two residues of gC1qC were modeled into the electron density (**Figure 2C**). All the water molecules except one correspond to those observed in the structure of the plasma-derived protein (PDB code 2wnv) (36). In the absence of calcium in the reservoir solution, the electron density filling the calcium-binding site is best modeled as a magnesium ion (**Figure 2D**). With a RMS deviation of 0.08 Å on the 340 Cα common positions, the two refined structures (**Table 1**) are almost identical except for the nature of the bound ion, which is either magnesium or calcium. Thus, this ion substitution does not alter the calcium-binding environment and is reversible (**Figure 2E**). The presence of a single calcium (or magnesium) ion at the top of the heterotrimeric assembly has been proposed to contribute to the stability of the recognition domain of C1q (10).

The X-ray crystal structure of a single-chain version of the homotrimeric globular head of adiponectin had validated the strategy used to generate the recognition domain of this C1q-related protein in a recombinant form (37). The fact that the 3D structure of C1q-scGR is virtually identical to that of the three-chain C1q-derived fragment shows that this strategy can be extended to other proteins containing trimeric gC1q domains.

Functional Properties of C1q-scGR

The interaction properties of C1q-scGR were analyzed by surface plasmon resonance (SPR) and compared to those of serum-derived C1q-GR, using known physiological ligands of C1q: the receptor for the globular heads of C1q (gC1qR), CRT, the long pentraxin PTX3, and heparin. All ligands were immobilized on the surface of a sensor chip and the serum-derived and recombinant forms of C1q-GR were used as soluble analytes. Both C1q-scGR and C1q-GR bound to the immobilized ligands with comparable association and dissociation rate constants, yielding comparable apparent K_D values in the sub-micromolar range (**Figure 3**; **Table 2**). This indicated that the recombinant single-chain protein retained the binding capacities of its serum-derived counterpart and was therefore fully functional. The K_D values obtained here for the interaction with CRT (494–510 nM) and gC1qR (304–344 nM) were in the same range as those reported previously for binding of C1q-GR to CRT (830 nM) (21) and gC1qR (370 nM) (38). The K_D value obtained for binding to heparin (51 nM) is slightly lower than that obtained previously for the interaction of C1q-GR with 6 kDa heparin (154 nM) (36), a difference that might be explained by the higher molecular weight heparin (15 kDa) used in the present study. Similar results were obtained when the binding experiments were performed in the absence of added calcium in the running buffer (not shown). In light of our structural data, it is likely that the calcium-binding site was still occupied under these conditions, since no chelating agent such as EDTA was used to remove the bound ion.

When the interaction experiments were performed using full-length C1q as soluble analyte, the binding affinities for all ligands, except CRT, were in the nanomolar range (**Figure 3**; **Table 2**). The observation that the C1q globular domain binds to immobilized gC1qR, PTX3, and heparin with a lower affinity (41- to 47-, 24- to 32-, and 32-fold, respectively) than intact C1q is consistent with the fact that C1q-scGR and C1q-GR lack the binding avidity of the hexameric C1q molecule. The decrease in affinity resulted mainly from a decrease in the k_a value, the k_d remaining essentially in the same range. A similar 44-fold decreased affinity has been

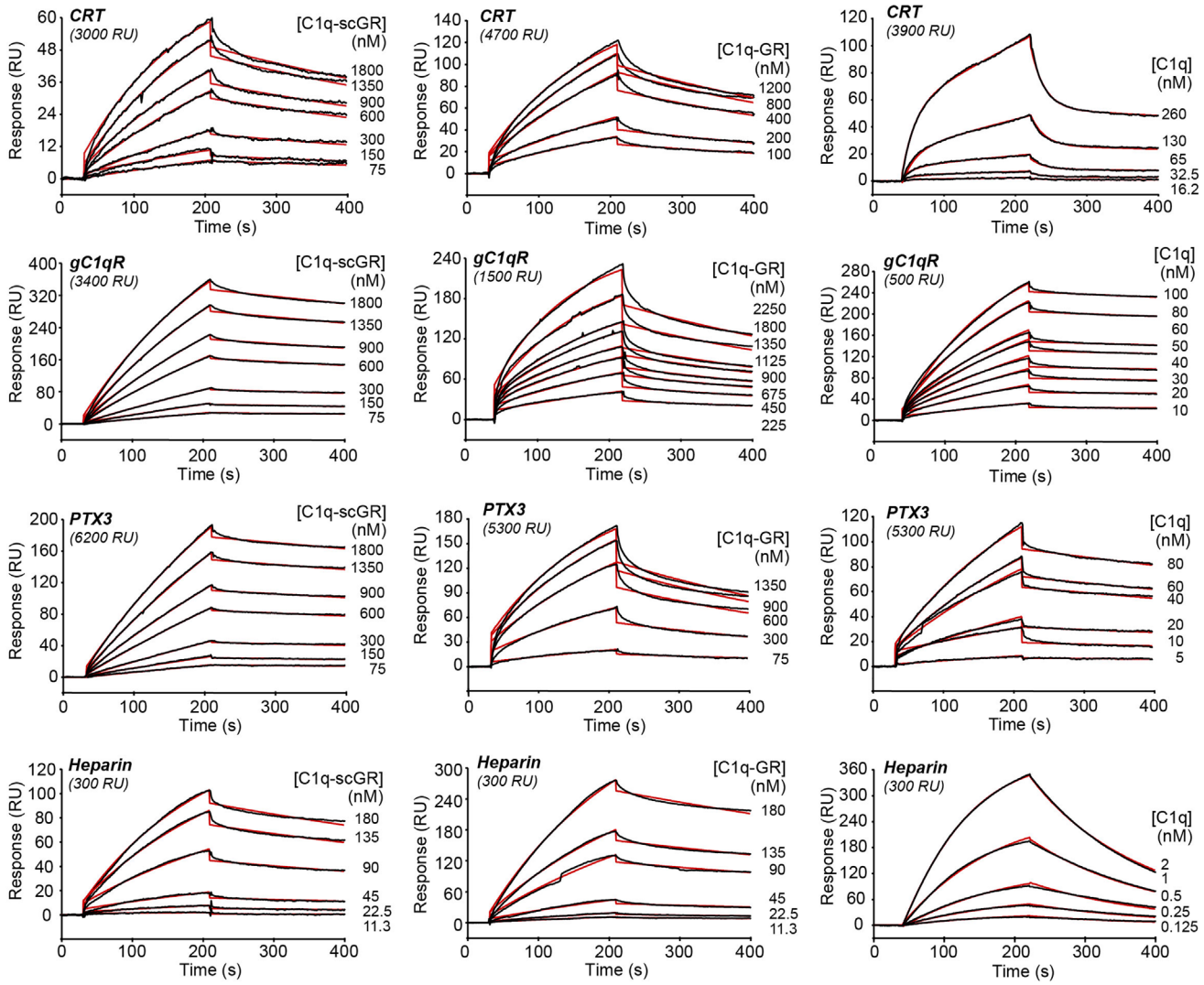

FIGURE 3 | Kinetic analysis of the interaction of C1q-scGR, C1q-GR, and C1q with immobilized CRT, gC1qR, PTX3, and heparin. The C1q samples (60 µl) were injected at the indicated concentrations over immobilized CRT, gC1qR, PTX3 in 50 mM Tris–HCl, 150 mM NaCl, 2 mM $CaCl_2$, 0.005% surfactant P20, pH 7.4, and over biotinylated heparin in 10 mM Hepes, 150 mM NaCl, 0.005% surfactant P20, pH 7.4. Fits are shown as red lines and were obtained by global fitting of the data using a 1:1 Langmuir binding model, except for the C1q–CRT interaction for which a two-state reaction (conformational change) model was used.

observed previously for the prion protein, another C1q ligand known to be recognized through C1q globular domain (39).

Proper kinetic analysis of the CRT–C1q interaction required the use of a two-state reaction binding model, taking into account conformational changes leading to an increasingly more stable complex formed in two steps, as reported previously for C1q binding to placenta-derived and recombinant CRT (21). The two groups of kinetic constants and the resulting apparent affinity constant (K_D), are listed in **Table 2**. As proposed previously (21), our data also suggest that CRT recognition by intact C1q implies conformational changes that do not take place in the isolated GR domains. Interestingly, the apparent K_D values obtained here for the interaction of CRT with C1q or its globular domain were all in the sub-micromolar range, suggesting an interaction mechanism differing from those involving other C1q ligands, such as gC1qR, PTX3, or the prion protein. It should be mentioned that a 2.4- to 7-fold increase in the C1q versus C1q-GR affinity to placenta-derived and recombinant CRT was observed previously, which corresponds anyway to a much lower avidity component compared to the other C1q ligands. Further investigation, including site-directed mutagenesis and/or structural analyses, will be needed to propose a relevant model for the CRT–C1q-GR interaction.

Of note, the same experimental SPR settings did not allow us to compare the binding affinity of C1q and its globular regions for IgG, a classical C1q ligand. Indeed, although full-length C1q readily bound to immobilized human IgG when injected at a concentration of 10 nM, only very weak binding of C1q-GR (either

TABLE 2 | Kinetic and dissociation constants for binding of C1q-scGR, C1q-GR, and C1q to immobilized C1q ligands.

Soluble C1q sample	Constants	Immobilized C1q ligands			
		CRT	gC1qR	PTX3	Heparin
C1q-scGR	k_a (M^{-1} s^{-1})	$2.80 \pm 0.33 \times 10^3$	$2.22 \pm 0.17 \times 10^3$	$1.32 \pm 0.24 \times 10^3$	$2.51 \pm 0.02 \times 10^4$
	k_d (s^{-1})	$1.36 \pm 0.04 \times 10^{-3}$	$6.70 \pm 0.31 \times 10^{-4}$	$5.52 \pm 0.66 \times 10^{-4}$	$1.29 \pm 0.06 \times 10^{-3}$
	K_D (nM)	494 ± 47	304 ± 26	444 ± 125	51.5 ± 2.7
C1q-GR	k_a (M^{-1} s^{-1})	$4.63 \pm 0.73 \times 10^3$	$4.40 \pm 0.77 \times 10^3$	$4.59 \pm 1.2 \times 10^3$	$2.09 \pm 0.22 \times 10^4$
	k_d (s^{-1})	$2.34 \pm 0.43 \times 10^{-3}$	$1.49 \pm 0.20 \times 10^{-3}$	$2.17 \pm 0.43 \times 10^{-3}$	$1.06 \pm 0.08 \times 10^{-3}$
	K_D (nM)	510 ± 88	344 ± 78	599 ± 21	51.5 ± 9.0
C1q	k_a (M^{-1} s^{-1})		$6.80 \pm 1.20 \times 10^4$	$3.87 \pm 1.27 \times 10^4$	$5.49 \pm 0.65 \times 10^6$
	[a]k_{a1} (M^{-1} s^{-1})	$7.82 \pm 0.12 \times 10^3$			
	[a]k_{a2} (s^{-1})	$4.72 \pm 0.90 \times 10^{-3}$			
	k_d (s^{-1})		$4.57 \pm 1.3 \times 10^{-4}$	$6.72 \pm 0.15 \times 10^{-4}$	$8.81 \pm 1.50 \times 10^{-3}$
	[a]k_{d1} (s^{-1})	$4.20 \pm 0.51 \times 10^{-2}$			
	[a]k_{d2} (s^{-1})	$4.82 \pm 1.12 \times 10^{-4}$			
	K_D (nM)	590 ± 105	7.20 ± 2.65	18.2 ± 2.6	1.60 ± 0.08

Values are the means ± SD of at least two separate experiments.

[a]The association (k_{a1}, k_{a2}) and dissociation (k_{d1}, k_{d2}) rate constants of the C1q–CRT interaction were determined by global fitting of the data using a two-state reaction binding model. The resulting dissociation constant was determined from the rate constants: $K_D = 1/[(k_{a1}/k_{d1})\ (1 + k_{a2}/k_{d2})]$.

serum-derived or recombinant) injected at concentrations in the micromolar range was observed (Figure S1 in Supplementary Material). This precluded determination of kinetic constants for C1q-GR binding to IgG, but revealed, here too, a difference between full-length C1q and its recognition domains. It is well known that, under physiological conditions, efficient complement activation is triggered by multivalent binding of C1q to antigen–IgG complexes. These conditions can be reproduced artificially in ELISA tests using adsorbed heat-aggregated IgG. Therefore, it is not totally unexpected that the globular regions bind only weakly to immobilized single IgG molecules. The immobilized gC1qR and PTX3 molecules are naturally trimers and octamers, respectively, and it is expected that each of these ligands can bind to a single globular head of C1q, although with less affinity than to full-length C1q.

CONCLUSION

The availability of a recombinant functional form of the heterotrimeric globular regions of C1q opens the way for deciphering the molecular basis of the binding versatility of C1q by mapping the residues involved in the recognition of its numerous targets using site-directed mutagenesis. Although it has been shown previously that the three isolated subunits mediate different individual binding properties (12), it is now possible to assess the effects of single residue mutations in the heterotrimeric context of C1q-scGR, as it occurs in native C1q. In addition, given the compact structure of the domain, it appears likely that recognition of certain ligands will involve residues contributed by several subunits (10), a hypothesis that can now be tested experimentally. The availability of two recombinant forms of C1q, the full-length protein (23) and its recognition domain, will allow comparison of their binding and effector properties, taking into account the avidity provided by the hexameric full-length C1q molecule.

In addition to basic research, such artificial gC1q molecules should be of interest for biomedical applications. The contribution of complement in the pathogenesis of many important diseases, including neurodegenerative, infectious, and autoimmune disorders, is now well recognized and C1q is an attractive target for anti-complement therapy (40). C1q-scGR molecules, possibly engineered to form multimers, could thus be used in the fluid phase as natural competitors to inhibit the classical complement pathway at the initial recognition step without any risk of triggering the immune effector mechanisms mediated by the collagen-like regions.

Engineered C1q-scGR molecules might also be used to functionalize magnetic nanobeads or hemoadsorption filters for *in vitro* blood cleansing, as described recently for the carbohydrate recognition domain of human MBL, a recognition protein of the lectin complement pathway (41, 42). MBL-coated devices were shown to efficiently capture bacteria, fungi, and endotoxins from whole human blood and are promising tools in sepsis therapy. Using C1q-scGR would broader the field of application of such devices beyond pathogenic microorganisms because of the capacity of C1q to recognize a variety of potentially noxious altered self elements such as amyloid fibrils and the toxic form of the prion protein. In addition, the fact that C1q specifically reacts with circulating immune complexes and acute-phase proteins such as pentraxins might open the way to the use of C1q-scGR hemoadsorption for the treatment of patients with severe autoimmune diseases such as SLE. It should be mentioned indeed that plasma immunoadsorption on a C1q-column (prepared with immobilized serum-purified porcine C1q) has been successfully used to treat a few SLE patients (43, 44). Using recombinant C1q-scGR, it is now possible to address the potential contamination risks associated with animal serum-derived proteins.

AUTHOR CONTRIBUTIONS

NT, CG, and IB designed the study; CM, IB, AC, and NT performed the research; CM, IB, CG, and NT analyzed the data; BB and BG contributed new reagents; NT, CG, and CM wrote the

manuscript; all authors revised and approved the final version of the manuscript.

ACKNOWLEDGMENTS

We thank Gérard Arlaud for helpful suggestions and discussions at the early stages of this project. This work used the platforms of the Grenoble Instruct center (ISBG; UMS 3518 CNRS-CEA-UJF-EMBL) with support from FRISBI (ANR-10-INSB-05-02) and GRAL (ANR-10-LABX-49-01) within the Grenoble Partnership for Structural Biology (PSB). We thank Luca Signor, Jean-Pierre Andrieu, and Aline Le Roy for assistance and access to the mass spectrometry, protein N-terminal sequencing, and analytical ultracentrifugation facilities, respectively. Access to the European Synchrotron Radiation Facility beamline ID23-eh1 is acknowledged. This work was supported by a grant from the French National Research Agency (ANR-09-PIRI-0021). The contribution of the Italian Health Ministry (RF-2010-2310888) is gratefully acknowledged.

SUPPLEMENTARY MATERIAL

The Supplementary Material for this article can be found online at http://journal.frontiersin.org/article/10.3389/fimmu.2016.00079

REFERENCES

1. Fraser DA, Tenner AJ. Directing an appropriate immune response: the role of defense collagens and other soluble pattern recognition molecules. *Curr Drug Targets* (2008) **9**:113–22. doi:10.2174/138945008783502476
2. Reid KB. Chemistry and molecular genetics of C1q. *Behring Inst Mitt* (1989) **84**:8–19.
3. Tacnet-Delorme P, Chevallier S, Arlaud GJ. Beta-amyloid fibrils activate the C1 complex of complement under physiological conditions: evidence for a binding site for A beta on the C1q globular regions. *J Immunol* (2001) **167**:6374–81. doi:10.4049/jimmunol.167.11.6374
4. Klein MA, Kaeser PS, Schwarz P, Weyd H, Xenarios I, Zinkernagel RM, et al. Complement facilitates early prion pathogenesis. *Nat Med* (2001) **7**:488–92. doi:10.1038/86567
5. Erlich P, Dumestre-Perard C, Ling WL, Lemaire-Vieille C, Schoehn G, Arlaud GJ, et al. Complement protein C1q forms a complex with cytotoxic prion protein oligomers. *J Biol Chem* (2010) **285**:19267–76. doi:10.1074/jbc.M109.071860
6. Biro A, Thielens NM, Cervenak L, Prohaszka Z, Fust G, Arlaud GJ. Modified low density lipoproteins differentially bind and activate the C1 complex of complement. *Mol Immunol* (2007) **44**:1169–77. doi:10.1016/j.molimm.2006.06.013
7. Korb LC, Ahearn JM. C1q binds directly and specifically to surface blebs of apoptotic human keratinocytes: complement deficiency and systemic lupus erythematosus revisited. *J Immunol* (1997) **158**:4525–8.
8. Taylor PR, Carugati A, Fadok VA, Cook HT, Andrews M, Carroll MC, et al. A hierarchical role for classical pathway complement proteins in the clearance of apoptotic cells *in vivo*. *J Exp Med* (2000) **192**:359–66. doi:10.1084/jem.192.3.359
9. Navratil JS, Watkins SC, Wisnieski JJ, Ahearn JM. The globular heads of C1q specifically recognize surface blebs of apoptotic vascular endothelial cells. *J Immunol* (2001) **166**:3231–9. doi:10.4049/jimmunol.166.5.3231
10. Gaboriaud C, Juanhuix J, Gruez A, Lacroix M, Darnault C, Pignol D, et al. The crystal structure of the globular head of complement protein C1q provides a basis for its versatile recognition properties. *J Biol Chem* (2003) **278**:46974–82. doi:10.1074/jbc.M307764200
11. Gaboriaud C, Frachet P, Thielens NM, Arlaud GJ. The human c1q globular domain: structure and recognition of non-immune self ligands. *Front Immunol* (2011) **2**:92. doi:10.3389/fimmu.2011.00092
12. Kishore U, Gupta SK, Perdikoulis MV, Kojouharova MS, Urban BC, Reid KB. Modular organization of the carboxyl-terminal, globular head region of human C1q A, B, and C chains. *J Immunol* (2003) **171**:812–20. doi:10.4049/jimmunol.171.2.812
13. Kojouharova MS, Tsacheva IG, Tchorbadjieva MI, Reid KB, Kishore U. Localization of ligand-binding sites on human C1q globular head region using recombinant globular head fragments and single-chain antibodies. *Biochim Biophys Acta* (2003) **1652**:64–74. doi:10.1016/j.bbapap.2003.08.003
14. Kojouharova MS, Gadjeva MG, Tsacheva IG, Zlatarova A, Roumenina LT, Tchorbadjieva MI, et al. Mutational analyses of the recombinant globular regions of human C1q A, B, and C chains suggest an essential role for arginine and histidine residues in the C1q-IgG interaction. *J Immunol* (2004) **172**:4351–8. doi:10.4049/jimmunol.172.7.4351
15. Roumenina LT, Ruseva MM, Zlatarova A, Ghai R, Kolev M, Olova N, et al. Interaction of C1q with IgG1, C-reactive protein and pentraxin 3: mutational studies using recombinant globular head modules of human C1q A, B, and C chains. *Biochemistry* (2006) **45**:4093–104. doi:10.1021/bi052646f
16. Roumenina LT, Popov KT, Bureeva SV, Kojouharova M, Gadjeva M, Rabheru S, et al. Interaction of the globular domain of human C1q with *Salmonella typhimurium* lipopolysaccharide. *Biochim Biophys Acta* (2008) **1784**:1271–6. doi:10.1016/j.bbapap.2008.04.029
17. Ge H, Xiong Y, Lemon B, Lee KJ, Tang J, Wang P, et al. Generation of novel long-acting globular adiponectin molecules. *J Mol Biol* (2010) **399**:113–9. doi:10.1016/j.jmb.2010.03.062
18. Arlaud GJ, Sim RB, Duplaa AM, Colomb MG. Differential elution of Clq, Clr and Cls from human Cl bound to immune aggregates. Use in the rapid purification of Cl subcomponents. *Mol Immunol* (1979) **16**:445–50. doi:10.1016/0161-5890(79)90069-5
19. Bottazzi B, Vouret-Craviari V, Bastone A, De Gioia L, Matteucci C, Peri G, et al. Multimer formation and ligand recognition by the long pentraxin PTX3. Similarities and differences with the short pentraxins C-reactive protein and serum amyloid P component. *J Biol Chem* (1997) **272**:32817–23. doi:10.1074/jbc.272.52.32817
20. Ghebrehiwet B, Jesty J, Xu S, Vinayagasundaram R, Vinayagasundaram U, Ji Y, et al. Structure-function studies using deletion mutants identify domains of gC1qR/p33 as potential therapeutic targets for vascular permeability and inflammation. *Front Immunol* (2011) **2**:58. doi:10.3389/fimmu.2011.00058
21. Paidassi H, Tacnet-Delorme P, Verneret M, Gaboriaud C, Houen G, Duus K, et al. Investigations on the C1q-calreticulin-phosphatidylserine interactions yield new insights into apoptotic cell recognition. *J Mol Biol* (2011) **408**:277–90. doi:10.1016/j.jmb.2011.02.029
22. Rossi V, Bally I, Thielens NM, Esser AF, Arlaud GJ. Baculovirus-mediated expression of truncated modular fragments from the catalytic region of human complement serine protease C1s. Evidence for the involvement of both complement control protein modules in the recognition of the C4 protein substrate. *J Biol Chem* (1998) **273**:1232–9. doi:10.1074/jbc.273.2.1232
23. Bally I, Ancelet S, Moriscot C, Gonnet F, Mantovani A, Daniel R, et al. Expression of recombinant human complement C1q allows identification of the C1r/C1s-binding sites. *Proc Natl Acad Sci U S A* (2013) **110**:8650–5. doi:10.1073/pnas.1304894110
24. Jacquet M, Lacroix M, Ancelet S, Gout E, Gaboriaud C, Thielens NM, et al. Deciphering complement receptor type 1 interactions with recognition proteins of the lectin complement pathway. *J Immunol* (2013) **190**:3721–31. doi:10.4049/jimmunol.1202451
25. Monaco S, Gordon E, Bowler MW, Delageniere S, Guijarro M, Spruce D, et al. Automatic processing of macromolecular crystallography X-ray diffraction data at the ESRF. *J Appl Crystallogr* (2013) **46**:804–10. doi:10.1107/S0021889813006195
26. McCoy AJ, Grosse-Kunstleve RW, Adams PD, Winn MD, Storoni LC, Read RJ. Phaser crystallographic software. *J Appl Crystallogr* (2007) **40**:658–74. doi:10.1107/S0021889807021206
27. Murshudov GN, Skubak P, Lebedev AA, Pannu NS, Steiner RA, Nicholls RA, et al. REFMAC5 for the refinement of macromolecular crystal structures. *Acta Crystallogr D Biol Crystallogr* (2011) **67**:355–67. doi:10.1107/S0907444911001314

28. Emsley P, Lohkamp B, Scott WG, Cowtan K. Features and development of Coot. *Acta Crystallogr D Biol Crystallogr* (2010) **66**:486–501. doi:10.1107/S0907444910007493
29. Adams PD, Afonine PV, Bunkoczi G, Chen VB, Davis IW, Echols N, et al. PHENIX: a comprehensive Python-based system for macromolecular structure solution. *Acta Crystallogr D Biol Crystallogr* (2010) **66**:213–21. doi:10.1107/S0907444909052925
30. DeLano WL. *The PyMOL Molecular Graphics System*. Palo Alto, CA: DeLano Scientific LLC (2002).
31. Rossi V, Bally I, Ancelet S, Xu Y, Fremeaux-Bacchi V, Vives RR, et al. Functional characterization of the recombinant human C1 inhibitor serpin domain: insights into heparin binding. *J Immunol* (2010) **184**:4982–9. doi:10.4049/jimmunol.0902016
32. Shapiro L, Scherer PE. The crystal structure of a complement-1q family protein suggests an evolutionary link to tumor necrosis factor. *Curr Biol* (1998) **8**:335–8. doi:10.1016/S0960-9822(98)70133-2
33. Sellar GC, Blake DJ, Reid KB. Characterization and organization of the genes encoding the A-, B- and C-chains of human complement subcomponent C1q. The complete derived amino acid sequence of human C1q. *Biochem J* (1991) **274**(Pt 2):481–90. doi:10.1042/bj2740481
34. Mizuochi T, Yonemasu K, Yamashita K, Kobata A. The asparagine-linked sugar chains of subcomponent C1q of the first component of human complement. *J Biol Chem* (1978) **253**:7404–9.
35. Pflieger D, Przybylski C, Gonnet F, Le Caer JP, Lunardi T, Arlaud GJ, et al. Analysis of human C1q by combined bottom-up and top-down mass spectrometry: detailed mapping of post-translational modifications and insights into the C1r/C1s binding sites. *Mol Cell Proteomics* (2010) **9**:593–610. doi:10.1074/mcp.M900350-MCP200
36. Garlatti V, Chouquet A, Lunardi T, Vives R, Paidassi H, Lortat-Jacob H, et al. Cutting edge: C1q binds deoxyribose and heparan sulfate through neighboring sites of its recognition domain. *J Immunol* (2010) **185**:808–12. doi:10.4049/jimmunol.1000184
37. Min X, Lemon B, Tang J, Liu Q, Zhang R, Walker N, et al. Crystal structure of a single-chain trimer of human adiponectin globular domain. *FEBS Lett* (2012) **586**:912–7. doi:10.1016/j.febslet.2012.02.024
38. Tacnet P, Cheong EC, Goeltz P, Ghebrehiwet B, Arlaud GJ, Liu XY, et al. Trimeric reassembly of the globular domain of human C1q. *Biochim Biophys Acta* (2008) **1784**:518–29. doi:10.1016/j.bbapap.2007.12.005
39. Blanquet-Grossard F, Thielens NM, Vendrely C, Jamin M, Arlaud GJ. Complement protein C1q recognizes a conformationally modified form of the prion protein. *Biochemistry* (2005) **44**:4349–56. doi:10.1021/bi047370a
40. Roos A, Ramwadhdoebe TH, Nauta AJ, Hack CE, Daha MR. Therapeutic inhibition of the early phase of complement activation. *Immunobiology* (2002) **205**:595–609. doi:10.1078/0171-2985-00157
41. Kang JH, Super M, Yung CW, Cooper RM, Domansky K, Graveline AR, et al. An extracorporeal blood-cleansing device for sepsis therapy. *Nat Med* (2014) **20**:1211–6. doi:10.1038/nm.3640
42. Didar TF, Cartwright MJ, Rottman M, Graveline AR, Gamini N, Watters AL, et al. Improved treatment of systemic blood infections using antibiotics with extracorporeal opsonin hemoadsorption. *Biomaterials* (2015) **67**:382–92. doi:10.1016/j.biomaterials.2015.07.046
43. Berner B, Scheel AK, Schettler V, Hummel KM, Reuss-Borst MA, Muller GA, et al. Rapid improvement of SLE-specific cutaneous lesions by C1q immunoadsorption. *Ann Rheum Dis* (2001) **60**:898–9.
44. Pfueller B, Wolbart K, Bruns A, Burmester GR, Hiepe F. Successful treatment of patients with systemic lupus erythematosus by immunoadsorption with a C1q column: a pilot study. *Arthritis Rheum* (2001) **44**:1962–3. doi:10.1002/1529-0131(200108)44:8<1962::AID-ART335>3.0.CO;2-R

Conflict of Interest Statement: The authors declare that the research was conducted in the absence of any commercial or financial relationships that could be construed as a potential conflict of interest.

frontiers in Immunology

ORIGINAL RESEARCH
published: 13 December 2016
doi: 10.3389/fimmu.2016.00567

Analysis of the Interaction between Globular Head Modules of Human C1q and Its Candidate Receptor gC1qR

Lina Pednekar[1], Ansar A. Pathan[1], Basudev Paudyal[1], Anthony G. Tsolaki[1], Anuvinder Kaur[1], Suhair M. Abozaid[1], Lubna Kouser[1], Haseeb A. Khan[2], Ellinor I. Peerschke[3], Mohamed H. Shamji[4], Gudrun Stenbeck[1], Berhane Ghebrehiwet[5] and Uday Kishore[1]**

[1] Biosciences, College of Health and Life Sciences, Brunel University London, London, UK, [2] Department of Biochemistry, College of Science, King Saud University, Riyadh, Saudi Arabia, [3] Department of Laboratory Medicine, Memorial Sloan-Kettering, Cancer Center, New York, NY, USA, [4] Allergy and Clinical Immunology, National Heart and Lung Institute, Imperial College London, London, UK, [5] Department of Medicine, State University of New York, Stony Brook, NY, USA

OPEN ACCESS

Edited by:
Cordula M. Stover, University of Leicester, UK

Reviewed by:
Robert Braidwood Sim, University of Leicester, UK
Goran Bajic, Harvard Medical School, USA

***Correspondence:**
Berhane Ghebrehiwet berhane.ghebrehiwet@stonybrookmedicine.edu; Uday Kishore uday.kishore@brunel.ac.uk, ukishore@hotmail.com

Specialty section:
This article was submitted to Molecular Innate Immunity, a section of the journal Frontiers in Immunology

Received: *04 July 2016*
Accepted: *22 November 2016*
Published: *13 December 2016*

Citation:
Pednekar L, Pathan AA, Paudyal B, Tsolaki AG, Kaur A, Abozaid SM, Kouser L, Khan HA, Peerschke EI, Shamji MH, Stenbeck G, Ghebrehiwet B and Kishore U (2016) Analysis of the Interaction between Globular Head Modules of Human C1q and Its Candidate Receptor gC1qR. Front. Immunol. 7:567. doi: 10.3389/fimmu.2016.00567

The heterotrimeric globular head (gC1q) domain of human C1q is made up of the C-terminal ends of the three individual chains, ghA, ghB, and ghC. A candidate receptor for the gC1q domain is a multi-functional pattern recognition protein, gC1qR. Since understanding of gC1qR and gC1q interaction could provide an insight into the pleiotropic functions of gC1qR, this study was undertaken to identify the gC1qR-binding site on the gC1q domain, using the recombinant ghA, ghB, and ghC modules and their substitution mutants. Our results show that ghA, ghB, and ghC modules can interact with gC1qR independently, thus reinforcing the notion of modularity within the gC1q domain of human C1q. Mutational analysis revealed that while Arg162 in the ghA module is central to interaction between gC1qR and C1q, a single amino acid substitution (arginine to glutamate) in residue 114 of the ghB module resulted in enhanced binding. Expression of gC1qR and C1q in adherent monocytes with or without pro-inflammatory stimuli was also analyzed by qPCR; it showed an autocrine/paracrine basis of C1q and gC1qR interaction. Microscopic studies revealed that C1q and gC1qR are colocalized on PBMCs. Cell proliferation assays indicated that ghA, ghB, and ghC modules were able to attenuate phytohemagglutinin-stimulated proliferation of PBMCs. Addition of gC1qR had an additive effect on the anti-proliferative effect of globular head modules. In summary, our results identify residues involved in C1q-gC1qR interaction and explain, to a certain level, their involvement on the immune cell surface, which is relevant for C1q-induced functions including inflammation, infection, and immunity.

Keywords: C1q, globular head, gC1qR, protein–protein interaction, cell proliferation

INTRODUCTION

C1q is the first subcomponent of the classical pathway of the complement system that links innate and adaptive immunity by virtue of recognizing IgG and IgM in the immune complexes (1). Structurally, human C1q (460 kDa) is made up of 18 polypeptides, i.e., 6A, 6B, and 6C chains. Each chain has a short N-terminal region, a collagen-like region (CLR), and a C-terminal globular head (gC1q) domain (2). A combination of interchain disulfide bond formation and triple-helical CLR gives rise to an ABC–CBA structural subunit. Three of these subunits associate to yield the hexameric

C1q molecule. The gC1q domain is a hetrotrimeric structure composed of C-terminal halves of A, B, and C chains. C1q is able to bind to an array of self, non-self, and altered-self ligands (3–7) *via* its gC1q domain (8). This ligand-binding versatility of C1q is offered by the modular organization of the individual globular head (gh) modules, ghA, ghB, and ghC, which are considered structurally and functionally independent (9–12).

A candidate receptor that binds to the gC1q domain of human C1q, called gC1qR (33 kDa), is a highly acidic, multi-ligand binding, and multi-functional protein. In addition to its role in the complement system, gC1qR is also involved in blood clotting *via* interaction with thrombin and vitronectin (13). Furthermore, as a high affinity receptor for high molecular weight kininogen and FXII, gC1qR present on the endothelial cells is able to serve as a major platform for the activation of the kinin/kallikrein, leading to the generation of the vasoactive peptide, bradykinin (14, 15).

Although the gC1q–gC1qR interaction has been described previously (16), the complementary binding sites and the precise nature of interaction remain to be fully established. The major gC1q-binding site on gC1qR has been shown to be located on residues 76–93 based on peptides studies (17). The availability of the recombinant individual gh modules, ghA, ghB, and ghC, which represent globular region of A, B, and C chains, respectively, without collagen region of C1q (18) has given us the opportunity to examine the gC1q–gC1qR interaction more closely. With respect to the structure/function relationship within the gC1q domain (19, 20), it is now known that ghA, ghB, and ghC are functionally independent modules. The modular organization of the gC1q domain offers C1q, the versatility required for binding to a range of self and non-self ligands. This is evident in the case of the HIV-1 gp41 peptide 601–613, which preferentially binds to ghA (20), and the β-amyloid peptide specifically interacting with ghB (20).

The crystal structure of gC1qR has revealed three monomers held together to form a trimer (21). Each monomer consists of seven anti-parallel β strands filled by an N-terminal and two C-terminal α helices. gC1qR has a distinct charge distribution, with the "solution face" of its "donut" shaped structure that is highly negatively charged and exposed to the plasma, while the reverse side or "membrane face" is neutral or basic (17). The C1q binding site, residues 76–93, is exposed only on the highly charged solution face (17). Since the C1q binding site on gC1qR has been identified, we sought to identify the complementary residues on the gC1q domain that are involved in the gC1q–gC1qR interaction. Previous studies have highlighted Arg^{B114} and Arg^{B129} of the B chain to be central in the C1q–IgG interaction (22). It has also been shown that C1q binding to gC1qR on platelets (23) and endothelial cells (24) induces complement activation independent of IgG. Furthermore, although gC1qR has been shown to bind to the gC1q domain of C1q, its physiological relevance still remains to be established.

Here, we have examined the interaction of recombinant forms of ghA, ghB, and ghC modules with gC1qR. We also used single residue substitution mutants for ghA, ghB, and ghC (19, 20, 22) that allowed us to identify residues on the gC1q domain that participate in the C1q–gC1qR interaction. A number of substitution mutants: ghA-R162A, ghA-R162E, ghB-R114A, ghB-R114Q, ghB-R163E, ghB-R163A, ghB-H117D, ghB-R129A, ghB-R129E, ghB-T175L, ghC-R156E, ghC-L170E, and ghC-H101A were tested for their interaction with gC1qR. The functional characterization of the point mutants identified an important role of Arg^{162} of ghA and Arg^{114} of ghB in the structure–function relationship involving C1q and gC1qR.

It is known that at sites of inflammation, adherent monocytes start to overexpress C1q. Thus, we performed a series of qPCR experiments to assess whether gC1qR expression was concomitant with C1q in adherent monocytes. gC1qR was upregulated, together with C1q on adherent monocytes, suggesting that both the ligand and the receptor are required under inflammatory conditions. The previously reported C1q-mediated anti-proliferative effect on T cells (25) could be reproduced qualitatively by the individual recombinant gh modules, which inhibited phytohemagglutinin (PHA)-stimulated proliferation of PBMCs. This anti-proliferative effect of gh modules was further enhanced by the addition of gC1qR, suggesting that gC1qR, in conjunction with C1q, can play an important role in modifying cellular immune responses.

EXPERIMENTAL PROCEDURES

Purification of Human C1q

C1q was purified from freshly thawed plasma, as published earlier (26). Briefly, plasma was made 5mM EDTA, pH 7.5, and centrifuged at 12,000 × *g* to remove aggregated lipids. The plasma was then incubated with non-immune IgG coupled to CNBr-activated Sepharose (GE Healthcare, UK) for 1 h at 4°C. The plasma was filtered through a sintered glass funnel, and C1q bound to IgG–Sepharose was then washed extensively with 10 mM HEPES, 140 mM NaCl, 0.5 mM EDTA, and pH 7.0. C1q was eluted with *N*-cyclohexyl-3-aminopropanesulfonic acid (CAPS) buffer (100 mM CAPS, 1 M NaCl, 0.5 mM EDTA, pH 11). The eluted C1q was then passed through a HiTrap Protein G column (GE Healthcare) to remove IgG contaminants and dialyzed against the washing buffer.

Expression and Purification of Wild-type ghA, ghB, ghC, and Substitution Mutants

The recombinant gh modules ghA, ghB, ghC, and their respective substitution mutants, were expressed in *Escherichia coli* BL21 fused to maltose-binding protein (MBP) in their monomeric forms (18). Bacterial cells were grown in 200 ml Luria–Bertani (LB) medium containing ampicillin (100 μg/ml) at 37°C on a shaker. Once grown to an OD_{600} of 0.6, the bacterial cells were induced with 0.4mM isopropyl β-D-thiogalactoside (IPTG) for 3 h and pelleted *via* centrifugation (4500 rpm for 15 min). The cell pellet was suspended in 25 ml of lysis buffer [20 mM Tris–HCl pH 8.0, 0.5 M NaCl, 1 mM EDTA, 0.2% v/v Tween 20, 5% glycerol, 0.1 mM phenylmethylsulfonyl fluoride (PMSF), and 100 μg/ml lysozyme] and incubated at 4°C for 1 h on a rotatory shaker. The cells were then sonicated (SoniPrep 150) at 60 Hz for 30 s with 2 min interval for 10 cycles. After centrifugation (13,000 rpm for 15 min), the supernatant was collected and diluted fivefold in buffer I (20 mM Tris–HCl, pH 8.0, 100 mM NaCl, 0.2% Tween

20, 1 mM EDTA, and 5% v/v glycerol) and passed through an amylose resin 15 ml bed column (New England Biolabs). The column was previously washed with three bed volumes of buffer I followed by buffer II (buffer I without Tween 20). The protein was then eluted in 1 ml fractions with 10 mM maltose in buffer II.

Cloning, Expression, and Purification of Human gC1qR

Recombinant mature gC1qR (residues 74–282) (27) was expressed in *E. coli* BL21 (λDE3) (Life Technologies). Bacterial cells were grown in 250 ml of LB medium at 37°C until an OD_{600} of 0.6 was reached and protein expression was induced with 0.5 mM IPTG. Following another 3 h incubation on a shaker, bacterial culture was spun down (4500 rpm, 15 min). The cell pellet was treated with lysis buffer (20 mM Tris pH 8.0, 0.5 M NaCl, 1 mM EDTA, 0.2% v/v Tween, 5% v/v glycerol, and 100 µg/ml lysozyme) and incubated for 1 h at 4°C with mild shaking. The resulting cell lysate was sonicated, as described above for gh modules. The sonicate was spun down at 13,000 rpm for 15 min, and the collected supernatant was dialyzed for 2 h against 20 mM Tris–HCl, pH 7.5. The dialyzed protein was subjected to an ion exchange chromatography using a Q-Sepharose column (Sigma). gC1qR was step-eluted at 0.45 M NaCl. Although we did not determine the oligomeric state of the recombinant gC1qR, it is likely to be a trimeric structure, based on the crystallization studies (21).

The purified fractions were passed through Pierce™ High Capacity Endotoxin Removal Resin (Thermo Fisher) to remove lipopolysaccharides (LPSs). Endotoxin levels in the protein preparations were determined using the QCL-1000 Limulus amebocyte lysate system (BioWhittaker Inc., USA). The assay was linear over a range of 0.1–1.0 EU/ml (10 EU = 1 ng of endotoxin) and the amount of endotoxin present in the preparations was estimated to be <4 pg/µg of the recombinant protein.

ELISA

Direct binding ELISA was performed to examine the interaction of C1q and gh modules with gC1qR. Microtiter wells (Maxisorp, Nunc) were coated with 1 µg of gC1qR (in 100 µl) in carbonate/bicarbonate buffer, pH 9.6, and left overnight at 4°C. Unbound proteins were removed and the wells were blocked with 2% w/v BSA in PBS for 2 h at 37°C. The plate was then washed three times with PBS + 0.05% Tween 20, and then different concentrations (2.5, 1.25, 0.625, and 0.312 µg/well) of ghA, ghB, or ghC modules (MBP as a control protein) were diluted in calcium buffer (50 mM Tris–HCl pH 8.0, 100 mM NaCl, and 5 mM $CaCl_2$) and added to the wells. The plate was kept first at 37°C for 1 h and then at 4°C for another hour. Following further washes, the bound protein was detected by anti-MBP monoclonal antibody (Sigma) (1:5000 dilution in PBS) and probed with rabbit anti-mouse IgG Horseradish peroxidase (HRP; 1:5000; Promega; #W402b) in PBS. Color was developed using *o*-phenylenediamine dihydrochloride (OPD) substrate (Thermo-Fisher Scientific) and the plate was read at 450 nm using iMark Microplate Absorbance reader (Bio-Rad).

Microtiter wells were coated with different concentrations of human C1q (5, 2.5, 1.25, and 0.625 µg/well in 100 µl) in carbonate/bicarbonate buffer, pH 9.6, and left overnight at 4°C. Unbound proteins were removed and the wells were blocked with 2% w/v BSA in PBS for 2 h at 37°C. The plate was then washed three times with PBS + 0.05% Tween 20, and then the wells were incubated with 2.5 µg of gC1qR in calcium buffer (50 mM Tris–HCl, pH 8.0, 100 mM NaCl, and 5 mM $CaCl_2$). The plate was kept first at 37°C for 1 h and then at 4°C for another hour. Following further washes, bound gC1qR was detected by anti-gC1qR polyclonal antibody (IgG fraction; 1:5000 dilution), followed by Protein A-HRP (1:5000 dilution) conjugate. MBP was used as a negative control protein.

Western Blotting

The immunoreactivity of the recombinant gC1qR (10 µg/lane) was assessed by western blotting. Following a 12% v/v SDS-PAGE gel, the protein was electrophoretically transferred onto PDVF membrane, followed by blocking for 1 h at room temperature with 5% non-fat milk in PBS. Recombinant human gC1qR was probed with rabbit anti-human gC1qR polyclonal antibodies (IgG fraction; 500 µg/ml concentration; 1:1000 dilution) and incubated at 37°C for 1 h. The membrane was washed three times in 0.02% PBS–Tween 20, 30 min each and probed with Protein A-HRP conjugate (Sigma, 1:1000 dilution in PBS) for 1 h at room temperature. Color was developed using 3,3′-diaminobenzidine (DAB).

Far-western blot was carried out to test the interaction of ghA, ghB, ghC, and key substitution mutants with gC1qR. Ten micrograms of each protein was run on a SDS-PAGE gel, followed by transferring and blocking as described above. Fifteen micrograms per milliliter of either the gh's modules or gC1qR was added in 10 ml calcium buffer (20 mM Tris–HCl, pH 7.5, 5 mM $CaCl_2$, and 100 mM NaCl) and incubated overnight at 37°C. Membranes were washed and probed with either polyclonal anti-gC1qR or rabbit anti-MBP (Life Technologies, 1:1000) polyclonal antibodies which were diluted in 2% w/v non-fat milk powder in PBS and incubated for 2 h at 37°C. The blots were developed as described above.

Fluorescence Microscopy

The binding of recombinant ghA, ghB, and ghC modules to gC1qR was examined microscopically using monocyte-derived human macrophages. Human PBMCs were separated from human blood from healthy volunteers (with ethical approval by the Institutional committee of Brunel University London) by Ficoll-paque (GE Healthcare) density gradient method. The separated PBMCs were suspended in complete medium (RPMI 1640, 2mM L-glutamine, 100 µg/ml Penicillin/Streptomycin, and 10% FCS). The 1×10^6 cells were seeded on 13 mm diameter cover slips and incubated for 14 days at 37°C in 5% CO_2 incubator.

PBMCs were treated with 10 µg of individual gh modules for 1 h at 37°C in serum-free medium. MBP (10 µg) was used as a negative control protein. Cells were then washed three times with PBS, fixed using 4% paraformaldehyde (PFA) for 10 min, and then rinsed with PBS three times. The coverslips were permeabilized using a buffer containing 20mM HEPES–NaOH pH 7.4, 300mM sucrose, 50mM NaCl, 3mM $MgCl_2$, 0.5% Triton X-100, and 10% sodium azide for 5 min on ice, and then blocked with 5% FCS

in PBS (wash buffer) for 30 min. The slides were then incubated with mouse anti-MBP (1:500 dilution in wash buffer) and rabbit anti-gC1qR antibodies (1:100 dilution in wash buffer) for 30 min. The slides were washed three times in wash buffer, 10 min each, and subsequently incubated with secondary antibodies: Alexa Fluor 647 conjugated donkey-anti-mouse antibody (Abcam; Cat: ab150111) 1:500 dilution in wash buffer and Alexa Fluor 488 conjugated goat anti-rabbit antibody (Abcam; Cat: ab150077) 1:500 dilution in wash buffer for 30 min. To stain the nucleus, Hoechst 33342 (Invitrogen, Cat: H3570 at 1:10,000 dilution) was used. The slides were then washed three times in the wash buffer 10 min each, mounted using Citifluor anti-fade (Citifluor, UK) and observed under a Leica DM4000 Fluorescent microscope using Leica Application Suite Software. In the merged images, the Alexa Fluor 647 color was set to red.

Quantitative RT-PCR

Whole blood (50 ml) was taken from healthy volunteers and 2 units/ml of heparin sodium (product details – PL 29931/015) (Wockhardt), was added to prevent blood clotting. Blood was then diluted with an equal volume of RPMI 1640. To isolate monocytes, blood in RPMI 1640 was separated on a Ficol column (Ficol-Plaque Plus, GE healthcare) by centrifugation at 2000 rpm for 16 min at room temperature. The top layer was removed and PBMCs interphase layer was carefully removed. An equal volume of RPMI 1640 was then added and the cells were pelleted by centrifugation at 1500 rpm for 10 min at room temperature. Cells were then re-suspended in 50 ml of RPMI 1640 and the cell concentration was determined using a hemocytometer (total yield 7×10^7 cells).

Then, 5×10^6 cells were added to each tissue culture well in a 24-well plate in 5 ml of RPMI 1640 containing 10% FCS, 100 µg/ml penicillin-streptomycin, and 2 mM L-glutamine, and incubated at 37°C with 5% CO_2 v/v atmosphere and left to adhere. Cells were then harvested at the following time points of incubation for adherence: 2 h, 24 h, 48 h, 72 h, 5 days, and 7 days. A similar experiment was also set up with the addition of 20 ng/µl of LPS (*Salmonella typhimurium*, Sigma-Aldrich). Adherent cells, with or without LPS, from each time point were harvested by removing the media from the plate and incubating cells in RPMI 1640 containing 0.025% trypsin/0.01% EDTA for 5 min at 37°C. Cells were removed using a cell scraper and an equal volume of RPMI 1640 containing 10% FCS was added to the harvested cells. Cells were pelleted by centrifugation at 1500 rpm for 10 min at room temperature and stored at −80°C until RNA extraction was carried out.

Total RNA was extracted using the GenElute Mammalian Total RNA Purification Kit (Sigma-Aldrich). Samples were then treated with DNase I (Sigma-Aldrich) to remove any contaminating DNA followed by heating at 70°C for 10 min to inactivate both DNase I and RNase, and then chilled on ice. The amount of total RNA was measured by determining the absorbance at 260 nm using the NanoDrop 2000/2000c (Thermo-Fisher Scientific) and the purity of the RNA was assessed using the ratio of absorbance at 260 and 280 nm. cDNA was synthesized using High Capacity RNA to cDNA Kit (Applied Biosystems) using 2 µg of total RNA.

Primer sequences were designed using the nucleotide Basic Local Alignment Search Tool and Primer (BLAST, http://blast.ncbi.nlm.nih.gov/Blast.cgi). The following primers were used: for 18S rRNA gene (endogenous control): forward (5′-ATG GCCGTTCTTAGTTGGTG-3′), reverse (5′-CGCTGAGCCAGT CAGTGTAG-3′); for C1q C chain gene: forward (5′-CAAA GGGCAGAAGGGAGAAC-3′), reverse (5′-ATCTGATCAGGC TGTTGGGT-3′); and for gC1qR gene: forward (5′-AACAA CAGCATCCCACCAAC-3′), reverse (5′-AGATGTCACTCTCA GCCTCG-3′).

PCR was performed on all samples in order to assess the quality of cDNA. The qPCR reactions, performed for measuring the expression level of C1q and gC1qR, consisted of 5 µl Power SYBR Green MasterMix (Applied Biosystems), 75nM of forward and reverse primer, 500 ng template cDNA in a 10 µl final volume, using a 7900HT Fast Real-Time PCR System (Applied Biosystems). The initial steps were 2 min incubation at 50°C, followed by 10 min incubation at 95°C. The template was then amplified for 40 cycles under these conditions: 15 s at 95°C and 1 min at 60°C. Samples were normalized using the expression of human 18S rRNA. Data were analyzed using the Relative Quantification (RQ) Manager Version 1.2.1 (Applied Biosystems). Cycle threshold (Ct) values for each target gene were calculated and the relative expression was calculated using the RQ value *via* the formula: $RQ = 2^{-\Delta\Delta Ct}$ for each target gene, and comparing relative expression with that of the 18S rRNA constitutive gene product. Assays were conducted twice in triplicate. Statistical analysis was performed using GraphPad Prism version 6.0 (GraphPad Software). An unpaired two-side *t*-test was used to compare the means of the expressed targets of the time points analyzed, using the 2 h time point as the calibrator. *p* Values were computed, and graphs compiled and analyzed.

Cell Proliferation Assay

PBMCs were re-suspended in serum-free medium containing RPMI 1640, Penicillin/Streptomycin and Sodium Pyruvate, and stimulated with PHA (Sigma; 11249738001) at a concentration of 1 µg/ml and 1×10^5 cells (100 µl) were aliquoted per well in a 96-well tissue culture plate. Next, the cells were treated with 20 µg/ml of ghA, ghB, ghC, or gC1qR in their respective wells. Different concentrations of gC1qR (1.25, 2.5, 5, and 10 µg) were also coincubated with 20 µg each of gh modules. At the 72 h time point, ^{3}H-methy thymidine (MP Biomedicals, USA) was added and the plate was pulsed for 16 h. Cells were subsequently harvested using a semi-automated cell harvester and the amount of ^{3}H-thymidine incorporated into DNA was measured using a liquid scintillation counter. Each experiment was conducted in triplicates.

RESULTS

Expression and Purification of Recombinant Human gC1qR in *E. coli* under Bacteriophage T7 Promoter

Recombinant expression of human gC1qR has been previously reported in *E. coli* as fusion to Glutathione-S-transferase (28).

Here, we expressed human gC1qR without any fusion partner under a strong bacteriophage T7 promoter. *E. coli* BL21 (λDE3) cells, containing the gC1qR construct, expressed a ~33 kDa protein following IPTG induction, compared to the uninduced cells (**Figure 1A**). The overexpressed protein appeared in the soluble fraction following cell lysis and sonication. Recombinant gC1qR was subsequently purified using Q-Sepharose. It was step-eluted at 0.45 M NaCl and appeared as a single band on SDS-PAGE under reducing conditions. The immunoreactivity of the purified recombinant gC1qR was confirmed by western blot using anti-gC1qR polyclonal antibodies that were raised against native human gC1qR (**Figure 1B**).

Recombinant gC1qR Binds Differentially to the Three Globular Head Modules of Human C1q

The recombinant gh modules ghA, ghB, ghC (**Figure 2A**) and their substitution mutants (**Figures 2B–D**) were expressed as MBP fusion proteins and purified on amylose resin. gC1qR bound full-length C1q in a dose-dependent manner (**Figure 3A**). When different concentrations of the ghA, ghB, and ghC modules were allowed to bind to a constant concentration of gC1qR, all modules bound to gC1qR independently in a dose-dependent manner (**Figure 3B**). ghA showed greater binding at 2.5 µg when compared with the other two modules, which is consistent with previous findings (29), which implicated ghA to be the most important gh region in the C1q–gC1qR interaction. To confirm the ELISA results, far-western blot was performed using recombinant gC1qR, ghA, ghB, and ghC proteins. Transferring gC1qR onto PDVF membrane and probing with gh modules revealed independent binding of ghA, ghB, and ghC to gC1qR (**Figure 3C**). Similarly, ghA, ghB, or ghC transferred onto PDVF membrane and individually probed with gC1qR confirmed the interaction (data not included) that each gh module binds specifically to gC1qR irrespective of their immobilized orientation on the membrane.

Arg^{A162} Is Crucial for C1q–gC1qR Interaction

Using ELISA, we examined the ability of gC1qR to interact with recombinant ghA and its single residue substitution mutants, ghA-R162A (i.e., Arg^{A162}Ala) and R162E. Different amounts of gC1qR were coated on microtiter wells and incubated with wild-type ghA, R162A and R162E. As shown in **Figure 4A**, the substitution of Arg^{A162} to Ala (R162A) resulted in up to 70% reduction in gC1qR binding at 1 µg/ml concentration, with respect to the background binding to MBP control protein. Substitution of Arg^{A162} with Glu (R162E) resulted in similar abrogation of binding when compared to wild-type ghA. To further confirm these observations, we carried out a far western blot (**Figure 4D**). Thus, 15 µg of gC1qR was transferred onto a PDVF membrane and probed with 10 µg each of ghA, R162E and R162A. **Figure 4D** shows a clear band for wild-type ghA. However, probing with the mutants revealed a very faint band for R162A while no band could be detected on the blot in the case of R162E.

Arginine and Histidine Residues within the ghB Module Appear Important for Stabilizing C1q–gC1qR Interaction

The ability of ghB and its single residue substitution mutants (R114Q, R114A, R163A, R163E, T175L, R129A, R129E, and H117D) to bind microtiter-coated gC1qR was examined using ELISA. The mutant Arg^{B114} to Gln (R114Q) bound better to gC1qR than the wild-type ghB (**Figure 4B**), suggesting that replacing a charged (polar) residue with an uncharged residue can strengthen binding between the two proteins. Substituting Arg^{B114} with Ala,

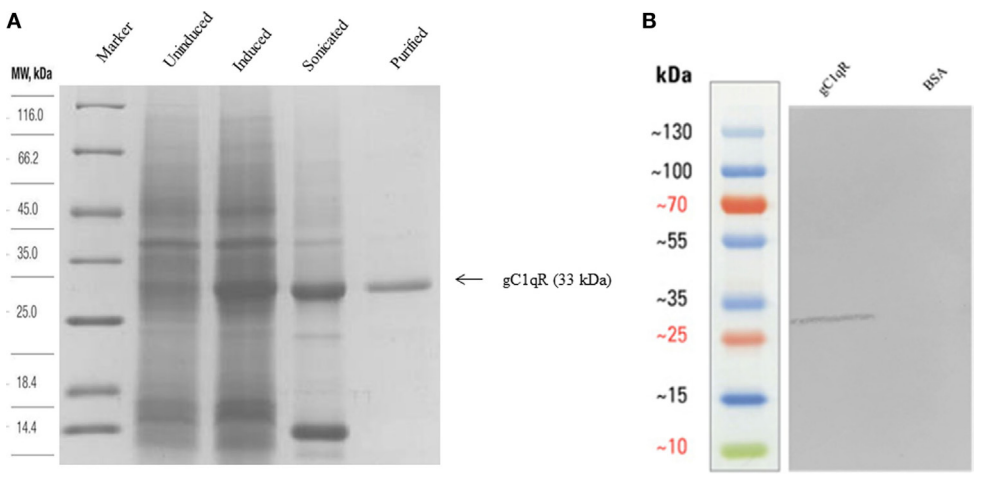

FIGURE 1 | **(A)** Expression and purification of recombinant gC1qR. Twelve percent (v/v) SDS-PAGE under reducing conditions. *E. coli* BL21 (λDE3) strain, transformed with plasmid T7-gC1qR and induced with IPTG, overexpressed a ~33 kDa protein (induced) as compared to uninduced cells. Following lysis and sonication of the bacterial cells, the overexpressed gC1qR appeared in the soluble fraction sonicate, which was further purified on a Q-Sepharose column. **(B)** Western blotting to show immunoreactivity of recombinant gC1qR: 10 µg of recombinant gC1qR protein was run on a 12% v/v gel and transferred onto a nitrocellulose membrane, which was probed with anti-gC1qR polyclonal antibody. BSA was used as a negative control protein.

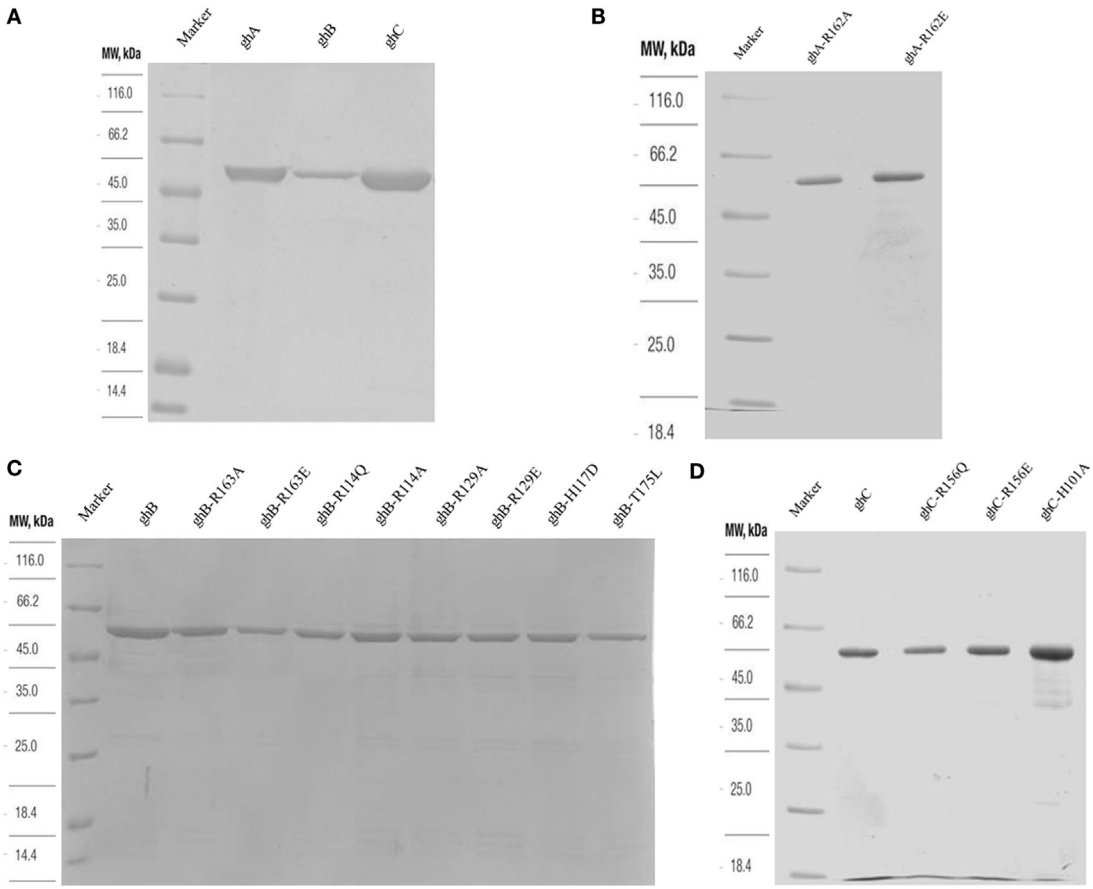

FIGURE 2 | SDS-PAGE (12% w/v) under reducing conditions of purified fusion proteins following affinity chromatography. MBP fusion proteins containing wild type and mutant globular head modules were purified using an amylose resin column **(A)**. Purified ghA, ghB and ghC **(B)** purified substitution mutants of ghA module; **(C)** purified mutants of ghB module, R163A, R163E, R114Q, R114A, R129A, R129E, H117D, and T175L; **(D)** purified ghC, R156Q, R156E, and H101A.

however, was not comparable with R114Q (**Figure 4B**). Out of all the ghB mutants, R114A, R129E, R163E, and H117D showed considerable reduction in binding. Thus, substituting arginine with glutamine had an adverse effect on the ghB–gC1qR interaction. Substituting His to Asp reduced ghB affinity for gC1qR by nearly 60%, which suggests that His^{B117} is very important for gC1qR binding. When comparing all the ghB substitution mutants, it was evident that the most significant effect was caused by the substitution of arginine to glutamine, suggesting that Arg^{B163} is crucial for gC1qR binding to C1q (**Figure 4B**). Similar observations were noted for the ghC mutants (**Figure 4C**).

Microscopy Studies

Since we established that ghA, ghB, and ghC individually bind to gC1qR, we performed microscopic studies to determine whether the gh's of C1q can colocalize with gC1qR on the surface of PBMCs. We first verified the interaction by identifying gC1qR on the surface using polyclonal antibodies against gC1qR (gC1qR in **Figure 5**). Incubation of the gh modules and probing with anti-MBP monoclonal antibodies showed the gh's bound on the surface of PBMCS with partial colocalization to gC1qR (**Figure 5**, arrows in merged images).

Transcriptional Expression of gC1qR and C1q in Adherent Monocytes

To examine a possible correlation between the temporal pattern of expression of C1q and gC1qR, qPCR analysis was performed in view of the fact that adherent monocytes upregulate C1q expression, a situation that mimics inflammation. In addition, the expression of C1q and gC1qR in the adherent monocytes was also assessed with and without LPS challenge (acting as a pro-inflammatory stimulus). C1q-RNA expression increased markedly in monocytes during adherence, peaking at 72 h with a $\log_{10}$ 3.5-fold difference compared to 2 h after adherence (**Figure 6A**). In contrast, incubation with LPS had a suppressive effect on C1q expression. There was also an increase in the gC1qR expression during monocyte adherence, with the pattern of expression appearing to be biphasic in nature with the peaks observed at 24 and 72 h (**Figure 6B**). In contrast to C1q, the presence of LPS elevated the expression of gC1qR, peaking at 24 h adherence,

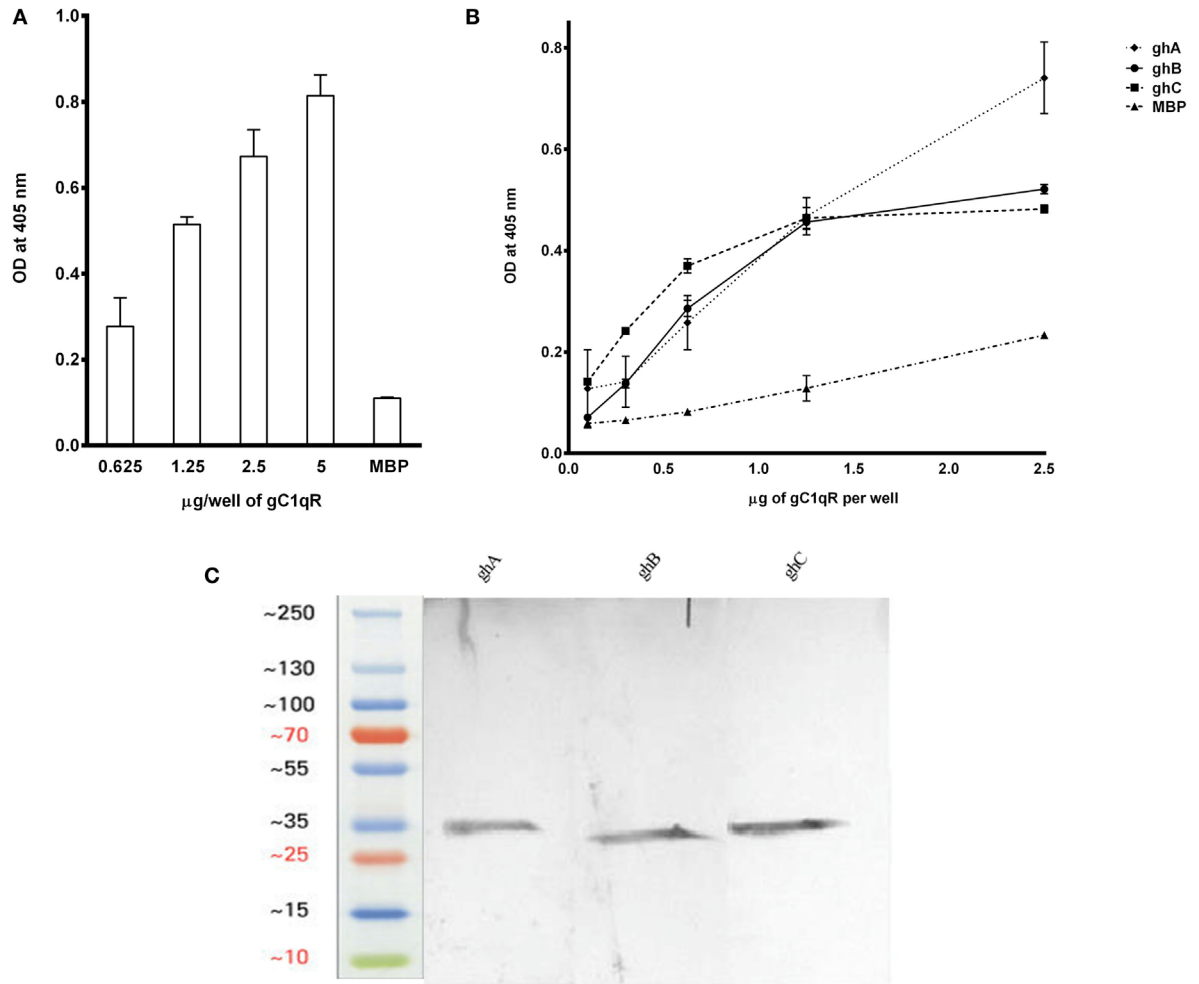

FIGURE 3 | **(A)** ELISA to show binding of gC1qR to C1q: microtiter wells, coated with different concentrations of human C1q (5, 2.5, 1.25, and 0.625 µg/well), were incubated with 2.5 µg of gC1qR. Bound gC1qR was detected by anti-gC1qR polyclonal antibody followed by Protein A-HRP conjugate. MBP was used as a negative control protein. **(B)** ELISA to assess interaction of gC1qR with ghA, ghB, and ghC modules. gC1qR (1 µg/well in 100 µl) was coated on microtiter wells and then incubated with various concentrations of wild type of ghA, ghB, and ghC. MBP was used as a negative control. Following washing, bound protein was detected using anti-MBP monoclonal antibody and goat anti-mouse IgG HRP conjugate. **(C)** Far-western blot analysis to show ghA, ghB, and ghC binding to gC1qR: 15 µg of gC1qR was first run on the SDS-PAGE under reducing conditions, transferred onto a PDVF membrane and then probed with 10 µg each of ghA, ghB, and ghC. Lanes 1 through 3 show interaction of gC1qR with ghA, ghB, and ghC, respectively.

more than twice the level observed without LPS. These results are consistent with an earlier study, showing enhancement of gC1qR surface expression on endothelial cells after 24 h (30). However, LPS seems to cause enhancement of gC1qR expression rather than inhibition, unlike C1q (**Figure 6A**), suggesting that gC1qR on its own may have a regulatory role in LPS-mediated inflammation.

ghA, ghB, ghC, and gC1qR Inhibit PHA-Stimulated Proliferation of PBMCs

Since C1q is known to have anti-proliferative effect on T cells (25), we examined if this inhibition is mediated through the gC1q domain. ghA, ghB, and ghC individually were able to inhibit PHA-stimulated proliferation of PBMCs (**Figure 7A**), as measured by thymidine uptake. The gh modules inhibited proliferation by >threefold when compared to PBMCs stimulated with PHA alone and MBP control. Next, we sought to determine whether the addition of different concentration of gC1qR to a fixed gh concentration would further inhibit proliferation. **Figure 7B** shows an inhibitory dose response for each gh module with the addition of gC1qR at different concentrations. The addition of 1.25 µg of gC1qR increased ghA and ghC mediated anti-proliferative effects by 40% (**Figure 7B**).

DISCUSSION

C1q, as a charge pattern recognition protein, is able to bind to a range of self and non-self-ligands through its heterotrimeric

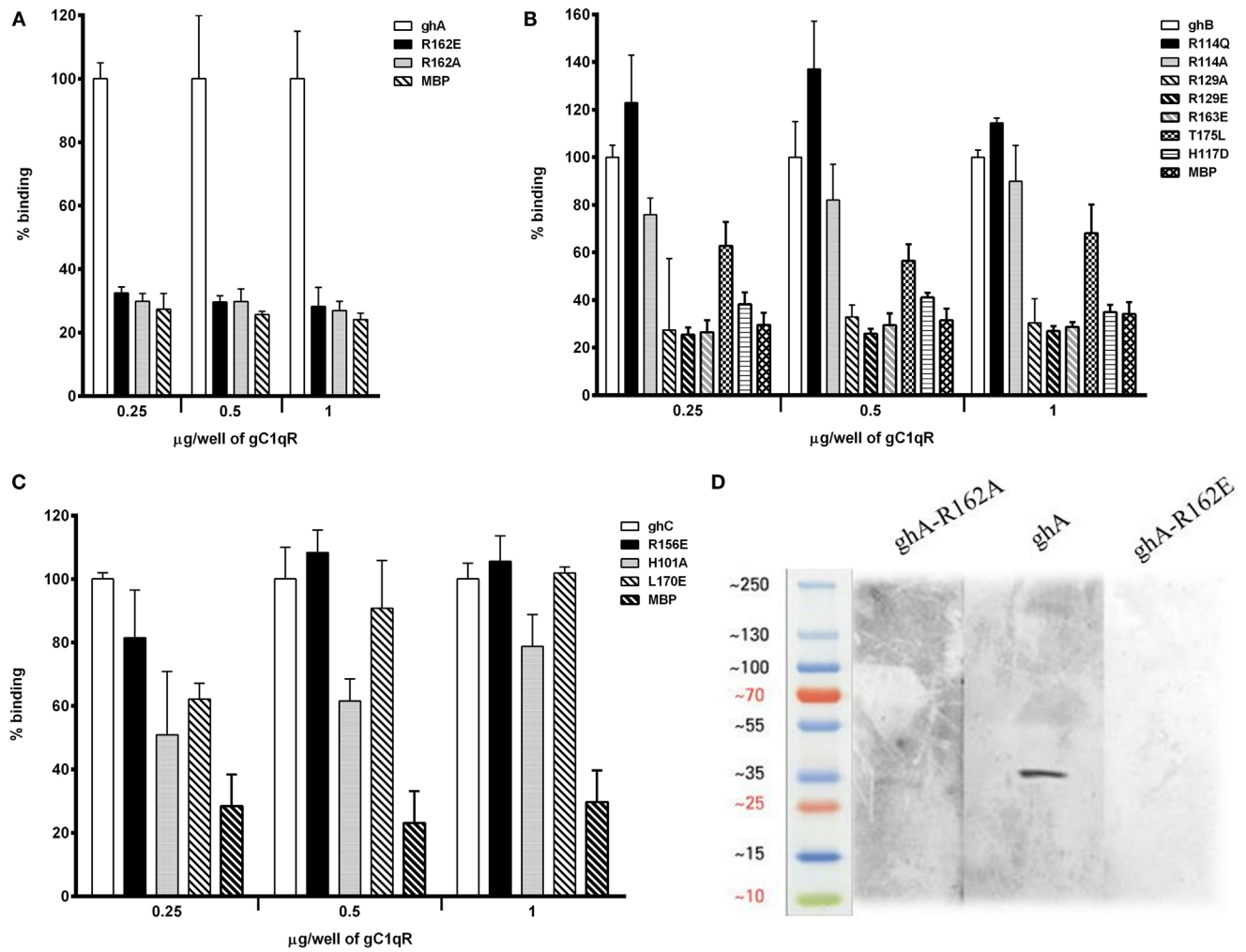

FIGURE 4 | ELISA to assess interaction between gC1qR and gh substitution mutants. Microtiter wells were coated with different quantities (0.25, 0.5, and 1 µg/well) of gC1qR. After blocking and washing, the wells were incubated with 2.5 µg/well of **(A)** ghA, R162A and R162E; **(B)** ghB, R114A, R114Q, R163A, R163E, R129A, R129E, T175L, and H117D; and **(C)** ghC, for 90 min at 37°C and 90 min at 4°C. Bound proteins were detected with anti-MBP monoclonal antibody followed by goat anti-mouse IgG–HRP conjugate. Data are representative of three experiments. **(D)** Ligand blot to show binding of ghA mutants R162A and R162E to gC1qR: PVDF membrane strips containing gC1qR were reacted with ghA, R162A and R162E, and then probed with anti-MBP monoclonal antibody followed by goat anti-mouse IgG–HRP.

gC1q domain (5, 31). The gC1q domain is also found in a range of non-complement proteins (22, 32, 33), including collagen VIII, precerebellin, and multimerin (2, 32–37). The crystal structure analysis of the gC1q domain shows a sphere-shaped, heterotrimeric arrangement with the N- and C-terminal ends of each domain residing at the base of the trimer (5). The crystal structure has also identified an exposed Ca^{2+} ion located at the apex; this has been considered important in the binding of gC1q to its ligands.

Out of several candidate receptors for C1q, calreticulin (cC1qR) binds to the collagen region of C1q, while gC1qR interacts with the gC1q domain (2, 13). However, the nature and the context of interaction between C1q and gC1qR have not been examined. Previous studies, using ligand blot analysis with C1q run under reducing conditions, have shown that gC1qR binds predominantly to the A chain and moderately to the C chain of C1q with the A chain Arg residue at positions 162 being critical for binding (28). The availability of the recombinant forms of ghA, ghB, and ghC (18) and their substitution mutants (22) gave us with the opportunity to fully explore the gC1q–gC1qR interaction.

Previous studies have shown that gC1qR inhibits aggregated IgG-mediated complement activation by binding to the gC1q site on C1q, thereby preventing IgG from binding to the gh's (28), suggesting that the binding sites for gC1qR and IgG on C1q may be identical or at least overlapping. It has also been shown that one of the IgG binding sites resides on Arg^{162} of the A chain (38), consistent with the mutational studies where the mutant R162E showed reduced the ability of C1q to bind to IgG by 35% (22).

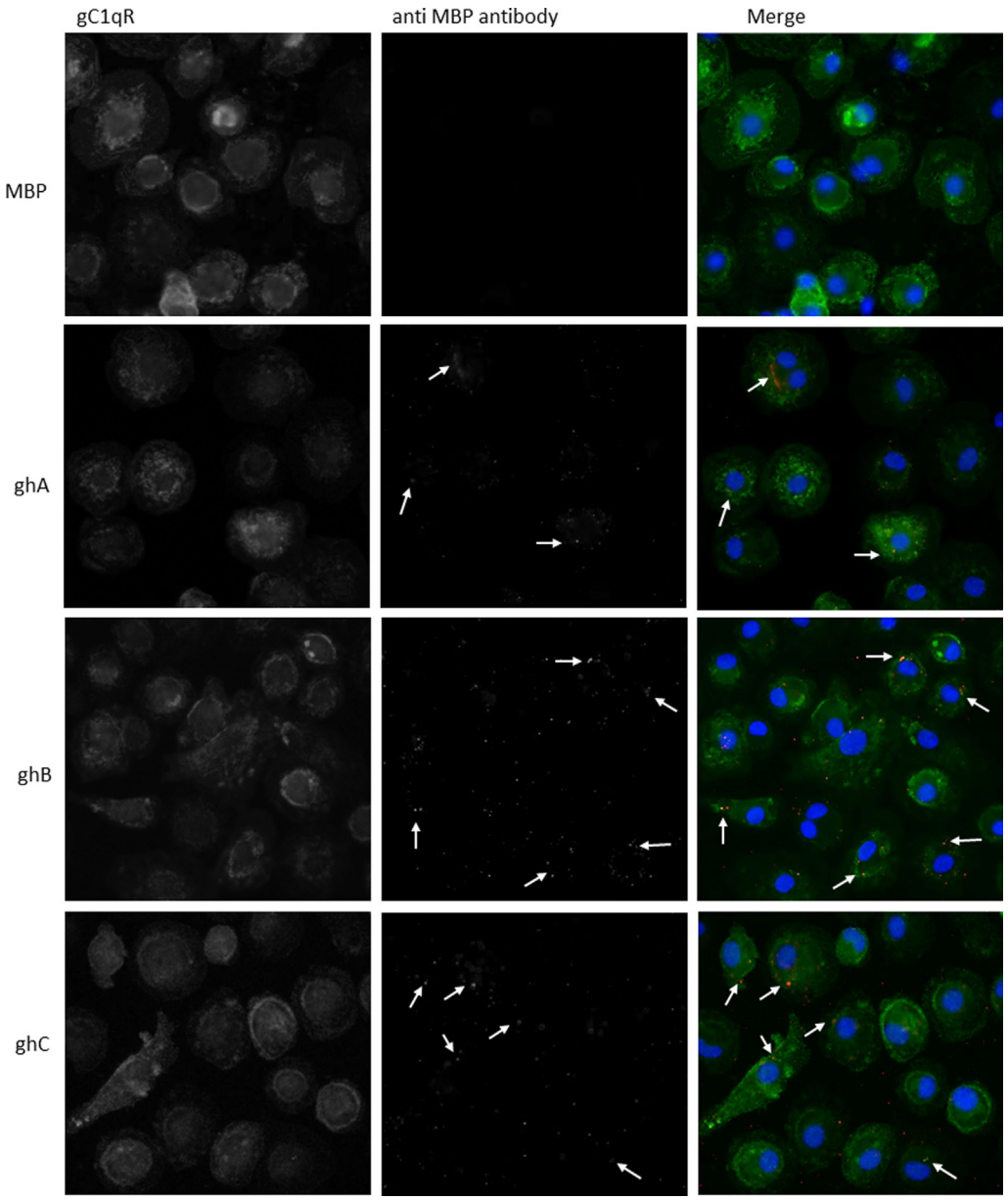

FIGURE 5 | **Interaction of ghA, ghB, and ghC with monocyte/macrophages**. PMBCs (1×10^6) were seeded on 13 mm coverslips and incubated in complete RPMI 1640 medium for 2 weeks at 37°C in 5% CO_2 incubator. Cells were treated with 10 μg of each globular head module and incubated with serum-free RPMI 1640 medium for 1 h at 37°C. After washing with PBS, cells were fixed with 4% PFA, permeabilzed with Triton X-100, and probed with anti-gC1qR polyclonal antibody and anti-MBP monoclonal antibody to reveal gC1qR and bound globular head modules, respectively. Cells were washed and treated with Alexa Fluor 488 conjugated secondary goat anti-rabbit antibody and Alexa Fluor 647 conjugated secondary donkey anti-mouse antibody and the nucleus was stained with Hoechst 33342. Cells were then examined under Leica fluorescence microscope with 40× magnification. In the merged images gC1qR is green; globular heads are red; and nucleus is blue. Arrows point to bound globular heads with colocalization of globular heads and gC1qR seen in orange in the merged images. Scale bars: 10 μm.

The importance of arginine residues in the ligand recognition of gC1q domain is consistent with the observation in this study (**Figure 3B**). Ghebrehiwet et al. have previously shown that the Arg^{162} in C1q A chain is significant in gC1qR binding (39). A peptide corresponding to the A chain with the Arg residue at position 162 substituted to Glu showed no binding to gC1qR. It has also been noted that residues 154–165 of the A chain are implicated in IgG binding (38), and inhibition studies have demonstrated that forming a complex between gC1qR and C1q prevented C1q binding to SRBCs, and hence, complement activation. These data are consistent with **Figure 4A**, which shows that substitution of the arginine residue in ghA reduces its binding to gC1qR considerably. We further examined the contributions of Arg^{114}, Arg^{163}, and His^{117} (of ghB) and Arg^{156} (of ghC) to the C1q–gC1qR

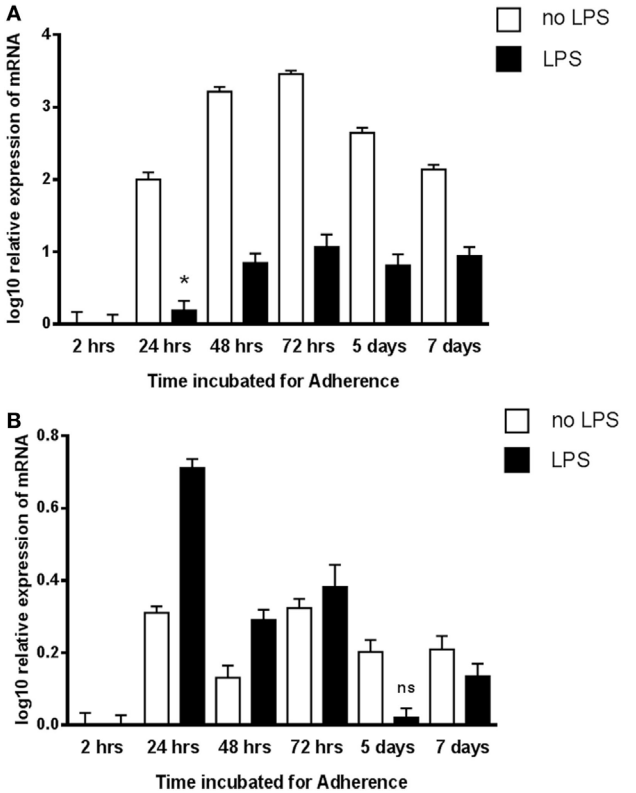

FIGURE 6 | Expression of C1q (A) and gC1qR (B) by adherent human monocytes *in vitro*. The expression of C1q and gC1qR was measured using real-time qPCR and the data were normalized *via* 18S rRNA gene expression as a control. Relative expression (RQ) was calculated by using the 2 h time point as the calibrator. The RQ value was calculated using the formula: $RQ = 2^{-\Delta\Delta Ct}$. Assays were conducted twice in triplicates. Error bars represent ±SEM. A two-side *t*-test was performed on the data. All samples showed significant expression compared to the calibrator ($p \leq 0.01$), except where noted: $^{*}0.01 < p < 0.05$; ns: not significant ($p \geq 0.05$). LPS was added to cultures at a 20 ng/μl concentration.

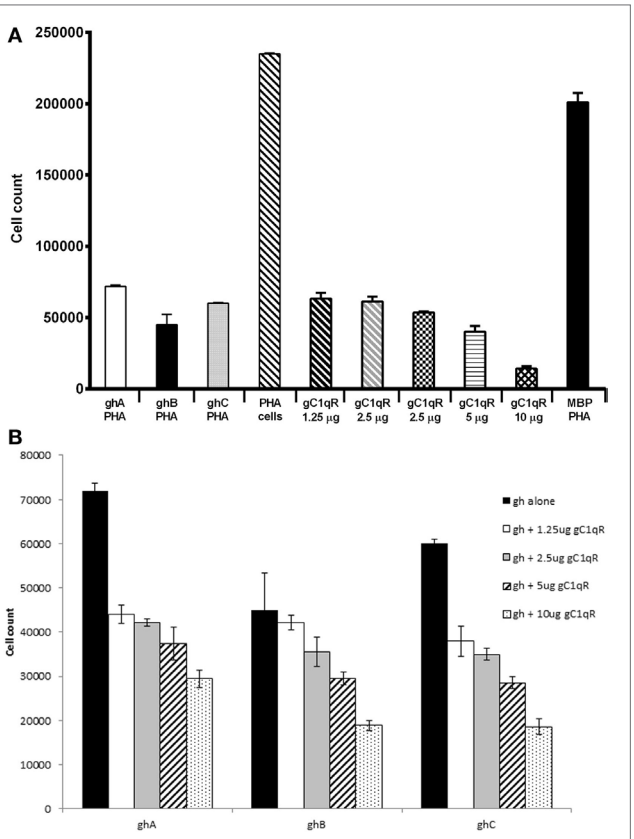

FIGURE 7 | Anti-proliferative effects of ghA, ghB, and ghC modules. Human PBMCs from healthy individuals were stimulated with PHA (1 μg/ml) for 3 days with or without recombinant gC1qR (1.25, 2.5, 5, 10, and 20 μg/ml), ghA, ghB, or ghC (20 μg/ml) followed by a 16 h pulse in the presence of tritiated methyl thymidine ([^{3}H]TdR). Each experiment was carried out in triplicates. **(A)** Each of ghA, ghB, ghC, and gC1qR inhibited PHA-stimulated proliferation of PBMCs; **(B)** ghA, ghB, and ghC coincubated with gC1qR inhibit PHA-stimulated proliferation of PBMCs.

interaction by substituting them with either neutral or negatively charged residues. Thus, the substitution of Arg to glutamine at amino acid 114 position of the B chain showed a much better binding to gC1qR than the wild-type ghB. The observation that a substitution mutant interacts better than the wild type is of great interest, offering an opportunity to neutralize the involvement of gC1qR in infection and inflammation. Experiments involving chemical modification have shown Arg^{11} of the B chain to be an important residue in IgG binding (38).

The qPCR-based mRNA expression studies appeared to suggest that both C1q and gC1qR are upregulated in adherent monocytes in a biphasic manner. It is likely that the two proteins are coexpressed under pro-inflammatory conditions and can regulate each other's functions, or may have distinct functions by recognizing unique self and non-self-molecular targets. When LPS was used in the assay, the expression of C1q was down-regulated, but gC1qR levels were upregulated, suggesting that C1q and gC1qR may have distinct roles in LPS-mediated immune response that are independent of each other.

Since C1q is known to exert an anti-proliferative effect on T cells (25), it was of interest to examine if individual gh modules were also anti-proliferative and if the addition of gC1qR in the assay could modulate this effect. Here, we show that ghA, ghB, and ghC modules also possess anti-proliferative properties of C1q (**Figure 7**). gC1qR had an additive effect on the anti-proliferative effects of gh modules in a dose-dependent manner (**Figure 7A**). The engagement of C1q with gC1qR, expressed on $CD4^{+}$ and $CD8^{+}$ T cells, is known to suppress cell proliferation (25). Therefore, further attenuation of cell proliferation by gC1qR is likely to be mutually beneficial for the immune regulation. Previously, it was thought that the "full-length" gC1qR (residues 1–282) was mostly resident in the mitochondria, which is then cleaved off to release the "mature form" (residues 74–282) expressed on the cell surface (16). However, subsequent studies have shown that the membrane associated-form is, in fact, the full-length gC1qR from which the mature form consisting of residues 74–282 is cleaved off and released as a soluble form into the pericellular milieu. On endothelial cells, the soluble form has been shown to induce bradykinin 1 receptor (B1R) expression by

binding to surface bound fibrinogen in an autocrine manner (40). Thus, the soluble gC1qR is capable of binding to immune cells and modulating various cellular immune responses, including cell proliferation. The anti-proliferative activity of gC1qR has also been demonstrated through the HCV core protein, which binds gC1qR on T cells and inhibits their growth, highlighting a role for gC1qR in host immune evasion (41). It is likely that the interaction of C1q with gC1qR provides a negative growth signal, which interferes with normal cell proliferation. This could prove useful in developing targeted therapies where uncontrolled proliferation of immune cells is a critical pathological issue.

The expression of gC1qR has been detected in several cellular compartments such as mitochondria (42), nucleus (43), and on the cell surface of neutrophils, mast cells, T and B lymphocytes, endothelial cells, monocytes, and platelets (44–48). However, since gC1qR is devoid of a transmembrane domain, it has been proposed to exert its signal across the membrane through a docking/signal interaction with CD44 (49). We carried out microscopy studies to investigate the colocalization of gC1qR with the gh modules on the cell surface of monocyte-derived macrophages, which revealed gC1qR's presence on the cell surface (**Figure 5**). We could also observe colocalization of individual gh with gC1qR. Although C1q has been shown to bind to residues 76–93 of gC1qR, it appears that there could be additional binding sites on gC1qR (50) involving residues 144–162. This paper together with the other studies, establishing the importance of C1q–gC1qR interaction in disease models, where complement activation is a critical factor in disease progression such as atherosclerosis and Alzheimer's disease, could be relevant for the development of novel therapeutic strategies.

AUTHOR CONTRIBUTIONS

LP, AP, BP, AT, AK, LK, SA, and GS carried out crucial experiments; HK, MS, and EP provided important reagents and facilities; UK and BG collaboratively designed and supervised most of the experiments, in addition to writing the manuscript.

FUNDING

This work was supported in part by the Brunel University London, the Deanship of Scientific Research at the King Saud University for funding *via* Group No. RGP-009 (HK), the National Institute of Allergy and Infectious Diseases R01 AI 060866 and R01 AI-084178 (BG and EP), and NIH/NCI Cancer Center support Grant P30 CA008748 (EP).

REFERENCES

1. Reid KB, Porter RR. Subunit composition and structure of subcomponent C1q of the first component of human complement. *Biochem J* (1976) 155:19–23. doi:10.1042/bj1550019
2. Kishore U, Reid KB. C1q: structure, function, and receptors. *Immunopharmacology* (2000) 49:159–70. doi:10.1016/S0162-3109(00)80301-X
3. Garlatti V, Chouquet A, Lunardi T, Vives R, Paidassi H, Lortat-Jacob H, et al. Cutting edge: C1q binds deoxyribose and heparan sulfate through neighboring sites of its recognition domain. *J Immunol* (2010) 185:808–12. doi:10.4049/jimmunol.1000184
4. Erlich P, Dumestre-Perard C, Ling WL, Lemaire-Vieille C, Schoehn G, Arlaud GJ, et al. Complement protein C1q forms a complex with cytotoxic prion protein oligomers. *J Biol Chem* (2010) 285:19267–76. doi:10.1074/jbc.M109.071860
5. Gaboriaud C, Frachet P, Thielens NM, Arlaud GJ. The human c1q globular domain: structure and recognition of non-immune self ligands. *Front Immunol* (2012) 2:92. doi:10.3389/fimmu.2011.00092
6. Nayak A, Pednekar L, Reid KB, Kishore U. Complement and non-complement activating functions of C1q: a prototypical innate immune molecule. *Innate Immun* (2012) 18:350–63. doi:10.1177/1753425910396252
7. Kishore U, Gaboriaud C, Waters P, Shrive AK, Greenhough TJ, Reid KB, et al. C1q and tumor necrosis factor superfamily: modularity and versatility. *Trends Immunol* (2004) 25:551–61. doi:10.1016/j.it.2004.08.006
8. Nayak A, Ferluga J, Tsolaki AG, Kishore U. The non-classical functions of the classical complement pathway recognition subcomponent C1q. *Immunol Lett* (2010) 131:139–50. doi:10.1016/j.imlet.2010.03.012
9. Kishore U, Ghai R, Greenhough TJ, Shrive AK, Bonifati DM, Gadjeva MG, et al. Structural and functional anatomy of the globular domain of complement protein C1q. *Immunol Lett* (2004) 95:113–28. doi:10.1016/j.imlet.2004.06.015
10. Gaboriaud C, Juanhuix J, Gruez A, Lacroix M, Darnault C, Pignol D, et al. The crystal structure of the globular head of complement protein C1q provides a basis for its versatile recognition properties. *J Biol Chem* (2003) 278:46974–82. doi:10.1074/jbc.M307764200
11. Kishore U, Kojouharova MS, Reid KB. Recent progress in the understanding of the structure-function relationships of the globular head regions of C1q. *Immunobiology* (2002) 205:355–64. doi:10.1078/0171-2985-00138
12. Kishore U, Leigh LE, Eggleton P, Strong P, Perdikoulis MV, Willis AC, et al. Functional characterization of a recombinant form of the C-terminal, globular head region of the B-chain of human serum complement protein, C1q. *Biochem J* (1998) 333:27–32. doi:10.1042/bj3330027
13. Lim BL, Reid KB, Ghebrehiwet B, Peerschke EI, Leigh LA, Preissner KT. The binding protein for globular heads of complement C1q, gC1qR. Functional expression and characterization as a novel vitronectin binding factor. *J Biol Chem* (1996) 271:26739–44. doi:10.1074/jbc.271.43.26739
14. Joseph K, Ghebrehiwet B, Peerschke EI, Reid KB, Kaplan AP. Identification of the zinc-dependent endothelial cell binding protein for high molecular weight kininogen and factor XII: identity with the receptor that binds to the globular "heads" of C1q (gC1q-R). *Proc Natl Acad Sci U S A* (1996) 93:8552–7. doi:10.1073/pnas.93.16.8552
15. Herwald H, Dedio J, Kellner R, Loos M, Muller-Esterl W. Isolation and characterization of the kininogen-binding protein p33 from endothelial cells. Identity with the gC1q receptor. *J Biol Chem* (1996) 271:13040–7. doi:10.1074/jbc.271.22.13040
16. Ghebrehiwet B, Lim BL, Peerschke EI, Willis AC, Reid KB. Isolation, cDNA cloning, and overexpression of a 33-kD cell surface glycoprotein that binds to the globular "heads" of C1q. *J Exp Med* (1994) 179:1809–21. doi:10.1084/jem.179.6.1809
17. Ghebrehiwet B, Jesty J, Peerschke EI. gC1q-R/p33: structure-function predictions from the crystal structure. *Immunobiology* (2002) 205:421–32. doi:10.1078/0171-2985-00143
18. Kishore U, Gupta SK, Perdikoulis MV, Kojouharova MS, Urban BC, Reid KB. Modular organization of the carboxyl-terminal, globular head region of human C1q A, B, and C chains. *J Immunol* (2003) 171:812–20. doi:10.4049/jimmunol.171.2.812
19. Bally I, Ancelet S, Moriscot C, Gonnet F, Mantovani A, Daniel R, et al. Expression of recombinant human complement C1q allows identification of the C1r/C1s-binding sites. *Proc Natl Acad Sci U S A* (2013) 110:8650–5. doi:10.1073/pnas.1304894110
20. Gadjeva MG, Rouseva MM, Zlatarova AS, Reid KB, Kishore U, Kojouharova MS. Interaction of human C1q with IgG and IgM: revisited. *Biochemistry* (2008) 47:13093–102. doi:10.1021/bi801131h
21. Jiang J, Zhang Y, Krainer AR, Xu RM. Crystal structure of human p32, a doughnut-shaped acidic mitochondrial matrix protein. *Proc Natl Acad Sci U S A* (1999) 96:3572–7. doi:10.1073/pnas.96.7.3572

22. Kojouharova MS, Gadjeva MG, Tsacheva IG, Zlatarova A, Roumenina LT, Tchorbadjieva MI, et al. Mutational analyses of the recombinant globular regions of human C1q A, B, and C chains suggest an essential role for arginine and histidine residues in the C1q-IgG interaction. *J Immunol* (2004) 172:4351–8. doi:10.4049/jimmunol.172.7.4351
23. Peerschke EI, Yin W, Grigg SE, Ghebrehiwet B. Blood platelets activate the classical pathway of human complement. *J Thromb Haemost* (2006) 4:2035–42. doi:10.1111/j.1538-7836.2006.02065.x
24. Yin W, Ghebrehiwet B, Weksler B, Peerschke EI. Classical pathway complement activation on human endothelial cells. *Mol Immunol* (2007) 44:2228–34. doi:10.1016/j.molimm.2006.11.012
25. Ghebrehiwet B, Habicht GS, Beck G. Interaction of C1q with its receptor on cultured cell lines induces an anti-proliferative response. *Clin Immunol Immunopathol* (1990) 54:148–60. doi:10.1016/0090-1229(90)90014-H
26. Tan LA, Yu B, Sim FC, Kishore U, Sim RB. Complement activation by phospholipids: the interplay of factor H and C1q. *Protein Cell* (2010) 1:1033–49. doi:10.1007/s13238-010-0125-8
27. Ghebrehiwet B, Peterson K, Peerschke EIB, Reddigari SR, Reid KBM. Purification and immunochemical characterization of soluble forms of the 2 types of c1q receptors – cc1q-r and gc1q-r. *FASEB* (1994) 8:A475.
28. Ghebrehiwet B, Lim BL, Kumar R, Feng X, Peerschke EI. gC1q-R/p33, a member of a new class of multifunctional and multicompartmental cellular proteins, is involved in inflammation and infection. *Immunol Rev* (2001) 180:65–77. doi:10.1034/j.1600-065X.2001.1800106.x
29. Ghebrehiwet B, Lu PD, Zhang W, Lim BL, Eggleton P, Leigh LE, et al. Identification of functional domains on gC1Q-R, a cell surface protein that binds to the globular "heads" of C1Q, using monoclonal antibodies and synthetic peptides. *Hybridoma* (1996) 15:333–42. doi:10.1089/hyb.1996.15.333
30. Ghebrehiwet B, Feng X, Kumar R, Peerschke EI. Complement component C1q induces endothelial cell adhesion and spreading through a docking/signaling partnership of C1q receptors and integrins. *Int Immunopharmacol* (2003) 3:299–310. doi:10.1016/S1567-5769(02)00270-9
31. Roumenina LT, Ruseva MM, Zlatarova A, Ghai R, Kolev M, Olova N, et al. Interaction of C1q with IgG1, C-reactive protein and pentraxin 3: mutational studies using recombinant globular head modules of human C1q A, B, and C chains. *Biochemistry* (2006) 45:4093–104. doi:10.1021/bi052646f
32. Mei J, Chen B, Yue H, Gui JF. Identification of a C1q family member associated with cortical granules and follicular cell apoptosis in *Carassius auratus gibelio*. *Mol Cell Endocrinol* (2008) 289:67–76. doi:10.1016/j.mce.2008.02.016
33. Colombatti A, Spessotto P, Doliana R, Mongiat M, Bressan GM, Esposito G. The EMILIN/Multimerin family. *Front Immunol* (2012) 2:93. doi:10.3389/fimmu.2011.00093
34. Carland TM, Gerwick L. The C1q domain containing proteins: where do they come from and what do they do? *Dev Comp Immunol* (2010) 34:785–90. doi:10.1016/j.dci.2010.02.014
35. Tom Tang Y, Hu T, Arterburn M, Boyle B, Bright JM, Palencia S, et al. The complete complement of C1q-domain-containing proteins in *Homo sapiens*. *Genomics* (2005) 86:100–11. doi:10.1016/j.ygeno.2005.03.001
36. Kishore U, Reid KB. Modular organization of proteins containing C1q-like globular domain. *Immunopharmacology* (1999) 42:15–21. doi:10.1016/S0162-3109(99)00011-9
37. Gerwick L, Reynolds WS, Bayne CJ. A precerebellin-like protein is part of the acute phase response in rainbow trout, *Oncorhynchus mykiss*. *Dev Comp Immunol* (2000) 24:597–607. doi:10.1016/S0145-305X(00)00016-1
38. Marques G, Anton LC, Barrio E, Sanchez A, Ruiz S, Gavilanes F, et al. Arginine residues of the globular regions of human C1q involved in the interaction with immunoglobulin G. *J Biol Chem* (1993) 268:10393–402.
39. Ghebrehiwet B, Lu PD, Zhang W, Keilbaugh SA, Leigh LE, Eggleton P, et al. Evidence that the two C1q binding membrane proteins, gC1q-R and cC1q-R, associate to form a complex. *J Immunol* (1997) 159:1429–36.
40. Ghebrehiwet B, Ji Y, Valentino A, Pednekar L, Ramadass M, Habiel D, et al. Soluble gC1qR is an autocrine signal that induces B1R expression on endothelial cells. *J Immunol* (2014) 192:377–84. doi:10.4049/jimmunol.1302031
41. Kittlesen DJ, Chianese-Bullock KA, Yao ZQ, Braciale TJ, Hahn YS. Interaction between complement receptor gC1qR and hepatitis C virus core protein inhibits T-lymphocyte proliferation. *J Clin Invest* (2000) 106:1239–49. doi:10.1172/JCI10323
42. Dedio J, Jahnen-Dechent W, Bachmann M, Muller-Esterl W. The multiligand-binding protein gC1qR, putative C1q receptor, is a mitochondrial protein. *J Immunol* (1998) 160:3534–42.
43. Matthews DA, Russell WC. Adenovirus core protein V interacts with p32 – a protein which is associated with both the mitochondria and the nucleus. *J Gen Virol* (1998) 79(Pt 7):1677–85. doi:10.1099/0022-1317-79-7-1677
44. Eggleton P, Ghebrehiwet B, Sastry KN, Coburn JP, Zaner KS, Reid KB, et al. Identification of a gC1q-binding protein (gC1q-R) on the surface of human neutrophils. Subcellular localization and binding properties in comparison with the cC1q-R. *J Clin Invest* (1995) 95:1569–78. doi:10.1172/JCI117830
45. Ghebrehiwet B, Kew RR, Gruber BL, Marchese MJ, Peerschke EI, Reid KB. Murine mast cells express two types of C1q receptors that are involved in the induction of chemotaxis and chemokinesis. *J Immunol* (1995) 155:2614–9.
46. Gupta S, Batchu RB, Datta K. Purification, partial characterization of rat kidney hyaluronic acid binding protein and its localization on the cell surface. *Eur J Cell Biol* (1991) 56:58–67.
47. Peerschke EI, Reid KB, Ghebrehiwet B. Identification of a novel 33-kDa C1q-binding site on human blood platelets. *J Immunol* (1994) 152:5896–901.
48. Peerschke EI, Ghebrehiwet B. Platelet membrane receptors for the complement component C1q. *Semin Hematol* (1994) 31:320–8.
49. Feng X, Tonnesen MG, Peerschke EI, Ghebrehiwet B. Cooperation of C1q receptors and integrins in C1q-mediated endothelial cell adhesion and spreading. *J Immunol* (2002) 168:2441–8. doi:10.4049/jimmunol.168.5.2441
50. Ghebrehiwet B, Jesty J, Vinayagasundaram R, Vinayagasundaram U, Ji Y, Valentino A, et al. Targeting gC1qR domains for therapy against infection and inflammation. *Adv Exp Med Biol* (2013) 735:97–110. doi:10.1007/978-1-4614-4118-2_6

Conflict of Interest Statement: The authors declare that the research was conducted in the absence of any commercial or financial relationships that could be construed as a potential conflict of interest.

The reviewer RS and handling Editor declared their shared affiliation, and the handling Editor states that the process nevertheless met the standards of a fair and objective review.

frontiers in Immunology

ORIGINAL RESEARCH
published: 22 December 2016
doi: 10.3389/fimmu.2016.00600

Complement Protein C1q Interacts with DC-SIGN *via* Its Globular Domain and Thus May Interfere with HIV-1 Transmission

*Lina Pednekar[1], Hrishikesh Pandit[2], Basudev Paudyal[1], Anuvinder Kaur[1], Maha Ahmed Al-Mozaini[3], Lubna Kouser[1], Berhane Ghebrehiwet[4], Daniel A. Mitchell[5], Taruna Madan[2] and Uday Kishore[1]**

[1] Biosciences, College of Health and Life Sciences, Brunel University London, Uxbridge, UK, [2] Department of Innate Immunity, National Institute for Research in Reproductive Health (ICMR), Mumbai, India, [3] Department of Infection and Immunity, King Faisal Specialist Hospital and Research Centre, Riyadh, Saudi Arabia, [4] Department of Medicine, State University of New York, Stony Brook, NY, USA, [5] Clinical Sciences Research Laboratories, University of Warwick, Coventry, UK

Dendritic cells (DCs) are the most potent antigen-presenting cells capable of priming naïve T-cells. Its C-type lectin receptor, DC-SIGN, regulates a wide range of immune functions. Along with its role in HIV-1 pathogenesis through complement opsonization of the virus, DC-SIGN has recently emerged as an adaptor for complement protein C1q on the surface of immature DCs *via* a trimeric complex involving gC1qR, a receptor for the globular domain of C1q. Here, we have examined the nature of interaction between C1q and DC-SIGN in terms of domain localization, and implications of C1q–DC-SIGN-gC1qR complex formation on HIV-1 transmission. We first expressed and purified recombinant extracellular domains of DC-SIGN and its homologue DC-SIGNR as tetramers comprising of the entire extra cellular domain including the α-helical neck region and monomers comprising of the carbohydrate recognition domain only. Direct binding studies revealed that both DC-SIGN and DC-SIGNR were able to bind independently to the recombinant globular head modules ghA, ghB, and ghC, with ghB being the preferential binder. C1q appeared to interact with DC-SIGN or DC-SIGNR in a manner similar to IgG. Mutational analysis using single amino acid substitutions within the globular head modules showed that Tyr^{B175} and Lys^{B136} were critical for the C1q–DC-SIGN/DC-SIGNR interaction. Competitive studies revealed that gC1qR and ghB shared overlapping binding sites on DC-SIGN, implying that HIV-1 transmission by DCs could be modulated due to the interplay of gC1qR-C1q with DC-SIGN. Since C1q, gC1qR, and DC-SIGN can individually bind HIV-1, we examined how C1q and gC1qR modulated HIV-1–DC-SIGN interaction in an infection assay. Here, we report, for the first time, that C1q suppressed DC-SIGN-mediated transfer of HIV-1 to activated pooled peripheral blood mononuclear cells, although the globular head modules did not. The protective effect of C1q was negated by the addition of gC1qR. In fact, gC1qR enhanced DC-SIGN-mediated HIV-1 transfer, suggesting its role in HIV-1 pathogenesis. Our results highlight the consequences of multiple innate immune pattern recognition molecules forming a complex that can modify their functions in a way, which may be advantageous for the pathogen.

Keywords: DC-SIGN, C1q, globular head domain, HIV-1, protein–protein interaction

OPEN ACCESS

Edited by:
Cees Van Kooten, Leiden University, Netherlands

Reviewed by:
Kenneth Reid, Green Templeton College University of Oxford, UK
Lubka T. Roumenina, INSERM UMRS 1138, Cordeliers Research Center, Complement and Diseases Team, France

****Correspondence:***
Uday Kishore
uday.kishore@brunel.ac.uk, ukishore@hotmail.com

Specialty section:
This article was submitted to Molecular Innate Immunity, a section of the journal Frontiers in Immunology

Received: *06 August 2016*
Accepted: *30 November 2016*
Published: *22 December 2016*

Citation:
Pednekar L, Pandit H, Paudyal B, Kaur A, Al-Mozaini MA, Kouser L, Ghebrehiwet B, Mitchell DA, Madan T and Kishore U (2016) Complement Protein C1q Interacts with DC-SIGN via Its Globular Domain and Thus May Interfere with HIV-1 Transmission. Front. Immunol. 7:600. doi: 10.3389/fimmu.2016.00600

INTRODUCTION

Dendritic cell-specific intracellular adhesion grabbing non-integrin (DC-SIGN) is a C-type lectin expressed on DCs that functions as a pattern recognition receptor (PRR). It can interact with a range of viral, bacterial, and fungal pathogens to primarily promote Th2 responses *via* activation of the mitogen-activated protein kinases Erk1 and Erk2 (1), leading to the clearance of pathogens. DC-SIGN also modulates TLR signalling by activating serine and threonine kinase Raf1, which acetylates the NF-κB subunit p65 upon interaction with pathogens, such as *Mycobacterium tuberculosis*, *Mycobacterium leprae*, *Candida albicans*, and measles virus (2, 3). Acetylation of p65 and increased IL-10 transcription leads to an enhanced anti-inflammatory cytokine response (2). DC-SIGN also mediates DC–T cell interaction *via* intracellular adhesion molecule-3 (ICAM-3) (4). In addition, DCs can adhere to endothelial cells expressing high levels of ICAM-2 *via* DC-SIGN. Further interactions between lymphocyte function-associated antigen-1 (LFA-1) and ICAM-1 with ICAM-2–DC-SIGN (5) promote trans-endothelial migration of DCs, allowing them to travel from the blood to the lymphatic system where they can induce T cell responses. Martinez et al. have shown that DC-SIGN stimulated CD3-activated T cells produce IL-2, which, in turn, enhances T cell differentiation (6). DC-SIGN can bind the cell wall component, glycolipid ManLAM of *M. tuberculosis*, and inhibit DC maturation through the suppression of TLR-4 (7). Such a cross talk between TLRs and DC-SIGN that generates anti-inflammatory immune response highlights the two-faced role of DC-SIGN in immune regulation.

DC-SIGN can bind to HIV-1 envelope protein gp120 through glycan structures (8) and mediate HIV transmission in *cis* and *trans* fashion. The *cis* mode supports DC-SIGN-mediated viral internalization and limited replication; in *trans* mode, viral particles are endocytosed and presented to $CD4^+$ cells (9). DC-SIGN, thus, allows DCs to carry HIV-1 to the lymph nodes where interactions between DCs and T cells leads to transmission of the virus to $CD4^+$ T cells, leading to their infection and eventual depletion (10). The hepatitis C virus (HCV) envelope glycoprotein E2 is another viral protein DC-SIGN engages with (11). This is achieved through utilizing its high quality endocytic capability to internalize the viral antigen, leading to the infection of DCs (12).

Structurally, DC-SIGN is composed of an extracellular domain (ECD), which exists as a tetramer, stabilized by an N-terminal α-helical neck region, followed by a carbohydrate recognition domain (CRD) (8). Its affinity for N-linked high mannose oligosaccharides is evident through its ligands HIV-1 gp120 and ICAM-3 being highly glycosylated, indicating that this binding is mediated through the CRD region (13, 14). Studies have shown that the interaction between gp120 and DC-SIGN triggers a drop in IL-6 production by immature DCs. In addition, gp120 binding to DC-SIGN has also been shown to suppress the anti-apoptotic activity of Nef and induce apoptosis in immature DCs (14). Thus, HIV pathogenesis heavily relies on the interplay of molecular mechanisms involving DC-SIGN.

Recently, it has emerged that DC-SIGN interacts with the complement classical pathway recognition protein, C1q (15), in conjunction with its globular head receptor, gC1qR, on the surface of immature DCs. C1q as well as gC1qR is known to associate with the viral envelope protein gp41 of HIV-1 (16, 17). C1q has been shown to interact with gp41 ectodomain *via* its globular head (gC1q) domain (18), specifically *via* the A chain (19), in a way similar to C1q–IgG interaction (20, 21). Similar to IgG, the ability of gp41 to form aggregates (16) leads to an enhanced activation of the C1 complex, as well as the function of gp41 to initiate the classical pathway on the surface of infected cells in an antibody-independent manner (22). The C1q binding site on gp41 resides within residues 601–613 of the immunodominant loop region (16), which contains hydrophobic side chains and forms a cleft (23).

gC1qR on its own has been shown to suppress the production of HIV-1 in MT-4 and H9 human T cell lines, and macrophages infected with $HIV\text{-}1_{IIIB}$ and $HIV\text{-}1_{Ba\text{-}L}$ (24) Suppression of virus production is further enhanced when gC1qR is preincubated with the target cell lines prior to HIV-1 challenge, suggesting that interference with viral entry by gC1qR occurs through interaction with CD4 (24). gC1qR is known to bind to a range of viral ligands including the HCV core protein (25), adenovirus core protein V (26) EBNA-1 (27), and rubella virus capsid protein (28). gC1qR can also act as a receptor for HIV-1 gp41 and target healthy $CD4^+$ T cells to natural killer (NK) cell-mediated lysis (17). This bystander effect of autologous killing occurs through the surface translocation of NKP44L, *via* activation of PI3K, NADPH oxidase, and p190 RhoGAP.

Recently, DC-SIGN, C1q, and gC1qR on immature DCs have been shown to form a tripartite complex, with a plausible role in DC differentiation through signaling *via* the NF-κB pathway (15). Given that each of these innate immune proteins (C1q, DC-SIGN, and gC1qR) can bind HIV-1, we set out to dissect the nature of interaction between C1q and DC-SIGN and examine how it can impact upon HIV-1 transmission.

MATERIALS AND METHODS

Expression and Purification of Soluble DC-SIGN and DC-SIGNR

The pT5T constructs expressing tetrameric and monomeric forms of DC-SIGN and DC-SIGNR were transformed into *Escherichia coli* BL21 (λDE3) (8). Protein expression was performed using bacterial culture in Luria-Bertani medium containing 50 μg/mL of ampicillin at 37°C until OD_{600} reached 0.7. The bacterial culture was induced with 10 mM isopropyl-β-D-thiogalactoside (IPTG) and incubated for a further 3 h. Bacterial cells (1 L) were centrifuged at 4,500 × *g* for 15 min at 4°C and cell pellet was treated with 22 mL of lysis buffer containing 100 mM Tris, pH 7.5, 0.5 M NaCl, lysozyme (50 μg/mL), 2.5 mM EDTA, pH 8.0, and 0.5 mM phenylmethylsulfonyl fluoride (PMSF), and left to stir for 1 h at 4°C. Cells were then sonicated for 10 cycles for 30 s with 2 min intervals and the sonicated suspension was spun at 10,000 *g* for 15 min at 4°C. The inclusion bodies, present in the pellet, were solubilized in 20 mL of 6 M urea, 10 mM Tris–HCl, pH 7.0, and 0.01% β-mercaptoethanol by rotating on a shaker for 1 h at 4°C.

The mixture was then centrifuged at 13,000 × *g* for 30 min at 4°C, and the supernatant was drop-wise diluted fivefold with loading buffer containing 25 mM Tris–HCl pH 7.8, 1 M NaCl, and 2.5 mM $CaCl_2$ with gentle stirring. This was then dialyzed against 2 L of loading buffer with three buffer changes every 3 h. Following further centrifugation at 13,000 × *g* for 15 min at 4°C, the supernatant was loaded onto a mannan-agarose column (5 mL; Sigma) pre-equilibrated with the loading buffer. The column was washed with five bed volumes of the loading buffer, and the bound protein was eluted in 1 mL fractions using the elution buffer containing 25 mM Tris–HCl pH 7.8, 1 M NaCl, and 2.5 mM EDTA. The absorbance was read at 280 nm, and the peak fractions were frozen at −20°C. Purity of protein was analyzed by 15% w/v SDS-PAGE.

Expression and Purification of Recombinant Wild-Type Globular Head Modules ghA, ghB, and ghC of Human C1q and Their Substitution Mutants

The recombinant globular head regions of human C1q, ghA, ghB, and ghC modules (19) and their respective mutants (29) were expressed in *E. coli* BL21 as fusion to maltose-binding protein (MBP). Bacterial cells were grown in 200 mL LB medium containing ampicillin (100 μg/mL) at 37°C, and induced with 0.4 mM IPTG at OD_{600} of 0.6 for 3 h, and then centrifuged (4,500 × *g* for 15 min). The cell pellet was suspended in 25 mL of lysis buffer (20 mM Tris–HCl pH 8.0, 0.5 M NaCl, 1 mM EDTA, 0.2% v/v Tween 20, 5% glycerol, 0.1 mM PMSF, and 0.1 mg lysozyme) and incubated at 4°C for 1 h on a rotary shaker. Cell suspension was then sonicated for 30 s with 2 min gaps for 10 cycles. After centrifugation (13,000 × *g* for 15 min), the supernatant was diluted fivefold in buffer I (20 mM Tris–HCl, pH 8.0, 100 mM NaCl, 0.2% Tween 20, 1 mM EDTA, and 5% glycerol), passed through an amylose resin column (15 mL; New England Biolabs), and then washed with three bed volumes of buffer I followed by buffer II (50 mL of buffer I without Tween 20). The protein was then eluted in 1 mL fractions with 10 mM maltose in 100 mL of buffer II and frozen at −20°C after determining protein concentration and purity *via* Nanodrop and 10% w/v SDS-PAGE, respectively.

Purification of Human C1q from Plasma

C1q was purified from freshly thawed plasma as described previously (19). Briefly, plasma was made 5 mM EDTA, pH 7.5, and centrifuged to remove aggregated lipids. It was then incubated with non-immune IgG coupled to CNBr-activated Sepharose (GE Healthcare, UK) for 1 h at 4°C. The plasma with IgG-Sepharose was filtered through a sintered glass funnel, and C1q-bound Sepharose was then washed extensively with 10 mM HEPES, 140 mM NaCl, 0.5 mM EDTA, pH 7.0. C1q was eluted with CAPS (N-cyclohexyl-3-aminopropanesulfonic acid) buffer (100 mM CAPS, 1 M NaCl, 0.5 mM EDTA, pH 11). The eluted C1q was then passed through a HiTrap protein G column (PierceNet, USA) to remove IgG contaminants and dialyzed against the washing buffer.

Expression and Purification of Human gC1qR

The recombinant mature gC1qR protein containing 74–282 residues was expressed in *E. coli* BL21 (λDE3) (30). Bacterial cells were grown in 250 mL of LB at 37°C until an OD_{600} of 0.6 was reached and induced with 0.5 mM IPTG. After 3 h, the bacterial cell culture was spun down (4,500 *g* for 15 min). The cell pellet was treated with lysis buffer (20 mM Tris–HCl pH 8.0, 0.5 M NaCl, 1 mM EDTA, 0.2% Tween, 5% glycerol, 0.1 mg lysozyme) and incubated for 1 h at 4°C with shaking. The cell lysate was then sonicated for 10 cycles at 30 s with 2 min intervals. The lysate was spun down at 13,000 *g* for 15 min, and the supernatant was collected and dialyzed for 2 h against 20 mM Tris–HCl, pH 7.5. The dialyzed protein was subjected to ion exchange using a DEAE column and gC1qR eluted at a peak of 0.45 M NaCl.

Direct Binding ELISA

Microtiter wells were coated overnight at 4°C with DC-SIGN or DC-SIGNR (5, 2.5, 1.25, and 0.625 μg/well) in carbonate–bicarbonate buffer, pH 9.6, and left overnight at 4°C. Wells were blocked with 100 μL of 2% w/v BSA in PBS for 2 h at 37°C. Following three washes with PBS + 0.05% Tween 20, ghA, ghB, ghC, or its substitution mutants (2.5 μg/100 μl) was added to each well in the buffer containing 50 mM NaCl, 100 mM Tris–HCl, pH 7.5, and 5 mM $CaCl_2$. MBP (Sigma) was used as a negative control. The plate was incubated at 37°C for 1.5 h and then at 4°C for 1.5 h. The wells were washed and the bound protein was detected with anti-MBP monoclonal antibodies in PBS (1:5,000, Sigma) followed by rabbit anti-mouse IgG-HRP conjugate (1:5,000; Sigma) for 1 h. The color was developed using o-phenylenediamine dihydrochloride (OPD, Sigma) and read at 415 nm.

Competitive ELISA

DC-SIGN and DC-SIGNR proteins were coated on microtiter wells by overnight incubation at 4°C using 5 μg/well (in 100 μL) in carbonate–bicarbonate buffer pH 9.6. Wells were blocked with 2% BSA in PBS for 2 h at 37°C. Following washing with PBS + 0.05% Tween, the plate was incubated with a steady concentration (5 μg/well) of one competing protein (gC1qR) and various concentrations (5, 2.5, 1.25, 0.625 μg/well) of the second competing protein (ghB) in calcium buffer to give a total of 100 μL/well. After incubating for 1.5 h at 37°C and 1.5 h at 4°C, the wells were washed and anti-gC1qR polyclonal antibody (1:1,000) in PBS was added and incubated for a further 1 h at 37°C. Bound protein was detected by Protein A-HRP conjugate (1:5,000), and the color was developed using OPD. Data were plotted to determine inhibition values of competitive ligand binding.

In order to examine if C1q and globular head modules can inhibit binding of DC-SIGN to gp120, microtiter wells were coated with 250 ng of gp120 (Abcam) in carbonate–bicarbonate buffer and left overnight at 4°C. Plate was blocked with 2% w/v BSA in PBS for 2 h at 37°C, followed by washing three times with PBS + 0.05% Tween 20. Various concentration of ghA, ghB, ghC, and C1q (10, 5, 2.5, 0 μg/mL) were co-mixed with 2.5 μg/mL of DC-SIGN and added to wells in calcium buffer

(100 µL/well). After incubation for 1 h at 37°C and 1 h at 4°C, the wells were washed again three times using PBS + 0.05% Tween 20. The binding of DC-SIGN to gp120 in the presence of globular heads and C1q was detected using rabbit anti-DC-SIGN antibody (1:500) and probed with Protein A-HRP conjugate (1:5,000). The color was developed using 3,3′,5,5′-tetramethylbenzidine (TMB) and read at 450 nm spectrophotometrically.

Western Blotting

Recombinant ghA, ghB, and ghC modules (15 µg), in addition to MBP and BSA as negative control proteins, were run separately on a 12% SDS-PAGE gel and transferred onto PDVF membrane for 1 h at 320 mA. Membrane was blocked in 5% non-fat milk (1 h at room temperature) and 50 µg of recombinant DC-SIGN (tetramer) in loading buffer (25 mM Tris–HCl, pH 7.8, 1 M NaCl, 2.5 mM $CaCl_2$) was added and incubated overnight at room temperature. The blot was washed three times for 10 min each in PBS containing 0.05% Tween 20 and then incubated with anti-DC-SIGN (1:1,000) polyclonal antibody (ProSci) in 1% non-fat milk (2 h at 37°C). Following subsequent washes, the membrane was incubated with Protein A-conjugated HRP (1:1,000) (1 h at room temperature). The blot was developed using 3, 3′-diaminobenzidine (DAB; Sigma D7679) as a substrate.

Fluorescent Microscopy

Binding of C1q Globular Head Modules to DC-SIGN Expressed on HEK Cells

DC-SIGN-expressing HEK 293 (DC-HEK) cells, as reported by Lang et al. (31) were grown in DMEM-F12 (Life Technologies, UK) containing 10% v/v FCS and blasticidin (5 µg/mL) (Gibco). The cells were grown on 13 mm glass cover slips till a monolayer of cells was formed and then incubated with 15 µg/mL of recombinant ghA, ghB, and ghC (MBP as a negative control) separately in serum free medium and left to incubate for 30 min in 37°C. Cells were washed with PBS and fixed using 4% v/v paraformaldehyde for 10 min, rinsed again with PBS three times, and then blocked with 5% FCS for 30 min. The slides were incubated for 30 min with mouse anti-MBP antibody to detect MBP fusion proteins and rabbit anti-DC-SIGN antibody to reveal expression of DC-SIGN in DC-HEK cells. After three washes for 30 min each and incubation with secondary antibodies: Alexa Fluor 568 conjugated goat anti-mouse antibody (Thermo Fisher) and Alexa Fluor 488 conjugated goat anti-rabbit antibody (Abcam) for 30 min, the slides were then washed in PBS, mounted, and observed under Leica DM4000 Fluorescent microscope using Leica Application Suite.

HIV-1 Transfer Assay with DC-HEK Cells and Pooled Peripheral Blood Mononuclear Cell (PBMC)

Pooled peripheral blood mononuclear cells (HiMedia Laboratories, India) were cultured in RPMI 1640 medium (Sigma Aldrich) containing 10% FBS, 1% Penicillin–Streptomycin (Complete RPMI medium), and stimulated with 5 µg/mL phytohemaglutinin (PHA) and 10 U/Ml of recombinant-human IL-2 (Gibco) for 24 h. PHA/IL-2 was washed off and activated PBMCs were cultured further for 3 days in complete RPMI 1640 medium.

DC-HEK cells were grown and maintained in DMEM-F12 (Sigma-Aldrich, USA) containing 10% FBS and blasticidin (5 µg/mL) (Gibco). Cells were sub-cultured every 3 days and those in the log phase were used for assays. DC-HEK cells were grown in a 12 well plate until 80% confluence. Indicated concentrations of C1q, ghA, ghB, ghC, and gC1qR individually, or in combination, in medium containing 5 mM $CaCl_2$ were added to each well and incubated for 2 h to allow binding. Excess protein was removed and cells were challenged with 5 ng/mL p24 of HIV-1 SF-162 strain (kindly provided by Dr. Jay Levy, NIH AIDS Program, National Institutes of Health, USA) for 1 h. MBP was added along with the virus as a negative protein control. Unbound virus was washed off and cells were co-cultured with PHA/IL-2 activated PBMCs for 24 h to facilitate viral transfer. PBMCs in the supernatant were then separated from the adhered DC-HEK monolayer and cultured further for 7 days and viral titer was determined using HIV-1 p24 antigen ELISA of supernatants collected on days 4 and 7 (XpressBio Life Science Products, Frederick, MD, USA). That the reduction in p24 levels was not due to cellular death was confirmed by MTT assay of cultured PBMCs on day 7.

Statistical Analysis

Viral transfer experiment data were plotted using GraphPad Prism version 5.0, and analyzed for statistical significance using one-way ANOVA. $P < 0.05$ was considered as statistically significant.

RESULTS

Both DC-SIGN and DC-SIGNR Bind to C1q

DC-SIGN and DC-SIGNR comprising of the entire ECD (**Figures 1A,C**) and the CRD region alone (**Figures 1B,D**) were expressed in *E. coli* and affinity-purified on mannose-agarose. The CRD regions of DC-SIGN and DC-SIGNR bound mannose weakly as majority of the proteins appeared in the flow through. The ECD domains of both DC-SIGN and DC-SIGNR bound to mannose with much greater affinity in the presence of Ca^{2+} and eluted with EDTA. Previously, Kang et al. have shown that DC-SIGNR interacts with C1q (32). Recently, work by Hosszu et al. revealed that DC-SIGN bound directly to C1q (15). Thus, we examined direct binding of both the tetrameric and monomeric variants of DC-SIGN and DC-SIGNR with purified human C1q on microtiter plates. Both DC-SIGN (**Figure 2A**) and DC-SIGNR (**Figure 3A**) in their tetrameric and monomeric forms were able to bind to C1q in a dose-dependent manner. Experiment showed a strong binding of the tetramers to C1q when compared to the CRD region alone, with the ability of C1q to bind nearly 50% more when the α-helical neck was intact. C1q bound to DC-SIGNR (**Figure 3A**) better than DC-SIGN (**Figure 2A**). The ability of the globular head modules to bind DC-SIGN was also examined *via* a far-western blot (**Figure 2D**), where ghA, ghB, and ghC, run on a SDS-PAGE and transferred on a nitrocellulose membrane, were probed with soluble DC-SIGN tetramer. ghA and ghB appeared to bind DC-SIGN well compared to the ghC module. MBP and BSA, used as negative control proteins, did not bind DC-SIGN tetramer.

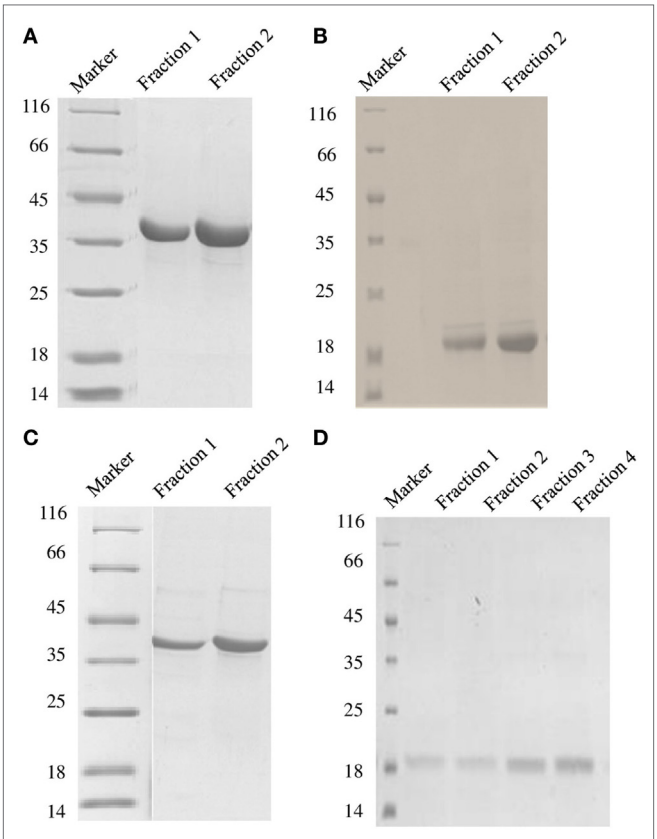

FIGURE 1 | SDS-PAGE under reducing conditions (12% v/v) showing purified fractions of soluble DC-SIGN tetramer (A), DC-SIGN monomer (B), DC-SIGNR tetramer (C), and DC-SIGNR monomer (D), following purification by mannose-agarose affinity chromatography.

DC-SIGN and DC-SIGNR Neck Region Is Required for Efficient Binding to C1q and Individual Globular Head Modules

Tetrameric (**Figure 2B**) and monomeric (**Figure 2C**) DC-SIGN and DC-SIGNR (**Figures 3B,C**) coated on microtiter wells were probed with ghA, ghB, and ghC to examine whether these globular head modules were able to bind to the ECD and CRD with similar avidity. ghA, ghB, and ghC bound with much greater affinity to DC-SIGN and DC-SIGNR tetramer in comparison to the monomers, indicating that the neck is required for the individual globular heads to bind efficiently. Like C1q, the ghA, ghB, and ghC modules bound DC-SIGNR better than DC-SIGN (**Figure 3B**).

DC-SIGN and DC-SIGNR Bind Preferentially to ghB Module

Since C1q bound to DC-SIGN and DC-SIGNR *via* its globular head region, as evident from the use of ghA, ghB and ghC modules, we sought to map their specificity for DC-SIGN and DC-SIGNR binding (**Figures 2B** and **3B**). When DC-SIGN and DC-SIGNR were coated on microtiter wells and probed with ghA, ghB, and ghC, all three globular heads bounds DC-SIGN and DC-SIGNR in a dose-dependent manner, indicating that all three heads are capable of binding to the ligands independently. Furthermore, ghB module was preferential in binding to DC-SIGN (**Figure 2B**); it bound much better to DC-SIGN compared to ghA and ghC. In addition, ghB was a better binder of DC-SIGNR, as was ghA for DC-SIGNR (**Figure 3B**) than DC-SIGN (**Figure 2B**), compared with the ghC module. Although binding of ghA, ghB, and ghC to the CRD domain was significantly lower, the ghB module was still a better binder of DC-SIGN (**Figure 2C**) and DC-SIGNR (**Figure 3C**) monomers.

The ghA Substitution Mutants Bind Differentially to DC-SIGN and DC-SIGNR

The ability of substitution mutants $Arg^{A162}Glu$ and $Arg^{A162}Ala$ to bind to DC-SIGN and DC-SIGNR was assessed by ELISA. Both substitution mutants bound DC-SIGN (**Figure 4A**) and DC-SIGNR (**Figure 5A**) in a dose-dependent manner. DC-SIGNR was able to interact with $Arg^{A162}Glu$ nearly as efficiently as it did with the wild-type ghA, showing a reduction in binding of only 15% at the highest concentration of 5 μg (**Figure 5A**). $Arg^{A162}Ala$, on the other hand, bound DC-SIGNR with much less affinity, showing a drop of 27% (**Figure 5A**). Considering DC-SIGN and DC-SIGNR are both highly conserved, $Arg^{A162}Glu$ was able to interact with DC-SIGN weakly than it did with DC-SIGNR (**Figures 4A** and **5A**), showing a ~35% reduced binding as opposed to ~5% (seen with DC-SIGNR.) The mutant $Arg^{A162}Ala$ bound DC-SIGN in a similar manner as it did to its homologue DC-SIGNR showing a reduced binding of ~25% (**Figure 4A**).

ghB Substitution Mutants Bind Differentially to DC-SIGN and DC-SIGNR

Using ELISA, we examined the ability of DC-SIGN to bind to the ghB substitution mutants $Arg^{B114}Gln$, ArgB114Ala, $Arg^{B163}Glu$, $Arg^{B163}Ala$, $Arg^{B129}Ala$, $Arg^{B129}Glu$, $His^{B117}Asp$, $Tyr^{B175}Leu$, and $Leu^{B136}Gly$ (29). All the ghB substitution mutants bound DC-SIGN (**Figure 4B**) and DC-SIGNR (**Figure 5B**) in a dose-dependent manner. Substituting Arg^{B114} to Gln and Ala resulted in a reduction of ~50% in the case of DC-SIGN (**Figure 4B**) and DC-SIGNR binding (**Figure 5B**), suggesting that the Arg residue at this position plays an important role in the C1q–DC-SIGN/DC-SIGNR interaction (**Tables 1** and **2**).

Substituting the ghB mutant Arg^{B129} with Glu and Ala caused a slight reduction of ~20% binding with DC-SIGN (**Figure 4B**) and up to ~40% with DC-SIGNR (**Figure 5B**). When Arg^{B163} was replaced with the negatively charged Glu, its affinity for DC-SIGN and DC-SIGNR was reduced by 50 and 35%, respectively (**Figures 4B** and **5B**) (**Tables 1** and **2**); substitution with Ala resulted in 30% reduction for DC-SIGN (**Figure 4B**) and increase by 20% for DC-SIGNR (**Figure 5B**) (**Tables 1** and **2**). A greater reduction in DC-SIGN and DC-SIGNR binding of ~60% was observed for the ghB mutant His^{B117} substituted for Asp. For the ghB module, Tyr^{B175} substitution to Leu had the most significant effect, showing a dramatic decrease of up to 90% in binding to DC-SIGN as well as DC-SIGNR at a concentration of 0.625 μg; this is not surprising due to its role in stabilizing the gC1q domain.

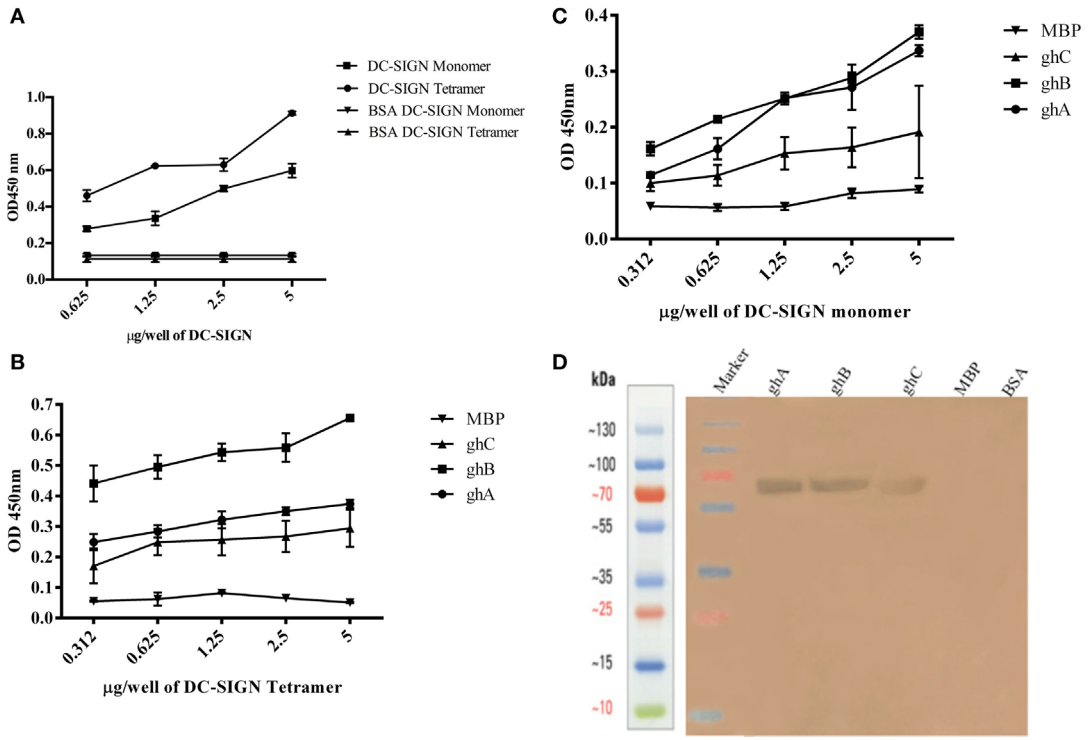

FIGURE 2 | Interaction of C1q, ghA, ghB, and ghC with DC-SIGN tetramer and monomer. **(A)** Microtiter wells coated with different concentrations (5, 2.5, 1.25, 0.625 µg/well) of DC-SIGN tetramer or monomer were probed with 2 µg/well of C1q. Bound C1q was detected with anti-C1q polyclonal antibodies (1:1,000 in PBS) and Protein A HRP conjugate (1:1,000 in PBS). BSA was used as a negative control protein. **(B)** Binding of ghA, ghB, and ghC to DC-SIGN tetramer and **(C)** DC-SIGN monomer involved coating a range of concentrations of the respective proteins on microtiter wells, which were then incubated with a fixed concentration of ghA, ghB, ghC, and MBP (2.5 µg/well in 5 mM $CaCl_2$ buffer) at 37°C. Binding was detected using anti-MBP monoclonal antibodies (1:5,000 in PBS) and then rabbit anti-mouse IgG-HRP (1:5,000 in PBS). **(D)** Far western blot to show DC-SIGN tetramer binding to membrane-bound ghA, ghB, and ghC: 15 µg of ghA, ghB, and ghC (BSA and MBP as negative control proteins) were run on a 12% SDS-PAGE gel and then transferred on to nitrocellulose membrane. The blot was incubated with 50 µg of DC-SIGN in PBS overnight at room temperature. The bound DC-SIGN protein was detected using anti-DC-SIGN polyclonal antibodies and Protein A HRP conjugate. Bands were developed using diaminobenzidine tablets dissolved in water.

Residue Leu^{136} on ghB, Important for IgG Binding, Is Also Involved in DC-SIGN Binding

Using a series of globular head single residue substitution mutants (29), we sought to examine that residues in the ghB chain offered complementary binding sites for DC-SIGN. Since Leu^{B136} and Tyr^{B175} residues are considered important in maintaining the gC1q structure as well as for IgG binding (33), we used Leu^{B136} substituted for Glu and Tyr^{B175} substituted for Leu in direct-binding ELISA. Leu^{B136}Gly showed ~50% less binding to DC-SIGN at the highest concentration (**Figure 4B**), suggesting that DC-SIGN and IgG binding sites on C1q (ghB) are overlapping.

The Contributions of ghC Substitution Mutants to DC-SIGN Binding

The substitution mutants His^{101}Ala, Arg^{156}Glu, and Leu^{170}Glu bound to DC-SIGN in a dose-dependent manner (**Figure 4C**). In fact, replacing Leu^{170} with Glu of the ghC chain reduced binding to DC-SIGN with a decrease in ~25% at the highest concentration. The ghC mutants His^{101}Ala reduced binding by 10%, suggesting that the contributions of His^{101} and Leu^{170} are comparable in the DC-SIGN–C1q interaction. The ghC substitution mutants also bound to DC-SIGNR in a dose-dependent manner.

The mutants His101Ala appeared to show ~10% better binding to DC-SIGNR with compared to wild type, whereas Leu170Glu and Arg156Glu showed reduced binding by up to 25% at the highest concentration of 5 µg of DC-SIGNR (**Figure 5C**; **Table 2**).

gC1qR and ghB Compete for the Same Binding Site on DC-SIGN

In view of the recent report of gC1qR, C1q, and DC-SIGN forming a trimeric complex on immature DCs (15), we examined whether DC-SIGN has complementary and overlapping binding site for C1q and gC1qR. We have recently mapped the gC1qR binding site on ghA, ghB, and ghC (30). Since ghB was found to be the preferential binder of DC-SIGN, ghB modules were tested in a competitive assay. When different concentrations of ghB and a constant concentration of gC1qR were challenged against DC-SIGN, probing with anti-gC1qR polyclonal antibody revealed that with decreasing concentration of ghB, more gC1qR was able to bind to solid-phase DC-SIGN (**Figure 6A**), thereby

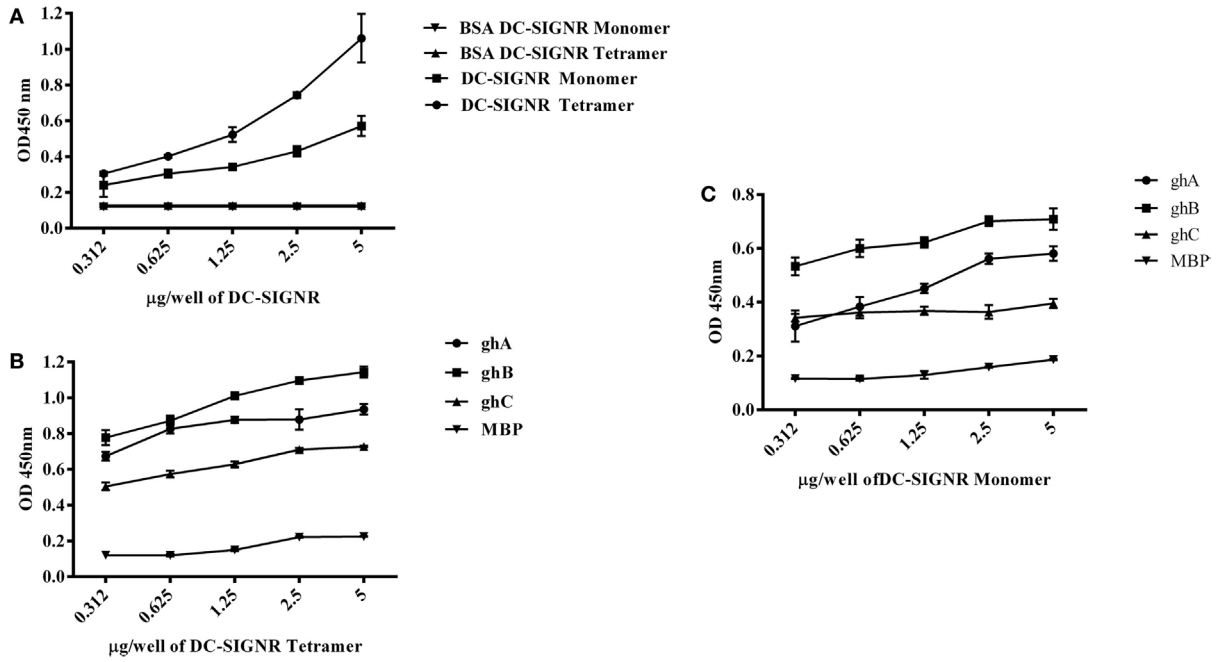

FIGURE 3 | **Interaction of C1q, ghA, ghB, and ghC with DC-SIGNR tetramer and monomer**. **(A)** ELISA to examine binding of C1q to DC-SIGNR tetramer and SIGN-R monomer: DC-SIGNR tetramer or monomer were coated at different concentrations, followed by addition of 2 µg/well of C1q. Bound C1q was probed with anti-C1q polyclonal antibodies (1:1,000 in PBS) and Protein A HRP (1:1,000 in PBS), and the color was developed using o-phenylenediamine dihydrochloride. **(B)** Binding of ghA, ghB, and ghC to DC-SIGNR tetramer and **(C)** SIGN-R monomer: different concentrations of DC-SIGNR tetramer **(B)** and DC-SIGNR monomer **(C)** were coated on microtiter wells in carbonate buffer and incubated overnight at 4°C and then incubated with ghA, ghB, ghC, and MBP (2.5 µg/well in 5 mM $CaCl_2$ buffer). Binding was detected using anti-MBP monoclonal antibody and rabbit anti-mouse IgG-HRP conjugate.

implying an overlapping binding site between the proteins. 5 µg of DC-SIGN and 5 µg of gC1qR were able to bind efficiently, showing an OD of 1 (data not shown); this binding appeared to be drastically reduced when 5 µg of gC1qR was allowed to compete with 5 µg of ghB.

C1q, ghA, ghB, and ghC Inhibit the Binding of DC-SIGN to gp120

C1q, ghA, ghB, and ghC were able to inhibit the binding of DC-SIGN to immobilized gp120 in a dose-dependent manner. The highest concentration of C1q, ghA, ghB, and ghC were able to significantly compete out the binding of DC-SIGN (**Figure 6B**).

The ghA, ghB, and ghC Modules Bind to Cell Surface-Expressed DC-SIGN

The binding of globular head modules to DC-SIGN was also performed using HEK 293 cells expressing DC-SIGN on the cell surface. The surface expression of DC-SIGN on DC-HEK cells was first confirmed with antibodies against DC-SIGN. To confirm the binding of individual globular head modules to DC-SIGN on DC-HEK cells, ghA, ghB, and ghC fused with MBP were added to the DC-HEK cells (**Figure 7**). Incubation of the globular head modules and probing with anti-MBP monoclonal antibodies showed that each globular head module bound on the surface of DC-HEK cells co-localizing with DC-SIGN expressed on DC-HEK cells unlike MBP (**Figure 7**).

C1q Inhibits DC-SIGN-Mediated Transfer of HIV-1 to PBMC in Culture

Since $CD4^+$ T cells and macrophages are the main cells targeted by HIV-1, we looked at the potential of C1q, ghA, ghB, ghC, and gC1qR to modulate DC-SING-mediated transfer of HIV-1 to activated PMBCs. As shown in **Figure 8A**, C1q considerably inhibited viral transfer to PBMCs in a dose-dependent manner on days 4 and 7. The globular head modules, ghA, ghB, and ghC, surprisingly did not interfere with HIV-1 transfer, neither individually nor collectively, when compared to untreated or MBP-treated control, suggesting that the collagen region of C1q and/or its multivalency of the gC1q domains are likely requirement for enforcing inhibitory properties. Addition of MBP in the control wells did not significantly affect the p24 levels in comparison with untreated controls (data not shown). Furthermore, during the assay period, cellular viability was not affected by any of the protein treatments, suggesting that differences in the infectivity were not due to cell death (data not shown).

We further examined the involvement of gC1qR with DC-SIGN in HIV-1 infection transmission (**Figure 8B**). gC1qR has previously been shown to inhibit CD4–gp120 interaction in HIV-1 isolates. It has also been recognized as a receptor on $CD4^+$ T cells that gp41 engages with in order to cause death of bystander $CD4^+$ T cells. We wanted to determine the role of gC1qR in DC-SIGN-mediated infection with or without C1q. **Figure 8B** shows that gC1qR alone did not mediate viral transfer

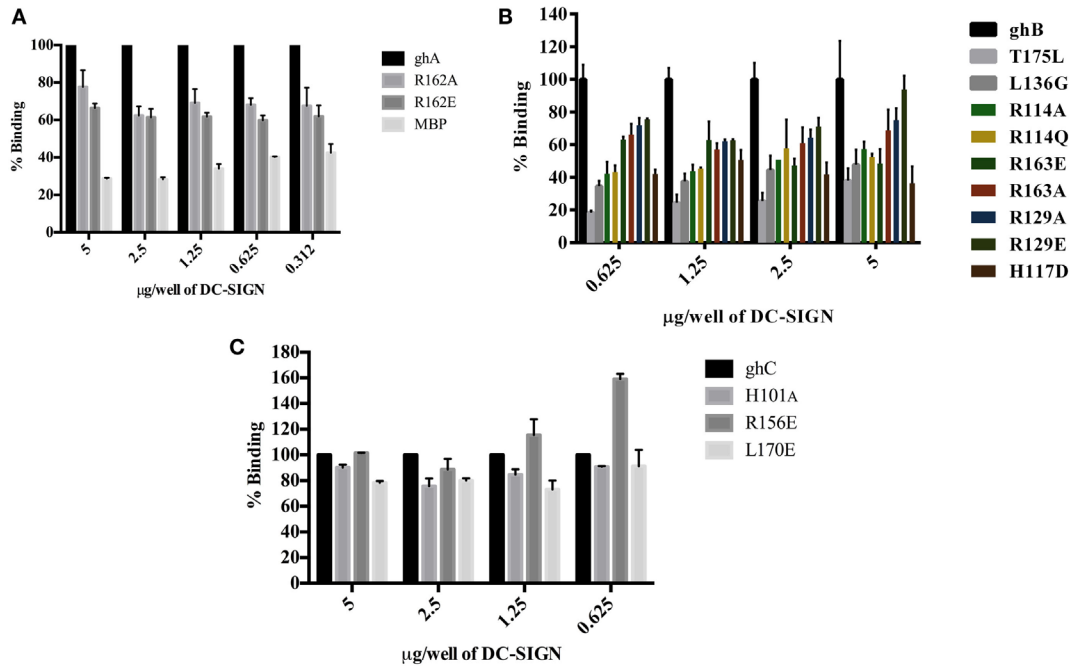

FIGURE 4 | Binding of globular head substitution mutants to DC-SIGN. Different concentrations of DC-SIGN tetramer were coated on microtiter wells in carbonate buffer overnight at 4°C. Wells were then incubated with 2.5 µg/well (in $CaCl_2$) of recombinant globular head wild type and mutant proteins and probed with anti-MBP monoclonal antibody and rabbit anti-mouse IgG-HRP conjugate. Percent binding was calculated for each mutant using binding of the wild-type globular head module as 100%. **(A)** Binding of ghA, ghA-R162E, and ghA-R162A to DC-SIGN; **(B)** binding of ghB mutants ghB-L136G, ghB-T175L, ghB-R114Q, ghB-R114A, ghB-R163A, ghB-R163E, ghB-R129E, ghB-R129A, and ghB-H117D to DC-SIGN; **(C)** binding of ghC mutants ghC-R156E, ghC-L170E, and ghC-H101A to DC-SIGN.

through DC-SIGN but significantly promoted viral transfer in the presence of C1q as well as the three globular head modules together for up to 7 days. This suggests that the tripartite interaction between C1q, gC1qR, and DC-SIGN enhances DC-SIGN-mediated viral transfer. Thus, association of these proteins on DCs may actually promote HIV-1 infection. In addition, involvement of gC1qR in the tripartite complex is likely to negate the protective effect of C1q.

DISCUSSION

The role of complement in HIV-1 pathogenesis is well-documented. Complement-opsonized HIV-1 causes enhanced viral infection of $CD4^+$ T cell lines (34), PBMCs, monocytes, and macrophages (35). DC-SIGN on the surface of immature DCs is involved in the capture of C3 opsonized R5 and X4 tropic HIV-1 and enhanced transmission to T cells (36). C1q can bind to gp41 directly in an antibody-independent manner and activate the classical pathway (16); however, this leads to an enhanced infection of complement receptor-bearing cells (37). To escape complement-mediated destruction, HIV-1 uses follicular DCs as a viral reservoir (38), following its internalization *via* CR2, and remains within its protective recycling endosome. Following emergence from the endosome to the cell surface, HIV-1 infects follicular T cells through CD4. HIV-1 opsonized with C3b interacts with CR1 on erythrocytes with factor I dissociating erythrocytes from this complex and converting C3b to iC3b and C3d. C3d opsonized HIV-1 is then able to bind to CR2 on B cells (39). In this study, we have examined complement-independent interaction of C1q with HIV-1 *via* DC-SIGN.

C1q is a charge pattern recognition protein that binds to a variety of ligands *via* its gC1q domain (19). Following its ability to interact with DC-SIGNR (32), Hosszu et al. recently have shown that C1q also recognizes a peptide derived from its homolog DC-SIGN (15). In the current study, we made use of the availability of recombinant individual globular head modules of C1q (ghA, ghB, and ghC) and its substitution mutants to establish that C1q binds DC-SIGN (and DC-SIGNR) *via* its gC1q domain.

Structure-function studies have demonstrated that the CRD region of DC-SIGN is the specific site for ligand binding and only funcions in the presence of the neck region within the ECD (12). We performed a series of binding experiments involving both the tetrameric forms of DC-SIGN and DC-SIGNR (comprising of the ECD and CRD region) as well as the monomeric forms, which only consist of the CRD region. We asked the question whether DC-SIGN and DC-SIGNR binding sites for C1q (and its gC1q domain) lies within their CRD region, or the α-helical neck region also plays an important role in these interactions. Both proteins have an increased affinity for glycoproteins containing high mannose oligosaccharides, such as mannan (40), gp120 (10), and ICAM-3 (41), *via* the CRD region. Here, individual globular head modules bound better to the tetrameric forms of DC-SIGN

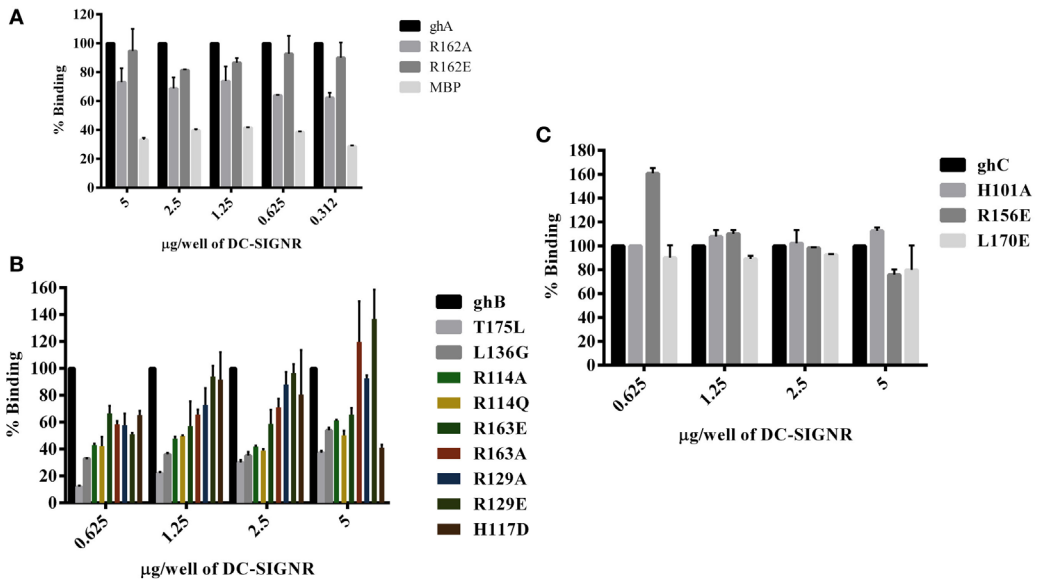

FIGURE 5 | Binding of globular head substitution mutants to DC-SIGNR. Different concentrations of DC-SIGNR tetramer were coated on microtiter wells in carbonate buffer overnight at 4°C and then incubated with 2.5 µg/well of recombinant globular head wild type and mutant proteins and probed with anti-MBP monoclonal antibody and rabbit anti-mouse IgG-HRP conjugate. Percent binding was calculated for each mutant using binding of the wild-type globular head module as 100%. **(A)** Binding of ghA, ghA-R162E and ghA-R162A to DC-SIGNR; **(B)** binding of ghB mutants ghB-L136G, ghB-T175L, ghB-R114Q, ghB-R114A, ghB-R163A, ghB-R163E, ghB-R129E, ghB-R129A, and ghB-H117D to DC-SIGNR; **(C)** binding of ghC mutants ghC-R156E, ghC-L170E, and ghC-H101A to DC-SIGNR.

TABLE 1 | Bindings of globular head modules and its mutants with DC-SIGN (% binding ± SD).

ghA	100.00 ± 0.0
R162A	77.71 ± 8.85
R162E	66.41 ± 2.38
ghB	100.0 ± 23.62
R129E	93.91 ± 8.34
R129A	75.05 ± 7.22
R163A	68.76 ± 12.78
R114A	57.37 ± 4.45
R114Q	52.46 ± 1.94
R163E	48.33 ± 8.89
L136G	47.74 ± 9.17
T175L	37.92 ± 7.50
H117D	36.35 ± 10.28
ghC	100.00 ± 0.00
R156E	101.41 ± 0.27
H101A	90.20 ± 2.27
L170E	78.32 ± 1.47

TABLE 2 | Bindings of globular head modules and its mutants with DC-SIGNR (% binding ± SD).

ghA	100.00 ± 0.00
R162E	94.78 ± 15.08
R162A	73.17 ± 9.54
ghB	100.00 ± 0.00
R129E	136.70 ± 21.82
R163A	119.68 ± 30.09
R129A	92.55 ± 2.26
R163E	65.69 ± 4.89
R114A	61.44 ± 0.38
L136G	53.99 ± 1.88
R114Q	50.27 ± 3.39
H117D	40.96 ± 2.26
T175L	37.23 ± 1.50
ghC	100.00 ± 0.00
H101A	112.60 ± 2.86
L170E	79.81 ± 20.40
R156E	75.77 ± 4.62

and DC-SIGNR as opposed to just the CRD region alone, indicating that the neck region, and hence, multimerization is needed to facilitate C1q binding. The neck region of DC-SIGN and DC-SIGNR interestingly differ most in their α helical structures (8) as the 23 amino acid repeats only show the first half of each repeat presenting a pattern of hydrophobic residues spaced at intervals, a feature that is abundant in most dimeric and trimeric coiled-coils (42).

We also found that the ghB module bound better to DC-SIGN and DC-SIGNR. Previous studies have identified ghB as a key module of the gC1q domain in binding to IgG, PTX3, and CRP (43, 44). Interestingly, C1q and ghB bound DC-SIGNR better than DC-SIGN, despite 77% sequence similarity. We also expressed and purified globular head mutants (29) where single amino acid residues were substituted in order to localize key residues involved in C1q interaction with its various ligands. These mutants were designed based on the crystal structure and are the residues known to be important in binding to various C1q ligands (43). It appears that IgG and DC-SIGN binding sites on ghB are overlapping and shared, including Lys^{136} and

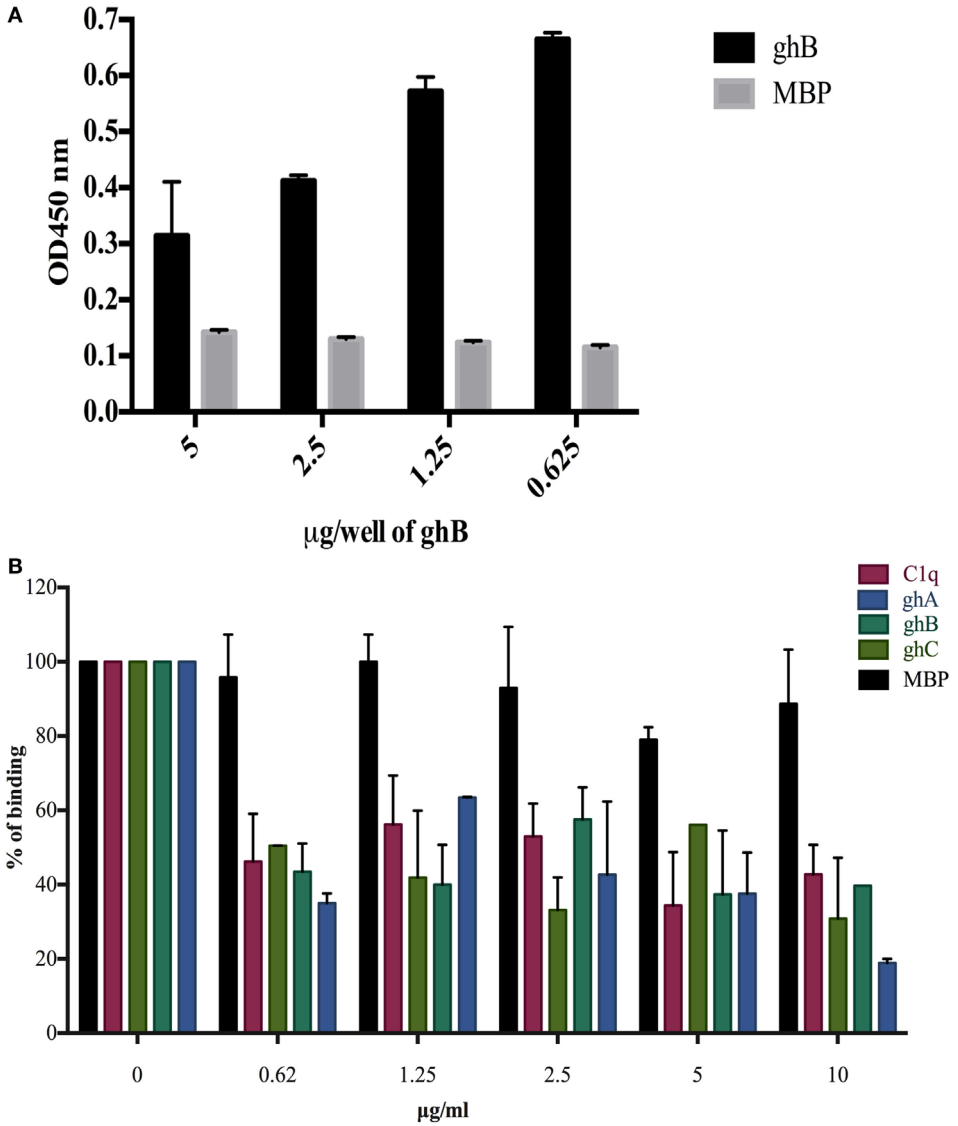

FIGURE 6 | **Competitive inhibition of DC-SIGN: HIV-1 gp120 interaction by globular head modules and gC1qR**. **(A)** ELISA to assess whether gC1qR and ghB directly compete for the same binding site on DC-SIGN: DC-SIGN was coated at 5 µg/well overnight at 4°C. Wells were blocked with 2% BSA in PBS for 2 h at 37°C. gC1qR (5 µg/well) and different concentrations of ghB (5, 2.5, 1.25, 0.625 µg/well) were added in buffer containing 5 mM $CaCl_2$. Incubation was carried out at 37°C for 1.5 h and 4°C for 1.5 h. Following repeated washes, bound gC1qR was probed using rabbit anti-gC1qR polyclonal antibodies (1:1,000) and Protein A-HRP (1:1,000). Color was developed using *o*-phenylenediamine dihydrochloride substrate; **(B)** competition between DC-SIGN tetramer and C1q globular head modules to bind solid-phase gp120. Microtiter wells were coated with 250 ng of gp120. Various concentrations of ghA, ghB, ghC, and C1q and constant 2.5 µg/mL of DC-SIGN were incubated at 37°C for 1 h and then at 4°C for 1 h. The binding of DC-SIGN to gp120 in the presence of globular heads or C1q was detected using rabbit anti-DC antibody (1:500), probed with Protein A HRP (1:5,000). DC-SIGN alone binding to gp120 was used as 100%.

Tyr^{175} on ghB, which have been previously shown to be important for binding to IgG (29) and for gC1q assembly (45). We also examined the roles of Arg^{114}, Arg^{129}, and Arg^{163} of the ghB module since arginine residues have previously been shown to be important for the C1q–IgG interaction (46). Moreover, Hosszu et al. have reported that C1q binds DC-SIGN *via* its IgG binding site (15). Our results highlighted the significance of Arg^{114} in C1q interaction with DC-SIGN and DC-SIGNR (**Figures 4B** and **5B**). Substituting Arg^{114} with the polar residue Glutamine and hydrophobic residue Ala led to ~80% reduction, highlighting a very important role for Arginine^{114} of B chain in C1q–DC-SIGN interaction. In addition, Tyr^{175} appears critical for C1q interaction with DC-SIGN and DC-SIGNR (**Figures 4B** and **5B**); the binding analysis revealed a dramatic reduction (82% for DC-SIGN and 90% for DC-SIGNR following substitution of Tyr with Leu). This is not the first time Tyr^{175} has been shown to be a critical residue in gC1q binding (33). Gadjeva et al. have shown that this residue mainly constitutes C1q binding to

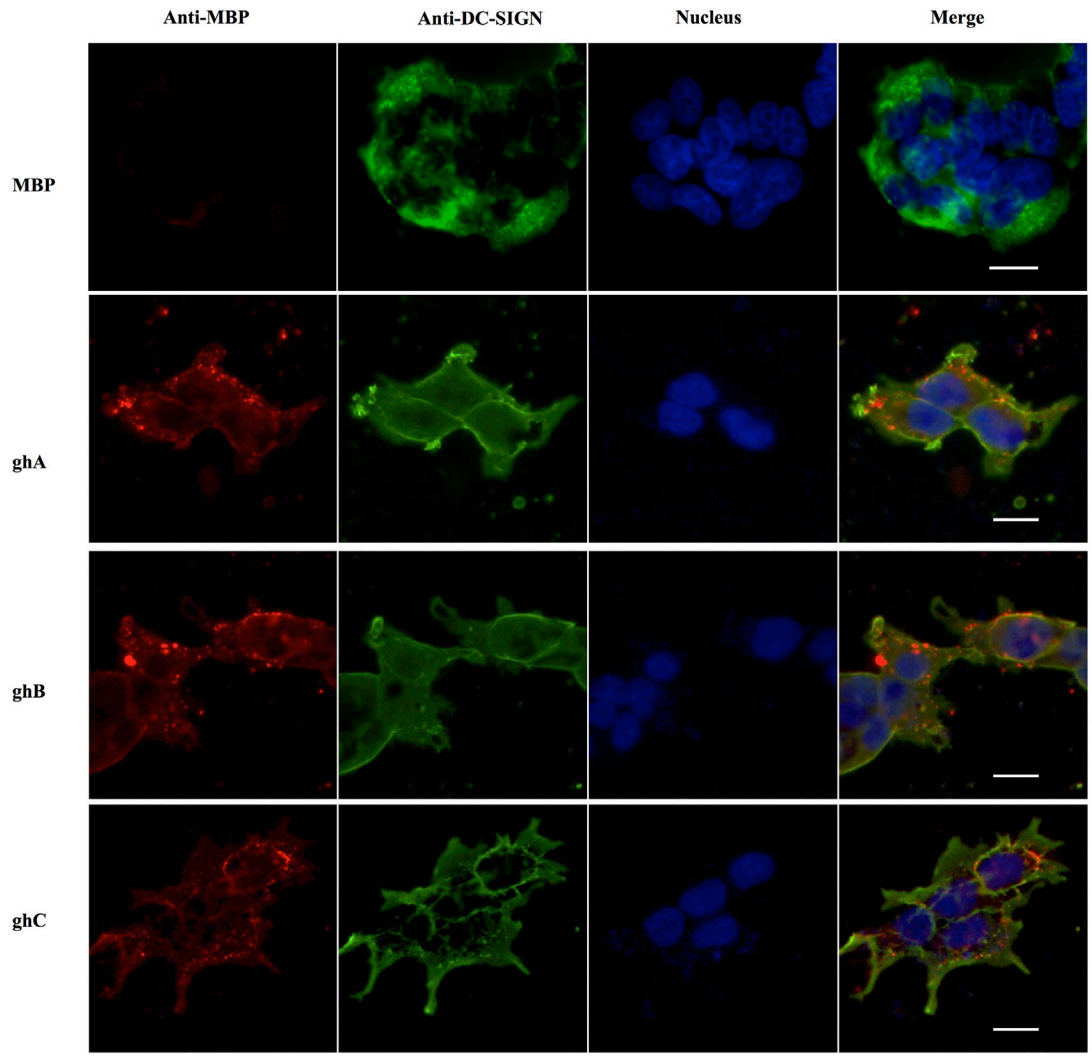

FIGURE 7 | ***In vitro*** **binding of globular heads modules to DC-SIGN expressed on HEK cells**. DC-SIGN-expressing HEK cells (DC-HEK cells) were incubated with recombinant globular head modules (ghA, ghB, ghC) and MBP as control for 30 min at 37°C. DC-HEK cells were fixed with 4% paraformaldehyde, washed and blocked with 5% FCS, and probed with mouse anti MBP antibody to detect the presence of MBP fused globular head modules and rabbit anti DC-SIGN to detect DC-SIGN expressed on the cells. Goat anti-mouse secondary antibody conjugated with Alexa Fluor 568 was used to detect binding of globular heads whereas DC-SIGN expression was visualized using goat anti-rabbit IgG conjugated with Alexa Fluor 488 antibody. Scale bar 20 μm.

IgM. Overall, our binding studies suggest that Tyr^{175} and Arg^{114} of ghB are critical for the C1q–DC-SIGN and C1q–DC-SIGNR interaction.

The known dual roles of DC-SIGN as a facilitator of adaptive immune response as well as promoter of HIV-1 infection prompted us to examine if innate immune soluble factors such as C1q and gC1qR can potentially modulate viral transmission *via* DC-SIGN (47), similar to reports involving $CD4^+$ T cells (48) and a lectin drug GRFT (*Griffithsia)* isolated from the red algae (49). We also included DC-SIGNR (DC-SIGN-related), a homolog of DC-SIGN, in our study. DC-SIGN-R is expressed on endothelium including liver sinusoidal (50), lymph node sinuses, and placental capillary (8). DC-SIGNR can bind ICAM-3 as well as gp120 to facilitate HIV-1 viral infection (50). As a receptor for bacterial dextrans (51) and capsular pneumococcal polysaccharide of *Streptococcus pneumoniae*, DC-SIGN-R can cause proteolysis of C3 (32). DC-SIGN-R is shown to be highly expressed by spleen marginal zone macrophages (MZM) and lymph node macrophages (52). SIGN-R1 (mouse homologue) in MZM interacts with C1q in the spleen and enhances apoptotic cell clearance *via* activation of the classical pathway (53).

The transmembrane envelope gp41 protein of HIV-1 is known to interact with C1q (54) through its A chain (19), leading to complement activation but no viral lysis (55). Instead, the virus is transmitted to complement receptor bearing cells such as macrophages and $CD4^+$ T cells allowing infection to take place (37, 54, 56, 57). HIV-1-infected $CD4^+$ T cells can activate the classical pathway *via* shedding of gp120, leading to unmasking of the gp41 epitope 601–613 available for interaction

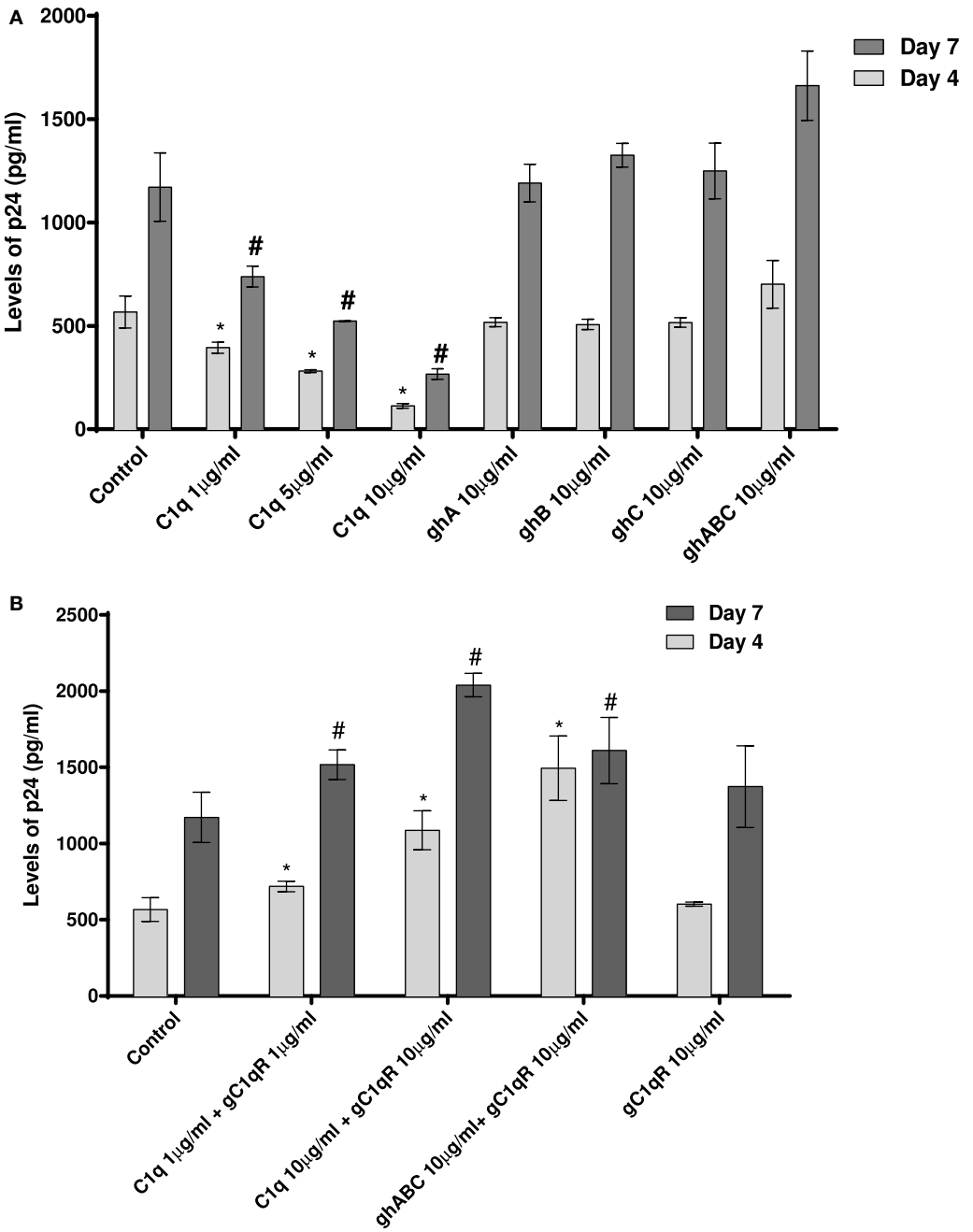

FIGURE 8 | HIV transfer assay mediated by DC-SIGN. Cell surface DC-SIGN expressing HEK (DC-HEK) cells were grown in a 12-well plate to form a confluent layer. Different concentrations of proteins were added to the cells and incubated for 2 h for binding. Unbound proteins were removed and cells were challenged with 2.5 ng/mL p24 of HIV-1 (SF-162 strain) for 1 h. Unbound virus was washed off and cells were co-cultured with PHA-activated PBMCs for 24 h. PBMCs were separated from the DC-HEK monolayer and cultured separately for 7 days to determine viral titer of the supernatants collected on days 4 and 7. **(A)** C1q, ghA, ghB, ghC, and ghABC; **(B)** gC1qR in presence of C1q, ghA, ghB, ghC, and ghABC. Data represent mean ± SD. $P < 0.05$ is considered significant. * and # indicate statistical significance in comparison to untreated controls of days 4 and 7, respectively.

with C1q (23). C1q is also involved in a range of processes independent to its complement functions (58, 59), including DC differentiation (60). C1q, along with its globular head receptor gC1qR and DC-SIGN, can co-localize on the surface of blood precursor DCs to promote DC differentiation (15). gC1qR, a multifunctional pathogen recognition receptor (61, 62), can also interact with gp41 of HIV-1 (17) on uninfected $CD4^+$ T cells and upregulate NK cell ligand NKP44-L, rendering healthy $CD4^+$ T cells susceptible to NK cell lysis. Since DC-SIGN is a receptor for HIV-1 through its binding to gp120, it is interesting that it

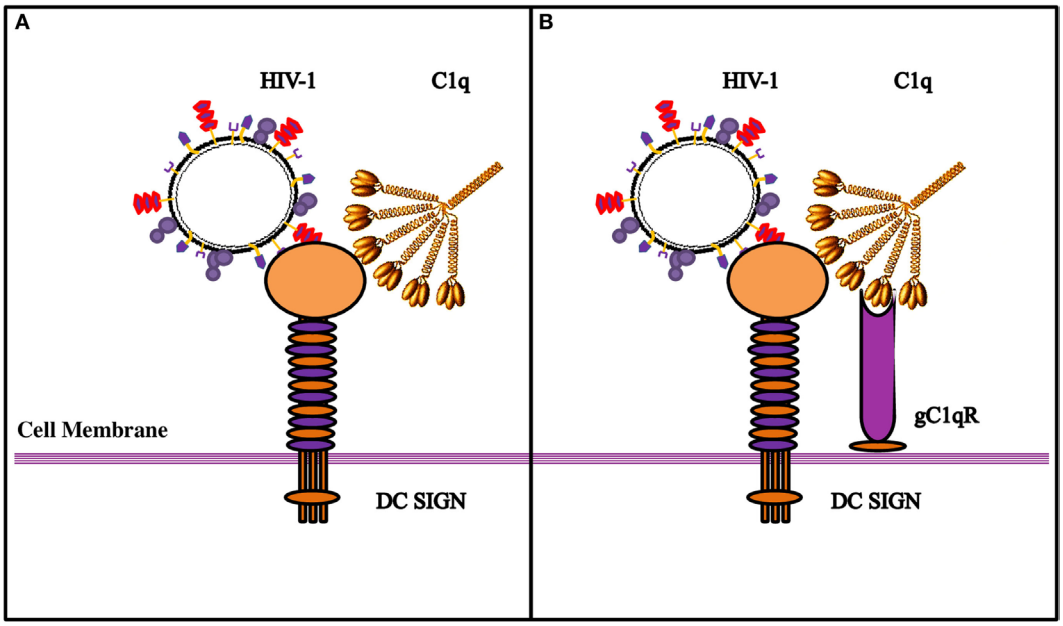

FIGURE 9 | Diagrammatic model explaining the possible implications of the tripartite molecular interplay between DC-SIGN, C1q, and gC1qR. (A) By virtue of its ability to bind to DC-SIGN on the cell surface, C1q is likely to inhibit interaction between DC-SIGN and HIV-1 gp120, resulting in the inhibition of viral transfer. **(B)** On the DC/Monocyte surface, a trimolecular receptor complex is formed between gC1qR, C1q, and DC-SIGN. Although each of these molecules can bind the HIV-1 virus independently, we postulate that it is the binding of the HIV-1 gp-41 to both gC1qR and C1q that initiates the membrane fusion before the final binding of gp120 to DC-SIGN and/or CD4, eventually allowing the internalization of the virus. It is possible that HIV-1 interaction with DC/monocytes causes recruitment of gC1qR to the cell surface, or its secretion, which in turn, can bind to C1q globular heads, thereby neutralizing the protection offered by C1q.

co-localizes with C1q and gC1qR, the two proteins, also known for HIV-1 binding and transmission of the viral infection. Such association forming a trimolecular unit on the target cell surface may create a vehicle that promotes pathogen entry and immunosuppression (15).

We wanted to examine if C1q–DC-SIGN interaction modulated HIV-1 transfer. We found that full length C1q but not its individual globular heads, suppressed DC-SIGN-mediated HIV-1 transfer to activated PBMCs. Curiously, addition of gC1qR negated the protective effects of C1q by enhancing DC-SIGN-mediated viral transfer. gC1qR, as an inhibitor of HIV-1 infection, can block the interaction between CD4 and gp120 and prevent viral entry (24). Since DC-SIGN binds to gp120 and gC1qR to gp41, both promoting infection, we can consider that even if gC1qR does interfere with the DC-SIGN-gp120 interaction, its active binding site for gp41 is still available to facilitate infection. The increased viral transmission of gC1qR seen when in association with C1q suggests that C1q bound to gC1qR can enhance its function. It is possible that C1q plays a protective role by blocking access of gp120 to DC-SIGN (**Figure 9**). This can happen if C1q shares binding sites on DC-SIGN. The globular heads, individually or in combination, did not appear to inhibit virus transmission unlike full length C1q, suggesting that the collagen domain of C1q and/or probably oligomeric form of C1q is required for the observed inhibitory effect.

In summary, we found that gC1qR can alter C1q–DC-SIGN interaction in a way that it promotes viral transfer, thus neutralizing the protective effect of C1q. The tripartite complex involving DC-SIGN–gC1qR-C1q probably leads to an increase in the distance between DC-SIGN and C1q that permits DC-SIGN interaction with gp120; this allows DC-SIGN and gC1qR to bind to the virus with enhanced affinity (**Figure 9**).

AUTHOR CONTRIBUTIONS

LP, HP, BP, and AK carried out crucial experiments; MA-M, LK, BG, and DM provided important reagents; TM supervised few experiments and helped with manuscript preparation; UK led the research, conceived the experiments, and drafted the manuscript.

FUNDING

BG would like to acknowledge support from the National Institute of Allergy and Infectious Diseases R01 AI 060866 and R01 AI-084178.

REFERENCES

1. Caparros E, Munoz P, Sierra-Filardi E, Serrano-Gomez D, Puig-Kroger A, Rodriguez-Fernandez J, et al. DC-SIGN ligation on dendritic cells results in ERK and PI3K activation and modulates cytokine production. *Blood* (2006) 107:3950–8. doi:10.1182/blood-2005-03-1252
2. Gringhuis SI, den Dunnen J, Litjens M, van HH, van Kooyk Y, Geijtenbeek TB. C-type lectin DC-SIGN modulates Toll-like receptor signaling via Raf-1 kinase-dependent acetylation of transcription factor NF-kappaB. *Immunity* (2007) 26:605–16. doi:10.1016/j.immuni.2007.03.012
3. den Dunnen J, Gringhuis SI, Geijtenbeek TB. Innate signaling by the C-type lectin DC-SIGN dictates immune responses. *Cancer Immunol Immunother* (2009) 58:1149–57. doi:10.1007/s00262-008-0615-1
4. Geijtenbeek TB, Torensma R, van Vliet SJ, van Duijnhoven GC, Adema GJ, van Kooyk Y, et al. Identification of DC-SIGN, a novel dendritic cell-specific ICAM-3 receptor that supports primary immune responses. *Cell* (2000) 100:575–85. doi:10.1016/S0092-8674(00)80693-5
5. Geijtenbeek TB, van Duijnhoven GC, van Vliet SJ, Krieger E, Vriend G, Figdor CG, et al. Identification of different binding sites in the dendritic cell-specific receptor DC-SIGN for intercellular adhesion molecule 3 and HIV-1. *J Biol Chem* (2002) 277:11314–20. doi:10.1074/jbc.M111532200
6. Martinez O, Brackenridge S, El-Idrissi Mel A, Prabhakar BS. DC-SIGN, but not sDC-SIGN, can modulate IL-2 production from PMA-and anti-CD3-stimulated primary human CD4 T cells. *Int Immunol* (2005) 17:769–78. doi:10.1093/intimm/dxh258
7. Maeda N, Nigou J, Herrmann JL, Jackson M, Amara A, Lagrange PH, et al. The cell surface receptor DC-SIGN discriminates between *Mycobacterium* species through selective recognition of the mannose caps on lipoarabinomannan. *J Biol Chem* (2003) 278:5513–6. doi:10.1074/jbc.C200586200
8. Mitchell DA, Fadden AJ, Drickamer K. A novel mechanism of carbohydrate recognition by the C-type lectins DC-SIGN and DC-SIGNR. Subunit organization and binding to multivalent ligands. *J Biol Chem* (2001) 276:28939–45. doi:10.1074/jbc.M104565200
9. Manches O, Frleta D, Bhardwaj N. Dendritic cells in progression and pathology of HIV infection. *Trends Immunol* (2014) 35:114–22. doi:10.1016/j.it.2013.10.003
10. Geijtenbeek TB, Kwon DS, Torensma R, van Vliet SJ, van Duijnhoven GC, Middel J, et al. DC-SIGN, a dendritic cell-specific HIV-1-binding protein that enhances trans-infection of T cells. *Cell* (2000) 100:587–97. doi:10.1016/S0092-8674(00)80694-7
11. Pohlmann S, Zhang J, Baribaud F, Chen Z, Leslie GJ, Lin G, et al. Hepatitis C virus glycoproteins interact with DC-SIGN and DC-SIGNR. *J Virol* (2003) 77:4070–80. doi:10.1128/JVI.77.7.4070-4080.2003
12. Lozach PY, Lortat-Jacob H, de Lacroix dL, Staropoli I, Foung S, Amara A, et al. DC-SIGN and L-SIGN are high affinity binding receptors for hepatitis C virus glycoprotein E2. *J Biol Chem* (2003) 278:20358–66. doi:10.1074/jbc.M301284200
13. Curtis BM, Scharnowske S, Watson AJ. Sequence and expression of a membrane-associated C-type lectin that exhibits CD4-independent binding of human immunodeficiency virus envelope glycoprotein gp120. *Proc Natl Acad Sci U S A* (1992) 89:8356–60. doi:10.1073/pnas.89.17.8356
14. Sarkar R, Mitra D, Chakrabarti S. HIV-1 gp120 protein downregulates Nef induced IL-6 release in immature dentritic cells through interplay of DC-SIGN. *PLoS One* (2013) 8:e59073. doi:10.1371/journal.pone.0059073
15. Hosszu KK, Valentino A, Vinayagasundaram U, Vinayagasundaram R, Joyce MG, Ji Y, et al. DC-SIGN, C1q, and gC1qR form a trimolecular receptor complex on the surface of monocyte-derived immature dendritic cells. *Blood* (2012) 120:1228–36. doi:10.1182/blood-2011-07-369728
16. Ebenbichler CF, Thielens NM, Vornhagen R, Marschang P, Arlaud GJ, Dierich MP. Human immunodeficiency virus type 1 activates the classical pathway of complement by direct C1 binding through specific sites in the transmembrane glycoprotein gp41. *J Exp Med* (1991) 174:1417–24. doi:10.1084/jem.174.6.1417
17. Fausther-Bovendo H, Vieillard V, Sagan S, Bismuth G, Debre P. HIV gp41 engages gC1qR on CD4+ T cells to induce the expression of an NK ligand through the PIP3/H2O2 pathway. *PLoS Pathog* (2010) 6:e1000975. doi:10.1371/journal.ppat.1000975
18. Thielens NM, Bally IM, Ebenbichler CF, Dierich MP, Arlaud GJ. Further characterization of the interaction between the C1q subcomponent of human C1 and the transmembrane envelope glycoprotein gp41 of HIV-1. *J Immunol* (1993) 151:6583–92.
19. Kishore U, Gupta SK, Perdikoulis MV, Kojouharova MS, Urban BC, Reid KB. Modular organization of the carboxyl-terminal, globular head region of human C1q A, B, and C chains. *J Immunol* (2003) 171:812–20.
20. Thielens NM, Tacnet-Delorme P, Arlaud GJ. Interaction of C1q and mannan-binding lectin with viruses. *Immunobiology* (2002) 205:563–74. doi:10.1078/0171-2985-00155
21. Pinter A, Honnen WJ, Tilley SA, Bona C, Zaghouani H, Gorny MK, et al. Oligomeric structure of gp41, the transmembrane protein of human immunodeficiency virus type 1. *J Virol* (1989) 63:2674–9.
22. Marschang P, Kruger U, Ochsenbauer C, Gurtler L, Hittmair A, Bosch V, et al. Complement activation by HIV-1-infected cells: the role of transmembrane glycoprotein gp41. *J Acquir Immune Defic Syndr Hum Retrovirol* (1997) 14:102–9. doi:10.1097/00042560-199702010-00002
23. Caffrey M. Model for the structure of the HIV gp41 ectodomain: insight into the intermolecular interactions of the gp41 loop. *Biochim Biophys Acta* (2001) 1536:116–22. doi:10.1016/S0925-4439(01)00042-4
24. Szabo J, Cervenak L, Toth FD, Prohaszka Z, Horvath L, Kerekes K, et al. Soluble gC1q-R/p33, a cell protein that binds to the globular "heads" of C1q, effectively inhibits the growth of HIV-1 strains in cell cultures. *Clin Immunol* (2001) 99:222–31. doi:10.1006/clim.2001.5013
25. Kittlesen DJ, Chianese-Bullock K, Yao ZQ, Braciale TJ, Hahn YS. Interaction between complement receptor gC1qR and hepatitis C virus core protein inhibits T-lymphocyte proliferation. *J Clin Invest* (2000) 106:1239–49. doi:10.1172/JCI10323
26. Matthews DA, Russell WC. Adenovirus core protein V interacts with p32 – a protein which is associated with both the mitochondria and the nucleus. *J Gen Virol* (1998) 79(Pt 7):1677–85. doi:10.1099/0022-1317-79-7-1677
27. Wang Y, Finan JE, Middeldorp JM, Hayward SD. P32/TAP, a cellular protein that interacts with EBNA-1 of Epstein-Barr virus. *Virology* (1997) 236:18–29. doi:10.1006/viro.1997.8739
28. Mohan KV, Ghebrehiwet B, Atreya CD. The N-terminal conserved domain of rubella virus capsid interacts with the C-terminal region of cellular p32 and overexpression of p32 enhances the viral infectivity. *Virus Res* (2002) 85:151–61. doi:10.1016/S0168-1702(02)00030-8
29. Kojouharova MS, Gadjeva MG, Tsacheva IG, Zlatarova A, Roumenina LT, Tchorbadjieva MI, et al. Mutational analyses of the recombinant globular regions of human C1q A, B, and C chains suggest an essential role for arginine and histidine residues in the C1q-IgG interaction. *J Immunol* (2004) 172:4351–8. doi:10.4049/jimmunol.172.7.4351
30. Pednekar L, Pathan AA, Paudyal B, Tsolaki AG, Kaur A, Kouser L, et al. Analysis of the interaction between globular head modules of human C1q and its receptor gC1qR. *Front Immunol* (2016) 7:567. doi:10.3389/fimmu.2016.00567
31. Lang SM, Bynoe MO, Karki R, Tartell MA, Means RE. Kaposi's sarcoma-associated herpesvirus K3 and K5 proteins down regulate both DC-SIGN and DC-SIGNR. *PLoS One* (2013) 8:e58056. doi:10.1371/journal.pone.0058056
32. Kang YS, Do Y, Lee HK, Park SH, Cheong C, Lynch RM, et al. A dominant complement fixation pathway for pneumococcal polysaccharides initiated by SIGN-R1 interacting with C1q. *Cell* (2006) 125:47–58. doi:10.1016/j.cell.2006.01.046
33. Gadjeva MG, Rouseva MM, Zlatarova AS, Reid KB, Kishore U, Kojouharova MS. Interaction of human C1q with IgG and IgM: revisited. *Biochemistry* (2008) 47:13093–102. doi:10.1021/bi801131h
34. Delibrias CC, Fischer EM, Kazatchkine MD. The enhancing role of complement in human immunodeficiency virus infection: soluble recombinant CR1 (CD35) inhibits complement-mediated enhancement of infection of a CD4-positive T-cell line with human immunodeficiency virus-1. *Scand J Immunol* (2000) 51:526–9. doi:10.1046/j.1365-3083.2000.00715.x
35. Bouhlal H, Galon J, Kazatchkine MD, Fridman WH, Sautes-Fridman C, Haeffner Cavaillon N. Soluble CD16 inhibits CR3 (CD11b/CD18)-mediated infection of monocytes/macrophages by opsonized primary R5 HIV-1. *J Immunol* (2001) 166:3377–83. doi:10.4049/jimmunol.166.5.3377
36. Bouhlal H, Chomont N, Requena M, Nasreddine N, Saidi H, Legoff J, et al. Opsonization of HIV with complement enhances infection of dendritic cells and viral transfer to CD4 T cells in a CR3 and DC-SIGN-dependent manner. *J Immunol* (2007) 178:1086–95. doi:10.4049/jimmunol.178.2.1086

37. Tacnet-Delorme P, Boyer V, Thielens NM, Hernandez JF, Bally I, Sim RB, et al. In vitro analysis of complement-dependent HIV-1 cell infection using a model system. *J Immunol* (1999) 162:4088–93.
38. Delibrias CC, Kazatchkine MD, Fischer E. Evidence for the role of CR1 (CD35), in addition to CR2 (CD21), in facilitating infection of human T cells with opsonized HIV. *Scand J Immunol* (1993) 38:183–9. doi:10.1111/j.1365-3083.1993.tb01711.x
39. Banki Z, Wilflingseder D, Ammann CG, Pruenster M, Mullauer B, Hollander K, et al. Factor I-mediated processing of complement fragments on HIV immune complexes targets HIV to CR2-expressing B cells and facilitates B cell-mediated transmission of opsonized HIV to T cells. *J Immunol* (2006) 177:3469–76. doi:10.4049/jimmunol.177.5.3469
40. Appelmelk BJ, van Die I, van Vliet SJ, Vandenbroucke-Grauls C, Geijtenbeek TB, van Kooyk Y. Cutting edge: carbohydrate profiling identifies new pathogens that interact with dendritic cell-specific ICAM-3-grabbing nonintegrin on dendritic cells. *J Immunol* (2003) 170:1635–9. doi:10.4049/jimmunol.170.4.1635
41. Geijtenbeek TB, Krooshoop DJ, Bleijs DA, van Vliet SJ, van Duijnhoven GC, Grabovsky V, et al. DC-SIGN-ICAM-2 interaction mediates dendritic cell trafficking. *Nat Immunol* (2000) 1:353–7. doi:10.1038/79815
42. McLachlan AD, Stewart M. Tropomyosin coiled-coil interactions: evidence for an unstaggered structure. *J Mol Biol* (1975) 98:293–304. doi:10.1016/S0022-2836(75)80119-7
43. Gaboriaud C, Juanhuix J, Gruez A, Lacroix M, Darnault C, Pignol D, et al. The crystal structure of the globular head of complement protein C1q provides a basis for its versatile recognition properties. *J Biol Chem* (2003) 278:46974–82. doi:10.1074/jbc.M307764200
44. Roumenina LT, Ruseva MM, Zlatarova A, Ghai R, Kolev M, Olova N, et al. Interaction of C1q with IgG1, C-reactive protein and pentraxin 3: mutational studies using recombinant globular head modules of human C1q A, B, and C chains. *Biochemistry* (2006) 45:4093–104. doi:10.1021/bi052646f
45. Gadjeva M, Zlatarova A, Ruseva M, Kishore U, Kojouharova M. Mutational analysis of ligand-binding activities of recombinant gC1q heterotrimer. *Mol Immunol* (2010) 47:2260–2260. doi:10.1016/j.molimm.2010.05.188
46. Burton DR, Boyd J, Brampton AD, Easterbrook-Smith S, Emanuel EJ, Novotny J, et al. The Clq receptor site on immunoglobulin G. *Nature* (1980) 288:338–44. doi:10.1038/288338a0
47. Balzarini J, Van Damme L. Microbicide drug candidates to prevent HIV infection. *Lancet* (2007) 369:787–97. doi:10.1016/S0140-6736(07)60202-5
48. Balzarini J, Van Laethem K, Daelemans D, Hatse S, Bugatti A, Rusnati M, et al. Pradimicin A, a carbohydrate-binding nonpeptidic lead compound for treatment of infections with viruses with highly glycosylated envelopes, such as human immunodeficiency virus. *J Virol* (2007) 81:362–73. doi:10.1128/JVI.01404-06
49. Hoorelbeke B, Xue J, LiWang PJ, Balzarini J. Role of the carbohydrate-binding sites of griffithsin in the prevention of DC-SIGN-mediated capture and transmission of HIV-1. *PLoS One* (2013) 8:e64132. doi:10.1371/journal.pone.0064132
50. Bashirova AA, Geijtenbeek TB, van Duijnhoven GC, van Vliet SJ, Eilering JB, Martin MP, et al. A dendritic cell-specific intercellular adhesion molecule 3-grabbing nonintegrin (DC-SIGN)-related protein is highly expressed on human liver sinusoidal endothelial cells and promotes HIV-1 infection. *J Exp Med* (2001) 193:671–8. doi:10.1084/jem.193.6.671
51. Kang YS, Yamazaki S, Iyoda T, Pack M, Bruening SA, Kim JY, et al. SIGN-R1, a novel C-type lectin expressed by marginal zone macrophages in spleen, mediates uptake of the polysaccharide dextran. *Int Immunol* (2003) 15:177–86. doi:10.1093/intimm/dxg019
52. Leavy O. Innate immunity: a new way to get complement. *Nat Rev Immunol* (2006) 4:490–1.
53. Prabagar MG, Do Y, Ryu S, Park JY, Choi HJ, Choi WS, et al. SIGN-R1, a C-type lectin, enhances apoptotic cell clearance through the complement deposition pathway by interacting with C1q in the spleen. *Cell Death Differ* (2013) 20:535–45. doi:10.1038/cdd.2012.160
54. Solder BM, Schulz TF, Hengster P, Lower J, Larcher C, Bitterlich G, et al. HIV and HIV-infected cells differentially activate the human complement system independent of antibody. *Immunol Lett* (1989) 22:135–45. doi:10.1016/0165-2478(89)90180-6
55. Banapour B, Sernatinger J, Levy JA. The AIDS-associated retrovirus is not sensitive to lysis or inactivation by human serum. *Virology* (1986) 152:268–71. doi:10.1016/0042-6822(86)90392-2
56. Gras GS, Dormont D. Antibody-dependent and antibody-independent complement-mediated enhancement of human immunodeficiency virus type 1 infection in a human, Epstein-Barr virus-transformed B-lymphocytic cell line. *J Virol* (1991) 65:541–5.
57. Boyer V, Desgranges C, Trabaud MA, Fischer E, Kazatchkine MD. Complement mediates human immunodeficiency virus type 1 infection of a human T cell line in a CD4-and antibody-independent fashion. *J Exp Med* (1991) 173:1151–8. doi:10.1084/jem.173.5.1151
58. Nayak A, Ferluga J, Tsolaki AG, Kishore U. The non-classical functions of the classical complement pathway recognition subcomponent C1q. *Immunol Lett* (2010) 131:139–50. doi:10.1016/j.imlet.2010.03.012
59. Nayak A, Pednekar L, Reid KB, Kishore U. Complement and non-complement activating functions of C1q: a prototypical innate immune molecule. *Innate Immun* (2012) 18:350–63. doi:10.1177/1753425910396252
60. Vegh Z, Kew RR, Gruber BL, Ghebrehiwet B. Chemotaxis of human monocyte-derived dendritic cells to complement component C1q is mediated by the receptors gC1qR and cC1qR. *Mol Immunol* (2006) 43:1402–7. doi:10.1016/j.molimm.2005.07.030
61. Ghebrehiwet B, Lim BL, Kumar R, Feng X, Peerschke EI. gC1q-R/p33, a member of a new class of multifunctional and multicompartmental cellular proteins, is involved in inflammation and infection. *Immunol Rev* (2001) 180:65–77. doi:10.1034/j.1600-065X.2001.1800106.x
62. Ghebrehiwet B, Jesty J, Xu S, Vinayagasundaram R, Vinayagasundaram U, Ji Y, et al. Structure-function studies using deletion mutants identify domains of gC1qR/p33 as potential therapeutic targets for vascular permeability and inflammation. *Front Immunol* (2011) 2:58. doi:10.3389/fimmu.2011.00058

Conflict of Interest Statement: The authors declare that the research was conducted in the absence of any commercial or financial relationships that could be construed as a potential conflict of interest.

frontiers in Immunology

ORIGINAL RESEARCH
published: 12 February 2018
doi: 10.3389/fimmu.2018.00131

Human Properdin Opsonizes Nanoparticles and Triggers a Potent Pro-inflammatory Response by Macrophages without Involving Complement Activation

*Lubna Kouser[1†], Basudev Paudyal[1,2†], Anuvinder Kaur[1], Gudrun Stenbeck[1], Lucy A. Jones[2], Suhair M. Abozaid[3], Cordula M. Stover[4], Emmanuel Flahaut[5], Robert B. Sim[6] and Uday Kishore[1]**

[1] Biosciences, College of Health and Life Sciences, Brunel University London, Uxbridge, United Kingdom, [2] Faculty of Science, Engineering and Computing, Kingston University, Kingston upon Thames, Surrey, United Kingdom, [3] Department of Infection and Immunity, King Faisal Specialist Hospital and Research Centre, Riyadh, Saudi Arabia, [4] Department of Infection, Immunity and Inflammation, University of Leicester, Leicester, United Kingdom, [5] Université de Toulouse, CNRS, INPT, UPS, UMR CNRS-UPS-INP N°5085, 3 Paul Sabatier, Bât. CIRIMAT, Toulouse, France, [6] Department of Biochemistry, University of Oxford, Oxford, United Kingdom

OPEN ACCESS

Edited by:
Cees Van Kooten, Leiden University, Netherlands

Reviewed by:
Mohamed Daha, Leiden University Medical Center, Netherlands
Arturo Ferreira, Universidad de Chile, Chile

***Correspondence:**
Uday Kishore
uday.kishore@brunel.ac.uk, ukishore@hotmail.com

[†]These authors are joint first authors.

Specialty section:
This article was submitted to Molecular Innate Immunity, a section of the journal Frontiers in Immunology

Received: *27 June 2017*
Accepted: *16 January 2018*
Published: *12 February 2018*

Citation:
Kouser L, Paudyal B, Kaur A, Stenbeck G, Jones LA, Abozaid SM, Stover CM, Flahaut E, Sim RB and Kishore U (2018) Human Properdin Opsonizes Nanoparticles and Triggers a Potent Pro-inflammatory Response by Macrophages without Involving Complement Activation. Front. Immunol. 9:131. doi: 10.3389/fimmu.2018.00131

Development of nanoparticles as tissue-specific drug delivery platforms can be considerably influenced by the complement system because of their inherent pro-inflammatory and tumorigenic consequences. The complement activation pathways, and its recognition subcomponents, can modulate clearance of the nanoparticles and subsequent inflammatory response and thus alter the intended translational applications. Here, we report, for the first time, that human properdin, an upregulator of the complement alternative pathway, can opsonize functionalized carbon nanotubes (CNTs) *via* its thrombospondin type I repeat (TSR) 4 and 5. Binding of properdin and TSR4+5 is likely to involve charge pattern/polarity recognition of the CNT surface since both carboxymethyl cellulose-coated carbon nanotubes (CMC-CNT) and oxidized (Ox-CNT) bound these proteins well. Properdin enhanced the uptake of CMC-CNTs by a macrophage cell line, THP-1, mounting a robust pro-inflammatory immune response, as revealed by qRT-PCR, multiplex cytokine array, and NF-κB nuclear translocation analyses. Properdin can be locally synthesized by immune cells in an inflammatory microenvironment, and thus, its interaction with nanoparticles is of considerable importance. In addition, recombinant TSR4+5 coated on the CMC-CNTs inhibited complement consumption by CMC-CNTs, suggesting that nanoparticle decoration with TSR4+5, can be potentially used as a complement inhibitor in a number of pathological contexts arising due to exaggerated complement activation.

Keywords: carbon nanotubes, complement, properdin, thrombospondin repeats, phagocytosis, inflammation, cytokines

INTRODUCTION

Nanoparticles including carbon nanotubes (CNTs) are considered attractive drug delivery platforms. However, their intended destination post-administration and associated cytotoxicity can be significantly altered by the innate immune system, which is likely to interact rapidly with the nanoparticles (1–3). A number of nanoparticles have been shown to activate a potent humoral wing of the innate

immunity called the complement system (4–6). The complement system can influence the pharmacokinetics and biodistribution of the therapeutic nanoparticles since complement proteins are potent opsonins, acting as a bridge between nanoparticles and a range of innate and adaptive immune cells (2, 7). This interaction not only brings about clearance of nanoparticles by phagocytic cells (8) but also influences the inflammatory response (9).

The complement system consists of more than 40 plasma proteins circulating in the blood and tissue fluids, many as inactive zymogens, which upon sequential activation help to defend against infection and mount an immune response (10). Complement activation takes place *via* the classical, lectin, and alternative pathways (**Figure 1A**) (10–13). In the alternative complement pathway, properdin is an upregulator of complement activation.

Properdin interacts with the surface-bound ligands C3b, C3bB, or C3bBb. Once properdin binds both C3b and Bb, the unstable C3 convertase, which has a half-life of about 90 s is strongly stabilized, its half-life increasing by 5- to 10-fold (14). Thus, the intermediates C3bP (where P stands for properdin) and C3bBP generate C3bBbP on the target surfaces (14). This allows the generation of C3b in an amplification loop, resulting in deposition of many copies of C3b on a complement-activating surface. One C3b binds to C3bBb itself, forming C3bBbC3b, homologous to the classical pathway C5 convertase C4b2a3b, thus leading to C5 cleavage and lytic pathway (10).

The C3 activation cascade is downregulated on host cells by membrane-bound regulatory proteins: complement receptor 1 (CR1), membrane cofactor protein (MCP) and decay accelerating factor (DAF), soluble factor H and factor I. Factor H inhibits C3bBb formation by binding to C3b; C3b in the factor H–C3b complex is cleaved by factor I to iC3b. In addition, factor H enhances the decay of convertase activity by displacing Bb from the complex, thus inhibiting the activation of complement alternative pathway (15). CR1, factor H, and DAF bind to C3b and dissociate the Bb fragment, while factor H, CR1 and MCP are cofactors for the factor I-mediated cleavage of C3b to iC3b, thus preventing the amplification of activation of complement on the host cell surface. Complement facilitates the recognition by phagocytic cells of complement-activating particles *via* bound complement components, which are recognized by the receptors CR1, CR2, CR3, CR4, and CRIg. CR1, expressed on macrophages and neutrophils, binds C3b, leading to phagocytosis in the presence of immune mediators such as C5a (10, 16).

Properdin is found at a concentration of 25 μg/mL in plasma (17). Due to this low level, its local production by a variety of stimulated cells, such as neutrophils, endothelial cells, peripheral blood monocytes, dendritic cells, and T cells, may be important in localized activation of the alternative pathway (18). Properdin is made up of identical subunits of 53 kDa associating with each other in a head-to-tail manner (19, 20) to form cyclic polymers (dimers, trimers, and tetramers) dispersed in a ratio of 26:54:20 (21). The human properdin monomer has seven thrombospondin type I repeats (TSR; TSR0–TSR6). A typical TSR is 60 amino acids long and has sequence similarities with thrombospondin, circumsporozoite protein of malaria parasite, and a domain of complement component C9 (22, 23) (**Figure 1B**). TSR4 and TSR5 in properdin play an important role in binding to C3b and in the stabilization of C3 convertase (24–26).

Carbon nanotubes and their functionalized derivatives can activate complement *via* the classical and alternative pathways (4–6). Complement deposition can enhance their uptake by complement receptor-bearing macrophages and B cells, while downregulating the pro-inflammatory response that is otherwise induced by CNTs (8, 9). We have shown previously that C1q, the recognition subcomponent of the classical pathway, and factor H, the downregulator of the alternative pathway, can bind CNTs directly (8). The structural organization of properdin (multisubunit, multiple potential binding domains, and potential multivalency) appears to suggest a possible role as a soluble pattern recognition receptor (PRR). It has been shown that properdin can bind apoptotic T cells *via* sulfated glycosaminoglycan (GAG) and augment phagocytosis by macrophages (27). Furthermore, properdin can also bind to DNA exposed on apoptotic and necrotic cells in a C3b-independent manner (28). Recently, it has been shown that properdin locally produced by DCs and tolerogenic DCs can bind to bind to necrotic cells, confirming previous reports to implicate properdin as an independent recognition molecule. Furthermore, treatment of DCs with siRNA targeting properdin reduced the proliferation of allogenic T cells, and this effect was more pronounced when combined with IFN-γ stimulation. Interestingly, IFN-γ reduced the production of properdin and factor H in both types of DCs (29). This demonstrates that local production of properdin is crucial for the DC and T cell responses. Furthermore, the production of properdin by neutrophils (29, 30) was comparable to DCs, whereas factor H production was very low (29).

Macrophages of properdin-deficient mice have reduced M1 phenotype (IL-1β) and an increased production in the M2 phenotype (arginase-1, MCP-1, and IL-10) associated with tumour-promoting activity. This suggests that the deficiency in properdin can modulate macrophages toward an M2 phenotype, which enhances the tumor environment (31).

Properdin binds to surfaces of several pathogens such as *Neisseria gonorrhoeae* (32), *Salmonella typhimurium* lipopolysaccharide (LPS), *Neisseria meningitidis* lipooligosaccharide (33), and *Chlamydia pneumoniae* (34), which leads to complement activation (15). In addition, recombinant properdin enhanced the opsonization of *N. meningitidis* and *S. pneumonia* by human serum *in vitro* (16). Properdin also binds to Zymosan, *Escherichia coli* (E. coli) strains, live human leukemia T cell lines, and rabbit erythrocytes, suggesting that properdin binding to these surfaces demonstrates its role as a PRR, initiating alternative pathway on target surfaces.

Properdin binds to NKp46 expressed on NK cells and innate lymphoid cell (ILC)1 and ILC3. The control of infection by properdin was dependent on NKp46 and group 1 ILCs. The control of meningococcal infection was not dependent on membrane attack complex, further confirming the pattern recognition role of properdin (35).

Here, we show that properdin acts as a pattern recognition receptor, binds to CNTs, *via* at least domains TSR4+5, and enhances their phagocytosis by macrophages (opsonizes), in addition to promoting a robust pro-inflammatory immune

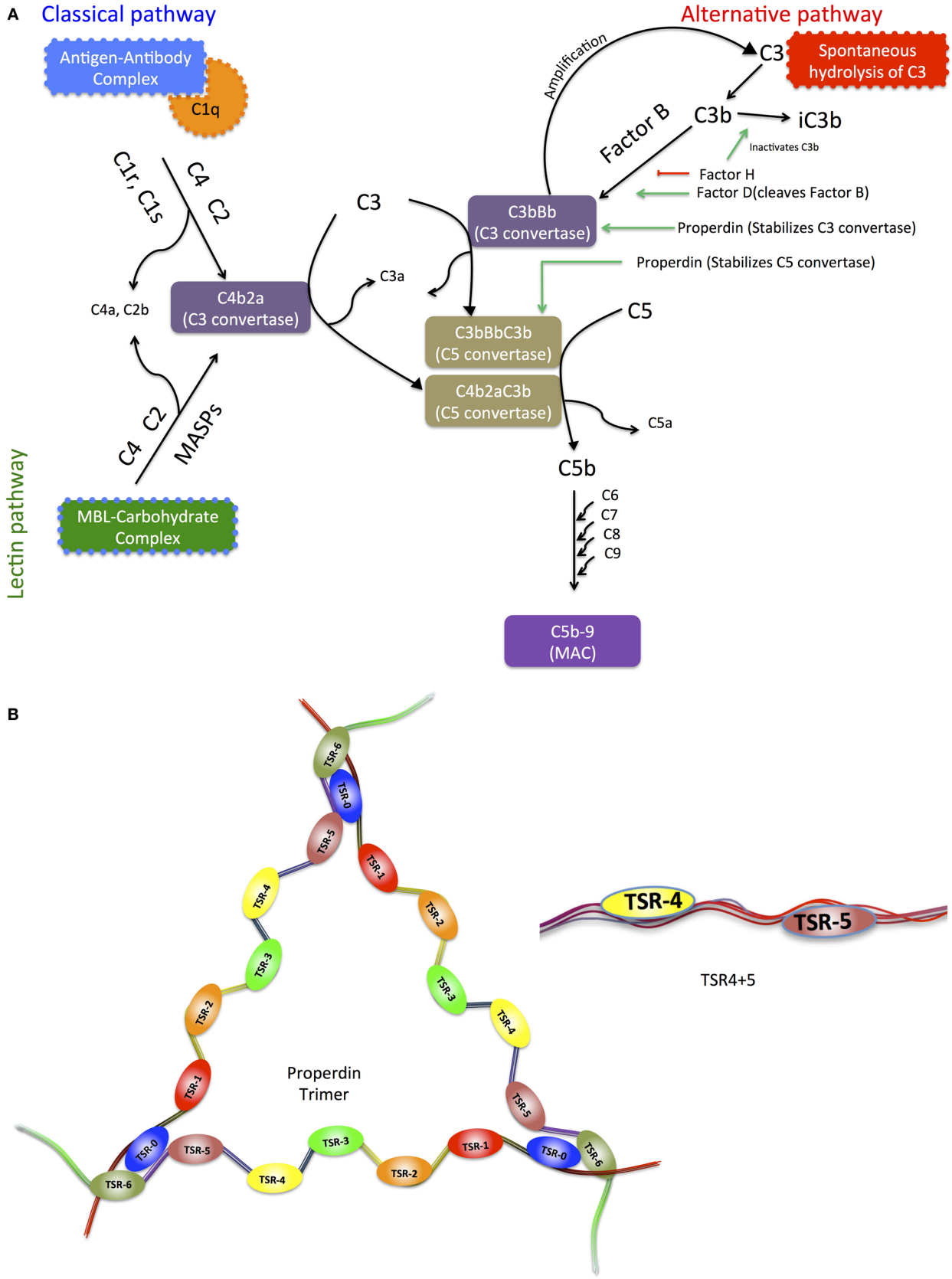

FIGURE 1 | Continued

FIGURE 1 | **(A)** Schematic diagram of the three pathways of the complement system, highlighting the upregulator (properdin) and downregulator (factor H) of the alternative pathway. The three complement systems, the classical, alternative, and lectin pathways merge in C5 convertase. C5 convertase cleaves C5 forming C5b, which combines with C6, C7, C8, and C9 to form the membrane attack complex (MAC). Activation of the classical pathway occurs upon recognition and binding of targets *via* C1q, which in turn activates C1r and C1s, and C1s cleaves C4 and C2. The lectin pathway is activated when mannose-binding lectin (MBL) or ficolins bind to microbial surfaces or other targets, and this binding activates MBL-associated serine proteases (MASPs), similar to C1s, which cleave C4 and C2. Classical and lectin pathway cleaved products of C4 and C2 form C3 convertase (C4bC2a), which cleaves C3 into C3b, the major opsonin of the complement system, binds covalently to targets. C3b also binds to C4b2a, altering its substrate preference to cleave C5 and thus forming C5 convertase C4b2a3b, which cleaves C5 into C5a and C5b. C5b assembles with C6, C7, C8, and C9 to form the MAC, which can cause disruption or lysis of target cells. The alternative pathway C3 convertase C3bBb is a homolog of C4b2a. It is formed by slow hydrolysis of C3 to form C3(H_2O), which is similar to C3b in conformation. C3(H_2O) forms a complex with factor B (FB), and FB in the complex is cleaved to form C3(H_2O)Bb, plus Ba, by factor D (FD). C3(H_2O)Bb itself cleaves C3 to form C3a plus C3b, and C3b then reacts with FB and FD to form C3bBb, in the same way as C3(H_2O)Bb is formed. C3bBb is unstable, but is stabilized by properdin, which holds together the C345C domain in C3b and the vWF domain in Bb, and also repositions the thioester-containing domain in C3b that is involved in the decay process of C3 convertase.
(B) Representative diagram of the modular organization of human properdin including thrombospondin repeats. Properdin is found in serum as monomers, dimers, trimers, and tetramers of a polypeptide made up of seven thrombospondin type I repeat (TSR) domains. It enhances alternative pathway activation by stabilization of C3 and C5 convertases. TSR0 is the *N*-terminal TSR. TSR4 and TSR5 modules expressed in tandem in E. coli have also been depicted.

response. The main C3b-binding domains of properdin, TSR4 and TSR5, when coated together on CNTs, acted as a potent inhibitor of complement alternative pathway activation, raising the possibility of regulating inflammatory response and complement activation on synthetic material surfaces.

MATERIALS AND METHODS

Expression and Purification of Recombinant Human Properdin in Human Embryonic Kidney (HEK) Cells

Full-length human properdin gene was subcloned as an EcoRI-XbaI cassette into pSecTag-C (Life Technologies), using terminal primers 5′-GAATTCGACCCCGTGCTCTGCTTCAC-3′ and 5′-TCTAGAGAGTTCCTCTTCC TCAGGGTCTTTG-3′, yielding the construct pLK-FL. The cDNA clone of human properdin was used as a template in the PCR reaction that was originally isolated from U937 cells stimulated by PMA and subcloned in the pBluescript vector (19, 24). HEK cells were plated in 24-well plates at a concentration of 0.5–1.25 × 10^5 cells per well in 0.5 mL of complete DMEM-F12 medium [10% v/v fetal calf serum (FCS), 2 mM L-glutamine, 100 U/mL penicillin, and 100 µg/mL streptomycin] and left at 37°C, 5% CO_2 in humidified atmosphere. Once the cells reached about 80% confluence, the growth medium was replaced with fresh 0.5 mL/well of complete DMEM-F12 medium. Up to 5 µg of pLK-FL DNA in 100 µL of Opti-MEM® I Medium (Gibco) without serum was added to each well for transfection. Up to 1.75 µL of Lipofectamine LTX® Reagent (Invitrogen) was added into the above-diluted Opti-MEM®-DNA solution, mixed gently, and incubated for 30 min at room temperature to form DNA-Lipofectamine LTX® Reagent complexes, 100 µL of which was added directly to each well containing HEK cells, swirled gently, and incubated at 37°C in CO_2 incubator for up to 24 h before examining for protein expression and secretion. Supernatant was collected and tested for the presence of properdin by direct ELISA.

Recombinant full-length properdin was purified by passing the supernatant through an antiproperdin IgG (monoclonal) affinity column, kindly provided by Dr. C. Koch, State Serum Institute, Copenhagen, Denmark. The column (anti-Properdin-Sepharose) was washed with three bed volumes of HEPES buffer (10 mM HEPES, 140 mM NaCl, 0.5 mM EDTA, pH 7.4). Bound properdin was eluted in 1 mL fractions using 3 M $MgCl_2$. The peak fractions were dialyzed against HEPES buffer overnight at 4°C. Minor contaminants were further removed by applying the dialyzate on to a DEAE Sepharose ion exchange column (GE Healthcare), which was first equilibrated with three bed volumes of Tris buffer (50 mM Tris–HCl, pH 7.5, 50 mM NaCl, 5 mM EDTA). Properdin did not bind to the DEAE Sepharose and was recovered in the flow-through, whereas other contaminants remained bound to the resin. SDS-PAGE analysis was carried out to confirm the purity of recombinant properdin.

Expression and Purification of Recombinant Human TSR4+5 Modules in Tandem, Fused to Maltose-Binding Protein *in E. coli*

Recombinant human TSR4+5 fused with maltose-binding protein (MBP) was expressed using *E. coli* BL21 strain (Life Technologies) (26). Overnight primary bacterial cultures were grown in Luria-Bertani medium with 100 µg/mL ampicillin with shaking (200 rpm) at 37°C until an A_{600} of 0.6–0.8 was reached. Expression was then induced with 0.4 mM isopropyl β-D-thiogalactoside (Sigma) and continued for 3 h at 37°C. The cell pellet, recovered after centrifugation at 4,500 rpm for 10 min, was resuspended in lysis buffer (20 mM Tris–HCl, pH 8.0, 0.5 M NaCl, 1 mM EDTA, 0.25% v/v Tween 20, 5% v/v glycerol) containing 100 µg/mL lysozyme (Sigma) and 0.1 mM phenylmethanesulfonyl fluoride (Sigma) and incubated for 1 h at 4°C on a rotary shaker. The lysate was then sonicated (using a Soniprep 150; MSE, London, UK) at 60 Hz for 30 s with an interval of 2 min on ice (12 cycles). The sonicate was centrifuged at 10,000 *g* for 15 min at 4°C. The supernatant was collected and diluted 5-fold with buffer I (20 mM Tris–HCl, pH 8.0, 100 mM NaCl, 1 mM EDTA, 0.25% v/v Tween 20) and passed through an amylose resin column (New England Biolabs), previously equilibrated in buffer I. The affinity column was washed with buffer I without Tween 20 and with 1 M NaCl, followed by buffer II (20 mM Tris–HCl, pH 8.0, 100 mM NaCl, 1 mM EDTA). The TSR4+5 fusion protein was then eluted with buffer II containing 10 mM maltose (Sigma). Minor contaminants were further removed by applying the fusion protein to a Q-Sepharose column (Sigma) equilibrated with three column volumes of low-salt buffer (50 mM Tris–HCl, pH 7.5, 100 mM NaCl, 5 mM EDTA, pH 7.5). After extensive washing with low-salt

buffer, the fusion protein was step eluted with 200 mM NaCl. The peak fractions were then passed through Pierce™ High Capacity Endotoxin Removal Resin to remove LPS. Endotoxin levels in the purified protein samples were analyzed using the QCL-1000 Limulus amebocyte lysate system (Lonza). The assay was linear over a range of 0.1–1.0 EU/mL (10 EU = 1 ng of endotoxin), and the endotoxin levels were <5 pg/μg of the recombinant proteins. MBP protein used as a control was expressed in *E. coli* using pMal-c vector (New England Biolab) and purified, as described above for MBP-TSR4+5.

Preparation and Transmission Electron Microscopy (TEM) of Carboxymethyl Cellulose-Coated Carbon Nanotubes (CMC-CNTs)

The synthesis and characterization of double-walled carbon nanotubes (DWNTs) has been described earlier (36, 37). After catalyst elimination by non-oxidizing HCl treatment, the DWNTs were washed with deionized water. For functionalization, wet DWNTs (corresponding to a dry amount of 100 mg) were added to a solution of 100 mg of carboxymethyl cellulose (CMC; Sigma 21901) in PBS. After mixing, the suspension was freeze dried to obtain a 50:50 homogeneous dry mixture of DWNTs and CMC. The samples were resuspended in PBS + 5 mM EDTA pH 7.4, and then centrifuged at 8,000 *g* for 5 min for the removal of aggregates. After centrifugation, the non-sedimented CNTs were washed to remove excess CMC by vacuum filtration using 0.2 μm Whatman polycarbonate filter with PBS-EDTA, pH 7.4. Functionalized CNTs (CMC-CNTs) were then resuspended in PBS-EDTA. For oxidized DWNTs, 100 mg of DWNTs were added to 100 mL of HNO_3 (3 M) and placed in ultrasonic bath for 30 min and refluxed at 130°C for 24 h. The solution was left to cool at room temperature. The solution was washed and filtered on a polypropylene membrane (0.45 μm). For electron microscopy, 2 μL of well-dispersed CMC-CNTs were adsorbed onto carbon-coated grids. Micrographs were recorded using a JEOL 2100 FEG-TEM operating at 80 Kv, and the images were processed using Gatan microscopy suite software (Gatan, Inc.). Surface visualization of CMC-CNTs was performed using a Zeiss Supra 35vP scanning electron microscope operating at 5 kev.

Coating of CMC-CNTs and Ox-CNTs with Properdin and TSR4+5

Purified properdin, TSR4+5, MBP, or BSA (Bovine serum albumin) were incubated in a w/w ratio of 2:1 with 100 μg of CMC-CNTs or Ox-CNTs in the affinity buffer (50 mM Tris–HCl, pH 7.5, 150 mM NaCl, 5 mM $CaCl_2$), overnight at 4°C. Excess protein was removed by repeated centrifugation and washing at 17,000 *g* for 10 min to wash away any unbound proteins trapped within the CNTs. CNTs were redispersed in affinity buffer between centrifugations.

Western Blotting to Detect Protein Binding to CNTs

Carbon nanotubes with bound protein were run on SDS-PAGE under reduced conditions, and protein bands were transferred on to a nitrocellulose membrane in transfer buffer (25 mM Tris, 192 mM glycine, 20% v/v methanol, pH 8.3) at 320 mA for 2 h. The membrane was then blocked with 5% semi-skimmed milk powder (Tesco, UK) in PBS, pH 7.4 (Sigma) overnight at 4°C. Rabbit anti-human properdin (0.92 mg IgG/mL) polyclonal antibodies were diluted 1:500 in PBS and incubated with the membrane for 2 h at room temperature. The membrane was washed three times, 10 min each, with PBS + 0.05% Tween 20 (PBST). Protein A–horseradish peroxidase (1:1,000; Thermo Scientific) in PBS was added and left at room temperature for 1 h. The blot was washed again with PBST three times, and the color was developed using 3,3′-diaminobenzidine (DAB) (Sigma-Aldrich).

Complement Consumption Assays

To measure complement consumption in human serum *via* the alternative pathway, properdin, TSR4+5, or MBP were precoated on CMC-CNTs in 1:1 w/w ratio in affinity buffer overnight at 4°C, followed by washing, as described above to remove unbound protein. Protein-coated CMC-CNTs and zymosan (positive control) were incubated with human serum (1/5 dilution) in DGVB-Mg-EGTA buffer (2.5 mM sodium barbital, 71 mM NaCl, 7 mM $MgCl_2$, 10 mM EGTA, 2.5% w/v glucose, 0.1% gelatin, pH 7.4) for 1 h at 37°C. Serum diluted 1/5 and incubated with no additions was the negative control. After incubation, CNTs were removed by centrifugation at 17,000 *g* for 10 min, and the ability of the supernatant to lyse rabbit erythrocytes (TCS Biosciences) was tested. Rabbit erythrocytes were washed by repeated centrifugation for 10 min, 700 g in PBS + 5 mM EDTA, pH 7.4 until the supernatant was clear. The cell concentration was adjusted to 1×10^9/mL in DGVB-Mg-EGTA. Then, 100 μL of these rabbit erythrocytes was added to 100 μL of serum supernatant samples or to undiluted normal human serum and incubated for 1 h at 37°C. After incubation, cells were centrifuged (700 *g*, 10 min) and released hemoglobin in the supernatant was measured at 541 nm. Total hemolysis (100%) was measured by lysing rabbit erythrocytes with undiluted normal human serum. Background spontaneous hemolysis was determined by incubating rabbit erythrocytes with DGVB-Mg-EGTA buffer. Percentage complement consumption was calculated using $(C - \mathrm{Ci})/C \times 100\%$, where C represents the % hemolysis of the negative control, and Ci is the % hemolysis with the CMC-CNT- or zymosan-treated sample.

To check whether the CMC-CNTs with bound properdin retained capacity to activate the complement alternative pathway, we used properdin-deficient serum obtained from the properdin gene-deficient mice (38). Genotyped mice were bled under terminal anesthesia. Blood was spun, and serum was transferred to a tube and stored at −20°. Properdin-coated CMC-CNTs (Properdin-CNT), TSR-coated CMC-CNTs (TSR4+5-CNT), and CMC-CNT alone were incubated with properdin-deficient serum (1/2 dilution) in DGVB-Mg-EGTA buffer and incubated for 1 h at 37°C. After incubation, CNTs were removed by centrifugation at 17,000 *g* for 10 min, and serum was collected. To each of the collected sera, purified properdin (1 μg/mL) was added, and the reconstituted sera were tested for the lysis of rabbit erythrocytes, as described above.

Biotinylation of CMC-CNTs

Carboxymethyl cellulose-coated carbon nanotubes were biotinylated as follows: 1 mg of CMC-CNTs was suspended in 1 mL 0.1 M MES buffer [2-(*N*-morpholino) ethanesulfonic acid, pH 5]. 1 mg of pentylamine biotin (Pierce, Thermo Fisher Scientific) in the presence of 4 µg EDC [1-Ethyl-3-(3-dimethylaminopropyl) carbodiimide] was added to the CMC-CNT suspension and stirred for 2 h at room temperature. The reaction was stopped by adding 50 µL of 0.1 M ethanolamine (Sigma). The resulting biotin-CMC-CNTs were dialyzed extensively against PBS (pH 7.4) to remove remaining reactants and MES.

Uptake of CMC-CNT into THP-1 Cells, Observed by Fluorescence Microscopy

Uptake of biotinylated CMC-CNTs, coated with properdin or MBP-TSR4+5, was examined using differentiated THP-1 macrophages. For fluorescence microscopy, 1×10^5 THP-1 cells were plated on 13-mm coverslips and treated for 24 h with 100 nM Phorbol myristate acetate (PMA; Sigma) in complete RPMI 1640 containing 10% v/v FCS, 2 mM L-glutamine, 100 U/mL penicillin, 100 µg/mL streptomycin, and 1 mM sodium pyruvate. Differentiated THP-1 cells were washed three times with PBS to remove excess PMA and then rested for 24 h in complete RPMI 1640 as above prior to exposure to the CNTs. Cells were washed three times with PBS and were exposed to 4 µg/mL biotinylated CMC-CNT coated with properdin (Properdin-CNTs), MBP-TSR4+5 (TSR4+5-CNT), or biotin-CMC-CNTs alone in 500 µL of serum-free RPMI 1640 medium for 2 h. Cells were washed twice with PBS, fixed with 4% paraformaldehyde for 10 min, washed, and processed for fluorescence microscopy. The cells on coverslips were permeabilized using permeabilizing buffer (20 mM HEPES, pH 7.4, 300 mM sucrose, 50 mM sodium chloride, 3 mM $MgCl_2$, 0.5% Triton X-100) for 5 min on ice. The cells were then stained for 30 min with 1.6 µM Hoechst 33342 (Life Technology), 2 µg/mL Alexa-Fluor546-conjugated wheat germ agglutinin (Invitrogen) and Alexa fluor 488-conjugated streptavidin (Thermo Scientific) to reveal biotinylated CMC-CNTs. Cells were washed twice, mounted using Citifluor anti-fade (Citifluor, UK), and observed under a Nikon Eclipse TE2000-S confocal microscope with 62 X oil lens.

To observe nuclear translocation of NF-κB, permeabilized cells were incubated with rabbit anti-NF-κB p65 polyclonal antibodies (Santa Cruz Biotech), followed by secondary Alexa Fluor 488-goat anti rabbit antibody, and observed with Leica Fluorescent microscope using LAS software (Leica Microsystems).

For quantification, 5×10^5 THP-1 cells were plated in 12-well plates and differentiated with PMA for 24 h and rested for 24 h in complete RPMI media. Cells were washed with PBS and exposed with 4 µg/mL biotinylated CMC-CNT coated with properdin (Properdin-CNTs), MBP-TSR4+5 (TSR4+5-CNT), or biotin-CMC-CNTs alone in 500 µL of serum-free RPMI 1640 medium for 2 h. Cells were washed three times with PBS and lysed with lysis buffer (10 mM HEPES, 20 mM NaCl, 0.5 mM EDTA, 1% v/v Triton X 100). An ELISA type assay was employed to quantify the amount of CNTs taken up by THP-1 cells (6). Microtiter wells (NUNC, polysorb) were coated with 100 µL Avidin (Pierce) at 50 µg/mL in 0.1 M carbonate bicarbonate buffer, pH 9 (Sigma) for 1 h at RT, followed by blocking with 0.05% of BSA for 1 h at RT. 50 µL of a solution or cell lysate containing biotin-CMC-CNTs and 50 µL of 0.05% BSA were added in each well and incubated for 1 h at RT. The plate was washed with PBS to remove unbound CNTs, and then incubated with 1:2,000 dilution of Streptavidin-HRP (Sigma) for 1 h at RT. Following washing again, O-phenylenediamine dihydrochloride (Sigma) was used as a substrate for the HRP, and the yellow 2, 3-diaminophenazine product was read at 450 nm.

Measurement of THP-1 Cell Cytokine and Transcription Factor mRNA Expression Using Quantitative RT-PCR

In a 12-well cell culture plate (Nunc), THP-1 cells (1×10^6/well) were differentiated with 100 nM PMA in RPMI 1640 complete medium for 24 h and then rested (without PMA) for 24 h. Cells were washed three times with PBS prior to the addition of 10 µg/mL of properdin-CMC-CNT, MBP-TSR4+5-CMC-CNT, or CMC-CNT alone to wells in serum-free RPMI 1640 medium and incubated for 30, 60, 120, or 360 min. Cells at each time point were washed with PBS and lysed within the wells using lysis buffer from GenElute Mammalian Total RNA Purification Kit (Sigma-Aldrich). Total RNA was extracted from the lysate using the GenElute Mammalian Total RNA Purification Kit (Sigma-Aldrich). To inactivate both DNase I and RNase, samples were heated at 70°C for 10 min and subsequently chilled on ice. A NanoDrop 2000/2000c spectrophotometer (Thermo-Fisher Scientific) was used to determine the amount and purity (260/280 nm ratio) of RNA. The cDNA was synthesized using High Capacity RNA to cDNA Kit (Applied Biosystems). Primers (**Table 1**) were designed using Primer-BLAST.[1]

The qPCR reaction mixture included 5 µL Power SYBR Green MasterMix (Applied Biosystems), 75 nM forward and reverse primers and 500 ng template cDNA in a 10 µL reaction volume. PCR was performed using a Step One Plus Real-Time PCR System (Applied Biosystems). Human 18S rRNA target was used as an endogenous control. Data were analyzed using the Step One software v2.3 (Applied Biosystems). Ct (cycle threshold) values for each cytokine target gene were calculated. Relative expression of each cytokine target gene was calculated using the relative

[1] http://blast.ncbi.nlm.nih.gov/Blast.cgi.

TABLE 1 | Terminal primers used for qPCR analysis.

Targets	Forward primer	Reverse primer
18S	ATGGCCGTTCTTAGTTGGTG	CGCTGAGCCAGTCAGTGTAG
IL-1β	GGACAAGCTGAGGAAGATGC	TCGTTATCCCATGTGTCGAA
IL-6	GAAAGCAGCAAAGAGGCACT	TTTCACCAGGCAAGTCTCCT
IL-10	TTACCTGGAGGAGGTGATGC	GGCCTTGCTCTTGTTTTCAC
IL-12	AACTTGCAGCTGAAGCCATT	GACCTGAACGCAGAATGTCA
TGF-β	GTACCTGAACCCGTGTTGCT	GTATCGCCAGGAATTGTTGC
TNF-α	AGCCCATGTTGTAGCAAACC	TGAGGTACAGGCCCTCTGAT
NF-κB	GTATTTCAACCACAGATGGCACT	AACCTTTGCTGGTCCCACAT
NLRP3	GCCATTCCCTGACCAGACTC	GCAGGTAAAGGTGCGTGAGA

quantification (RQ) value, using the equation $RQ = 2^{-\Delta\Delta Ct}$ for each cytokine target gene and comparing relative expression with that of the 18S rRNA constitutive gene product. Assays were conducted in triplicate.

Multiplex Cytokine Array Analysis

Supernatant from THP-1 cells, incubated with non-biotinylated CMC-CNT, properdin-CMC-CNT, and MBP-TSR4+5-CMC-CNT for 24 and 48 h, were collected for measuring secreted cytokines, chemokines, growth factors, and other ligands and receptors. The analytes were measured using MagPix Milliplex kit (EMD Millipore) following the manufacturer's protocol. 25 µL of assay buffer was added to each well of a 96-well plate, followed by addition of 25 µL of standard, control, or supernatant of THP-1 cells. 70 µL of a mixture of 36 individual capture magnetic beads was added to 3.5 mL of diluent buffer, vortexed, and 25 µL of the magnetic beads coupled to analytes were added to each well containing assay buffer, samples, and controls and incubated for 18 h at 4°C. The plate was washed with assay buffer, and 25 µL of detection antibodies (EMD Millipore) were incubated with the beads for 1 h at room temperature. 25 µL of streptavidin–phycoerythrin was then added to each well and incubated for 30 min at room temperature. Following the washing step, 150 µL of sheath fluid was added to each well, and the plate was read using the Luminex Magpix instrument. Assays were carried out in duplicate.

Statistical Analysis

Statistical analysis was conducted using GraphPad Prism version 7.0 (GraphPad Software). An unpaired two-sided *t*-test and multiple *t*-test using Holm–Sidak method was used on the data for any significant difference between uncoated and protein coated CNTs. *P* values were computed and graphs compiled and analyzed.

RESULTS

Recombinant Full-Length Properdin and MBP-TSR4+5 Bind CMC-CNTs

Functionalized DWNTs were well dispersed in aqueous solution. High-resolution TEM images of pristine DWCNTs (**Figure 2A**) and CMC-coated DWCNTs (**Figure 2B**) revealed the places where the CMC coating on the nanotubes was easily visible. In general, following CMC coating, the image seems blurred and shows much less details.

We analyzed the binding of purified properdin as well as TSR4+5 modules (**Figure 3A**) to CNTs after preincubation of the proteins with CMC-CNTs followed by washing with PBS extensively *via* centrifugation. Western blot analysis revealed that properdin and MBP-TSR4+5 bound CMC-CNTs and appeared in the 12% SDS-PAGE at their expected molecular weight at ~55kDa (**Figure 3B**). CNTs remained in the loading wells. Furthermore, properdin and TSR4+5 also bound to Ox-CNTs efficiently (data not shown). This suggested that the properdin and TSR4+5 interaction with CNTs is likely to be through charge pattern/polarity recognition of the CNT surface and not due to CMC.

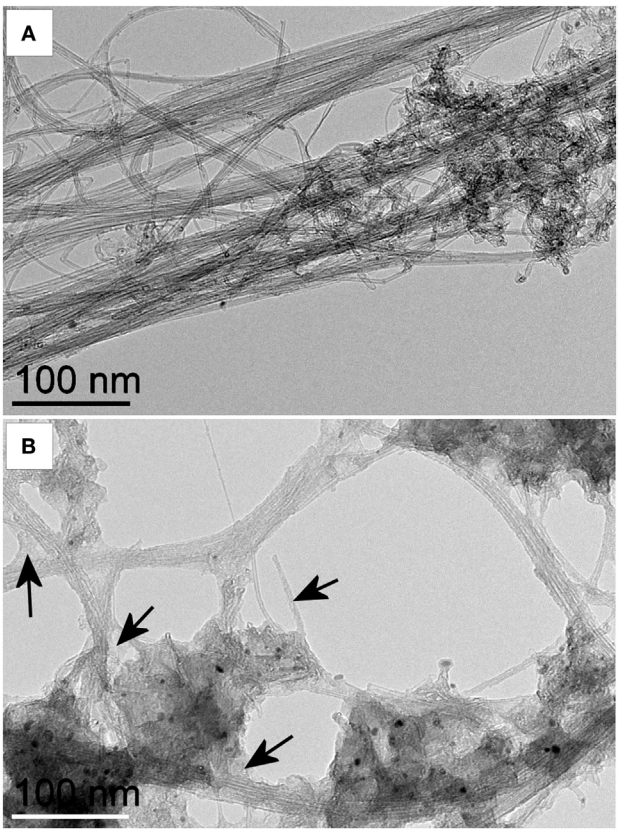

FIGURE 2 | Transmission electron microscopy (TEM) images of pristine and carboxymethyl cellulose-coated carbon nanotubes (CMC-CNTs). High-resolution TEM image of **(A)** pristine DWCNTs and **(B)** CMC-coated DWCNTs. Images were acquired at the same magnification. Black arrows indicate examples of places where the carboxymethyl cellulose (CMC) coating on the nanotubes is easily visible. In general, after CMC coating, the image seems blurred and shows much less details. Double-walled carbon nanotubes were coated with CMC and dispersed in water. Suspended CMC-CNTs were adsorbed on a carbon grid. The images were recorded with a Jeol 2100 transmission electron microscope operating at 80 kV. Scale bar is 100 nm.

MBP-TSR4+5 Coated on CMC-CNTs Inhibited Complement Consumption *via* the Alternative Pathway

Properdin-coated and MBP-TSR4+5-coated CMC-CNTs were assessed for their ability to activate the complement alternative pathway (**Figure 4A**) compared with uncoated CMC-CNTs. Zymosan was used as a positive control that consumed complement. Properdin coating of CMC-CNT did not interfere with the alternative pathway activation; it allowed complement consumption by the CNTs to the same extent as CMC-CNT alone. MBP also did not diminish consumption. However, TSR4+5-coated CMC-CNTs showed ~60% less complement consumption, suggesting that the CNT-surface bound TSR4+5 acted as an inhibitor of the complement alternative pathway, similar to its inhibitory properties in solution (26). These results suggest that properdin is likely to bind to CNTs *via* TSR4+5 and that precoated TSR4+5 can inhibit the binding of properdin (from the serum), and thereby

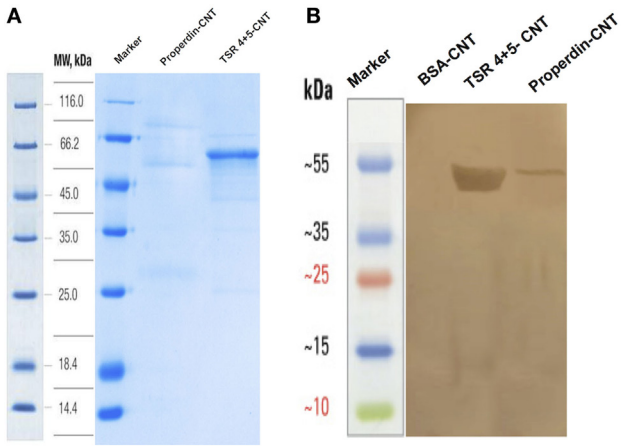

FIGURE 3 | Carboxymethyl cellulose-coated carbon nanotubes (CMC-CNTs) stably bind to purified human properdin and recombinant TSR4+5, as shown *via* SDS-PAGE **(A)** and western blot **(B)**. **(A)** CMC-CNTs were incubated with recombinant human properdin, or thrombospondin type I repeat (TSR) 4 + 5-MBP fusion protein and BSA overnight in the affinity buffer. Carbon nanotubes (CNTs) were washed extensively *via* centrifugation and run on an SDS-PAGE (12%) under reduced conditions. Properdin migrated at ~55 kDa and MBP-TSR4+5 migrated as a single band at ~53 kDa. **(B)** In parallel, the SDS-PAGE was transferred onto nitrocellulose membrane for 2 h at 320 mA. The blot was probed with anti-human properdin (polyclonal) antibodies, followed by protein A–HRP conjugate and developed using 3,3′-diaminobenzidine.

diminish alternative pathway activation. Properdin-coated CMC-CNTs also consumed complement (activated complement) *via* the alternative pathway (**Figure 4B**) when properdin-deficient serum was used. Complement consumption was increased by ~60% compared to uncoated CMC-CNTs. TSR4+5-coated CNTs were not significantly different in consumption from uncoated. This suggested that the CNT-bound properdin still retained its activity of promoting alternative pathway activation.

Figure 4 suggests that properdin binding is a dominant factor in alternative pathway activation by CMC-CNT. In **Figure 4A** (using normal human serum), it is shown that CMC-CNT, P-CMC-CNT, and MBP-CMC-CNT all consume about 60% of the (alternative pathway) complement activity in the serum, whereas TSR4+5-CMC-CNT consume only about 15%. In **Figure 4B** (properdin-deficient mouse serum), only P-CMC-CNT allow extensive consumption: CMC-CNT and TSR4+5 CMC-CNT show much lower consumption. Therefore, properdin (on the P-CMC-CNT) has a very large effect.

Properdin, but Not TSR4+5, Enhanced CMC-CNT Uptake by THP-1 Cells

Although properdin and TSR4+5 bound to nanoparticles, only full-length properdin, and not TSR4+5, was able to enhance uptake of CNTs by differentiated THP-1 cells at 2 h (**Figure 5**) in the absence of added complement (serum). Previous studies have reported an enhanced phagocytosis of nanoparticles in a complement-dependent and complement-independent manner. Precoating with C1q enhanced uptake of CNTs by U937 monocytic cells and human monocytes, whereas factor H, a negative regulator of the complement system, did not (8). As shown in **Figure 5**, Alexa Fluor 488-conjugated streptavidin-labeled biotin-CMC-CNT (green) did not show a significant level of uptake at 2 h. Properdin-CMC-CNT showed considerably enhanced uptake by THP-1 cells, compared to CMC-CNT alone and TSR4+5-CMC-CNT. The CMC-CNTs (green) were observed within the cell membrane stained with Alexa Fluor 546-conjugated wheat germ agglutinin (red) and the nucleus (Hoechst, blue). The qualitative confocal sections (right panel) with higher magnification revealed properdin-CMC-CNT within the cell; however, very few CMC-CNTs could be seen intracellularly in the case of TSR4+5-CMC-CNT (**Figure 5**), suggesting that an intact properdin molecule is required for this function as an "opsonin." This also indicates that interaction of properdin with macrophage may not be limited to TSR4+5 only, and other TSR modules may be involved.

Pro-inflammatory Cytokines Are Upregulated by Properdin-Coated CMC-CNTs, as Revealed by qPCR Analysis

Having found properdin acting as an opsonin for CNTs, we next examined the pro- and anti-inflammatory cytokine response by THP-1 cells *via* qPCR analysis. TNF-α, IL-1β, IL-6, and IL-12 mRNA expression were significantly upregulated at 6 h by properdin-CMC-CNT and TSR4+5, and CMC-CNTs from 30 min onward (**Figure 6A**). In contrast, IL-10 and TGF-β were initially upregulated at 30 min, but decreased by 6 h, suggesting that the anti-inflammatory response was dampened (**Figure 6B**). Consistent with the upregulation of TNF-α, NF-κB was also upregulated by 6 h, when CMC-CNTs were coated with properdin or TSR4+5. However, the NLRP3 mRNA expression was not significant, suggesting that the activation of NLRP3 inflammasome was weak.

Multiplex Array Analysis Revealed Dramatic Upregulation of Pro-inflammatory Cytokines/Chemokines by THP-1 Cells When Challenged with CMC-CNTs Coated with Properdin or TSR4+5

Multiplex array analysis using supernatants that were collected at 24 and 48 h time points from the phagocytosis assay revealed a dramatic increase in the levels of pro-inflammatory cytokines (IL-6, IL-12p40, IL-12p70, IL-1α, IL-1β, TNF-α, IL-13, IL-15, and IL-9) for properdin-CMC-CNT or TSR4+5-CMC-CNT. Properdin and TSR4+5-coated CMC-CNTs also enhanced chemoattractants such as IL-8, I-TAC, MIG, and MCP-1 (**Figure 7**). A number of anti-inflammatory cytokines, chemokines, growth factors, and immune ligands were also differentially upregulated by protein-coated CNTs (**Figure 7**).

Properdin or TSR4+5-Coated CMC-CNTs Induced Nuclear Translocation of NF-κB in THP-1 Cells

THP-1 cells were used to assess the translocation of NF-κB following challenge with Properdin-CMC-CNT or TSR4+5-CMC-CNT, using fluorescent staining. The transcription factor, NF-κB, regulates the signaling pathway of many pro-inflammatory

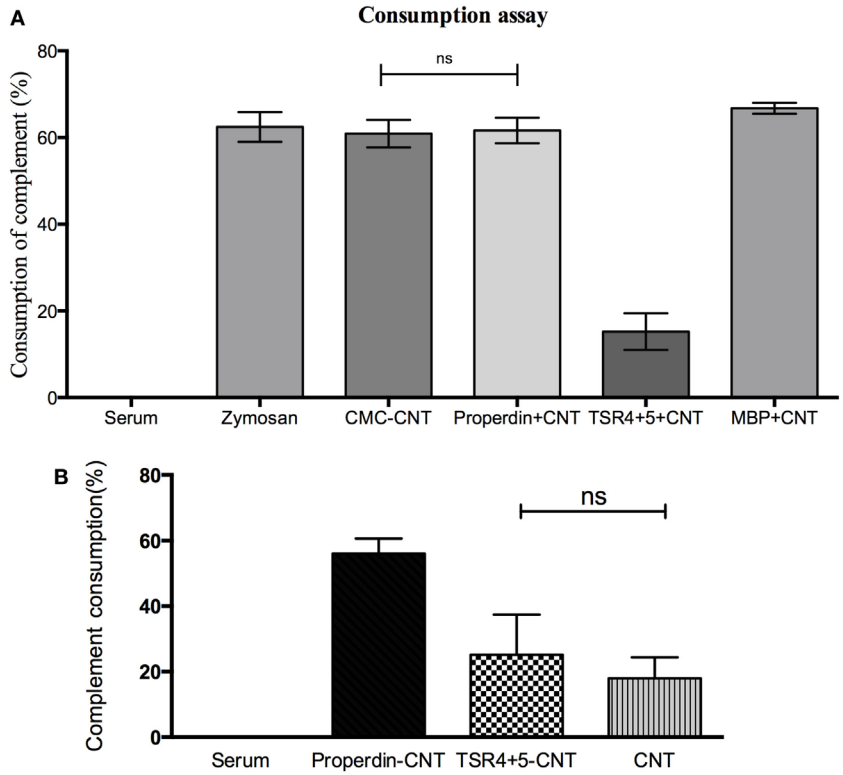

FIGURE 4 | **(A)** Carboxymethyl cellulose-coated carbon nanotube (CMC-CNT) bound properdin activates the alternative pathway, while thrombospondin type I repeat (TSR)4 + 5-coated carbon nanotubes (CNTs) fail to consume complement: Properdin, TSR4+5, or maltose-binding protein (MBP)-coated CMC-CNTs were incubated with human serum (1/5 dilution in DGVB-Mg-EGTA buffer) for 1 h at 37°C. Samples were spun down, and serum was collected for consumption assay. Zymosan without CNTs was used as a positive control, and serum alone without CNTs was used as a negative control (zero consumption). **(B)** Only properdin-coated CNTs allow complement consumption in the presence of properdin-deficient serum derived from properdin gene knockout mice. Protein-coated CMC-CNTs were incubated with properdin-deficient serum diluted (1:2) with DGVB-Mg-EGTA buffer for 1 h at 37°C. The samples were centrifuged and properdin-deficient serum supernatant was collected. Properdin was added to the serum to give a final concentration of 1 μg/mL. Serum with reconstituted properdin was assayed for complement consumption. The experiments were repeated three times; error bars represent ± SD. A two-tailed, unpaired *t*-test was performed on the data to determine significant differences in complement consumption of properdin coated CNTs and TSR4+5-coated CNTs with CNTs only. All these comparisons were significant ($P < 0.05$), except where shown [not significant (ns), $P > 0.05$].

cytokines when exposed to external stimuli. Properdin-CMC-CNT or TSR4+5-CMC-CNT incubated with THP-1 cells at 2 h were fluorescently stained with an antibody against the p65 subunit of NF-κB (green) (**Figure 8**). The merged image shows induction of translocation of NF-κB to the nucleus (blue), which is significantly enhanced by properdin-CMC-CNT and TSR4+5-CMC-CNT, compared to CMC-CNT alone (**Figure 8**). Properdin and TSR4+5-coated CMC-CNTs also induced an upregulation of NF-κB mRNA levels at 360 min by THP-1 cells (**Figure 6B**). This is consistent with the nuclear localization of NF-κB (**Figure 7**). This reflects on the upregulation of the pro-inflammatory response by TNF-α, IL-1β, IL-2, and IL-6 (**Figures 6** and **7**).

DISCUSSION

Previous reports have established an important role for the classical pathway in the recognition and phagocytic clearance of functionally derivatized CNTs (6, 8). CNTs, pristine and derivatized, appeared to offer a molecular charge pattern for C1q to bind and activate the classical pathway. On its own, C1q appeared to bind CNTs *via* its globular head (gC1q) domain, enhanced uptake of CNTs by macrophages, and upregulated the pro-inflammatory immune response (8). Although complement factor H also bound to derivatized CNTs, it did not enhance uptake while exerting an anti-inflammatory effect. CNTs, coated with recombinant forms of globular head modules corresponding to the *C*-terminal ends of the A, B, and C chains of C1q [ghA, ghB, and ghC, respectively (39)], were able to inhibit classical pathway activation *via* the nanoparticle surface. In addition, they also enhanced uptake of CNTs leading to considerable downregulation of a pro-inflammatory response. Thus, nanoparticles precoated with recombinant globular heads have been proposed to be a good strategy to avoid quick clearance of nanotherapeutics by phagocytes due to complement deposition with concomitant suppression of pro-inflammatory cytokine/chemokine response (8). Here, we have examined whether properdin can interact with nanoparticles, thus potentially acting as a pattern recognition innate immune molecule, similar to C1q and factor H, and modulate CNT handling by macrophages.

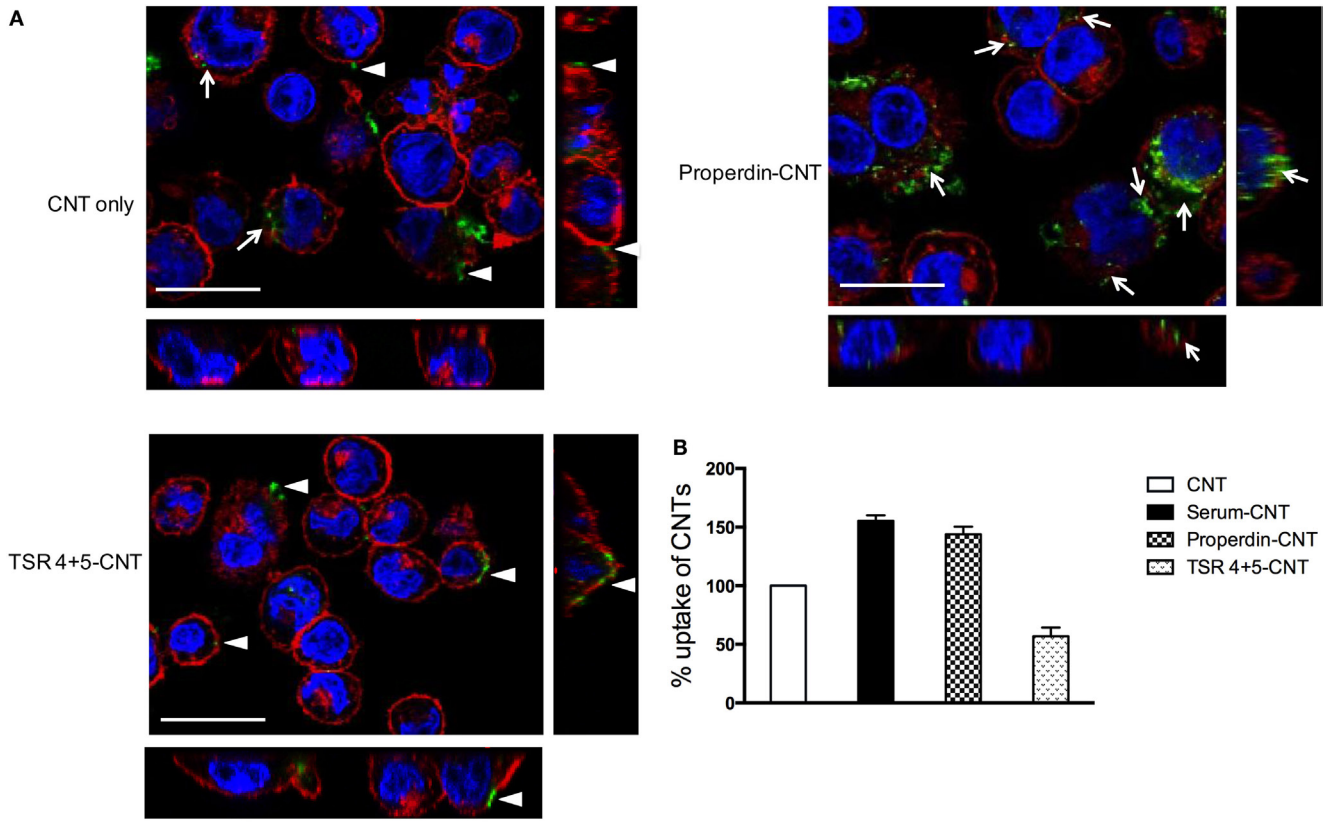

FIGURE 5 | **(A)** Properdin-coated carboxymethyl cellulose-coated carbon nanotube (CMC-CNT) show enhanced uptake by THP-1 cells. To observe internalization of carbon nanotubes (CNTs), PMA-differentiated THP-1 cells were treated with properdin or MBP-TSR4+5-coated biotinylated CMC-CNTs and uncoated biotinylated CMC-CNTs for 2 h. Cells were washed, fixed, permeabilized, and stained with Alexafluor-488-labeled Streptavidin (green) to reveal internalized biotin-CMC-CNTs (arrows). Alexafluor546-conjugated wheat germ agglutinin was used to reveal plasma membrane (red), and the nucleus was stained with Hoechst 33342 (Blue). Images shown are single sections (including side images) taken with a Nikon confocal microscope; scale bar, 20 μm arrow heads point to the CNTs adhering to the plasma membrane. **(B)** TSR4+5-coated CNTs show reduced uptake by THP-1 cells. To quantify the amount of uptake of protein coated or uncoated CMC-CNTs, THP-1 cells were incubated with 4 μg/mL of protein-coated biotin CMC-CNTs or uncoated CMC-CNTs for 2 h. The cells were lysed, and the amount of CNTs was quantified by an ELISA type assay. All experiments were done in triplicate; error bars represent mean ± SEM. A two-tailed, unpaired *t*-test was performed on the data to determine significant differences in uptake of CNTs between properdin-coated CNTs and TSR4+5-coated CNTs with CNTs only. All these comparisons were significant ($P < 0.05$), except where shown [not significant (ns), $P > 0.05$].

Pluronic-corona nanoparticles stimulate complement activation *via* the alternative pathway. The hydroxyl-containing nanoparticles are strong activators of C3, and the core thiols enhance the release of C3a (40, 41). Fe MWNTs coated with CMC, RNA or PL-PEG-NH_2 activate both the classical (predominantly) and alternative pathways (6). The consumption of C3 and C5 on the CNT surface suggests that there would be binding sites for C4b and C3b. C3b and C4b bind to nucleophilic groups, such as OH, and NH_2 groups; however, C3b does not form covalent adducts with high-molecular-weight proteins when bound to CNT. Thus, it may bind *via* hydrophobic interactions with CNTs or covalently to unesterified cholesterol in adsorbed HDL. Serum opsonization or complement deposition enhanced the uptake of CNTs by macrophages compared to non-opsonized CNTs, leading to an anti-inflammatory cytokine response (6).

Properdin is a highly positively charged molecule at neutral pH, with an isoelectric point of >9.5 (21). It binds to several self and non-self-target ligands such as Zymosan (42), rabbit erythrocytes, *N. gonorrhoeae* (32), T cells (27), human proximal tubular epithelial cells (43), and cartilage oligomeric matrix protein (44). Properdin engagement with surface-bound C3b recruits more C3b to form the C3 convertase complex, C3bBb. Properdin has also been proposed to act as a pattern recognition molecule for initiating alternative pathway other than just stabilizing the already formed C3bBb convertase (14). Properdin can directly interact with target ligands such as GAGs (28), including heparin (45), heparan sulfate (27, 46), dextran sulfate, fucoidan (47), and chondroitin sulfate (27). Properdin binding to activated platelets appears to occur *via* surface GAGs; when surface GAGs are removed, there is reduction in properdin binding to activated platelets (48). Properdin can bind DNA on late apoptotic and necrotic cells (42) and also bacterial LPS (33). Properdin's direct interaction with cell surface molecules may indicate it is a selective pattern recognition molecule. Thus, properdin may be a key innate immune molecule that can bind to a wide range of nanotherapeutics.

Nanoparticles are hydrophobic but are made biocompatible by coating with CMC, which is negatively charged, making the particles water soluble, less toxic, and more biodegradable and biotolerable (49). Many cell surface molecules identified so far that interact directly with properdin are negatively charged. Properdin and TSR4+5 were able to bind CNTs (CMC-CNT and Ox-CNT) directly and stably (**Figure 3**), in a conformation that retained their biological activity (**Figure 4**). We next assessed the uptake of properdin-CMC-CNT and TSR4+5-CMC-CNT by THP-1 macrophages (**Figure 5**). Properdin, but not TSR4+5, was able to enhance the phagocytosis of nanoparticles considerably. It is likely that the properdin-mediated enhancement of phagocytosis requires additional TSR modules or multimers of properdin. This may be due to the requirement for additional receptors or more widespread engagement of receptors binding to whole properdin. Although uptake of nanoparticles was exclusive to properdin, TSR4+5 was also able to trigger the pro-inflammatory cytokine response similar to properdin. This may indicate that additional receptors need to be engaged for phagocytic uptake, which are not necessarily required for the cytokine response. CMC-CNTs on their own were not able to produce a significant signal for these cytokines; however, IL-10 mRNA was upregulated at 30 min, which may be dampening the activation of macrophages, thus explaining lesser uptake of uncoated CMC-CNTs alone. TNF-α, IL-1β, and IL-6 transcripts were dramatically upregulated at 6 h, suggesting that properdin or TSR4+5 coated CMC-CNTs may alter the immune response. Once the early response of nanoparticles was revealed by qPCR, we further analyzed the secreted cytokine levels at 24 and 48 h following THP-1-CMC-CNT interaction, using multiplex array analysis (**Figure 7**). Interestingly, a dramatic upregulation of pro-inflammatory cytokine response was observed consistent with the early mRNA response for TNF-α, IL-1β, and IL-6 (**Figure 6**), which are potent inducers of GM-CSF (50). GM-CSF was dramatically upregulated by

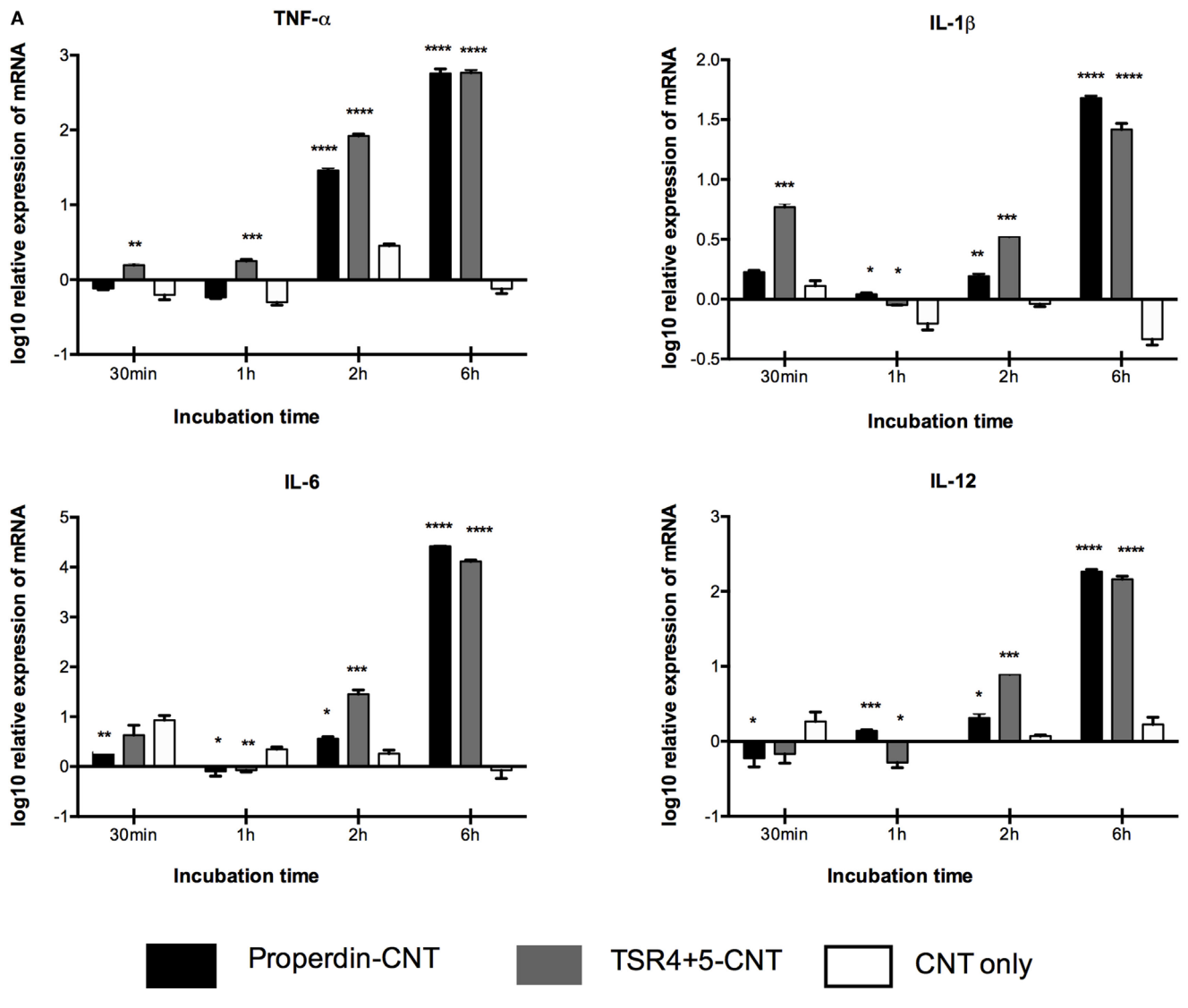

FIGURE 6 | Continued

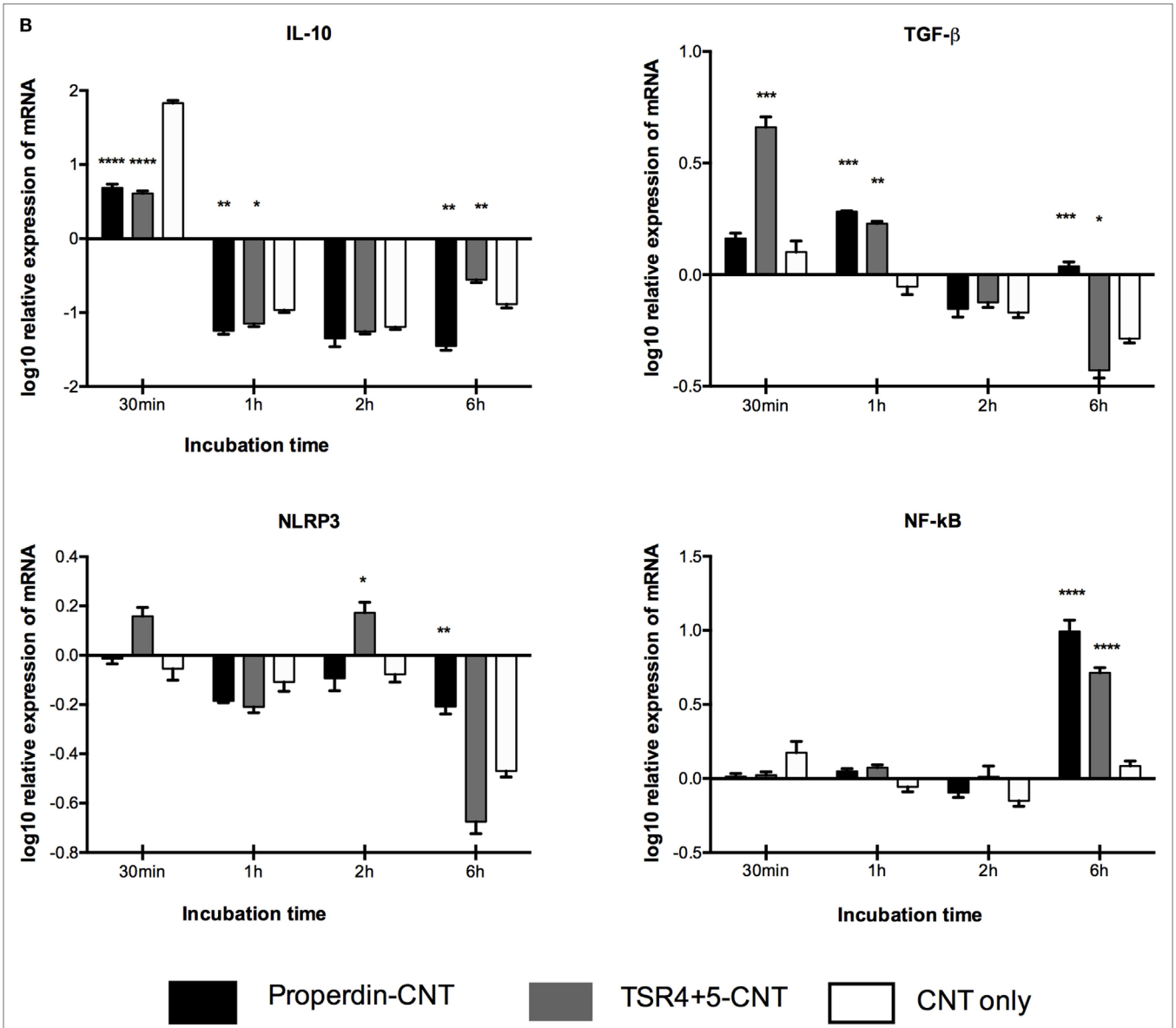

FIGURE 6 | Transcriptional upregulation of pro-inflammatory cytokines by properdin or thrombospondin type I repeat (TSR)4 + 5-coated carboxymethyl cellulose-coated carbon nanotubes (CMC-CNTs). For the measurement of mRNA expression of **(A)** pro- and **(B)** anti-inflammatory target genes, THP-1 cells were incubated with coated and uncoated CMC-CNTs for 30 min, 1 h, 2 h, and 6 h (*X*-axis). The expression of cytokines was measured using real-time qPCR, and the data were normalized using as endogenous control; 18S rRNA gene expression assays were conducted in triplicate. Error bars represent ±SEM. A multiple *t*-test using Holm–Sidak method was performed to determine significance differences in expression between each uncoated and protein-coated carbon nanotubes (CNTs) of different time points. All these comparisons were significant: $^{*}P < 0.05$, $^{**}P \leq 0.01$, $^{***}P \leq 0.001$, and $^{****}P \leq 0.0001$.

Properdin-CMC-CNT as well as TSR4+5-CMC-CNT. GM-CSF is produced by macrophages in response to immune stimuli, which can recruit neutrophils and lymphocytes. IL-1α and IL-1β (**Figure 7**) induce an inflammatory pathway initiated *via* Myd88 activation and triggered by NF-κB transcription of inflammatory genes. In addition, IL-8, a chemoattractant for neutrophils, may induce local production of properdin by neutrophils and enhance activation of the alternative pathway (30).

Although nanoparticles are considered highly promising drug delivery platforms in a variety of disease conditions, their systemic administration into the human body and their intended target tissue can be affected by innate and adaptive immune components. It has been shown in many studies that CNTs potently activate complement. Complement deposition leads to enhanced particle uptake by complement receptor-bearing macrophages and B cells (9). Subsequently, it was found that complement deposition on CNTs was in fact advantageous due to suppression of the pro-inflammatory response and upregulation of anti-inflammatory cytokine production (9). Functionally derivatized CNTs (CMC-CNT and RNA-CNT) activated

complement and became coated with complement proteins when treated with serum, while gold nanowires of similar size (51) were found to be poor activators of complement, while mounting a robust pro-inflammatory response, in contrast to complement-activating nanoparticles. We have shown here that properdin can act as an opsonin for nanoparticles without involving complement recruitment and activation and enhance their uptake and clearance by a macrophage cell line. It is possible that THP-1 cells synthesize a sufficient quantity of complement proteins (e.g., C3) to contribute to this apparent opsonization.

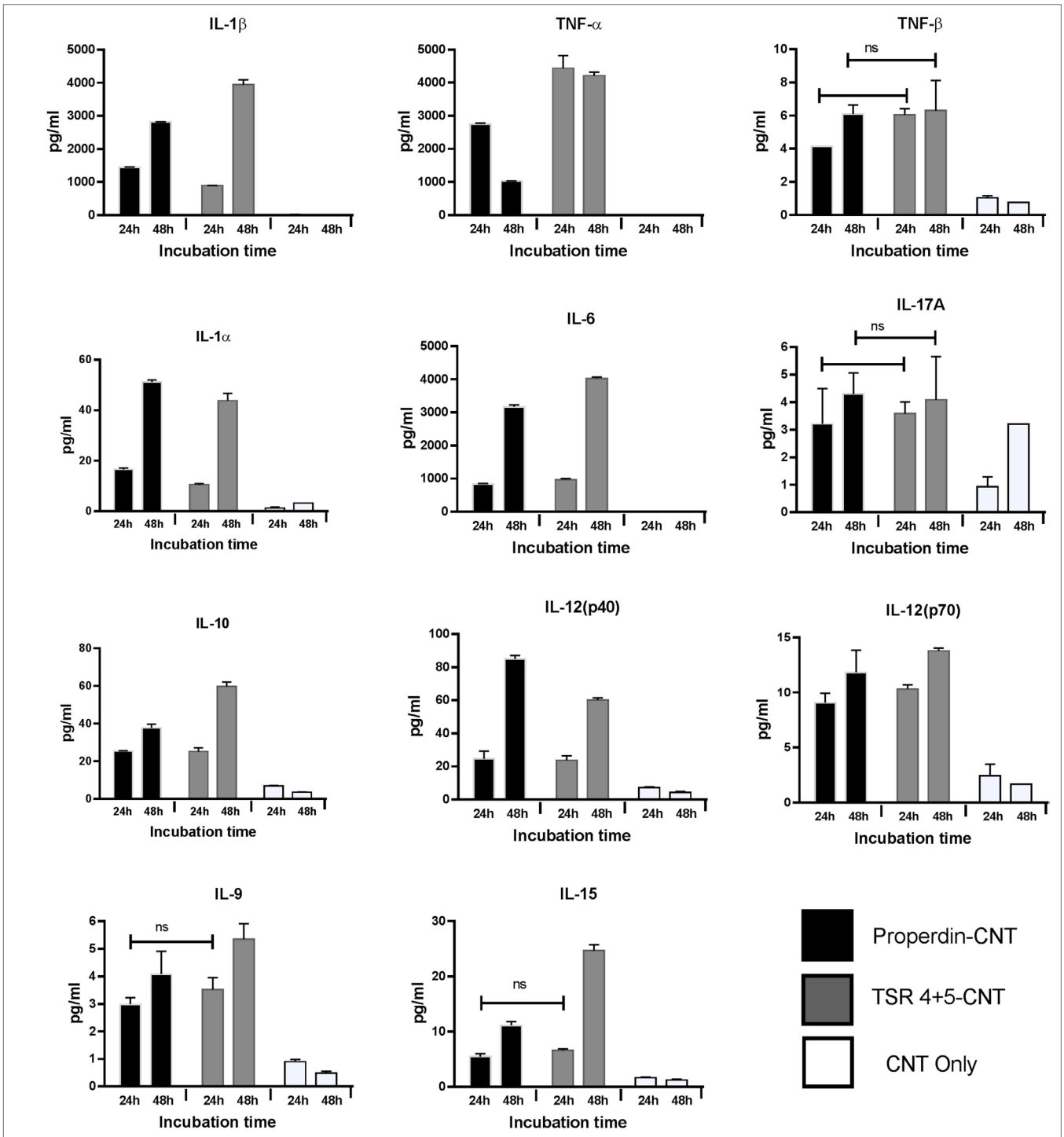

FIGURE 7 | Continued

The World Protein Atlas[2] reports that Properdin RNA and trace C3 RNA is found in these cells. However, Takizawa et al. found that the addition of serum as a complement source was necessary to observe phagocytosis of apoptotic cells by activated THP-1 cells (52). In addition, we have shown complement deposition on CNTs invariably modulates an otherwise pro-inflammatory response toward anti-inflammatory immune response dominated by IL-10 (9). Interesting, pulmonary surfactant protein SP-D can also opsonise CNTs and induce a potent pro-inflammatory response by macrophages. However, SP-D bound CNTs, when treated with serum, continued to

[2]http://www.proteinatlas.org.

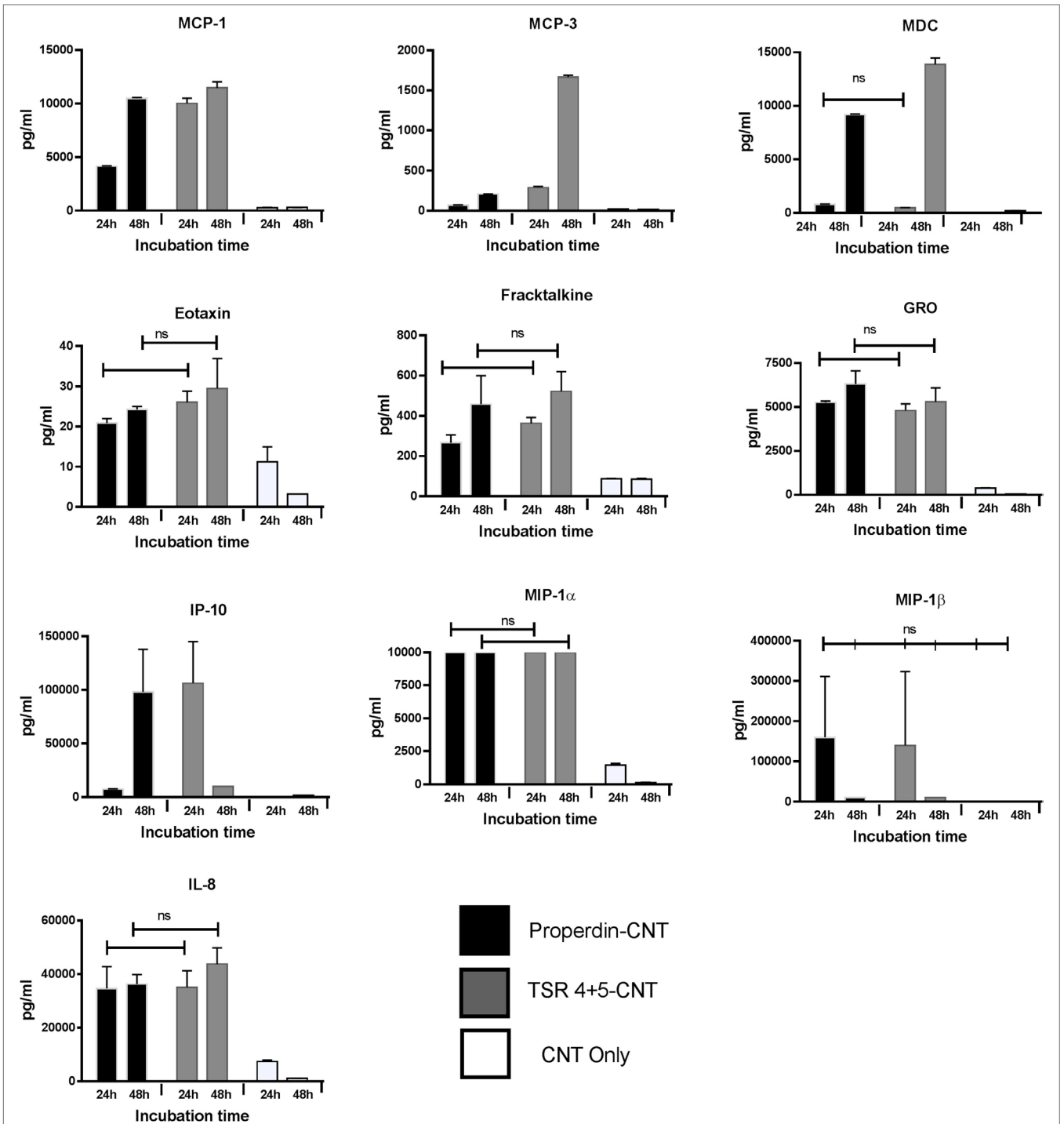

FIGURE 7 | Continued

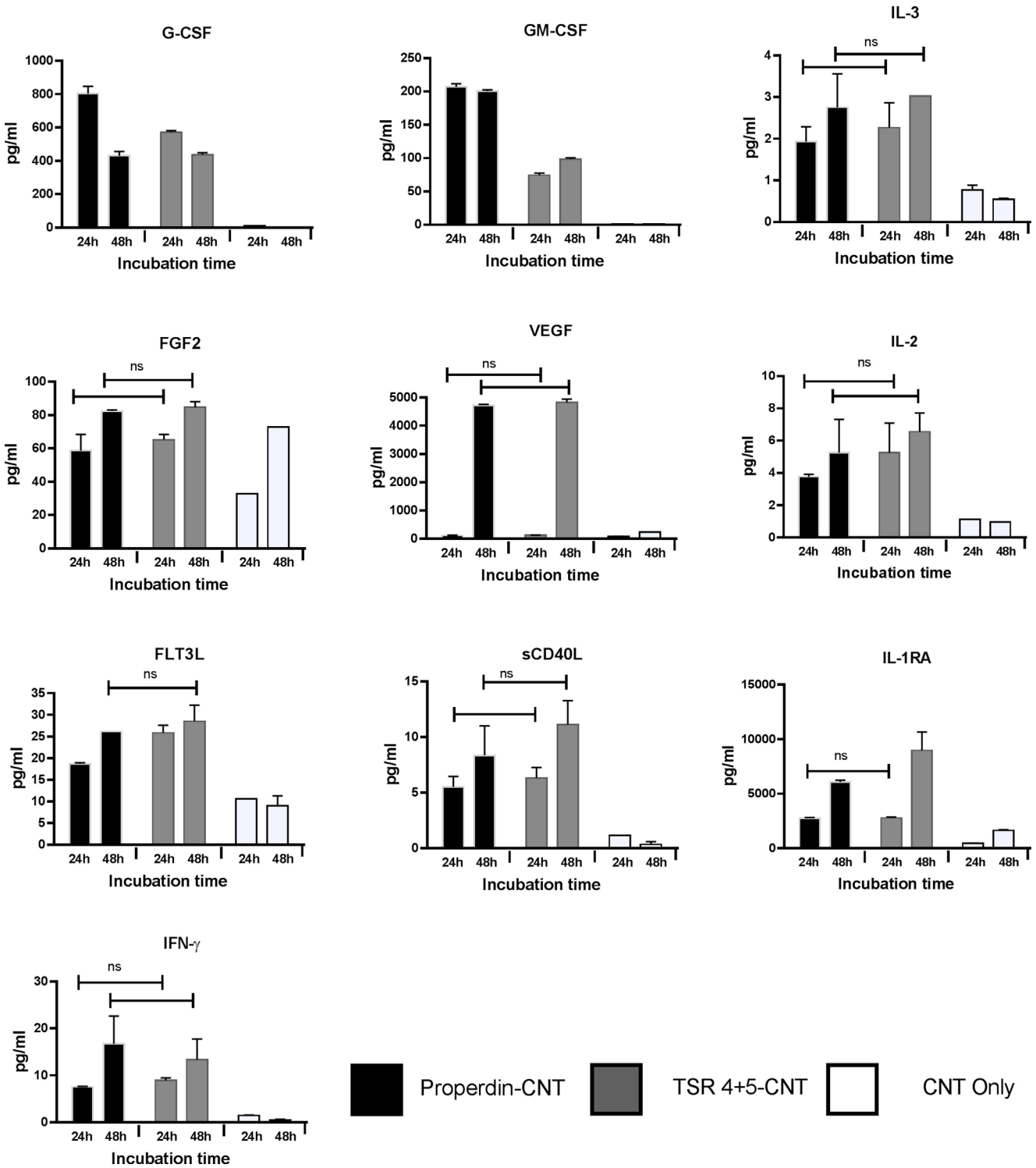

FIGURE 7 | Properdin or thrombospondin type I repeat (TSR)4 + 5-coated carboxymethyl cellulose-coated carbon nanotubes (CMC-CNTs) induce secretion of pro-inflammatory cytokines and chemokines by THP-1 cells. Protein-coated carbon nanotubes (CNTs) were incubated with THP-1 cells for 30 min, 1 h, 2 h, 6 h, 12 h, 24 h, and 48 h. Cells from early time points (30 min, 1 h, 2 h, and 6 h) were used for quantitative expression of different cytokines. Supernatant from late time points (24 and 48 h) (*X*-axis) were used for the measurement of the levels of cytokines (IL-6, IL-10, IL12p40, IL12p70, IL-1α, IL-1β, TNF-α, IL-15, IL-17A, IL-9, and TNF-β), chemokines (MCP-3, MDC, eotaxin, fractalkine, GRO, IL-8, IP-10, MCP-1, MIP-1α, and MIP-1β), growth factors (IL-2, FGF-2, G-CSF, GM-CSF, IL-3, and VEGF), and related ligands and receptors (IFN-γ, FLT-3L, IL-1RA, and sCD40L) by using a commercially available MagPix Milliplex kit (EMD Millipore). A multiple *t*-test using Holm–Sidak method was performed to determine significance differences in expression between expression between properdin or TSR4+5-coated and uncoated nanoparticles of different time points. All these comparisons were significant ($P < 0.05$), except where shown [not significant (ns), $P > 0.05$].

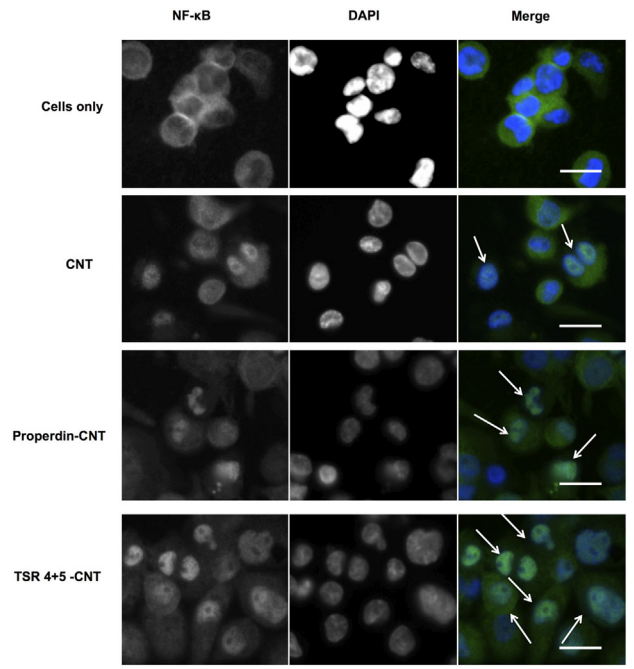

FIGURE 8 | Carboxymethyl cellulose-coated carbon nanotubes (CMC-CNTs) coated with properdin or thrombospondin type I repeat (TSR) 4 + 5 cause translocation of transcription factor NF-κB from cytoplasm to nucleus of THP-1 cells (arrows in merged images). Differentiated THP-1 cells were treated with properdin-coated or TSR4+5-coated CMC-CNTs for 2 h. Cells were washed, fixed, permeabilized, and incubated with rabbit anti-NF-κB p65 antibodies, followed by secondary Alexa Fluor 488-goat anti-rabbit antibody (Green). The nucleus was stained with Hoechst 33342 (Blue). Scale bar: 20 μm. Hoechst 33342 was used to stain the nucleus instead of DAPI.

activate complement, suggesting that SP-D binding site on the CNTs is distinct from that required for complement deposition. Even more interestingly, complement deposition on SP-D-bound CNTs downregulated the pro-inflammatory cytokine and chemokine production; instead, the immune response by macrophages became anti-inflammatory as revealed by multiplex array analysis and NF-kB nuclear translocation assay (53). These points appear to suggest complement-independent effects of properdin when bound to CNTs. It is worthwhile to clarify here that we are examining here the functions of properdin as a PRR, in a context where local synthesis of properdin may be intended for its non-complement functions, where all complement components may not be present for the alternative pathway activation.

Another important data that merit discussion here, which is not the main thrust of this study, is that TSR4+5-bound CNTs dampened the alternative pathway activation *in vitro*. The recombinant TSR4+5 has recently been shown to compete with properdin in binding to C3b (and other ligands) and inhibit the alternative pathway in solution phase (26). In this study, TSR4+5 bound to the CNTs and inhibited the alternative pathway activation on the surface of the bound nanoparticles, suggesting that the nanoparticles may be exploited to present a potential complement inhibitor as an arrayed drug delivery platform (**Figure 4**). These results are of pathophysiological significance because properdin deficiency has been linked with a range of bacterial infections especially *Neisseria* (54). The properdin gene-deficient mice have been found to be susceptible to bacterial infections (38). Properdin-CNTs used as a platform for drug delivery may mediate a protective role in disease mice models deficient in properdin. This will pave the way for further testing of its prophylactic and therapeutic values in murine models where properdin deficiency renders the mice susceptible to a range of infections.

Inhibition of complement alternative pathway has been previously reported to be beneficial in various pathological conditions. For example, mAb 1379, an anti-mouse factor B antibody, has been shown to provide protection against anti-phospholipid antibody-induced complement activation and fetal loss (55). Anti-C5 monoclonal antibody eculizumab is used as a therapeutic for paroxysmal nocturnal hemoglobinuria. We have reported in this study that TSR4+5:CMC-CNT are able to inhibit the alternative pathway by inhibiting consumption of complement on nanoparticles, which may have potential implications on therapeutic drug delivery in conditions with alternative pathway related diseases. Recently, a significant contribution of complement proteins to the tumor microenvironment has become a focus of intense research. Tumor cells thrive on an immunosuppressed microenvironment. To this effect, conditioned medium from melanoma B16F10 tumor cells has been shown to prime M1 macrophages, characterized by upregulation of iNOS, IL-1β, TNF-α, IL-12, IL-23, CXCL-9, and CXCL-10 (31). Thus, the tumor microenvironment could potentially be modulated by properdin-CNTs.

AUTHOR CONTRIBUTIONS

LK and BP carried out crucial experiments, plotted the data, and wrote the first draft. AK, GS, LJ, EF, SA, CS, and RS provided crucial reagents and expertise. UK led the work, designed experiments, analyzed the data, and finalized the manuscript.

REFERENCES

1. Lee YK, Choi EJ, Webster TJ, Kim SH, Khang D. Effect of the protein corona on nanoparticles for modulating cytotoxicity and immunotoxicity. *Int J Nanomedicine* (2014) 10:97–113. doi:10.2147/IJN.S72998
2. Pondman KM, Sim RB, Kishore U. Interaction of the immune system with nanoparticles. In: Bhushan B, editor. *Encyclopedia of Nanotechnology*. Dordrecht: Springer Netherlands (2015). p. 1–8.
3. Pondman KM, Salvador-Morales C, Paudyal B, Sim RB, Kishore U. Interactions of the innate immune system with carbon nanotubes. *Nanoscale Horizons* (2017) 2:174–86. doi:10.1039/C6NH00227G
4. Salvador-Morales C, Flahaut E, Sim E, Sloan J, Green ML, Sim RB. Complement activation and protein adsorption by carbon nanotubes. *Mol Immunol* (2006) 43:193–201. doi:10.1016/j.molimm.2005.02.006
5. Moghimi SM, Andersen AJ, Ahmadvand D, Wibroe PP, Andresen TL, Hunter AC. Material properties in complement activation. *Adv Drug Deliv Rev* (2011) 63:1000–7. doi:10.1016/j.addr.2011.06.002
6. Pondman KM, Sobik M, Nayak A, Tsolaki AG, Jakel A, Flahaut E, et al. Complement activation by carbon nanotubes and its influence on the phagocytosis and cytokine response by macrophages. *Nanomedicine* (2014) 10:1287–99. doi:10.1016/j.nano.2014.02.010

7. Kommareddy S, Amiji M. Biodistribution and pharmacokinetic analysis of long-circulating thiolated gelatin nanoparticles following systemic administration in breast cancer-bearing mice. *J Pharm Sci* (2007) 96:397–407. doi:10.1002/jps.20813
8. Pondman KM, Pednekar L, Paudyal B, Tsolaki AG, Kouser L, Khan HA, et al. Innate immune humoral factors, C1q and factor H, with differential pattern recognition properties, alter macrophage response to carbon nanotubes. *Nanomedicine* (2015) 11:2109–18. doi:10.1016/j.nano.2015.06.009
9. Pondman KM, Tsolaki AG, Paudyal B, Shamji MH, Switzer A, Pathan AA, et al. Complement deposition on nanoparticles can modulate immune responses by macrophage, B and T cells. *J Biomed Nanotechnol* (2016) 12:197–216. doi:10.1166/jbn.2016.2124
10. Carroll MV, Sim RB. Complement in health and disease. *Adv Drug Deliv Rev* (2011) 63:965–75. doi:10.1016/j.addr.2011.06.005
11. Kishore U, Reid KB. Modular organization of proteins containing C1q-like globular domain. *Immunopharmacology* (1999) 42:15–21. doi:10.1016/S0162-3109(99)00011-9
12. Kjaer TR, Thiel S, Andersen GR. Toward a structure-based comprehension of the lectin pathway of complement. *Mol Immunol* (2013) 56:222–31. doi:10.1016/j.molimm.2013.05.220
13. Alcorlo M, Tortajada A, Rodriguez de Cordoba S, Llorca O. Structural basis for the stabilization of the complement alternative pathway C3 convertase by properdin. *Proc Natl Acad Sci U S A* (2013) 110:13504–9. doi:10.1073/pnas.1309618110
14. Hourcade DE. The role of properdin in the assembly of the alternative pathway C3 convertases of complement. *J Biol Chem* (2006) 281:2128–32. doi:10.1074/jbc.M508928200
15. Sim RB, Kolble K, McAleer MA, Dominguez O, Dee VM. Genetics and deficiencies of the soluble regulatory proteins of the complement system. *Int Rev Immunol* (1993) 10:65–86. doi:10.3109/08830189309051172
16. Janeway C, Travers P, Walport M, Shlomchik M. *Immunobiology: The Immune System in Health and Disease*. New York: Garland Science (2001).
17. Pillemer L, Blum L, Lepow IH, Ross OA, Todd EW, Wardlaw AC. The properdin system and immunity. I. Demonstration and isolation of a new serum protein, properdin, and its role in immune phenomena. *Science* (1954) 120:279–85. doi:10.1126/science.120.3112.279
18. Kouser L, Abdul-Aziz M, Nayak A, Stover CM, Sim RB, Kishore U. Properdin and factor H: opposing players on the alternative complement pathway see-saw. *Front Immunol* (2013) 4:93. doi:10.3389/fimmu.2013.00093
19. Nolan KF, Kaluz S, Higgins JM, Goundis D, Reid KB. Characterization of the human properdin gene. *Biochem J* (1992) 287(Pt 1):291–7. doi:10.1042/bj2870291
20. Discipio RG. Properdin is a trimer. *Mol Immunol* (1982) 19:631–5. doi:10.1016/0161-5890(82)90232-2
21. Smith CA, Pangburn MK, Vogel CW, Muller-Eberhard HJ. Molecular architecture of human properdin, a positive regulator of the alternative pathway of complement. *J Biol Chem* (1984) 259:4582–8.
22. Goundis D, Reid KB. Properdin, the terminal complement components, thrombospondin and the circumsporozoite protein of malaria parasites contain similar sequence motifs. *Nature* (1988) 335:82–5. doi:10.1038/335082a0
23. Sun Z, Reid KB, Perkins SJ. The dimeric and trimeric solution structures of the multidomain complement protein properdin by X-ray scattering, analytical ultracentrifugation and constrained modelling. *J Mol Biol* (2004) 343:1327–43. doi:10.1016/j.jmb.2004.09.001
24. Higgins JM, Wiedemann H, Timpl R, Reid KB. Characterization of mutant forms of recombinant human properdin lacking single thrombospondin type I repeats. Identification of modules important for function. *J Immunol* (1995) 155:5777–85.
25. Perdikoulis MV, Kishore U, Reid KB. Expression and characterisation of the thrombospondin type I repeats of human properdin. *Biochim Biophys Acta* (2001) 1548:265–77. doi:10.1016/S0167-4838(01)00238-2
26. Kouser L, Abdul-Aziz M, Tsolaki AG, Singhal D, Schwaeble WJ, Urban BC, et al. A recombinant two-module form of human properdin is an inhibitor of the complement alternative pathway. *Mol Immunol* (2016) 73:76–87. doi:10.1016/j.molimm.2016.03.005
27. Kemper C, Mitchell LM, Zhang L, Hourcade DE. The complement protein properdin binds apoptotic T cells and promotes complement activation and phagocytosis. *Proc Natl Acad Sci U S A* (2008) 105:9023–8. doi:10.1073/pnas.0801015105
28. Xu W, Berger SP, Trouw LA, de Boer HC, Schlagwein N, Mutsaers C, et al. Properdin binds to late apoptotic and necrotic cells independently of C3b and regulates alternative pathway complement activation. *J Immunol* (2008) 180:7613–21. doi:10.4049/jimmunol.180.11.7613
29. Dixon KO, O'Flynn J, Klar-Mohamad N, Daha MR, van Kooten C. Properdin and factor H production by human dendritic cells modulates their T-cell stimulatory capacity and is regulated by IFN-gamma. *Eur J Immunol* (2017) 47:470–80. doi:10.1002/eji.201646703
30. Wirthmueller U, Dewald B, Thelen M, Schafer MK, Stover C, Whaley K, et al. Properdin, a positive regulator of complement activation, is released from secondary granules of stimulated peripheral blood neutrophils. *J Immunol* (1997) 158:4444–51.
31. Al-Rayahi IA, Browning MJ, Stover C. Tumour cell conditioned medium reveals greater M2 skewing of macrophages in the absence of properdin. *Immun Inflamm Dis* (2017) 5:68–77. doi:10.1002/iid3.142
32. Spitzer D, Mitchell LM, Atkinson JP, Hourcade DE. Properdin can initiate complement activation by binding specific target surfaces and providing a platform for de novo convertase assembly. *J Immunol* (2007) 179:2600–8. doi:10.4049/jimmunol.179.4.2600
33. Kimura Y, Miwa T, Zhou L, Song WC. Activator-specific requirement of properdin in the initiation and amplification of the alternative pathway complement. *Blood* (2008) 111:732–40. doi:10.1182/blood-2007-05-089821
34. Cortes C, Ferreira VP, Pangburn MK. Native properdin binds to *Chlamydia pneumoniae* and promotes complement activation. *Infect Immun* (2011) 79:724–31. doi:10.1128/IAI.00980-10
35. Narni-Mancinelli E, Gauthier L, Baratin M, Guia S, Fenis A, Deghmane AE, et al. Complement factor P is a ligand for the natural killer cell-activating receptor NKp46. *Sci Immunol* (2017) 2:eaam9628. doi:10.1126/sciimmunol.aam9628
36. Bortolamiol T, Lukanov P, Galibert A, Soula B, Lonchambon P, Datas L, et al. Double-walled carbon nanotubes: quantitative purification assessment, balance between purification and degradation and solution filling as an evidence of opening. *Carbon N Y* (2014) 78:79–90. doi:10.1016/j.carbon.2014.06.051
37. Flahaut E, Bacsa R, Peigney A, Laurent C. Gram-scale CCVD synthesis of double-walled carbon nanotubes. *Chem Commun (Camb)* (2003) 12:1442–3. doi:10.1039/B301514A
38. Stover CM, Luckett JC, Echtenacher B, Dupont A, Figgitt SE, Brown J, et al. Properdin plays a protective role in polymicrobial septic peritonitis. *J Immunol* (2008) 180:3313–8. doi:10.4049/jimmunol.180.5.3313
39. Kishore U, Gupta SK, Perdikoulis MV, Kojouharova MS, Urban BC, Reid KB. Modular organization of the carboxyl-terminal, globular head region of human C1q A, B, and C chains. *J Immunol* (2003) 171:812–20. doi:10.4049/jimmunol.171.2.812
40. Thomas SN, van der Vlies AJ, O'Neil CP, Reddy ST, Yu SS, Giorgio TD, et al. Engineering complement activation on polypropylene sulfide vaccine nanoparticles. *Biomaterials* (2011) 32:2194–203. doi:10.1016/j.biomaterials.2010.11.037
41. Toda M, Kitazawa T, Hirata I, Hirano Y, Iwata H. Complement activation on surfaces carrying amino groups. *Biomaterials* (2008) 29:407–17. doi:10.1016/j.biomaterials.2007.10.005
42. Ferreira VP, Cortes C, Pangburn MK. Native polymeric forms of properdin selectively bind to targets and promote activation of the alternative pathway of complement. *Immunobiology* (2010) 215:932–40. doi:10.1016/j.imbio.2010.02.002
43. Gaarkeuken H, Siezenga MA, Zuidwijk K, van Kooten C, Rabelink TJ, Daha MR, et al. Complement activation by tubular cells is mediated by properdin binding. *Am J Physiol Renal Physiol* (2008) 295:F1397–403. doi:10.1152/ajprenal.90313.2008
44. Happonen KE, Saxne T, Aspberg A, Morgelin M, Heinegard D, Blom AM. Regulation of complement by cartilage oligomeric matrix protein allows for a novel molecular diagnostic principle in rheumatoid arthritis. *Arthritis Rheum* (2010) 62:3574–83. doi:10.1002/art.27720
45. Yu H, Munoz EM, Edens RE, Linhardt RJ. Kinetic studies on the interactions of heparin and complement proteins using surface plasmon resonance. *Biochim Biophys Acta* (2005) 1726:168–176.

46. Zaferani A, Vives RR, van der Pol P, Navis GJ, Daha MR, van Kooten C, et al. Factor h and properdin recognize different epitopes on renal tubular epithelial heparan sulfate. *J Biol Chem* (2012) 287:31471–81. doi:10.1074/jbc.M112.380386
47. Holt GD, Pangburn MK, Ginsburg V. Properdin binds to sulfatide [Gal(3-SO4) beta 1-1 Cer] and has a sequence homology with other proteins that bind sulfated glycoconjugates. *J Biol Chem* (1990) 265:2852–5.
48. Saggu G, Cortes C, Emch HN, Ramirez G, Worth RG, Ferreira VP. Identification of a novel mode of complement activation on stimulated platelets mediated by properdin and C3(H_2O). *J Immunol* (2013) 190:6457–67. doi:10.4049/jimmunol.1300610
49. Bourdiol F, Mouchet F, Perrault A, Fourquaux I, Datas L, Gancet C, et al. Biocompatible polymer-assisted dispersion of multi walled carbon nanotubes in water, application to the investigation of their ecotoxicity using Xenopus laevis amphibian larvae. *Carbon N Y* (2013) 54:175–91. doi:10.1016/j.carbon.2012.11.024
50. Chung EY, Kim SJ, Ma XJ. Regulation of cytokine production during phagocytosis of apoptotic cells. *Cell Res* (2006) 16:154–61.
51. Pondman KM, Maijenburg AW, Celikkol FB, Pathan AA, Kishore U, Haken Bt, et al. Au coated Ni nanowires with tuneable dimensions for biomedical applications. *J Mater Chem B* (2013) 1:6129–36. doi:10.1039/C3TB20808G
52. Takizawa F, Tsuji S, Nagasawa S. Enhancement of macrophage phagocytosis upon iC3b deposition on apoptotic cells. *FEBS Lett* (1996) 397:269–72. doi:10.1016/S0014-5793(96)01197-0
53. Pondman KM, Paudyal B, Sim RB, Kaur A, Kouser L, Tsolaki AG, et al. Pulmonary surfactant protein SP-D opsonises carbon nanotubes and augments their phagocytosis and subsequent pro-inflammatory immune response. *Nanoscale* (2017) 9:1097–109. doi:10.1039/c6nr08807d
54. Soderstrom C, Braconier JH, Sjoholm AG, Thuresson B. Granulocyte functions and *Neisseria meningitidis*: influence of properdin-deficient serum. *APMIS* (1991) 99:965–71. doi:10.1111/j.1699-0463.1991.tb01285.x
55. Thurman JM, Kraus DM, Girardi G, Hourcade D, Kang HJ, Royer PA, et al. A novel inhibitor of the alternative complement pathway prevents antiphospholipid antibody-induced pregnancy loss in mice. *Mol Immunol* (2005) 42:87–97. doi:10.1016/j.molimm.2004.07.043

Conflict of Interest Statement: The authors declare that the research was conducted in the absence of any commercial or financial relationships that could be construed as a potential conflict of interest.

The reviewer MD and handling editor declared their shared affiliation.

frontiers in Immunology

ORIGINAL RESEARCH
published: 08 May 2018
doi: 10.3389/fimmu.2018.00533

Human Properdin Modulates Macrophage: *Mycobacterium bovis* BCG Interaction *via* Thrombospondin Repeats 4 and 5

Maha Ahmed Al-Mozaini[1,2], Anthony G. Tsolaki[1], Munirah Abdul-Aziz[1,3], Suhair M. Abozaid[1,2], Mohammed N. Al-Ahdal[2], Ansar A. Pathan[1], Valarmathy Murugaiah[1], Evgeny M. Makarov[1], Anuvinder Kaur[1], Robert B. Sim[3], Uday Kishore[1] and Lubna Kouser[1]**

[1] College of Health and Life Sciences, Brunel University London, London, United Kingdom, [2] Department of Infection and Immunity, King Faisal Specialist Hospital and Research Centre, Riyadh, Saudi Arabia, [3] Department of Biochemistry, Oxford University, Oxford, United Kingdom

Mycobacterium tuberculosis can proficiently enter macrophages and diminish complement activation on its cell surface. Within macrophages, the mycobacterium can suppress macrophage apoptosis and survive within the intracellular environment. Previously, we have shown that complement regulatory proteins such as factor H may interfere with pathogen–macrophage interactions during tuberculosis infection. In this study, we show that *Mycobacterium bovis* BCG binds properdin, an upregulator of the complement alternative pathway. TSR4+5, a recombinant form of thrombospondin repeats 4 and 5 of human properdin expressed in tandem, which is an inhibitor of the alternative pathway, was also able to bind to *M. bovis* BCG. Properdin and TSR4+5 were found to inhibit uptake of *M. bovis* BCG by THP-1 macrophage cells in a dose-dependent manner. Quantitative real-time PCR revealed elevated pro-inflammatory responses (TNF-α, IL-1β, and IL-6) in the presence of properdin or TSR4+5, which gradually decreased over 6 h. Correspondingly, anti-inflammatory responses (IL-10 and TGF-β) showed suppressed levels of expression in the presence of properdin, which gradually increased over 6 h. Multiplex cytokine array analysis also revealed that properdin and TSR4+5 significantly enhanced the pro-inflammatory response (TNF-α, IL-1β, and IL-1α) at 24 h, which declined at 48 h, whereas the anti-inflammatory response (IL-10) was suppressed. Our results suggest that properdin may interfere with mycobacterial entry into macrophages via TSR4 and TSR5, particularly during the initial stages of infection, thus affecting the extracellular survival of the pathogen. This study offers novel insights into the non-complement related functions of properdin during host–pathogen interactions in tuberculosis.

Keywords: complement, cytokine, properdin, macrophage, *Mycobacterium tuberculosis*, *Mycobacterium bovis* BCG, phagocytosis, thrombospondin repeats

OPEN ACCESS

Edited by:
Cees Van Kooten,
Leiden University, Netherlands

Reviewed by:
Michael Kirschfink,
Universität Heidelberg, Germany
Lubka T. Roumenina,
INSERM UMRS 1138, France

***Correspondence:**
Uday Kishore
uday.kishore@brunel.ac.uk,
ukishore@hotmail.com;
Lubna Kouser
lubna_k@hotmail.co.uk

Specialty section:
This article was submitted to Molecular Innate Immunity, a section of the journal Frontiers in Immunology

Received: *03 July 2017*
Accepted: *01 March 2018*
Published: *08 May 2018*

Citation:
Al-Mozaini MA, Tsolaki AG, Abdul-Aziz M, Abozaid SM, Al-Ahdal MN, Pathan AA, Murugaiah V, Makarov EM, Kaur A, Sim RB, Kishore U and Kouser L (2018) Human Properdin Modulates Macrophage: Mycobacterium bovis BCG Interaction via Thrombospondin Repeats 4 and 5. Front. Immunol. 9:533. doi: 10.3389/fimmu.2018.00533

INTRODUCTION

Properdin is an upregulator of the alternative pathway of complement activation. In one of the three pathways of the complement system, the alternative pathway, the activation of the major complement opsonin, C3, is driven by a complex serine protease, C3bBb, also called the C3 convertase, which is bound to the surface of the complement-activating target. To form C3bBb, factor B associates

with C3b in the presence of Mg^{2+} and factor D, a serine protease, which cleaves factor B into Bb and Ba fragments producing a C3 convertase C3bBb (1). This complex, which has a half-life of 90 s, is stabilized by the binding of properdin, which increases the half-life by 5- to 10-fold (2). Furthermore, C3b molecules are generated by C3bBb and deposited near to the surface-bound convertase leading to the opsonization of the target and formation of C5 convertase, producing C5a and C5b, leading on to the lytic pathway and cell lysis (3).

The monomer of human properdin (53 kDa) has a flexible rod-like structure with a length of 26 nm and a diameter of 2.5 nm, composed of seven thrombospondin type I repeats (TSR). Each TSR is of about 60 amino acids, typically containing six conserved cysteine residues: these occur in TSR1–TSR6 (4–6), but the N-terminal domain, TSR0, is truncated. TSR4 is crucial for binding to C3bBb and TSR5 for binding to C3bBb, suggesting that both TSRs may be important for stabilizing the C3 convertase complex (5). Recently, TSR4+5, expressed as a double domain, has been shown to bind to properdin ligands such as C3b and inhibit the alternative complement pathway (7). These studies demonstrate the important role that these TSRs may play in the alternative pathway and in their interaction with pathogens.

Properdin circulates in plasma at a concentration of about 4–25 μg/ml existing as cyclic oligomers, dimer, trimer, and tetramer in a ratio of 26:54:20 (4). The dissociation and reassociation of properdin upon denaturation–renaturation cycles stimulated by guanidine or low pH indicates properdin ratio stability in solution (8). The interaction between properdin monomers involves the N-terminal end of one monomer and the C-terminal end of another (9). Properdin can also bind to microbial surfaces of several pathogens, including *Neisseria gonorrhoeae* (10), *Salmonella typhimurium* lipopolysaccharide (LPS), *Neisseria meningitidis* lipooligosaccharide (11), and *Chlamydia pneumoniae* (12). Binding of properdin to microbial surfaces results in the recruitment of fluid phase C3b, inducing assembly of C3 convertase C3bBb and causing further deposition of C3b on the pathogen surface (13–15), subsequently generating a C5 convertase, MAC formation, and cell lysis. At 10 μg/ml, recombinant properdin enhanced complement deposition on *N. meningitidis* and *S. pneumoniae* and dramatically enhanced serum lysis of these bacteria, and in the mouse model, significantly reduced bacteremia and increased survival rates (16).

Although *Mycobacterium tuberculosis* and its close-relative *Mycobacterium bovis* have significant interaction with components of the innate immune system, e.g., toll-like receptors, complement, surfactant proteins SP-A and SP-D (17), the initial stages of tuberculosis pathogenesis remain poorly understood. Many bacteria have evolved mechanisms to evade immune responses: by inhibiting complement activation by proteolytic cleavage of complement proteins, having their own complement inhibitors (18), or binding complement regulatory proteins like factor H (15, 19).

Mycobacterium tuberculosis is a highly specialized intracellular pathogen and may exploit complement proteins to enhance its uptake by macrophages. Although it has been shown that *M. tuberculosis* can activate all three pathways of the complement system (20, 21), it is unclear how the pathogen uses complement proteins in tuberculosis pathogenesis. *M. tuberculosis* has been shown to bind to complement receptors (CR) CR1, CR3, and CR4 and gain entry into macrophages (22–24). There is also evidence that enhanced phagocytosis of *M. tuberculosis* by human alveolar and monocyte-derived macrophages results from C3 opsonization (24). The ability of *M. tuberculosis* to bind to CR3 non-opsonically has also been shown which may be important for bacterial invasion when complement is sparse, for example, in the lung (25). Properdin has recently been considered as a pattern recognition receptor (PRR) on its own, i.e., binding to recognition patterns without need for prior deposition of C3b or C3bBb (26–28). Therefore, we investigated the role of properdin in tuberculosis pathogenesis, by using the model organism *M. bovis* BCG.

Here, we show, for the first time, that properdin and recombinant form of TSR4+5 expressed as a two-module protein binds to *M. bovis* BCG, demonstrating its role as a soluble PRR. Properdin and TSR4+5 were found to inhibit the uptake of *M. bovis* BCG by macrophages during phagocytosis, altering the pro- and anti-inflammatory cytokine response, and thus, possibly shaping the adaptive immune response in tuberculosis pathogenesis.

MATERIALS AND METHODS

Purification of Native Properdin

The affinity columns, IgG Sepharose and anti-properdin monoclonal antibody Sepharose, were prepared as described previously (7). The IgG-Sepharose column was prepared from human non-immune IgG (~26 mg IgG/ml of Sepharose) coupled to CNBr-activated Sepharose (GE Healthcare, UK). For preparation of the anti-human properdin column, CNBr-activated Sepharose (GE Healthcare Life Sciences, UK) was used to couple to anti-properdin mouse monoclonal antibody (2 mg/ml). One liter of human plasma (TCS Biosciences) containing 5 mM EDTA was filtered through Whatman filter paper before applying to IgG Sepharose to deplete C1q (which would otherwise have bound to the IgG on the anti-properdin Sepharose). The column was washed with three bed volume of HEPES buffer (10 mM HEPES, 140 mM NaCl, 0.5 mM EDTA, and pH 7.4). Plasma was then applied to the monoclonal anti-properdin column and washed with the same HEPES buffer. Bound properdin was eluted with 3 M $MgCl_2$ and the peak fractions were dialyzed against HEPES buffer overnight at 4°C. Contaminants were further removed by applying the pooled protein fractions to a HiTrap Q FF-Sepharose (GE Healthcare) ion-exchange column, followed by washing the column with three bed volumes of 50 mM Tris–HCl, pH 7.5, 50 mM NaCl, and 5 mM EDTA. Properdin did not bind to the Q Sepharose column and appeared in the flow-through free from contaminants as demonstrated by SDS-PAGE.

For the size exclusion chromatography analysis, 50 μl of the proteins at the concentrations varying from 0.3 mg/mL to 1.0 mg/mL were applied to a TSKgel G2000SWXL, 5 μm, 7.8 × 300 mm column (Tosoh Bioscience). The column was equilibrated with buffer containing 50 mM sodium phosphate, pH7.0 and 300 mM NaCl at the flow rate 0.3 ml/min using SCL-10Avp HPLC system

(Shimadzu). The absorbance was detected at 230 and 280 nm. The Bio-Rad Gel Filtration Standard (Cat # 151-1901) were used for the protein molecular weight calibration of the column.

Expression and Purification of TSR4+5

The recombinant maltose-binding protein (MBP) fusion proteins MBP-TSR4+5, MBP-TSR4, or MBP-TSR5 were expressed in *Escherichia coli* as described previously (7, 29). The *E. coli* BL21 bacterial cells (Life Technologies) were grown in 1 L of Luria–Bertani medium with 100 µg/ml ampicillin, shaking at 37°C until an optical density at 600 nm (OD_{600}) of between 0.6 and 0.8 was reached. Protein expression was then induced in the bacterial cell culture with 0.4 mM isopropyl β-D-1-thiogalactopyranoside (IPTG) (Sigma-Aldrich) for 3 h shaking at 37°C. The cells were then pelleted at 4,500 rpm, 4°C for 10 min, lysed using 50 ml lysis buffer [20 mM Tris–HCl, pH 8.0, 0.5 M NaCl, 1 mM EDTA, 0.25% v/v Tween 20, 5% v/v glycerol, 100 µg/ml lysozyme (Sigma-Aldrich), and 0.1 mM phenylmethanesulfonyl fluoride (Sigma-Aldrich)], and incubated for 1 h at 4°C on a rotary shaker. The cell lysate was then sonicated using a Soniprep 150 (MSE, London, UK) at 60 Hz for 30 s with an interval of 2 min (12 cycles) and then centrifuged at 13,000 rpm for 15 min at 4°C. The supernatant was diluted five-fold with buffer A (20 mM Tris–HCl, pH 8.0, 100 mM NaCl, 1 mM EDTA, and 0.25% v/v Tween 20) and passed through an amylose resin column (25 ml bed) (New England Biolabs) that was equilibrated in buffer A. The affinity column was washed with buffer A without Tween 20 and with 1 M NaCl, 20 mM Tris–HCl, pH 8.0, 1 mM EDTA, followed by buffer B (20 mM Tris–HCl, pH 8.0, 100 mM NaCl, 1 mM EDTA). The MBP-TSR4+5 fusion protein was eluted with 100 ml of buffer B containing 10 mM maltose (Sigma-Aldrich) (affinity elution buffer). Trace contaminants were further removed by applying the fusion protein to a DEAE Sepharose column. Thus, the affinity purified fusion protein in affinity elution buffer was applied to the ion-exchange (5 ml bed) column and washed with three column volumes of low salt buffer containing 50 mM Tris–HCl, pH 7.5, 100 mM NaCl, 5 mM EDTA, at pH 7.5. After extensive washing with low salt buffer, the fusion protein eluted at 0.2 M NaCl using a NaCl gradient (50 mM to 1 M). The peak elutions were then passed through Pierce™ High Capacity Endotoxin Removal Resin (Qiagen) to remove LPS. Endotoxin levels were determined using the QCL-1000 Limulus amebocyte lysate system (Lonza), and the assay was linear over a range of 0.1–1.0 EU/ml (10 EU = 1 ng of endotoxin). The endotoxin levels were less than 4 pg/µg of the MBP-TSR4+5.

Mycobacterial Cell Culture

Mycobacterium bovis BCG (Pasteur strain) were grown in liquid culture using Middlebrook 7H9 media (Sigma-Aldrich), supplemented with 0.2% (v/v) glycerol, 0.05% (v/v) Tween-80, and 10% (v/v) albumin dextrose catalase (ADC) (BD BBL, Becton Dickinson). Green fluorescent protein (GFP)-expressing *M. bovis BCG* (Danish Strain 1331) containing the pGFPHYG2 plasmid was a kind gift from B. Robertson, Imperial College, London, UK. GFP-*M. bovis* BCG was grown in the above conditions/media but with the addition of 50 µg/ml of hygromycin to maintain the plasmid. Cultures were incubated at 37°C with agitation (~120 rpm) for 7–10 days until the bacteria had reached the exponential growth phase at $OD_{600nm} = 0.60–1.00$.

Assay of Human Properdin and TSR4+5 Binding to Mycobacteria

Mycobacterium bovis BCG, harvested and washed in PBS, was adjusted to a concentration of 1.25×10^9 cells/ml in PBS ($OD_{600} = 1$ equates to approximately 1×10^9 cell/ml). Then 200 µl of bacterial suspension was dispensed into individual microtiter wells of a 96-well plate (Maxisorp™, NUNC). Plates were incubated at 4°C overnight and washed with buffer 1 [10 mM HEPES pH 7.5, 140 mM NaCl, 0.5 mM EDTA, and 100 µg/ml hen ovalbumin (Sigma-Aldrich)]. Wells were blocked for 2 h at 37°C with buffer 1 + 10% (w/v) Marvel Dried Milk powder.

Human properdin (up to 50 µg/ml) or TSR4+5 (up to 30 µg/ml) were added, in two-fold serial dilutions (100 µl/well) in buffer 1 and incubated for 2 h at 37°C. Individual TSR4 and TSR5 proteins, MBP and BSA were used as negative controls. Microtiter wells were washed three times with buffer 1. Mouse anti-properdin monoclonal antibody (1.19 mg/ml) diluted 1/2,500 in buffer 1 (29) was added to the wells containing properdin. Mouse anti-MBP monoclonal antibody (Sigma-Aldrich) was added to wells containing TSR4+5, TSR4 and TSR5, diluted 1/5,000 in buffer 1, and incubated for 1 h at 37°C. For the BSA negative control, mouse anti-BSA monoclonal antibody (Sigma-Aldrich) was used (1/5,000 dilution). Plates were washed an additional three times in buffer 1 and then incubated with goat anti-mouse IgG-horseradish peroxidase conjugate (Sigma-Aldrich), diluted 1/5,000 in buffer 1. The substrate *p*-nitrophenol phosphate (Sigma-Aldrich) was then added to each well, and the plates read at 405 nm.

Fluorescence Microscopy for TSR4+5 Binding to Mycobacteria

Mycobacterium bovis BCG bacteria (approximately 10^6 cells) were spotted on poly-L-lysine coated microscope slides (Sigma-Aldrich) and incubated at 37°C for cells to adhere. After washing three times with PBS, bacterial cells were then fixed with 4% paraformaldehyde for 5 min. Slides were washed three times with PBS and then incubated at 37°C for 1 h with 0, 1, or 10 µg/ml of TSR4+5, or 10 µg/ml of BSA (negative control) in buffer 1. Slides were washed three times with PBS, and then the primary monoclonal antibody (mouse anti-MBP) added at 1/500 dilution and incubated for 1 h at room temperature. After washing three times with PBS, goat anti-mouse conjugated with AlexaFluor488 (1/500 dilution) was added as the secondary antibody and incubated for 1 h at room temperature. Slides were then washed three times with PBS and mounted with antifade (Citifluor AF3) PBS solution and viewed using a LeicaDM4000 Fluorescence microscope. Images were processed using Image J.[1]

[1] http://imagej.nih.gov/ij.

Phagocytosis Assay

THP-1 macrophage cells were cultured in RPMI-1640 (Gibco) (RPMI) containing 10% (v/v) fetal bovine serum (FBS) (Sigma-Aldrich), 2 mM L-glutamine (Sigma-Aldrich), 100 U/ml penicillin (Sigma-Aldrich), 100 μg/ml streptomycin (Sigma-Aldrich), and 1 mM sodium pyruvate (Sigma-Aldrich) and left to grow in 5% CO_2 at 37°C for approximately 3 days before passaging. Cells were resuspended in RPMI and adjusted to 1×10^6 cells/well (in 1.8 ml) in a 24-well plate. To induce adherence onto the wells, THP-1 cells were treated with 50 ng/ml of phorbol 12-myristate 13-acetate (PMA) (Sigma-Aldrich) into RPMI-1640 without FBS, penicillin or streptomycin and left to settle for at least 30 min before adding 200 μl of bacterial culture (1×10^9 bacteria/ml).

M. bovis BCG bacteria were pelleted at mid-exponential phase, at an $OD_{600nm} = 0.6–1.0$ by centrifugation at 1,000 × *g* for 10 min at 4°C. The mycobacterial pellet was resuspended in the buffer 1. This mycobacterial culture was then separated into different microfuge tubes and treated with varying concentrations of properdin (2 or 20 μg/ml) or MBP-TSR4+5 (1 or 5 μg/ml). Control samples were left untreated, and all were incubated for 2 h at 37°C for binding to occur. The mycobacterial suspension was washed once in growth medium before resuspending in RPMI medium without FBS, penicillin, or streptomycin. 200 μl of the mycobacterial suspension was added to each well of THP-1 cells. Mycobacterial concentration was adjusted to give approximate multiplicity of infection (MOI) ratio of 10:1.

Plates were gently swirled and incubated at 37°C, 5% CO_2 for up to 48 h to allow mycobacterial uptake. THP-1 cells were sampled at 15, 30, and 45 min and 1, 2, and 6 h. Supernatants were collected after 24 and 48 h of incubation for multiplex analysis. Plates were washed three times with PBS to remove extracellular bacteria. THP-1 cells were then lifted by adding 1 ml of 0.25% trypsin to the wells and incubated for 10 min at 37°C, 5% CO_2. THP-1 cells were collected by centrifugation at 1,000 × *g* for 10 min at 4°C.

To recover and count the ingested mycobacteria, THP-1 cells were lysed by resuspending the cell pellets in 1 ml of sterile water, followed by a series of vortex mixing for 10 min at room temperature. 24-well plates containing 2 ml Middlebrook 7H10 agar with 10% Oleic Acid+ADC (OADC) (BD, BBL, Becton Dickinson) were prepared. Four serial 1/10 dilutions were made, and 10 μl of the concentrated mycobacterial suspension and diluted suspension from each time point was spotted onto the 7H10 agar wells. The 24-well plates were secured with parafilm and wrapped in aluminum foil, inverted and incubated at 37°C for 10–14 days. Wells were photographed, and the colony-forming unit (CFU) count determined. The same procedure was used to quantify the initial input number of bacteria incubated with THP-1 cells.

Fluorescence Microscopy for Phagocytosis Assay

THP-1 cells were cultured as described above and seeded at 1×10^5 cells per 13 mm coverslip and differentiated with PMA as described above. GFP-expressing *M. bovis* BCG was incubated with 0, 1, 10 μg/ml of TSR4+5 for 2 h at 37°C in buffer 1. Cells were also incubated with 10 μg/ml of BSA as a negative control.

TABLE 1 | Primers used for quantitative real-time PCR.

	Forward primer	Reverse primer
18S	5′-ATGGCCGTTCTTAGTTGGTG-3′	5′-CGCTGAGCCAGTCAGTGTAG-3′
IL-1β	5′-GGACAAGCTGAGGAAGATGC-3′	5′-TCGTTATCCCATGTGTCGAA-3′
IL-6	5′-GAAAGCAGCAAAGAGGCACT-3′	5′-TTTCACCAGGCAAGTCTCCT-3′
IL-10	5′-TTACCTGGAGGAGGTGATGC-3′	5′-GGCCTTGCTCTTGTTTTCAC-3′
IL-12	5′-AACTTGCAGCTGAAGCCATT-3′	5′-GACCTGAACGCAGAATGTCA-3′
TGF-β	5′-GTACCTGAACCCGTGTTGCT-3′	5′-GTATCGCCAGGAATTGTTGC-3′
TNF-α	5′-AGCCCATGTTGTAGCAAACC-3′	5′-TGAGGTACAGGCCCTCTGAT-3′

Cells were washed twice in PBS and then resuspended in plain RPMI media. 1×10^6 GFP-*M. bovis* BCG was added to the THP-1 cells (MOI of 10:1) and incubated for phagocytosis for 2 h at 37°C. THP-1 cells were then washed three times in PBS to remove extracellular bacteria and then fixed in 4% paraformaldehyde for 5 min. After washing three times in PBS, THP-1 cells were incubated with 2 μg/ml of AlexaFluor546-conjugated wheat germ agglutinin (Invitrogen) to reveal the plasma membrane. Cells were then washed three times and mounted using Vectashield antifade with DAPI (Vector Labs) to reveal nucleus. Slides were observed under a Leica DM4000 fluorescence microscope at 40× magnification. Images were processed using Image J (see text footnote 1).

Quantitative Real-Time PCR (qPCR) Analysis of mRNA Expression of Cytokines

THP-1 cell pellets were collected from each time point as described above. RNA extraction was performed using the GenElute Mammalian Total RNA Purification Kit (Sigma-Aldrich) according to the manufacturer's protocol. Samples were then treated with DNase I (Sigma-Aldrich) to remove any contaminating DNA according to the manufacturer's protocol. The amount of RNA was measured using the NanoDrop 2000/2000c spectrophotometer (Thermo Fisher Scientific) at 260 nm, and the ratio of absorbance at 260 and 280 nm was used to assess the purity of the RNA. Complementary DNA (cDNA) was synthesized using High Capacity RNA to cDNA Kit (Applied Biosystems, UK) according to the manufacturer's protocol. Primer sequences (**Table 1**) were designed and analyzed for specificity using the nucleotide Basic Local Alignment Search Tool and Primer-BLAST.[2]

PCR was performed on all cDNA samples to assess the quality of the cDNA. The qPCR assays were performed for the expression of pro- and anti-inflammatory cytokines. The qPCR reaction consisted of 5 μl Power SYBR Green MasterMix (Applied Biosystems), 75 nM of forward and reverse primer, 500 ng template cDNA in a 10 μl final reaction volume. qPCR was performed in a 7900HT Fast Real-Time PCR System (Applied Biosystems). The initial steps were 2 min incubation at 50°C followed by 10 min incubation at 95°C, the template was then amplified for 40 cycles under these conditions: 15 s incubation at 95°C and 1 min incubation at 60°C. Samples were normalized using the expression of human 18S rRNA. Data were analyzed using the relative quantification (RQ) Manager Version 1.2.1 (Applied Biosystems). Cycle threshold (Ct) values for each cytokine target

[2]http://blast.ncbi.nlm.nih.gov/Blast.cgi.

gene were calculated, and the relative expression of each cytokine target gene was calculated using the RQ value, using the formula: $RQ = 2^{-\Delta\Delta Ct}$ for each cytokine target gene, and comparing relative expression with that of the 18S rRNA constitutive gene product. Assays were conducted twice in triplicate.

Multiplex Analysis

Supernatants were collected from the phagocytosis assay at 24 and 48 h to determine the levels of secreted cytokines (IL-6, IL-10, IL-12p40, IL-12p70, IL-1α, IL-1β, TNF-α, IL-13, IL-15, IL-17A, IL-9, and TNF-β), chemokines (MCP-3, MDC, Eotaxin, Fractalkine, GRO, IL-8, IP-10, MCP-1, and MIP-1α), growth factors (IL-2, EGF, FGF-2, G-CSF, GM-CSF, IL-3, IL-4, IL-5, IL-7, and VEGF), and other related ligands and receptors (IFN-α2, IFN-ϒ, FLT-3L, IL-1RA, and sCD40L). MagPix Milliplex kit (EMD Millipore) was used to measure immune response following the manufacturer's protocol. 25 µl of assay buffer was added to each well of a 96-well plate, followed by the addition of 25 µl of standard, controls or supernatants of cells treated with *M. bovis* BCG in the presence or absence of properdin and MBP-TSR4+5. 25 µl of magnetic beads coupled to analytes of interest was added in each well and incubated for 18 h at 4°C. The 96-well plate was washed with the assay buffer, and 25 µl of detection antibodies was incubated with the beads for 1 h at room temperature. 25 µl of streptavidin–phycoerythrin was then added to each well and incubated for 30 min at room temperature with shaking at 750 rpm. Following a washing step, 150 µl of sheath fluid was added to each well, and the plate was read using the Luminex Magpix instrument. Assays were conducted in duplicate.

Statistical Analysis

Analysis of data for statistical significance was conducted using GraphPad Prism 6 for Windows (GraphPad Software, Inc.). Statistical analyses were made using two-way ANOVA for mRNA expression data and a one-way ANOVA for the multiplex data. p Values < 0.05 were considered statistically significant, unless otherwise stated (non-significant).

RESULTS

Human Properdin and TSR4+5 Bind to Mycobacteria

Human properdin was purified from human plasma. SDS-PAGE, followed by western blotting using antihuman properdin polyclonal antibodies, showed a distinct band at 55 kDa (**Figure 1A**), which was the expected molecular weight of the glycosylated monomer. The two biologically active modules of properdin TSR4 and TSR5 were expressed together in tandem as previously described, fused to MBP (7), and is also shown on an SDS-PAGE gel, which has a molecular weight of 55 kDa (**Figure 1B**). Using gel filtration chromatography, we found that human properdin eluted as a mixture of monomer, dimer and trimer; a negligible amount probably formed aggregates. Nearly 60% of MBP-TSR4+5 appeared as a monomer while nearly 40% was found to migrate as a dimer (data not shown).

The binding of properdin to *M. bovis* BCG was observed to be in a dose-dependent manner; BSA was used as a negative control that showed almost no binding (**Figure 2A**). TSR4+5 binding was also observed to be in a dose-dependent manner. MBP was used as a negative control (**Figure 2B**). The two binding curves cannot be compared quantitatively, as different detection antibodies were used. Because the MBP-TSR4+5 recombinant protein and properdin monomer have about the same molecular weight, 5 µg of TSR4+5 corresponds in molar terms to about 5 µg of properdin monomer (**Figures 1A,B**). The binding of a mixture of the two separately expressed TSR4, and TSR5 is much lower than that of the combined expressed TSR4+5 (**Figure 2B**). For this comparison, the same detection antibody was used. These results suggest that both TSR4 and TSR5 modules contribute to the interaction with *M. bovis* BCG, and that TSR4+5 binds

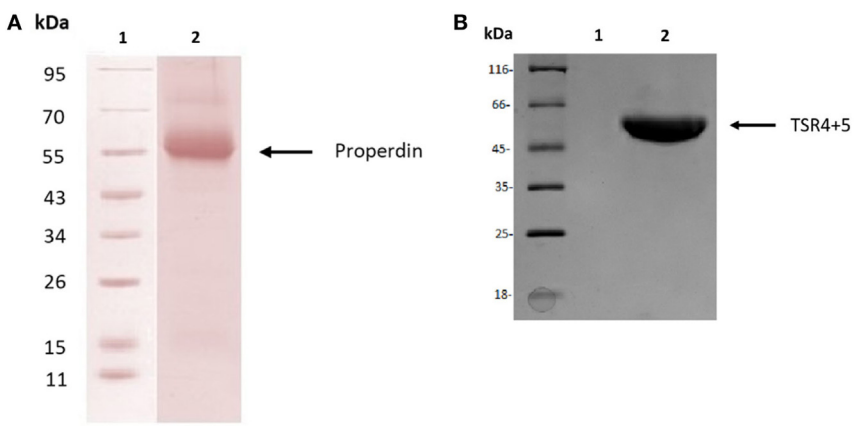

FIGURE 1 | Purified human properdin and recombinant maltose-binding protein (MBP)-thrombospondin repeats (TSR) 4+5. **(A)** Properdin was purified from human plasma. Filtered plasma was applied to a non-immune IgG-Sepharose column, then to a mouse monoclonal anti-properdin Sepharose column; properdin was eluted with 3 M $MgCl_2$. The eluted samples were dialyzed against HEPES buffer (10 mM HEPES, 140 mM NaCl, 0.5 mM EDTA, pH 7.4) overnight at 4°C. Contaminants were removed by applying the protein to a Q Sepharose column, and the product appears as a single band on SDS-PAGE and western blot at about 55 kDa. **(B)** MBP-TSR4+5 was purified *via* an amylose resin column, and the purified fusion protein also appears on SDS-PAGE as a band of about 55 kDa.

with similar characteristics to that of whole properdin on *M. bovis* BCG surface. These results were further confirmed using microscopy where TSR4+5 specifically bound to *M. bovis* BCG in a dose-dependent manner (**Figure 2C**).

Properdin Inhibits Uptake of *M. bovis* BCG by THP-1 Cells

Properdin inhibited the uptake of *M. bovis* BCG by THP-1 cells. At a concentration of 20 μg/ml, uptake of *M. bovis* BCG was significantly reduced by properdin (**Figure 3A**). TSR4+5 was also able to substantially inhibit uptake of *M. bovis* BCG by THP-1 cells (**Figure 3B**). The effect of properdin and

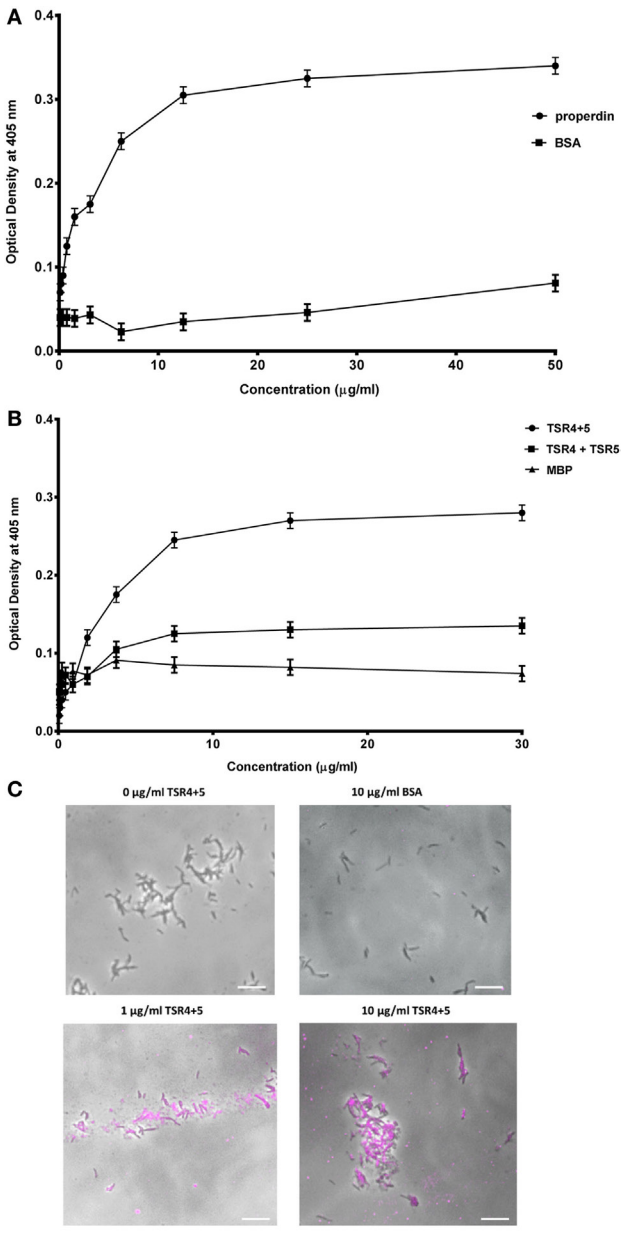

FIGURE 2 | Continued

FIGURE 2 | Human properdin binds mycobacteria *via* thrombospondin repeats (TSR) 4+5. **(A)** Properdin binding to mycobacteria; BSA was used as a negative control protein. **(B)** Comparison between TSR4+5 and individual TSR4 and TSR5 binding to mycobacteria; maltose-binding protein (MBP) as negative control. Assays were conducted in 10 mM HEPES, 140 mM NaCl, 0.5 mM $CaCl_2$ + 0.5 mM $MgCl_2$, 100 μg/ml hen ovalbumin, and pH 7.5. Serial dilutions of properdin were incubated in mycobacteria coated wells followed by incubation with mouse anti-properdin monoclonal antibody and mouse anti-BSA monoclonal antibody, respectively; serial dilutions of TSR4+5, TSR4 or TSR5 were incubated in another set of mycobacteria coated wells followed by incubation with mouse anti-MBP monoclonal antibody. Anti-mouse IgG conjugated with alkaline phosphatase and substrate *p*-nitrophenol phosphate were incubated in both sets of wells, and the color was measured at 405 nm using a plate reader. Assay was conducted in quadruplicate. Error bars represent SD. **(C)** Differential direct binding of 0, 1, and 10 μg/ml of TSR4+5 to *Mycobacterium bovis* BCG. 10 μg/ml of BSA was used as a negative control. Cells were incubated for 2 h with either TSR4+5 or BSA. Cells were washed, fixed, and stained with mouse anti-MBP monoclonal antibody followed by goat anti-mouse 1gG-conjugated with AlexaFluor488. Images are shown as single sections taken using a Leica DM4000 microscope; bar scale 10 μm.

TSR4+5 on the phagocytosis of *M. bovis* BCG was dose dependent. The input number of *M. bovis* BCG was about 7.8×10^6 CFU/ml, which was the total number of bacteria added to THP-1 cells. Without properdin or TSR4+5, 5.0×10^6 CFU/ml of *M. bovis* BCG was phagocytosed which was approximately 66% efficiency of phagocytosis compared with the input number. At the highest concentration tested, properdin showed an inhibition of uptake of approximately 60% compared with *M. bovis* BCG with no properdin (**Figure 3A**). For TSR4+5, the effect on *M. bovis* BCG was slightly lower at approximately 40% inhibition (**Figure 3B**). These results were also confirmed by microscopy, with TSR4+5 having a suppressive effect on the uptake of GFP-expressing *M. bovis* BCG by THP-1 cells (**Figure 3C**). PMA stimulation was used to induce differentiation of THP-1 cells before incubation with *M. bovis* BCG. PMA has been shown to activate protein kinase C and increase cell adherence and expression of surface markers associated with macrophage differentiation (30). These data show that (i) properdin has an anti-opsonic effect on *M. bovis* BCG, inhibiting phagocytosis; and (ii) TSR4+5 modules play a major role in this interaction of *M. bovis* BCG and macrophages. These observations demonstrate, for the first time, a novel, non-complement-related role for properdin in host–pathogen interactions in tuberculosis.

Properdin Induces a Pro-Inflammatory Response During the Early Phase of Phagocytosis of *M. bovis* BCG by THP-1 Cells

The effect of properdin on the inflammatory response during the phagocytosis of *M. bovis* BCG was measured. The gene expression of key pro- and anti-inflammatory cytokines in tuberculosis was determined using quantitative real-time PCR. Our data showed that properdin significantly enhanced the upregulation of pro-inflammatory cytokines TNF-α, IL-1β, and IL-6 from THP-1 cells challenged by *M. bovis* BCG (**Figure 4A**), particularly at the

initial stage of uptake (within the first hour of phagocytosis), which decreased gradually toward the later stages of phagocytosis. The increase in TNF-α transcript was particularly striking as TNF-α is well known for activating macrophages for killing of intracellular mycobacteria. In addition, TNF-α is a key mediator in the early stages of granuloma formation. By contrast, the anti-inflammatory cytokines measured from THP-1 cells (IL-10 and TGF-β) were shown to be downregulated in the presence of properdin, when challenged by *M. bovis* BCG (**Figure 4B**). IL-12 also appeared to be downregulated (**Figure 4A**). Properdin, therefore, appears to play an important role in pro-inflammatory cytokine production by macrophages infected by *M. bovis* BCG, which may have significant implications in shaping the adaptive immune response during *M. tuberculosis* infection.

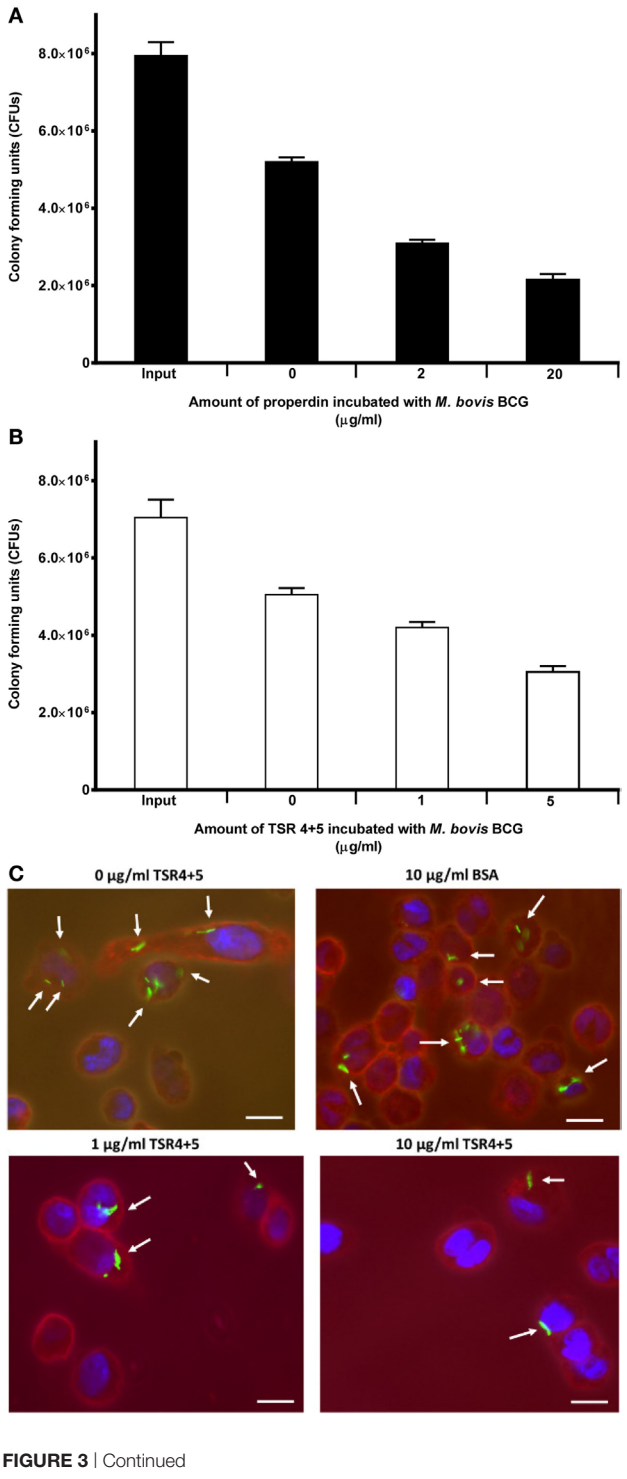

FIGURE 3 | Continued

FIGURE 3 | Effect of properdin and thrombospondin repeats (TSR) 4+5 on the phagocytosis of *Mycobacterium bovis* BCG by THP-1 cells. **(A)** *M. bovis* BCG was treated with properdin at concentrations of 0, 2, and 20 μg/ml or with **(B)** TSR4+5 at concentrations 0, 1, and 5 μg/ml. The mycobacteria were incubated with macrophage for 2 h. After THP-1 cell lysis, surviving internalized *M. bovis* BCG were measured by plating lysates on 7H10 media to obtain colony-forming units (CFUs). The input value is the starting number of *M. bovis* BCG added to the THP-1 cells, before phagocytosis. A one-way ANOVA test was performed on the data to determine significant differences in CFU count by properdin or TSR4+5. All comparisons were significant ($p < 0.05$), unless where shown (ns, not significant, $p > 0.05$). Samples were analyzed in triplicate. **(C)** Differential uptake of GFP-*M. bovis* BCG by THP-1 macrophages after treatment with 0, 1, and 10 μg/ml of TSR4+5, or 10 μg/ml of BSA, used as a negative control. Cells were incubated for 2 h. Cells were then washed, fixed, and stained with AlexaFluor546-conjugated wheat germ agglutinin to reveal the plasma membrane (red), and the nucleus was stained with DAPI (blue). Images are shown as single sections, taken using a Leica DM4000 microscope; bar scale 10 μm.

Cytokine gene expression by THP-1 cells infected with *M. bovis* BCG were also studied in the presence of TSR4+5, which revealed that TSR4+5 also has a significant effect on the pro-inflammatory response. TNF-α was upregulated (**Figure 5A**), while IL-10 was found to be downregulated (**Figure 5B**), during the first hour of phagocytosis. IL-12 was also shown to be significantly downregulated (**Figure 5A**). These data mirror the observations for properdin, and hence, validate the importance of TSR4+5 in the binding of properdin to *M. bovis* BCG and in its modulation of the inflammatory response. These data are also similar to recent published observations of another complement regulatory protein, factor H (19), thus offering potentially novel insights into the involvement of these proteins in host–pathogen interactions in tuberculosis.

Multiplex Analysis of Cytokine Secretion

The inflammatory response during the phagocytosis of *M. bovis* BCG by THP-1 cells was further determined by measuring the secretion of cytokines, chemokines, and other growth factors using the Multiplex analysis of supernatants collected at 24 and 48 h post phagocytosis (**Figures 6A–D**). The secretion of pro-inflammatory cytokines TNF-α, IL-1β, and IL-1α was significantly enhanced by treatment with properdin or TSR4+5 at the 24 h time point (**Figure 6A**). The enhancement of these pro-inflammatory cytokines can be critical for controlling mycobacterial infection, particularly in the formation of the granuloma. However, by 48 h, there was a decrease in the production of pro-inflammatory cytokines (IL-6, IL-12p40, IL-12p70, IL-1α, IL-1β, TNF-α, IL-13, IL-15, and IL-9) in the presence of properdin- and TSR4+5-treated *M. bovis* BCG (**Figure 6A**). Properdin and TSR4+5 also downregulated the

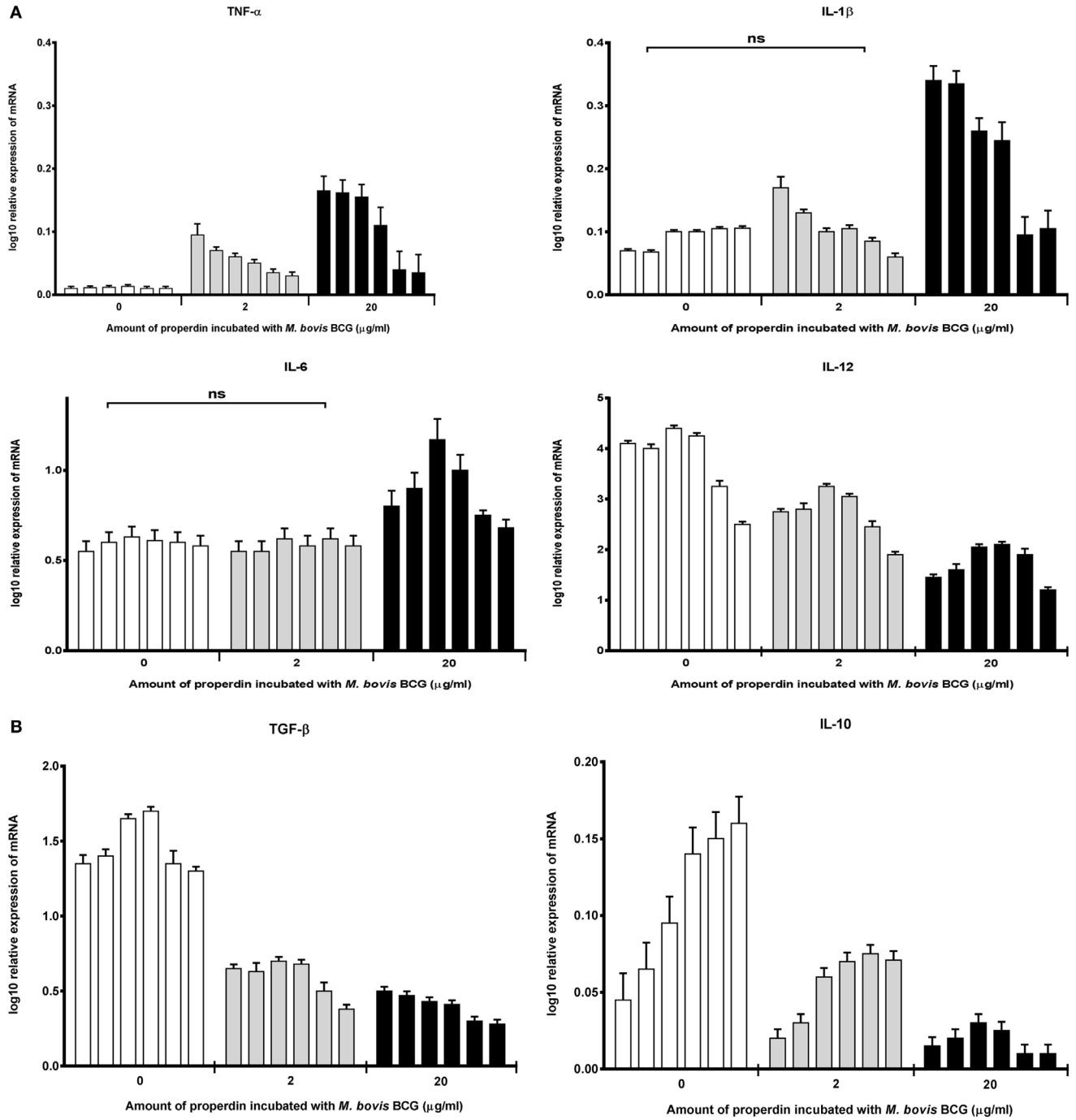

FIGURE 4 | Temporal mRNA expression profile of cytokines produced by THP-1 cells incubated with different concentrations of properdin and *Mycobacterium bovis* BCG. **(A)** Pro-inflammatory cytokines: TNF-α, IL-1β, IL-6, and IL-12; **(B)** anti-inflammatory cytokines: TGF-β and IL-10. The expression of each cytokine was measured using qPCR, and the relative expression [relative quantification (RQ)] calculated by normalizing the data using human 18S rRNA expression as a control. The RQ value was calculated using the formula: $RQ = 2^{-\Delta\Delta Ct}$. Assays were conducted twice in triplicates. Error bars represent SD. A two-way ANOVA test was performed on the data to determine significant differences in expression of cytokine production by properdin. All comparisons were significant ($p < 0.05$), unless where shown (ns, not significant, $p > 0.05$).

anti-inflammatory response such as IL-10 after 24 and 48 h of phagocytosis, although this was less pronounced for IL-12 at 48 h (**Figure 6A**). These observations again mirror the initial responses observed in cytokine gene expression of during the first few hours of phagocytosis, in the presence of properdin or TSR4+5 (**Figures 5A,B**). The effect of properdin and TSR4+5 also led to marked downregulation of a number of growth factors MCP-3 (24 h), MDC, Eotaxin, Fractalkine (24 h), GRO

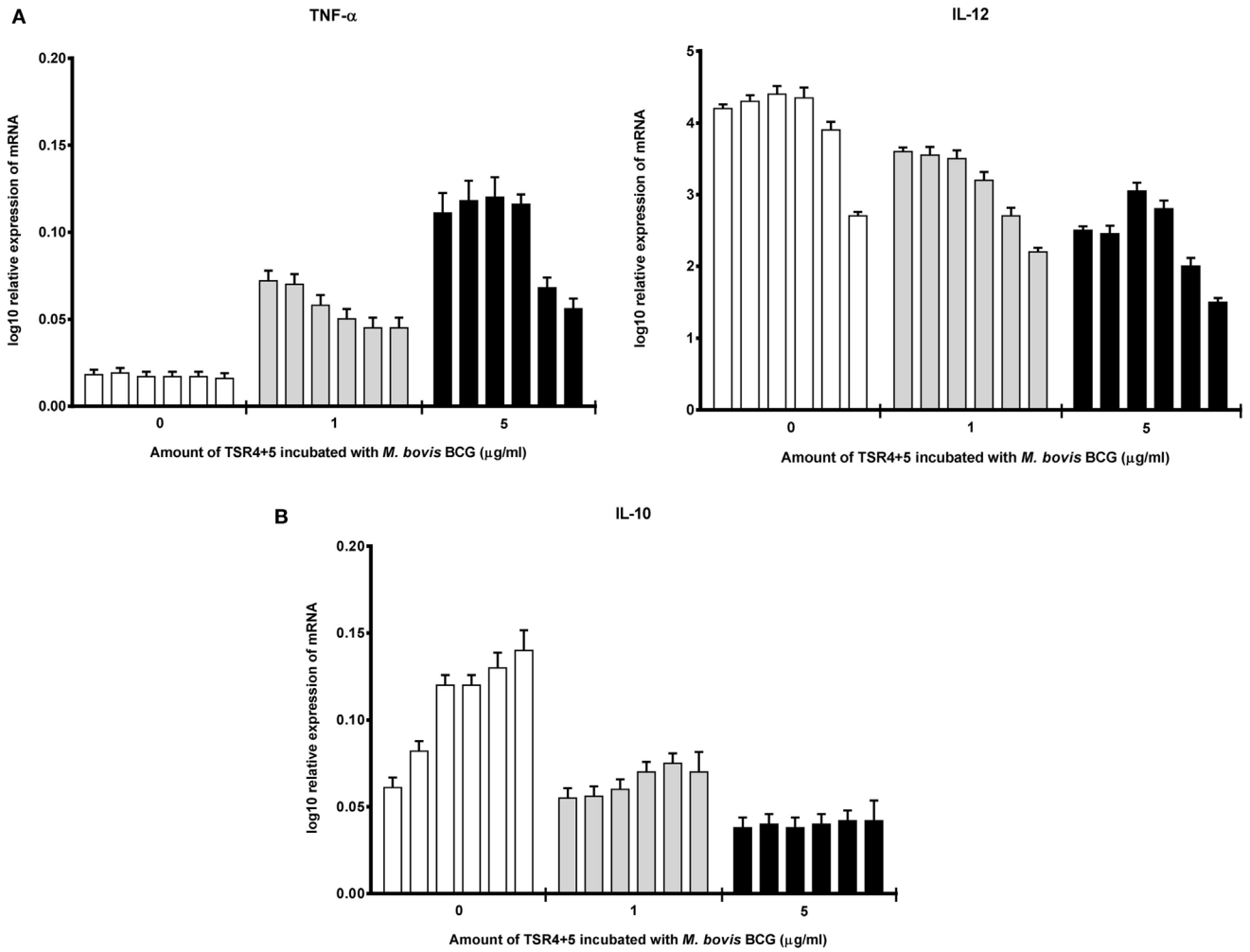

FIGURE 5 | Temporal mRNA expression profile of cytokines produced by THP-1 cells incubated with different concentrations of thrombospondin repeats (TSR) 4+5 and *Mycobacterium bovis* BCG. **(A)** Pro-inflammatory cytokines: TNF-α and IL-12; **(B)** anti-inflammatory cytokine: IL-10. The expression of each cytokine was measured using qPCR, and the relative expression [relative quantification (RQ)] calculated by normalizing the data using human 18S rRNA expression as a control. The RQ value was calculated using the formula: $RQ = 2^{-\Delta\Delta Ct}$. Assays were conducted twice in triplicates. Error bars represent SD. A two-way ANOVA test was performed on the data to determine significant differences in expression of cytokine production by TSR4+5. All comparisons were significant ($p < 0.05$), unless where shown (ns, not significant, $p > 0.05$).

(24 h), IP-10, MCP-1, MIP-1, VEGF, G-CSF (48 h), GM-CSF (48 h), and VEGF (24 h) (**Figures 6B,C**). Additional ligands and receptors (IFN-α2, IFN-γ, FLT-3L, IL-1RA, and sCD40L) did not show any significant changes (**Figure 6D**).

DISCUSSION

We have previously shown that a complement regulatory protein, factor H, can bind to *M. bovis* BCG and inhibit its uptake by THP-1 macrophages (19). Factor H can also enhance the pro-inflammatory response during this host–pathogen interaction (19). This study highlighted a novel complement-independent property of factor H as an anti-opsonin and in the modulation of the inflammatory response against a pathogen. With the goal of further elucidating the role of complement control proteins in the early stages of mycobacterial infection, this study looked at the role of properdin, an upregulator of the alternative complement pathway. Properdin and thrombospondin repeat (TSR) modules TSR4+5 were shown to bind to *M. bovis* BCG and inhibit bacterial uptake by THP-1 cells, augmenting the inflammatory response. These observations are similar to what has been observed previously with factor H (19), which is intriguing, since properdin and factor H have opposing effects on the regulation of complement activation (3). These findings were also consistent with previous reports, which have demonstrated that properdin deficient mice have a reduced M1 (IL-1β) and increased M2 (arginase-1, MCP-1, IL-10) profile, crucial for the tumor microenvironment (31). This suggests that the production of IL-1β and reduction in IL-10 mediated by properdin may be required for protection against *M. tuberculosis* in the initial phase of infection.

The functions of properdin have been extensively investigated within the remit of the complement alternative pathway, and

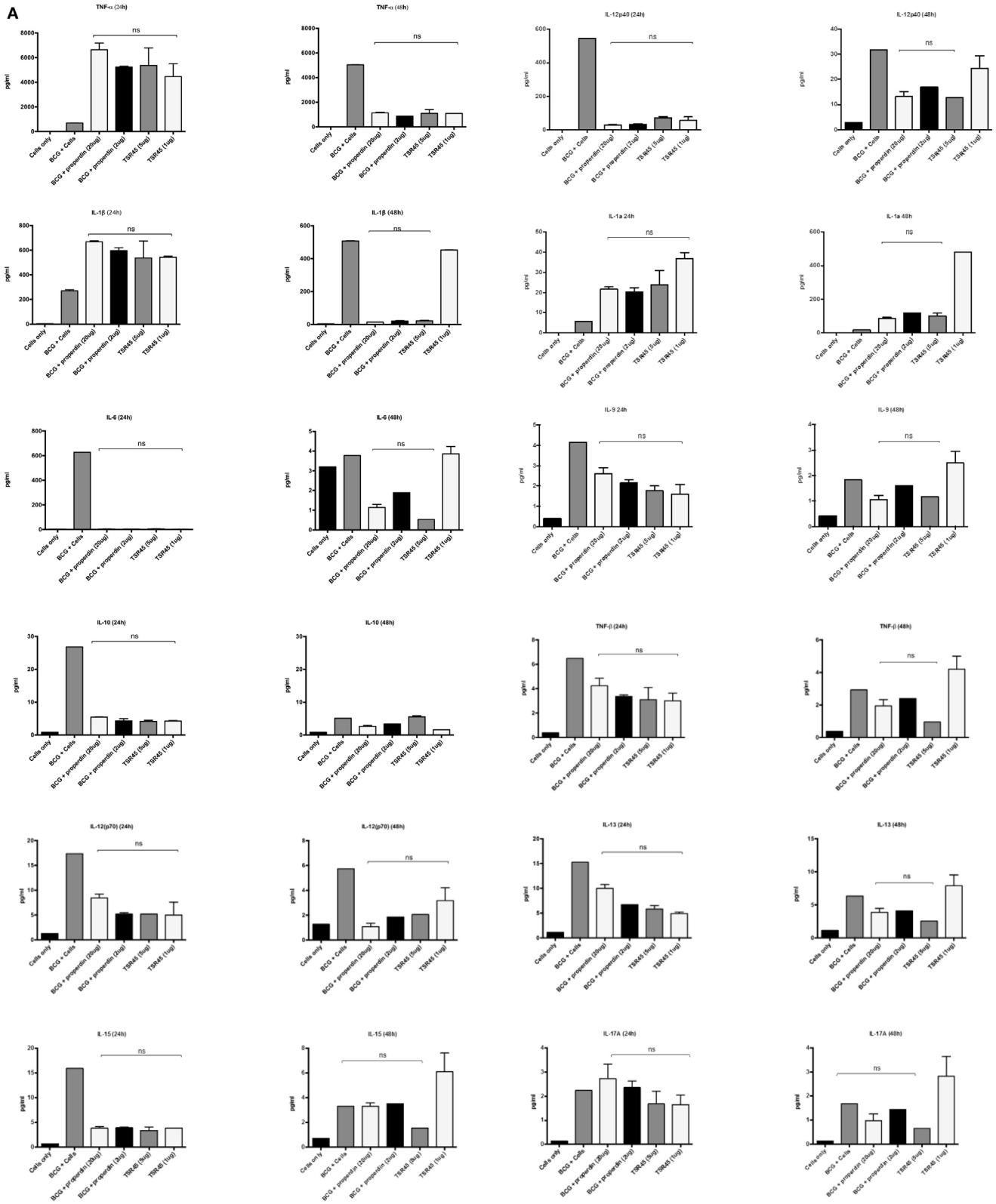

FIGURE 6 | Continued

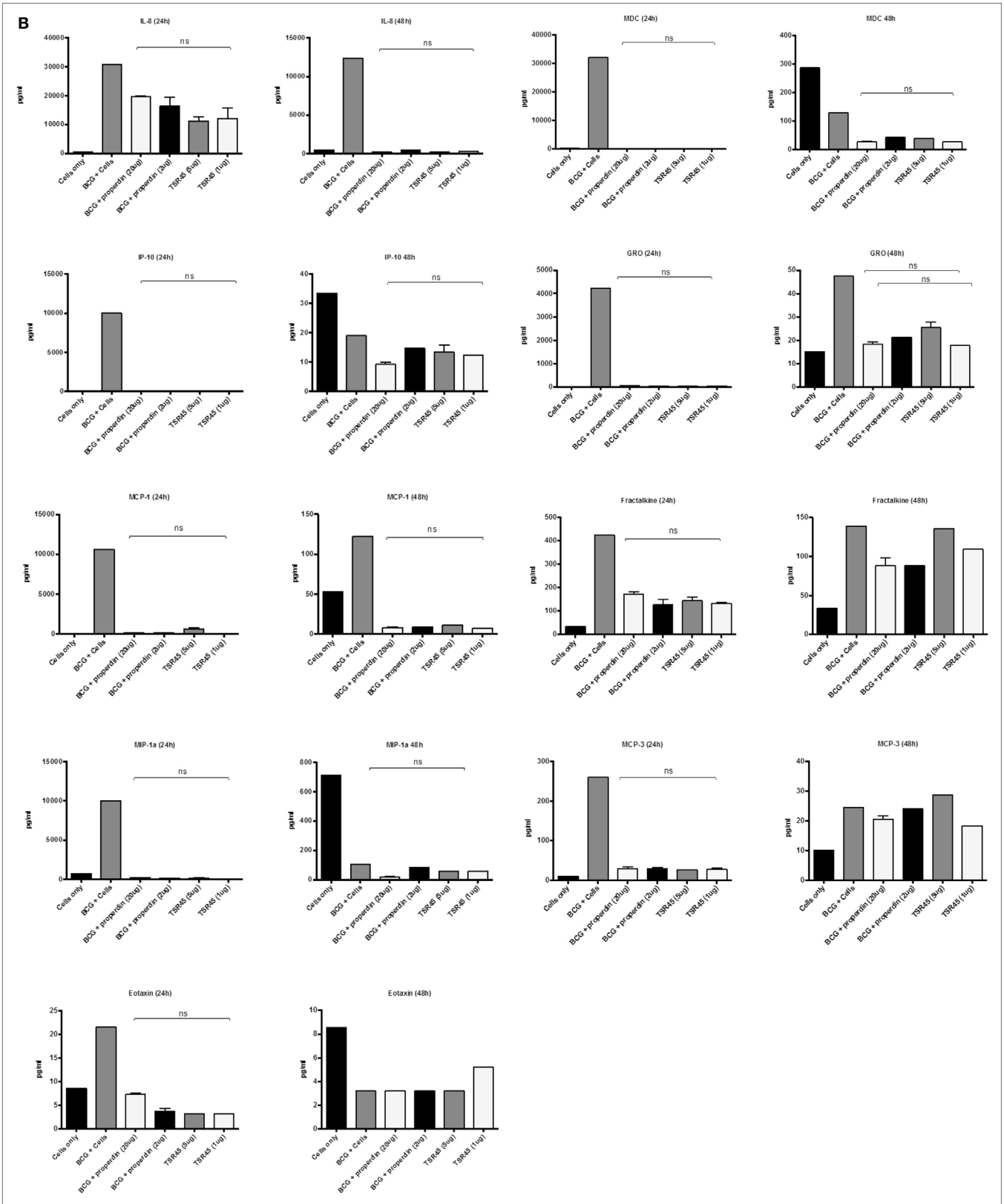

FIGURE 6 | Continued

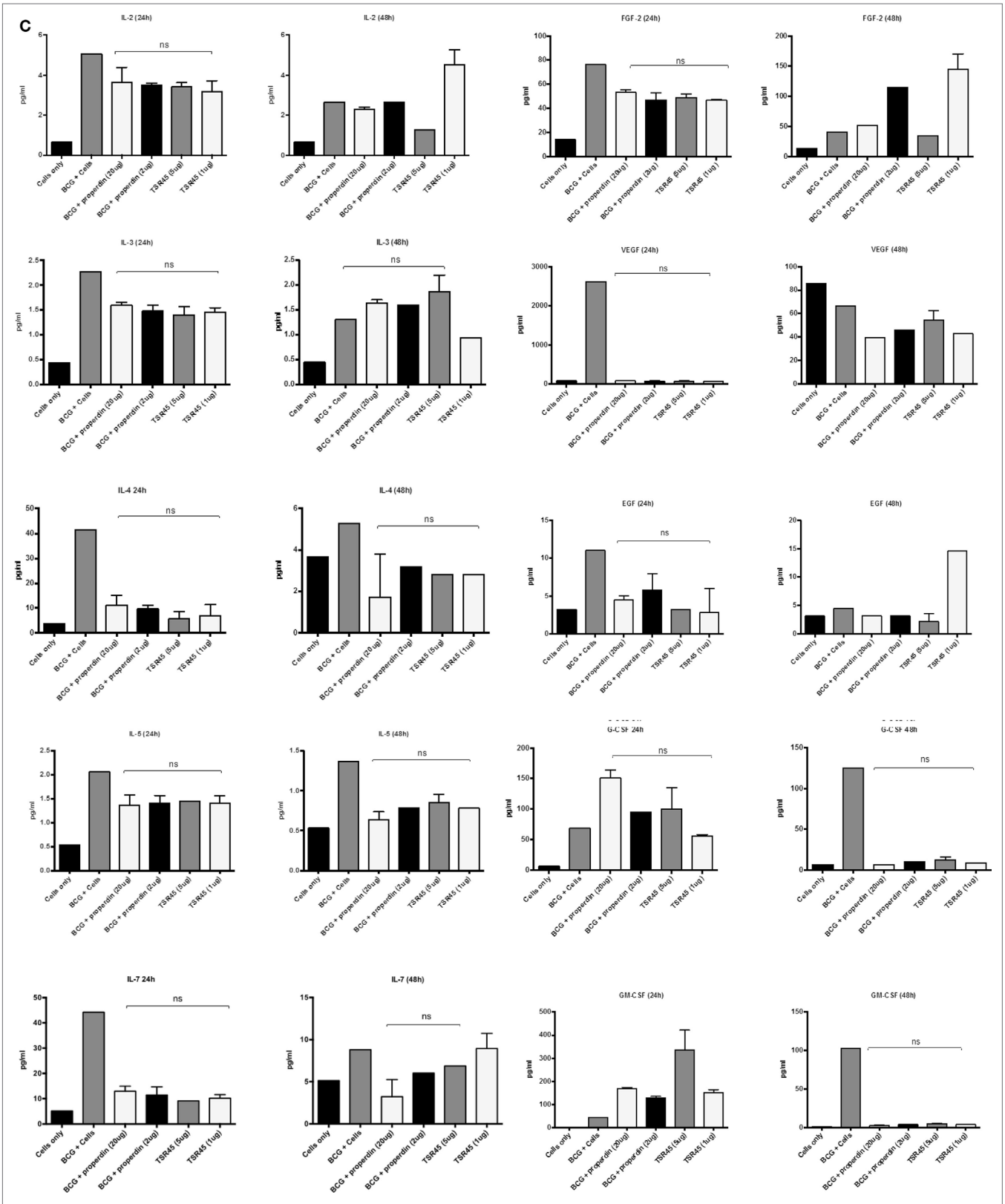

FIGURE 6 | Continued

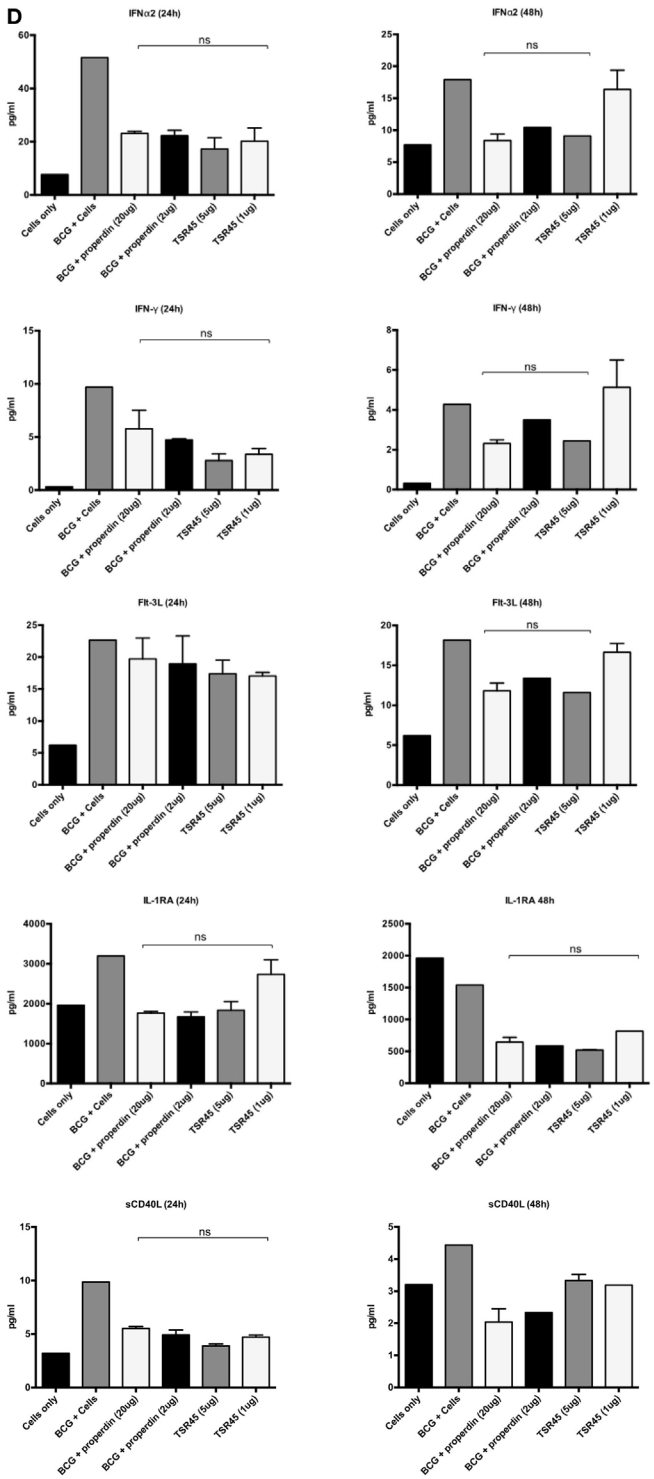

FIGURE 6 | Multiplex cytokine analysis of supernatants collected at 24 and 48 h phagocytosis of *Mycobacterium bovis* BCG by THP-1 cells incubated with or without properdin and thrombospondin repeats (TSR) 4+5. The supernatants were collected from phagocytosis assay of *M. bovis* BCG in the presence or absence of properdin and TSR4+5 at 24 and 48 h time point. The levels of cytokine production were measured for **(A)** (IL-6, IL-10, IL-12p40, IL-12p70, IL-1α, IL-1β, TNF-α, IL-13, IL-15, IL-17A, IL-9, and TNF-β), **(B)** chemokines (MCP-3, MDC, Eotaxin, Fractalkine, GRO, IL-8, IP-10, MCP-1, and MIP-1α), **(C)** growth factors (IL-9, IL-2, EGF, FGF-2, G-CSF, GM-CSF, IL-3, IL-4, IL-5, IL-7, and VEGF), and **(D)** related ligands and receptors (IFN-α2, IFN-γ, FLT-3L, IL-1RA, and sCD40L) using multiplex analysis. Error bars represent SD. A one-way ANOVA test was performed on the data to determine significant differences in expression of cytokine production by properdin or TSR4+5. All comparisons were significant ($p < 0.05$), unless where shown (ns, not significant, $p > 0.05$). Supernatants were analyzed in duplicate.

its involvement with pathogens has largely been characterized as complement dependent. In this study, we aimed to look at the complement-independent interaction of properdin with mycobacteria (i.e., effects in the absence of other complement proteins), with a view to examining its possible role in the pathogenesis of tuberculosis. The role of complement in tuberculosis has been examined, but little is understood about the role of the individual complement proteins in tuberculosis infection, especially complement control proteins. Properdin has been shown to play a role in a number of pathogenic infections such as those by *C. pneumoniae*, in which properdin promotes complement C3b deposition and opsonization (12). A recent study also demonstrated that a low dose of properdin, which is highly polymerized, is able to protect against *N. meningitidis* and *Streptococcus pneumoniae*, by assembling the alternative complement pathway (16). The central premise in these recent studies is that properdin is an upregulator of the complement alternative pathway, and thus, when in contact with pathogens, the alternative pathway is triggered and stabilized by properdin.

Properdin has also been shown to enhance the uptake of apoptotic T cells by dendritic cells (DCs) and macrophages, thus promoting phagocytosis (27). Properdin may also bind to the DNA found to be exposed on apoptotic and necrotic cells, suggesting that this may also be a crucial site for alternative pathway activation (32). There is recent evidence to suggest that properdin, locally produced by tolerogenic DCs, binds to necrotic cells, confirming its role a pattern recognition molecule of the innate immunity. In addition, properdin is also involved in the interaction of DC and T cell responses. Interestingly, silencing of properdin by treating DCs with siRNA in the presence/absence of IFN-γ reduced the proliferation of allogenic T cells (33). Properdin binds to early apoptotic cells via sulfated GAGs, resulting in C3b deposition and uptake by phagocytes. Activation of neutrophils drives the deposition of properdin, which binds apoptotic T cells. Since properdin has been shown to bind apoptotic cells via GAGs (27) or DNA, it remains unclear what other ligands and receptors are involved in properdin–apoptotic cell interaction. It is likely that properdin as a soluble factor is acting as an adaptor molecule. Furthermore, properdin also binds to NKp46 expressed on natural killer cells, innate lymphoid cells (ILC)1 and ILC3. This study demonstrated that the control of meningococcal infection was dependent on NKp46 and group 1 ILCs, further elucidating the role of properdin as an independent pattern recognition molecule (34).

In our study, we show that purified native properdin and TSR4+5 bind to *M. bovis* BCG in a dose-dependent manner, suggesting that the binding of properdin to *M. bovis* BCG may be *via* TSR4+5. The physiological concentration of properdin in serum is about 25 μg/ml (35). We also demonstrate that coating of *M. bovis* BCG with properdin inhibits the uptake of the bacterium by THP-1 cells; however, only about 60% inhibition was achieved at the highest dose of native properdin. TSR4+5 was also able to mirror the effects of properdin, in inhibiting the uptake of *M. bovis* BCG by macrophages by up to 40%.

The recruitment of properdin by mycobacteria may be particularly crucial in the initial stages of tuberculosis infection, when after inhalation, the first host cell *M. tuberculosis* encounters is the alveolar macrophage.

In the lungs, mycobacteria are phagocytosed by alveolar macrophages, which are unable to completely eliminate them, and so produce crucial chemoattractants (36), which recruit inflammatory cells such as neutrophils, macrophages, γδ-T cells, and natural killer cells that stimulate inflammation and tissue remodeling (36–38). Our findings may be indicative of the early inflammatory processes *in vivo*, involved in granuloma formation, which are nodular-type lesions that cordon-off *M. tuberculosis* infection, and provide an environment for the bacilli to persist and survive as a latent infection. TNF-α and IFN-γ are involved in recruitment of cells in the granuloma (39, 40). Thus, properdin may play a role in granuloma formation by promoting pro-inflammatory cytokines. Inflammatory balance is essential particularly of Th2/Th1 cytokines, which are required to maintain a protective granuloma (41). This is determined by the balance in IFN-γ/TNF-α versus IL-4/IL-10/TGF-β within the granuloma. Properdin and TSR4+5 may be implicated in maintaining this balance. It is not known whether complement proteins reside in the granuloma; however, during infection, complement proteins may be produced locally at sites of infection. Properdin may be secreted by neutrophils, monocytes and T cells locally at the site of infection (3). Thus, innate immune molecules residing in or being recruited at sites of infection may play a role in the balance of Th1/Th2, which may cause granuloma necrosis and replication of *M. tuberculosis* (41–43).

TNF-α was dramatically increased in the first 24 h of phagocytosis in the presence of properdin and TSR4+5, compared to non-treated mycobacteria. TNF-α plays a major role in granuloma formation and our results suggest that properdin may have a role in potentiating the pro-inflammatory response that results in granuloma formation. These observations are further strengthened by the concurrent increase in IL-1α levels over 24 h which have been shown to be key in macrophage proliferation and maturation during granuloma formation (44).

During phagocytosis, pro- and anti-inflammatory cytokines were produced by THP-1 cells when treated with properdin or TSR4+5. In the initial stages of infection by *M. bovis* BCG, pretreated with properdin, during phagocytosis, the expression of TNF-α was significantly enhanced. Other pro-inflammatory responses that were also elevated in the presence of properdin at initial stages of infection are IL-1β and IL-6. IL-1β is a mediator of inflammation and is required for host resistance to *M. tuberculosis* infection (45). IL-6 is a biomarker for tuberculosis, as increased levels are observed in patients with tuberculosis (46) that is required for a T cell response against *M. tuberculosis* infection (47, 48). Conversely, IL-10, IL-12, and TGF-β were downregulated by properdin, thus suppressing the anti-inflammatory response. The downregulation of IL-12 by properdin *in vivo* may suppress the Th1 response. TSR4+5 was also able to mimic the cytokine response like properdin, suggesting that the modules responsible for the major part of the interaction with *M. bovis* BCG may be TSR4+5.

Macrophages play a significant role in the innate immune response to pathogens and so are also crucial for an adaptive immune response (49). However, *M. tuberculosis* can evade the innate immune defense, inhibiting phagosome maturation (36), resisting anti-microbial agents damaging the bacterial cell wall

and facilitating replication within the host and escaping early immune recognition. Thus, these pathogens interfere with the early immune response and the induction of pro-inflammatory cytokines (49).

IL-10 and TGF-β suppression by properdin may enhance the clearance of mycobacteria by the host during the early stages of *M. tuberculosis* infection. After phagocystosis of *M. tuberculosis*, IL-10 has been shown to block phagolysosome maturation and antigen presentation by macrophages, thus aiding the survival of the pathogen (50, 51). Furthermore, IL-10 can inhibit the generation of reactive oxygen and nitrogen intermediates in IFN-γ activated macrophages, which are required for intracellular killing (52, 53). The enhanced levels of IL-10 and TGF-β in the lungs of active tuberculosis patients demonstrate a weakened immune response to *M. tuberculosis*, and hence, a role in the pathogenesis and disease progression (54, 55). VEGF was also found to be at a significantly higher level in tuberculosis patients with extrapulmonary tuberculosis (EPTB) than those with pulmonary disease (56). In our study, properdin and TSR4+5 seems to result in a marked elevation of VEGF after 48 h. Since our data also shows that mycobacteria have a reduced phagocytosis by macrophages, the resulting extracellular bacteria may be encouraged by VEGF to disseminate. The beneficial effect of properdin may be to inhibit the mechanisms involved in evasion and, thus, facilitate a protective response against mycobacterial infection.

The downregulation of IL-12 by properdin or TSR4+5 may be due to the reduced phagocytosis of *M. bovis* BCG, thus, downregulating the Th1 response. This may be necessary for the Th1/Th2 homeostasis in the protective granuloma (41, 57, 58). Both IL-10 and TGF-β levels were supressed, whilst TNF-α was elevated during the first 24 h after phagocytosis.

Although *M. bovis* BCG shares 99% genome homology to *M. tuberculosis*, there are some genetic differences which lead to its avirulence. The major difference between *M. bovis* BCG and *M. tuberculosis* is the large genomic deletion RD1, which causes the loss of various virulent genes coding for proteins such as ESAT-6, CFP-10 and also a bacterial secretion system (59, 60). Therefore the findings in our study will need to be validated using virulent strains of *M. tuberculosis*.

Properdin deficiency renders the host susceptible to a range of bacterial infections, especially *Neisseria* species. Three types of properdin deficiency have been reported: type I (absence of the properdin protein), type 2 (low level of properdin about 1–10% found in the serum), and type 3 deficiency (normal levels of protein being produced, but functionally defective). The most commonly reported deficiency is the type I properdin deficiency that exhibits fulminant infections. The incidence of tuberculosis has not been reported in properdin deficient subjects, possibly due to the majority of studies being in Scandinavia or western Europe, in populations where there is a low incidence of tuberculosis.

The data in this study suggest that properdin, *via* TSR4+5, may help in the clearance of mycobacterial infection by circumventing pathogen immune evasion strategies by upregulating the pro-inflammatory response. Properdin may also promote the formation and maintenance of the protective granuloma. The data in this study give further insights into the involvement of complement regulatory proteins in shaping the cellular immune response against mycobacteria in a complement activation-independent manner. Further studies are needed to fully characterize the nature and extent of involvement of properdin in tuberculosis pathogenesis, particularly in the early stages of infection.

The complement-independent interaction between human properdin and mycobacteria is a novel observation, which is independent of C3b deposition and aggregation of properdin (61). This is consistent with our recent study where we have shown that properdin can recognize chemical patterns on nanoparticles *via* TSR4+5 and modulate immune response by THP-1 cells (26) without involving complement activation/deposition. In conclusion, properdin may be involved in modulating host-pathogen interactions in tuberculosis. However, further studies are needed on pathogenic *M. tuberculosis* and *in vivo*, to understand the precise role of this complement regulatory protein in pathogenesis, which may give new insights into therapies against this formidable disease.

AUTHOR CONTRIBUTIONS

MA-M, AT, MA-A, and LK carried out crucial experiments. SA, MNA-A, AAP, VM, EMG, AK, and RBS provided crucial reagents and expertise. UK, AT and LK wrote the manuscript in addition to designing the experiments.

FUNDING

MA-A has been supported by the Ministry of Higher Education, Malaysia and the Universiti Sains Malaysia.

REFERENCES

1. Pangburn MK, Muller-Eberhard HJ. The C3 convertase of the alternative pathway of human complement. Enzymic properties of the bimolecular proteinase. *Biochem J* (1986) 235:723–30. doi:10.1042/bj2350723
2. Pillemer L, Blum L, Lepow IH, Ross OA, Todd EW, Wardlaw AC. The properdin system and immunity. I. Demonstration and isolation of a new serum protein, properdin, and its role in immune phenomena. *Science* (1954) 120:279–85. doi:10.1126/science.120.3112.279
3. Kouser L, Abdul-Aziz M, Nayak A, Stover CM, Sim RB, Kishore U. Properdin and factor h: opposing players on the alternative complement pathway "see-saw". *Front Immunol* (2013) 4:93. doi:10.3389/fimmu.2013.00093
4. Smith CA, Pangburn MK, Vogel CW, Muller-Eberhard HJ. Molecular architecture of human properdin, a positive regulator of the alternative pathway of complement. *J Biol Chem* (1984) 259:4582–8.
5. Higgins JM, Wiedemann H, Timpl R, Reid KB. Characterization of mutant forms of recombinant human properdin lacking single thrombospondin type I repeats identification of modules important for function. *J Immunol* (1995) 155:5777–85.
6. Goundis D, Reid KB. Properdin, the terminal complement components, thrombospondin and the circumsporozoite protein of malaria parasites contain similar sequence motifs. *Nature* (1988) 335:82–5.
7. Kouser L, Abdul-Aziz M, Tsolaki AG, Singhal D, Schwaeble WJ, Urban BC, et al. A recombinant two-module form of human properdin is an

inhibitor of the complement alternative pathway. *Mol Immunol* (2016) 73:76–87. doi:10.1016/j.molimm.2016.03.005
8. Pangburn MK. Analysis of the natural polymeric forms of human properdin and their functions in complement activation. *J Immunol* (1989) 142:202–7.
9. Alcorlo M, Tortajada A, Rodriguez de Cordoba S, Llorca O. Structural basis for the stabilization of the complement alternative pathway C3 convertase by properdin. *Proc Natl Acad Sci U S A* (2013) 110:13504–9. doi:10.1073/pnas.1309618110
10. Gulati S, Agarwal S, Vasudhev S, Rice PA, Ram S. Properdin is critical for antibody-dependent bactericidal activity against *Neisseria gonorrhoeae* that recruit C4b-binding protein. *J Immunol* (2012) 188:3416–25. doi:10.4049/jimmunol.1102746
11. Kimura Y, Miwa T, Zhou L, Song WC. Activator-specific requirement of properdin in the initiation and amplification of the alternative pathway complement. *Blood* (2008) 111:732–40. doi:10.1182/blood-2007-05-089821
12. Cortes C, Ferreira VP, Pangburn MK. Native properdin binds to *Chlamydia pneumoniae* and promotes complement activation. *Infect Immun* (2011) 79:724–31. doi:10.1128/IAI.00980-10
13. Ferreira VP, Cortes C, Pangburn MK. Native polymeric forms of properdin selectively bind to targets and promote activation of the alternative pathway of complement. *Immunobiology* (2010) 215:932–40. doi:10.1016/j.imbio.2010.02.002
14. Saggu G, Cortes C, Emch HN, Ramirez G, Worth RG, Ferreira VP. Identification of a novel mode of complement activation on stimulated platelets mediated by properdin and C3(H_2O). *J Immunol* (2013) 190:6457–67. doi:10.4049/jimmunol.1300610
15. Carroll MV, Lack N, Sim E, Krarup A, Sim RB. Multiple routes of complement activation by *Mycobacterium bovis* BCG. *Mol Immunol* (2009) 46:3367–78. doi:10.1016/j.molimm.2009.07.015
16. Ali YM, Hayat A, Saeed BM, Haleem KS, Alshamrani S, Kenawy HI, et al. Low-dose recombinant properdin provides substantial protection against *Streptococcus pneumoniae* and *Neisseria meningitidis* infection. *Proc Natl Acad Sci U S A* (2014) 111:5301–6. doi:10.1073/pnas.1401011111
17. Tsolaki AG. Innate immune recognition in tuberculosis infection. *Adv Exp Med Biol* (2009) 653:185–97. doi:10.1007/978-1-4419-0901-5_13
18. Rooijakkers SH, van Strijp JA. Bacterial complement evasion. *Mol Immunol* (2007) 44:23–32. doi:10.1016/j.molimm.2006.06.011
19. Abdul-Aziz M, Tsolaki AG, Kouser L, Carroll MV, Al-Ahdal MN, Sim RB, et al. Complement factor H interferes with *Mycobacterium bovis* BCG entry into macrophages and modulates the pro-inflammatory cytokine response. *Immunobiology* (2016) 221:944–52. doi:10.1016/j.imbio.2016.05.011
20. Ferguson JS, Weis JJ, Martin JL, Schlesinger LS. Complement protein C3 binding to *Mycobacterium tuberculosis* is initiated by the classical pathway in human bronchoalveolar lavage fluid. *Infect Immun* (2004) 72:2564–73. doi:10.1128/IAI.72.5.2564-2573.2004
21. Ramanathan VD, Curtis J, Turk JL. Activation of the alternative pathway of complement by mycobacteria and cord factor. *Infect Immun* (1980) 29:30–5.
22. Cywes C, Godenir NL, Hoppe HC, Scholle RR, Steyn LM, Kirsch RE, et al. Nonopsonic binding of *Mycobacterium tuberculosis* to human complement receptor type 3 expressed in Chinese hamster ovary cells. *Infect Immun* (1996) 64:5373–83.
23. Hu C, Mayadas-Norton T, Tanaka K, Chan J, Salgame P. *Mycobacterium tuberculosis* infection in complement receptor 3-deficient mice. *J Immunol* (2000) 165:2596–602. doi:10.4049/jimmunol.165.5.2596
24. Schlesinger LS, Bellinger-Kawahara CG, Payne NR, Horwitz MA. Phagocytosis of *Mycobacterium tuberculosis* is mediated by human monocyte complement receptors and complement component C3. *J Immunol* (1990) 144:2771–80.
25. Cywes C, Hoppe HC, Daffé M, Ehlers MR. Nonopsonic binding of Mycobacterium tuberculosis to complement receptor type 3 is mediated by capsular polysaccharides and is strain dependent. *Infect Immun* (1997) 65:4258–66.
26. Kouser L, Paudyal B, Kaur A, Stenbeck G, Jones LA, Abozaid SM, et al. Human properdin opsonizes nanoparticles and triggers a potent pro-inflammatory response by macrophages without involving complement activation. *Front Immunol* (2018) 9:131. doi:10.3389/fimmu.2018.00131
27. Kemper C, Hourcade DE. Properdin: new roles in pattern recognition and target clearance. *Mol Immunol* (2008) 45:4048–56. doi:10.1016/j.molimm.2008.06.034
28. Kemper C, Atkinson JP, Hourcade DE. Properdin: emerging roles of a pattern-recognition molecule. *Annu Rev Immunol* (2010) 28:131–55. doi:10.1146/annurev-immunol-030409-101250
29. Perdikoulis MV, Kishore U, Reid KB. Expression and characterisation of the thrombospondin type I repeats of human properdin. *Biochim Biophys Acta* (2001) 1548:265–77. doi:10.1016/S0167-4838(01)00238-2
30. Daigneault M, Preston JA, Marriott HM, Whyte MK, Dockrell DH. The identification of markers of macrophage differentiation in PMA-stimulated THP-1 cells and monocyte-derived macrophages. *PLoS One* (2010) 5:e8668. doi:10.1371/journal.pone.0008668
31. Al-Rayahi IA, Browning MJ, Stover C. Tumour cell conditioned medium reveals greater M2 skewing of macrophages in the absence of properdin. *Immun Inflamm Dis* (2017) 5:68–77. doi:10.1002/iid3.142
32. Xu W, Berger SP, Trouw LA, de Boer HC, Schlagwein N, Mutsaers C, et al. Properdin binds to late apoptotic and necrotic cells independently of C3b and regulates alternative pathway complement activation. *J Immunol* (2008) 180:7613–21. doi:10.4049/jimmunol.180.11.7613
33. Dixon KO, O'Flynn J, Klar-Mohamad N, Daha MR, van Kooten C. Properdin and factor H production by human dendritic cells modulates their T-cell stimulatory capacity and is regulated by IFN-gamma. *Eur J Immunol* (2017) 47:470–80. doi:10.1002/eji.201646703
34. Narni-Mancinelli E, Gauthier L, Baratin M, Guia S, Fenis A, Deghmane AE, et al. Complement factor P is a ligand for the natural killer cell-activating receptor NKp46. *Sci Immunol* (2017) 2(10):eaam9628. doi:10.1126/sciimmunol.aam9628
35. Agarwal S, Specht CA, Haibin H, Ostroff GR, Ram S, Rice PA, et al. Linkage specificity and role of properdin in activation of the alternative complement pathway by fungal glycans. *MBio* (2011) 2(5):e00178-11. doi:10.1128/mBio.00178-11
36. Russell DG. *Mycobacterium tuberculosis*: here today, and here tomorrow. *Nat Rev Mol Cell Biol* (2001) 2:569–77. doi:10.1038/35085034
37. Feng CG, Kaviratne M, Rothfuchs AG, Cheever A, Hieny S, Young HA, et al. NK cell-derived IFN-gamma differentially regulates innate resistance and neutrophil response in T cell-deficient hosts infected with *Mycobacterium tuberculosis*. *J Immunol* (2006) 177:7086–93. doi:10.4049/jimmunol.177.10.7086
38. Eum SY, Kong JH, Hong MS, Lee YJ, Kim JH, Hwang SH, et al. Neutrophils are the predominant infected phagocytic cells in the airways of patients with active pulmonary tuberculosis. *Chest* (2010) 137:122–8. doi:10.1378/chest.09-0903
39. Smith D, Hansch H, Bancroft G, Ehlers S. T-cell-independent granuloma formation in response to *Mycobacterium avium*: role of tumour necrosis factor-alpha and interferon-gamma. *Immunology* (1997) 92:413–21. doi:10.1046/j.1365-2567.1997.00384.x
40. Algood HM, Chan J, Flynn JL. Chemokines and tuberculosis. *Cytokine Growth Factor Rev* (2003) 14:467–77. doi:10.1016/S1359-6101(03)00054-6
41. Ehlers S, Schaible UE. The granuloma in tuberculosis: dynamics of a host-pathogen collusion. *Front Immunol* (2012) 3:411. doi:10.3389/fimmu.2012.00411
42. Dannenberg AM Jr. Delayed-type hypersensitivity and cell-mediated immunity in the pathogenesis of tuberculosis. *Immunol Today* (1991) 12:228–33. doi:10.1016/0167-5699(91)90035-R
43. Sanghi S, Grewal RS, Vasudevan B, Lodha N. Immune reconstitution inflammatory syndrome in leprosy. *Indian J Lepr* (2011) 83:61–70.
44. Huaux F, Lo Re S, Giordano G, Uwambayinema F, Devosse R, Yakoub Y, et al. IL-1α induces CD11b(low) alveolar macrophage proliferation and maturation during granuloma formation. *J Pathol* (2015) 235(5):698–709. doi:10.1002/path.4487
45. Mayer-Barber KD, Barber DL, Shenderov K, White SD, Wilson MS, Cheever A, et al. Caspase-1 independent IL-1beta production is critical for host resistance to *Mycobacterium tuberculosis* and does not require TLR signaling in vivo. *J Immunol* (2010) 184:3326–30. doi:10.4049/jimmunol.0904189
46. Correia JW, Freitas MV, Queiroz JA, PereiraPerrin M, Cavadas B. Interleukin-6 blood levels in sensitive and multiresistant tuberculosis. *Infection* (2009) 37:138–41. doi:10.1007/s15010-008-7398-3
47. Leal IS, Smedegard B, Andersen P, Appelberg R. Interleukin-6 and interleukin-12 participate in induction of a type 1 protective T-cell response during vaccination with a tuberculosis subunit vaccine. *Infect Immun* (1999) 67:5747–54.

48. Appelberg R, Castro AG, Pedrosa J, Minoprio P. Role of interleukin-6 in the induction of protective T cells during mycobacterial infections in mice. *Immunology* (1994) 82:361–4.
49. Bhatt K, Salgame P. Host innate immune response to *Mycobacterium tuberculosis*. *J Clin Immunol* (2007) 27:347–62. doi:10.1007/s10875-007-9084-0
50. Shaw TC, Thomas LH, Friedland JS. Regulation of IL-10 secretion after phagocytosis of *Mycobacterium tuberculosis* by human monocytic cells. *Cytokine* (2000) 12:483–6. doi:10.1006/cyto.1999.0586
51. O'Leary S, O'Sullivan MP, Keane J. IL-10 blocks phagosome maturation in *Mycobacterium tuberculosis*-infected human macrophages. *Am J Respir Cell Mol Biol* (2011) 45:172–80. doi:10.1165/rcmb.2010-0319OC
52. Moore KW, de Waal Malefyt R, Coffman RL, O'Garra A. Interleukin-10 and the interleukin-10 receptor. *Annu Rev Immunol* (2001) 19:683–765. doi:10.1146/annurev.immunol.19.1.683
53. Gazzinelli RT, Oswald IP, James SL, Sher A. IL-10 inhibits parasite killing and nitrogen oxide production by IFN-gamma-activated macrophages. *J Immunol* (1992) 148:1792–6.
54. Almeida AS, Lago PM, Boechat N, Huard RC, Lazzarini LC, Santos AR, et al. Tuberculosis is associated with a down-modulatory lung immune response that impairs Th1-type immunity. *J Immunol* (2009) 183:718–31. doi:10.4049/jimmunol.0801212
55. Barnes PF, Lu S, Abrams JS, Wang E, Yamamura M, Modlin RL. Cytokine production at the site of disease in human tuberculosis. *Infect Immun* (1993) 61:3482–9.
56. Ranaivomanana P, Raberahona M, Rabarioelina S, Borella Y, Machado A, Randria MJD. Cytokine biomarkers associated with human extra-pulmonary tuberculosis clinical strains and symptoms. *Front Microbiol* (2018) 9:275. doi:10.3389/fmicb.2018.00275
57. Aly S, Mages J, Reiling N, Kalinke U, Decker T, Lang R, et al. Mycobacteria-induced granuloma necrosis depends on IRF-1. *J Cell Mol Med* (2009) 13:2069–82. doi:10.1111/j.1582-4934.2008.00470.x
58. Rook GA. Th2 cytokines in susceptibility to tuberculosis. *Curr Mol Med* (2007) 7:327–37. doi:10.2174/156652407780598557
59. Gordon SV, Brosch R, Billault A, Garnier T, Eiglmeier K, Cole ST. Identification of variable regions in the genomes of tubercle bacilli using bacterial artificial chromosome arrays. *Mol Microbiol* (1999) 32:643–55. doi:10.1046/j.1365-2958.1999.01383.x
60. Brodin P, Majlessi L, Marsollier L, de Jonge MI, Bottai D, Demangel C, et al. Dissection of ESAT-6 system 1 of *Mycobacterium tuberculosis* and impact on immunogenicity and virulence. *Infect Immun* (2006) 74:88–98. doi:10.1128/IAI.74.1.88-98.2006
61. Harboe M, Johnson C, Nymo S, Ekholt K, Schjalm C, Lindstad JK, et al. Properdin binding to complement activating surfaces depends on initial C3b deposition. *Proc Natl Acad Sci U S A* (2017) 114(4):E534–9. doi:10.1073/pnas.1612385114

Conflict of Interest Statement: The authors declare that the research was conducted in the absence of any commercial or financial relationships that could be construed as a potential conflict of interest.

Advantages of publishing in Frontiers

OPEN ACCESS
Articles are free to read for greatest visibility and readership

FAST PUBLICATION
Around 90 days from submission to decision

HIGH QUALITY PEER-REVIEW
Rigorous, collaborative, and constructive peer-review

TRANSPARENT PEER-REVIEW
Editors and reviewers acknowledged by name on published articles

Frontiers
Avenue du Tribunal-Fédéral 34
1005 Lausanne | Switzerland

Visit us: www.frontiersin.org
Contact us: info@frontiersin.org | +41 21 510 17 00

REPRODUCIBILITY OF RESEARCH
Support open data and methods to enhance research reproducibility

DIGITAL PUBLISHING
Articles designed for optimal readership across devices

FOLLOW US
@frontiersin

IMPACT METRICS
Advanced article metrics track visibility across digital media

EXTENSIVE PROMOTION
Marketing and promotion of impactful research

LOOP RESEARCH NETWORK
Our network increases your article's readership